NARASARAOPETA ENGINEERING COLLEGE
(AUTONOMOUS)

PROCEEDINGS

INTERNATIONAL CONFERENCE

EMERGING TRENDS IN MECHANICAL ENGINEERING AND INDUSTRIAL AUTOMATION

NEC-ICETMEIA-2K21

30th & 31st July, 2021

Editors-in-Chief

Dr. M.Sreenivasa Kumar
Principal & Professor, Dept. of Mechnical Engineering

Dr. D.Jagadish
Professor, Dept. of Mechnical Engineering

Editors

Dr. D.Suneel
Vice-Principal & Professor, Dept. of ME

Dr. P.Suresh Babu
Professor, Dept. of ME

Dr. B.Venkata Siva
Professor & HoD Dept. of ME

Mr. M.Venkanna Babu
Associate Professor, Dept. of ME

Organized by

Department of **Mechanical Engineering**

In Association with **The Institution of Engineers (India)**

ISBN : 978-93-91420-02-4

Proceedings of

International Conference on

Emerging Trends in Mechanical Engineering and Industrial Automation

NEC-ICETMEIA- 2K21

30th – 31stJULY2021

Chief Editors

Dr.M.Sreenivasa Kumar Principal and Professor Department of Mechanical Engineering Narasaraopeta Engineering College Narasaraopet-522601	**Dr.D.Jagadish** Professor Department of Mechanical Engineering Narasaraopeta Engineering College Narasaraopet-522601

Editors

Dr.D.Suneel
Dr.B.Venkata Siva
Dr.P.SureshBabu
Mr.M.VenkannaBabu

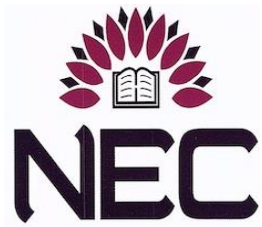

Organized By

Department of Mechanical Engineering

NARASARAOPETA ENGINEERING COLLEGE (AUTONOMOUS)

NARASARAOPET–522 601, ANDHRA PRADESH, INDIA

www.nrtec.in

Rs. /-

ISBN: 978-93-91420-02-4

First Edition: 2021

PublishedbySurneniMohanNaiduforSpectrumPublicationsandprintedatStudentsHelplineGroup,Hyderabad-38

SPECTRUM PUBLICATIONS™

knowledge at your hands...

#326/C, Surneni Nilayam, Near BK Guda Park, S.R.Nagar
Hydeabad-500038, India
Tel:+914023710657,32494570,23800657
Cell:+919440575657,9392575657
Fax:+914023810657
E-mail:studentshelpline.org@gmail.com

ACKNOWLEDGEMENT

It is my pleasure to record my sincere thanks to **Mr M.S.Chakravarthi, Hon'ble Vice Chairman**, NEC Group for his valuable guidance and encouragement throughout the proceedings of the conference. My sincere thanks to **Dr.M.Sreenivasa Kumar, Principal**, **NEC**, **Dr D. Suneel, Vice Principal NEC** and **Dr.B.Venkata Siva H.O.D., Mech.** for their whole hearted administrative support.

It's my privilege to thank the Keynote Speakers, Invited Speakers and Chairpersons of various technical sessions for their support in organizing the event. My sincere thanks to all the individual members of the Scientific Advisory Committee and Organizing Committee for their constructive ideas while designing the Conference Program. My special thanks to **Dr.Jose I. Rojas**, Division of Aerospace Engineering, Universitat politecnica de catalunya, Spain and **Dr. Naresh Kakur**, Department of Aerospace Engineering, Khalifa University of Science and Technology, UAE for sparing their valuable time. I thank all the participants who submitted the scientific and technical papers for sharing their ideas.

NEC-ICETMEIA 2K21conference would have been impossible without the support of academic institutions and industrial organizations both in terms of manpower and ideas. This support is greatly acknowledged. I thank my management **Sri M.V.Koteswara Rao** Garu, Chairman and **Sri M.Ramesh Babu** Garu Secretary for their kind support and encouragement for the conference.

My heartfelt thanks to my colleagues and all my research team members whose efforts and hard work in organizing and managing the conference are gratefully acknowledged. I thank Co-Conveners and Organizing Committee forrenderingtheirsupporttotheconference.

I sincerely thank M/S Spectrum Publications Hyderabad for bringing out the Souvenir and Pre Conference Proceedings well in time.

Finally, I thank all the people and institutions who are directly and indirectly involved in organizing the Conference.

I thank one and all

Dr.D.Jagadish
Professor
Department of Mechanical Engineering
Narasaraopeta Engineering College (Autonomous)
Chief Editor
NEC-ICETMEIA- 2K21

Chief Patron

SrM.S.Chakravarthi, B.Tech, MS(US),eMBA(ISB-Hyd)
Vice -Chairman, NEC Group

Patrons

Sri M.V.Koteswara Rao, B.Sc
Chairman, NEC Group

Sri M.Ramesh Babu, B.Com
Secretary, NEC Group

Co-Patrons

Dr.M.Sreenivasa Kumar, M.Tech, Ph.D(UK),MISTEE,FIE(I)
Principal, NEC

Dr.D.Suneel, M.Tech, Ph.D, FIE(I),MISTEE,MRSI
Vice Principal, NEC

Convener

Dr.B.Venkata Siva, M.Tech, Ph.D, FIE (I), MISTE, ISNT
Head, Dept. of ME

Co-Conveners

Dr.D.Jagadish,M.E, Ph.D,
Professor, Dept. of ME
Dr. P.Suresh Babu,M.Tech, Ph.D
Professor, Dept. of ME

Organizing Committee

Mr.M.VenkannaBabu	Mr.B.Rajiv Kumar
Mr.M.Venkaiah	Mrs.P.Sravani
Mr.P.Srinivasarao	Mr.ShaikBajan
Mr.Ch.Sekhar	Mr.T.Ashok Kumar
Mr.K.Kiran Chand	Mr.B.Ramababu
Mr.N.VijayaSekhar	Mr.T.N.V.MaheshBabu
Mr.K.JohnBabu	Mr.D.Mojeswara Rao
Mr. SK.NagulMeeravali	Mr. P.Sarath Chandra

Conference Advisory Committee

Prof.MarinaL.Galano,
Dept. of Material Science, UNIVERSITY OF OXFORD, UK

Dr.RukminiSrikantRevuru,
Assoc Prof. University of Northern Lowa, Cedar Falls, IA, USA

Jose I.Rojas,
Department of Physics – Division of Aerospace Engineering,
Universitatpolitecnica de catalunya, Spain

Kishore Kumar Sadasivuni,
Department of ME & IE, Qatar University, Qatar

Prof. N Siva Prasad,
Pro Vice Chancellor, GITAM University, Hyderabad

Dr.K.Srinivasa Reddy,
Professor, Dept of ME, IIT Madras

Prof. V.V.Subbarao,
Principal, UCEN, JNTUK, Narasaraopet

Dr.A.Gopala Krishna,
Professor, Director (R&D), JNTUK

Dr.D.Chakradhar,
Asst. Prof. Dept. of ME, IIT, Palakkad

Dr. K.L.Sahoo,
Sr.Prinicpal Scientist, CSIR, NML, Jamshedpur

Dr. Y. Ravi Kumar,
Asoc. Prof. Dept. of ME, NIT, Warangal

Dr.Y.Naresh,
Asst. Prof. Dept. of ME, SVNIT, Surat

Dr.Ramakrishna Ramachandran,
Assoc. Prof. Dept. pf D&A, VIT, Vellore

Dr. P.S. Rama Sreekanth,
Dept. of ME, VIT, A.P

Mr. Jnanananda Rao Kadi,
Deputy Manager, Bharat Dynamics Ltd., Hyderabad

Dr.Srinivasu Gangisetty,
Asst. Prof. Dept. of ME, NIT, Raipur

Conference Papers Review Board

Dr.M.Sreenivasa Kumar, Professor, Principal, NEC

Dr.D.Suneel, Professor, Vice Principal, NEC

Dr.B.Venkata Siva, Professor, Head, Dept. of ME, NEC

Dr.D.Jagadish, Professor

Dr.P.Suresh Babu, Professor

M.Venkaiah, Associate Professor

P.Srinivasarao, Assistant Professor

Ch.Sekhar, Assistant Professor

M.Venkanna Babu, Assistant Professor

K.Kiran Chand, Assistant Professor

P.Sravani, Assistant Professor

T.Ashok Kumar, Assistant Professor

N.Vijaya Sekhar, Assistant Professor

B.Rajiv Kumar, Assistant Professor

K.John Babu, Assistant Professor

Shaik Bajan, Assistant Professor

P.Sarath Chandra, Assistant Professor

SK.Nagul Meeravali, Assistant Professor

Mr.B.Ramababu, Assistant Professor

Mr.T.N.V.Mahesh Babu, Assistant Professor

Mr.D.Mojeswara Rao, Assistant Professor

PREFACE

International Conference on “Emerging Trends in Mechanical Engineering and Industrial Automation” **NEC-ICETMEIA-2K21** provides an excellent international forum for sharing knowledge and results in theory, methodology and applications impacts and challenges of Mechanical Engineering. The purpose of this conference is to bring together the mechanical engineering community to explore, disseminate and strengthen initiatives in new directions under the broad areas of Manufacturing, Thermal Sciences, Mechanical Design, Robotics, Mechatronics and Industrial Automation.

The objective of this conference is to create an international conglomeration of scientists, engineers and institutional experts. This forum serves as platform where people can share information about latest diverse technological advancements, innovations and achievements in the areas of Mechanical Engineering and allied fields of Engineering. Further it would also facilitate the discussion that centers on the developments and challenges in the fields of design, manufacturing, thermal, robotics, mechatronics fields of Engineering. The focus of this conference is to provide technical platform that encourages the scientific research and educational activities that would cater the needs of both society and the industry. Most importantly, NEC-ICEMEIA-2K21 is invested in the advancement of a common man’s life by utilizing the theory and practice of mechanical engineering and allied streams of Engineering. The conference includes Keynote addresses and guest lectures by eminent speakers around the globe who would deliberate the recent trends and challenges in the fields of Mechanical Engineering and Industrial Automation.

Message from Vice Chairman

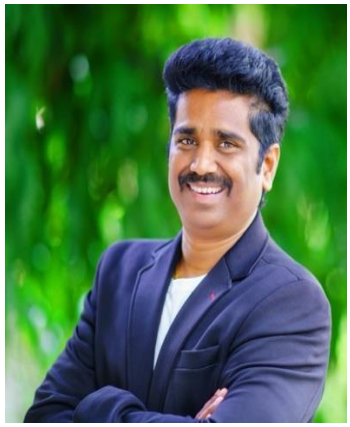

I am glad to know that Department of Mechanical Engineering of Narasaraopeta Engineering College is organizing “International Conference on Emerging Trends in Mechanical Engineering and Industrial Automation” [NEC-ICETMEIA2K21]. I hope this e-conference can congregate academicians, industry personnel and research scholars to share their findings and insights about innovations in Mechanical Engineering. The theme of the conference emphasizes on key aspects of Manufacturing, Thermal Sciences, Mechanical Design, Robotics, Mechatronics and Industrial Automation. I hope this initiative by Department of Mechanical Engineering will pave way to exceptional deliberations and other activities to enhance the power of knowledge and ideology in the field of engineering.

I wish the organizers great success for the conference.

Mr.M.S.Chakravarthi
Vice Chairman
NEC-Group

Message from Principal

I am glad to know that the Department of Mechanical Engineering of Narasaraopeta Engineering College organizing an International Virtual Conference on "Emerging Trends in Mechanical Engineering and Industrial Automation" [NEC-ICETMEIA2K21] during 30th& 31st of July 2021. The unprecedented ongoing pandemic situation prevailing all over the globe has driven the professionals to continue their research and knowledge dissemination virtually. I believe that such virtual conferences will be one of the finest opportunities for academicians, scientists, professionals, students and researchers from all over the globe to share and express their views, discuss the practical challenges and possible solutions in Science & Engineering fields.

The theme of the conference emphasizes the necessity of engineering innovation Mechanical Engineering in these difficult times all over the globe. I hope the scientific deliberations, discussions and other activities that happen during the conference will enrich the participants and definitely leave new milestones.

I wish the organizers the very best for the success of the Conference

Dr. M.Sreenivasa Kumar
Professor & Principal
Narasaraopeta Engineering College

Message from Vice Principal

It gives immense pleasure to write a message for the International Conference on "Emerging Trends in Mechanical Engineering and Industrial Automation" [NEC-ICETMEIA2K21] organized by Department of Mechanical Engineering, Narasaraopeta Engineering College (Autonomous) during 30th& 31st of July 2021. There are truly amazing innovations and breakthrough nowadays in the selected fields of Mechanical Engineering. I expect the present International Conference will explore students and research scholars to focus much on the field of Mechanical Engineering and Industrial Automation. I have gone through some of the abstracts and could see its rich qualitative academic content. I am also able to envisage its great potential to discuss and learn some new innovations in the fields of Mechanical Engineering.

It is important to inculcate an attitude towards research in the minds of younger generation and this conference would be a stepping stone towards this attainment in the field of Mechanical Engineering.

I wish the conference a great success. I am sure the conference is a grand scientific extravaganza and great feast for the student community.

Dr.D.Suneel
Professor & Vice Principal
Narasaraopeta Engineering College

Message from Head of the Department

I am very much delighted in welcoming the delegates for the 2 day virtual international conference on “Emerging Trends in Mechanical Engineering and Industrial Automation” [NEC-ICETMEIA2K21]. The pursuit for knowledge has been from the beginning of time but knowledge only becomes valuable when it is disseminated and applied to benefit of humankind. The prime focus of this conference is to bring together academicians, researchers and industry professional to join hands in finding the scope, challenges and opportunities and solutions that are encountered in the fields of Mechanical Engineering.

Our technical sessions are rich and varied in the domains of Machine Design, Production Engineering, Thermal Engineering and Automation. As a conference Convener, I know that the success of the conference depends ultimately on the many people who have worked with us in planning and organizing both the technical program and virtual technical deliberations. In particular, we thank the review and advisory committee for their wise advice and brilliant suggestion on organizing the technical program; the Program Committee for their thorough and timely reviewing of the papers and publishing them in a conference proceeding. It is envisaged that the intellectual discourse will result in future collaborations between Universities, research institutions and industry globally towards the recent technological developments of Mechanical Engineering, during this pandemic situation.

Dr.B.Venkata Siva
Professor & Head
Department of ME
Convener, ICETMEA-2K21

LIST OF FULL LENGTH PAPERS SELECTED FOR PROCEEDINGS

International Conference on Emerging Trends in Mechanical Engineering and Industrial Automation

NEC-ICETMEIA- 2K21

***

 ISBN: 978-93-91420-02-4

Effectiveness of Compression-Ignition Engine Fuelled with Pond Water Algae Biodiesel

Katta Murali Krishna Prasad and P. Sravani
Department of Mechanical Engineering, Narasaraopeta Engineering College (AUTONUMOUS), Narasaraopet, A.P.

***Abstract*—Algae are the fast-growing florae around the globe. Microalgae are largely a diverse group of microorganisms comprising eukaryotic photoautotrophic protists and prokaryotic cyanobacteria (sometimes called blue-green algae). These microbes contribute to half of global photosynthetic activity and are virtually found in euphotic niches. The viability of biodiesel from pond water algae (PWA) as a third-generation biodiesel feedstock is examined in current investigation. Primarily, the oil is extracted from the algal biomass and then it is subjected to two stage trans-esterification technique. Ethanol is mixed up with the attained algal bio oil in order to reduce its viscosity. The processed algal oil is blended with diesel in various proportions. Later, by direct-injection into compression-ignition, the engine's performance and emission characteristics are assessed at varying loads (25, 50 and 100%) and CRs (15.5, 16.5, 17.5 and 18.5) using these prepared blends. Results have depicted that performance indices of engine are enhanced and emission parameters are reduced with the increase of algal biodiesel proportion in diesel fossil fuel.**

Keywords: Selective catalytic reactor, honeycomb, catalyst, space velocity, NOx conversion efficiency, ammonia slip.

I. INTRODUCTION

Energy executes a noteworthy role in development. The fiscal development of any nation relies on its energy consumption. It is vital in every sector around the world, i.e. transportation, manufacturing, agriculture sector etc. BP Statistical Review reported that primary energy consumption by fuel is 13276.3 M toe. However, total proven oil reserves are 1706.7 thousand million barrels in the world till the end of 2016, which is sufficient to meet 5to6 decades of world energy demand [1].The world energy consumption is drastically increased from ~1687.7 kg in 2003 to 1873.7 kg in2010 (per capita kg of oil equivalent). However, diesel fuel consumption per capita increased by ~ 37% between 2003 and 2010 for the automotive diesel engine [2,3]. It has been found 900 million vehicles (except two-wheelers) throughout the world that produces almost 26% greenhouse gases (GHGs) emissions [4]. Nearly all types of automobiles operated by diesel and petrol play a vital role in air pollution. To curbs out pollution hazards, many countries adopted and implemented the updated emission standards, and made a policy to use alternative energy sources. In India, Bharat Stage VI (BS-VI) standards are going to be implemented from 2020, surpassing BS-V to control the continuous increasing pollution hazards from automobiles. Various worldwide emission standards (Bharat Stage, China, and Euro) for cars and light trucks (diesel vehicles) for the last decade are shown in Fig.1[5]. A flow chart of transportation activities and their emission are presented in Fig. 2, and the vehicle population growth (commercial~29.6%and passenger~34.9) from 2010t o 2020 are shown in Fig. 3 [6].

II. REVIEW OF LITERATURE

Saharetal. [19] Studied the technique for biodiesel production and analysis from used cooking oil with feedstock pretreatment method, transesterification process, whereas Mohadesi et al. [20] examined the impact of KOH/Cl inoptilolite as a catalyst to produce biodiesel using used cooking oil. Kassaby and Allah[21] examined the effect of varying compression ratios (CR14, CR16, CR18) at different speeds (1000, 1250,1500, 1750, and 2000 rpm) on CI engine fueled with different blends (B0, B10, B20,B30, B50) and ensured that the 20% biodiesel blended safely with diesel fuel and delivered almost the same performance and exhaust emissions when compared with diesel.

III. EXPERIMENTALINVESTIGATION

A. Biodiesel preparation

Blends of fossil fuel diesel, PWA oil and ethanol are employed in CI engine as fuels. Initially, Algae was collected from local pond (PWA) present in Krishna district of Andhra Pradesh state, India. Preparation of PWA biodiesel is depicted through Fig. 6.Collected PWA were ground with motor as much as possible. The ground PWA were dried for 20 min at 80°C in an incubator for releasing water. Hexane and ether solution (20 and 20 mL) were mixed with the dried PWA to extract oil. Then the mixture was kept for24 h for settling. The biomass was collected after filtration and weighted.

The extracted oil was evaporated in vacuum to release hexane and ether solutions using rotary evaporator. 0.25 g NaOH was mixed with 24 mL methanol and stirred properly for 20 min. The mixture of catalyst and methanol was poured into the algal oil in a conical flask in order to lessen its viscosity. Later, transesterification reaction process is carried out. The conical flask containing solution was stirred for 3h by electric shaker at 300rpm. The reaction process step is indicated in Fig. 1.

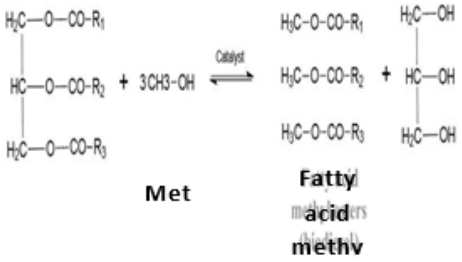

Fig.1. Transesterification reaction

 ISBN: 978-93-91420-02-4

A. ENGINESETUPAND INSTRUMENTATION

Fig. 2 depicts the schematic of computerized multifuel 4-stroke VCR engine. This setup comprises single-cylinder,variablecompression ratio direct-injection compression-ignition engine which the loading is done by dynamometer of eddy current type. There is no need to stop the engine in order to alter its compression ratio (CR). Air box fitted with orifice plate makes the way for air to enter the engine. The instrumentation box comprises gaging instruments for engine speed, air & fuel consumption,torque, temperature and coolant flowrates. Sensors will record these parameters and values will be sent to data acquisition device,which exhibits these data in computer using LabView software.The technical specifications of engine aretabulatedin Table 2.

Specification	Details
Make	Kirloskar
Engine cylinder/stroke	1/4
Maximum fuel injection pressure	220bars
D* L	87.5 * 110 mm
Compression ratio	15.5-18.5
Rated output	4.5kWat1500 rpm
Rated speed	1500rpm

IV. EXPERIMENTALTESTPROCEDURE

The prepared fuel blends are tested under various engine loads. Prior to each experimentation, the engine is run with diesel for 10 min to ensure the reliability of attained data. The experiment values are taken after the engine reached to a steady state condition. The stationary multi fuel engine employed here is operated to run at its maximum speed of 1500 rpm. The temperature and relative humidity of intake air is measured with the aid of RTD sensors and the velocity is measured using velocity sensors.

All tailpipe exhausts are evaluated in a real-time manner. The engine load was managed via the load cell. The engine's fuel consumption was estimated by calculating the decrease in the fuel level and in the measurement container over a specified period of time.

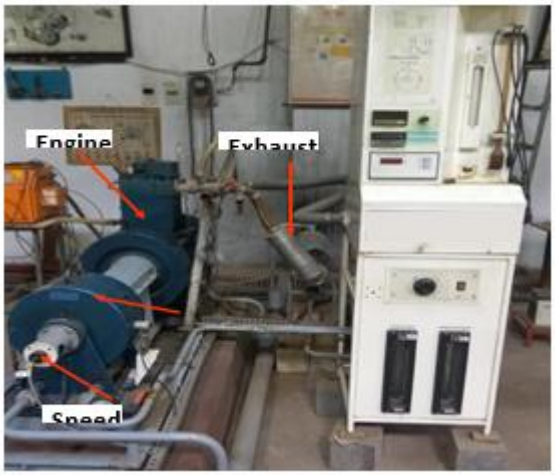

Fig.2. Engine setup

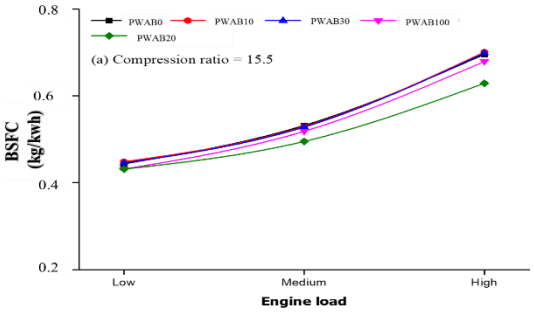

RESULTS

The prepared blends (PWAB0, PWAB100, PWAB10, PWAB20 and PWAB30) are examined experimentally using VCR diesel engine at various CRs of 15.5and 17.5at different engine loads of 25, 50 and 100% by maintaining uniform speed of 1500 rpm. The performance attributes viz., BTE and BSFC and emission parameters viz., EGT, CO_2, PM, and NO_X are investigated for analyzing the PEC of the engine.

A. Brakethermal efficiency

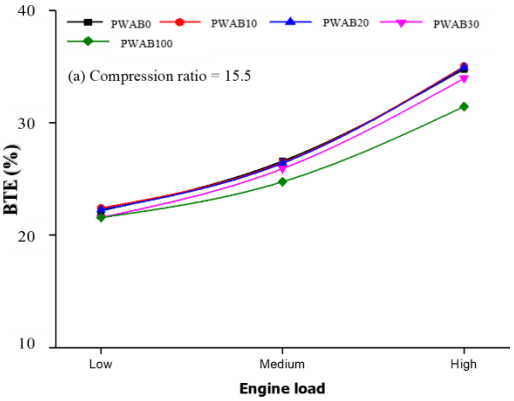

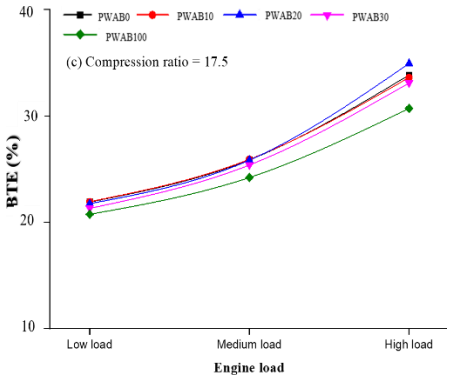

B. Brakespecificfuelconsumption

 ISBN: 978-93-91420-02-4

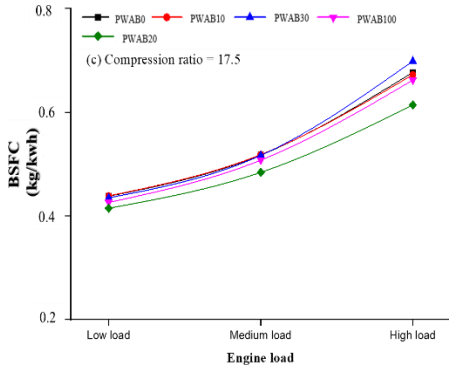

Fig. 3. BSFC at various engine load with different Compression Ratio

The variation of fuel NOX emission with engine load for the engine compression ratio at 15.5 and 17.5 are given in Figure 3 (a, c). The comparison of NO_X emissions with the low, medium and high engine load shows for PWAB0 (diesel), PWAB 10 (90% diesel + 10 PWA oil), PWAB20 (80% diesel + 20% PWA oil), PWAB30 (70% diesel +30% PWA oil) and PWAB100 (100% PWA biodiesel). TheNOXemission of a blend of PWAB10, PWAB30 and PWAB100 found to be lower from those of diesel and PWAB20 for the entire range of engine load. NOX emissionraised with enhancement in engine load due to elevated combustion temperature. Theincreasing compression ratio in the engine than NOXemission increased due to the improved combustion characteristics [50-52]. The NOX emission (ppm) produced for PWAB0 is 3663.9 at CR15.5, 3828.4 at CR17.5. The NO_X emission (ppm) for PWAB10 is3941.9 at CR15.5,4061.5 at CR17.5 , and PWAB20 is 2588.4 at CR15.5, 1960.5 at CR17.5 and 1703.1 at full load condition.

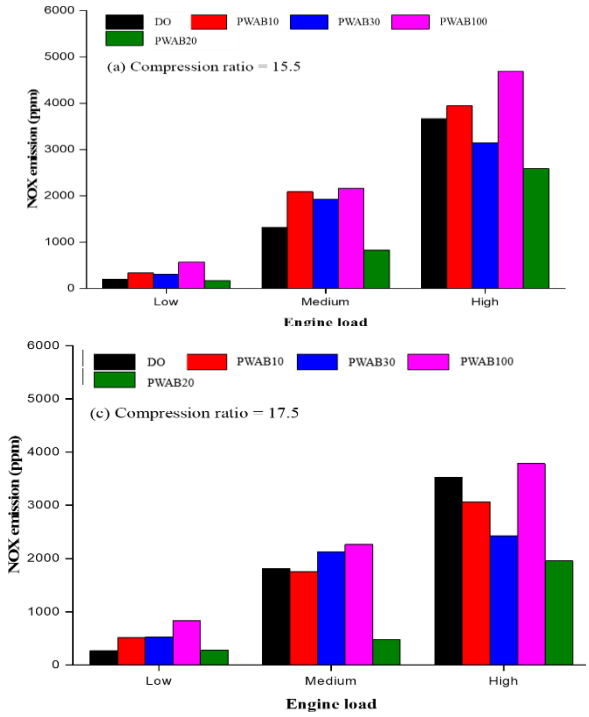

Figure4.Engineload Vs. NOx emission with different compression ratio

SUMMARY AND CONCLUSIONS

According to the investigation results obtained from the present study, performance and emission characteristics of BTE, BSFC and PM, CO2, EGT & NO_X emissions of CI engine charged with pond water algae diesel for various engine loads and CR has been summarized below.

- The reduction in exhaust gas temperature has been found for the PWA biodiesel blends than diesel fuel at all engine loads. Maximum EGT was observed at 15.5 CR, 1500 rpm and high engine load.
- Less BSFC has been noticed from the CI engine fuelled with PWA biodiesel blends than CI engine charged with diesel at all engine loads.
- PM from tail pipe of CI engine has been declined with the addition of PWA biodiesel to the diesel fuel. PM emissions decrease with increased compression ratio in the present investigation.
- Due to increase in compression ratio of the engine, CO_2 emission decreases as thermal efficiency increases and fuel consumption reduces.
- Escalation of CR from 15.5 to 117.5 leads to increase in NOXemission by5.04%and3.57%for diesel fuel and PWA biodiesel blend(PWAB10),respectively, indicating improved biodiesel combustion at higher CR. NOX emission escalates with rise in the engine load due to elevated combustion temperature.
- TheriseinengineCRescalatesthetailpipeemissionsbecauseofimprovementin combustion of biodiesel in engine at higher CR.

VII. REFERENCES

1. Dudley BDS. BP Statistical Review of World Energy: 49.n.d.
2. Energy use (kg of oil equivalent per capita) n.d.https://data.worldbank.org/indicator/EG.USE.PCAP.KG.OE(accessed April1, 2021).
3. ChintalaV,Subramanian KA. Assessment of maximum available work of a hydrogen fueled compression ignition engine using exergy analysis. Energy 2014; 67:162–75.
4. Nesamani KS. Estimation of automobile emissions and control strategies in India.SciTotal Environ 2010; 408:1800–11.
5. Emission Standards-Summary of worldwide engine and vehicle emission standards n. d. https://www.dieselnet.com/standards/(accessed April3, 2021).
6. Wagner I. Number of passenger cars and commercial vehicles in use worldwide from 2006 to 2015 in (1,000 units) n.d. https://www.statista.com/statistics/281134/number-of-vehicles-in-use-worldwide/(accessedApril3, 2021).
7. Venkanna, B. K., and Venkataramana Reddy, C., 2011. Performance, emission and combustion characteristics of DI diesel engine running on blends of calophylluminophyl lumlinn oil(honeoil)/dieselfuel/kerosene.Int.J.RenewableEnergyTechnology,2(3): 294-305.
8. Silvio, C.A. de A., Belchior, C.R., Nascimento, M.V.G., Vieira, L. dos S.R. andFleury, G. 2002, Performance of a diesel generator fuelled with palm oil, Fuel,81:2097–2102.
9. Nwafor, O.M.I., Rice, G. and Ogbonna, A.I. 2002. Effect of advanced injection timing on the performance of rapeseed oil in diesel engines, Renewable Energy,21: 433–444.

 ISBN: 978-93-91420-02-4

Design and Analysis of Disc Brake of an Electric Go-Kart

Suvikram Pradhan, Deepankar Mahato, G. Avinash Sharma and Anshuman Nayak
Department of Mechanical Engineering
GIET University, Gunupur,Odisha, Pin-765022, India

***Abstract*— As technologies are emerging day by day there is a large development in the automobile sector. And even the technologies for all of the vehicles such as bike, car, and luxury vehicles are improving day by day. And now even some of the vehicles are running using some of the non-conventional sources of energy such as bio diesel, battery or even solar energy. As a result of all the advancement in the automobile industries some of the companies are using microprocessors as well as microcontrollers and some pre-defined nano-computers to do some of the tasks. But the most important concern in today's date is safety of the person those who will be riding the vehicle. So it is one of the major concerns to develop a brake which is not only capable of stopping the vehicle at a least possible distance but also have some of the most desirable characteristics. Thus the paper is presented for the analysis {static and thermal} of the disc brakes which are one of the most efficient brakes and we can say a miracle of Engineering. Modeling was done using CATIA V5R21 software and Static and Transient Thermal Analysis was done using ANSYS software.**

Keywords—Disc brake, Thermal analysis, Static analysis.

I. INTRODUCTION

A brake is a device which is used stop the vehicle at a minimum possible distance and should have a good amount of the anti-fading characteristics. In general when the brake is applied 2 pistons force the rotating disc to stop and the energy is converted to thermal or heat energy and it start to decelerate.

Properties of brake required:

1) Should have good anti-fade characteristics.
2) Easy of operation.
3) Should able to stop the vehicle at the least possible distance.

Classification:

4) As per actuation
   - Mechanical
   - Pneumatic
   - Vacuum
   - Servo
   - Hydraulic
5) As per fitting
   - At the transmission system
   - At the wheels
6) As per purpose
   - Primary Brakes
   - Secondary Brakes
7) As per construction
   - Drum Brakes
   - Disc Brakes

Brakes are one of the it should maintain a good anti-fading characteristics important parts of an automobile control system that is used to stop the vehicle at the least possible distance and also and moreover it should be requiring very less amount of maintenance or no maintenance and should be economic.

OBJECTIVES:

- V5R21 software. Design the go-kart disc brake using CATIA
- Static structural analysis of the disc brake using ANSYS software to calculate the resulting value of principal and vonmises stresses.
- Thermal structural analysis of the disc brake using ANSYS software to calculate the resulting value of heat distribution and various parameters.

II. LITERATURE REVIEW

STABILITY OPTIMIZATION OF A DISC BRAKE SYSTEM WITH HYBRID UNCERTAINTIES FOR SQUEAL REDUCTION BV RUI LII AND DEJIE YU ON 28 JANUARY 2016

It is clearly mentioned about how Brake squeal is a noise problem which is caused due to self-friction and some number of induced vibrations which may help in inducing squealing noise. It is also been mentioned about the previous Researchers been carried out on brake sequel and several representative mechanisms that have been attributed to break squeal phenomenon, like stick- slip, sprag-slip, hammering, mode coupling, and time delay [2-5]. However, even after conducting several experiments on brake squeal it is not fully understood because of various Complexities.

From the mentioned studies, due to some uncertain Factors present in the structure and systems, as well in the brake system. So, for avoiding such uncertainties, RBDO was introduced which is basically the revised form of First Order Reliability Method (FORM)and is a double loop strategy; the reliability analysis (inner loop) and the structural optimization (outer loop). Therefore, it is considered as the best method for improving the performance, stability of an uncertain due to disc brake systems in order to reduce the sequel.

DESIGN AND ANALYSIS OF DISC BRAKE, BY G. VENKAT KUMAR, R. DILIP KURIAN, R. HARISH KUMAR, M.G.MOHAN RAO, ON 1 FEBRUARY 2018;

It is clearly mentioned about the development of disc brake which was patented by Frederick William Manchester in his Birmingham factory in the year 1902 and was been successfully used a Lanchester car. It is successful application started in airplanes and in tanks during the world War 2. While in Britain, Daimler company used the disc brakes on its armored car in the year 1939. Those disc brakes were made by girdling company, and it became necessary for the four-wheel drive (4 * 4) vehicle where the

epicyclic final drive was present in the wheel hubs and no room was left for the conventional hub mounted drum brake. Then at Germany's Argus motoren, Hermann Klave (1912-2001) thin patented disc brakes on his name in the year 1940. After that Chryster developed unique braking system, from 1949 to 1953.It was first used in racing in 1951, the one BRM type 15, using a Girling produced set, and for a formula one car. Then the first mass production was done 1955 on the Citroen ds, which featured the front disc brake caliper type, which is one of many Innovations. The model was sold up to 1.5 million units over a period of 20 yrs. with the same setup.

REVIEW PAPER ON THERMAL ANALYTICS OF VENTILATED DISC BRAKE BY VARYING DESIGN PARAMETERS, BY SUBHASISSARKAR, PROF. (DR)PRAVIN RATHOD, ON 12 DECEMBER 2013.

TING-LONG, HD-ET at (1974): - It has been mentioned on the investigational marks been carried out by on effect of frictional heating on brake material (aircrafts). Here metallographic study apparatus is used. It has been discovered that a minimum surface temperature which would result the minimum value of (1/pc) and (1/kpc) when the area of contact is maximum and by higher load – lower friction system.

Masahiro Kubota et al (2000): - here it is mentioned about the uses of CFD analysis (computational fluid dynamics) approach which is used for visualizing the actual process. Short and ground sharped arrangement and been used and the result showed the anti-squeal property was improved and also a weight reduction was seen when compared with respect to baseline rotor shape without giving cooling performance and heat resistance factor to determinate.

Oder G.et al.(2009): - it is mentioned on the work on the terminal and analysis of streak on the break disc in railway vehicles. And then in addition centrifugal load is considered. Here finite element method (FEM) approach has also been used. 3D model was modelled for analyzing purpose brake disc is of rounded graphite material. They are also fulfilling the buyer's requirements in order for safety purposes. The investigation done didn't considered shearing forces, residual and cyclic loads, during the entire lifespan of brake discs, the results were needed to be compared with respect to experimental results.

Comparative life cycle assessment of car disc brake systems-case study results and method discussion about comparative LCAS, BY Katja Tasala Gradin, Anna Hedlund Astrom; ON 11 October 2019;

Here, it is mentioned about two-disc brakes that were assessed under the guidelines of the ISO 14040: 2006 Standard (ISO 2006). Here it is mentioned of the life cycle and it impact on the new disc brake and then it was compared to the life cycle of the reference disc brake that was taken. i.e., from cradle to the grave, which also included processes of material extraction until the waste management and for comparing the impact of environment sima Pro version 9.0.0.47 (PRE-Consultants 2019) was used?

Then in the case study it was found that in Phu LOW BRASYS (Low environmental Impact BRAKE System) project (LOWBRASYS 2017) was considered, the objectives of one of the projects was in order to develop a new disc brake which helps in reducing particular generation while braking condition. The wear testing for the project partner, indicated about 16% decrease in the particulate formation.

RESEARCH PAPER ON MODELING AND SIMULATION OF DISC BRAKE TO ANALYSE TEMPERATURE DISTRIBUTION USING FEA, BY SUBHASIS SARKAR (DR), PRAVIN P. RATHOD A.I. MODI. 2014 ISSUE 03, VOL. 2 OF IISRD;

Here it is mentioned of a paper presented by Talati and Talalifar (2009), about the heat conduction in a disc brake system, here the governing heat equations applied for the disk and then the pad an extracted which are in a form of transient heat equations with some amount of heat generation And then the conclusion made was that the heat that was generated because of friction generated between the disc and the pad must be ideally dissipated to the environment in order for avoiding the decrease in friction coefficient between the dire and pad to avoid rise in value of temperature and excessive heating leading to brake fluid vaporization.

III. MATERIALS USED FOR MANUFACTURING OF DISC BRAKE

There are various materials that can be used for manufacturing of brakes but the materials are chosen in such a way that it should be economic as well as having a high wear and tear resistance and cannot fade in a short period of time while it should be able to stop the vehicle at a minimum possible distance:

1) CAST IRON

2) STAINLESS STEEL

These are the most common materials that are being used for manufacturing of disc brakes.

DESIGN PARAMETERS OF DISC BRAKE

It is designed using the CATIA software and the CAD model is shown below: {Diameter 190mm}

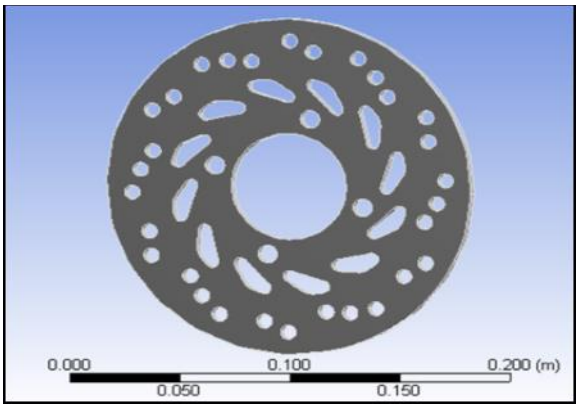

IV. ANALYSIS OF DISC BRAKE

The analysis of the disc brake is done using the FEM meaning finite element analysis in ANSYS MECHANICAL and has calculated most of the parameters that are responsible of the failures of the braking equipment. In this paper we analyzed static and transient thermal analysis of disc brake system. In material section of disc brake is to be Grey cast iron. Both analysis has done using ANSYS software.

 ISBN: 978-93-91420-02-4

A. STATIC STRUCTURE ANALYSIS

Through static structural analysis we can get the resulting values of the various stresses acing on the disc and most important fact is that we can find the values of the maximum and minimum values of the resulting stress. This method uses FEM as a base method and does the calculation using various failure criteria so we can say failure theories.

CAE RECORDS (static):

1) Stainless Steel

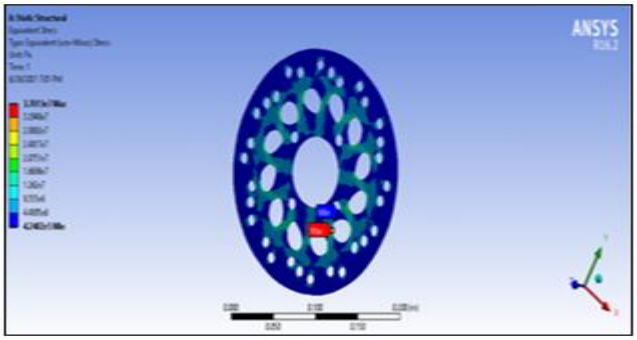

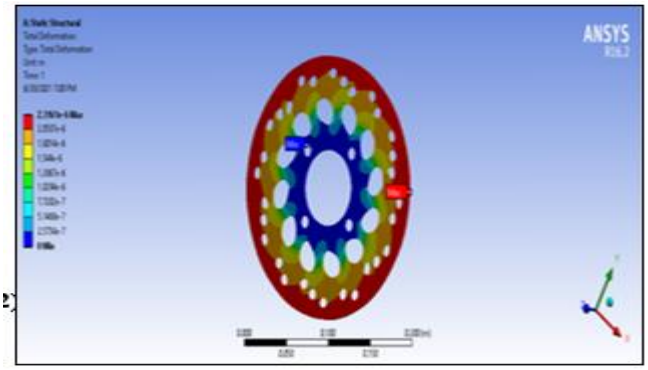

2) Cast Iron

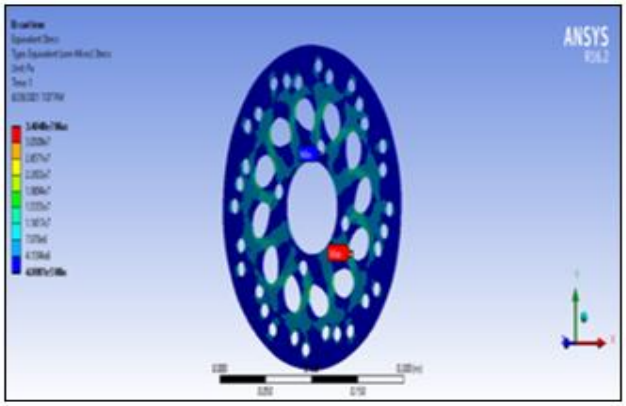

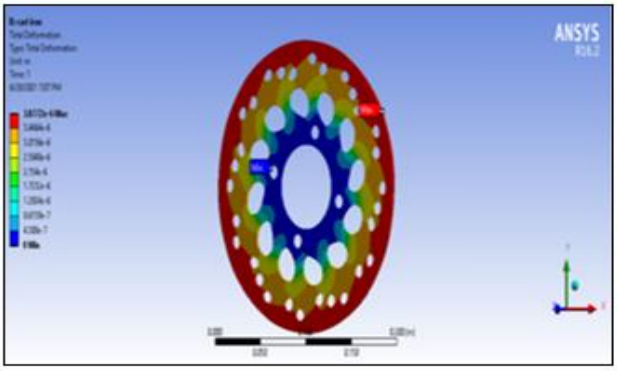

B. THERMAL ANALYSIS

Through thermal structural analysis we can get the resulting values of the various thermal properties acing on the disc and most important fact is that we can find the values of the maximum and minimum values of the thermal parameters. This method uses FEM as a base method and does the calculation using various failure criteria so we can say failure theories.

CAE RECORDS (thermal):

1) Stainless steel

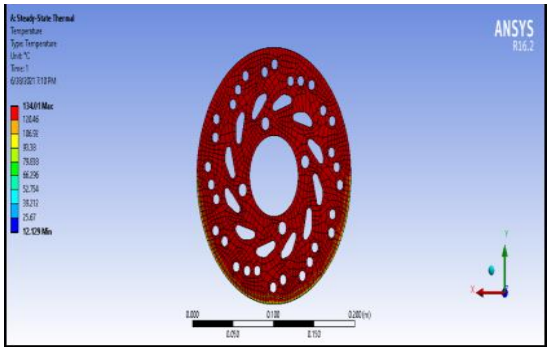

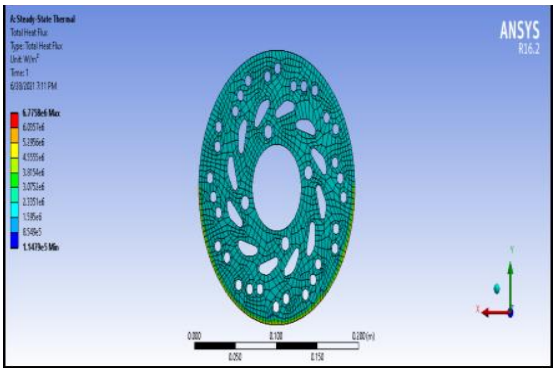

2) Cast iron

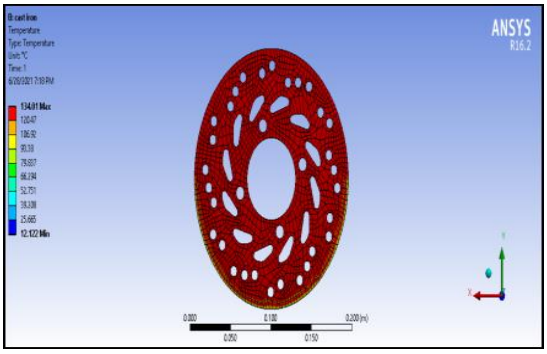

 ISBN: 978-93-91420-02-4

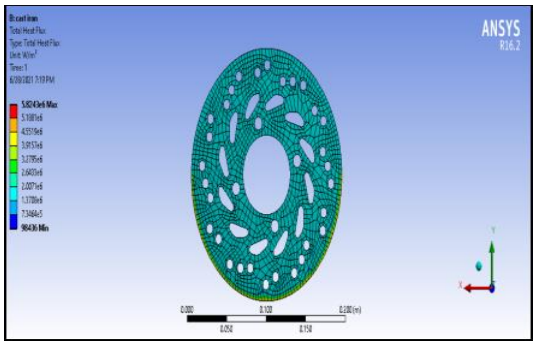

V. RESULTS

From the above experiments we have formulated the CAD model of the brake disc that is used in the electric go-karts and have done the analysis of the brake disc using ANSYS software and got the values of various parameters as specified below table.

S.NO	PARAMETERS	STAINLESS STEEL	CAST IRON
1.	**EQUIVALENT STRESS**	MAX-3.7013e7 Pa MIN-4.2402e7 Pa	MAX-3.4048e7 Pa MIN-4.0081e7 Pa
2.	**TOTAL DEFORMATION**	MAX-2.3161e-6 M MIN-2.5734e-7 M	MAX-3.8772e-6 M MIN-0 M
3.	**TEMPERATURE DISTRIBUTION**	MAX-134.01 C MIN-12.129 C	MAX-134.01 C MIN-12.122 C
4.	**TOTAL HEAT FLUX**	MAX-6.7758e6 W/m^2 MIN-1.1479e5 W/m^2	MAX-5.8243e6 W/m^2 MIN-98436 W/m^2

VI. CONCLUSION

The steady state thermal and static structural analysis of the disc brakes is recurrent in brake application that has been performed in conjunction with the theoretical style. Supported the results from ANSYS it can be concluded that being the 2 major materials for manufacturing of brakes cast iron is better as compared to stainless steel as from the results from ANSYS analysis systems.

The study will give a helpful style tool and improve the brake performance of braking system. Comparing the different results obtained from analysis, it's over that disc brake of cast iron material is t the very best combination for the current application over the stainless steel.

REFERENCES

[1] Daniel Das. A, Christo Reegan Raj. V, Preethy. S, Ramya Bharani. G, "Structutal and Thermal Analysis of Disc Brake in Automobile", International Journal of Latest Trends in Engineering and Technology (IJLTET) Vol. 2, Issue 3 May 2013.

[2] M. L. Aggarwal, Atul Sharma, "Deflection and stress Analysis of Brake Disc using Finite Element Method", Oct 19-20, 2012.

[3] Ch. Lakshmi Srinivas, Ameer Fareed Basha Shaik, "Structural and Thermal Analysis of Disc Brake with and without cross drilled rotor of race car", International Journal of Advanced Engineering Research and Studies IJAERS/ Vol. 1/Issue 4 / July-sept., 2012.

[4] Subhasis Sarkar, Pravin P. Rathod, "Review paper on Thermal Analysis of Ventilated Disc Brake by varying Design parameter", International Journal of Engineering Research and Technology (IJERT) Vol. 2, Issue 12, December – 2013.

[5] International Journal of Technical Innovation in Modern Engineering & Science (IJTIMES) Impact Factor: 5.22 (SJIF-2017), e-ISSN: 2455-2585 Volume 4, Issue 6, June-2018 IJTIMES-2018@All rights reserved 8 Thermal Analysis of Disc brake Using ANSYS Avinash Singh Thakur1 , Asst. Prof. P.S. Dhakad2 , 1Mechanical Engineering Department, NITM, Gwalior 2 Mechanical Engineering Department, NITM, Gwalior

[6] IJIRST –International Journal for Innovative Research in Science & Technology| Volume 3 | Issue 12 | May 2017 ISSN (online): 2349-6010 All rights reserved by www.ijirst.org 68 Thermal Analysis of Disc Brake Mr. Sumeet Satope Mr. Akshaykumar Bote UG Student UG Student Department of Automobile Engineering Department of Automobile Engineering R.M.C.E.T. (Ambav) R.M.C.E.T. (Ambav) Prof. Swapneel D. Rawool Assistant Professor Department of Automobile Engineering R.M.C.E.T. (Ambav)

[7] International Research Journal of Engineering and Technology (IRJET) e-ISSN: 2395 -0056 Volume: 04 Issue: 07 | July -2017 www.irjet.net p-ISSN: 2395-0072 Design and Thermal Analysis of Disc Brake for Minimizing Temperature Deepak S. Hugar1, Prof. U. B. Kadabadi2.

 ISBN: 978-93-91420-02-4

A Comprehensive Review on Recent Research on Semi Solid Processed Aluminum 7 Series Alloys

Devarapalli Raviteja[1], I Veeranjaneyulu[2], V.Venkata.Kamesh[3]and Sekhar chinthamreddy[4]
[1,2,3] Department of Mechanical Engineering , Aditya Engineering College (A), Surampalem, India
[4]Department of Mechanical Engineering, Narasaraopeta Engineering College (A), Narasaraopet, India

Abstract – At present for industries it is a challenge to produce products of good quality and should have high durability. In this engineering world there is great a great need of various engineering materials to satisfy these engineering needs. The material usage mainly depends on the material strength and properties. Aluminium 7 series alloy has good mechanical properties and low density; it is mainly used in transportation applications like aerospace, marine and automobile manufacturing. The aim of this work is to discuss the manufacturing process for different 7075 alloys required to obtain the spheroidal grain structure suitable for thixoforging. A literature review the semi-solid processed Al 7 series alloys is displayed. Application of the compo casting process led to a transformation of a dendritic to a no dendritic structure of the base alloy. The mechanical properties of the composite are improved in relation to the base alloy.

Keywords: Aluminum-7075, Thixoforging, Casting, Semi Solid

Abbreviations

Al	-	Aluminium
SSM	-	Semi Solid Metal
RC	-	Rheocast
USV	-	Ultrasonic Vibrations
dT	-	temperature difference
dfs	-	composition
GISS	-	Gas Induced Semi – Solid
SSR	-	Semi Solid Rheocasting
SSD	-	Semi Solid Processing
SST	-	Semi Solid Temperature
SIMA	-	Strain Induced Melt Activated
MMC	-	Metal Matrix Composite
Mg	-	Magnesium
Si	-	Silicon
TRT	-	Technique – Thermal Rate Treatment

I. Introduction

A lot of researches have been focused on the semi-solid metal (SSM) processing since it was invented in 1970s at Massachusetts Institute of Technology. Components produced by this unique technique have various advantages compared with the conventional liquid casting, such as low porosity, heat treatability and superior mechanical properties. The Rheocasting process becomes popular in recent years, because it possesses several advantages over thixoforming process, including increasing mould life, low cost, enhancing casting precision and qualities. Rheocasting involves stirring the melt during solidification to produce a non-dendritic semi-solid slurry, then injecting the slurry directly into a mould or die to give a final product. The ultrasonic vibration (USV) for making semi-solid slurry is a relatively new method in rheocasting process. This novel technology requires less expensive equipment for production and it is easy to be introduced into the melt. The alloys commonly used for SSM processing are certain cast Al alloys, and some wrought Al alloys of 2000 or 7000 series. However, little study has been conducted to process 5000 series Al alloys by SSM processing. The 5000 alloys have been found a large variety of applications including architectural, household appliances, marine craft, and automotive structures due to its excellent combination of weldability and corrosion resistance. They are generally classified as a non-heat treatable aluminium alloys, and their strength are not high enough to be used as structural components. Therefore, it is necessary to adopt proper processing to obtain higher mechanical properties for these series alloys. Compared with conventional casting and forging processes, semi-solid forming offers significant advantages, such as increased die life, reduced micro-segregation, and improved mechanical properties.

A new method named Semi-solid metal casting (SSM) is a near net shape variant of die casting. The process is used today with non-ferrous metals, such as aluminum, copper, and magnesium, but also can work with higher temperature alloys for which no currently suitable die materials are available. The process combines the advantages of casting and forging. The potential for this type of process was first recognized in the early 1970s.

SSM is done at a temperature that puts the metal between its liquids and solidus temperature. Ideally, the metal should be 30 to 65% solid. The semi-solid mixture must have a low viscosity to be usable, and to reach this low viscosity the material needs a globular primary surrounded by the liquid phase. The temperature range possible depends on the material and for aluminum alloys can be as much as 50 °C.

Semi-solid casting is typically used for high-end applications. For aluminum alloys, typical parts include structural medical and aerospace parts, pressure containing parts, defense parts, engine mounts, air manifold sensor harnesses, engine blocks, and oil pump filter housings. The below flow chart gives a clear idea of semi-solid processing of metals.

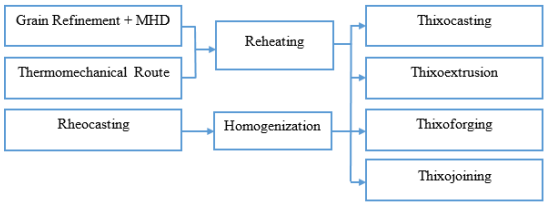

Fig 1.1 Semi Solid Processing of Metals

 ISBN: 978-93-91420-02-4

The process relies on the thixotropic behavior of alloys with a spheroidal rather than a dendritic microstructure in semisolid state. Flemings and his students were the first to discover accidentally this thixotropic behavior in the early 1970s while performing continuous hot tearing test of solidifying Sn-15% Pb. In thixotropic condition, an alloy decreases in viscosity if it is sheared but it will thicken again if it is allowed to stand. This process requires uniform heating and partial re melting of the alloy slug to obtain a homogeneous consistency throughout. This technology promises some advantages such as prolonged die life due to less thermal shock and also provides more laminar cavity fill which could lead to reduced gas entrapment. This process also can improve the usage of feedstock materials and it can contribute to the reduction of processing cost of thixoformed parts. Viscous flow is improved in semisolid metal processing because this process can provide additional laminar cavity fill, which can reduce gas entrapment.

The automotive component illustrated in figure 1.2 is an example where the near-net-shape, mechanical integrity, high strength, optimum ductility and high volume of production characteristics of thixo forming have enabled a cost effective design solution to be achieved. The issue for potential industrial users is therefore to evaluate accurately the full extent of the costs and benefits to be gained through implementing the technology. The difficulties in achieving this arise from the reliability of predictions of future cash flows and evaluation of what are often considered to' be 'intangible' benefits.

Fig 1.2 Automobile Component Made of Thixo formed Process

Alloying in SSM Casting

In addition, the process temperature (slurry temperature) must be the temperature at which the liquid portion of the slurry has a mostly eutectic composition. The reason for this is that to obtain the stability of the slurry at working temperature, the solid fraction sensitivity (dfs/dT) should be as small as possible. Fig 1.3 Illustrates the amount of heat that is produced at the temperature at which (dfs/dT) is the smallest, i.e. the 'knee point' of the solidification curve. This helps to stabilize the solid fraction, as the amount of heat needed to form the eutectic phase is large and, for this reason, the slurry becomes more stable during casting process.

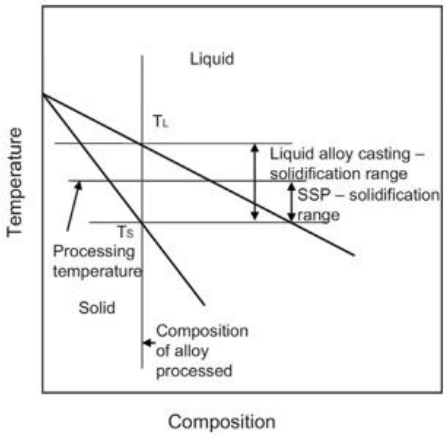

Fig 1.3 Typical solidification range in semi-solid processing and processing temperature

Technologies in slurry preparation

The above figure schematically shows different branches of the method in SSM casting methods developed during last four decades. In the early stages of the commercialization of the SSM casting process, thixocasting evolved into a process capable of preparing slurries with excellent thixotropic characterization. Despite of good process controllability in thixocasting, a high degree of industrialization has not been achieved. This arises from the production restriction, mainly due to the cost of the preformed thixoformed billet and the inability to recycle scrap in-house. In contrast to the initial stages of developing process of the SSM casting, direct slurry formation from molten metal or rheocasting process as a means of decreasing primary investment was developed during the last decade. In this type of SSM casting, the key point to be more effective is to cool down the melt to a semi-solid temperature for the production of slurry by extraction of heat from the melt in very time-efficient ways. However, most of the rheocasting processes have been designed based on temperature-control mechanisms that generally utilise by thixocasting processes. In this method, the cooler surroundings extracts heat, generate solid particle, and by applying the shear force at the same time prepare the slurry. Such methods are often time- consuming, complex and slow the processes.

In contrast, newly developed approaches such as semi-solid rheocasting (SSR), the gas- induced semi-solid (GISS) and RheoMetalTM process apply shear force when copious nucleation starts to form by means of an internal heat absorber. For instance, RheoMetalTM process is characterized by a low need for process control, short slurry forming times, and favorable microstructure characteristics, which altogether means that it is possible to produce high integrity rheo cast components in an effective way.

SSD Processes

There are a number of different techniques to produce semi-solid castings. For aluminum alloys the more common processes are thixocasting and rheocasting.

 ISBN: 978-93-91420-02-4

a) Thixocasting

Thixocasting utilizes a pre-cast billet with a non-dendritic microstructure that is normally produced by vigorously stirring the melt as the bar is being cast. Induction heating is normally used to re-heat the billets to the semi-solid temperature range, and die casting machines are used to inject the semi-solid material into hardened steel dies. Thixocasting is being performed commercially in North America, Europe and Asia. Thixocasting has the ability to produce extremely high quality components due to the product consistency that results from using pre-cast billet that is manufactured under the same ideal continuous processing conditions that are employed to make forging or rolling stock. The main disadvantage is that it is expensive due to the special billets that must be used. Other disadvantages include a limited number of alloys, and scrap cannot be directly reused.

b) Rheocasting

Unlike thixo casting, which re-heats a billet, rheocasting develops the semi-solid slurry from the molten metal produced in a typical die casting furnace. This is a big advantage over thixo casting because it results in less expensive feedstock, in the form of typical die casting alloys, and allows for direct recycling. However, rheocasting also poses process control issues such that after an initial surge of activity, very little material is processed via rheocasting. Rheocasting is the Cost-effective Semi Solid Processing Route used now a days.

c) Thixomolding

For magnesium alloys, thixo moulding uses a machine similar to injection moulding. In a single step process, room temperature magnesium alloy chips are fed into the back end of a heated barrel through a volumetric feeder. The barrel is maintained under an argon atmosphere to prevent oxidation of the magnesium chips. A screw conveyor located inside the barrel feeds the magnesium chips forward as they are heated into the semi-solid temperature range. The screw rotation provides the necessary shearing force to generate the globular structure needed for semi-solid casting. Once enough slurry has accumulated, the screw moves forward to inject the slurry into a steel die.

d) Strain-induced melt-activated (SIMA)

In the SIMA method the material is first heated to the SMM temperature. As it nears the solidus temperature the grains recrystallize to form a fine grain structure. After the solidus temperature is passed the grain boundaries melt to form the SSM microstructure. For this method to work the material should be extruded or cold rolled in the half-hard tempered state. This method is limited in size to bar diameters smaller than 37 mm (1.5 in)

Advantages

The advantages of semi-solid casting are as follows:

1. Complex parts produced net shape
2. Porosity free
3. Reduced shrinkage
4. Excellent mechanical performance
5. Tight tolerances
6. Thin walls
7. Good surface finish

Composite Material

A composite material is a macroscopic combination of two or more distinct materials, having a recognizable interface between them. Composite is a multiphase material that exhibits significant proportion of the properties of both constituent phases such that a better combination of properties is realized. This is termed as the principle of combined action. There are different types of composites namely:

1. Fibre Reinforced Composites
2. Metal Matrix Composites
3. Ceramics Matrix Composites
4. Carbon Composites

Metal Matrix Composites

The matrix in a metal matrix composite (MMC) is usually an alloy, rather than a pure metal. A metal matrix composite (MMC) is a composite material with at least two constituent parts, one being a metal. The other material may be a different metal or another material, such as a ceramic or organic compound.

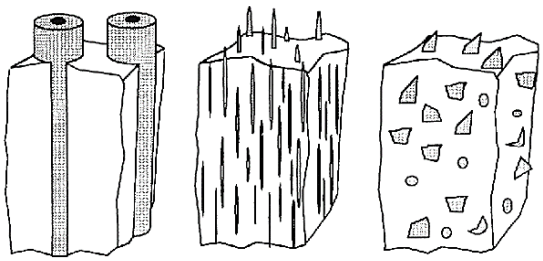

a) Monofilaments b) Whiskers/short fibres c) Particle

Fig 1.4 Schematic presentation of three shapes of metal matrix materials

Need of Metal Matrix Composite

The need for composite materials has become a necessity for modern technology, due to the improved physical and mechanical properties. Metal matrix composites (MMC) have been developed in recent years. Metal Matrix Composites have emerged as a class of material capable of advanced structural, aerospace, automotive, electronic, thermal management and Wear applications. A composite material is a material consisting of two or more physically and/or chemically distinct phases. The composite generally has superior characteristics than those of each of the individual components. Usually, the reinforcing component is distributed in the continuous or matrix component. When the matrix is a metal, the composite is termed a metal-matrix composite (MMC).

 ISBN: 978-93-91420-02-4

Application of Metal Matrix Composites

Metal composite materials have found application in many areas of daily life. Metal Matrix Composites (MMCs) are increasingly found in the automotive industry. These materials are produced in situ from the conventional production and processing of metals. Metal matrix composites (MMCs) are a class of materials with the ability to blend the properties of ceramics (high strength and high modulus) with those of metals or alloys (ductility and toughness) to produce significant improvements in the mechanical properties of the composite over those of the monolithic metal or alloys.

Table 1.1 Reinforcement materials for metal matrix materials

METAL MATRIX MATERIALS	REINFORCEMENT MATERIALS
Magnesium	Carbide
Copper	Alumina oxide
Nickel	Boron nitride
Zinc	Graphite

Literature Survey

Misra and Oswalt [1] have studied the aging characteristic of the alloy, and their observations are reproduced here. Ti refined Al-Mg-Si alloys consists of two different precipitates namely like TiAl2 and platelets Mg2Si.When the structure consists entirely of Mg2Si precipitates, material exhibits maximum strength properties Normally the alloys are artificially aged to attain acceptable combination of tensile strength and acceptable elongation. Solution treated specimen contains only TiAl2 needles, which acts as nucleation agents. As precipitation process progresses, density of TiAl2 continuously decrease while that of Mg2Si platelets increases. When only Mg2Si precipitates are observed, the microstructure corresponds to best possible elongation, with peak strengths. Combination of this with low "Dendrite Arm Spacing" gives the maximum tensile properties.

Hanliang Zhu, et.al [2] in his paper has conducted experiments on mechanical properties and metallurgical properties of Al-7Si-Mg cast alloys at different aging conditions. It was noticed that strength properties vary with aging. Aging at 165 °C gives the optimum balance of strength and ductility. Planar slip bands and (GP) zones were observed using TEM. Coarse slip bands increased with increase in aging temperature or time. They used over aging treatment to enhance tensile strength properties. From his studies it is concluded that over-aging treatment can used to improve the overall tensile properties.

Witthaya Eidhed [3] in their studies on the effect of solution treatment time on microstructure and hardness of Al-12Si-1.3Cu-1.1Ni alloy produced by permanent mold casting found maximum hardness with microstructure at short solution time between 4 and 6 hr. The solutionizing temperature selected was 520o C with holding times of 0.5, 1, 1.5, 2, 4, 6, 8 and 10hr. This was followed water quenching and aging at 175ºC for 15 hr.

M. N. Mazlee, J. B. Shamsul, H. Kamarudin [4] studied the influence of superheat treatment on the microstructure and dynamic mechanical properties of A357 alloys. Optical microscopic studies showed larger eutectic Si particles and larger α-Al dendrites in non-superheated A357 alloy than superheated alloy. Dynamic mechanical properties have shown high damping capacity of superheated A357.

Haga and Suzuki [5] casted Aluminum alloys via a cooling slope by pouring alloy between 640ºC and680°C. They concluded that the cooling rate affects the spheriodity of primary α-Al particles. It was clarified that the primary crystal became globular when the ingot cast using the cooling slope was re melted into the semisolid state. Casting factors, which affected the sphericity of the primary crystal when the ingots were re melted, were investigated. The cooling rate of the ingot in the mold was found to be the most important factor in making primary crystal globular when the ingot was re melted.

Chirita et.al [6] studied the hypo and hyper eutectic Al-Si alloys mechanical properties produced by centrifugal and gravity die casting processes. The centrifugal castings showed better rupture strength, % elongation and modulus of elasticity than die cast specimen.

H. Budiman, et.al [7] Studied the "Effect of Water Cooling on the Production of Al-Si Thixotropic Feedstock'' and they observed that metallic alloys with non- dendritic microstructure in the semi-solid state are required for semi-solid processing. Then only they can be sheared to flow to fill the die cavity and thicken after cooling. In their experiments Al-Si alloy was melted in a graphite crucible with dry argon degassing and poured on boron nitride coated mild steel cooling slope. They investigated effect of water cooling on cooling slope and it was concluded that the water cooling influence the volume, size, and shape factor of α-Al particle.

Erhard Ogris [8] in his PhD thesis investigated on the development of new ductile Al-Si-Mg alloys from semi-solid metal. The silicon spheroidization and its influence on mechanical properties was theoretically and experimentally described. Modeling as well as experimental investigations of the silicon spheroidization show that well modified eutectic silicon spheroidizes within minutes of soaking time between 500°C and 540°C. The application of this silicon spheroidization treatment (SST) to thixo formed components resulted in outstanding fracture elongation values (up to 18%) at good yield strength level (~230MPa). FEM simulations of the short high temperature heat treatment confirm a short process time for successful SST even for components with notably variable wall thicknesses.

Geng Haoran et.al. [9], studied a new melting technique-thermal rate treatment (TRT) in connection with Al-Si based alloys and they noticed that TRT treatment improves impact toughness of the material, refines primary silicon phase and increases amount of α phase.

H. Moller et.al [10] studied the semi-solid metal (SSM) high-pressure die casting (HPDC), the newly developed heat treatment cycles, and the traditional heat treatment cycles indicating that similar values of hardness can be obtained by using significantly shorter heat treatment cycles. The tensile properties obtained for SSM- HPDC were compared with those manufactured by gravity die-casting. It was inferred that the changed microstructures (globular or dendrite) do not have a noteworthy effect on the heat treatment response and this implies that the short heat treatment cycles originally developed for globular SSM-HPDC A356 castings can be successfully applied to dendritic liquid A356 castings too.

M.WESSÉN et.al [11] in their work the microstructure and tensile properties were investigated in a thick-walled section (approximately 45 mm×43 mm) of a rheocast component. Prolonged solidification period of may lead to coarse Al-Si eutectic. To reduce the coarseness of the eutectic sodium was used as a modifier. They prepared tensile test specimen from 1) As cast, 2) Na modified melt cast and 3) modified melt cast 30 min after Na addition. The material was studied in as cast condition and in T6 condition. The results show that Na addition even after a fading time of 30 min, refined Al-Si eutectic. But Na modification reduced yield strength by more than 30%.

M. Hitchcock et.al [12] studied Solidification behavior of Al–7Si–0.6Mg slurry and effect of rheo die casting on microstructure .They characterized the 2017 aerospace aluminum alloy through metallographic investigations. For the 2017 alloy precipitation strengthening by solution treatment at 550ºC and age-hardening heat treatment processes were conducted. Microstructure of the heat-treated samples showed uniform distribution of fine θ' particles in the α-matrix of the aluminum alloy; this precipitation strengthening and age-hardening heat-treatment processes enabled2017 aluminum alloy for aerospace application.

Aleksandar Vencl [13] tested microstructural, wear and mechanical properties of thixocast and heat-treated Al-Si alloy A356 (Al-Si7-Mg0.3). Results of tribological tests were compared with that of grey cast iron. Plastic flow of the alloy was noticed under dry sliding conditions and lubricated conditions showed less plastic deformation with a low coefficient of friction.

Z. Fan, X. Fang, S. Ji [14] studied a new semisolid metal (SSM) processing technology, the rheo-die casting process. In this direct shaping of the semisolid slurry into required component was carried out using cold chamber die casting process. The RDC process can be applied for cast and wrought Al-alloys. In this paper, they presented the microstructure and mechanical properties of the RDC Al-alloys under as cast, and heat treatment conditions. The results indicated that the RDC samples have negligible porosity, fine and uniform microstructure in the as-cast condition. When compared with conventional high-pressure die casting or any other process, RDC samples have shown better tensile strength and ductility. It was also found that heat treatment of these Al-alloys, under T5 and T6 conditions improved strength but with a slight decrease in ductility.

Tim Basner [15] the most popular aluminum alloys for semi-solid automotive components are A356 and A357. The density of rheocast semi-solid A357 is higher than die cast A357 and allows for both T5 and T6 heat treatment. The mechanical properties of rheocast semi-solid A357 was found to be more dependent upon the heat treat schedule and casting soundness than by the solid content of the semi-solid slurry or the globule shape.

M.A. Bayoumi [16] made their studies on extruded semi solid as cast A356 alloy. Extrusion temperatures selected were 560°C, 570°C, 580 °C, and three isothermal holding times selected were 5min 30min and 60 min respectively. Extrusion reduction ratios selected were of 5.3 and 17. Modification improved hardness and impact strength, wear resistance and fatigue strength of the alloy when compared to conventional cast alloys. They observed fractured surfaces of tensile specimen using SEM.

G.T. Abdel-Jaber1, et.al [17] investigated solidification behavior and mechanical behavior of Al-Si alloy (Si3-15%) at different moulding conditions. microstructural studies and wear studies carried out by using a pin on disc tribometer to investigate the effect of the alloying element content and the molding conditions on the wear resistance and the coefficient of friction of the alloy. The results showed that the solidification time increased with the increasing of silicon content up to 12%. However, an increase of both the ultimate tensile strength and the hardness is obtained by the increase of the silicon content. Wear rate decreased and coefficient of friction increased with increase in silicon content.

Madhusudhan Reddy and Srinivasa Rao. K [18] investigated the feasibility of locally modifying the surface properties of cast aluminium alloy A356 using friction stir processing (FSP).Hardness plots have showed40% increase in hardness, compared to the as-cast metal. Uniform micro-hardness, excellent wear resistance and excellent pitting corrosion resistance were observed in the friction stir processed A356 aluminum alloy. This could be due to homogenous distribution of fine Si particulates throughout the α-Al matrix.

D.R. Gunasegaram, et.al [19] in their studies observed that high pressure die-cast (HPDC) aluminium components that respond to age hardening cannot be solution treated at high temperatures due the presence of internal porosity and entrapped gases. Due to swelling components may be dimensionally inaccurate. This can be avoided by using modified shorter solution treatment procedures. In this present paper, the roles of critical alloying elements are considered in both current commercial and experimental alloy compositions in this series. It is shown that values of 0.2% proof stress exceeding 400 MPa may be readily achieved by heat treating conventionally produced HPDC components.

Chen Zhongwei and Zhang Ruijie [20] studied the effect of strontium on primary dendrite and eutectic temperature of A357 aluminium alloy and their results were summarized here. They modified A357 alloy with strontium. It was observed that Sr modifies the Al-Si eutectic, affects the primary α-Al dendritic matrix and growth temperature of α - Al dendrite. Al-Si eutectic decreases more prominently at higher cooling rates.

K.N. Prabhu and P. Hemanna [21] in their studies on "Heat Transfer during Quenching of Modified and Unmodified Gravity Die-Cast A357 Cylindrical Bars", heat transfer during quenching of chill-cast modified and unmodified A357 Al-Si alloy was examined using a computer-aided cooling curve analysis. Water at 60 °C and a vegetable oil (Palm oil) were used as quench media. The investigation clearly showed that the heat transfer during quenching depends on the casting history. The modification changed the silicon morphology this could be the reason for increase in the cooling rate and peak heat flux. The increase in electrical conductivity of modified samples than unmodified samples confirmed this. But modification decreased ultrasound velocity.

Q. G. WANG et.al. [22] studied on ''The effect of Mg content on the solidification and precipitation behaviour of both as cast and Sr- modified Al-7Si-Mg casting alloys with Mg concentrations covered the range from 0.3 % to 0.7%, at various solidification rates using cooling curve analysis, optical and electron microscopy. They observed that increasing Mg content or cooling rate lowers the liquidus and binary Al-Si eutectic transformation temperatures. Si present in the alloy influences the latent heat of fusion of these alloys but Mg does not. At Mg levels of 0.6% and higher only ternary reaction is observed. Mg levels above 0.5% did not affect yield strength but precipitates increased with Mg content.

Wislei R. et.al [22] noticed that hypoeutectic Al-Si alloys can have significant improvements in mechanical properties by inducing structural modification in the normally occurring eutectic. The modification not only affects the mechanical properties but also the corrosion resistance of these alloys. Modification changes grain size and inter dendritic spacing which in turn influence the corrosion resistance of alloys. In their present study, modified and as cast samples of an Al 9 wt. % Si alloy were solidified under similar solidification conditions. The corrosion resistance was tested by electrochemical impedance spectroscopy technique and the Tafel extrapolation method. Test was carried out in a 0.5 M NaCl test solution at 25°C. The impedance parameters and corrosion rate were obtained from an equivalent circuit analysis. The corrosion resistance of as cast alloy was better than that of modified alloy.

Girish Kumar et.al. [23] Modified Al– Si alloys to improve their mechanical properties. Thermal analysis is used to determine the effectiveness of modification. In their present study, (A357) alloy solidification behavior with or without chilling was observed. They concluded that effect of modification and chilling on Thermal analysis parameters were more. A theoretical model was used to predict growth velocities. The eutectic grain sizes were calculated using the model and they were in good agreement with those measured from ASTM standard casting microstructures.

A.Thirugnanama, et.al [24] observed that the microstructural aspects of cast A356/357 alloys strongly depend on the %Mg, and the fracture behaviour of these alloys depends on the size and shape of eutectic silicon particles and iron-rich inter- metallic. Magnesium content increases both the matrix strength and eutectic particle size but decreases the ductility. The combined effect of modification and grain refinement improves the overall mechanical properties. Increasing the cooling rate refines the eutectic, Fe bearing phases improve ductility. Porosity defect is detrimental to mechanical properties and an increased level of porosity is reported to accompany the modification of A356/357 cast alloys. Heat treatment of A356/357 aluminium alloys strengthens mechanical properties. The fracture toughness of Al-Si- Mg alloys depends on silicon particle cracking. Microstructural aspects and fracture behavior of A356/A357 alloys was studied in this paper.

Conclusions

Here in this paper different literature review was discussed on the semi-solid processing of Aluminium 7 series and it constituent's alloys in the application of automobile, aerospace, marine and defense applications. It is hereby declared that the manufacturing process also effect the mechanical and thermal properties of the material when subjected to loads. It is also said that these alloys behave differently with filler materials that increases the strength and decreases the porous nature of the material. Heat treatment increases the better malleability of the material and good microstructural properties for better applications in defence. These materials can be used as the armour of the tanks for better durability of the vehicle.

References

[1] OSWALT, KJ, and MS MISRA. "Dendrite Arm Spacing (DAS): A nondestructive test to evaluate tensile properties of premium alloy (Al-Si-Mg) castings." AFS International Cast Metals Journal 6.1 (1981): 26-40.

[2] Zhu, H., Guo, J. & Jia, J. Correlation of the aging characteristics and deformation behavior of A357 alloy. J. of Materi Eng and Perform 10, 186–191 (2001). https://doi.org/10.1361/105994901770345204

[3] Eidhed, Witthaya. "Modification of β-Al5FeSi compound in recycled Al-Si-Fe cast alloy by using Sr, Mg and Cr additions." J. Mater. Sci. Technol 24.1 (2008): 45-47.

[4] Mazlee, M.N., Shamsul, J.B., & Kamarudin, H. (2017). Comparison of Dynamic Mechanical Properties of Non-Superheated and Superheated A357 Alloys. arXiv: Materials Science.

[5] Haga, Toshio & Suzuki, Shinsuke. (2001). Casting of aluminum alloy ingots for thixoforming using a cooling slope. Journal of Materials Processing Technology - J MATER PROCESS TECHNOL. 118. 169-172. 10.1016/S0924-0136(01)00888-3.

[6] Chirita, G. & Stefanescu, I. & Cruz, D. & Soares, D. & Silva, Filipe. (2010). Sensitivity of different Al–Si alloys to centrifugal casting effect. Materials & Design. 31. 2867-2877. 10.1016/j.matdes.2009.12.045.

[7] El Mahallawi, Iman & Mahmoud, T. & Gaafer, A. & Mahmoud, Fouad. (2015). Effect of Pouring Temperature and Water Cooling on the Thixotropic Semi-solid Microstructure of A319 Aluminium Cast Alloy. Materials Research. 18. 10.1590/1516-1439.304114.

[8] Ogris, Erhard. (2002). Development of Al-Si-Mg alloys for semi-solid processing and silicon spheroidization treatment (SST) for Al-Si cast alloys [D]. Zurich: Swiss Federal Institute of Technology.

[9] Geng, Haoran & Wang, R. & Yang, Zhongxi & Chen, J.H. & Sun, C.J. & Wang, Y.. (2005). Temperature dependence of viscosity of Al-Si alloy melts. Acta Metallurgica Sinica (English Letters). 18. 159-163.

[10] Möller, Heinrich & CURLE, U.A. & MASUKU, E.P... (2010). Characterization of surface liquid segregation in SSM-HPDC aluminium alloys 7075, 2024, 6082 and A201. Transactions of Nonferrous Metals Society of China. 20. 10.1016/S1003-6326(10)60593-6.

[11] Östklint, Mattias & Wessén, Magnus. (2012). Microstructure Characteristics and Semi-Solid Slurry Formation in Binary Mg-Al Alloys Produced by the RheoMetal Process. Solid State Phenomena. 192-193. 482-487. 10.4028/www.scientific.net/SSP.192-193.482.

[12] Hitchcock, M. & Wang, Y. & Fan, Zhongyun. (2007). Secondary solidification behaviour of the Al–Si–Mg alloy prepared by the rheo-diecasting process. Acta Materialia. 55. 1589-1598. 10.1016/j.actamat.2006.10.018.

[13] Vencl, Aleksandar. (2009). Tribological properties of thixocasted and heat treated hypoeutectic Al-Si alloy A356. Scientific Problems of Machines Operation and Maintenance. 44. 15-23.

[14] Fan Z, Liu G, Wang Y, Ji S, and Bevis M, Method and apparatus for making metal alloy castings, J Mater Sci 41 (2006) 3631.

[15] Basner, Tim. (2000). Rheocasting of Semi-Solid A357 Aluminum. 10.4271/2000-01-0059.

[16] Bayoumi, M.A. & Negm, M.I. & El-Gohry, A.M.. (2009). Microstructure and mechanical properties of extruded Al–Si alloy (A356) in the semi-solid state. Materials & Design. 30. 4469–4477. 10.1016/j.matdes.2008.11.025.

[17] Abdel-Jaber, G. T., Omran, A. M., Khalil, K. A., Fujii, M., Seki, M., & Yoshida, A. (2010). An investigation into solidification and mechanical properties behavior of Al-Si casting alloys. International Journal of Mechanical and Mechanics Engineering, 10(4), 34-41.

[18] Madhusudhan Reddy, G., Srinivasa Rao, K. Enhancement of wear and corrosion resistance of cast A356 aluminium alloy using friction stir processing. Trans Indian Inst Met 63, 793–798 (2010). https://doi.org/10.1007/s12666-010-0121-y

[19] Lumley, Roger & O'Donnell, R.G. & Gunasegaram, Dayalan & Givord, Michel. (2007). Heat Treatment of High-Pressure Die Castings. Metallurgical and Materials Transactions A. 38. 2564-2574. 10.1007/s11661-007-9285-4.

[20] Zhongwei, Chen & Ruijie, Zhang. (2010). Effect of strontium on primary dendrite and eutectic temperature of A357 aluminum alloy. China Foundry. 7. 149-152.

[21] Prabhu, K. & Hemanna, P. (2006). Heat Transfer during Quenching of Modified and Unmodified Gravity Die-Cast A357 Cylindrical Bars. Journal of Materials Engineering and Performance. 15. 311-315. 10.1361/105994906X108729.

[22] Wang, Q.G., Davidson, C.J. Solidification and precipitation behaviour of Al-Si-Mg casting alloys. Journal of Materials Science 36, 739–750 (2001). https://doi.org/10.1023/A:1004801327556

[23] Osorio, Wislei & Cheung, Noé & Spinelli, José & Goulart, Pedro & Garcia, A. (2007). The effects of a eutectic modifier on microstructure and surface corrosion behavior of Al-Si hypoeutectic alloys. Journal of Solid State Electrochemistry. 11. 1421-1427. 10.1007/s10008-007-0300-x.

[24] Arunachalam, Thirugnanam & Sukumaran, K. & Raghukandan, K & Pillai, U.T.s & Pai, Chandrasekhar. (2005). Microstructural aspects and fracture behavior of A356/357 alloys - An overview. Transactions of the Indian Institute of Metals. 58.

 ISBN: 978-93-91420-02-4

A study on microstructure and mechanical Properties A7075 Reinforced with Fly ash/Sic hybrid metal matrix composite

Devarapalli Raviteja[1], I Veeranjaneyulu[2], V.Venkata.Kamesh[3]and Sekhar chinthamreddy[4]
[1,2,3] Department of Mechanical Engineering (A), Aditya Engineering College (A), Surampalem, India
[4]*Department of Mechanical Engineering (A), Narasaraopeta Engineering College (Autonomous), Narasaraopet,* India

***Abstract*—An experiments have been performed under laboratory condition to study the mechanical behavior and microstructure of the hybrid composite with aluminium matrix A7075 alloy, reinforced with silicon carbide (Sic) and Flyash. The fabricating the samples has been done by using stir casting technique. Scanning electron microscopy (SEM) was used for microstructure analysis. Mechanical properties were carried out on both the base alloy and composite. Enhanced hardness was observed for the composite. Interestingly improved tensile results were obtained for the composite than alloy. The hardness of the composite is increased due to dispersion of (Sic) and Flyash particles in aluminium matrix.**

Keywords -- A7075 alloy, (Sic) and Fly ash, (SEM) Scanning electron microscopy, (XRD) X-ray diffraction.

Nomenclature

ρ_{MMC} = density of composite
m= mass of the composite
m_1= mass of the composite in distilled water
ρ_{H2O}= density of distilled water
Vr = weight ratio of reinforcement
ρ_r = density of reinforcement
ρ_c = density of composite
ρ_m is the density of the unreinforced alloy

I. INTRODUCTION

Composites have wide variety of application in aerospace, defense and it in automotive industries because of its unique properties such as high specific strength, wear resistance, strength-to-weight, strength-to-cost, etc. (1). By introduce hard ceramic particulates like SiC, Al_2O_3 and B_4C into aluminium based matrix, results in to enhanced the various properties. From the literature study reveals that among the reinforcements SiC is chemically compatible with aluminium and forms an adequate bond with the matrix without developing inter- metallic phase and has other advantages such as excellent thermal conductivity, good workability and low cost (2). In order to attain high strength to low weight ratios in materials the usage of Aluminium metal matrix composites (AMMCs) are used very extensively which can be used for sophisticated aerospace and automobile structures because of their properties which can be customized in the course of the accumulation of preferred reinforcements . Al_2O_3 is one of the widely used second reinforcement. But it has its own demerits like poor wetting behavior with aluminium and more weight percentage leads to increase in porosity (3). They share a good fraction in automobile and aerospace applications (4-6). Among these particles reinforced metal matrix composites have found unique interest due to their elevated specific stiffness and specific strength at normal or elevated temperature. Normally micron sized ceramic particles are used as reinforcement to improve the properties of the MMCs.

Due to their high heat resistant properties, ceramic particles are mainly used as reinforcements. Out of various ceramics used fly ash is one of the economic as well as low density reinforcement which is available in plenty as waste derivative during incineration of charcoal at thermal power plants. Ibrahim et al. (7) in his review observed that the properties of material obtained by means of metal matrix. A composites with varying reinforcement percentage up to 20% in increment of five, by considering dissimilar alloys A6061, A2014, and A356. It is concluded that by rising reinforcement percentage the tensile properties like yield, and ultimate strengths has been increased whereas the elongation of alloy found to be decreased. Lloyd et al. (8) W.H et al. (9) and D Silva et al. (10), particle induced damage in MMCs has been studied, with Metal matrix composites with a size superior to 10 μm. The cracking of particles has been observed which indicate the dominant damage mechanism. Accordingly properties of metal matrix composites will depend on the particulate size. An attempt has been made to fabricate Al/TiB_2/Al_2O_3 composite in our previous work. In this present work an attempt has been made to introduce SiC an outstanding reinforcement among all the other reinforcements.

This present work analyses the various mechanical properties on both base alloy and hybrid composite.

II. EXPERIMENTAL

A. Fabrication of composites

Aluminium based hybrid MMC having Sic and Fly ash particles of 53μm and 3% weight was fabricated by eddy process. A7075 was used as base material and chemical composition is shown in table1.

TABLE 1. Elemental analysis of A 7075 alloy by wt. %.

Elemental analysis of A 7075 alloy by wt. %.										
Zn	Cu	Mg	Si	Cr	Mn	Fe	Pb	Sn	Ti	Al
5.1	1.2	2.1	0.4	0.18	0.3	0.5	0.029	0.012	0.2	balance

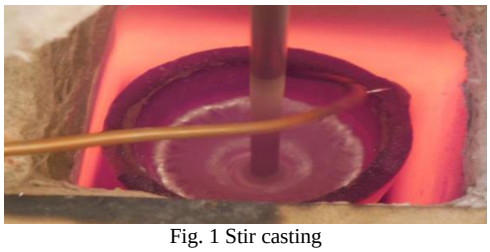

Fig. 1 Stir casting

 ISBN: 978-93-91420-02-4

Fig. 2 Casted fingers

The composite was produced by stir casting as shown in "Fig. 1". Small sized ingots of aluminium zinc alloy are loaded into a crucible made of graphite and placed in an electric furnace in which the melting was performed. A pool is created in the middle of graphite crucible using a stirrer operated mechanically and the temperature should be maintained around770°C throughout the casting.

The preheated particulates of SiC and fly ash were dropped uniformly into the melt. To ensure continuous and smooth flow of the particles proper care should be taken to avoid the agglomeration. The inert gas shielding should be maintained throughout to avoid the oxidation as the casting is exposed to the atmosphere during the stirring time approximately 2 to 3 minutes. Still, the melt with reinforcement was in stirring condition the same was casted into cast iron mold which is preheated to 200 ^{0}C as shown in "Fig. 2". The fabricated ingots were homogenized at 110^{0}C for 24hrs to minimize the chemical in homogeneities and to remove any internal stresses induced in the castings.

III. CHARACTERIZATION OF COMPOSITES

A. Metallography and hardness

A Scanning electron microscopy (SEM) (Model: Hitachi S-3400N - Japan) was used, to evaluate the morphological changes and elemental analysis of the composite and base alloy. Brinell hardness tester (Model No: RAB250) is used to find the hardness of the composite and base alloy by taking 3 readings on an average.

B. Density studies

By using the technique of Archimedes principle the densities of composite and base alloy were found by using the relation:

$\rho_{MMC} = (m) / \{(m-m_1) \times \rho_{H2O}\}$

By using the concept of rule of mixtures the theoretical density calculations was done using following relation.

$\rho_{composite} = V_r \rho_r + (1-V_r) \rho_m$

C. Tensile tests

Tensile properties of alloy and composite was determined by means of FIE/UTN-40 testing machine as per ASTM B557 standards. Plotting has done continuously through a data attainment system with an electronic extensometer.

IV. RESULTS AND DISCUSSIONS

A. Microstructures

"Fig. 3(a-d)" shows the SEM micrographs of fly ash, SiC particles, and hybrid composite varying with wt. percentage. We can observe that, addition of particulates of the SiC and fly ash in the base alloy, i.e. by increasing the reinforcement content by weight percent which can be seen noticeably, "Fig. c", shows the microstructure of the base alloy and whereas the "Fig. d", shows the addition of the particulates to the base alloy, difference was noticed clearly in the microstructures.

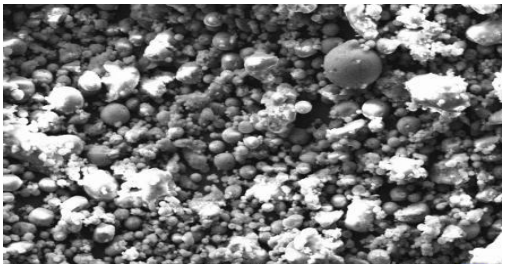

(a)

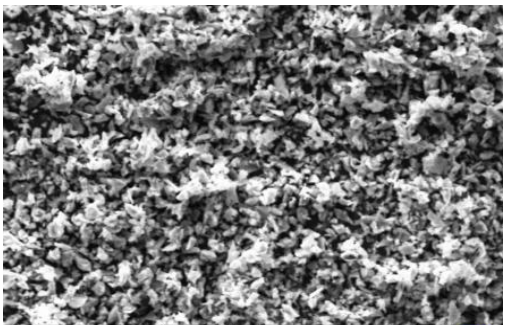

(b)

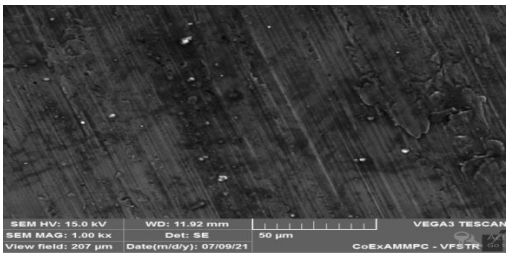

(c)

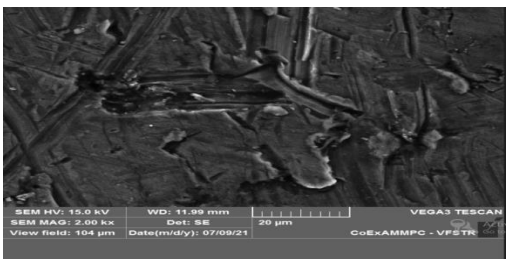

(d)

Fig 3. (a) Microstructure of flyash particles (b) SiC particles (c) base (d) 3% Flyash/SiC composite

B. XRD analysis

The XRD analysis in "Fig. 4", shows a mineralogical composition. In the presence of silica SiO2, alumina Al2O3, and mullite 3Al2O3·2SiO2,silica SiO_2 and hematite are seen. The peaks which are represented with miller indices are corresponding to the characteristic peaks of the flyash

 ISBN: 978-93-91420-02-4

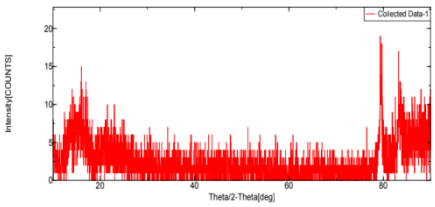

Fig 4. XRD of composite

C. Density studies

The average theoretical and measured values of the density for the base alloy and composites are shown in table 2. It was observed that the SiC and flyash particulate addition to the base alloy drastically decreases the density of the resultant composite when compared to the base.

TABLE 2. Densities of alloy and composites

S.No.	Specimen	Measured density (g/cc)	Theoretical density (g/cc)
1	Alloy 7075	2.81	2.81
2	3% FA+3% SiC composite	2.73	2.78

By increasing the reinforcement percentage in base alloy the density was found to be decreased due to the low density of flyash particulates, also the decrease may be attributed to the increase of porosity with flyash. The obtained densities were checked by measured densities and found lower than theoretical ones as depicted in table2.

D. Hardness studies

Due to the presence of hard SiC and flyash, the hardness was found to be increased from 115 to 120 BHN from base alloy to composite with 3 % reinforcement. The result reported by Hassan, S. F *et al.* and Ma, NG *et al*. [11, 12] is in the similar lines.

TABLE 3. Densities of alloy and composites

S.No.	Specimen	BHN
1	Alloy 7075	115
2	3% FA+3% SiC composite	120

E. Tensile studies

Tensile test specimen type is flat were machined from extruded materials. “Fig. 5”, represents the line diagram of sample.Tensile properties of both alloy and composites were determined by means of FIE/UTM-40 testing machine as per ASTM B557 standards. Plotting has done continuously through a data attainment system with an electronic extensometer.

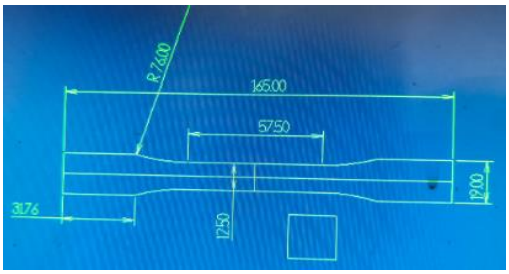

Fig 5. Tensile specimen measurements as per ASTM B557

TABLE 4. Mechanical behaviour of alloy and composite

S.No.	Specimen	Yield strength (YS), MPa	Ultimate tensile strength (UTS), Mpa	Elongation (%)
1	Alloy 7075	114.7	173.4	0.12
2	3% FA/ SiC composite	121.8	174.4	0.98

From table 4 it is evident that the composite exhibited superior properties when compared to the base alloy. A decrease in elongation is observed with the increase in reinforcement content and appears to be quite noticeable from the enhanced hardness allied with increased Silicon carbide content.

V. CONCLUSIONS

1. Successfully hybrid composite was fabricated by using stir casting technique.
2. Identified the reinforcement particles have been uniform distributing in the matrix phase.
3. SEM figures have clearly shows that there was a good interfacial bonding between the particles and matrix phase.
4. The density of the composite was found to be decreased with an addition of reinforcement by compared with the base alloy.
6. The composite hardness was increased by increase in the reinforcement content.
7. The tensile properties are enhanced to the composite like yield strength and ultimate tensile strength when compared to the base alloy.

 ISBN: 978-93-91420-02-4

REFERENCES

[1] S. Das, 2004. Development of Aluminium Alloy Composite for Engineering Applications, Indian Institute of Meterials, 27 (4), pp. 325-334.

[2] K.Umanath, Analysis of dry sliding wear Behavior of Al6061/SiC/Al2O3 hybrid metal matrix composites. Bhrath University, Chennai, India.

[3]A.V Smith, Titanium di boride particle-reinforced aluminium with high wear resistance, Composite materials research Laboratory, State university of New York, USA.

[4] Ma, NG, Deng, CJ, Yu, P, Kwok, WY, Aravind, M, Ng, DHL, Chan, SLI, Formation of Mg-Mg2Cu nanostructured eutectic in Mg-based metal matrix composite, Journal of Materials Research, 188. (2003)1934-1942

[5] MV Rotti, Synthesis and characterization of aluminium alloy A356 and SiC metal matrix composite, 2nd International conference on industrial technology and management, Singapore DOI: 10.7763/IPCSIT V49.3, 2012.

[6] Syed Hafeez and Khalid, Tensile response of Al reinforced with sub-micron alumina metal matrix Composites, in: Proceedings of ICRAME-05, 2005,1-5.

[7] E.J. Lavernia, Particulate reinforced metal matrix composites-a review, Journal of materials science, 26, 199, 1137-1156.

[8] Lloyd, Particulate reinforced aluminum and magnesium matrix composites,International Materials Reviews 39, 1994.

[9] Whitehouse, and Clyne, Cavity formation during Tensile Straining of Particulate andShort Fibre Metal Matrix Composites Acta Metallurgy & Material Science, 41,1993, 1701-1711.

[10] H. Ribes, R. Da Silva, M. Suéry and T. Bretheau, Effect of interfacial oxide layer in Al–SiC particle composites on bond.

[11] Khalid A Al-Dheylan, Amro AI-Qutubb, Syed Hafeez, Tensile response ofaluminum reinforced with submicron A1203 metal matrix Composites, in:Proceedings of ICRAMME- 05, 2005, pp. 1–5.

[12] J. Llorca, C. Gonzalez, Microstructural factors controlling the strength and ductility ofparticle-reinforced metal-matrix composites, J. Mech. Phys. Solids 46 (1998) 1–28.

 ISBN: 978-93-91420-02-4

Establishment of SCR Test facility and Evaluation of 8mm pitch Honeycomb Type Catalyst in a 20 Liter capacity SCR Test facility

Tellamekala Anitha, Donepudi Jagadish and M.Sreenivasa Kumar
Department of Mechanical Engineering, Narasaraopeta Engineering College, Narasaraopet, India

***Abstract*—The objective of this project was to establish the 20 litre capacity SCR test facility and generate the data required for evaluating the performance of in-house developed 8mm pitch honeycomb type SCR catalyst with dust concentration of about 30 to 52 g/nm^3 in coal based flue gas. SCR test facility is capable to process up to 60 Nm^3/hr of flue gas generated from coal combustion process with 30-60 grams /Nm^3 of dust concentration. The NOx removal efficiency, ammonia slip and differential pressure across honeycomb catalyst was investigated with dust concentration of 30-52 grams/Nm^3 in flue gas by varying the space velocities (2500-1500 per hr.) and flue gas temperatures (300–350^{0}C) using anhydrous ammonia as reducing agent and the ratio of ammonia (NH_3) to Oxides of Nitrogen (NOx) was maintained as 0.9 to 1.0 for all the experiments. The result shows that the NOx reduction efficiency achieved with honeycomb was 81.89 – 86.75% at 2500-1500 per hr. space velocities and the ratio of ammonia (NH3) to oxides of nitrogen (NOx) was maintained at 0.9. NOx reduction efficiency achieved with honeycomb was 82.72–88.23% at 2500-1500 per hr. space velocities and the ratio of ammonia (NH_3) to oxides of nitrogen (NOx) was maintained at 1.0.Ammonia slip measured was in the range of 1.3 to 1.9 ppm for honeycomb catalyst at 0.9 for ammonia to oxides of nitrogen.The total Differential Pressure (DP) across Honeycomb SCR catalyst was 28-38 mmWc over a 2250mm length.**

Keywords—Selective catalytic reactor, honeycomb, catalyst, space velocity, Nox conversion efficiency, ammonia slip.

I. INTRODUCTION

Fossil fuels play a crucial role in the energy mix, and will continue to play a major role in decades to come. Coal is the most common source for heat and power production, and the role of coal will continue to be very important in the near future. According to EIA statistics for 2016, coal remains the second largest energy source worldwide until 2030 and from 2030 through 2040, it is the third-largest energy source. World coal consumption increases from 2012 to 2040 at an average rate of 0.6%/year [1]. The coal combustion generates solid and gaseous combustion products and is inevitably associated with environmental pollutants among which Oxides of Nitrogen (NOx) are major ones. The nitrogen monoxide (NO), nitrogen dioxide (NO2) and nitrous oxide (N_2O) molecule belongs to the family of nitrogen oxides (NOx) compounds. NOx is used to refer to the total amount of nitrogen oxides. About 95 % of oxides of nitrogen from industrial activities come from combustion processes. NOx can cause severe health problems and have strong environmental impacts. The main effects are: Formation of ground-level ozone, formation of acid aerosols, formation of acid rain, deterioration of water quality, formation of toxic chemicals and global warming. In view of severe health issues and strong environmental impacts, the Ministry of Environment and Forest (MOEF), GOI issued notification for implementation of emission norms for particulate matter (PM), sulphur di-oxide (SO2), oxides of nitrogen (NOx) and mercury (Hg). The final emission limits under Title IV, promulgated in February 1998, are shown in Table 1, 2 & 3.

Table 01:TPPs (units) regulatory norms installed before 31st December, 2003

Parameter	Standards
Particulate Matter	100 mg/Nm3
Sulphur Dioxide (SO2)	600 mg/ Nm3 (Units Smaller than 500 MW capacity units) 200mg /Nm3 (for units having capacity of 500MW and above)
Oxides of Nitrogen (NOx)	600 mg/ Nm3
Mercury (Hg)	0.03 mg/ Nm3 (for units having capacity of 500 MW and above)

Table 02: TPPs regulatory norms installed after 1st Jan, 2003, up to 31st Dec, 2016

Parameter	Standards
Particulate Matter	50 mg/Nm3
Sulphur Dioxide (SO2)	600 mg/ Nm3 (Units Smaller than 500 MW capacity units). 200 mg /Nm3 (for units having capacity of 500MW and above).
Oxides of Nitrogen (NOx)	300 mg/ Nm3
Mercury (Hg)	0.03 mg/ Nm3

Table 03: TPPs (units) regulatory norms to be installed form 1st January, 2017

Parameter	Standards
Particulate Matter	30 mg/ Nm3
Sulphur Dioxide (SO2)	100 mg/ Nm3
Oxides of Nitrogen (NOx)	100 mg/ Nm3
Mercury (Hg)	0.03 mg/ Nm3

To maintain stringent regulatory norms imposed by the Ministry of Environment and Forest (MOEF), GOI for Oxides of Nitrogen (NOx), BHEL has formed CFT committee and identified the solution.

NOx Removal techniques: Oxides of Nitrogen (NOX) can be controlled by using the following methods:

- Combustion controls; and
- Post-combustion controls;

Combustion controls: The NOX emissions are reduced by changing the process parameters while combustion process. The combustion process parameters are air, coal and residence time. Under this method the maximum conversion efficiency less than 50% and also this method is least expensive.

 ISBN: 978-93-91420-02-4

Post-Combustion controls: In this method the NOx emissions which are generated in combustion process are converted in to nitrogen (N2). This method occurs after combustion process and it requires chemical reactions to convert the NOX in to nitrogen (N2). These techniques introduce a reagents like ammonia (or) urea into the flue gas stream to selectively react with the NOX. The reaction may be completed either with or without the use of a catalyst. Under this technology there are two sub technologies available, they are: (1) Selective Non-Catalytic Reduction (SNCR) and (2) Selective Catalytic Reduction (SCR).

Table 4: Summary of Post-Combustion Control Technologies.

Control Technology	Application	NOX Reduction (%)
SNCR	Boilers/Process Heaters	40 - 50
SCR	Boilers/Process Heaters	80 - 90

From the above NOx removal techniques, SCR technology has more efficient, very low consumption of ammonia, very high dioxin reduction and the emission levels can be achieved below 100 mg/Nm^3.

II. METHODS AND MATERIALS

A. Sub Bituminous Coal:

Raw sub bituminous coal of grade E and of –10 mm size from Singareni calories was obtained for this experimentation. The various analysis of coal has been pursued using in-house available techniques and shown in table 4, 5, 6, 7 & 8. The raw coal was crushed and sieved to 0.5 mm to – 4 mm sizes and used for generation of flue gas for testing of in-house developed catalyst.

Table 5: Physical properties of Sub-bituminous coal

S.No	properties of Sub-bituminous coal	
1	The mean diameter of the particle (mm)	1.75
2	Bulk Density of coal (kg/m3)	810.04
3	Particle Density of coal (kg/m3)	1665.1

Table 6. Proximate analysis of Sub-bituminous coal:

S.N	Proximate analysis of Sub-bituminous coal	
1	Moisture (%)	2.55
2	Ash (%)	29.25
3	Volatile Matter (%)	28.93
4	Fixed Carbon (%)	39.27

Table 7. Ultimate analysis of Sub-bituminous coal:

S.N	Ultimate analysis of Sub-bituminous coal	
1	Carbon (%)	49.82
2	Hydrogen (%)	3.64
3	Nitrogen (%)	1.02
4	Sulphur (%)	0.58
5	Oxygen (%)	13.14

III. EXPERIMENTAL SYSTEM DESCRIPTION

The experiments were conducted in 20 litres capacity Selective Catalytic Reduction (SCR) test facility with 8mm pitch honeycomb type SCR catalysts. The 8mm pitch honeycomb type catalyst supplied by BHEL Corp. R&D, CTI Group Bangalore and is installed in 20 litres capacity Selective Catalytic Reduction (SCR) test facility to evaluate the performance. The existing 200mm dia pilot plant was operated in a combustion mode and generated flue gas for testing of 20 litres capacity honeycomb type catalysts for NOx reduction. The Process and Instrumentation Diagram (P&ID) for De-NOx process is shown in Figure 1. The performance of honeycomb type catalyst was tested with dust concentration of 30-52 grams/Nm^3 in flue gas. The experimental setup comprises of the following systems/sub-systems and are explained subsequently

Table 7: The experimental setup systems/sub-Systems

S.No	Sub System
01	Ø200mm Pilot Plant Test Facility
02	Flue Gas Cooler-I & II
03	On-line Dust Monitoring system
04	NOx Measurement System
05	Ammonia Injection system
06	Static Mixture
07	SCR Reactor Housing
08	SCR Catalyst
09	Venturi Flow Meter
10	Ammonia Slip measurement System

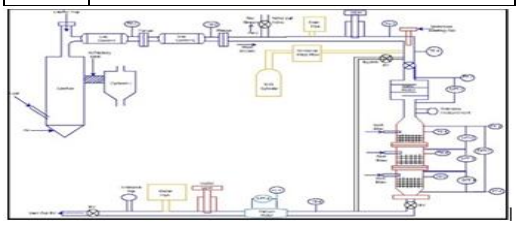

Figure 1: Process and flow diagram of 20 Ltrs capacity pilot plant.

A. NOx Measurement System:

A flue gas analyser is used to measure the oxides of nitrogen from flue gas at inlet and outlet of SCR reactor. A flue gas analyser is a portable electronic device, which measures and displays the products of combustion from both domestic and commercial fossil fuelled appliances. Additionally, they can measure the ambient air quality in rooms or buildings. Flue gas analysers are used for measure the following composition from flue gas i.e. O_2, CO, CO_2, SOx and NOx and these components are measured using NDIR (Non- Dispersive Infrared) Technology.

B. Ammonia Injection System:

Anhydrous ammonia is used as reducing agent for De-NOx system in SCR technology. In this system, a 0.5mm nozzle is used for injecting the ammonia in to flue gas pipe line with the help of ammonia mass flow controller.

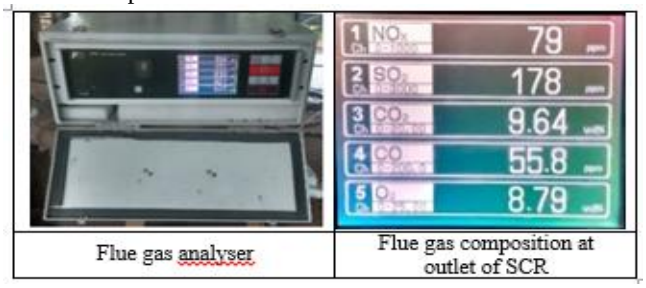

Figure2: Flue gas analyser and measured composition

The anhydrous ammonia injection nozzle and mass flow controller is shown in figure 4(a) & 4(b) respectively.

 ISBN: 978-93-91420-02-4

Figure 3: Anhydrous ammonia injection nozzle and mass flow controller

C. Static Mixture:

Static mixture is an equipment which is used to mix thoroughly the Oxides of Nitrogen (NOx) available in flue gas with an-hydrous ammonia. The performance of the catalyst is totally depends upon the quality of mixing in the static mixture.

D. SCR Reactor Housing:

The honeycomb catalyst is enclosed in a fabricated stainless steel housing called SCR reactor. The size of the SCR reactor is 100 mm x 100 mm x 900 mm of 3 modules.

Figure 4. Pictorial View of SCR reactor

E. SCR Catalyst:

Catalyst is the heart of DeNOx process. There are two types of catalysts are available; Honeycomb type catalyst. The Honeycomb type catalysts with 8mm pitch has been used for reduction of oxides of nitrogen (NOx) from flue gas. Anhydrous gaseous ammonia reacts with NOx in flue gas to form nitrogen (N_2) and water vapor (H_2O) in presence of honeycomb type SCR catalyst. The primary base material of catalyst is titanium dioxide (TiO_2), with smaller amounts of other metal oxides including tungsten oxide (WO_2) for thermal support and vanadium pentoxide (V_2O_5), which is the primary active material.

The size of honeycomb catalyst is offered with 94mm X 94mm X 750mm of 3 Modules with 8mm pitch and 1mm wall thickness. The total volume of honeycomb catalyst is 0.0198 m^3 (or) 19.8 litres (0.094*0.094*0.75 *3). The pictorial view of 8mm pitch honeycomb type SCR catalysts have been shown in figure 06. To provide a large gas contact area with a minimum pressure loss, the honeycomb catalyst is provided as 64 elements containing a large number of parallel channels (corrugated or extruded honeycomb catalysts).

Figure 5: Pictorial view of 8mm Honeycomb & plate type SCR catalysts

IV. EXPERIMENTAL PROCEDURE:

The existing Ø200mm Pilot Plant Test Facility was operated in a combustion mode and generated flue gas for testing of 8mm pitch honeycomb type SCR catalysts. The Process and Instrumentation Diagram (P&ID) and Pictorial view of SCR test facility for De-NOx process is shown in Figure 1. The performance of honeycomb type SCR catalysts were tested with high dust (30-52 grams/Nm^3) concentration in flue gas.

For testing of honeycomb type catalyst with dust, flue gas generated from the combustor and sent directly to dust measurement system where the dust concentration was measured with help of on-line dust monitoring system. Once the dust measured using on-line dust measurement system, the flue gas was sent to immersion heating coil to heat the flue gas to a required SCR inlet temperature (300 to 350 Deg.C). Then the inlet NOx concentration was measured using flue gas analyser and is shown in figure 2. Subsequently the required quantity of Anhydrous Ammonia was admitted with help of ammonia mass flow controller in to flue gas pipe line through ammonia injection nozzle. The pictorial view of ammonia mass flow controller and ammonia flow nozzle is shown in figure 3 (a) & 3 (b). The quantity of anhydrous ammonia is calculated based on the flue gas flow rate and NOx concentration in the flue gas. Once the anhydrous ammonia injected in to flue gas, the mixture of Ammonia (NH_3) and Oxides of Nitrogen (NOx) gas was sent to static mixture for better mixing of ammonia and oxides of nitrogen in the flue gas. Then the mixture sent in to SCR reactor to reduce the oxides of nitrogen (NOx) in presence of honeycomb type SCR catalysts for NOx reduction at required SCR inlet temperatures. The line diagram and pictorial view of 20 liter capacity SCR reactor module is shown in Figure 4. The temperature, pressure and differential pressures are measured across the SCR reactor using E-type thermocouples, pressure transmitters and differential transmitters respectively. Once the reaction completed in SCR reactor, the flue gas passes through gas Venturi flow meter to measure the flue gas flow rate for calculating the space velocity. The outlet NOx concentration and ammonia slip also measured before vent off to the atmosphere using flue gas analyzer and ammonia gas analyzer respectively. The NOx conversion rate was calculated based on the inlet and outlet NOx concentration of the SCR reactor.

V. EXPERIMENTAL RESULTS

The existing Ø200mm Pilot Plant Test Facility was operated in a combustion mode and generated flue gas for testing of 8mm honeycomb type catalyst for generating the

performance curves. The size of the each honeycomb is 94mm X 94mm X 750 mm long to get about 20 liter catalyst volume. The Process and Instrumentation Diagram (P&ID) of 20 litres SCR test Facility for De-NOx system is shown in Figure 1. Coal was procured from Singareni calories, to generate the flue gas for testing of in-house developed catalyst. Feed particle size has been maintained more or less same for all the experiments and which was + 0.5 to –4.0 mm. The performance of honeycomb type catalyst was evaluated by varying the dust concentration from 30-52 grams/nm3 in flue gas. For testing of honeycomb catalyst the flue gas flow rate varied at 31.80, 41.75 & 51.70 Nm^3/hr and space velocity 1500-2500 /hr respectively. Also the SCR inlet temperature varied in the range of 300 to 350 Deg.C and the molar ratio of ammonia (NH_3) to oxides of nitrogen (NOx) varied in the range of 0.9 to 1.0 for all experiments. The Ø200mm Pilot Plant Test Facility generates the flue gas by operating in combustion mode. The flue gas composition consists of carbon di-oxide (CO_2), water (H_2O), oxygen (O_2), nitrogen (N_2), nitrous oxide (NO), nitrogen di-oxide (NO_2), sulphur di-oxide (SO_2), and Argon (Ar). The generated flue gas composition in volume percentage wise is shown in table 8.

Table 15: The typical flue gas composition

Flue Gas Composition (Vol %)	
Carbon di-oxide (CO_2)	12
Water (H_2O)	8.5
Oxygen (O_2)	6.24
Nitrogen (N_2)	71.9755
Oxides of Nitrogen (NOx)	0.04
Oxides of Sulphur (SOx)	0.03
Argon (Ar)	1.2
Average Molecular Weight	29.46952

The generated flue gas was sent to honeycomb type SCR catalysts to generate the performance curves. Also measured the anhydrous ammonia flow rate, flue gas flow rate, inlet NOx, Outlet NOx, Inlet dust concentration, pressures, differential pressures across static mixture & SCR reactor and ammonia slip at out let of the SCR reactor.

VI. RESULTS AND DISSCUSSION

The NOx reduction reaction takes place in presence of SCR catalyst. The SCR reactor contains a honeycomb catalyst of 94 X 94 X 750 mm size of 3 modules. When the mixture (Flue gas and ammonia) is admitted in to SCR reactor, the available NOx in the flue gas is reacted with ammonia in presence of catalyst and converted in to nitrogen (N_2) and water (H_2O). The catalytic reduction process consists of primary and secondary reactions and those are shown below:

A. Primary reactions:

$4NO + 4NH_3 + O_2 \rightarrow 4N_2 + 6H_2O$

$2NO_2 + 4NH_3 + O_2 \rightarrow 3N_2 + 6H_2O$

$NO + NO_2 + 2NH_3 \rightarrow 2N_2 + 3H_2O$

B. Secondary reactions:

$2SO_2 + O_2 \rightarrow 2SO_3$

$2NH_3 + SO_3 + H_2O \rightarrow (NH4)_2SO_4$

$NH_3 + SO_3 + H_2O \rightarrow NH_4HSO_4$

C. NOx Removal Efficiency (η_{NOx}):

The NOx removal efficiency, represented as η_{NOx}, is determined from the inlet and outlet NOx concentration of SCR. The equation for the NOx removal efficiency is given by:

$$\text{NOx Removal Efficiency } \eta_{NOx} : \frac{\text{NOxin - NOxout}}{\text{NOxin}}$$

Where:

η_{NOx} = NOx removal efficiency, fraction

NOxin = Inlet NOx rate to the SCR,

NOxout = outlet NOx rate from the SCR.

D. Space Velocity (1/hr):

The space velocity is defined as the ratio of volumetric flow rate of flue gas and the catalyst volume. It is commonly regarded as the reciprocal of the residence time. The units are per hour.

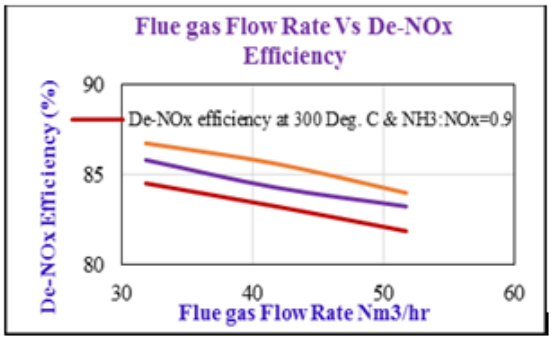

Figure 6. Flue gas flow rate Vs De-NOx efficiency

Figure 6. Shows the De-NOx efficiency as a function of flue gas flow rate. This experiment was conducted in a 20 litre capacity SCR test facility by varying the flue gas flow rate of 31.80, 41.75 & 51.70 Nm^3/hr. Also the SCR inlet temperature varied in the range of 300 to 350 Deg.C and the molar ratio of ammonia (NH_3) to oxides of nitrogen (NOx) varied in the range of 0.9 to 1.0 but reported only 0.9 (NH_3: NOx=0.9) due to avoid more ammonia slip.

The results show that the De-NOx efficiency increases with decrease in flue gas flow rate which could be attributed due to less residence time. The residence time is the major parameter which greatly affects the DeNOx efficiency in SCR catalyst. When the flue gas flow rate increases, the residence time decreases which means the flue gas spent very less time in SCR reactor which leads to reduction in reaction rate between NOx and NH_3. When the flue gas flow rate increases from 31.80 to 51.70 Nm^3/hr, the De-NOx efficiency decreased from 86.75 to 81.89% at different temperatures (300-350 Deg.C).

 ISBN: 978-93-91420-02-4

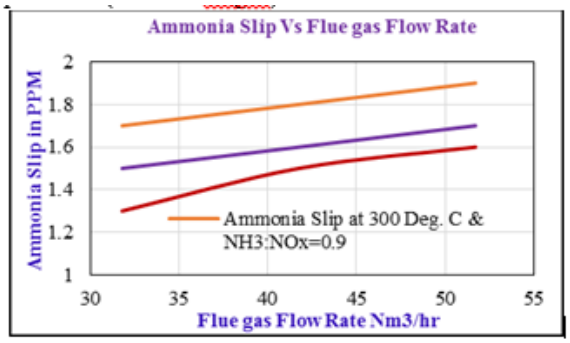

Figure 7: Ammonia slip Vs Flue gas flow rate

Figure 7. Shows the ammonia slip as a function of flue gas flow rate. This experiment was conducted in a 20 litre capacity SCR test facility by varying the flue gas flow rate of 31.80, 41.75 & 51.70 Nm^3/hr. Also varied the SCR inlet temperature in the range of 300-350 deg. C and the molar ratio of ammonia (NH_3) to oxides of nitrogen (NOx) in the range of 0.9 to 1.0 but reported only 0.9 (NH_3: NOx=0.9) due to avoid more ammonia slip.

The results show that the Ammonia slip increases as the flue gas flow rate increases which could be attributed due lower residence time. When the flue gas flow rate increases from 31.8 to 51.70 Nm^3/hr, the ammonia slip increases from 1.3 to 1.9ppm at the molar ratio of ammonia (NH_3) to oxides of nitrogen (NOx) in the range of 0.9. When the flue gas flow increases, the residence time decreases when the residence time decreases the reactivity also decreases. When the reactivity decreases the ammonia slip increases. Ammonia slip also increases as the catalyst activity decreases. The allowable ammonia slip approximately less than 2 ppm [4].

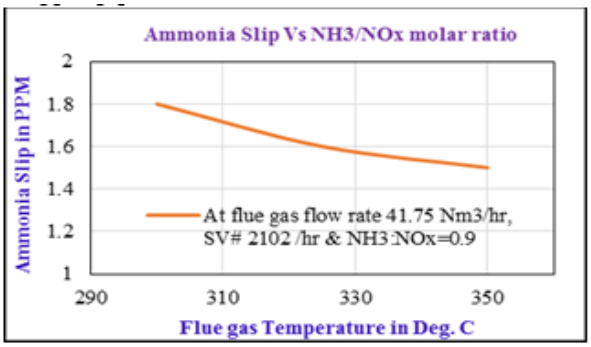

Figure 8. Ammonia slip Vs flue gas temperature

Figure 8. Shows the ammonia slip as a function of flue gas temperature. This experiment was conducted in a 20 litre capacity SCR test facility by maintained the flue gas flow rate of 41.75 Nm^3/hr and space velocity 2102 /hr. Also the SCR inlet temperature has been varied from 300 to 350 deg. C and the molar ratio of ammonia (NH_3) to oxides of nitrogen (NOx) also varied in the range of 0.9 to 1.0 but reported only 0.9 (NH_3: NOx=0.9) due to avoid more ammonia slip.

The results show that the ammonia slip decreases with increase in SCR inlet temperature which could be attributed due higher reaction kinetics at high temperatures. When the SCR inlet temperature increases from 300 to 350 Deg.C, the ammonia slip decreases from 1.8 to 1.5 ppm at a space velocity of 2102 /hr & NH_3: NOx = 0.9. The higher temperatures favor the reactions between ammonia and oxides of nitrogen. When the SCR inlet temperature increases, the De-NOx efficiency increases due to more reactions, which in turn affects the ammonia consumption. When the ammonia consumption increases, the ammonia slip decreases.

E. Gas flow rate Vs pressure drop across SCR reactor:

Figure 9. Shows the pressure drop across SCR reactor as a function of flue gas flow rate. This experiment was conducted in a 20 litre capacity SCR test facility by varying the flue gas flow rate at 31.80, 41.75 & 51.70 Nm^3/hr and space velocity of 1600, 2102 & 2600 /hr respectively.

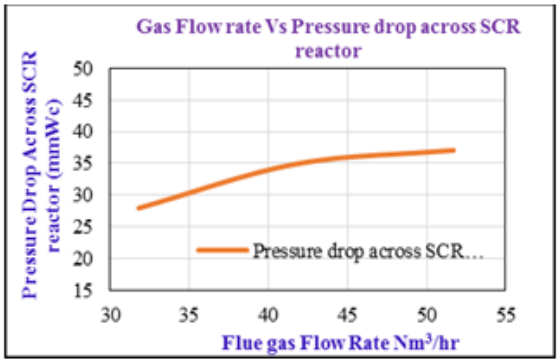

Figure 9: Flue gas flow rate Vs pressure drop across SCR reactor

The results show that the pressure drop across SCR catalyst increases with increase in flue gas flow rate. The pressure drop across SCR catalyst is a function of the length of the catalyst, catalyst configuration and deposition of fly ash over the catalyst. The measured dust concentration at a flow rate of 31.80, 41.75 & 51.70 Nm3/hr was 30-32, 45-47 and 50-52 grams/nm^3 respectively.

It also been observed that the pressure drop across SCR reactor is varying from 28 mmWc to 38 mmWc over a 2250mm catalyst length.

CONCLUSIONS

Experiments were carried out to generate the performance curves with in-house developed 8mm Pitch Honeycomb type catalyst in a 20 liter volume capacity SCR test facility. The flue gas was generated with coal from Ø200mm Pilot Plant test Facility by operating in combustion mode. The NOx removal efficiency and ammonia slip was investigated with dust concentration of 30-52 grams/Nm^3 in flue gas by varying the space velocities (2500-1500 per hr.) and flue gas temperatures (300–350^{0}C) using anhydrous ammonia as reducing agent.

- In-house developed 8mm pitch honeycomb type SCR catalysts were tested in a 20-liter capacity SCR test facility with dust concentration in the range of 30-52 grams/nm^3 by varying the space velocities (2500-1500 per hr.) and flue gas temperatures in the range of 300–350^{0}C using anhydrous ammonia as reducing agent.
- NOx reduction efficiency achieved with honeycomb was 81.89 – 86.75% at 2500-1500 per hr. space velocities and the ratio of ammonia (NH_3) to oxides of nitrogen (NOx) was maintained at 0.9.
- NOx reduction efficiency achieved with honeycomb was 82.72– 88.23% at 2500-1500 per hr. space

velocities and the ratio of ammonia (NH_3) to oxides of nitrogen (NOx) was maintained at 1.0.

- Ammonia slip measured was in the range of 1.3 to 1.9 ppm for honeycomb catalyst at 0.9 for ammonia to oxides of nitrogen.
- The total Differential Pressure (DP) across Honeycomb SCR catalyst was 28-38 mmWc over a 2250mm length.

Finally, it can be concluded that, the 8mm pitch honeycomb type SCR catalysts are very much suitable for reduction of Oxides of Nitrogen (NOx) in the range of 80-90% in flue gas with dust concentration of 30-52 grams/Nm^3 which are meeting the NTPC requirements. Hence, based on the performance achieved in 20 litre SCR test facility, the honeycomb type SCR catalysts were selected and finalized for establishment of 1500 Nm^3/hr slip stream De-NOx system in Left Hand (LHS) side and Right Hand (RHS) Side at Unit-2 of NTPC Simhadri power plant as per MOU.

REFERENCES

[1] International Energy Outlook 2016, report no. DOE/EIA-0484(2016) I May 2016.

[2] The Cadmus Group, Inc., Bechtel Power Corporation, and Science Applications International Corporation. Selective Catalytic Reduction for NOx Control on Coal-fired Boilers, Draft Report. Prepared for the U.S. Environmental Protection Agency. May 1998.

[3] Selective Catalytic Reduction Draft public comment. Prepared by John L. Sorrels, Air Economics Group Health and Environmental Impacts Division Office of Air Quality Planning and Standards U.S. Environmental Protection Agency. June 2015.K. Elissa, “Title of paper if known,” unpublished.

[4] Institute of Clean Air Companies (ICAC). White Paper. Selective Catalytic Reduction (SCR) Control of NOx Emissions from Fossil Fuel-Fired Electric Power Plants. May 2009

 ISBN: 978-93-91420-02-4

A Review on NVH Issues and Technological Challenges in Electric Vehicle and Hybrid Electric Vehicle Powertrain

Gangaraju Moopuri[1] and Vijayalakshmi C[2]
[1]Department of Mechanical Engineering, Sree Vidyanikethan Engineeing College, Tirupati, India.
[2]Department of GEBH, Sree Vidyanikethan Engineeing College, Tirupati, India.

***Abstract*— This article guided with the proposals for how future measurements of NVH (Noise, Vibration & Harshness) from electric and hybrid electric vehicles be performed and what aspects of this NVH need future investigations. The coordination of diesel motor innovation into a hybrid electric vehicle arrangement indicates guarantee as an approach to meet efficiency and outflow of energy necessities. Because of the high multifaceted nature of different hybrid systems, it is critical to examine the new NVH difficulties and recognize proper counter measures. The goal is to identify the viable methods of energy transfer from the diverse sources of excitation through numerous interfaces to given target places.**

Keywords— hybrid electric vehicles, Transfer Path Analysis, Noise distribution, Noise Transfer Function Introduction.

I. INTRODUCTION

It seems that the global population may increase with current trend, may increase from 6 billion to 10 billion by 2050. And also vehicles in use may increase from 700 million to 2.5 billion by 2050.if all the vehicles are internal combustion engine vehicles then all cities may be covered with permanent smog with entire air pollution. According to Air Research Board (ARB) in 2001 around 9000 people die per year due to fine particle matters in California. So there is a necessity to think ahead. Then there is one of the promising solutions is sustainable transport. It means it has low or zero emission vehicles, promotion of public transport so that very less vehicles on the road and use of renewable energy sources i.e less depending on fossil fuels.

II. BENEFITS OF USING ELECTRIC VEHICLES:

A. Energy sources

The main alternative and transitional energy sources for transportation have the importance to discuss major challenges that the present world faces i.e energy security, sustainability and pollution. The comparison of energy sources (storage) used for transportation is as follows

Table 1: Different types of energy sources and its significance in the energy transmission.

S.No	Energy Source	Phase of energy source	Remarks
1	Gasoline (Petrol) Diesel	Liquid fuels	As diesel is having more energy density it is more fuel economical compared to petrol
2	Compressed Natural Gas (CNG) & Hydrogen	Gaseous fuels	CNG has higher specific energy compared to liquid fuels. But it has low energy density.
3	Ultra-Capacitors	Electrical energy in electrostatic form.	It typically stores 10 to 100 times more energy per unit volume or mass than electrolytic capacitors.
4	Batteries	Chemical Energy	Specific energy and energy density are very low compared with petro i.e (75% & 25% less compared with petrol)
5	Ultra-flywheel	Stores energy in mechanical form at very high speeds.	It is very less liable. For safety concern these are used inside the EVs.

B. Pollutantsand Greenhouse Gases:

There are various types of pollutants and greenhouse gases which are released as pollutants from the vehicles and they are reasons for smoke and air pollution and some of them are particulate matter (PMx), CO, CO2, CH4, NOx(N2O NO and NO2), volatile organic compounds and SOx(SO2) gases. Particulate matter or Particle are released as part of combustion cycle. These particles are extremely small in the range of micro meters. Therefore, they can't be filtered by human throat and nose and enters the body and effects heart and lungs. Diesel engine releases more PMx Particles (PM10, PM2.5) which are more dangerous. Due to presence of the gases infrared radiations are trapped in to the atmosphere and cause greenhouse effect cause global warming. There is an increase in electric and hybrid electric vehicles especially from last 10 years, it shows its significance.

III. NVH & ACOUSTICS

In 2011 by Greg Goetchius gave his prediction of where the challenges of NVH on electric cars would be, where we have to deal with powertrain noise proportionally with road noise, wind noise and other ancillary noise corresponding to power steering and wiper etc. In electric vehicle road noise and wind noise significantly increase and powertrain noise is less importance compared with internal combustion engine vehicles. In the case of electric vehicles ancillary system noise increases 5 to 10 percent and wind noise increase by almost 20 to 30 percent and totally added to 110 percent i.e the additional 10% noise is not fully known. However the function of frequency range and other function of vehicle speed in both ICE and EVs are discussed using the following charts. In ICE car green band is indicating the engine structure and engine air born noise contributions being wide important. Wide range of frequencies from 20 to 80 kHz and also really being dominant in the low speed range of 60km/h, followed by the road noise and tire noise in the frequency range 60 to 100km/h. But in the case of electric vehicles

power train noise significantly decrease especially in the low frequency range basically there is no contribution of engine noise. In lower speeds the road noise and tire noise contributions are very high. In higher frequency range almost greater than 100km/h wind noise is taken off [1-3].

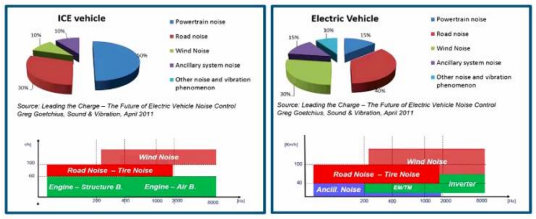

Fig. 1. Sources of Noise distribution in ICE and Electric vehicle

IV. CONTROL MEASURES FOR VIBRATION REDUCTION

A. Transfer Path Analysis(TPA):

Transfer path analysis is really mathematical description of source transfer receiver approach. Source transfer receiver approach is actually fundamental approach considering at noise and vibration problems i.e. any NVH issue would be an issue if it is perceived by receiver, as long as a receiver don't have any issue then there is no any NVH problem. Any of these problems or issues would be caused because of by cause of source that could be engine, tire interaction, exhaust system or power steering system[4]. As long as source is faraway or completely decoupled from receiver there is no problem so there must be some way of transfer of vibration energy that is created in source to the receiver before it is actually really becomes problem. That is essentially what TPA does it. It is really describes the source, transfer and receiver idea with mathematical equations and it is essentially multiplied by source with transfer functions through with receiver response. By the knowledge of transfer path analysis and its applications that there are other ways of looking at noise and vibration issues saying with the help of problem frequency[5-6]. TPA is one that the equation which path is the actual energy takes, which also look at panel contribution analysis i.e which panel is vibrating the most and radiating more energy in to the interior. The simulation also look at grid contribution analysis which grid is actually contributing. Operating deflection shape analysis is also done using transfer path analysis by which we can understand which path the energy will takes place and actual contribution comes out in the form of actual operating deflection shape. With this we can understand how the structure vibrates can be obtained.

B. Fundamentals of Transfer Path Analysis:

So as to clarify the basic standards behind Transfer Path Analysis it is essential to comprehend the basic components from Source path receiver model. Air borne Noise: Sound at receiver resulting from sound radiated by source. Structure borne noise: Sound at receiver resulting from vibrations generated by a source [7].

$$Source\ (F_i, Q_j) X\ Transfer\ Function (NTF) - - - - > Receiver\ (Y_k)$$

C. Measurement of Noise Transfer Function (NTF):

That is there is a need to measure transfer functions that describes the functional parameters depends to transfer the energy from source to receiver side, for that the most traditional way of doing that of using model hammer to exite different force input locations that is defiantly through the measurement error. That is when we hit the structure not always with the same direction not always with the same force and when different people are doing the measurements may set different results[8-9].

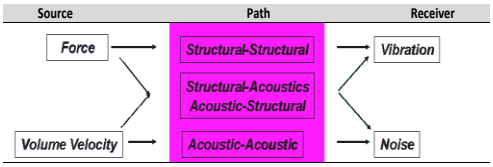

Fig. 2. The Source-Transfer-Receiver Concept.

Therefore that the small shakers have been developed the time like the ones that we distribute from two sources which allows to access the instrument. The force input locations without shakers can get much more repeatable and consistent measurement data from that [10]. It is interesting to notice that when we are measuring transfer functions, the theory says that when it is considered as exiting point A and measuring point B, if it is inverse that exiting point B and measuring point A also would get same noise transfer function. When it is comes to the noise transfer function to the cabin it is interesting to put one source at receiver location and measure all the responses of the force input points at the same time. That can be known with the acoustic sources, it again from that we use from sources allows to measure all these transfer functions in one go. It is also important to know that when some cases like in a methodology that you set in to we need localized transfer function measurements, we still need to measure locally either with hammer or with other small shakers[11-12].

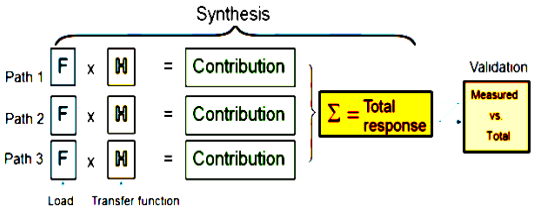

Fig. 3. TPA-Synthesis Method.

D. Determination of Sources:

One could think of using four cells in the source location so in the path input locations. If there is four cells, these cells are measuring those forces directly. That would be a good idea but biggest issue with that is that in order to put those four transducers in there we need usually to modify the structure in some way and actually as such you could modifying the actual forces. So much more used are two methodologies one is mount stiffness method and other is Matrix inversion method [13-15].

V. LOAD IDENTIFICATION METHODS

A. Mount Stiffness Method:

In mount stiffness method we are going to measure over a mount or path, if we want measure active and passive side across that mount is pushing, integrating the accelerations twice and multiplying with mount stiffness would give us the actual force passing through the path. It is the mount stiffness method it requires mount stiffness value it comes from supplier. It also requires enough isolation of the mass and frequency response functions to targets only. The

 ISBN: 978-93-91420-02-4

measurements of forces on both active and passive side will be carried. Sufficient isolation over the mount i.e ≈20dB at least required[16-18].

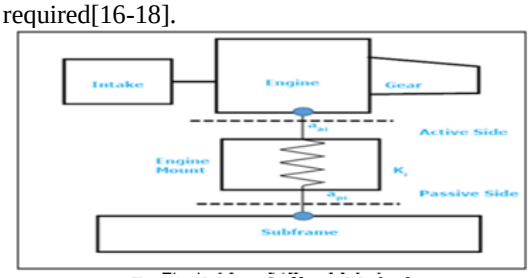

Fig. 4. Mount Stiffness Method

$$F_t(\omega) = K_t(\omega) \times \frac{(a_{ai}(\omega) - a_{pi}(\omega))}{-\omega^2} \quad \text{---------- (1)}$$

B. Matrix Inversion Method:

In matrix inversion method a diminutive of different approach, here we don't measure the forces on the active side we actually do all the measurements on the passive side only. Both the structure if we want and from all those acceleration measurements there we are going to back to calculate actual force that is being applied. That is going to be assumption that each of these accelerations that are measuring here are actually caused by the forces acting on the structure. If we know the noise transfer function between, their force input locations and these accelerations which we called as indicators, we can inverse that matrix and back calculate the actual forces have to be in order to cause that accelerations. In matrix inversion method need to capture enough dynamics of the structure and need to determine more accelerations than the actual [19-21].

$$\{F(\omega)\} = [H(\omega)]^{-1}.\{a(\omega)\} \text{ ---------- (2)}$$

C. Advanced load identification Methods:

1) Strain Sensors:

Whereas accelerations are driven by the global dynamics of the structure, the acceleration responses are dominated by a limited amount of global structural body modes. Strain measurements especially capture much localized defects. So that they can be very useful in cases where there are little dynamics in the structure and there is lower frequencies over where the paths are very close to gather on the passive side, Where it will be very difficult to distinguish between two paths using just accelerations. Indicator for quality of the matrix inversion is that the condition number of the matrix. Condition number is the ratio between the highest and lowest singular value that is calculated from that matrix inversion. Overall lower condition number is worthy and higher condition number is not worthy. As a guideline it wants to be below on hundred. In the case of strain indicators strain measurements are dominated by great amount of confined structural body modes and in this method, there is extended possibilities for load separation/identification possibilities are there.

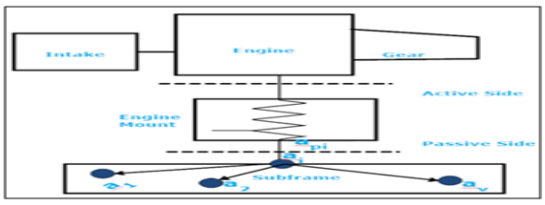

Fig. 5. Matrix inversion method

D. OPAX Method:

Several attempts have been made to speed up the TPA process. One example is the operational path analysis (OPA or OTPA) approach. This approach requires only operational data measured at the path references (for example, passive-side mount accelerations, pressures close by vibrating surfaces, nozzles and apertures, etc.) and target points. The OPA method is time efficient, but has several limitations that make the reliability and accuracy unpredictable: difficult transmissibility estimation, neglected cross-coupling between paths, effect of missing paths and OPA sum as a quality indicator. As described in the section on OPAX, Simcenter Testlab OPAX software is an alternative, fast and test-based procedure that supports troubleshooting of vibroacoustic problems in an efficient manner. The Simcenter Testlab OPAX solution separates loads and transfer paths. By doing so, the vibro-acoustic energy can be traced back to the source. This method has proven its reliability and efficiency, especially for soft-mount applications (for example, powertrain structure-borne paths).

The traditional transfer path analysis (TPA) is based on the superposition principle that is valid for linear, time invariant systems. The individual path contribution to the sound pressure (or vibration response) in point m from force acting in point n in direction k is given by

$$with\ P_{mnk}(\omega) = H_{mnk} \times F_{nk}(\omega) \text{ --- (3)}$$

Where P_{mnk} is the (complex) sound pressure spectrum, H_{mnk} is the (complex) frequency response function (NTF) of the receiving system when decoupled at interfacing DOFs and F_{nk} is the complex force spectrum. The total response (e.g. sound pressure) is then obtained as [23]

$$P_m(\omega) = \sum_{n=1,k=1}^{N,3} P_{mnk}(\omega) = \sum_{n=1,k=1}^{N,3} H_{mnk}(\omega)\ F_{nk}(\omega) \text{ --(4)}$$

The determination of operating forces for each DOF is done indirectly, and can be performed in three different ways. The first and most common method is to use resilient connecting elements as "force transducers", provided that the complex dynamic transfer stiffness [22-24] is known for the different DOFs. The forces are then obtained as

$$F_{nk}(\omega) = K_{nk}(\omega)x_{nk1}(\omega) - x_{nk2}(\omega) \text{ --(5)}$$

x_{nk1} is the operating displacement at the source side and x_{nk2} is the operating displacement at the receiver side.

The second method is to use inversion of the measured FRF matrix between structural and and exciting forces response acting at all interfacing DOFs on the receiver side. This inverted matrix is then multiplied with the vector of operational measurements of vibration on the receiver side. The matrix inversion method has to be used when the transfer paths include rigid connections or the mounts are very stiff compared to the receiving structure, since the relative displacement across the mount becomes too small to use Equation (6). The forces are obtained as

$$\begin{Bmatrix} F_1 \\ \vdots \\ F_N \end{Bmatrix} = \begin{bmatrix} H_{11} & H_{12} & \cdots & H_{1N} \\ \vdots & \ddots & & \vdots \\ H_{M1} & \cdots & \cdots & H_{MN} \end{bmatrix}^{-1} \begin{Bmatrix} \ddot{x}_1 \\ \vdots \\ \ddot{x}_M \end{Bmatrix} \quad (6)$$

Where the number of responses M can and should be larger than the number of force DOFs N. An over determination factor of about 2 is often used.

VI. CONCLUSION

EVs and HEVs have specific NVH behavior. To improve its NVH performance the source transfer receiver approach must be adopted. In which we need to take in to account specific NVH of electric and hybrid electric vehicle. With the high focus on sound quality we can adjust sound level. We need to explore new engineering methodologies and chose such as signal capturing of electric & power signals and signal analysis. We need to look at high frequency test and simulation methods and also adopt system integration based, multidisciplinary approaches to include control strategies of gears, clutch and brakes in to the analysis of the complete vehicle. Transfer path analysis (TPA) has been a key method in NVH engineering for the past decades. Evolutions kept TPA up to date ready. Some time ago faster analysis with tools like OPAX and time domain TPA for transient defense for example start/Stop events. Now a days combining 3D and 1D models to allow contribution analysis much more in detail and applying it throughout development of vehicle.

REFERENCES

[1] Kinnear Road, Columbus, OH 43212 On the Control of Engine Start/Stop Dynamics in a Hybrid Electric Vehicle, Journal of Dynamic Systems, Measurement, and Control NOVEMBER 2009, Vol. 131 / 061005-1

[2] Recent research on vehicle noise and vibration Int. J. Vehicle Noise and Vibration, Vol. 8, No. 4, 2012.

[3] https://www.fhwa.dot.gov/pavement/sustainability/articles/tire_noise.cfm

[4] An Introduction to Tire/Pavement Noise of Asphalt Pavement, Robert Bernhard, Purdue University Roger L. Wayson, University of Central Florida.

[5] https://www.researchgate.net/publication/304494555_NVH_of_Hybrid_Vehicles_Key_Challenges_and_Conceptual_Approaches [accessed Sep 15 2018].

[6] Takayoshi yoshioka Noise and Vibration Reduction Technology in Hybrid Vehicle Development SAE International, Document Number: 2001-01-1415

[7] Masashi komada, takayoshi yoshioka Noise and Vibration Reduction Technology in New Generation Hybrid Vehicle Development SAE International, Document Number: 2005-01 - 2294

[8] Essamallam, ibrahimahmed Noise Characteristics for Hybrid Electric Vehicle Induction Motor SAE Technical papers 2007-01-2261

[9] Roceedinges of the American Control Conference SeaUIe. Washington June 1995 TA6 A Hybrid Electric Vehicle Powertrain Dynamic Model* by K.E. Bailey and B.K. Powell

[10] Design, demonstrations and sustainability impact assessments for plug-in hybrid electric vehicles Thomas H. Bradleya, Andrew A. Frankb

[11] Williamson SS, Lukic SM, Emadi A. Comprehensive drive train efficiency analysis of hybrid electric and fuel cell vehicles based on motor – controller efficiency modeling. IEEE transactions on power electronics 2006; 21:730-40.

[12] Emadi A. Hand book of automotive power electronics and motor drives. Florida: Taylor & Francis Group, CRC Press; 2005.

[13] Brandl, Stephan & Graf, Bernhard & Rust, Alfred & Resch, Thomas. (2015). NVH of Hybrid Vehicles – Key Challenges and Conceptual Approaches.

[14] Nuria Campillo-Davo and Ahmed Rassili, Shaker Verlag Publications (2016) NVH Analysis Techniques for Design and Optimization of Hybrid and Electric Vehicles, ISBN 978-3-8440-4356-3,

[15] A comprehensive overview of hybrid electric vehicle: Powertrain configurations, powertrain control techniques and electronic control units, Energy Conversion and Management 52 (2011) 1305–1313.

[16] Recent Improvements in Road Noise Control Arnaud Gaudin and Laurent Gagliardini PSA- Peugeot-Citroën SAE International.

[17] Fernandez del rincon, A. ... et al, 2016. Experimental approaches for NVH study of Electric and Hybrid Electric Vehicles, Annex 3A: Transfer Path Analysis for vehicle NVH refinement: Application on EV / HEV vehicles. IN: Campillo-Davo, N. and Rassili, A. (eds). NHV Analysis Techniques for Design and Optimization of Hybrid and Electric Vehicles. Aachen: Shaker, pp. 67-98.

[18] Geluk, T., Van der Linden, P., Vige, D., Caudano, M., Gottardi, S., Ciraolo, F., & Mir, H. (2011). "Noise Contribution Analysis at Suspension Interfaces Using Different Force Identification Techniques." SAE International, 2011-01-1600.

[19] Van der Seijs, M., de Klerk, D., Rixen, D.J. (2016) "General framework for transfer path analysis: History, theory and classification of techniques." Mechanical Systems and Signal Processing, 68:69, 2017:244.

[20] Transfer path analysis - Qualifying and quantifying vibro-acoustic transfer paths; www.siemens.com/simcenter.

[21] Geluk, T., Van der Linden, P., Vige, D., Caudano, M., Gottardi, S., Ciraolo, F., & Mir, H. (2011) "Noise Contribution Analysis at Suspension Interfaces Using Different Force Identification Techniques." SAE International, 2011-01-1600

[22] Bianciardi, F., Janssens, K., & Britte, L. (2013). "Critical asessment of OPA: effect of coherent path inputs and SVD truncation." 20th international congress on Sound & Vibration. Bangkok, Thailand.

[23] Plunt, Juha. (2005). Examples of Using Transfer Path Analysis(Tpa) Together With Cae- Models to Diagnose and Find Solutions for NVH Problems Late in the Vehicle Development …. 10.4271/2005-01-2508.

[24] ISO10846-1/2 1997. Acoustics and Vibration - Laboratory measurement of vibro-acoustic transfer properties of resilient elements. Part 1: Principles and guidelines. Part 2: Dynamic stiffness of elastic supports for translatory motion – Direct Method.

 ISBN: 978-93-91420-02-4

Design and Analysis of Cantilever Beam

K.L.N. Murthy and N. Vijaya Sekhar
Department of Mechanical Engineering, A.M. Reddy College of Engineering College, Guntur, Andhra Pradesh, INDIA,
Department of Mechanical Engineering, Narasaraopeta Engineering College, Guntur, Andhra Pradesh, INDIA

Abstract: In this project static and Modal analysis is a process to detect project, statics, strain and deformation. Vibration characteristics (natural frequencies and mode shapes) of a structure or a machine component while it is being designed. It has become a major alternative to provide a helpful contribution in understanding control of many vibration phenomena which encountered in practice.
In this work we compared the stress and natural frequency for different material having same I, C and T cross- sectional beam. The cantilever beam is designed and analyzed in ANSYS. The cantilever beam which is fixed at one end is vibrated to obtain the natural frequency, mode shapes and deflection with different sections and materials.

Key words: Finite element analysis, cantilever beam, static and model analysis.

1. INTRODUCTION

1.1 BEAM

A **beam** is a structural element that is capable of withstanding load primarily by resisting against bending. The bending force induced into the material of the beam as a result of the external loads, own weight, span and external reactions to these loads is called a bending moment. Beams are characterized by their profile (shape of cross-section), their length, and their material. Beams are traditionally descriptions of building or civil engineering structural elements, but smaller structures such as truck or automobile frames, machine frames, and other mechanical or structural systems contain beam structures that are designed and analyzed in a similar fashion.

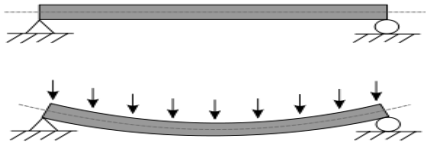

A statically determinate beam, bending (sagging) under a uniformly distributed load.

2. LITERATURE REVIEW

The dynamic analysis of a beam with multiple degree of freedom (MDOF) are studied in this paper. Due to the destructive effects of vibration in machines and structures due to resonance. In multiple degree of freedom system, there are n natural frequencies and the concept of resonance is complicated by the effect of mode shapes. In the present work cantilever beam of different materials and dimensions is considered for the dynamic analysis of free vibration at no load condition as well as comparison between materials. The modelling, simulation and analysis of cantilever beam is done by using ANSYS and theoretically by finite element method (FEM) for the evaluation of natural frequency and mode shape.

3. PROBLEM DESCRIPTION:

The objective of this project is to make a 3D model of the cantilever beam and study the static and model behavior of the cantilever beam by performing the finite element analysis.3D modeling software(PRO-Engineer) was used for designing and analysis software (ANSYS) was used for static and modal analysis.

The methodology followed in the project is as follows:

- Create a 3D model of the cantilever beam assembly using parametric software pro-engineer.
- Convert the surface model into Para solid file and import the model into ANSYS to do analysis.
- Perform static analysis on the cantilever beam.
- Perform model analysis on the existing model of the cantilever beam.

4. INTRODUCTION TO CAD/CAE:

Computer-aided design (**CAD**), also known as **computer-aided design and drafting** (**CADD**), is the use of computer technology for the process of design and design-documentation.

4.1. INTRODUCTION TO PRO-ENGINEER

Pro/ENGINEER Wildfire is the standard in 3D product design, featuring industry-leading productivity tools that promote best practices in design while ensuring compliance with your industry and company standards. Integrated Pro/ENGINEER CAD/CAM/CAE solutions allow you to design faster than ever, while maximizing innovation and quality to ultimately create exceptional products.

Different modules in pro/engineer

Part design, Assembly, Drawing&Sheet metal.

4.2. INTRODUCTION TO FINITE ELEMENT METHOD:

Finite Element Method (FEM) is also called as Finite Element Analysis (FEA). Finite Element Method is a basic analysis technique for resolving and substituting complicated problems by simpler ones, obtaining approximate solutions Finite element method being a flexible tool is used in various industries to solve several practical engineering problems. In finite element method it is feasible to generate the relative results.

5. RESULTS AND DISCUSSIONS:

5.1. Models of cantilever beam using pro-e wildfire 5.0:

The cantilever beam is modeled using the given specifications and design formula from data book. The cantilever beam outer casing body profile is sketched in sketcher and then it is extruded using extrude option.

 ISBN: 978-93-91420-02-4

Cantilever beam 3D model
I-Section:

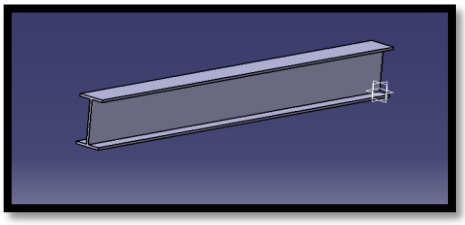

C-Section

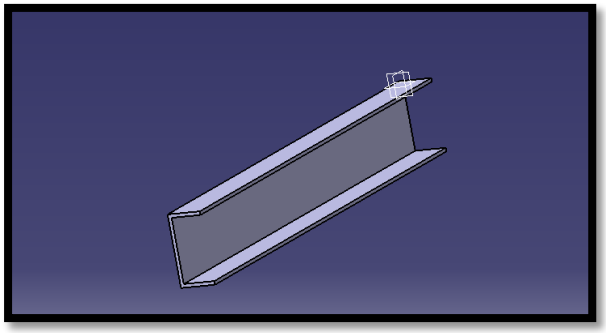

T-Section

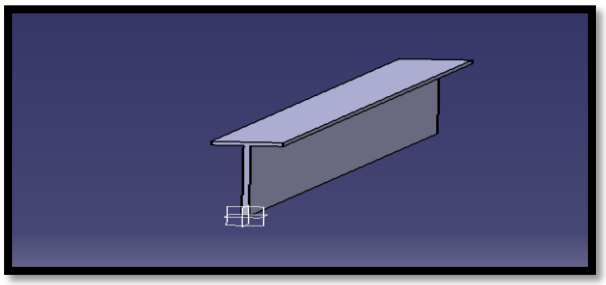

5.2. STRUCTURAL ANALYSIS OF CANTILEVER BEAM
MATERIAL-Steel

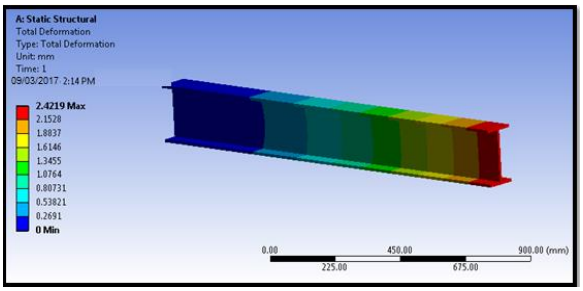

According to the above contour plot, the deformation is maximum at the free end of the beam and the deformation is minimum at the fixed end. At this condition the maximum deformation of the beam is 2.429.

STRESS

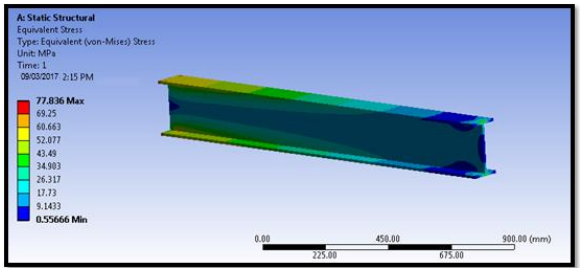

According to the above contour plot, the maximum stress is at the fixed the fixed end because we are applying the loads at the free end.

STRAIN

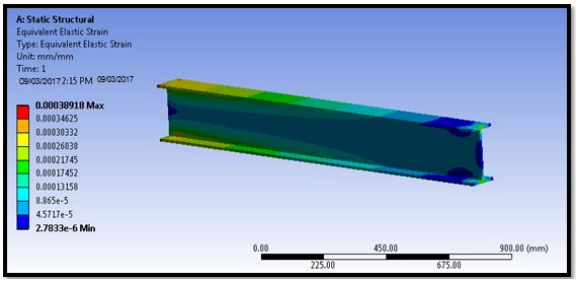

According to the above contour plot, the maximum strain occurs at the fixed end of the beam i.e., 0.00038918.

5.3 MODAL ANALYSIS OFCANTILEVER BEAM
Material-Steel
Total Deformation-1

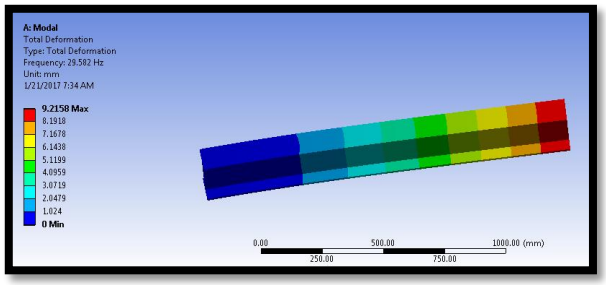

Total deformation-2

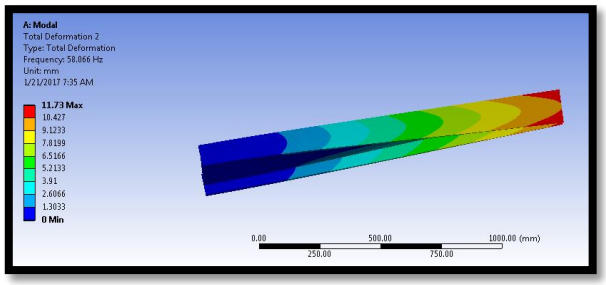

Total deformation-3

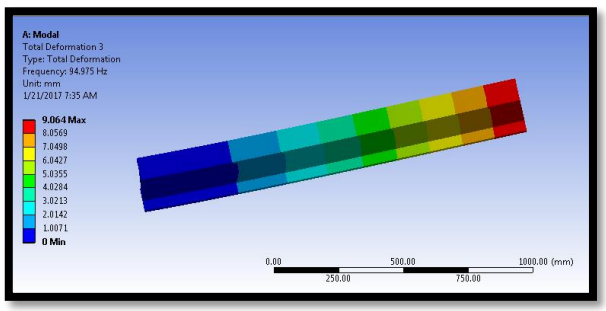

MATERIAL PROPERTIES:

Steel material properties

Density	:	7850kg/m^3
Young's modulus	:	205000Mpa
Poisson's ratio	:	0.3

IMPORTED MODEL

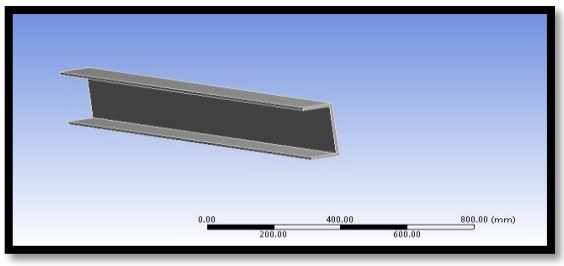

MESHED MODEL

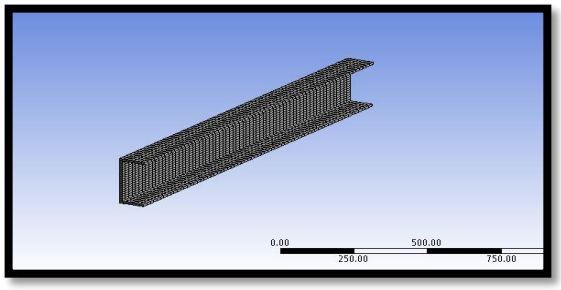

Finite element analysis or FEA representing a real project as a "mesh" a series of small, regularly shaped tetrahedron connected elements, as shown in the above fig. And then setting up and solving huge arrays of simultaneous equations. The finer the mesh, the more accurate the results but more computing power is required.

6. RESULTS AND DISCUSSIONS

Static analysis results

I-section

Material	Deformation(mm)	Stress (N/mm^2)	Strain
Steel	2.4219	77.836	0.00038918
Stainless steel	2.5099	78.313	0.00040577
Cast iron	4.4028	76.871	0.00069883

C-section

Material	Deformation(mm)	Stress (N/mm^2)	Strain
Steel	10.361	169.52	0.00084759
Stainless steel	10.778	170.35	0.00088267
Cast iron	18.696	167.77	0.0015251

T-section

Material	Deformation(mm)	Stress (N/mm^2)	Strain
Steel	4.7314	207.08	0.0010354
Stainless steel	4.9027	208.22	0.0010789
Cast iron	8.6034	204.75	0.0018614

Modal analysis results

Material	Total Deformation 1(mm)	Total Deformation 2(mm)	Total Deformation 3(mm)
Steel	9.2158	11.7	9.06
Stainless steel	9.2752	11.8	9.12
Cast iron	9.6225	12.23	9.466

C-section

Material	Total Deformation 1(mm)	Total Deformation 2(mm)	Total Deformation 3(mm)
Steel	9.9427	14.092	11.479
Stainless steel	10.012	14.192	11.553
Cast iron	10.37	14.691	11.987

T-section

Material	Total Deformation 1(mm)	Total Deformation 2(mm)	Total Deformation 3(mm)
Steel	13.151	13.465	10.829
Stainless steel	13.053	13.37	10.76
Cast iron	13.599	13.941	11.236

7. CONCLUSION

In this work we compared the stress and natural frequency for different material having same I, C and T cross- sectional beam. The cantilever beam is designed and analyzed in ANSYS. The cantilever beam which is fixed at one end is vibrated to obtain the natural frequency, mode shapes and deflection with different sections and materials.

By observing the static analysis the deformation and stress values are less for I-section cantilever beam at cast iron material than steel and stainless steel.

By observing the modal analysis results the deformation and frequency values are less for I-section cantilever beam more for T-section.

So it can be conclude the cast iron material is better material for cantilever beam in this type I-section model.

REFERENCES

[1] Chandradeep Kumar, Anjani Kumar Singh, Nitesh Kumar, Ajit Kumar, "Model Analysis and Harmonic Analysis of Cantilever Beam by ANSYS" Global journal for research analysis, 2014, Volume-3, Issue-9, PP:51- 55.

[2] Yuan, F.G. and R.E. Miller. A higher order finite element for laminated composite beams. Computers & Structures, 14 (1990): 125-150.

[3] Dipak Kr. Maiti& P. K. Sinha. Bending and free vibration analysis of shear deformable laminated composite beams by finite element method. Composite Structures, 29 (1994): 421- 431

[4] Teboub Y, Hajela P. Free vibration of generally layered composite beams using symbolic computations. Composite Structures, 33 (1995): 123– 34.

[5] Banerjee, J.R. Free vibration of axially loaded composite Timoshenko beams using the dynamic stiffness matrix method. Computers & Structures, 69 (1998): 197-208

[6] Bassiouni AS, Gad-Elrab RM, Elmahdy TH. Dynamic analysis for laminated composite beams. Composite Structures, 44 (1999): 81–7.

 ISBN: 978-93-91420-02-4

Analysis of Static and Fatigue Strength of Aluminum Alloy Wheel

K.L.N. Murthy and N. Vijaya Sekhar
Department of Mechanical Engineering, A.M. Reddy College of Engineering College, Guntur, Andhra Pradesh, INDIA,
Department of Mechanical Engineering, Narasaraopeta Engineering College, Narasaraopet, INDIA

Abstract—The present thesis summarizes the application of Finite Element Analysis technique for analysing stress distribution and fatigue life of Aluminium alloy wheels subject to radial loads. Alloy wheels intended for use on passenger cars stipulate two types of fatigue tests, the Dynamic cornering fatigue test and the Dynamic radial fatigue test. As wheels undergo inconsistent, varying loads during their service life, fatigue behaviour is a key consideration in the design and performance evaluation. But, alloy wheels have more complex shapes than regular steel wheels, so it is difficult to assess fatigue life by analytical methods. Hence, Finite Element Analysis has been used to evaluate the performance of wheels over their life. The deflection for Alloy wheel Al 2024-T351 of this project is found to be around 0.164 mm which is much less than that of Aluminium A356.2 alloy wheel which is 0.2833mm.This shows that Al 2024-T351 is stiffer than Aluminium A356.2 alloy wheel. Static analysis results showed that the maximum shear stress and von- Mises stresses of A356.2 alloy wheel are 78.6% and 50% higher than the Al 2024-T351 alloy wheel.

Keywords—Alloy wheel, Fatigue life, Fatigue tests

I. INTRODUCTION

Wheel is an important structural member of the vehicular suspension system that supports the static and dynamic loads encountered during vehicle operation. Since the rims, on which cars move, are the most vital elements in a vehicle, they must be designed carefully. Safety and economy are particularly of major concerns when designing a mechanical structure so that the people could use them safely and economically. Style, weight, manufacturability and performance are the four major technical issues related to the design of a new wheel and/or its optimization. The wheels are made of either steel or cast/forge Aluminum alloys. Aluminum is the metal with features of excellent lightness, corrosion resistance, etc. In particular, the rims, which are made of Aluminum casting alloys, are more preferable because of their weight and cost. In the real service conditions, the determination of mechanical behavior of the wheel is important, but the testing and inspection of the wheels during their development process is time consuming and costly.

II. LITERATURE SURVEY

Fatigue analysis as we know it today has come a long way, 178 years ago, in 1837, Wilhelm Albert published the first article on fatigue, establishing a correlation between applied loads and durability. Two years later, in 1839, Jean-Victor Poncelet, designer of cast iron axles for mill wheels, officially used the term "fatigue" for the first time in a book on mechanics.In19th century, it was considered to be mysterious that fatigue fracture did not show a visible plastic deformation. Systematic fatigue fractures tests were done in laboratories, notable by August Wohler. Fatigue was considered to be an engineering problem. Fatigue is also the initiation and growth of a crack, or growth from a pre-existing defect, which progresses until a critical size is reached. In narrow sense, the term fatigue of materials and structural components means damage and damage due to cyclic, repeatedly applied stresses.

III FATIGUE ANALYSIS

It has been observed that material fail under fluctuating stresses. It is a stress magnitude which is lower than the ultimate tensile strength of the material the decreased resistance of the materials to fluctuating stresses is called FATIGUE. There is a basic difference between failure due to static load and that due to fatigue. The failure due to static load is illustrated by the simple tension test. And there is sufficient time for elongation of fibres. In this case the load is gradually applied. The fatigue failure begins with a crack at some point in the material. The crack is more likely to occur in the regions of discontinuity, such as oil holes, key ways, screw threads and regions in machining operations, such as scratches on the surface, stamp mark, inspection marks, internal crack due to defects in materials like holes etc. These regions are subjected to stress concentration due to the crack. The crack spreads due to fluctuating stresses, until the cross section of the component is so reduced that the remaining portion is subjected sudden fracture.

A. FATIGUE LIMIT (ENDURANCE LIMIT)

The problem with Aluminium is it doesn't have a typical 'fatigue limit'. The more stress cycles that are imposed on Aluminium, the lower the stress cycles need to be to eventually result in failure. This is different than steel which has some distinct endurance limit. If a plot is drawn between peak alternating bending stress on y- axis against a log scale of life cycle on x- axis a knee in the curve at around 10^7 cycles is appeared as shown in Fig.1, so by 10^8cycles, the graph is almost flat. For Aluminium it isn't flat though, it continues to decline, meaning that as it continue to impose more cycles on test specimen, the peak alternating bending stress needed to result in failure continues to drop.

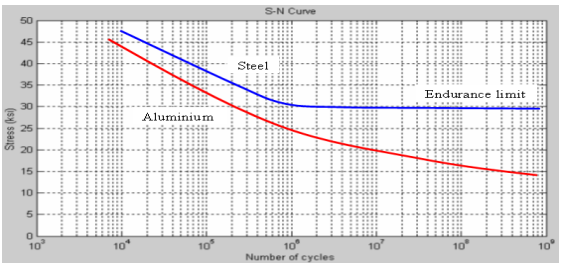

Fig.1 FATIGUE LIMIT

 ISBN: 978-93-91420-02-4

B. FATIGUE FAILURE

Failure is one of most important aspects of material behaviour because it is directly influence the selection of material for certain application, the method of manufacturing and service life of component. Fatigue, or metal fatigue, is the failure of a component as a result of cyclic stress. The failure occurs in three phases: crack initiation, crack propagation, and catastrophic overload failure. The duration of each of these three phases depends on many factors including fundamental raw material characteristics, magnitude and orientation of applied stresses, processing history, etc. Fatigue failures often result from applied stress levels significantly below those necessary to cause static failure. Fatigue failures are typically characterized as either low-cycle (<1,000 cycles) or high-cycle (>1,000 cycles). The threshold value dividing low- and high-cycle fatigue is somewhat arbitrary, but is generally based on the raw material's behaviour at the micro structural level in response to the applied stresses. Low cycle failures typically involve significant plastic deformation.

Fig.2 FATIGUE FAILURE ON A WHEEL RIM

Fatigue failure is also due to crack formation and propagation. A fatigue crack will typically initiate at a discontinuity in the material where the cyclic stress is a maximum. Fatigue fracture typically occurs in material of basically brittle nature. External or internal cracks develop at pre-existing flaws or fault of defects in the material; these cracks then propagate and eventually they lead to total failure of part. The fracture surface in fatigue is generally characterized by the term "beach marks". Fatigue failure on a wheel rim is shown in Fig.2.

IV .MODALING OF ALLOY WHEEL USING CATIA

FEATURES OF CATIA

- Easy accessible software
- Predefined shapes
- Powerful in surfacing
- User pattern facilities
- Supports CSG and feature based
- Retrieving data is very easy

This is powerful program used to create complex designs with a great precision. The design intent of any 3-D modal of any assembly defined by its specification CATIA can be used to capture the design. Intent of any complex modal by incorporating intelligence to the design. Tomake the designing process simple and easy.The 3-D modal of the wheel was created in CATIA and the file was exported in the IGES (International Graphics Exchange Specification) format into ANSYS.

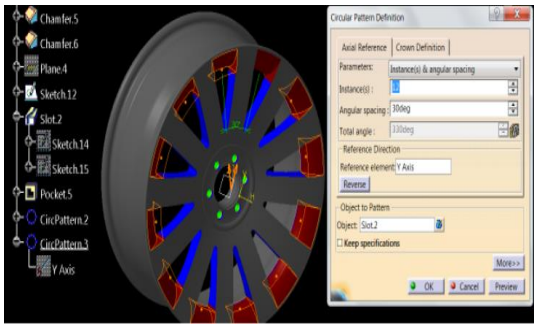

Fig.3 A 3-D model wheel created in CATIA

V. FATIGUE ANALYSIS USING FEA PACKAGE

The Finite Element Analysis is a mathematical method for solving ordinary and partial differential equations. Because it is a numerical method, it has the ability to solve complex problems that can be represented in differential equation form as these types of equations occur naturally. In virtually all fields of the physical sciences, the applications of the Finite Element Method are limitless as regards the solution of practical.Now a days, even the most simple products rely on the Finite Element Method for design evaluation. This is because contemporary design usually cannot be solved as accurately & cheaply as FEM, using any other method that is currently available. Physical testing was the norm in years gone by, but now it is simply too expensive and time consuming.

The finite element method is a very important tool for those involved in engineering design; it is now used routinely to solve problems in the following areas:

- Structural Strength design
- Structural interaction with fluid flows
- Analysis of shock (underwater & in materials)
- Acoustics
- Thermal analysis
- Vibrations
- Crash simulations
- Fluid flows
- Electrical analyses
- Mass diffusion

VI.RESULTS

Static and Fatigue results are shown in Table1 and Table 2

TABLE1

STATIC STRUCTURAL RESULTS

Definition							
Type	Von – Mises stress	Shear stress	Total deformation		Directional deformation		
Results							
Alloys							
	A 356.2	Al 2024	A 356.2	Al 2024	A356.2	Al 2024	
Minimum	3.8842 e-002MPa	3.8842 e-002MPa	-48.241MPa	-48.241MPa	0 mm	0 mm	-0.20193mm
Maximum	163.97MPa	81.985MPa	48.195MPa	24.097MPa	0.283 mm	0.164mm	0.20205mm

 ISBN: 978-93-91420-02-4

TABLE 2
FATIGUE RESULTS

Definition					
Type	Life		Safety factor	Equivalent alternating stress	
Design life	1.e+009 cycles				
Results					
Alloys	A 356.2	Al 2024		A 356.2	Al 2024
Minimum	1.653e+005cycles	1.653e+005cycles	0.60985	3.88e-002MPa	3.88e-002MPa
Maximum	1.766e+006cycles	1.767e+006cycles	15	163.97 MPa	128.88 MPa

B. RESULTS WITH IMAGES

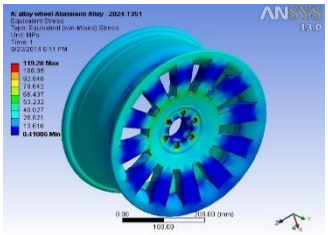

Fig. 4 Equivalent Stress on the Wheel

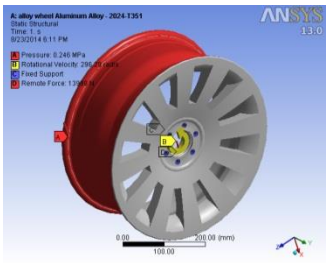

Fig.5 Pressure acting on the Wheel

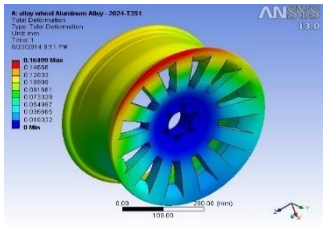

Fig. 6 Total Deformation of the Wheel

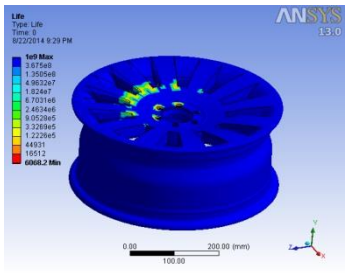

Fig7 Life of the Wheel

VII.CONCLUSIONS

- The wheel is analyzed for the calculated loading condition and the relevant stress is obtained
- In the case of pressure loading along with radial load, Von Mises stress obtained shows the maximum stress the wheel experiences under the pressure load and on the portion of the rim there is a gradual transition from compression to tension.
- For predicting the fatigue life of Aluminum alloy wheel the S – N curve approach is used.
- The proposed safety factors will be useful for manufacturers/ designers for reliable fatigue life prediction of similar structural components subjected to radial fatigue load.
- . From the analysis, finally, it can be concluded that as the speed increases Stress, displacement increases and life decreases.

VIII.REFERENCES

1. IS 5057 INDIAN STANDARD method of rotating bending fatigue testing of metals1985
2. Fatigue life analysis of Aluminium wheels by simulation of Rotary Fatigue test by LiangmoWang – Yufa Chen – ChenzhiWang – Qingzheng Wang school of mechanical Engineering Nanjing University of Science And Technology, China. Strijniski – vestnik – Journal of Mechanical Engineering 57(2011) 31 – 39
3. Evaluation of fatigue life of Aluminium alloy wheels under radial load Engineering Failure Analysis 14(2007) 791 – 800
4. Prediction of Fatigue Failures of Aluminium Disc Wheels Using the Failure Probability Counter Based on historical test data by Yeh-Liang Hsu, Ming-Sho Hsu, Shu-Gen Wang, Tzu – ChiLiu in Journal of the Chinese Institute of Industrial Engineers, Vol. 21, No. 6, Pp 551- 558
5. J.Stearns et al performed experimental work on wheels on radial Fatigue test in April 2000
6. Mehrdad Zoroufi Ali Fatemi, an expert work to produce S – N curve and also durability Test for the components to compare Fatigue strength of three different metals
7. International Journal of Mechanical and Industrial Engineering (IJMIE), ISSN No. 2231–6477, Vol-2, Issue-1, 2012
8. Timoshenko, S. (1954), Stress concentration in the history of strength of Materials. The William M. Murray Lecture. Proc. SESA, Vol.12, pp.1-12.

 ISBN: 978-93-91420-02-4

Design of Automated Braking System Based on Vehicle Over Speed Using PLC Ladder Method

Sivasankara Raju R, Sreeramulu, Srihari P and C J Rao
Department of Mechanical Engineering, Aditya Institute of Technology and Management, Tekkali - 532201

***Abstract*— This work emphasize on design of a speed controller with an automatic braking system in the vehicle. The speed control in the automatic braking system experiences proved the electronic circuits such as sensor, relay, control system, programmable logic controller (PLC), signal transmitter, receiver, and Ladder Circuits. The software WPL Soft is used to model the circuit. The perception in performing the ride control and automatic braking process is vital rule of a circumstance being instruments. It helps the ultrasonic sensor for disclosure by the interference and infra-red (IR) sensor for automatic braking system purpose. The conception of Automatic Over speed Control System (AOCS) is based on stresses developing in clutch and brake. The speed of a vehicle increased afar a pre-interpreted strategic top speed; the Microcontroller actuates the clutch as well brake and bring speed of vehicle down to a reliable ride.**

Keywords: Speed Sensor, PLC, IR Sensor, WPL Software, Microcontroller.

VII. INTRODUCTION

Automation is largely converting the role of people in plenty of systems, and riding isn't always any exception. A developing amount of automobiles are being prepared with pace manipulate structure. This device use ultrasonic sensor to discover the impediment or affecting automobile beforehand and warn toward motive force on crash risk. When subsequent a few other car, the velocity manage device (SCS) will mechanically offers sign about distance among vehicle with obstruction during LED show to the driver to lessen the pace of vehicle[1]–[3].

Nowadays manufacturers of Cars similarly to Motor cycles moreover anticipate such technology and machine's which assures safety at immoderate pace. The use of right braking gadget and via the use of managed tempo discount strategies is the important thing to solve such troubles. The utilization of Anti-lock braking mechanism in motors is the present day style to boom protection of the car. There are also different answers like Automatic Braking Systems which can be beneficial as well as useful. Automatic braking technology coalesce sensors and brake controls to assist save human immoderate momentum impact. Some computerized braking structures can save collisions on the whole, but maximum of them are intended to actually reduce the cost of a medium earlier than it hits some component[4]–[7].

Dhanya et al. [8] proposed an era of improve automatic braking system with sensor fusion idea. In this they represent operation of the residences of every capacitive and ultrasonic sensor for identifying the difficulty for measuring the distance many of the car and the interference. This distance range is applied to deal with computerized braking system for security program. In this apparatus they adopt the 32-bit micro-controller with ARM processor (LPC2138) because the thoughts of this gadget for controlling performance and complete the register through using c-language.

Bhumkar et al. [9] implements a scheme of about accidents avoidance and disclosure on streets. This device is ready growth generation in vehicles for performing it more clever and interactive for avoiding accidents on highways. ARM7 is the usage of making this design more active, steady and powerful. In this process, they heard described real-time online protection prototypes that rule the car pace underneath motive pressure exhaust. The principle of this machine is to avoid injuries.

Sairam et al. [10] provides a technique which can adorn the security of an automobile. This machine offer solution can reinforce the operator via caution the purpose force impediment and gathering adjacent to a vehicle that could produce collision to this. Moreover implementing and automobile are retarding in device, which supports in heading off calamities. In this device ultrasonic sensor, motor purpose of pressure and LCD are adopted.

Muqaddas Bin Tahir [11] have come up with an ingenious method distance measuring (Hurdle Detection) for comfy surroundings in car via ultrasonic rays. In this strategy, 8 ultrasonic sensors are employed to sense the unique find of a thing. By enforcing a rise in safety strategy in automobile, sensor may be able of achievement typically until the sensor detects workable possibility. In this the sensor does not allow output or sign till the car comes interior 75 feet of an item, at which timer sends records of hurdle to driver. The sensor nicely shows an object; it's miles as much as person or purpose pressure to cope with the hurdle.

The primary objective of the ultrasonic braking technique is that motors should brake while the sensors sense the obstruction. This is a technology for motors to receive an impending head collision with some new automobile or a hindrance, and to impede the vehicle for this infer, that's covered by controlling the braking circuit. This instrument includes ultrasonic sensors viz. Ultrasonic wave emitter and rapid wave receiver. The ultrasonic wave emitter provided in a frontal segment of a certain braking automobile, designing and emitting ultrasonic waves in a fixed distance in facade of the vehicle. The meditated wave (detection pulse) meant to obtain the distance among automobile and the hurdle. The 8051 micro-controller is exploited to wield the DC motor based on detection pulse statistics, and the servomotor controls the damp of the automobile, but the vehicle can prevent by sensing the boundaries to keep away from a twist of fate.

The objective of this work is:

- To develop a safety car braking system using ultrasonic sensor
- To design a vehicle with less human attention to

 ISBN: 978-93-91420-02-4

the driving

- To develop a model showing working of ultrasonic sensor based braking system.
- To propose a low cost automation system which can be implemented easily in today's cars to provide safety and accuracy while driving and parking.

VIII. DESIGN AND IMPLEMENTATION

A. PLC Programming

Programmable Logic Controllers (PLC's) are straightforward to compute. They employ a relay ladder language that's remarkably akin to hypnotic relay circuitry. Engineers, consultants, and electricians can determine to compute the PLC without considerable study or practice. There are many influences in adopting Programmable Logic Controllers versus a relay or solid-state electronics. In a PLC, transformations can be achieved, and in most arguments, without hardware alterations to the controller. PLC's are recyclable and signal lights on the PLC at principal diagnostic points help regulate. Its stable, performed for the modern situation and easy to maintain. Along with its cost savings, the PLC is flexible and apt to produce various functions.

B. PLC Wiring

Generally, in electrical wiring concept we have two major types. They are Sourcing and Sinking: When choosing the type of input or output module for your PLC system, it is very significant to have a firm sympathetic of sinking and sourcing concepts. Uses of these terms occur often in conversation of input or output circuits.

Sinking & Source is used exclusively with Digital DC circuits and shown in Fig. 1 and Fig. 2 respectively. If, the common pin is + polarity called as sourcing circuit and – polarity called a sinking circuit. PLC is generally having 2 different output types such as Relay type output and Transistor type output. In transistor type having two types such as NPN (Sinking) and PNP (Sourcing)

C. WPL SOFTWARE

WPLSoft is program-editing software carried out for the Delta DVP-PLC series used under WINDOWS, illustrated in Fig. 3. Except for general program design and separate general operates (e.g. cut, paste, copy, multi-windows, etc.) of WINDOWS, WPLSoft, in addition, has implemented numerous Chinese/English commentary-editing and diverse special functions (e.g. survey and publishing the recorded file, the system, the data readout, the file saving, and monitor and set up diagrams of varied reaches, etc.).

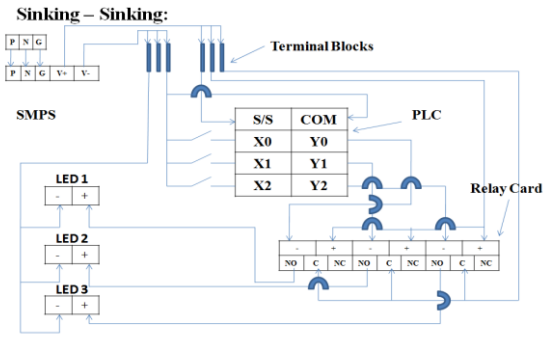

Fig. 1. Sinking Circuit diagram

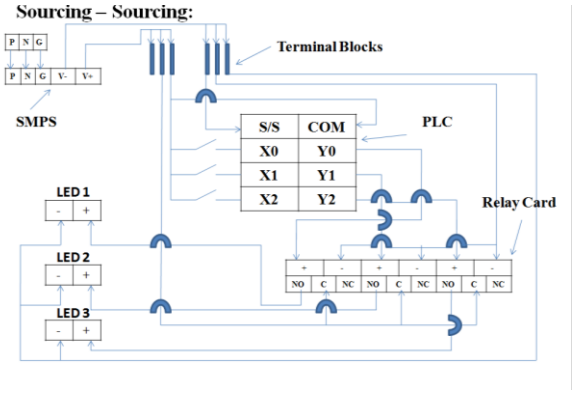

Fig. 2. Sourcing Circuit diagram

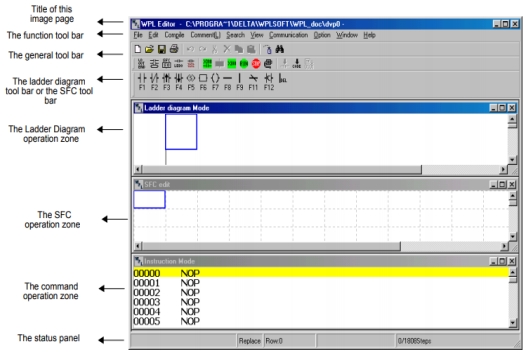

Fig. 3. WPL Editor Window

IX. STEPS IN CIRCUIT DESIGNING

A. CIRCUIT DIAGRAM AND EXPLANATION

STEP-1: In this first step we need to start car as per logic, so the car should start when all doors are closed and the key should also kept starting the car, vide in Fig. 4. So M50, M51, M52, M53 are the doors of the car and M1 is car as we designed in the first line, M is known as the memory allocation which act as dummy switch and M1 is load, when all switches are in ON position then the load(car) is applied. In the second line M1(load) act as switch it act like key or acceleration in if we rotate the key then car be stop, so we used counter here.

Fig. 4. Start and closing doors of car logic circuit

 ISBN: 978-93-91420-02-4

STEP-2: As we observed in step 1 the car starts in step 1, in step 2 counters will act as switch and M1 act as acceleration then the light will be on and in second line M2 act as load (vide in Fig. 5) if we stop key then it will reset the system so we latched RST to the 3rd line

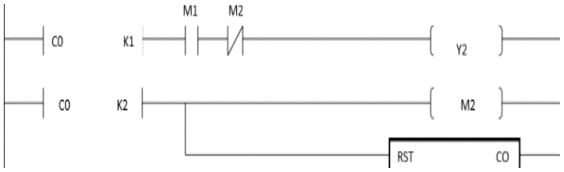

Fig. 5. Acceleration of PLC circuit

STEP-3: In this step the car speed should be increment when we press acceleration so X2 and Y2 will act as sensor and Y0 as an engine of the car, shown in Fig. 6.

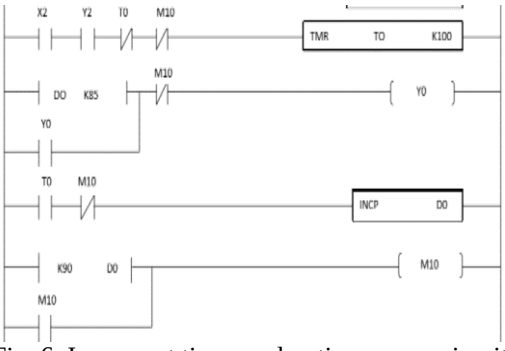

Fig. 6. Increment ting acceleration sensor circuit

STEP-4: In this step (Fig. 7) according to the logic when speed of the car reaches to speed 100kmph then the decrement of speed should be done automatically for every 50sec it should reduces upto 10kmph speed. So decrement had connected to this line and this should done according to timer so we added timer to the motor means M10.

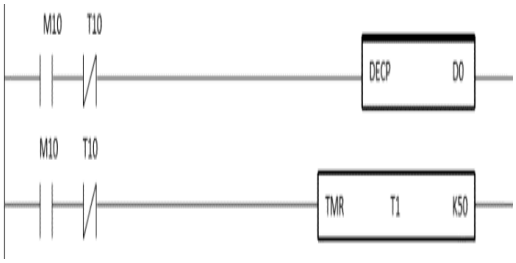

Fig. 7. Decremented speed and timer sensor

STEP-5: In this step (Fig. 8.) when any obstacle come infront or behind the car then buzzer should be activated sudden and if car touch any object then air bags in the car should come out. Then automatically brake should activated and the must stop. In this M4 and M3 will works as sensor and Y3 will act as air bags and Y1 as buzzer.

The model block diagram of PLC circuit and fabricated design board are shown in Fig. 9 and Fig.10, respectively.

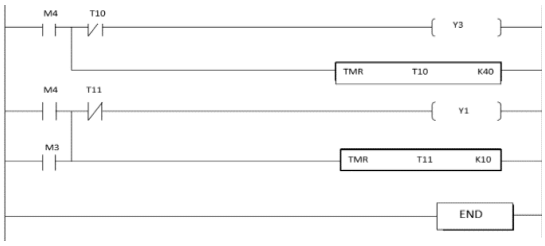

Fig. 8. Automatically brake and stop circuit

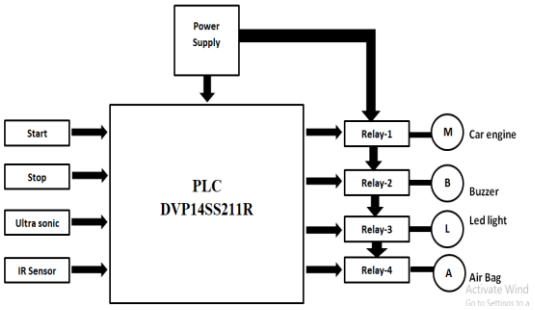

Fig. 9. Block Diagram of PLC Circuit

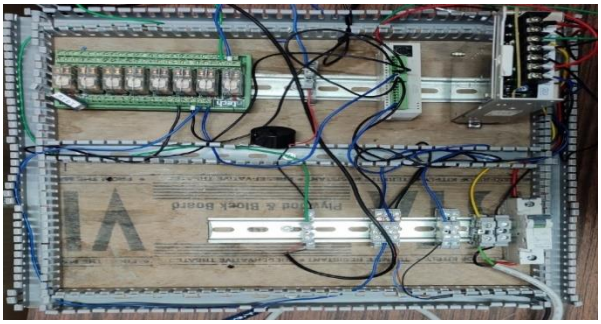

Fig. 10. PCB design of Activation of automatic braking system

B. Ladder Diagram Monitor

1. If users are to monitor the PLC status under the PC window, they firstly will present the ladder diagram window on PC (as shown follows Fig. 11.), then click on “Ladder diagram monitor start” under the “Communication” function on the function panel, or click on the icon

2. When the monitoring has started (Fig. 12.), the green portion displayed in the window is an indication that the contact of the device is at the continuity status or that the output coil is at the exciting-magnet status, or even, that the application commands are under process. On the contrary, if the green color does not display on the location of the contact, the output coil, and the application command, it means that this portion is currently not in motion. Moreover, the current value of the register will be shown on the upper part of the register, as shown Fig. 12.

Finally run the program after connected to PLC carefully. These are the various steps used in the working of this project AUTOMATED BRAKING SYSTEM DEPENDING ON OVER SPEED After uploading program into PLC we can disconnect the cable it will run by itself. Before upload we need check in the simulation

Procedure	The Ladder Symbols	Location of the Cursor	Input through the clicking on the Function Keys		Input through the Keyboard
1	⊣ ⊢	Row: 0, Line: 1	F1 *Footnote 1	Device name: X Device number: 1	LD X1
2	—( )	Row: 0, Line: 2	F7	Device name: Y Device number: 1	OUT Y1
3	⊣ ⊢	Row: 1, Line: 1	F1	Device name: X Device number: 2	LD X2
4	|	Row: 1, Line: 2	F9		F9
5	—( )	Row: 1, Line: 2	F7	Device name: Y Device number: 2	OUT Y2
6	⊣ ⊢	Row: 2, Line: 1	F1	Device name: X Device number: 1	LD X1
7	⊣ ⊢	Row: 3, Line: 1	F1	Device name: M Device number: 0	LD M0
8	—▭	Row: 3, Line: 2	F6 *Footnote 2	Application command MOV Operand 1: D Device value: 1 Operand 2: D Device value: 2	MOV D1 D2
9		Row: 4, Line: 0		Double click the mouse to input P0	P0
10	⊣↑⊢	Row: 4, Line: 1	F3	Device name: M Device number: 1	LDP M1
11	|	Row: 4, Line: 2	F9		F9
12	—▭	Row: 4, Line: 2	F6	Counting command CNT Operand 1: C Device value: 0 Operand 2: K Device value: 100	CNT C0 K100
13	⊣↓⊢	Row: 5, Line: 1	F4	Device name: M Device number: 1	LDF M1
14	—▭	Row: 6, Line: 1	F6	Application command END	END

Fig. 11. Operation Procedure of the Ladder Diagram

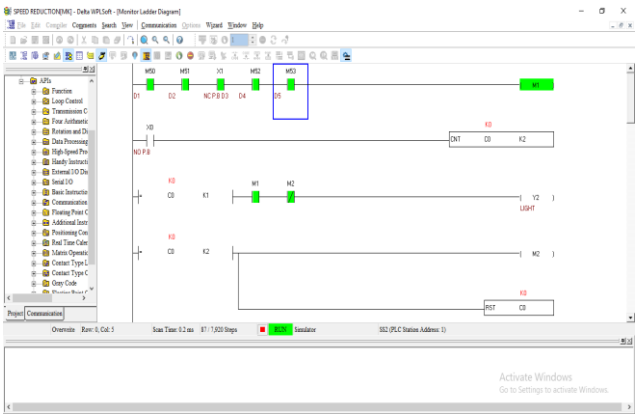

Fig. 12. Monitoring PLC window display

X. CONCLUSIONS

The designing of the "Automated Braking System Depending on Vehicle Over Speed" Circuit by logical from the fact solve by using the WPL soft software and made easy by using PLC Ladder method to Solve, by using PLC we can detect the object/obstacle by using ultrasonic sensor and also we can control the speed of engine by using PLC and we can make alert to the driver by using IR sensor and we observed the working of PLC and also the simulation of the ladder circuit by using WPL soft software we can also make implementation in car by using PLC in our car . This Automated Braking System Depending On Vehicle over Speed is implemented in tesla cars not only speed reduction but also we can control the car by using PLC and also this make driver safe from accidents also and this project will save many life from accidents.

The introduced braking system in this work is very cheap and is affordable for anybody. But the actual importance for the safety increases the value of this system. Due to this the various changes, modifications, new ideas are introduced. These changes are observed and analyzed the importance of this system. So these automobile industries are about to launching the various intelligent systems to increase safety of customers.

Acknowledgements. The Authors are grate thankful to the management of Aditya Institute of Technology and Management, for establishing ARC laboratory collaborating with APSSDC – European centre for Mechatronics APS GMBH, Aachen.

REFERENCES

[1] A. P. Correia, C. H. Llanos, R. W. de Carvalho, S. A. Alfaro, C. Koike, and E. D. Moreno, "A control design approach for controlling an autonomous vehicle with FPGAs," *J. Comput.*, vol. 5, no. 3, pp. 360–371, 2010.

[2] D. Webster, "A Pulsed Ultrasonic Distance Measurement System based upon Phase Digitizing," *IEEE Trans. Instrum. Meas.*, vol. 43, no. 4, pp. 578–582, 1994.

[3] H. Ahmad Al_Issa, "Sensors Application Using PIC16F877A Microcontroller," *Am. J. Remote Sens.*, vol. 4, no. 3, p. 13, Jul. 2016.

[4] C. C. Chang, C. Y. Chang, and Y. T. Cheng, "Distance measurement technology development at remotely teleoperated robotic manipulator system for underwater constructions," in *International Symposium on Underwater Technology, UT'04 - Proceedings*, 2004, pp. 333–338.

[5] D. H. K. Hoomod and S. M. M. Al-Chalabi, "Achieving Real-Time Tracking Mobile Wireless Sensors Using SE-KFA," in *Journal of Physics: Conference Series*, 2018, vol. 1003, no. 1, p. 012039.

[6] N. Amin and M. Borschbach, "Quality of obstacle distance measurement using Ultrasonic sensor and precision of two Computer Vision-based obstacle detection approaches," in *International Conference on Smart Sensors and Systems, IC-SSS 2015*, 2017, pp. 1–6.

[7] G. L. Gissinger, C. Menard, and A. Constans, "A mechatronic conception of a new intelligent braking system," *Control Eng. Pract.*, vol. 11, pp. 163–170, 2003.

[8] D. Thakur and A. P. Thakare, "A Review on Implementation of FPGA for Automatic Reverse Braking System," *Int. J. Sci. Res. ISSN (Online Index Copernicus Value Impact Factor*, vol. 14, no. 1, pp. 2319–7064, 2013.

[9] S. P. Bhumkar, V. V Deotare, and R. V Babar, "Accident Avoidance and Detection on Highways," *Int. J. Eng. Trends Technol.*, vol. 3, no. 2, pp. 247–252, 2012.

[10] G. V Sairam, B. Suresh, C. H. S. Hemanth, and K. Krishna, "Intelligent Mechatronic Braking System," *Int. J. Emerg. Technol. Adv. Eng.*, vol. 3, no. 4, pp. 3–8, 2013.

[11] M. Bin Tahir and M. Abdullah, "Distance Measuring (Hurdle detection System) for Safe Environment in Vehicles through Ultrasonic Rays," *Glob. J. Res. Eng. Automot. Eng.*, vol. 12, no. 1, pp. 1–5, 2012.

 ISBN: 978-93-91420-02-4

The Analysis on Concentric Pipe Heat Exchanger

Shaik Chand Mabhu Subhani and Pilli Sravani
Department of Mechanical Engineering, Narasaraopeta engineering college (Autonomous),Narasaraopet, Guntur, A.P.

***Abstract*—A Heat Exchanger is a device which is used to transfer heat from one fluid to another, whether the fluids are separated by a solid wall so that they never mix, or the fluids are directly in contact. Every year Heat exchanger technology is growing to develop efficient, compact and economical heat exchangers, all over the world. Updating the community for this development needs an interaction. These days concentric tube heat exchangers are used with forced convection for lowering the working fluid's temperature by raising the cooling medium's temperature.**

The purpose of this project is to use ANSYS FLUENT software and practical calculations to analyze the temperature drops as a function of both inlet velocity and inlet temperature and how each varies with the other. Each heat exchanger model was designed and simulated for both parallel flow and counter flow heat exchanger models. The results were compared between parallel and counter flow heat exchangers. CFD analysis was utilized to find the outlet temperatures of parallel and counter flow heat exchangers for the inlet velocity and inlet temperature of the fluid medium used. "Computational Fluid Dynamics (CFD) is a science of predicting fluid flow, heat transfer, mass transfer, and related phenomena by solving the mathematical equations which govern these processes using a numerical processes". These outlet temperature values obtained were used to determine the overall heat transfer coefficient. Theoretical calculations are done by the values obtained through the experiment conducted on the heat exchanger setup for both parallel and counter flow

Keywords— Heat Exchangers, Parallel flow, Counter flow, temperature , CFD Analysis , ansys

I. INTRODUCTION

Today's demand of higher energy consumption and reduced availability of fossil fuel resources increase the impact of thermal performance of heat exchanger day by day. Heat exchangers are very effective for the transfer of heat from one medium to another without even intermixing one fluid with another. One of the most promising devices for heat transfer is the counter flow heat exchanger mostly adapted by the chemical plants, petrochemical plants, oil refineries etc. Reducing the temperature of hot outlet fluid without affecting the cost is a big task for various industries that could be only possible by the proper selection of input. Typically, in a heat exchanger two segregated fluids at different temperature with a solid boundary, exchange thermal energy from one fluid to another via surface without even intermixing. There are numerous configurations of classifying heat exchanger. In context with the flow configuration, there exists three primary types for heat transfer: parallel flow, counter flow and. cross flow. According to Fourier for the conduction states the more the area of heat exchanger, the more will be the heat transfer rate.

By second law of thermodynamics only transfer of sensible heat occurs in the heat exchanger. One of the greatest advantages of the counter flow heat exchanger is higher uniform temperature difference as well as that the mass flow rate and time for the interaction of one fluid with other increases, the heat transfer also goes up as compared to parallel flow heat exchanger. Maximization of surface area and minimization of flow resistance lead to better effectiveness of heat exchanger, which is the main focus for designing. On the contrary, the increase in area increases the space for the installation and correspondingly manufacturing cost will get increased. On the other hand, reduction in flow resistance can be achieved by improving the surface finishing of the heat exchanger. Many experiments have been carried out on the counter flow heat exchanger citing the flow in either laminar or turbulent manner, for achieving its better configuration. However, very limited CFD simulation has been done on the counter flow heat exchanger at different flow configuration to verify the thermo-hydraulic performance or to check the heat transfer and velocity distribution inside the flow domain.

Direction of Flow: According to the relative direction of two fluid streams the heat exchangers are classified into the following three categories:

1. Parallel flow
2. Counter flow
3. Cross – flow

A. Parallel flow heat exchangers:

In parallel flow heat exchangers the fluids both hot and cold travel in same direction. The flow arrangement for hot and cold fluids from inlet to outlet is shown in fig 1.1. In parallel flow heat exchangers the temperature difference from hot to clod fluid decreases. This type of heat exchangers requires large space and hence it is rarely used in practical applications. Eg: Oil coolers, oil heaters, water heaters etc, are examples of parallel flow heat exchanger.

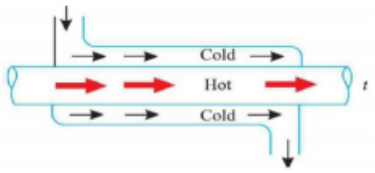

Fig 1.1. Parallel flow heat exchanger

B. Counter flow heat exchangers

In a counter flow heat exchanger, the two hot and cold fluids enter at opposite ends. The flow arrangement and temperature distribution for such a heat exchanger are shown schematically in fig. 1.2. the temperature difference between the two fluids remains more or less nearly constant. This type of heat exchanger, due to counter flow, gives maximum rate of heat transfer f or a given surface area. Hence such a heat exchangers are most favored for heating and cooling of fluids.

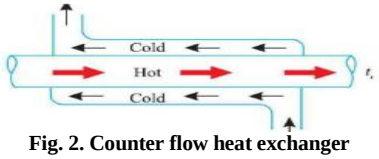

Fig. 2. Counter flow heat exchanger

C. Cross - flow heat exchanger

When two fluids crosses one another in space at right angles such type of heat exchanger is known as cross flow heat exchanger. In cross flow heat exchanger there is no mixing of fluid streams and hot fluid flows in spate tubes and cold fluid is mixes perfectly as it flows through the

 ISBN: 978-93-91420-02-4

exchanger. The temperature of this mixed fluid will be uniform across any section and will vary only in the direction of flow. The cooling unit of refrigeration system is an example of cross-flow heat exchanger.

II. LITERATURE SURVEY

Praveen Kumar Kanti et al, [1] investigated CFD analysis of shell and tube heat exchanger. Analysing shell and tube heat exchanger without baffle plates by changing their outer material. The calculations and simulations are done for counter flow of the heat exchanger.

D.Bhanuchandrarao et al, [2] investigated CFD analysis and performance of parallel and counter flow in concentric tube heat exchangers. The results were compared between each model and between parallel and counter flow with fouled piping. Turbulent flow was also analysed during the development of the heat exchangers to determine its effect on heat transfer. While as expected the fouled heat exchanger had a lower performance and therefore cooled the working fluid less, the performance of the counter heat exchanger unexpectedly of the parallel heat exchanger.

Oon et al. [3] have done a CFD simulation in fluent to avoid the backflow in an annular passage from the sudden expansion of pipe. The Nusselt number and the Reynolds numbers have been considered for the investigation and to show the uniform heat transfer from the sudden expansion. Then the heat flux approach was used in the fluent set up to show the heat transfer in the tubular pipe.

Nagarsheth et al. [4] used a systematic approach on a cross flow water tube in tube heat exchanger with a string of basic instrument like PID controller to regulate the temperature. PID controller is a kind of sensor which works in a closed loop feedback mechanism in industrial control system

Hwang et al [5] measured pressure drop and heat transfer coefficient in fully developed laminar pipe flow using constant heat flux conditions. Based on the experimental results they showed that the experimental friction factor was in good agreement with the theoretical predictions using the Darcy equation.

Bianco et al [6] observed only a maximum of 11% difference between single and two phase results for the laminar regime.

Akbari et al [7] for the first time compared three different two phase models and the single phase model in the laminar regime. Single and two phase models were found to be predicting identical hydrodynamic fields but very different thermal ones.

III. PROBLEM STATEMENT

The double pipe heat exchanger is used in industry such as condenser for Chemical process and cooling fluid process. This double pipe heat exchanger is designed in a large size for large application in industry. To make this small double pipe heat exchanger type become practicality, the best design for this small double pipe heat exchanger is choose. Heat transfer is considered as transfer of thermal energy from physical body to another. Heat transfer is the most important parameter to be measured as the performance and efficiency of the concentric tube heat exchanger. By using CFD simulation software, it can reduces the time and operation cost compared by Analytical calculations in order to measure the optimum parameter and the behaviour of this type of heat exchanger.

A. Objectives

The objective of the present study is to provide more complete understanding Flow misdistribution in tubular heat exchanger by studying area weighted and mass weighted temperature profiles for mal distribution without back flow and mal distribution with back flow. And comparison of average temperature profiles of flow mal distribution with the average temperature profiles of uniform mass flow distribution. This numerical investigation was carried out for the concentric tube arrangement with different diameter of tubes. A finite volume numerical scheme is used to predict the conjugate heat transfer and fluid flow characteristics with the aid of the computational fluid dynamics (CFD) commercial code, FLUENT. An effective model, the standard based k-ε turbulence model was applied in this investigation. the available relevant literature is quite limited With respect to the analytical and it is still difficult to predict the physics of the flow mal distribution within the circular tube banks. Therefore, temperature distributions within the bundle were studied numerically. The objective of this study is to develop a CFD simulation to predict heat Transfer in concentric tube heat exchanger by using different fluids.

B. Scopes of research

The scopes of this research are as follows:

i. Study on heat transfer for heat exchanger specific to double pipe heat exchanger types.
ii. Design the double pipe heat exchanger by using ANSYS WORKBENCH.
iii. Simulation in double pipe heat exchanger by using FLUENT software.
iv. Analysis the heat exchanger specific to flow rate of hot and cold fluid.
v. To simulate heat transfer in concentric tube heat exchanger by using CFD-Fluent software.
vi. To analyze the heat transfer in concentric tube heat exchanger by comparing the simulation result to the Analytical calculations. Validate simulation results to the Analytical calculations within 5% error.

IV. GEOMETRY AND MODELING

The layout diagram for practical analysis on parallel flow and counter flow heat exchanger is as shown below

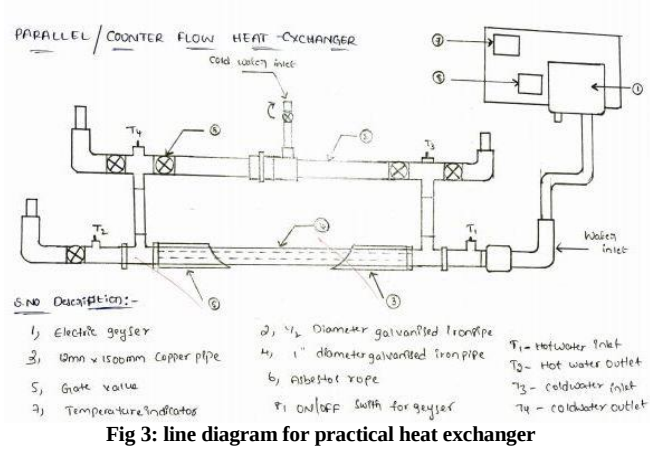

Fig 3: line diagram for practical heat exchanger

A. Modeling of heat exchanger by using ANSYS

The geometry made in ANSYS workbench. This geometry imported to Ansys fluent and repairs the geometry

 ISBN: 978-93-91420-02-4

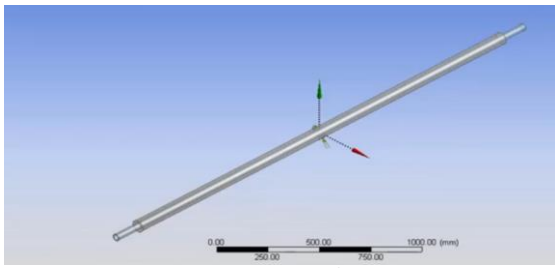

Fig 4: Geometric modeling of heat exchanger

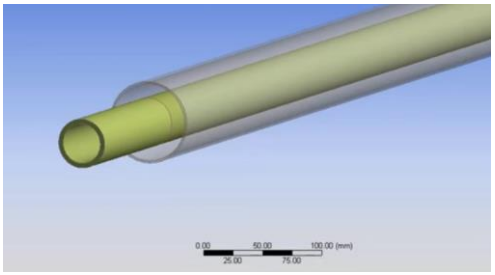

Fig 5: Geometric modeling of heat exchanger close view

B. Defining Material Properties

Water was used as the base fluid flowing through tubing or piping. Its material properties were derived from tables based on the temperature which was being calculated in the model. The material was defined in FLUENT using its material browser. For the different flow arrangement problem model certain properties were defined by the user prior to computing the model, these properties were: thermal conductivity, density, heat capacity at constant pressure, ratio of specific heats, and dynamic viscosity. For the modified Graetz problem with pipe wall conduction as well as for the heat exchanger models the material library properties in FLUENT were used.

TABLE I. FLUID PROPERTIES

Different fluids properties	Density (ρ) kg/m3	Thermal conductivity(K) W/mk	Specific heat CP j/kgK	Dynamic viscosity (μ) kg/m
Water	998.2	***0.6***	4182	0.001003
Transformer oil	826	0.134	2328	0.009

TABLE II. MATERIAL PROPERTIES

Different material properties	Density (ρ) kg/m3	Thermal conductivity(K) W/mk	Specific heat (C_P) j/kgK
Copper	8978	387.6	381
Galvanized iron	7850	520.1	470

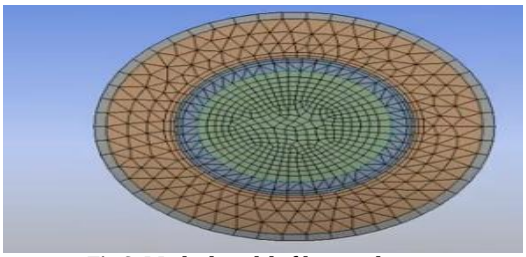

Fig 6: Meshed model of heat exchanger

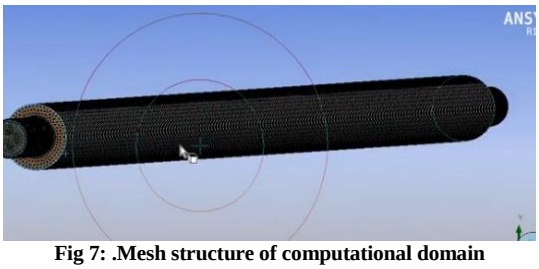

Fig 7: .Mesh structure of computational domain

C. Finite volume methods

The mass, momentum, and scalar transport equations are integrated over all the fluid elements in a computational domain using CFD. The finite volume method is a particular finite differencing numerical technique, and is the most common method for calculating flow in CFD codes. This section describes the basic procedures involved in finite volume calculations.

The finite volume method involves first creating a system of algebraic equations through the process of discretizing the governing equations for mass, momentum, and scalar transport. To account for flow fluctuations due to turbulence in this project, the RANS equations are discretized instead when the cases are run using the k-epsilon turbulence model. When the equations have been discretized using the appropriate differencing scheme for expressing the differential expressions in the integral equation (i.e. central, upwind, hybrid, or power-law, or other higher order differencing schemes), the resulting algebraic equations are solved at each node of each cell.

Numerical procedure and computational methodology:

The governing differential transport equations were converted to algebraic equations before being solved numerically. After the specification of the boundary condition, the solution control and the initialization of the solution have to be given before the iteration starts. The solution controls like the pressure velocity coupling and the discrimination of the different variables and the relaxation factors have to be specified.

The solutions sequential algorithm (called the segregated solver) used in the numerical computation requires less memory that the coupled solver. Since we are using the segregated solver for our problem, the default under relaxation factors are used and the SIMPLE scheme for the pressure velocity coupling is used and the second discrimination is used for the momentum and the standard scheme is used for the pressure.

V. RESULTS AND DISCUSSIONS

A. Experimental values Obtained for water From Practical Heat Exchanger

For parallel flow:
Hot water flow rate: 50CC
Cold water flow rate: 40cc
Inlet temperature Thi = 49^0 C
Outlet temperature Tho = 42^0C
Inlet temperature Tci = 25^0 C
Outlet temperature Tco = 30^0C
For counter flow:
Hot water flow rate: 50CC
Cold water flow rate: 40cc
Inlet temperature Thi = 49^0C
Outlet temperature Tho = 41^0 C
Inlet temperature Tci = 25^0 C
Outlet temperature Tco = 30.5^0 C

 ISBN: 978-93-91420-02-4

B. Experimentalvalues Obtained For Transformer Oil From Practical Heat Exchanger

For parallel flow:
Hot Transformer oil flow rate: 50CC
Cold water flow rate: 40cc
Inlet temperature Thi = 49^0 C
Outlet temperature Tho = 45^0C
Inlet temperature Tci = 25^0 C
Outlet temperature Tco = 28^0C
For counter flow:
Hot transformer oil flow rate: 50CC
Cold water flow rate: 40cc
Inlet temperature Thi = 49^0C
Outlet temperature Tho = 43^0 C
Inlet temperature Tci = 25^0 C
Outlet temperature Tco = 28.5^0C

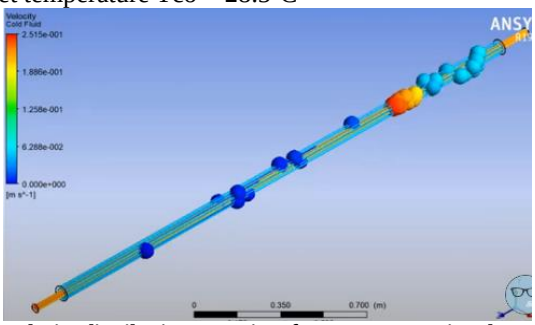

Fig 8: velocity distribution over pipes for water –water in tubes

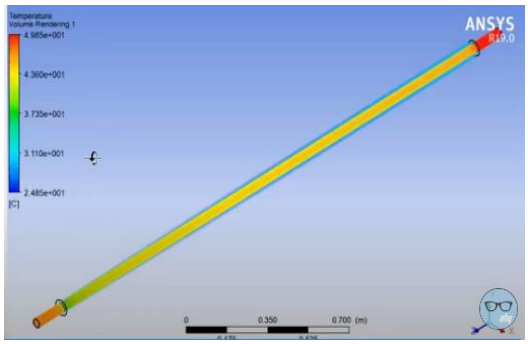

Fig 9: Temperature distribution for parallel flow heat exchanger

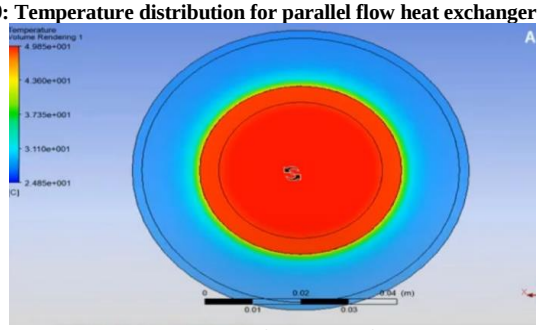

Fig 10: Temperature distribution for parallel flow heat exchanger

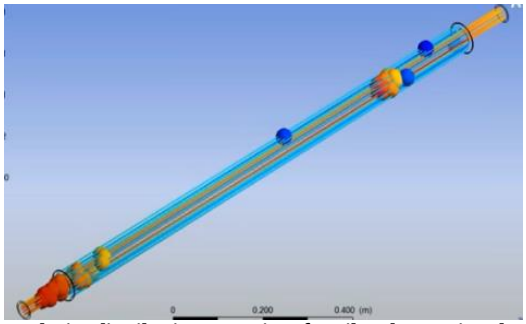

Fig 11: velocity distribution over pipes for oil and water in tubes

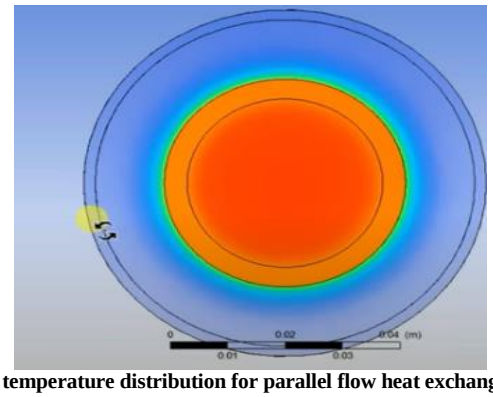

Fig 12: temperature distribution for parallel flow heat exchanger

C. Results for practical analysis on heat exchanger

TABLE III. CASE 1- PARALLEL FLOW HEAT EXCHANGER WATER - WATER

s.no	Water flow rate in CC	Inlet temperature in ^{0}C	Out let temperature in ^{0}C	Temperature difference in ^{0}C
Cold water	40	25	30	5
Hot water	50	49	43	6

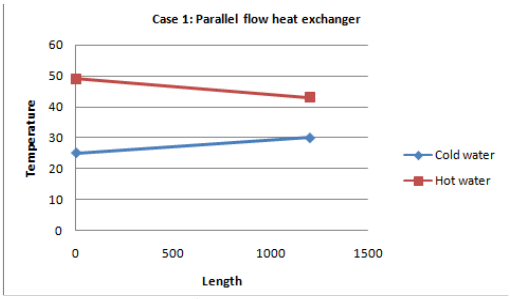

Graph 5.1: Case 1- Parallel flow heat exchanger water - water

TABLE IV. CASE 2 - COUNTER FLOW HEAT EXCHANGER WATER - WATER

s.no	Water flow rate in CC	Inlet temperature in ^{0}C	Out let temperature in ^{0}C	Temperature difference in ^{0}C
Cold water	40	25	30.5	5.5
Hot water	50	49	41	7

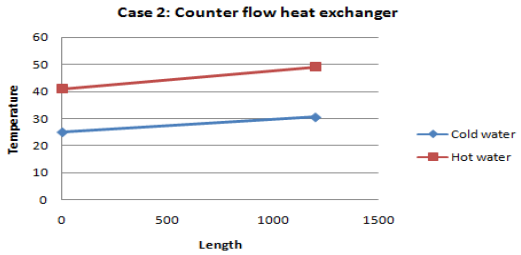

Graph 5.2: Case 2- Counter flow heat exchanger water - water

 ISBN: 978-93-91420-02-4

TABLE V. CASE 3- PARALLEL FLOW HEAT EXCHANGER TRANSFORMER OIL - WATER

s.no	Water flow rate in CC	Inlet temperature in ^{0}C	Out let temperature in ^{0}C	Temperature difference in ^{0}C
Cold water	40	25	28	3
Transformer oil	50	49	45	4

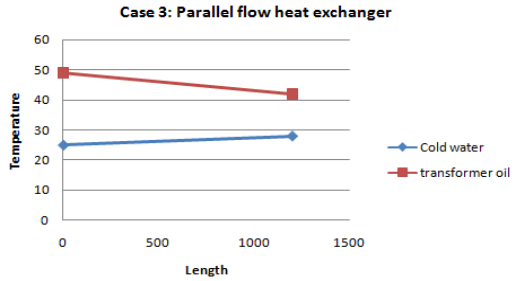

Graph 5.3: Case 3- Parallel flow heat exchanger Transformer oil - water

TABLE VI. CASE 4 - COUNTER FLOW HEAT EXCHANGER TRANSFORMER OIL - WATER

s.no	Water flow rate in CC	Inlet temperature in ^{0}C	Out let temperature in ^{0}C	Temperature difference in ^{0}C
Cold water	40	25	29.5	4.5
Transformer oil	50	49	43	6

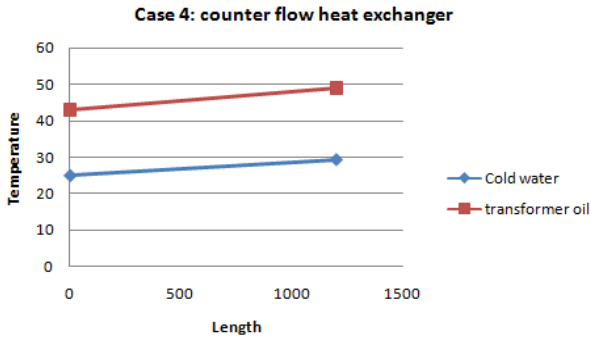

Graph 5.4: Case 4 - Counter flow heat exchanger Transformer oil - water

D. Results for CFD analysis on heat exchanger

TABLE VII. CASE 5 - PARALLEL FLOW HEAT EXCHANGER WATER - WATER

s.no	Water flow rate in CC	Inlet temperature in ^{0}C	Out let temperature in ^{0}C	Temperature difference in ^{0}C
Cold water	40	25	30.5	5.5
Hot water	50	49	43	6

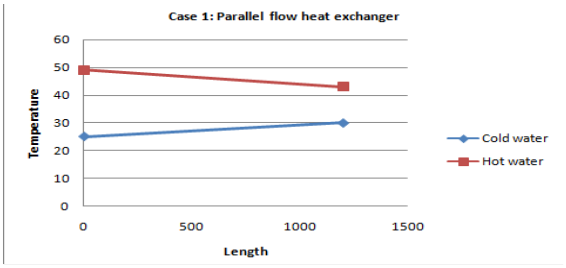

Graph 5.5: Case 1- Parallel flow heat exchanger water – water

TABLE VIII. CASE 6 - COUNTER FLOW HEAT EXCHANGER WATER - WATER

s.no	Water flow rate in CC	Inlet temperature in ^{0}C	Out let temperature in ^{0}C	Temperature difference in ^{0}C
Cold water	40	25	31	6
Hot water	50	49	42	7

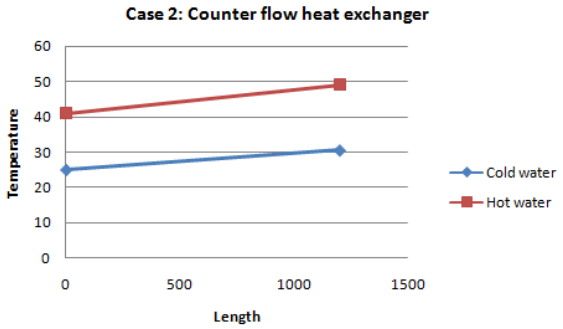

Graph 5.6: Case 6- Counter flow heat exchanger water - water

TABLE IX. CASE 7- PARALLEL FLOW HEAT EXCHANGER TRANSFORMER OIL - WATER

s.no	Water flow rate in CC	Inlet temperature in ^{0}C	Out let temperature in ^{0}C	Temperature difference in ^{0}C
Cold water	40	25	28	3
Transformer oil	50	49	45	4

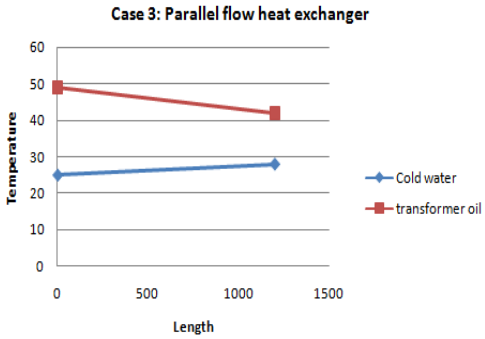

Graph 5.7: Case 7 - Parallel flow heat exchanger Transformer oil - water

TABLE X. CASE 8 - COUNTER FLOW HEAT EXCHANGER TRANSFORMER OIL - WATER

s.no	Water flow rate in CC	Inlet temperature in ^{0}C	Out let temperature in ^{0}C	Temperature difference in ^{0}C
Cold water	40	25	29	4
Transformer oil	50	49	43	5

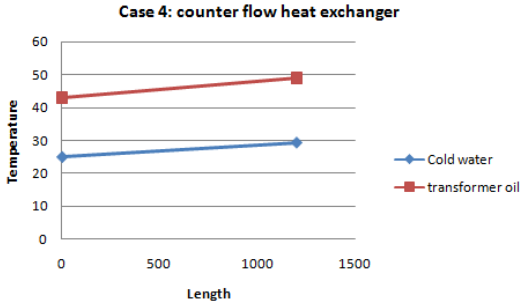

Graph 5.8: Case 8 - Counter flow heat exchanger Transformer oil - water

Conclusion

The performance, practical and CFD analysis of different fluids were investigated on parallel and counter flow in concentric tube heat exchanger.

In the present work the counter flow heat exchanger using CFD analysis has been investigated. The heat transfer and flow distribution of 3-D model counter flow heat exchanger is discussed in detail and compared with the previous literature in view of varying the inlet temperature and flow rate. The discretized 3-D model outcome are in agreement with the previous literature and hence are validated for proposed heat exchanger using fluent simulation tool of ANSYS. The present work observes the better heat transfer and comprehensive understanding of a heat exchanger.

The conclusions of the investigating at are as follows.

1. The main objective of this project was to analyses the fluid flow in double pipe heat exchangers and the subsequent performance of these heat exchangers.
2. This review is done on both practical and CFD analysis
3. Modeling the double pipe heat exchanger by using ANSYS WORKBENCH.
4. To simulate heat transfer in concentric tube heat exchanger by using CFD-Fluent software.
5. The ANSYS FLUENT results were found to be• fairly consistent with hard calculations with most of the values within 5% of each other
6. The results in practical and as well as in cfd are nearly equal
7. As the cold fluid temperature goes down, the steady state condition for heat transfer can be achieved at a faster rate
8. The pressure and temperature contours show the higher velocity and pressure magnitudes along the outer pipes as compared to the inner pipe.

Moreover, new materials with better thermal properties for the construction of counter flow heat exchanger could lead to bright and improved changes of heat transfer. The present work can further be enhanced by considering Nusselt and Reynolds number stress models to improve the flow characteristics in the system and comparing the results with other computational methods.

REFERENCES

[1] Praveen Kumar Kanti, Karthika.U.P, Sabeer Ali, SanathKumar.N, ShyamChandran C“CFD analysis of shell and tube heatexchanger”, ISSN: 2319- 6890)(online),2347-5013, VolumeNo.5Issue:Special 6, pp: 1129 -1254, 20 May 2016

[2] D.Bhanuchandrarao, M.Ashokchakravarthy, Dr. Y. Krishna, Dr. V .V. SubbaRao, T.HariKrishna “CFD Analysis And PerformanceOf Parallel And Counter Flow In Concentric Tube Heat Exchangers”, ISSN: 2278-0181,Vol. 2 Issue 11, November – 2013

[3] C. S. Oon, H. Togun, S. N. Kazi, A. Badarudin and E. Sadeghinezhad, “Computational simulation of heat transfer to separation fluid flow in an annular passage”, Int. Commun. Heat Mass, Vol. 46, pp. 92-96, (2013).

[4] S. Nagarsheth, U. Pandya and H. Nagarsheth, “Control Analysis Using Tuning Methods for a Designed, Developed and Modeled Cross Flow Water Tube Heat Exchanger”, Int. J. Mech., Aero, Ind. Mechatron. Eng., World Academy of Science and Technology, Vol. 8, No. 12, pp. 1889- 1894, (2014).

[5] K.S.Hwang, S.K.Jang, S.U.S.Chio, Flow and convective heat transfer characteristics of water-based Al2O3 nanofluids in fully developed laminar flow regime, International Journal of Heat and Mass Transfer, 52 (2009) 193-199.

[6] V. Bianco, F. Chiacchio, O. Manca, S. Nardini, Numerical investigationof nanofluids forced convection in circular tubes, Applied Thermal Engineering, 29 (2009) 3632 – 3642.

[7] M. Akbari, N. Galanis, A. Behzadmehr, Comparative analysis of singleand two-phase models for CFD studies of nanofluid heat transfer, International Journal of Thermal Sciences, 50 (2011) 1343-1354

 ISBN: 978-93-91420-02-4

Design and Finite Element Analysis of Gas Turbine Blade

Mojeswararao Duduku and B.Rambabu
Department of Mechanical Engineering, Narasaraopeta Engineering College (A), Narasaraopet, India

***Abstract*— Gas turbines are extensively used for air craft propulsion, land based power generation and industrial applications. Thermal efficiency of gas turbine improved by increasing turbine rotor inlet temperature. The current rotor inlet temperature in advanced gas turbine is for above the melting point of blade material. A sophisticated cooling scheme must be developed for continuous safe operation of gas turbines with high performance.**

Gas turbines are cooled externally and internally. Several methods have been suggested for the cooling of blades and vanes. The techniques that involve cooling the blades and vanes by using cooling methods is to have radial holes to pass high velocity cooling air along the blade span.

In this thesis a turbine blade is designed and modeled in CREO parametric **software. The turbine blades are designed using film cooling. The** turbine **blade with film cooling for no holes, 3 holes, 7 holes, 13 holes is modeled.**

CFD, Thermal analysis is done to determine the heat transfer rates, heat **transfer coefficients of the blade. The present used material for blade is chromium steel. In this thesis, it is replaced with Nickel alloys. CFD analysis, Thermal analysis is done in ANSYS.**

Keywords: Gas turbine blade, Vanes, CREO, nickel alloy.

INTRODUCTION

A gas turbine, also called a combustion turbine, is a type of internal combustion engine. It has an upstream rotating compressor coupled to a downstream turbine, and a combustion chamber in-between.Gas turbines are sometimes referred to as turbine engines. Such engines usually feature an inlet, fan, compressor, combustor and nozzle (possibly other assemblies) in addition to one or more turbines.

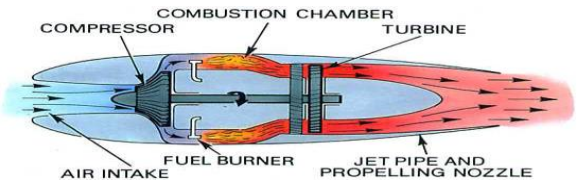

Fig: 1 Gas Turbine

I. SELECTION OF MATERIAL

Chromium Steel Thermal conductivity = 24.38W/m-k
Nickel Alloy 617 Thermal conductivity = 13.6W/m-k

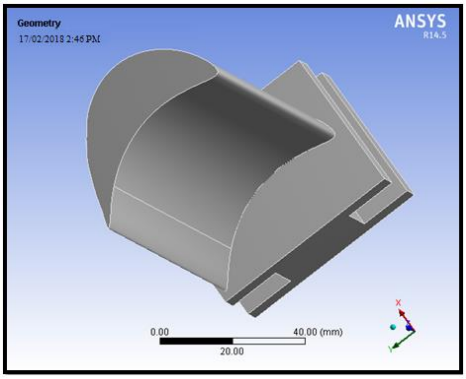

Fig: 2 Imported Model

II.FINITE ELEMENT ANALYSIS

FEA consists of a computer model of a material or design that is stressed and analyzed for specific results. It is used in new product design, and existing product refinement. A company is able to verify a proposed design will be able to perform to the client's specifications prior to manufacturing or construction. Modifying an existing product or structure is utilized to qualify the product or structure for a new service condition. In case of structural failure, FEA may be used to help determine the design modifications to meet the new condition.

There are generally two types of analysis that are used in industry: 2-D modeling, and 3-D modeling. While 2-D modeling conserves simplicity and allows the analysis to be run on a relatively normal computer, it tends to yield less accurate results. 3-D modeling, however, produces more accurate results while sacrificing the ability to run on all but the fastest computers effectively. Within each of these modeling schemes, the programmer can insert numerous algorithms (functions) which may make the system behave linearly or non-linearly. Linear systems are far less complex and generally do not take into account plastic deformation. Non-linear systems do account for plastic deformation, and many also are capable of testing a material all the way to fracture. Points of interest may consist of: fracture point of previously tested material, fillets, corners, complex detail, and high stress areas. The mesh acts like a spider web in that from each node, there extends a mesh element to each of the adjacent nodes.

 ISBN: 978-93-91420-02-4

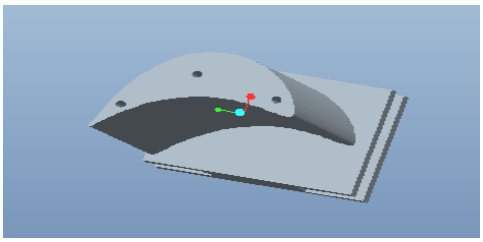

Fig: 3 Turbine blade with 3 holes

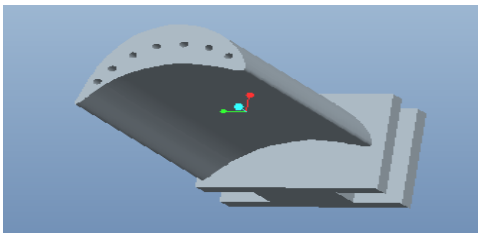

Fig: 4 Turbine blade with 7 holes

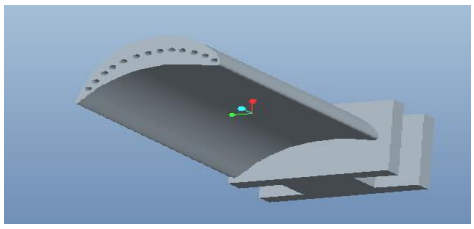

Fig: 5 Turbine blade with 13 holes

RESULTS AND ANALYSIS

TABLE I. CFD ANALYSIS

Models	Materials	Results		
		Temperature(°C)		Heat flux(W/mm^2)
		Max.	Min.	
No-holes	Chromium steel	812	22.459	9.3625
	Nickel alloy	812	22.059	6.4744
3-holes	Chromium steel	812	22.595	9.8363
	Nickel alloy	812	22.078	6.8431
7-holes	Chromium steel	812	22.331	10.517
	Nickel alloy	812	22.04	7.2644
13-holes	Chromium steel	812	22.39	7.9833
	Nickel alloy	812	22.048	5.224

TABLE II. THERMAL ANALYSIS

Turbine models	Results				
	Pressure(Pa)	Velocity(m/s)	Heat transfer coefficient(W/m^2-k)	Mass flow rate (kg/s)	Heat transfer rate(W)
No-holes	2.63e^{+05}	1.79 e^{+03}	2.86e^{+03}	0.3660354 6	289848
3-holes	6.51e^{+05}	1.96 e^{+03}	2.66e^{+03}	1.3362656	1468896
7-holes	3.59e^{+05}	1.98 e^{+03}	3.06e^{+03}	0.2184982 3	173056
13-holes	2.61e^{+05}	1.82 e^{+03}	2.88e^{+03}	0.1821594 2	144232

In this thesis a turbine blade is designed and modeled in Pro/Engineer software. The turbine blades are designed using cooling holes. The turbine blade is designed with no holes, 3 holes, 7 holes, 13 holes. The present used material for blade is chromium steel. In this thesis, it is replaced with Nickel alloy. Thermal and CFD analysis is done to determine the heat transfer rates and heat transfer coefficients of the blade.

CONCLUSION

By observing the CFD analysis results, the pressure gradient is more for blade with 3 holes than blade with 7 & 13 holes. Due to high pressure gradient, the heat transfer coefficient and heat transfer rate are more for blade with 3 holes.

REFERENCES

1. Design and Analysis of Gas Turbine Blade by Theju V, Uday P S, PLV Gopinath Reddy, C.J.Manjunath
2. Heat Transfer Analysis of Gas Turbine Blade through Cooling Holes by K Hari Bahamian, M.Lava Kumar
3. The design and analysis of gas turbine blade by pedaprolu venkata vinod

Investigation on Mechanical Properties of Glass fiber and Carbon Nano Tubes Sandwich Composite Material

Rajiv Kumar Busa
Department of Mechanical Engineering, Narasaraopeta Engineering College(A), Narasaraopeta, India

Abstract—Sandwich epoxy composite material is a combination of two or more different materials which consists of three layers i.e. two face sheets and one core material as in the form of layer. These Composites are widely used because of their light weight and good strength which are suitable for the applications like aerospace, marine, automobile, architecture panel etc. In order to improve the properties of the sandwich epoxy composites several particulate and fiber based fillers/reinforcing materials are used.

This research work involves in improving the mechanical properties of Epoxy /Glass Fiber composite by adding Multi Walled Carbon Nano Tubes (MWCNT) and thus reducing the cost of the hybrid nano composite.

In this research work high magnesium content and low weight aluminum sheet of 0.5mm thickness sheet is used as face material and Carbon nanotubes which is low weight material and glass fiber of woven type is used as core material in order to improve mechanical properties. In addition to this, Carbon nanotubes have high electrical conductivity than copper by adding Carbon nanotubes electrical properties can also be improved.

Formability analysis is done to find out forming parameters by using Erickson cupping test. .Experimental investigation helps in identifying the some of the parameters such as density, Poisson's ratio, yield strength, ultimate tensile stress, total elongation, strain hardening coefficient, plastic strain ratio, etc. of materials.

Keywords—Epoxy, Carbon Nano Tubes, Glass Fiber.

I. INTRODUCTION

Sandwich composite material is a combination of two or more different materials which consists of three layers i.e. two face sheets and one core material as in the form of layer. These materials have great advantages such as low weight and considerably higher shear stiffness to weight ratio than an equivalent beam made of only the core material or the face-sheet material and also high tensile strength to weight ratio. The high stiffness of the face-sheet leads to a high bending stiffness to weight ratio for the composite.

There are different manufacturing processes for sandwich composite materials .They are cold working and hot working process. In cold working process there in no external heat is used in hot working process external heat is supplied to the material to improve its properties and also to minimize curing time.

Materials used for manufacturing are as in the form of sheets and some- times core materials are in the form of granulated powder. Mostly aluminum is used in manufacturing of sandwich composite material due to its low weight and easy deformation on applying of load. Depending up on the requirement number of layers are increased in general it is a three layer composite

II. SANDWICH STRUCTURE

Sandwich structures can be classed as composite materials in that they consist of two or more individual components of differing properties which when combined result in a high performance material. In contrast to monolithic composites - which consist of an intimate mixture of fibres (glass, kevlar, carbon, metal, etc.) supported within a continuous matrix (e.g. thermoplastic or thermoset resin) - sandwich structures have a discrete structure in which a core material is bonded to, and faced with, a skin material.

The skin material usually has a high stiffness, whereas the core typically has high compressive and shear strength. When these are bonded together, this combination gives the sandwich structure a high flexural modulus.

Skin material can vary but common forms include:

FRP (fibre reinforced polymer - thermoplastic and thermoset).

Polymer

Wood

Aramid sheet

Metals (aluminium, titanium, steel, etc.)

Ceramic

Stone

The core can exist in a number of structures and materials:

Expanded/extruded foam (polymer - polyurethane, epoxy; metal - aluminium)

Honeycomb structure (metal - aluminium, steel; Nomex - aramid fibre dipped in resin (epoxy, phenolic or polyamide) to form a paper-like material)

Solid (wood - balsa; polymer - epoxy)

The skins are bonded to the core with film, liquid or paste adhesives and normally cured using heat and pressure, although some adhesives can cure at room temperature. It is important to note that the chosen adhesive needs to have the appropriate mechanical and thermal properties to achieve compatibility between the skin and

core materials, especially with respect to thermal expansion differences.

Sandwich panels are used in preference to conventional composites where the characteristics of low weight and high resistance to bending are required.

SANDWICH THEORY

Sandwich theory describes the behavior of a beam, plate, or shell which consists of three layers - two face sheets and one core. The most commonly used sandwich theory is linear and is an extension of first order beam theory. Linear sandwich theory is of importance for the design and analysis of sandwich panels, which are of use in building construction, vehicle construction, airplane construction and refrigeration engineering.

SOME ADVANTAGES OF SANDWICH CONSTRUCTION ARE

i) Sandwich cross sections are composite. They usually consist of a low to moderate stiffness core which is connected with two stiff exterior face-sheets. The composite has considerably higher shear stiffness to weight ratio than an equivalent beam made of only the core material or the face-sheet material. The composite also has a high tensile strength to weight ratio.

ii) The high stiffness of the face-sheet leads to a high bending stiffness to weight ratio for the composite.

The behavior of a beam with sandwich cross-section under a load differs from a beam with a constant elastic cross section as can be observed in the adjacent figure. If the radius of curvature during bending is large compared to the thickness of the sandwich beam and the strains in the component materials are small, the deformation of a sandwich composite beam can be separated into two parts

i) Deformations due to bending moments or bending deformation, and

ii) Deformations due to transverse forces, also called shear deformation.

III.CARBON NANO TUBES

Carbon Nanotube is a tube shaped material, made of carbon, having a diameter measuring on the nanometer scale. A nanometer is one billionth of a meter, or about one ten thousandth of the thickness of a human hair. The graphite layer appears somewhat like a rolled up chicken wire with a continuous unbroken hexagonal mesh and carbon molecules at the apexes of the hexagons.

Carbon Nanotubes have many structures, differing in length, thickness, and in the type of helicity and number of layers. Although they are formed from essentially the same graphite sheet, their electrical characteristics differ depending on these variations, acting either as metals or as semiconductors. As a group, Carbon nanotubes typically have diameters ranging from <1 nm up to 50 nm. Their lengths are typically several microns, but recent advancements have made the nanotubes much longer, and measured in centimeters.

CARBON NANO TUBES IN COMPOSITES

Carbon nanotubes have high Young's modulus and axial tensile strength but they are also very flexible. So that they can be knotted tightly without breakage and exhibit a plastic behavior, in contrast with conventional carbon fibers.

It has been verified that carbon nanotubes improve thermal and flammability properties of a number of polymers.

CNTs show outstanding mechanical properties: stiffness, strength and resilience exceeds any current material .CNTs also have superior thermal and electrical properties: thermal stability up to 2,800◦C in vacuum thermal conductivity about twice as high as diamond, electric current-carrying capacity 1,000 times higher than copper wires.

CNT has lot of applications due to is extensive properties compared with other materials by adding CNT to any composite its properties can be improved. It has high electrical conductivity than copper so it is used in many electrical applications.

CNT CAN BE CATEGORIZED BY THEIR STRUCTURES

- Single wall Nanotubes (SWNT)
- Multiwall Nanotubes (MWNT)
- Double wall Nanotubes (DWNT)

In this research work multiwall carbon nanotubes powder is used.

PROPERTIES OF A CARBON NANOTUBE

The intrinsic mechanical and transport properties of Carbon Nanotubes make them the ultimate carbon fibers. The following tables compare these properties to other engineering materials.

Overall, Carbon nanotubes show a unique combination of stiffness, strength, and tenacity compared to other fiber materials which usually lack one or more of these properties. Thermal and electrical conductivity are also very high, and comparable to other conductive materials.

Fiber material	Strength (Tpa)	Specific density (g/cm^3)	E (TPa)	Strain at Break (%)
Carbon Nanotube	10-60	1.3-2	1	10
HS steel	4.1	7.8	0.2	<10
Carbon fiber-PAN	1.7-5	1.7-2	0.2-0.6	0.3-2.4
Carbon fiber-Pitch	2.2-3.3	2-2.2	0.4-0.96	0.27-0.6
E/S- glass	2.4/4.5	2.5	0.07/0.08	4.8
Kevlar 49	3.6-4.1	1.4	0.13	2.8

Comparison of mechanical properties of carbon nanotubes with different material

Material	Electrical Conductivity (s/m)	Thermal Conductivity(W/m.k)
Carbon Nanotubes	106-107	>3000
Carbon Fiber-Pitch	2 -8.5 × 106	1000
Carbon Fiber-PAN	6.5 - 14 ×106	8 - 105

Copper	6 × 107	400

Comparison of transport properties of carbon nanotubes with different material

POTENTIAL APPLICATIONS FOR CARBON NANOTUBES

Carbon Nanotube Technology can be used for a wide range of new and existing applications:

Conductive plastics
Structural composite materials
Flat-panel displays
Gas storage
Antifouling paint
Micro- and nano-electronics
Radar-absorbing coating
Technical textiles
Ultra-capacitors
Atomic Force Microscope (AFM) tips
Batteries with improved lifetime
Biosensors for harmful gases
Extra strong fibers.

APPLICATIONS OF NANOCOMPOSITES

Wind-turbine blades,
Boats,
Architectural moldings
Automobile
Structural panels for Aerospace applications.

PROPERTIES TO BE INVESTIGATED

Tensile properties
Flexural properties
Impact properties
Hardness
Formability

MATERIALS USED IN PREPARATION OF HYBRIDSANDWICH COMPOSITE SHEETS:

- Aluminum sheet (AA5052-H32) of 0.5mm thickness.
- Glass fiber of woven type.
- Adhesive (resin and hardener type) EPOXY (LY556) and Hardener (HY951).
- Multi walled CNT (carbon nanotubes) powder (Inside Diameter: 5 to 10 nm, Out Side Diameter: 10 to 20 nm, Length: 10 to 30 µm, Purity: 99.8%).

METHODS USED FOR PREPARATION OF SANDWICH SHEET:

- Hand Lay-up
- Vacuum Bagging
- Spray Lay-up
- Filament Winding
- Pultrusion
- Resin Transfer
- Infusion Processes

In this research work hand lay out technique is used for preparation of sandwich sheet which is a simple and low cost method for manufacturing of sandwich sheets.

COMBINATIONS PREPARED:

- AA (5052)-H32/GF/AA (5052)-H32.
- AA (5052)-H32/CNT/GF/CNT/AA (5052)-H32. (3%, 4%, 5%)

ACCESSORIES NEEDED FOR PREPARATION OF SANDWICH SHEETS:

i) Measuring tape: To measure and mark dimensions of aluminum and glass fiber.
ii) Tin cutter: To cut aluminum sheet.
iii) Emery paper: To rub aluminum sheet.
iv) Box plaster: To keep glass fiber without de-lamination while cutting.
v) Scissor: To cut glass fiber.
vi) Mugs: For mixing of resin and hardener.
vii) Gloves and face mask for safety purpose
viii) Stirrer: For mixing of resin and hardener.
ix) Plastic cover: To cover sandwich sheet so extra resin squeeze cannot stick to ply wood.
x) Ply wood: To cover sandwich sheet for equal distribution of pressure.
xi) Measuring jar: To measure ethyl alcohol.
xii) Electronic weighting machine: To check weight of resin and hardener.

 ISBN: 978-93-91420-02-4

STEPS INVOLVED IN PREPARATION OF SANDWICH SHEET:

CUTTING OF ALUMINUM SHEET:

The actual sheet dimension is 1220mm length and 1020mm width. With tin cutter cut the sheet into 9 pieces of each has dimensions of 406 mm length and 340mm width.

PREPARATION OF SHEET SURFACE:

By using high quality emery paper rub the shine surface side of sheets which provides scratches in order to provide grip to sandwich sheet without causing de-lamination. With the help of emery paper manually can rub the sheet.

CUTTING OF GLASS FIBER:

As glass fiber used is of woven type it will simply delaminate while cutting in order to prevent this use 5cm box tape (plaster) and paste it on glass fiber which helps in preventions of de-lamination of glass fiber and by using a strong scissor or glass fiber cotter is used to cut the glass fiber to required dimension upon the pasted box tape on glass fiber.

(Note: The dimension of glass fiber should be more than sheet)

MIXING OF RESIN AND HARDNER:

Before starting work with epoxy ware face mask and rubber gloves why because resin and hardener smell is very bitter and it is difficult to work with it without wearing face mask which helps in covering your nose and chemicals in resin and hardener are highly reactive while coming in contact to skin leads skin diseases and allergies in order to overcome this wear gloves, allow proper work space i.e. prepare sheet at proper ventilation area.

For 1000gms of resin mix 400 grams of hardener and stirrer the combination using stirrer for 20 to 30 minutes. Now epoxy mix is ready to apply.

APPLYING OF RESIN HARDNER MIX TO ALUMINUM SHEET:

Take proper quantity of resin hardener mixture by using spoon and pour it on aluminum sheet after that by using a roller, distribute mixture to all the sheet without any gaps and place the glass fiber piece upon it repeat the step and place the another sheet upon glass fiber so as aluminum sheets are placed on both sides of glass fiber.

Now cover the both sides of sandwich sheet with plastic cover which helps in removing of sheet easily after curing why because by application of load upon sheet leads to squeeze the epoxy mixture to outer edges of sheet which will stick to other surfaces in order to overcome this plastic cover is used to cover both sides of sandwich sheet.

APPLICATION OF LOAD ON SHEETS:

After completion of above steps place a plywood piece which is larger in dimension of sheet upon the sandwich sheet, on application of load upon wood leads to equal distribution of load to all sides of sheet. After that apply load of around 40 to 50kgs and allow the sheets to curing gas curing time is 19 hours, after curing remove the sheets and cut the extra glass fiber on each edges of sandwich sheet gently and sandwich sheet is ready for testing. Load can be applied by using any weight, but approximately 40kgs and above has to be applied.

(Note: After curing resin squeezes out sticks to glass fiber and plastic sheet covered plastic sheet can be removed easily but cutting of glass fiber will be difficult the scissor used for cutting of glass fiber cannot be used glass fiber cutter or tin cutter can also be used)

PREPARATION OF CNT IMPREGATED SANDWICH SHEET:

The above procedure is same for all type of sheets prepared but only resin hardener mixing is to be changes while preparation of carbon nanotubes impregnated sandwich sheets. This project involves in preparation of different sandwich sheets with different percentages of CNT power in core material.

In order to prepare 3% of CNT sandwich sheet 30gms of resin is to be removed from 1000gms and then CNT is poured into resin and mixed for some time and then hardener is mixed and further work is continued as described as above.

In this project CNT reinforced sheets with 3%, 4% and 5% are to be manufactured. For 4% sheets 40gms of resin has to be removed and for 5% sheets 50gms of resin

has to be removed. And for proper epoxy mix respective amount of hardener has also be removed improper mixing or low quantity mixing leads to damages such as de-lamination of sheet can takes place.

WEIGHING OF RESINE:

An electronic weighing machine is used to measure resin and remaining resin is poured into another bottle with lid or closed container for further application. After opening of seal resin or hardener can be used only up to 3 months so extra resin removed can be used within 3 months.

WEIGHTING OF HARDNER:

In order to get proper mix and good adhesion respective amount of hardener is also to be removed and poured in another bottle with lid or a closed container. If 30gms of resin is removed from the 1000gms bottle then 12gms of hardener has to be removed from the 400gms of hardener. If 40gms of resin is removed from the 1000gms bottle then 16gms of hardener has to be removed from the 400gms of hardener. If 50gms of resin is removed from the 1000gms bottle then 20gms of hardener has to be removed from the 400gms of hardener. Why this is because the resin and hardener mix ratio is 1000gms of resin to 400gms of hardener.

(Note: Improper mixing leads to damage of work and proper strength can be achieved).

PROBLEMS ARISED DURING PREPARATION OF CNT SANDWICH SHEETS:

As resin and hardener is highly reactive by mixing of CNT into it leads to some chemical reaction and lot of heat is generated and within 20 minutes total resin and hardener mix get solidified as like as solid plastic. In addition to this lot of heat is generated and after solidification also heat cannot be reduced for a long time. For manufacturing purpose 20 minutes cannot be enough to prepare sandwich sheets.

This process was tried on 3% CNT mixture and 4% CNT and 5% CNT mixture but when CNT percentage is reactive time is reducing from 40 minutes to 20 minutes for solidification, which was enough to prepare one or two sheets, but in order to prepare more sheets time is not enough.

PROBLEM RECTIFICATION:

In order to rectify the above problem dispassion solution is used which will increase the reaction time to 2 hours so within 2 hours work can be finished but dispassion solution cannot be mixed directly to resin and hardener or CNT powders a method called sonication or ultra-sonication. Sonication process is used in which dispassion solution is heated to rise its temperature and CNT powder is mixed into it and allow to stirrer for 30 minutes to 1 hour and then solution is ready so that all powder poured into it gets equally dissipated, the solution is poured into the resin and further work is done as mentioned above. In this project ethyl alcohol is used as dispassion solution and 200ml is used for 1000 grams of resin.

(Note: while working with 4% and 5% CNT 300ml is used.)

SONICATION PROCESS:

Sonication can be used to speed dissolution, by breaking intermolecular interactions. It is especially useful when it is not possible to stir the sample. Sonication is commonly used in nanotechnology for evenly dispersing nanoparticles in liquids.

CLEANING AFTER PREPARATION:

Even though gloves are used as epoxy mix have high adhesive property sometimes gloves may tore due to sharp edges of aluminium sheet and epoxy mix can come in contact to skin during such time acetone can be used to clean where it comes in contact and also after completion of sheet preparation process and sonication process stirrer and measuring jars and other equipment's which are in contact with epoxy mix can be cleaned by using acetone liquid.

EXPERIMENTAL WORK

TESTS CONDUCTED:

- Tensile Test.
- Flexural Test.
- Impact Resistance Test.
- Ericission Cupping Test.

TENSILE TEST:

The ASTM standard for tensile test is D638

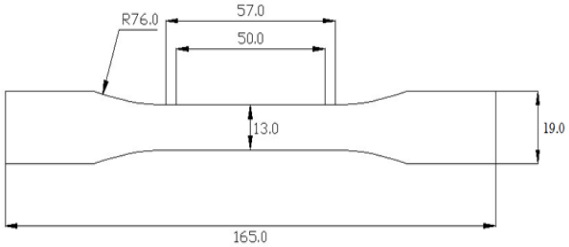

ASTM standard figure for tensile test

 ISBN: 978-93-91420-02-4

Tensile testing setup

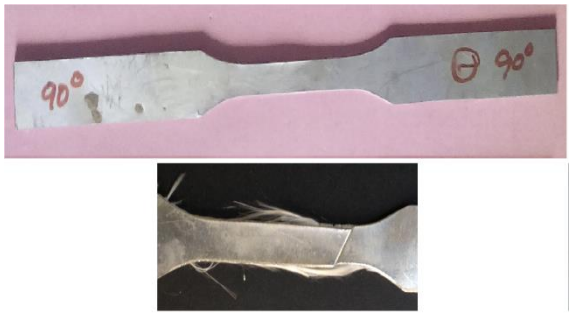

Tensile test specimens before and after testing.

FLEXURAL TEST

The ASTM standard for flexural test is [D790] all dimension are in mm.

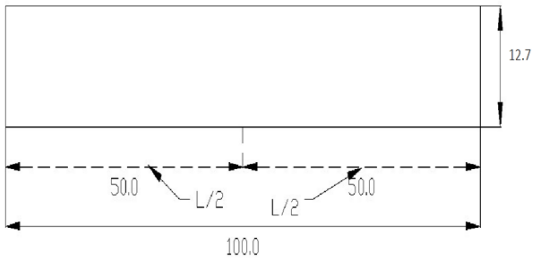

ASTM standard figure for flexural test

Flexural test specimens before and after testing

IMPACT RESISTANCE TEST

Test conditions:

Temperature: Room temperature (25 ± 2^{0}C).
Diameter of impact core: 12.7mm.
Height of weight fall (1kg): 100cm & 150cm.

Impact Resistance test setup

Impact resistance specimens before and after testing

ERICISSION CUPPING TEST

Test method: IS10175

Ericission cupping test setup

Ericission cupping test specimen before and after testing

OBJECTIVES

The epoxy resin is proposed as the core material in this research due to its cheaper cost. This research work will be carried out in room temperature condition and with simple cost effective experimental setup (Hand Layup Technique) Glass Fiber (GF) will be used as reinforcement in the core (epoxy). The mechanical properties of the core shall be improved by adding Carbon Nano Tubes (CNT).

OBSERVATIONS

It has been found that by mixing of CNT powder to epoxy causes curing time to reduce due to the chemical reaction. It has been found that by mixing of CNT powder to epoxy, mechanical properties of sandwich sheets can be improved. It has been found that by mixing of various

percentages of CNT (by increasing percentage of CNT powder) mixed to epoxy, impact resistance can be reduced. It has been found that flexural strength of sandwich sheets can be improved by increasing in percentage of CNT powder mixed to epoxy. It has been found that ductility of sandwich sheets can be improved by varying in percentage of CNT powder mixed to epoxy.

RESULTS AND DISCUSSION

Impact Strength of Epoxy/GF/Steel Slag has improved compare to other composite materials. Hardness Results of Epoxy/GF/CNT very much improved compare to other combination of composite materials. Addition of Nano filler such as CNT gives better results compare to pure Epoxy/ Glass fiber. Mechanical Properties of AA/GF/AA sandwich sheets have been improved by adding of carbon nanotubes powder. Mechanical Strength for CNT sandwich sheets is more compare to GF sandwich sheets. Flexural strength of CNT impregnated sandwich sheets is more when compared to GF impregnated sandwich sheets.CNT impregnated sandwich sheets have more ductility when compared to glass fiber impregnated sandwich sheets.

SCOPE

The cost of MWCNT is high and not available in India. The research on CNT material in Epoxy Composite is not done. Very less literature is on using CNT in the Epoxy Composites. There is no work reported on improving the Mechanical properties of the Epoxy by using CNT. There is no study on synergetic effect of reinforcement fillers on the carbon nanotubes powder used in the Epoxy Composite materials. The research work made on combinations manufactured using CNT is not done yet.

REFERENCES

1) Cristiane Becker et al. (ELSEVIER, Vol. Part A 42, pp. 196-202, 2011). Mechanical and flame- retardant properties of epoxy/Mg-Al LDH Composites.

2) Mahmood M. Shokrieh et.al (ELSEVIER, Vol. 40, pp. 443- 452, 2012).Fabrication and mechanical properties of clay/epoxy Nano composite and its polymer concrete.

3) KwangSeon Shin, KeeJoo Kim, Suk-Woo Choi and Meung Ho Rhee. Mechanical Properties of Aluminum/Polypropylene/Aluminum Sandwich Sheets.

4) Nadir Ayrilmis · Jan T. Benthien · HeikoThoemen ·Robert H. White. Effects of fire retardants on physical, mechanical, and fire properties of flat-pressed WPCs.

5) K.J. Kim, D. Kim, S.H. Choi , K. Chung, K.S. Shin ,F. Barlat , K.H. Oh, J.R. Youn.Formability of AA5182/polypropylene/AA5182 sandwich sheets.

6) Jun Yanagimoto, KatsuyoshiIkeuchi. Sheet forming process of carbon fiber reinforced plastics for lightweight parts.

7) Jianguang Liu, Wei Liu, Wei Xue. Forming limit diagram prediction of AA5052/polyethylene/AA5052 sandwich sheets.

8) K.P. Jacksona, J.M. Allwooda, M. Landertb.Incremental forming of sandwich panels.

9) K. Logesh, V.K.Bupesh Raja. Investigation of Mechanical Properties of AA8011/PP/AA1100 Sandwich Materials.

10) A S Singha and Vijay Kumar Thakur. Mechanical properties of natural fibre reinforced polymer composites.

11) AutarK.Kaw. Mechanics of composite material (CRC Press).

12) KrishanK.Chawala. Composite materials, science and engineering (Springer).

13) P.K.Mallick. Fiber reinforced composites, Materials, Manufacturing and design by (CRC Press).

CFD Analysis of Super Utiliy Vehicle to Determine Aerodynamic Behaviour

Peruopgu Manoj Kumar and Dr. B. Venkata Siva
Department of Mechanical Engineering, Narasaraopeta Engineering College (A), Narasaraopet, India

***Abstract*— a steady increase in global energy demand has a direct influence on the fuel prices. This together with the environmental problems caused by the exhaust gases of cars is the main motives behind needs to reduce fuel consumption of roads vehicles. Reducing aerodynamic drag can lead to reduction in fuel consumption leading to less environment problems.**

Keywords—Aerodynamics, CFD analysis, Super Utility Vehicle.

I.INTRODUCTION

Aerodynamic, the study of the motion of air, partially it interaction with a solid object such as an airplane wing. Aerodynamic is a sub-field of fluid dynamic and gas dynamics, is often used synonymously with gas dynamics, the difference being that "gas dynamics" applies to study of the motion of all gases, and is not limited to air. The formal study of aerodynamic began in the modern sense in the eighteen century, although observations of fundamental concepts such as aerodynamic drag were recorded much earlier. Most of the early efforts in aerodynamic were directed towards achieving behavior-than-air flight, which was first demonstrated by Wilbur & Orville Wright in 1903. Since then, the use of aerodynamics through mathematical analysis, empirical approximations, wind tunnel experimentation, and computer simulation has formed a rational basis for the development of heavier-than-air flight & a number of other technologies. Recent work in aerodynamics has focused on issues related to compressible flow, turbulence, & boundary layers and has become increasingly computational in nature.

Fig1.A vortex is created by the passage of an aircraft wing, revealed by smoke. Vortices are one of the many phenomena associated with the study of aerodynamics

II.MODELING OF EXTERNAL BODY OF SUV

The external body models of SUV's Brezza & Eco sport are modelled. The model are modified by adding lip kits to the front bumper the analyses are carried out using a commercial CFD solver, ANSYS Fluent. The solver is based on finite volume method with second order discretization. The convergence criteria for continuity, momentum and other parameters were set to 10^{-3}, while the convergence of energy equation was set to 10^{-6}. In most

Cases, the momentum and other residuals were less than 10^{-5} and the highest residual was $7*10^{-4}$.

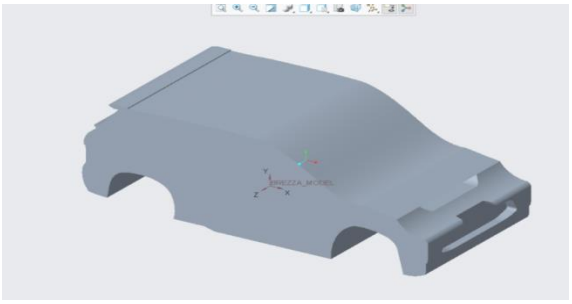

Fig2. Layout of Steam Power Plant

III.CFD ANALYSIS ON SUV MODELS

CFD analysis is performed on all the models of SUV and compared for the better model by observing results of pressure, velocity, lift and drag.

Turbulence models are known to replace the time-dependent Navier–Stokes equations by averaging them and simplifying the equations to reduce the complexities in calculation of the required quantities. Though these turbulence models are simplified and averaged, these models are able to predict the effects of turbulence accurately in many applications that are developed and implemented within commercial CFD software. The 'two-equation' models are most common and widely used models. These two equations represent two transport equations to solve for turbulent properties of the flow. Generally, one of the turbulent properties is the mean turbulent kinetic energy 'k' and the second property depends on the type of turbulence model. It is either dissipation rate 'e', for k-e turbulence model or the specific dissipation, 'x', which is a measure of the inverse time scale of the eddies, for k-x turbulence model.

3.1 .Boundary Conditions:

Analysis is performed by varying the speed of air speed of air -80km/hr, 120kmlhr & 160km/hr

3.2 .Brezza original model

→→Ansys → workbench→ select analysis system → fluid flow fluent → double click

→→Select geometry → right click → import geometry → select browse →open part → ok→

Select Tools – Select Enclosure and enter dimensions

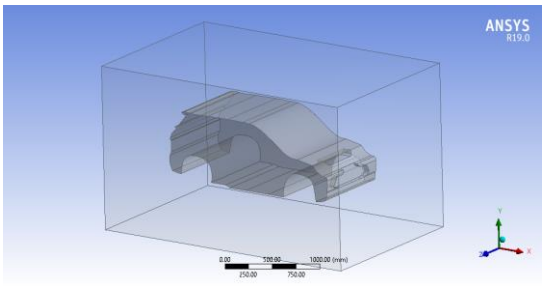

Fig3.Imported geometry of Brezza original model with enclosure from Creo 6.0

3.3. Right click on Setup in main window and Edit

The solver setup includes
Following steps:-
1. Type of analysis: For aerodynamic analysis 3D model analysis which pressure based steady state analysis with relative velocity formulation is carried out.
2. Models: here the type of numerical model used for the analysis is defined. For aerodynamic analysis Viscous based numerical model. The type of viscous based model used is realizable k-epsilon and scalable wall function model
3. Materials: here the material for the model is defined. In this work the analysis is carried out on Air which is the surrounding fluid. Here properties of the material can be retrieved from ANSYS Library.4. Boundary conditions: this is the core part of ANSYS Solver here the initial boundary conditions are defined. The initial boundary values for our analysis are:-

a. Inlet fluid velocity: - 80km/hr, 120km/hr, 160km/hr.
b. Wall: - Stationary
5. Solution methods:-
a. Pressure-Velocity Coupling
b. Scheme: Simple
c. Gradient: - Least Square Cell Based
d. Pressure: - second order
e. Momentum: - second order upwind

After carrying out all these initial set-ups run the calculation with required number of iterations. More the number of iterations the obtained result will be more close to the actual values.

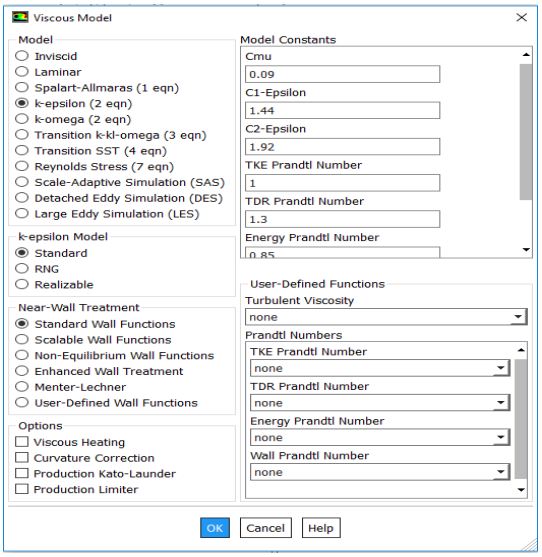

Fig4. K-epsilon is considered as viscous model

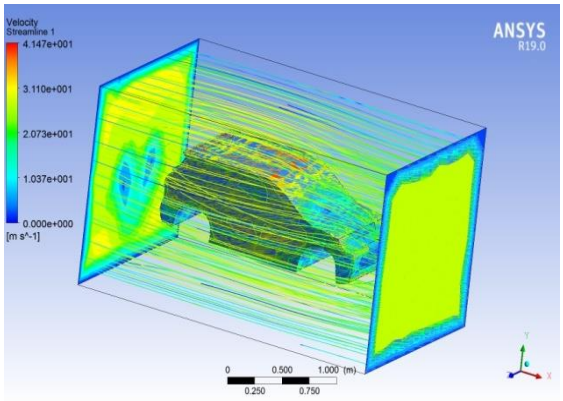

Fig5. Air flow path stream line on Brezza original model at 80km/hr

Drag force

	Forces (n)	Coefficients
Zone	Pressure	Viscous
Total	Pressure	Viscous
Total		
Wall-12 (0 0 0)	(0 0 0)	(0 0 0)
(0 0 0)	(0 0 0)	(0 0 0)

Wall-13 (-0.0024922251 0.0011541762 0.0055057006)
(-0.00031071517 1.2817594e-05 3.5113998e-07)
(-0.0028029403 0.0011669938 0.0055060517)
(-0.004068939 0.0018843694 0.0089888989)
(-0.00050729007 2.0926685e-05 5.7328976e-07)
(-0.0045762291 0.001905296 0.0089894722)
Wall-fluid (-7.3822244e-15 -128.47145 1.3418452)
(-16.02031 0.034087086 0.0032452923)
(-16.02031 -128.43737 1.3450905)
(-1.2052611e-14 -209.74931 2.1907676)
(-26.155608 0.055652385 0.0052984364)
(-26.155608 -209.69366 2.1960661)

Lift force

	Forces (n)	Coefficients
Zone	Pressure	Viscous
Total	Pressure	Viscous
Total		
Wall-12	(0 0 0)	(0 0 0)
(0 0 0)	(0 0 0)	(0 0 0)

Wall-13 (-0.0024922251 0.0011541762 0.0055057006)

(-0.00031071517 1.2817594e-05 3.5113998e-07)
(-0.0028029403 0.0011669938 0.0055060517)
(-0.004068939 0.0018843694 0.0089888989)
(-0.00050729007 2.0926685e-05 5.7328976e-07)
(-0.0045762291 0.001905296 0.0089894722)
Wall-fluid (-7.3822244e-15 -128.47145 1.3418452)
(-16.02031 0.034087086 0.0032452923) (-16.02031 -128.43737 1.3450905) (-1.2052611e-14 -209.74931 2.1907676)
(-26.155608 0.055652385 0.0052984364) (-26.155608 -209.69366 2.1960661)

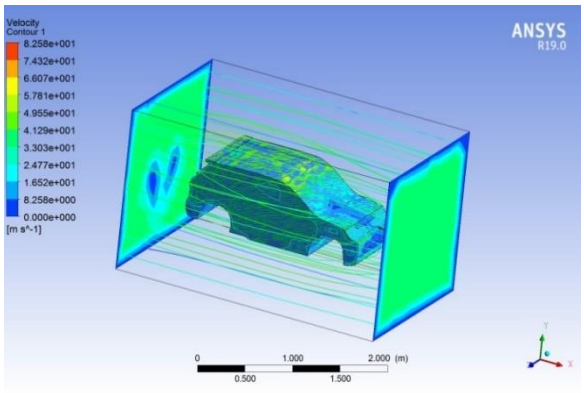

Fig6. Air flow path streamline on Brezza original model at120Km/hr

Wall-fluid (-1.6521427e-14 -287.73915 2.2050127)
(-32.634523 0.071008865 0.0055725886) (-32.634523 -287.66814 2.2105852) (-2.6973759e-14 -469.7782 3.6000207)
(-53.280854 0.11593284 0.0090981039) (-53.280854 -469.66227 3.6091188)
Net (-497.49599 -123.84141 5.7629931)
(-43.383338 1.3106357 -0.021196116)
(-540.87933 -122.53077 5.741797)
(-812.23835 -202.19006 9.4089683)
(-70.82994 2.1398134 -0.034605904)
(-883.06829 -200.05024 9.3743624)

Forces - Direction Vector (1 0 0)

	Forces (n)			Coefficients		
Zone	Pressure	Viscous	Total	Pressure	Viscous	Total
Wall-12	0	0	0	0	0	0
Wall-13	(-0.00569847)	(-0.00067397237)	(-0.0063724424)	(-0.0093036245)	(-0.0011003631)	(-0.010403988)
Wall-fluid	(-1.6521427e-14)	(-32.634523)	(-32.634523)	(-2.6973759e-14)	(-53.280854)	(-53.280854)
Net	(-497.49599 -43.383338)	(-540.8793-812.23835)	(-70.82994-883.06829)			

Lift force

Force (n)			Coefficients		
Zone	Pressure	Viscous	Total	Pressure	Viscous	Total
Wall-12	(0 0 0)	(0 0 0)	(0 0 0)	(0 0 0)	(0 0 0)	(0 0 0)
Wall-13	(-0.00569847 0.0025426239 0.012422399)	(-0.00067397237 2.8976924e-05 -1.2574405e-06)	(-0.0063724424 0.0025716008 0.012421142)	(-0.0093036245 0.0041512227 0.020281468)	(-0.0011003631 4.7309263e-05 -2.0529641e-06)	(-0.010403988 0.004198532 0.020279415)

Wall-fluid (-1.6521427e-14 -287.73915 2.2050127)
(-32.634523 0.071008865 0.0055725886)
(-32.634523 -287.66814 2.2105852)
(-2.6973759e-14 -469.7782 3.6000207)
(-53.280854 0.11593284 0.0090981039)
(-53.280854 -469.66227 3.6091188)
Net (-497.49599 -123.84141 5.7629931)
(-43.383338 1.3106357 -0.021196116)
(-540.87933 -122.53077 5.741797)
(-812.23835 -202.19006 9.4089683)

Forces - Direction Vector (0 1 0)

Forces (n) Coefficients

Zone	Pressure	Viscous	Total Pressure	Viscous Total
Wall-12	0	0	0	0
Wall-13	(0.0025426239)	(2.8976924e-05)	(0.0025716008)	

(0.0041512227) (4.7309263e-05) (0.004198532)

Wall-fluid (-287.73915) (0.071008865) (287.66814) (-469.7782) (0.11593284) (-469.66227)

Net (-123.84141 1.3106357) (-122.53077-202.19006)(2.1398134-200.05024)

IV.CALCULATIONS

4.1 Ecosport Modified Model

Velocity – 22.22m/s (80Km/hr)

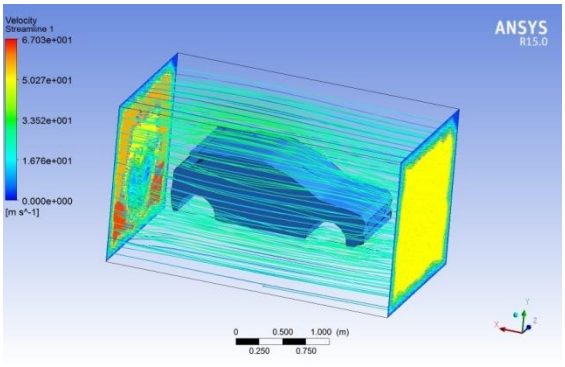

Fig7. Air flow path streamline on Ecosport modified model at 80Km/hr

Drag force

Forces (n)

Coefficients

Zone Pressure Viscous Total Pressure Viscous Total

Wall-kit (0 0 0) (0 0 0) (0 0 0) (0 0 0) (0 0 0) (0 0 0)

Wall-car (0 0 0) (0 0 0) (0 0 0) (0 0 0) (0 0 0) (0 0 0)

Wall-enclosure (296.47998 -95.926269 -2.0658168) (23.68417 0.096242478 0.024856249) (320.16415 -95.830026 -2.0409606) (484.04894 -156.61432 -3.3727622) (38.668032 0.15713058 0.040581631) (522.71698 -156.45719 -3.3321806)

Net (296.47998 -95.926269 -2.0658168) (23.68417 0.096242478 0.024856249) (320.16415 -95.830026 -2.0409606) (484.04894 -156.61432 -3.3727622) (38.668032 0.15713058 0.040581631) (522.71698 -156.45719 -3.3321806)

Forces - Direction Vector (1 0 0)

Forces (n) Coefficients

Zone Pressure Viscous Total Pressure Viscous Total

Wall-kit 0 0 0 0 0 0

Wall-car 0 0 0 0 0 0

Wall-enclosure (296.47998) (23.68417) (320.16415) (484.04894) (38.668032) (522.71698)

Net (296.47998) (23.68417) (320.16415) (484.04894) (38.668032) (522.71698)

Lift force

"Force Report"

Forces

Forces (n) Coefficients

Zone Pressure Viscous Total Pressure Viscous Total

Wall-kit (0 0 0) (0 0 0) (0 0 0) (0 0 0) (0 0 0) (0 0 0)

Wall-car (0 0 0) (0 0 0) (0 0 0) (0 0 0) (0 0 0) (0 0 0)

Wall-enclosure (296.47998 - 95.926269 -2.0658168)

(23.68417 0.096242478 0.024856249) (320.16415 -95.830026 -2.0409606) (484.04894 -156.61432 -3.3727622) (38.668032 0.15713058 0.040581631) (522.71698 -156.45719 -3.3321806)

Net (296.47998 -95.926269 -2.0658168) (23.68417 0.096242478 0.024856249) (320.16415 -95.830026 -2.0409606) (484.04894 -156.61432 -3.3727622) (38.668032 0.15713058 0.040581631) (522.71698 -156.45719 -3.3321806)

Forces - Direction Vector (0 1 0)

Forces (n) Coefficients

Zone	Pressure	Viscous	Total	Pressure	Viscous	Total
Wall-kit	0	0	0	0	0	0
Wall-car	0	0	0	0	0	0
Wall-enclosure	(-95.926269)	(0.096242478)	(-95.830026)	(-156.61432)	(0.15713058)	(-156.45719)
Net	(-95.926269)	(0.096242478)	(-95.830026)	(-156.61432)	(0.15713058)	(-156.45719)

I. RESULTS AND DISCUSSIONS

A. From CFD analysis, the pressure, velocity, drag and lift forces are observed for all the models of SUV.

B. The results are tabulated as follows:

TABLE 1.1: CFD RESULTS OF BREZZA ORIGINAL MODEL AT DIFFERENT SPEEDS

Speed (Km/hr)	Pressure (Pa)	Velocity (m/s)	Drag (N)	Lift (N)
80	229.2	36.79	395	89.82
120	514.4	40.34	883	200.05
160	912.5	53.84	1557.68	364.28

TABLE 1.2: CFD RESULTS OF BREZZA MODIFIED MODEL AT DIFFERENT SPEEDS

Speed (Km/hr)	Pressure (Pa)	Velocity (m/s)	Drag (N)	Lift (N)
80	223.5	26.96	395.19	91.611
120	502.7	40.48	879.54	208.189
160	892.9	53.99	1557.12	372.22

By comparing results of original and modified Brezza models, the pressure & velocity are decreasing and lift is increasing for the modified model (attaching lip kit for the front bumper) when compared with original model. The change in drag is very less for the modified model. The change in velocity is also very less for higher speeds 120km/hr and 160km/hr.

For the modified model, the pressure is reducing by about 2.5%, the velocity is reducing by about 26.7%, and the lift is increasing by about 2%.

CFD RESULTS OF ECOSPORT ORIGINAL MODEL AT DIFFERENT SPEEDS

Speed (Km/hr)	Pressure (Pa)	Velocity (m/s)	Drag (N)	Lift (N)
80	241.1	28.42	492.4	77.29
120	539.1	42.65	1097.43	84.99
160	956	56.01	2226.90	176.16

CFD RESULTS OF ECOSPORT MODIFIED MODEL AT DIFFERENT SPEEDS

Speed (Km/hr)	Pressure (Pa)	Velocity (m/s)	Drag (N)	Lift (N)
80	249.9	29.37	522.71	156.45
120	556.2	44.07	1163.08	344.27
160	993.5	58.76	2059.85	601.94

By comparing results of original and modified Ecosport models, the pressure, velocity, drag and lift are increasing for the modified model (attaching lip kit for the front bumper) when compared with original model.

For the modified model, the pressure is increasing by about 3.5%, the velocity is increasing by about 3%, the lift is increasing by about 50.6% and the drag is increasing by about 5.8%.

 ISBN: 978-93-91420-02-4

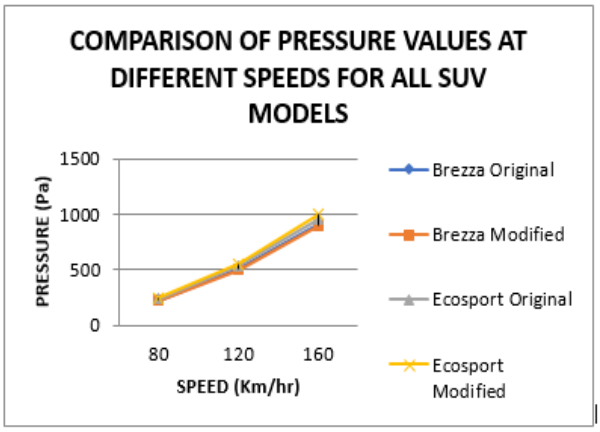

Graph 1.1: Comparison of pressure values at different speeds for all SUV models

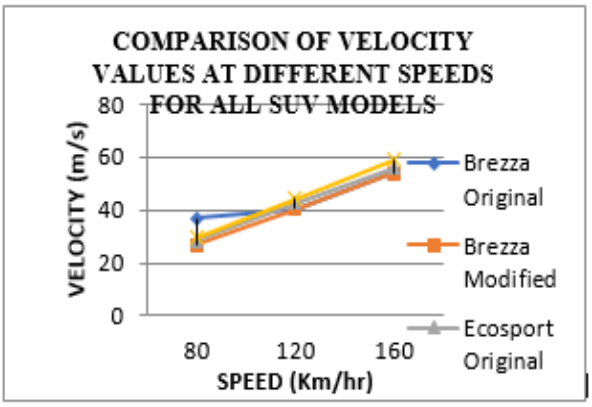

Graph 1.2: Comparison of velocity values at different speeds for all SUV models

V.CONCLUSION

CFD analysis is done by applying different inlet speeds 80Km/hr, 120Km/hr and 160Km/hr. the original models of Brezza and Ecosport are modified by attaching a lip kit for front bumper.

The modification of the models by attaching lip kit showed significant difference on Ecosport model than Brezza model. The lift has been increased and drag force has been reduced by the attachment for Ecosport model. But the pressure and velocity are increasing for modified Ecosport model in reverse with the Brezza model where pressure and velocity are decreased for modified model.

REFERENCES

[1] Pramod Krishnani, CFD Analysis of Drag Reduction for a Generic SUV, Proceedings of IMECE2009 2009 ASME International Mechanical Engineering Congress and Exposition November 13-19, 2009, Lake Buena Vista, Florida, USA IMECE2009-10170

[2] Vipul Kshirsagar, Jayashri V. Chopade, Aerodynamics of High Performance Vehicles, International Research Journal of Engineering and Technology (IRJET) e-ISSN: 2395-0056, Volume: 05 Issue: 03 | Mar-2018 www.irjet.net p-ISSN: 2395-0072

[3] Pikula, Boran & Filipovic, Ivan & Kepnik, Goran. (2011). Research of the external aerodynamics of the vehicle model, Research Gate.

Devlopment of Code for Automated HVAC System using Digital Controller

Venkaiah Mandula
Department of Mechanical Engineering, Narasaraopeta Engineering College (AUTONUMOUS), Narasaraopet, A.P.

Abstract—the present work is intended to develop a code to automate the HVAC System. To achieve that, advanced industrial controller (PLC) software called WPL soft is used, which is the most widely used tool in industries. This software requires a dedicated programming language called Ladder diagram. By using WPL soft, a program in Ladder diagram is developed to automate the HVAC system, also this program will take care the different requirements of industries such as controlling temperature, selection of proper compressor based on the requirement.

Keywords—HVAC, Ladder diagram, PLC.

I.INTRODUCTION TO HVAC

Heating, Ventilating and Air Conditioning, HVAC, is a huge field. HVAC systems include a range from the simplest hand-stoked **stove**, used for comfort heating, to the extremely reliable total air-conditioning systems found in submarines and space shuttles. Cooling equipment varies from the small domestic unit to refrigeration machines that are 10,000 times the size, which is used in industrial processes

Depending on the complexity of the requirements, the HVAC designer must consider many more issues than simply keeping temperatures comfortable. This chapter will introduce **you** to the fundamental concepts that are used by designers to make decisions about system design, operation, and maintenance.

II.HVAC OBJECTIVE & ITS COMPONENTS

A. Objective of HVAC

Before starting to design a system, it is critical that you know what your system is to achieve. Often, the objective is to provide a comfortable environment for the human occupants, but there are many other possible objectives: creating a suitable environment for farm animals; regulating a hospital operating room; maintaining cold temperatures for frozen food storage; or maintaining temperature and humidity to preserve wood and fibre works of art.

Whatever the situation, it is important that the objective criteria for system success are clearly identified at the start of the project, because different requirements need different design considerations.

B.Components of HVAC
The components of HVAC system are shown in below figure:

1.Air Conditioner Equipment

Evaporator Coil: In a system with a furnace, the evaporator coils sit on top of the furnace and is the critical component that cools the air inside a home. The furnace blower passes air across the evaporator coil. During this process, the air cools as it comes in contact With the cold coil and heat transfers from the air to the refrigerant.
Condenser Coil: This part of the air conditioning system **cools** (removes heat) from refrigerant and is located in the outdoor condenser unit.

Compressor: A machine used to supply air or other **gas** at increased pressure, located in the outdoor condenser unit.
Fan: A mechanical device that creates a current of air.

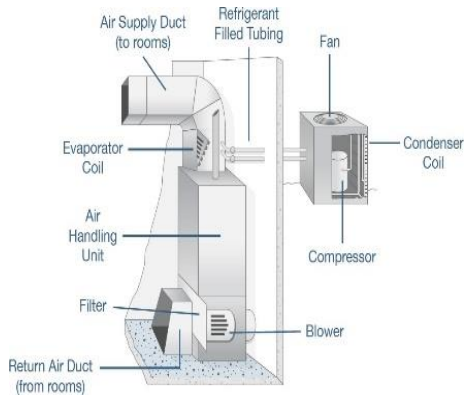

Fig: II.I Components of HVAC

Refrigerant Filled Tubing: Circulates refrigerant **between** outdoor condenser unit and indoor evaporator coil
Gas Forced Air Furnace **Equipment**
Return Air Duct: A duct carrying air from a conditioned space to the mixing air duct or plenum unit.
Filter: A porous device for removing impurities or solid particles from the air that passes through it.
Blower: a mechanical device that creates a current of air. See the fan also.
Air Handling Unit (AHU): a device used to **condition** and circulate air as part of a heating, ventilating, and air-conditioning (HVAC) system. An air handler is usually a large metal box containing a blower, heating or cooling elements, filter racks or chambers, sound attenuators, and dampers. Air handlers usually connect to a ductwork ventilation system that distributes the conditioned air through the building and return it to the AHU.
Air Supply Duct: A **duct** that carries conditioned air from air supply units to room diffusers or grilles.

III.PROGRAMMABLE LOGIC CONTROLLER

PLC **manufacturer**. Once the program has been written A Programmable Logic Controller (PLC) is a small, self–contained, rugged computer designed to control processes and events in an industrial environment – that is, to take over the job previously done with relay logic controllers. Wires from switches, sensors and other input devices are attached directly to PLC. Each PLC contains a microprocessor that has been programmed to drive the output (O/P). Terminals in a specified manner, based on the signals from the input terminals. The PLC program is usually developed on a separate programmer (PG) computer such as a Personal Computer (PC), using special software provided by the, it is transferred or downloaded into the PLC.

III.I PLC Hardware:

The PLC is basically a programmed interface between the field input devices like limit switches, sensors, **transducers**, push buttons etc. And the final control elements like actuators, solenoid valves, dampers, drives, LED's, etc. Programmable controller consists of the following modules:

1. Input modules
2. Output modules
3. CPU with processor and program memory
4. Power supply
5. Bus system

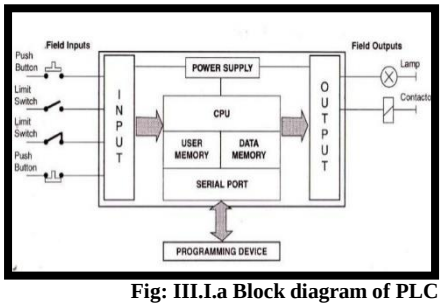

Fig: III.I.a Block diagram of PLC hardware

III.II Operation of PLC:

C. Bringing Input Signal Status to the Internal Memory of CPU:

The field signals are connected to input module. At the output of input module, the field status is converted into a voltage level that is required by the CPU. At the beginning of each cycle the CPU brings in all the field-input signals from input module and stores into its internal memory as process image of input signal. This internal memory of CPU is called as PII (Process Image Input). The programmable controller operates cyclically i.e. when the program has been scanned, it starts again at the beginning of the program.

IV.PROCESSING OF SIGNALS USING PROGRAM & *UPDATING* PIQ:

Once the field-input status is brought into the internal memory of CPU i.e. in PII, the execution of user program, statement-by-statement begins. Based on the user program the CPU performs logical and arithmetic operation on the date from PII. It also processes times and counts as well as flag states based on the instructions. The results of the user program scan i.e. decision are then stored in the internal memory of CPU. This internal memory is called Process Image Output or PIQ.

D.Sending *Process Output Image to Output Module*:

At the end of the program run i.e. at the end of scanning cycle, the CPU transfers the signal states in the process image output to the output module and further to field control.

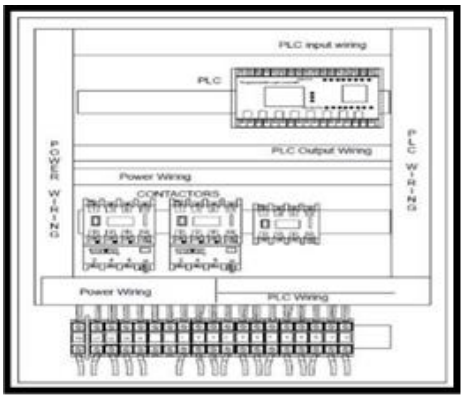

Fig: III.II.a PLC Kit

Programmable logic controller: Delta dvp12sa2

MPU points : 12 (8DI + 4DO)
Max. I/O points : 492 (12 + 480)
Program capacity : 16k steps

High-Speed Pulse Output:
Supports 2 points (Y0, Y2) of 100 kHz and 2 points (Y1, Y3) of 10kHz independent high-speed pulse output.

Extendable to Maximum 8 Modules: DVP-SA2 is extendable to analogue I/O, temperature measurement, input DIP switch, PROFIBUS/ Device Net communication modules and single-axis motion control functions

V.Delta PLC

Programmable logic controller (PLC) is a control system using electronic operations. It's easy storing procedures, handy extending principles, functions of sequential/position control, timed counting and input/output control are widely applied to the field of industrial automation control. Delta's DVP series programmable logic controllers offer high-speed, stable and highly reliable applications in all kinds of industrial automation machines. In addition to fast logic operation, bountiful instructions and multiple function cards, the cost-effective DVP- PLC also supports various communication protocols, connecting Delta's AC motor drive, servo, human machine interface and temperature controller through the industrial network in to a complete "Delta Solution" for all users.

Delta's DVP series programmable logic controllers offer high-speed, stable and highly reliable applications in all kinds of industrial automation machines. In addition to fast logic operation, bountiful instructions and multiple function cards, the cost-effective DVP-PLC also supports various communication protocols, connecting Delta's AC motor drive, servo, human machine interface and temperature controller through the industrial network in to a complete "Delta Solution" for all users

Figure no: IV.1a DVP-12SA2

Components of Delta PLC:

Miniature Circuit Breakers (MCB)
Switch Mode Power Supply
Relay card
Terminal Block
Ground Terminal blocks
Fused connection terminals
Wire duct

IV.II Programming languages:

Based on the "International Electro Technical Commission (IEC)" standard, PLC programming languages are classified into five main standards.

1. Ladder diagram (LD)
2. Instruction List (IL)
3. Structured Text (ST)
4. Function Block Diagram (FBD)
5. Sequential Function Charts (SFC)

These languages are accepted internationally. Among all of them, mostly Ladder diagram (LD) programming language is used in the industry.

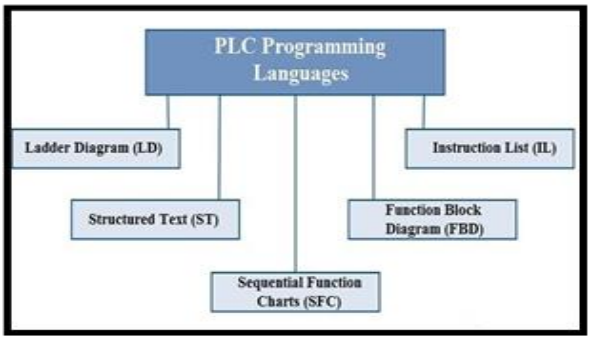

Figure no: IV.1b PLC programming language

Ladder diagram (LD):

Ladder diagram (LD) is also known as "Ladder Logic ". It is used with programmable logic controllers.

Generally, Ladder diagram is most popular all over the world (including India). This language is easy to learn. If you look at the ladder diagram, it looks similar to the electrical circuit diagram

Ladder Diagrams:

The ladder diagram is the universal programming language of PLC. It has a short abbreviation as LD and also known as Ladder Logic. It is one of the oldest programming languages for PLC. In the ladder diagram, the programming language that used to create the program to control the PLC system is known as Ladder Diagram Language or Ladder Logic Language. It has signified by the graphical representation, just like electrical wiring for logic control. (At the end of this article, I will share LD examples that will get you a clear understanding.)

Different Symbols used in Ladder Diagram:

This programming uses different graphic elements. These graphic elements are also called as Symbols.

Basic ***Important Parts of Ladder Diagram in PLC Programming:***

- Rungs
- Branches
- Inputs and Outputs for PLC programming

Rungs

In Ladder diagram, the horizontal lines called Rungs. You can put as many numbers of rungs as per your project requirements.

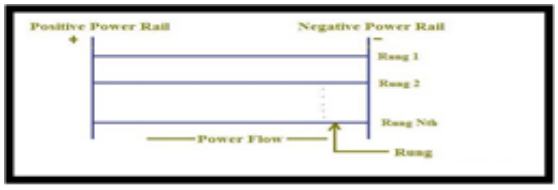

Figure no: IV.II.a The above diagram is shown with 'N' number of rungs.

Branches

There are three types of branches. They are as follows.

Series **Branch:** In the series branch, inputs or outputs are connected in the series.

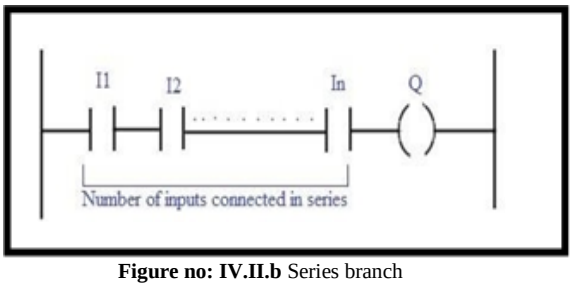

Figure no: IV.II.b Series branch

Parallel Branch

In the parallel branch, inputs or outputs are connected parallels.

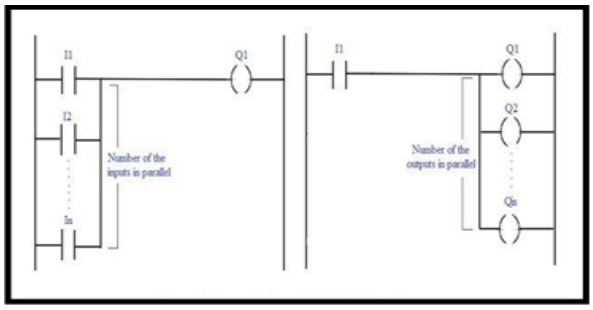

Figure no: IV.II.c Parallel branch

Nest Branch

The combination of series and parallel branches in the same or different rungs are called as Nest Branch.

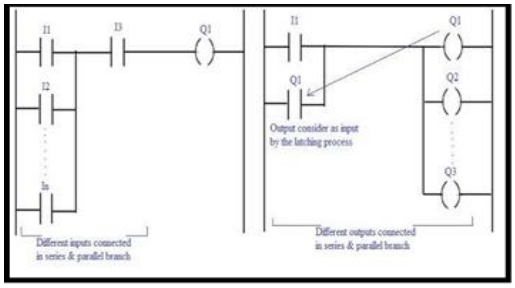

Figure no: IV.II.d Nest branch

Inputs and Outputs for PLC Programming

For writing the program, Inputs and outputs are playing the most important role.

Inputs refer to the switch or Push Button (PB).
Output referred to the Coil or Lamp or Load.
Input is Normally Open (NO) Contact or Normally Closed (NC) Contact.

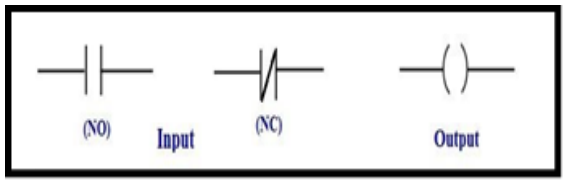

Figure no: IV.II.e Inputs and Outputs

WPL Software:

Here the software used is DELTA WPL Soft by DVP programmable logic controllers. This is the official software used to create and simulate the ladder diagrams which are dumped in Delta PLC's. For this, the WPL Soft is to be installed in the laptop. And the software is opened. By clicking on the file button, we can create a new file and then the ladder diagram is generated according to our requirement.

Rules **of ladder diagram programming:**

There are 6 Rules for PLC Ladder Diagram Programming.

1. Inputs can be used in Series as well as Parallel to form a connection
2. Outputs (or coil) can be used only in Parallel
3. One Input can be used in multiple times in one program
4. One Output cannot be used multiple times in one program, except in Set/Reset and Latch/ Unlatch functions
5. Input Address cannot be used as an Output Address
6. Outputs Address can be used as Inputs Address

VI. EXPERIMENTAL PROCEDURE:

Here the case studies are regulating temperature of room by two compressors, limiting the level co2 by using smoke sensor. The compressors and smoke sensor is controlled by plc. The ladder diagram created by using WPL software. After creating ladder diagram its simulated in software itself to know whether the created code is write or wrong.

Case **1***:*

The average level **co2** should be maintained in a room that must be less than *1000* ppm. To decrease the level of co2 in a room a smoke sensor is used. If the co2 level increase more than permissible level indication is made by the smoke sensor and the compressor gets started.

Case 2:

In this case study, the temperature of the room must be maintained below 33° C. if the temperature of the room increases more than 33° c the compressor gets started. The compressor runs on three different speeds based on the temperature in a room.

Temperature between 33 to 35° c compressor 1 runs with normal speed.
Temperature between 36 to 38° c compressor 1 runs with medium speed.
Temperature between 39 to 41° c compressor 1 runs with high speed.

Case 3:

Within 10 minutes if compressor 1 could not able to maintain below 33° c the HVAC immediately gets shifted to a backup compressor is also running on three different speeds.

Temperature between 33 to 35° c compressor 1 runs with normal speed.
Temperature between 36 to 38° c compressor 1 runs with medium speed.
Temperature between 39 to 41° c compressor 1 runs with high speed.

VII. RESULT AND DISCUSSION:

Ladder diagram ***for automated HVAC system***

The ladder diagram of automated HVAC system is programmed by using WPL software is shown in below.

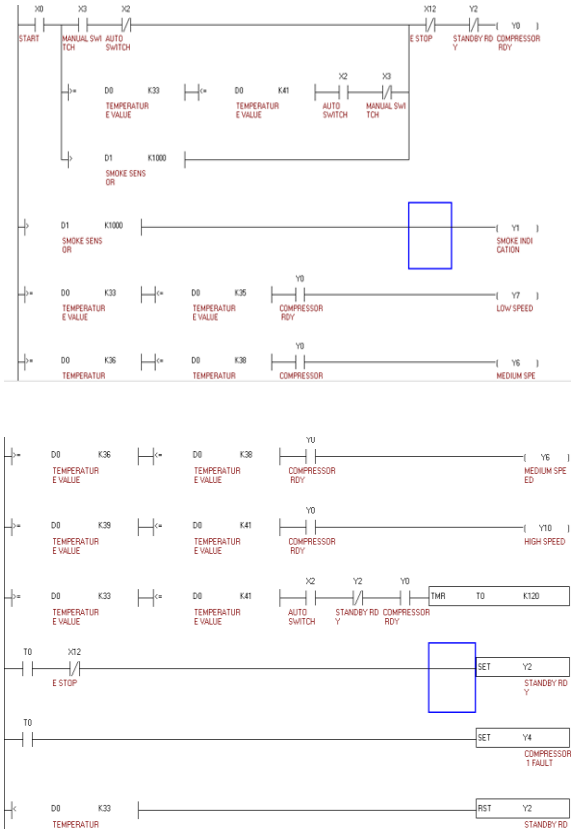

1. The current enter into the circuit through the main switch (xo) as a manual switch is on the Condition and auto switch, Estop, standby is off Condition.
2. The temperature sensor of HVAC system monitors temperature of room every minute
3. A timer is also works along with compressor.
4. The compressor runs on three different speeds Based on the temperature in a room.

Temperature between 36 to 38° c compressor runs with medium speed.

Temperature between 39 to 41° c compressor 1 runs with high speed.

If temperature of room isn't maintained below given limit after 10 minutes work of compressor 1 then it shifts to standby compressor.

The smoke sensor detects co2 level if level increase more than1000 ppm then it send signal plc. And plc. activate compressor.

II. CONCLUSION:

In this paper, PLC programs are successfully developed for different industrial applications. In case study one PLC program is developed for limiting the co2 levels in the room, in case study 2 PLC program is developed for regulation temperature by compressor 1 and case study 3 PLC program is developed for regulation temperature by standby compressor an automated HVAC system will continuously monitors the room temperature. The PLC is programmed by using ladder diagram with the help of WPL software then the ladder diagram is dumped into PLC to obtain results. The Ladder diagram is extensively used and easy to understand. The compressors of HVAC system are controlled by PLC, when the temperature raises than the permissible limit, then the compressor start working, by removing heat they reduce the temperature and get stopped. . A smoke sensor is also used to limit the co2 level in the room. Thus an automated HVAC not only monitoring room temperature but saves the power.

References

1. International Journal of Research in Engineering, Science and Management Volume-2, Issue-1, January-2019 www.ijresm.com | ISSN (Online): 2581-5792
2. ODuran, and A. Batocchio, "Object oriented development methodology for PLC software", Advances in Information and Communication Technology, 1995, 265-272.
3. R. Augustin, "Programmable Logic Controllers versus Personal Computers for process control", Computers in Industrial Engineering, Elsevier Science Ltd., 33, 1997, 421- 42.
4. Georg Frey, "Formal methods in PLC control demonstrated at a flexible manufacturing line", Marik et.al(eds.), Knowledge and Technology Integration in Production and Services © Springer Science Business Media, New York, 2002,501-508.
5. S N Sivanandam, S Sumathi, and S N Deepa, "Design and implementtion of PLC cum micro-controller based electrically synchronized lift", Indian Journal of Engineering and Materials Sciences, 12, Aug. 2005, 269 – 277.
6. 6. Suresh Kumar, Jitendra Prasad Rajwar, Abhay Kumar Thakur, "Building Management System using PLC and SCADA", Int. J. Scientific and Engineering Research, 4(5), May. 2013, 217-219.
7. 7. Adrian Ioannou, (1984) HVAC system. In: Ioannou A. (eds) HVAC Specifications. Springer, Boston, MA.Douglas M. Considine, Glenn D. Considine, Part of the Chapman and Hall Advanced HVAC Technology Series book series (AITS).
8. 8. Mortimer J., Rooks B. (1987) HVAC system Specifications. In: The International HVAC system Report. Springer, Berlin, Heidelberg.Cheng Ding, Jianhua Wu, Part of the Lecture Notes in Computer Science book series (LNCS, volume 10985).
9. 9.Hartley J. (1984) HVAC. In: Flexible Automation in Japan. Springer, Berlin, Heidelberg.
10. 10.International Journal for Research in Applied Science & Engineering Technology (IJRASET). HVAC Modern Trailer Bharth G, Sunil Kumar K, Srinivasa Chari V.
11. 11.International Journal for Research in Applied Science & Engineering Technology (IJRASET). HVAC Modern Trailer Lakshiminarayana T.
12. 12.https://blog.bisresearch.com/heating-ventilation-air-conditioner-market-future-multi- billion-dollar-industry

Performance and Emission Characteristics of Diesel Engine with Linseed Oil –Diesel blends as Fuel with VCR

[1]K.Kiran chand, [2]P.Srinivasa Rao, [3]Thirupathi Reddy.K and [4]Jyothu Naik
[1,2] *Department of Mechanical Engineering*, Narasaraopeta Engineering College (A),Narasaraopet, India
[3]*Department of Mechanical Engineering*, RGM College of Enginering and Technology, Nandhyal, India.
[4]*Department of Mechanical Engineering*, Rayalaseema University College of Engineering, Kurnool, India

Abstract— **this paper investigates the performance and emission characteristics of a diesel engine with Linseed oil and its diesel blends. The Linseed oil-diesel blends C5 (5% Linseed l oil and 95% diesel), C10 (10% Linseed oil and 90% diesel), L15 (15% Linseed oil and 85% diesel), and L20 (20% Linseed oil and 80% diesel) was prepared to test in diesel engines. The present experimental results were obtained on the performance and the emissions of CO, HC and NOx in diesel engine. The results showed that the brake thermal efficiency was decreased as the blend increased, and the brake specific fuel consumption was slightly higher than the diesel fuel. The CO and HC emissions are higher than diesel. However, NOx emissions of the blends were found to be decreased significantly compared to diesel as blend ratio increased. Smoke emission was found to be increased slightly when compared to diesel.**

Keywords— Diesel engine, Linseed oil, Diesel blend.

Introduction

The energy demand increases day by day in India due to increase in population as well as increase in modernization of the world. Today India is much dependent on petrochemical reserve (*i.e.* coal, gasoline, crude oil etc.) to satisfy our energy demand. In our country we have a very limited crude oil reserve. So to satisfy our demand we are fully dependent on crude oil import from foreign countries. Among various gasoline fuels, diesel fuel is most widely used as it proves higher energy density (*i.e.* more energy can be extracted from diesel as compared with the same volume of gasoline fuel) than other gasoline. Therefore diesel engines have versatile uses in heavy-duty transportation, power generation and also in agricultural sectors. That's why the consumption of diesel is much higher than other gasoline. As the underground crude oil reserve is non-renewable, so its reserve is decreasing rapidly due to gradual increase in its consumption. This phenomenon drives us to search for an alternative and renewable substitute of diesel fuel.

The use of vegetable oils as an alternative fuel for diesel engines dates back to around a century. Due to rapid decline of crude oil reserve and increase in price, the use of vegetable oils is again prompted in many countries. Depending upon soil condition and climate, different nations are looking for different vegetable oils- for example, soybean oil in U.S.A., rapeseed and sunflower oil in Europe, palm oil in Malaysia and

Problems associated with using straight vegetable oil (SVO) in diesel engine can be classified in two groups, namely: operational and durability problems. Operational problems are related to starting ability, ignition, combustion and performance. Durability problems are related to deposit formation, carbonization of injection tip, ring sticking and lubrication oil dilution [2, 3]. Various researchers have shown that the use of vegetable oil and their derivatives is competitive compared to mineral diesel [4, 5]. Many researchers have tried to use biodiesel derived from mahua oil as fuel for diesel engine. In most of the countries including India, biodiesel is expensive than the diesel and also biodiesel is not available commercially in the market. Most of the work reported in the literature involves only the laboratory studies [6-8]. Pramanik *et al.* Have studied the performance and emissions of a diesel engine with Jatropha methyl ester at various blends. It has been reported that 50% of Jatropha oil blends can be substituted for diesel fuel in a C.I. engine. It has been reported that the Jatropha oil exhibited higher specific fuel consumption and lower exhaust gas temperatures compared with diesel fuel. Etherification is one of the methods to convert the vegetable oil into its methyl ester, known as biodiesel. Several researchers have used biodiesel as an alternate fuel in the existing CI engines without any modifications the objectives of this experimental study are to assess the performance and emission characteristics of a diesel engine with Castrol oil diesel blends and compared with diesel fuel.

Experimental setup and procedure:

The engine test was conducted on a four stroke, single cylinder, water-cooled direct injection, Kirloskar Engine diesel engine. The specifications of the test engine are given in Table 2. The schematic of the experimental set up is shown in Fig. 1 A three whole injector nozzle was located at the center of the combustion chamber with high pressure fuel pump and has an operating pressure of 180 bar. The engine was coupled to an electrical dynamometer and loaded by electrical resistance to apply different engine brake loads. AVL DI 444 exhaust gas analyzer was used for this experiment is to measure the exhaust emissions like CO, HC, NO. The measuring method is based on the principle of light absorption in the infrared region, known as "non-dispersive infrared absorption". The broadband infrared radiation produced by the light source passes through a chamber filled with gas, generally methane or carbon dioxide. Smoke opacity was measured by AVL 437C model. The

measurement is based on the principle of light absorption by particle. Photo electronic smoke detection is based on the principle of optical detection. It is also known as the "scattered" light principle.

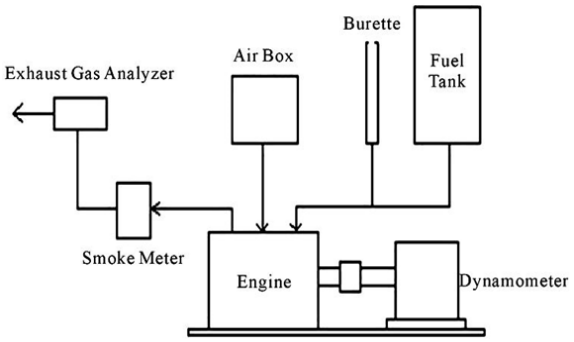

Fig. 2: Schematic view of experimental setup

Table 4: Specification details of Kirloskar TV1 engine

Type	**Vertical, single cylinder 4 stroke**
Number of cylinders	01
Rated power (kW)	3.7
Bore(mm)/Stroke (mm)	80/110
Compression ratio	16.5:1
Speed (rpm)	1500
Type of cooling	Water cooling
Injection pressure	180bar
Injection timing	23^{o} bTDC

To estimate the performance parameters, operating parameters such as engine speed, power output, and fuel consumption were measured. Significant engine performance parameters such as Brake specific fuel consumption (BSFC) and Brake thermal efficiency (BTE) for the test fuels were calculated. Emission parameters such as CO, HC, NO and smoke opacity were observed for various fuel blends. Initially, experimental tests were conducted with neat diesel, in the next phase, the engine was operated diesel-mustard oil blend ratio of 95:05 (L5), 90:10 (L10), 85:15 (L15) and 80:20 (L20).

RESULTS AND DISCUSSION

Brake thermal efficiency

The variations of BTE at different loads and various fuel blends are shown in Fig. 3. The BTE for diesel is higher than that of all other Linseed oil diesel -blends at all loads. It is observed that the BTE is decreases with increase in Linseed oil diesel blends at full load. The BTE for L5 blend is higher than other blends L10, L15 and L20 blends. The reason for this higher viscosity, lower calorific value of the blends and low cetane number of fuel blends. The BTE of L5, L10, L15 and L20 are 26.6%, 25.5%, 24.2% and 23.2% respectively, whereas for diesel is 28.1% at full load. At 75% of the load all the fuel blends have higher brake thermal efficiency than full load conditions.

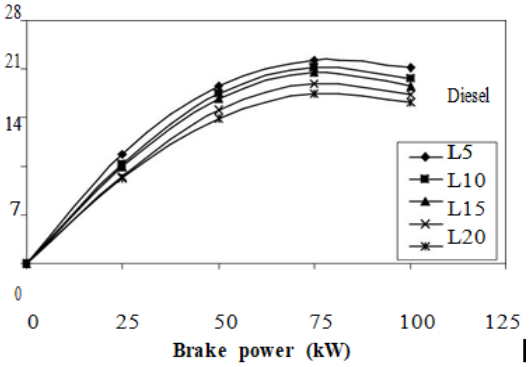

Fig. 3: Brake thermal efficiency Vs brake power

Brake specific fuel consumption:

The variation in BSFC for the test fuels with respect to brake power is shown in Fig. 4 for diesel and various Linseed oil-diesel blends. The BSFC of all fest fuels are decreases with increase in loads. At 75% of the load Linseed oil diesel blends have lower specific fuel consumptions. The BSFC of all Linseed oil-diesel blends are higher than diesel fuel at full load. This may be due to poor atomization and vaporization of high viscosity, low cetane number and lower calorific value of the blends. The BSFC of L5, L10, L15 and L20 are 0.32 kg/kWh, 0.346 kg/kWh, 0.362 kg/kWh and 0.387 kg/kWh respectively, whereas for diesel is 0.306 kg/kWh.

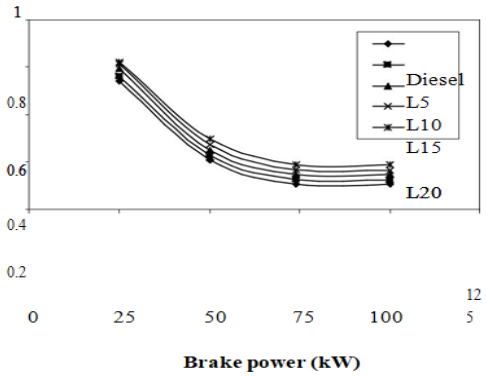

Fig. 4: Brake specific fuel consumption Vs Brake power

Exhaust gas temperature

Fig. 10 shows the variation between exhaust gas temperature and brake power for different fuels. It is seen that the exhaust gas temperature increases with increase in load for all test fuels. At higher % load condition, L20 shows higher exhaust gas temperature than other fuel blends. The exhaust gas temperature of L5, L10, L15 and L20 are 345^{o}C, 358^{o}C, 368^{o}C and 382^{o}C, respectively, whereas for diesel is 338^{o}C at full load.

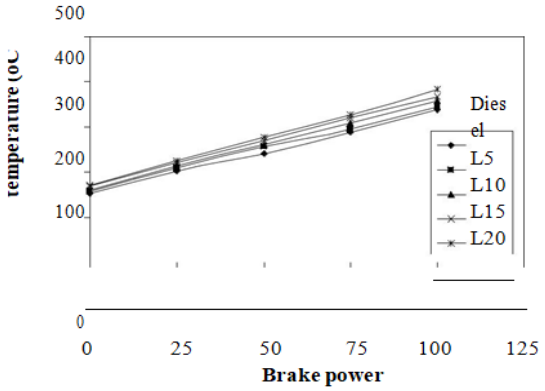

Fig. 5: Exhaust gas temperature Vs brake power

This may be due to slow burning of high viscous Linseed oil blends, resulting in higher exhaust gas temperature.

Carbon monoxide emission (CO)

The variation of CO emission with brake power for diesel and different blends of Linseed oil is shown in Fig. 6. It is observed that the CO emissions increase with increase in load for all the test fuels. The CO emissions for L5, L10, L15 and L20 are 0.17% Vol, 0.24% Vol, 0.32% Vol and 0.39% Vol, respectively, whereas for diesel is 0.11% Vol at full load. Linseed oil-diesel blends have higher CO emissions due to poor atomization and vaporization due to its high viscosity and have less time to undergo complete combustion.

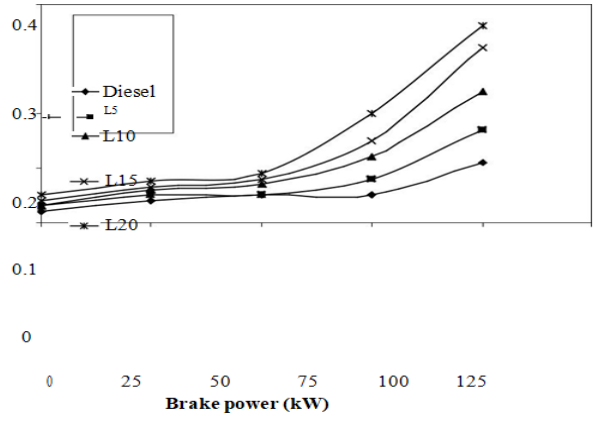

Fig. 6: Carbon monoxide emission Vs brake power

Hydrocarbon emission (HC)

The Fig. 7 shows the variation of hydrocarbon emission with respect to brake power for diesel and different blends of Castrol oil. It can be seen that the HC emission for all the Linseed oil- diesel blends are higher than that of diesel for medium and higher loads. This may be due to incomplete combustion of vegetable oil blends due its high viscosity and poor atomization of the blends. The HC emission for L5, L10, L15 and L20 are 0.17% Vol, 0.24% Vol, 0.32% Vol and 0.360% Vol, respectively, whereas for diesel is 0.11% Vol at full load.

Nitrogen oxides emissions (NO)

The variations of nitrogen oxide emissions with brake power for diesel and different Linseed oil blends is shown in Fig. 8. The NOx emission is a function of lean fuel with higher temperature, high peak combustion temperature and spray characteristics. A fuel with high HRR at rapid combustion and lower HRR at mixing controlled combustion will causes of NOx emission. NOx emission increases with increase in load for all test fuels. The NO emission for L5, L10, L15 and L20 blend is 9.6%, 21%, 29% and 37, respectively lower than neat diesel at full load. The decrease in NO emission due to slower burning of high viscosity of Linseed oil diesel blends, resulting in lower peak combustion temperature.

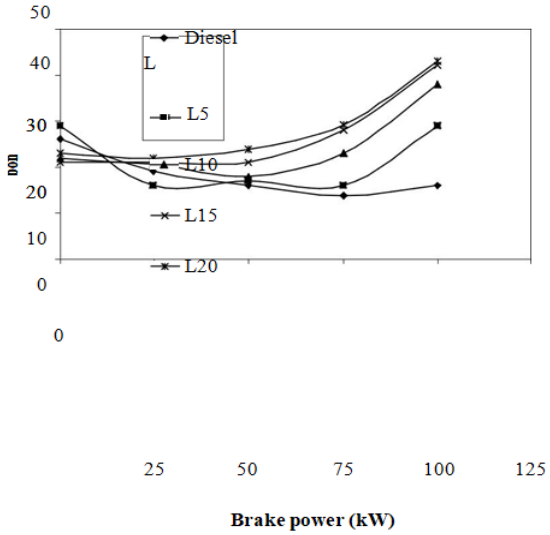

Fig. 7: Hydrocarbon emission Vs brake power

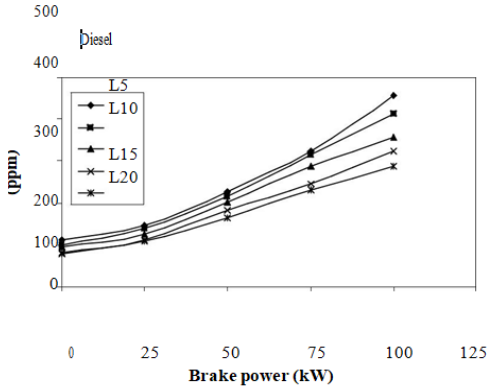

Fig. 8: Nitrogen oxide emission vs. brake power

Smoke opacity

The variation of smoke opacity with brake power for all the test fuels is shown in Fig. 9. The smoke is produced due to incomplete combustion of fuel. It can be seen that at higher load, the smoke intensity for blended fuels are higher compare to neat diesel. The smoke opacity of L5, L10, L15 and L20 are 4 BSU, 4.3 BSU, 4.5 BSU and 4.9 BSU respectively, whereas for diesel is 3.6 BSU at full load. This may be due to poor atomization and of high viscosity and low volatility of Linseed oil blends, resulting in higher smoke emission at full load.

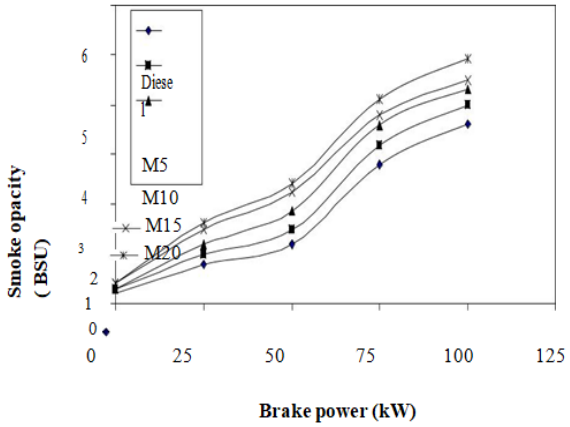

Fig. 9: Smoke opacity vs. brake power

CONCLUSION

In the present investigations the Linseed oil –diesel blends were prepared by blending methods by vol/vol. Fuel properties were determined for the Linseed oil diesel blends. Performance and emission characteristics were investigated on diesel engine by smoke analyzer and gas analyzer. The results of the experimental study were concluded as follows: The brake thermal efficiency of all Linseed oil diesel blends was slightly higher than diesel due to high viscosity, and low calorific value of the fuel. Brake specific fuel consumption of the blends were determined to be higher for all blends at full load. The exhaust temperature was increased with L10. L15 and L20 biodiesel mixture reduced the temperature as the blend ratio increased. The CO and HC emissions of all blends were higher than diesel. The smoke emissions were found to be slightly higher than diesel fuel. When compared to diesel, NOx emissions of all the blends of Linseed oil were found to be increased. As the blend ratio increased, the NOx emissions were also increased respectively.

REFERENCES

1.V.K.Shahira, C.P.Jawaharb, V.Vinodc ,P.R.Sureshc Experimental Investigations on the Performance and Emission Characteristics of a Common Rail Direct Injection Engine Using Tyre Pyrolytic Biofuel Journal of King Saud University - Engineering Sciences (2018), doi:

2.Shivashimpi, M. M., Banapurmath, N. R. and Alur, S. A. (2019). Effect of Injection Parameters: Injection Timing and Injection Pressure on the Performance, Emission and Combustion Characteristics of CRDI Diesel Engine Operate with Palm Oil Methyl Ester (POME). European Journal of Sustainable Development Research, 3(3), em0091. https://doi.org/10.20897/ejosdr/3977.

3.A. S. Divakar Shetty, , L. Dineshkumar, , Sandeep Koundinya, and , and Swetha K. ManeExperimental investigation on CRDI engine using butanol-biodiesel-diesel blends as fuel International Conference on Functional Materials, Characterization, Solid State Physics, Power, Thermal and Combustion Energy AIP Conf. Proc. 1859, 020028-1–020028-7; doi: 10.1063/1.4990181 Published by AIP Publishing. 978-0-7354-1533-1/$30.00.

4.Divakar Shetty A. S , Ravi Kumar R, Kumarappa S, Antony A.J IOP Conf. Series: Materials Science and Engineering 149 (2016) 012223 doi:10.1088/1757-899X/149/1/012223.

5. B. Ashoka, K. Nanthagopala,D. Arumuga Perumalb, J.M. Babuc, Anmol Tiwaria, Akhil Sharmaa https://doi.org/10.1016/j.enconman.2018.11.047 Received 29 August 2018; Received in revised form 30 October 2018; Accepted 19 November 2018.

6. Ananthakumar, S., Jayabal, S. and Thirumal, P., 2017. Investigation on performance, emission and combustion characteristics of variable compression engine fuelled with diesel, waste plastics oil blends. Journal of the Brazilian Society of Mechanical Sciences and Engineering, 39(1), pp.19-28.

7. Mani, M., Subash, C. and Nagarajan, G., 2009. Performance, emission and combustion characteristics of a DI diesel engine using waste plastic oil. Applied thermal engineering, 29(13), pp.2738-2744.

8. Damodharan, D., Sathiyagnanam, A.P., Rana, D., Kumar, B.R. and Saravanan, S., 2017. Extraction and characterization of waste plastic oil (WPO) with the effect of n-butanol addition on the performance and emissions of a DI diesel engine fueled with WPO/diesel blends. Energy conversion and management, 131, pp.117-126.

9 .R.JyothuNaik, and K.Thirupathi Reddy. Experimental Study on the Effect of Inlet Air Temperature on Waste Plastic Pyrolysis Oil with Diesel Fuelled HCCI Combustion Engine, International Journal of Recent Technology and Engineering (IJRTE), ISSN: 2277-3878, Volume-7, Issue-ICETESM, March 2019.

10. Jyothunaik Ramavathu & Thirupathi Reddy Kota 2019 .Combustion performance and emission characteristics on HCCI engine of waste plastic pyrolysis oil biodiesel blends with external PFI and vaporiser, International Journal of Sustainable Engineering, 12(5):1-14.

11. Ramavathu, J. N., & Kota, T. R. (2020). Influences of pilot injection, main injection and EGR on performance combustion and emissions in an HCCI-DI combustion engine using with Diesel and WPPO biodiesel blends. International Journal of Ambient Energy, pp.1-38.

Experimental Investigation in Single Cylinder VCR Multifuel Engine Using Bio-Diesel as Linseed Oil

[1]Donepudi Jagadish, [2]M.Venkaiah, [3]Ch. Shekar and [4]Jyothu Naik
[1,2,3]Department of Mechanical Engineering, Narasaraopeta Engineering College (A), Narasaraopet, India.
[4]Department of Mechanical Engineering, Rayalaseema University College of Engineering, Kurnool, A.P. India

***Abstract*— The linseed oil is characterized for engine performance, combustion and emission analysis at various compression ratios (CR-14, 16, and 18) and fuel blends (B9, B18, B27, B36%, and Diesel). The brake thermal efficiency (BTHE) at CR18 is higher at full load condition for all blend ratios that may be due to lower brake specific fuel consumption (BSFC) and complete combustion of mixture with excess oxygen in the biodiesel. The BSFC is decreased on increasing brake power (BP) and CR. The exhaust gas temperature is decreased (3%) on increase in CR from 14 to 18. The cylinder peak pressures and net heat release rate are lower than that of diesel because of lower heating value. The hydro carbon (HC), carbon monoxide (CO), and carbon dioxide (CO2) emissions decreases while increasing the compression ratio, however, nitrogen oxide (NOx) emission is increased with CR for all fuel blends and these properties were progressively lower for higher concentration of biodiesel. Overall engine performance is optimum at CR of 18 for B18 fuel blend.**

Keywords— VCR Engine, Multi Fuel, Fuel Efficiency.

I. INTRODUCTION

A VCR engine has been widely tested these days to bring out the best fuel efficiency and also to minimize the pollutants[1-2]. Various tests have been made these days by the researchers using this VCR engines to bring out the comparison results using petrol or diesel. This works investigates on a single cylinder multi fuel VCR Engine at 2 compression ratios 16:1 and 18:1 respectively. Petrol engines have the tendency to limit the max pressure during a compression stroke which would result in detonation rather than burning, and hence to achieve this max

Power output along with its same speed, more amount of fuel is to be burnt. This would result in the requirement of more amount of air for burning the fuel[3-7]. This brings in the use of the turbochargers and superchargers for increasing the pressure at the inlet. This would result in decrease in the compression ratio of the detonation in the fuel or air mixture i.e. the volume above the piston is made greater. This can be done to a greater or lesser extent with a very massive increase in power being possible.

Variable Compression Ratio is becoming very much desirable as the oil cost increase and car owners have an interest in fuel economy[12]. In addition to this, the Global Climate Warming may require some measures from the international community. In this Automobile industry, it has stricter limits in the case of car emissions, especially the emission of carbon di oxide. VCR is one cost effective way of to achieve these targets of pollutants. In addition, VCR permits the use of blended diesel with ethanol[8-11]. The cylinder head of an VCR engine is varied by the hydraulic system that is connected to the crank shaft and it could also provide some potential in order to control the temperature of the emitted exhaust gas, contributing to protecting component temperatures. A VCR Engine's efficiency and its performance can be continuously varied by the compression ratio by changing the combustion chamber volume..

- MATERIALS AND METHODOLOGY

The VCR engine which is capable of varying the compression ratio has been used to test the performance of diesel at two compression ratios (16:1 and 18:1). This test is then compared with one another to obtain the best performance results. Compression Ratio can be changed in a number of ways:

- Changing the piston head design.
- Changing the stroke length of the cylinder
- Changing cylinder diameter
- Changing the air fuel ratio.

Table 1 Engine Specification

Parameter	Specification
Compression Ratio	Variable from 5:1 to 20:1
No of Cylinder	Single Cylinder
Cooling	Water Cooling
Spark Timing	Variable from 0 to 70 Deg.
Fuel	Petrol / Diesel
Speed	1400 to 1500 RPM
Lubrication	Forced
Ignition Type	Spark Ignition or Compression Ignition

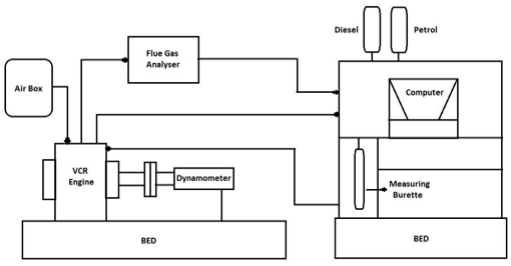

Figure 1 Set up of the VCR Engine

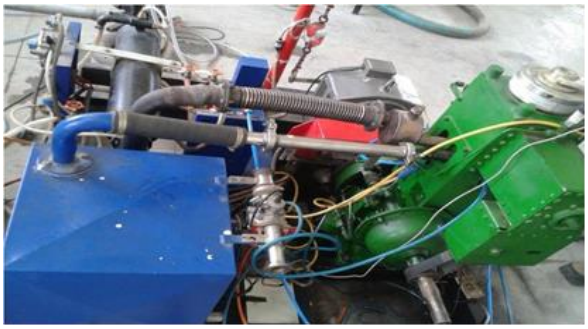

Figure 2 VCR Engine

RESULT AND DISCUSSION

- *For Compression Ratio 18:1*

Table 2 Engine Performance using diesel at compression ratio 18:1

Load (Kg)	Speed (rpm)	BP (KW)	IP (Kw)	FP (Kw)	Air (Kg/hr)	SFC (Kg/Kw hr)
0	1620	0	1.76	1.76	24.88	0
2.52	1590	1.081888	2.47	1.39	24.26	0.45
4.97	1560	2.100679	3.48	1.42	23.19	0.28
7.51	1560	3.171527	4.48	1.25	22.92	0.28
10.04	1560	4.238695	5.33	1.188	21.82	0.29

Table 3 Engine Performance using diesel at compression ratio 18:1

Load (Kg)	Max Pressure (bar)	Mech (%)	BTE (%)	Vol (%)	Calorific value (KJ/Kg)	Cooling water (ml/sec)
0	57.31021	0	0	92.61602	44000	60
2.524037	59.33685	43.66655	18.14223	92.00136	44000	60
4.978955	60.94967	59.00144	27.61648	89.62067	44000	60
7.517039	61.18668	71.79788	34.0362	88.59778	44000	60
10.0464	61.24949	77.60807	36.61852	84.35046	44000	60

Brake power = T*ώ, Indicated power can be defined as the theoretical maximum output power of an engine. The indicated power is the total power obtained from the extension of the gases in the cylinders by avoiding any abrasion, heat loss or entropy of the system. In thermodynamics, the thermal efficiency (η_{th}) can be described as an dimensionless rate of performance of a device that consumes thermal energy like an internal combustion engine, a steam turbine or a steam engine, a boiler, a furnace, or a refrigerator. In other words, efficiency means how well an energy change or transfer process is achieved. Mechanical efficiency = BHP/IP, BSFC is a rate of fuel ability of a shaft reciprocating engine. It is defined as the measure of fuel consumption to the measure of power produced. It can be also known as power- specific fuel consumption.

For Compression Ratio 16:1

The above tabular column shows the engine performance of standard diesel with compression ratio 16:1 Horsepower (hp) is the name of measurement of power for several units, the rate at which work is done. The conventional conversion factor, generally for electrical power, is 1 hp=746 watts. Mechanical efficiency is defined as the measure of effectiveness of a machine to transform the energy and power from the input of the device into the output force and movement. Efficiency could be defined as the ratio of measure of output performance to the performance of an ideal machine. *Volumetric* efficiency can be used to define the comparison performance or other measurable parameter per unit of the physical volume.

Table 4 Engine Performance using diesel at compression ratio 16:1

Load (Kg)	Speed (rpm)	BP (KW)	IP (Kw)	FP (Kw)	Air (Kg/hr)	SFC (Kg/Kw hr)
0	1620	0	3.28	3.28	22.26	0
2.49	1590	1.07	3.85	2.80	21.80	0.67
5.00	1560	2.11	5.03	2.92	21.06	0.44
7.49	1560	3.16	5.73	2.66	19.87	0.37
10.02	1530	4.14	6.27	2.11	17.09	0.37

Table 5 Engine Performance using diesel at compression ratio 16:1

Load (Kg)	Max Pressur (bar)	Mech (%)	BTE (%)	Vol (%)	Calorific value (KJ/Kg)	Cooling water (ml/sec)
0	46.87	0	0	82.8	44000	60
2.47	48.47	27.95	12.06	82.67	44000	60
5.00	49.59	41.58	18.51	81.22	44000	60
7.47	50.80	53.79	21.95	76.81	44000	60
10.02	51.36	66.17	21.61	67.38	44000	60

Table 6 Engine Performance using diesel at compression ratio 14:1

Load (Kg)	Speed (rpm)	BP (KW)	IP (Kw)	FP (Kw)	Air (Kg/hr)	SFC (Kg/Kw hr)
0	1620	0	3.28	3.24	22.26	0
2.49	1590	1.07	3.85	2.85	21.80	0.67
5.00	1560	2.11	5.037	2.95	21.06	0.44
7.49	1560	3.16	5.78	2.67	19.81	0.37
10.02	1530	4.14	6.26	2.17	17.07	0.37

Table 7 Engine Performance using diesel at compression ratio 14:1

Load (Kg)	Max Pressure (bar)	Mech (%)	BTE (%)	Vol (%)	Calorific value (KJ/Kg)	Cooling water (ml/sec)
0	57.31	0	0	92.61	44000	60
2.52	59.33	43.66	18.14	92.00	44000	60
4.97	60.94	59.00	27.61	89.62	44000	60
7.51	61.18	71.79	34.03	88.59	44000	60
10.04	61.24	77.60	36.61	84.35	44000	60

- Mechanical Efficiency = (Brake Power/Indicated Power)*100
- Sample Calculation: At CR 16:1
- Load = 2.5Kg, BP=1.073KW, IP=3.853KW

- Mechanical Efficiency = (1.073/3.853)*100
- Mechanical Efficiency at load 2.5Kg = 27.28%

Real devices can dissipate power through friction, wear and also by part deformation. It can be seen in fig that the mechanical efficiency of compression ratio 18:1 is more when compared with the compression ratio 16:1

- Brake Thermal Efficiency = 3600*Brake Power*100/(Fuel Consumption*Calorific Value)
- Sample calculation at CR16:1
- Load=2.5 Kg BP=1.073KW FC=0.728 Kgs/Hr CV= 44000 KJ/Kg
- Brake Thermal Efficiency=3600*1.073*100/(0.728*44000)
- Brake Thermal Efficiency = 12.062%

It can be seen in fig 3.3 that the Brake Thermal efficiency using compression ratio 18:1 at different loads is more when compared with the compression ratio 16:1

It is observed that the brake thermal efficiency increases with increase in load. This may be due to the friction torque is constant at all loads because, as the load increases, forms a smaller proportion of the indicated torque. The factors such as lower heating values and higher viscosity of the esters may affect the mixture formation process and hence the result in slow combustion hence reducing the brake thermal efficiency.

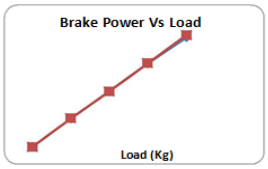

Figure 3 Break power vs Load

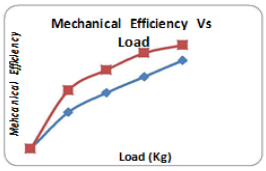

Figure 4 Mechanical Efficiency vs Load

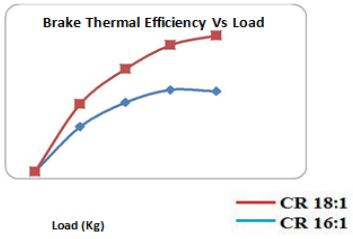

Figure 4 BTE vs Load

CONCLUSIONS

This experiment is done varying the load from 0 kg to 10 kgs and their respective efficiencies are obtained. The brake power, mechanical efficiency and also the brake thermal efficiency are found to be more for the case of 18:1 Compression ratio. The study concludes that the compression ratio at 18:1 has a better engine performance when compared to that of 16:1 when fueled with diesel. Same kind of tests could also be performed with biodiesel as different blends and at different compression ratios.

REFERENCES

1.Thiago Hoeltgebaum, Roberto Simoni, Daniel Martins, "Reconfigurability of Engines: A Kinematic Approach to Variable Compression Ratio Engines", Advances in Reconfigurable Mechanisms and Robots II pp 1061-1071, 24 November 2015

2.Chavan Supriya Baburao, R.Rohith Renish, Shinde Chandrakant Anna, Kumbhar Rajendra Rayappa, "Application of an Ecofriendly Heterogeneous Catalyst (CaO) for Synthesis of Biodiesel and its Characterization on VCR Engine", International Review of Mechanical Engineering (I.RE.M.E.), Vol. 9, N. 3, May 2015

3.Abhishek Reddy G, Nirmal Pratap Singh, Kolluri R V Sai Krishna, Anurag Priyedarshi, SN Singh, "Effect Of Compression Ratio On The Performance Of Diesel Engine At Different Loads", Abhishek Reddy G et al. Int. Journal of Engineering Research and Applications, ISSN: 2248-9622, Vol. 5, Issue 10, (Part - 2) October 2015, pp.62-68

4. Ajeet Kumar, S.K. Shukla, J.V. Tirkey, "Performance and Emission Characteristics of Coconut Biodiesel and Diesel Blends on VCR Engine", International Journal of Innovative Research in Engineering & Management (IJIREM) ISSN: 2350-0557, Volume-3, Issue-5, September-2016

5. D Balajee, G Sankaranarayanan, P Harish, N Jeevarathinam, "Performance and combustion characteristics of ci engine with variable compression ratio fuelled with pongamia and jatropha and its blends with diesel", int. J. Mech. Eng. & rob. Res. 2013, ISSN 2278 – 0149, vol. 2, no. 3, july 2013

6. G.Lakshmikanth, A.K.Thajudeen, S.Santhanakrishnan, G.Arunkumar "Performance and emission characteristics of mahua oil biodiesel on acompression ignition engine", International Journal of Engineering Research & Technology (IJERT), ISSN: 2278-0181, Vol. 2 Issue 10, October - 2013

7. K Satyanarayana, Naik RT2 and SV Uma-Maheswara Rao," Performance and Emissions Characteristics of Variable Compression Ignition Engine", Adv Automob Eng 2016, 5:2, 10.4172/2167-7670.10001463, July 08, 2016.

8. Supriya B.Chavan, Rajendra Rayappa Kumbhar,Ashutosh Kumar,and Yogesh C. Sharma," Study of Biodiesel Blends on Emission and PerformanceCharacterization of a Variable Compression Ratio Engine",ACS Publications, May 27, 2015.

9. Rupesh L. Raut, Babaso N. Naik, Shekhar D. Thakare, Amol A. Gawali," Emission analysis of bio-diesel blends on variable compression ratio engine", IJRET: International Journal of Research in Engineering and Technology ,eISSN: 2319-1163, Volume: 03 Issue: 05 | May-2014.

10 S. Nagaraja, K. Sooryaprakash, R. Sudhakaran, "Investigate the Effect of Compression Ratio over the Performance and Emission Characteristics of Variable Compression Ratio Engine Fueled with Preheated Palm Oil - Diesel Blends", Procedia Earth and Planetary Science 11 (2015) 393 – 401.

11. Yogesh Tamboli, Dr. G. R. Selokar, Amitesh Paul, Jehan Zala, "Feasibility Testing of VCR Engine using various blend of Neem Oil", International Journal of Innovations in Engineering and Technology (IJIET), Vol. 2 Issue 3 June 2013

12. Venkateswara Rao P, "Compression ratio effect on Diesel Engine working with Biodiesel (JOME)-Diesel blend as fuel, Research Journal of Chemical Sciences", ISSN 2231-606 Vol. 5(7), 48-51, July (2015)

13.C.S. Padmavat, Dr. R. B.Yarasu and Dr. P.M. Khodke An Empirical Model for Performance of Single Cylinder Variable Compression Ratio Diesel Engine International Journal of Mechanical Engineering and Technology, 8(5), 2017, pp. 767–777.

14. Ravinder Kumar and Navdeep Sharma Dugala. Exhaust Gas Diesel on Single Cylinder Diesel Engine. International Journal of Mechanical Engineering and Technology, 8(7), 2017, pp. 140-1

TRIBOLOGICAL PROPERTIES OF TEXTURED SURFACE

V.Sambasiva Rao, A.Sirisha, K.V.L.S.N.Vyahruth and K.Naga Teja
Department of Mechanical Engineering, Vasiredddy Venkatadri Institute of Technology, A.P, India

Abstract- **Work drained this project is to improve the tribological properties by surface texturing on cylindrical body. The textured surface contains different or single scale micro level dimples on the surface of the contact body. The performance of a textured surface depends on the shape, geometry and pattern of the surface texture. In this paper we analyzed the tribological properties in ansys by creating non-textured and textured bodies and analyzed the static pressure, dynamic pressure, cell Reynolds number, total energy, wall shear stress, skin friction coefficient. The different texture shape, different texture area ratio and patterns, different lubrication regims with different contact geometries and materials have been subjected to theoretical and experimental researches for many years. This project studies about the process of surface texturing and its analysis.**

1. INTRODUCTION

The word trilogy came from Greek word tribe mean rubbing. Tribology is branch of science which deals with the Friction, Lubrication and Wear. Sometimes we want to reduce the friction. For example, in gears, cams, bearing, car engine applications we need to reduce friction, so we use lubrication in this areas to decrease friction. Sometimes we need to increase the friction for example in brakes, to stop moving objects we use brakes where the friction need to increase. Here in some application we need friction to increase and in some applications some we need to decrease the friction. By texturing the surface we can reduce friction and also we can increase the friction. The reduction of friction depends on the pattern of the dimples in many experimental studies conclude the textured surface is more adoptable to reduce the friction.

2. LITERATURE WORK

Bowden was a pioneer of tribology field. His work with Taylor explored that making a surface roughness or smother not always affect the sliding friction. For some materials the rough surfaces may decrease friction and some other materials making smoother increase friction. Here they conclude that the surface with texturing with micro level dimples can reduce the friction.

On this paper on Friction reduction through biologically inspired scale-like laser surface Textures Source: doi: 10.3762/bjnano.9.238, Published online 2018 Sep 26. In this contribution, biologically inspired scale-like morphologies were manufactured on bearing steel surfaces by laser light. When they did test on the textured surface under lubrication they concluded that reduction in the friction coefficient varied between 20–30% for speeds between 20 to 80 mm/s.

3. TEXTURING

Surface texturing is surface modification technique, in order to improve, in order to improve, among other things, its tribological performance. This obtained through different patterns, which can be on micro or non-scales created on contact surface .The performance of a textured surface depends on the shape, geometry and pattern of surface.

3.1. *Single Scale Texturing:*

The single scale texturing defined as the texturing on the surface is done in the only in single dimple pattern.

3.2 *Multi Textured Surface:*

The multi scale texturing defined as the texturing on the surface is done in the multiple different types of dimple patterns.

4. SOFTWARE EMPLOYED

Software used for doing the Analysis in Ansys19.2.

Ansys is mechanical finite element analysis software is used to simulate computer model of structures, machine components for analyzing strength, toughness,elasticity,temperature distribution, fluid flow and other attributes on the components.

Ansys is used to determine how the product is functioning, analysis is done in the software. In ansys we can get more accuracy and no parallax error, we can faster and more accurately in ansys.

4.2 *Considerations:*

A cylindrical work-piece with dimensions Diameter 10mm and Length 30mm is considered for Analysis purpose.

- Material selected for analysis is Aluminum.
- Analysis is done with Steady state flow, Reynolds Equation.
- Inlet velocity is 5m/s and pressure at ambient conditions

 ISBN: 978-93-91420-02-4

4.2. *Analysis of Non-Textured Surface:*

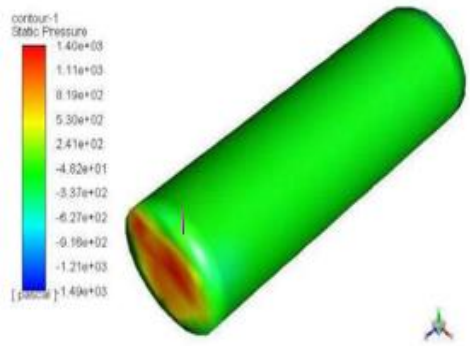

Figure 4.2.1Contour of Static Pressure

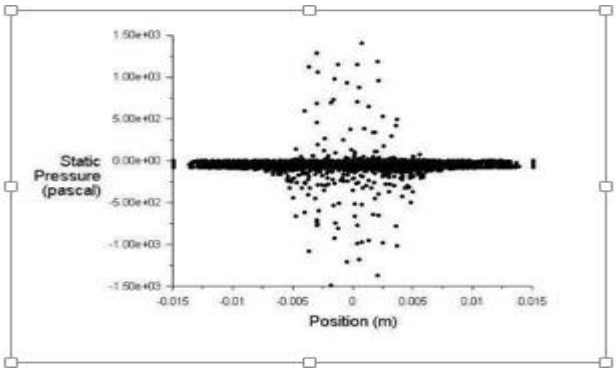

Figure 4.2.2 Plot of Static Pressure

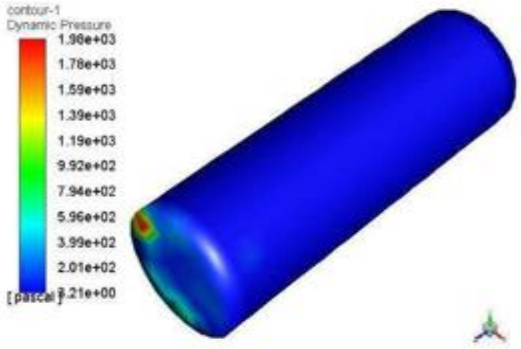

Figure 4.2.3 Contour of Dynamic Pressure

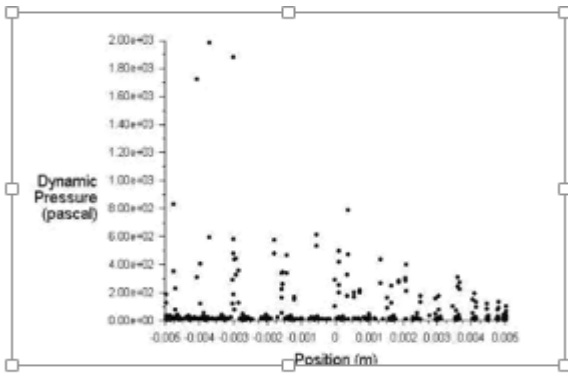

Figure 4.2.4 Plot of Dynamic Pressure

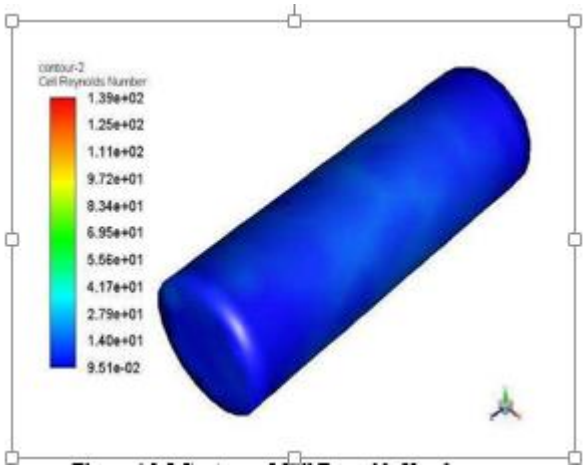

Figure 4.2.5 Contour of Cell Reynolds Number

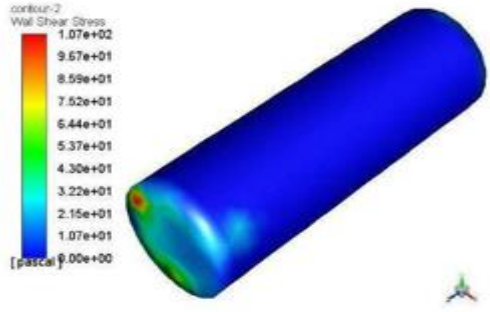

Figure 4.2.6 Contour of Wall Shear Stress

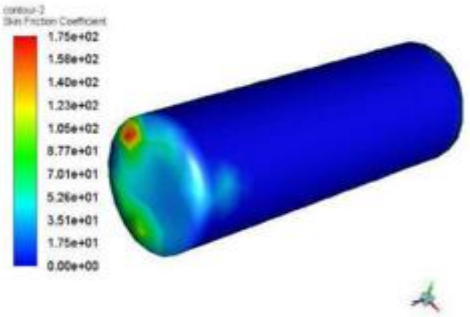

Figure 4.2.7 Contour of Skin Friction Coefficient

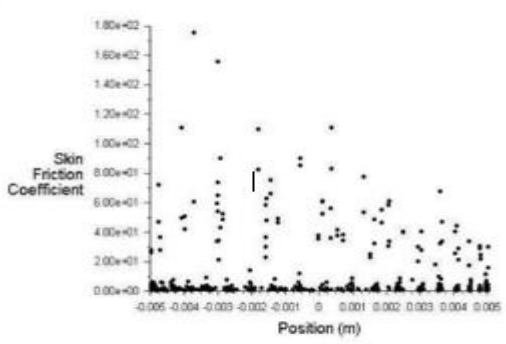

Figure 4.2.8 Plot of Skin Friction Coefficient

 ISBN: 978-93-91420-02-4

4.3Analysis of *textured surface:*

Surface Texturing made: Circular Dimples of radius 30µm and depth 30µm.

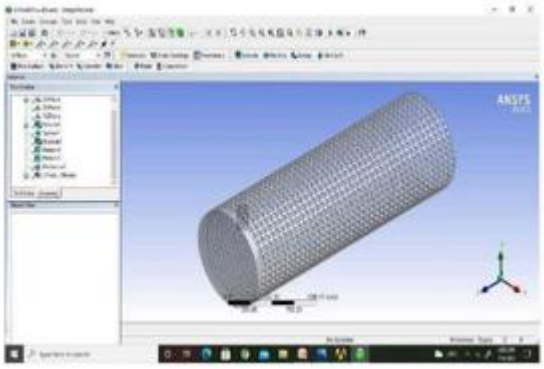

Figure: 4.3.1 Textured Surface

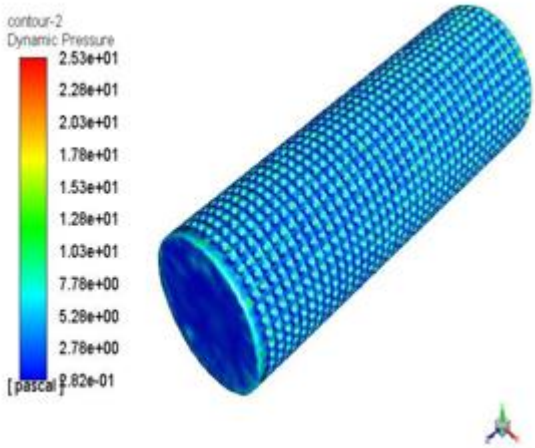

Figure: 4.3.2 Contour of Static Pressure

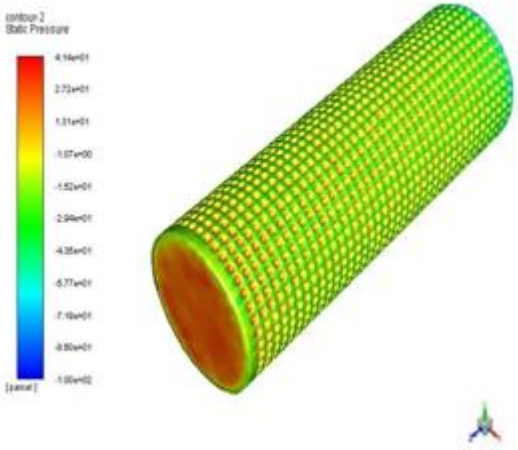

Figure: 4.3.3 Plot of Static Pressure

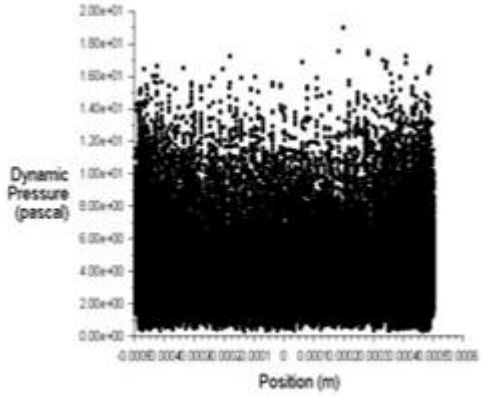

Figure: 4.3.4 Contour of Dynamic Pressure

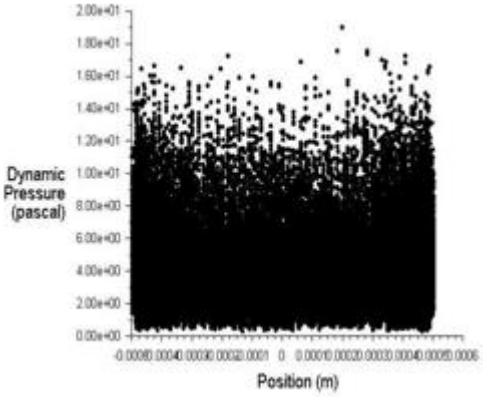

Figure: 4.3.5 Contour of Static Pressure

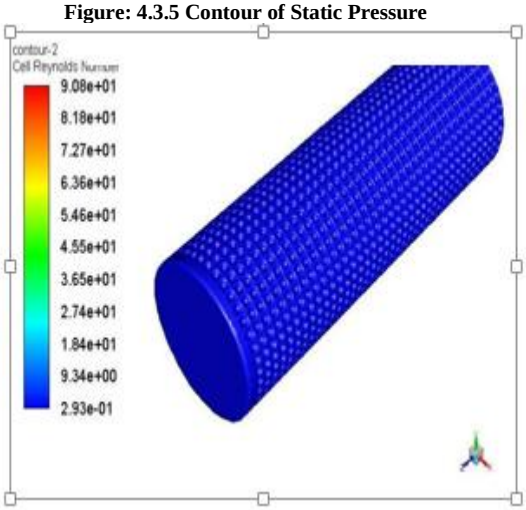

Figure: 4.3.6 Contour of Reynolds Number

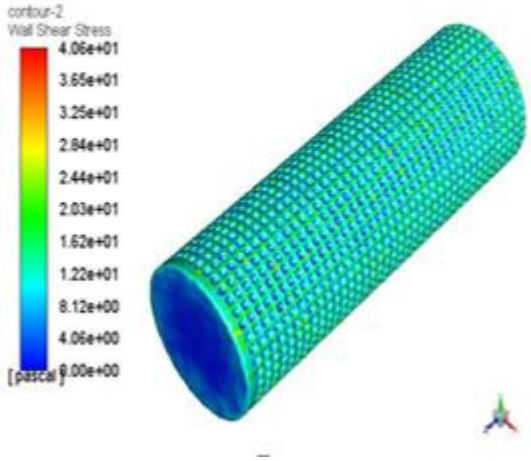

Figure: 4.3.7 Contour of Wall Shear Force

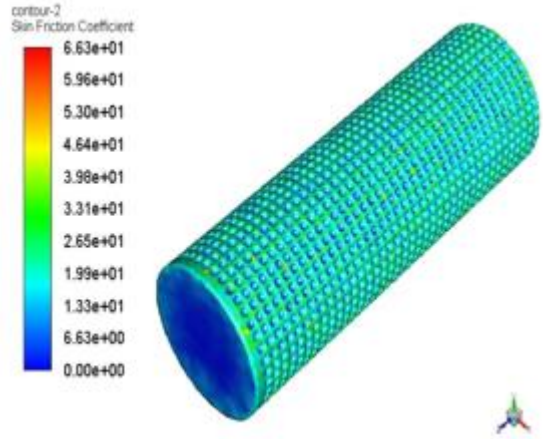

Figure: 4.3.8 Contour of Skin Friction Coefficient

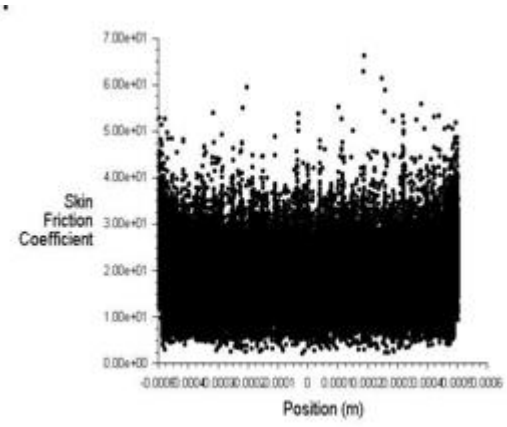

Figure: 4.3.9 Plot of Skin Friction Coefficient

5. RESULT

By observing the analysis results of circular textured surface and Non-Textured surface in ansys workbench that the values of the Static pressure, Dynamic pressure, Cell Reynolds Number, Wall Shear Stress, Skin Friction Coefficient, are reduced in circular textured surface compared to the Non-Textured surface.

So by the observing analysis values we are concluding that the friction wear parameters also can be reduced. So it better to choose the textured surface over the Non-textured surface.

6. REFERENCE

1. A Review of Surface Texturing in Internal Combustion Engine Piston Assembly– Journal.
2. Tribological performance of surface texturing in mechanical applications—a review–Journal
3. Dowson, D. History of Tribology; Longman: London, UK, 1979; ISBN 978-0-582-44766-0.
4.
5. Amontons, G. De la résistance causée dans les machines. Mémoires l'Académie R. A 1699, 257– 282
6. Bowden, F.P.; Tabor, D. Mechanism of metallic friction. Nature 1942, 150, 197–199. [CrossRef]
7.
8. Archard, J.F. Contact and rubbing of flat surfaces. J. Appl. Phys. 1953, 24, 981–988. [CrossRef]
9.
10. Greenwood, J.A.; Williamson, J.B.P. Contact of Nominally Flat Surfaces. Proc. R. Soc. A Math. Phys. Eng. Sci.1966, 295, 300–319.
11.
12. Nosonovsky, M.; Bhushan, B. Multiscale Dissipative Mechanisms and Hierarchical Surfaces;
13.
14. Nano science and Technology; Springer: Berlin/Heidelberg, Germany, 2008; ISBN 978-3-540-78424-1.
15. Prodanov, N.; Gachot, C.; Rosenkranz, A.; Mücklich, F.; Müser, M.H. Contact mechanics of laser-textured
16. Surfaces: Correlating contact area and friction. Tribol. Lett. 2013, 50, 41–4

Thermal Analysis and Experimental Investigation of Pin Fin made of Brass

GSSSR Vamsi, K Vishnu Nayak
Dr. G.Sulochana, University College of Engineering, Narasaraopet-JNTUK, Narasaraopeta, India.
Mr.ch.venkata Prasad, Velagapudi Ramakrishna Siddhartha Engineering College, Vijayawada, India.

***Abstract*— Industrial components often fail due to overheating because of less heat dissipation. This paper emphasizes on the experimental investigation of the temperature distribution along the pin fin made of brass. The analysis is performed on a 150mm long, 12 mm diameter brass pin fin, having a thermal conductivity of 110.7 W/m K. The influence of the mode of convection viz., natural and forced convection is evaluated. Temperature at different lengths along the fin is evaluated experimentally (both natural and forced), analytically and using ANSYS. The temperature distribution along the fin is then compared with one another. Analysis and graphical representation of heat transfer, efficiency and effectiveness is then presented.**

Keywords*— *natural convection, forced convection, heat transfer coefficient, efficiency, effectiveness

II. INTRODUCTION

Many of the industrial components generate some amount of energy. At elevated temperatures, the system may fail due to overheating. For continuous and efficient working of any industrial component, the generated heat must be dissipated to the surroundings and the temperatures should be kept within the permissible limits. Thermal analysis is the process of finding the values of temperature at different points when the material is in steady state condition. A steady state is the material condition where there is input heat energy equal to output heat energy.

Fins or extended surfaces are employed on the industrial components in order to increase the surface area available for convection. This increases the heat dissipation to the surroundings thereby keeping the system safe. Depending on the application, different geometrical configurations of fins are available as uniform cross-section (rectangular and pin) fin and non-uniform cross-section (triangular, elliptical and trapezoidal) fin. The important factors which mainly affect the heat transfer rate are the thermal conductivity of material, size of material etc., Different materials have different thermal conductivity and it affects the rate of heat transfer.

By increasing the length and diameter of the pin fin, the heat transfer rate can be improved but the fin faces the difficulty of increased self-weight and size.

Many researches are going on the heat transfer analysis of pin fin although very less information about the temperature distribution over the fin length and influence of operating conditions on the heat transfer rate was found. Therefore, in this work, an experimental and analytical investigation is carried out to evaluate temperature distribution across the fin length at variable operating conditions. The experiments are conducted for both natural and Forced convection. The experimental findings were then compared with the analytical results and represented graphically.

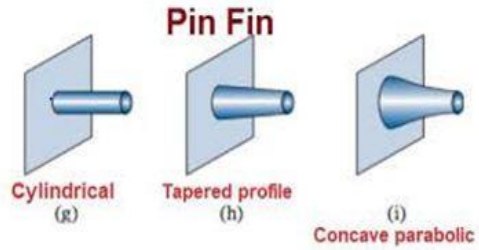

III. EXPERIMENTAL SET-UP

The apparatus is equipped with a blower that provides air flow at different rates. A control valve is also provided to regulate the flow from the blower. The equipment consists of a rectangular channel in conjunction with a nozzle attached to the blower. A 150 mm long pin fin of 12 mm diameter made up of brass is fitted at the base to a rectangular channel. A controlled amount of heat is supplied to the flange by means of an electric heater, which can be varied with the help of a variance. Six thermocouples were installed over the length of the fin as shown in fig. 2. The brass fin is kept inside a rectangular duct. An ammeter and voltmeter are also provided to record the current and voltage readings at a particular heat input. To vary the heat input the voltage may be increased or decreased with the help of a regulator.

The analytical relations and solutions for uniform area fin are available in several literatures [16-18]. In this study, the fin of finite length with insulated tip was considered. The analytical relations were made by considering some of the assumptions as listed below:

- 1-D conduction in the y-direction.
- The fin material is having constant thermal conductivity.
- No internal heat source is placed inside the fin.
- Radiation heat transfer is neglected.

 ISBN: 978-93-91420-02-4

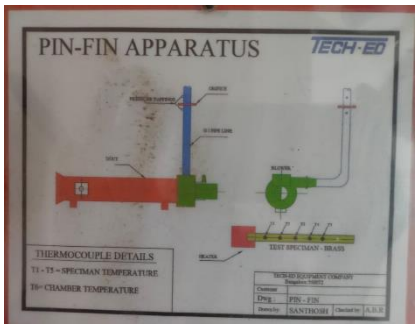

Heat transfer mechanism that does not need any external agent to generate fluid motion, the flow movement is solely by density difference due to temperature gradient is termed as free convection. Two dimensionless numbers that dominate the free convection heat transfer are Prandtl and Grashof number, can be written as:

- Prandtl number, $Pr = \frac{hd}{k}$
- Grashoff number, $Gr = \frac{\rho^2 d^3 g \beta \Delta T}{\mu^2}$
- Nusselt number, $u = 0.59(GrPr)^{0.25}$

IV. FORCED CONVECTION

In convection mode of heat transfer if the movement of surrounding fluid is provided by some external agents like fans, blower, pumps etc. then it is termed as forced convection. The fluid flow may be of the laminar or turbulent type. The motion of fluid amplify the heat transfer, flow with higher velocity will increase the heat dissipation rate. Forced convection is dominated by two dimensionless numbers named as Prandtl and Reynolds numbers, can be expressed as:

Prandtl number, $Pr = \frac{hd}{k}$

Reynold's number, $Re = \frac{\rho v d}{\mu}$

Nusselt number, $N_u = 0.683(Re)^{0.466}\,(Pr)^{0.333}$

The case of flow over vertical cylinder is considered to obtain temperature distribution over the fin length.

Temperature distribution for finite length fin with insulated tip is expressed as:

$$\frac{T - T_\infty}{T_0 - T_\infty} = \frac{cos\, h[m(L - x)]}{cosh(mL)}$$

Where m is fin parameter which is given by;

$$m = \sqrt{\frac{hP}{kA}}$$

Heat Transfer Rate, Q = $\sqrt{hPkA}\, Tanh(mL)\,(T_0 - T_{\infty})$

Effectiveness of the Fin, $\epsilon = \frac{Tanh(mL)}{mL}$

Efficiency of the fin, $\eta = \sqrt{\frac{hp}{kA}}\, tanh\,(mL)$

Results and Discussion

A. *Case A: Free Convection*

In this case, the investigation of temperature distribution over the fin length is performed under the natural circulation of air due to density difference. The temperature distribution at the various section of the fin was experimentally observed at constant heat input supplied by the heater. The experimental results are compared with the analytical solutions for the case of free convection heat transfer over pin fin made of brass.

FREE CONVECTION (BRASS)

Column1	T1	T2	T3	T4	T5	T6
Experimental	124.00	117.00	109.00	102.00	98.00	46.00
Mathematical	130.50	122.00	116.00	111.90	109.90	46.00
ANSYS	130.00	124.00	116.00	113.00	110.00	46.00

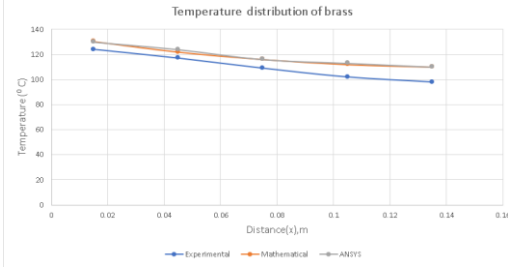

B. *Forced Convection*

In this case, the air is forced to flow over the fin by employing a blower. The temperature profile at the different section of fin length is observed at variable heat input. Thermal analysis is also performed using ANSYS. Experimental results are compared with the findings obtained by employing widely accepted relations and also ANSYS. The variation of temperature distribution over the fin length by experimental, analytical approach and ANSYS at given heat input is represented. It can be depicted that the results by analytical relation predict comparatively lesser than that of experimental observations, the dominance of forced convection heat transfer increases as the distance of length section from the fin base increases while conduction mode is more responsible for heat dissipation near the fin base region. The dominance of different modes of heat transfer leads to the variation in experimental and analytical thermal behavior.

 ISBN: 978-93-91420-02-4

FORCED CONVECTION (BRASS)

Column1	T1	T2	T3	T4	T5	T6
Experimental	133.00	115.40	105.80	96.00	93.20	44.00
Analytical	129.80	111.10	99.00	90.40	86.60	44.00
ANSYS	130.00	112.00	100.00	94.00	88.00	44.00

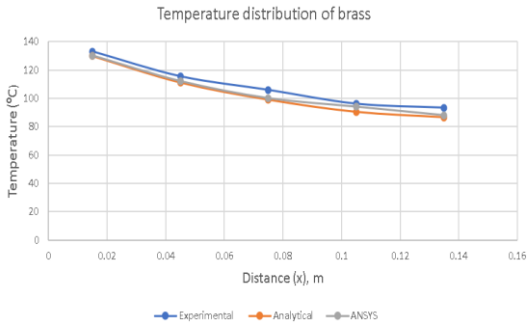

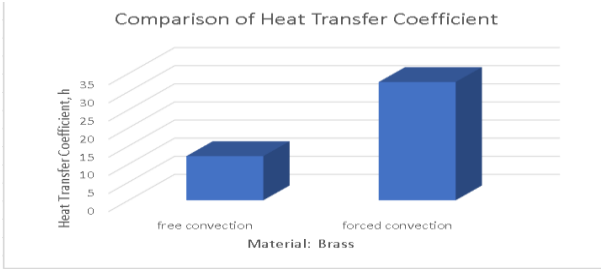

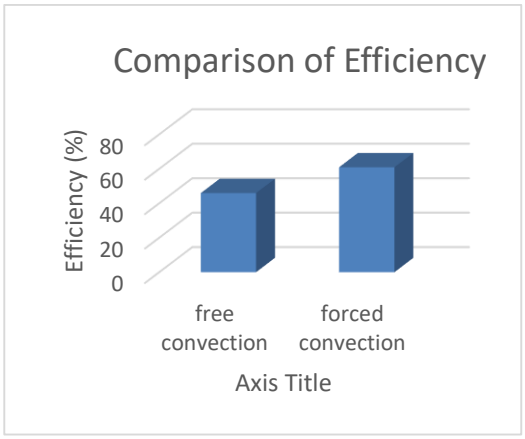

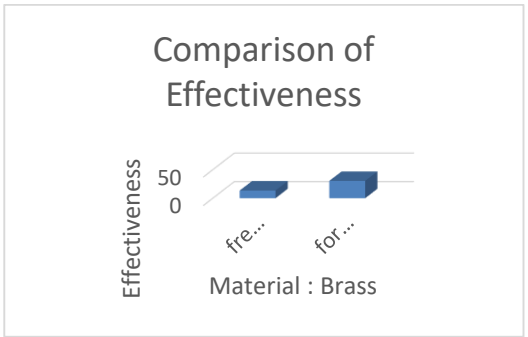

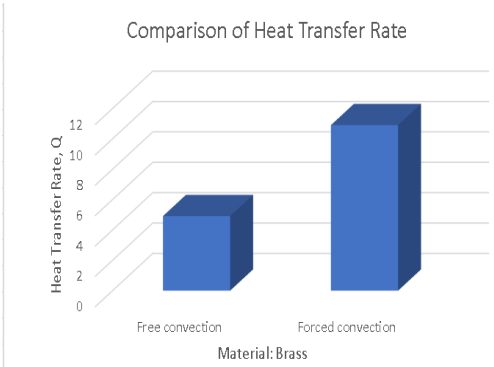

Nomenclature:

Cp=specific heat of the fluid

μ=viscosity of fluid

k_s=thermal conductivity of the material of the fin 32.65 $W/m^2 K$

L=characteristic length of fin

ρ=Density of Fluid

ϑ =kinematic viscosity of fluid

d= Fin diameter

V=Air Velocity

T_0 =Base Temperature

T_{atm}=Atmospheric Temperature

K=Thermal conductivity of Brass

h=Convective heat transfer coefficient

P=Perimeter of fin

A=Fin Area

CONCLUSION

From the above observations and results, we can conclude that

- The results by widely accepted analytical relations were in better agreement with the experimental findings for natural convection.
- Forced convection in a brass pin fin when used with a fluid velocity of 1.74 m/s, can dissipate 122% more heat than in the free convection, with improved efficiency (32.68%) and effectiveness (125.67%).
- Convection mode of heat transfer was found to be more dominating than conduction at the region away from the fin base.

References

1. Vikas Kannojiya Experimental Investigation of Temperature Distribution along the Length of the Pin Fin", IOP Conference Series: Material Science and Engineering, 2018.
2. Lakshmi Kant Chavan, Niranjana Purane, "Thermal Analysis of Pin Fin Using Different Materials", International Journal of Science and Research, 2013.
3. Y. Pratapa reddy, G. Raju, Ch. Srinivasa Rao, "Thermal Analysis of Composite Fin, International Journal of Core Engineering and Management, 2014.
4. Naser Sahiti, "Thermal and Fluid Dynamic
5. Performance of Pin Fin Heat Transfer Surface", 2006.
6. US Gawai Mathew V K, Murtuza S D, "Experimental Investigation of Heat Transfer by PIN FIN",2013.

Experimental and Simulation of wear test on GPR Material

T. Sunil Kumar and R.Bala Ganesh
Dept. of Mechanical Engineering, Geethanjali Institute of Science and Technology, Nellore, Andhra Pradesh, India.

Abstract: Wear rate is defined as the volume lose per unit distance and unit time. The current design/manufacturing field looking for value added/engineering projects. In this project an attempt has been made on GPR material to predict the wear rate in helicopter rotor, wind turbines and sports equipment Etc. The wear rate of a material can be estimated by using pin on disc by factorial method. The tangential load and the coefficient of friction values are taken from pin on disc experiment and estimate the wear rate by factorial method. During the wear testing the total deformation, directional deformation, elastic strain and shear strain are estimated using ansys software at different conditions. These results should provide good understanding of wear prediction and durability of the material.

Keywords: glass reinforced polymer, wear rate, sliding contact.

INDRODUCTION

INTRODUCTION TO PIN ON DISC:

Microsystems and micro-machines in particular are a rapidly emerging technology, finding a wide variety of applications. Various investigations on micro-machines show that the tribological behaviour plays a key role in the performance of micro-machines 1–4. At present, in-situ wear measurements are the most realistic methods to predict wear in micro-components. In 5 a detailed in-situ study of the tribological performance of poly-silicon micro-engines can be found. Moreover, the manufacture of prototypes is highly expensive both in terms of time and money for such in-situ studies.

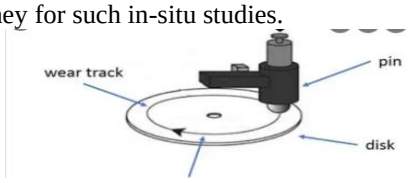

Fig 1: Pin on disc setup

INTRODUCTION TO WEAR*:*

Wear is the damaging, gradual removal or deformation of material at solid surfaces. Causes of wear can be mechanical (e.g., erosion) or chemical (e.g., corrosion). The study of wear and related processes is referred to as tribology. Wear in machine elements, together with other processes such **as** fatigue and creep, causes functional surfaces to degrade, eventually leading to material failure or loss of functionality. Thus, wear has large economic relevance as first outlined in the Just Report. Abrasive wear alone has been estimated to cost 1-4% of the gross national product of industrialized nations.

Wear of metals occurs by plastic displacement of surface and near-surface material and by detachment of particles that form **wear debris**. The particle size may vary from millimeters to nanometers. This process may occur by contact with other metals, non-metallic solids, flowing liquids, solid particles or liquid droplets entrained in flowing gasses. The **wear rate** is affected by impact,static,dynamic),typeof motion (e.g., sliding, rollin g), temperature and lubrication, in particular by the process of deposition and wearing out of the boundary lubrication layer. Depending on the tribosystem, different **wear types** and **wear mechanisms** can be observed.

Wear types and mechanisms *:*

Wear is commonly classified according to so-called wear types, which occur in isolation or complex interaction. Common types of wear include:

- Adhesive wear
- Abrasive wear
- Surface fatigue
- Fretting wear
- Erosive wear
- Corrosion and oxidation wear

Other, less common types of wear are impact-, cavitation- and diffusive wear. Each wear type is caused by one or more wear mechanisms. For example, the primary wear mechanism of adhesive wear is adhesion. Wear mechanisms and/or sub-mechanisms frequently overlap and occur in a synergistic manner, producing a greater rate of wear than the sum of the individual wear mechanisms.

Factorial technique:

The wear rate for the glass reinforced polymer can be calculated by using the formula

Wear rate = co efficient of friction / density * sliding distance

The co-efficient of friction can be calculated by using the formula (μ) = Tangential load / Applied load.

Boundary conditions:

Boundary conditions applied in ansys are given below

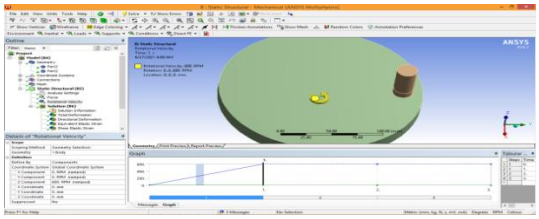

Fig 2: part-1

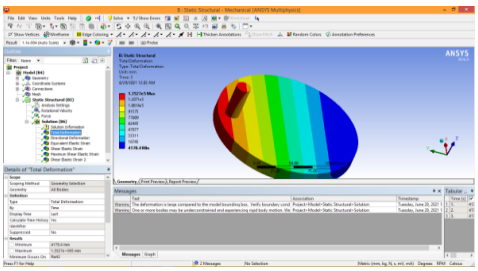

Fig 3: part-2

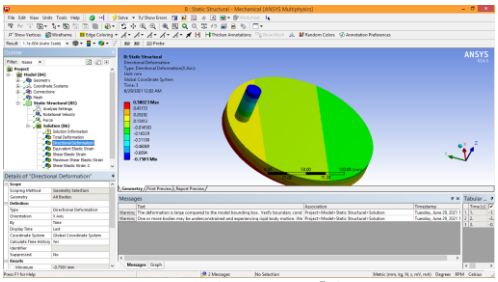

Fig 4: Meshing

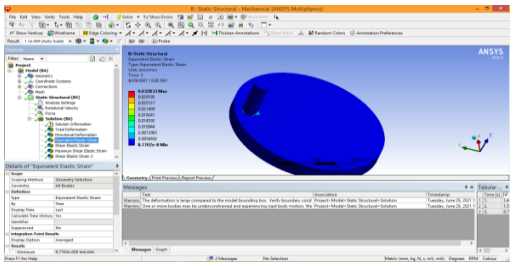

Fig 5: Force

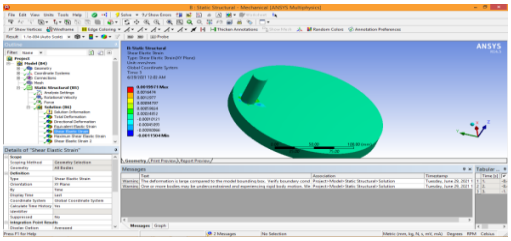

Fig 6: Rotational Velocity

Results: The results obtained by using ansys are shown below

At Speed 200rpm and Load 1 KN

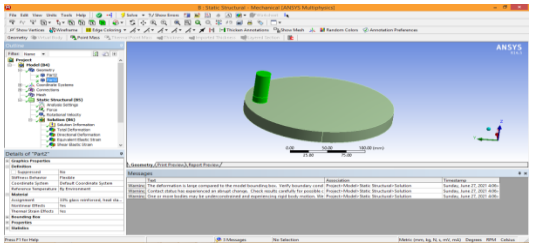

Fig 7: Total deformation

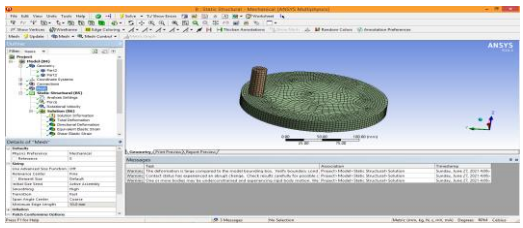

Fig 8: Directional deformation

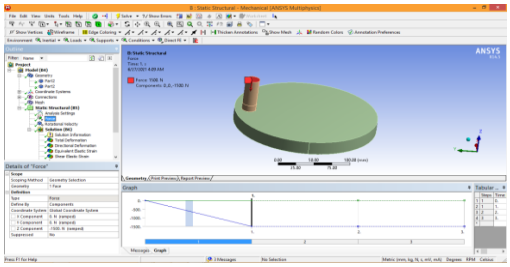

Fig 9: Equivalent Elastic Strain

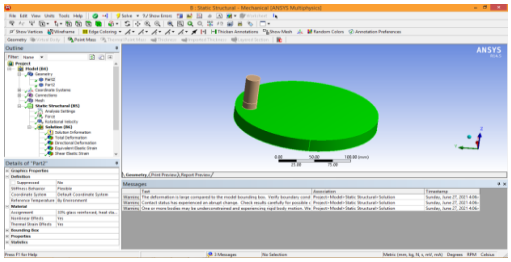

Fig 10: Shear elastic strain

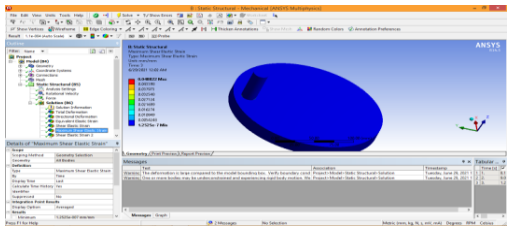

Fig 11: Max shear elastic strain

The results obtained are tabulated as shown below:

The values of the terms provided by ansys are recorded and tabulated as given below

Table no 1: Observations for each set of results in ansys

SL NO	Speed (rpm)	Load (kn)	Deformation (mm)		Equivalent elastic strain	Shear elastic strain	Maximum shear elastic strain
			Total deformation	Directional deformation			
1	200	1	1.3527e^5	0.58125	0.032841	0.001997 5	0.048834
		1.5	2.0286e^5	4.2649	0.10845	0.006665	0.16133
		2	2.7032e^5	17.687	0.25377	0.015708	0.37757
2	400	1	1.3527e^5	0.58032	0.032829	0.001996 8	0.048816
		1.5	2.0286e^5	4.2545	0.10842	0.006664 2	0.16127
		2	2.7032e^5	17.694	0.25378	0.015706	0.37758
3	600	1	1.3527e^5	0.57987	0.032817	0.001995 8	0.048798
		1.5	2.0286e^5	4.2572	0.10841	0.006663	0.16125
		2	2.7032e^5	17.691	0.25372	0.015703	0.37749

The values of wear rate are calculated by using the formula mentioned in the factorial technique and by varying the tangential load for 5 different samples at 1, 1.5 and 2 KN loads and the values are obtained as shown in the table below.

Table no: 2 Wear rate values for five samples

SAMPLE	LOAD (P) (KN)	SPEED (N) (RPM)	COFFICIENT OF FRICTION (μ)	WEAR RATE
1	1	200	0.26	0.0000013
	1.5	400	0.19	0.0000009
	2	600	0.038	0.0000001
2	1	200	0.42	0.0000021
	1.5	400	0.156	0.0000008
	2	600	0.025	0.0000001
3	1	200	0.188	0.0000009
	1.5	400	0.16	0.0000008
	2	600	0.17	0.0000008
4	1	200	0.26	0.0000013
	1.5	400	0.32	0.0000016
	2	600	0.017	0.0000001
5	1	200	0.65	0.0000033
	1.5	400	0.847	0.0000044
	2	600	1.35	0.000007

CONCLSION

The values of wear rate for glass reinforced polymer (GPR) at different compositions (or) samples are calculated and noted in the table 5.2. From the table we can observe that the values of wear rate decrease with increase in speed as we can see that the wear rate is lower at 200rpm and decreases

when speed is increased to 400rpm. The reason is when the sliding velocity continue sly increases the coefficient of friction is decreased causing the decrease in wear loss at high speed. From the table 5.2 we can also conclude that 45%glass fibre reinforced polyamide has the least wear rate values when compared to the other composition samples. Hence we can say that products made of 45%glass fibre reinforced polyamide has high durability than other compositions of the glass reinforced polymer (GPR). In addition the values for total deformation, directional deformation, equivalent elastic strain, shear elastic strain and maximum shear elastic strain are determined at different speeds and lods by using ansysand the relation between these terms and the lads and speed are determned. Total deformation is same when there is a change of speed but increases when the load applied increases. The values of directional deformation are proportional to the load and inversely proportional to the speed of the disc. The equivalent elastic strain, shear elastic strain and maximum shear elastic strain is proportional to the load and inversely proportional to the speed of the disc.

The helicopter rotor, wind turbines and sports equipment like kayaks are more durable when the material used to prepare them is 45%glass fiber reinforced polyamide of GRP materials.

References

1. ANSYS User's Manual for Version 10.0.

2. Ashraf, M. A., Najafabadi B. S., Gol O., Sugumar D. (2008) Time-to-failure prediction for a polymer– polymer swivelling joint. International Journal of Advanced Manufacturing Technology, 39(3-4): 271-278.

3. Ashraf, M. A., Najafabadi, B. S., Gol, O., Sugumar, D. (2007) Finite element analysis of a polymer sliding contact for Schallamach wave and wear. Key Engineering Materials, 348–349:633–636.

4. Ashraf, M.A., Najafabadi, B.S., Hsu, H.Y. (2006) Surface-surface contact wear prediction using FEA. In Research in Interactive Design, Springer, Paris.

5. Ashraf, M.A., Najafabadi, B.S., Hsu, H.Y. (2006) Wear prediction: A methodical approach. In Research in interactive design, Springer, Paris.

6. Bayer, R.G. (2002) Wear analysis for engineers. HNB Publishers, New York.

7. Cantizano, A., Carnicero, A., Zavarise, G. (2002) Numerical simulation of wear-mechanism maps. Computational Materials Science, 25:54-60.

8. Hegadekatte, V., Huber, N., Kraft, O. (2005) Finite element-based simulation of dry sliding wear. Modelling and Simulation in Materials Science and Engineering, 13 (1):57-75.

9. Hutchings, I.M. (1992) Tribology: friction and wear of engineering material. Edward Arnold Publishers, London.

10. Kim, N.H., Won, D., Burris, D., Holtkamp, B., Gessel, G.R., Swanson, P., Sawyer, W.G. (2005) Finite element analysis and experiments of metal/metal wear in oscillatory contacts. Wear, 258:1787–1793.

11. Lydersen, S., Rausand, M. (1987) A systematic approach to accelerated life testing. ReliabEng 18(4):285–293.

12. Meng, H.C., Ludema, K.C. (1999) Wear models and predictive: Their form and content. Wear, 181- 183:443-457.

13. Podra, P., Andersson, S. (1999) Simulating sliding wear with finite element method. Tribology International, 32:71-81.

14. Rabinowicz, E. (1995) Friction and wear of materials. Wiley, New York.

15. Sfantos, G.K., Aliabadi, M.H. (2007) Total hip arthroplasty wear simulation using the boundary element method. Journal of Biomechanics, 40: 378–389.

16. Unal, H., Mimaroglu, A., Kadroglu, and Ekiz, H. (2004) Sliding Friction and Wear Behaviour of Polytetrafluoroethylene and its Composites under Dry Conditions. Material and Design, 25:239-245.

17. Williams, J.A. (2005) Wear and wear particles-Some fundamentals. Tribology International, 38(10): 863–870.

18. Zhang, W.M., Meng, G. (2006) Friction and wear study of the hemispherical rotor bushing in a variable capacitance micro motor. Microsystem Technologies, 12(4):283–292.

19. Zhang, W.M., Meng, G. (2006) Numerical simulation of sliding wear between the rotor bushing and ground plane in micro motors. Sensors and Actuators A: Physical, 126(1):15–24.

20. Wear – Materials, Mechanisms and Practice Editor::Gwidon W. Stachowiak first published: 11 November 2005 ISBN: 9780470016282 online ISBN: 9780470017029 DOI: 10.1002/9780470017029

21. Friction and Wear of Materials, 2nd Edition Ernest Rabinowicz ISBN: 978-0-471-83084-9

 ISBN: 978-93-91420-02-4

CFD Analysis of Two Pass Double Pipe Heat Exchanger with TiO_2/Ethylene Glycol Nano Fluid

Gopi Nerusu and Pathuri Srinivasa Rao
Department of Mechanical Engineering, Narasaraopeta Engineering College (A), Narasaraopet, India.

***Abstract*- This paper deals with the numerical simulation of cold fluid forced convection heat transfer under turbulent flow condition with different flow rates of 8, 10, 12, 14, 16 lpm and at various Nano fluid volume-fractions of 0.03%, 0.1%, 0.2%, 0.3% and 0.4% with constant hot fluid flow rate of 8 lpm. In this study, TiO2/Ethylene Glycol Nano fluid is used as cold fluid and pure water is used as hot fluid around initial temperatures of 27 °C and 60 °C, respectively. The objective is to augment the heat transfer coefficient and friction-factor of 2 pass Double pipe heat exchanger at various Reynolds numbers range of 9,000 to 25,000 using Computational Fluid Dynamics (CFD). The present study explored that the effect of volume concentration in 2 pass Double pipe counter flow heat exchanger on convective heat transfer and friction characteristics in a tube. The simulations were done for these flow rates at different volume concentrations. The results showed that an enhancement in heat transfer coefficient is increased by 34.93% at 0.4% volume concentration at Reynolds number range of 9000 to 24,000 when compared to water. The maximum friction factor obtained is 1.34 times at 0.3% volume-fraction of TiO2/Ethylene Glycol Nano fluid at Reynolds number of 10,833, when compared to water.**

Keywords: Heat Pipe, Nano fluid, CFD Analysis, Double pipe heat pipe.

I INTRODUCTION

Heat exchangers are essential engineering devices in several process industries as the efficiency and economy of the process largely depends on the performance of the heat exchangers and other important engineering applications in heat exchangers such as power plants, air-conditioning, petrochemical industry, natural gas processing, refrigeration, solar water heater, chemical reactors, sewage treatment, shell and tube heat exchangers in nuclear reactors. The design method for heat exchangers is very critical, as it needs perfect analysis on rate of heat transfer and pressure drop estimations. The rate of heat transfer can be enriched by producing a disturbance in the flow of fluid by breaking the viscous boundary and thermal boundary layers, this problem can be rectified in the other type as there exists a fairly constant difference in temperature. Double pie heat exchanger is a simple exchanger which consists of two pairs of pipes are arranged in the hairpin alignment, for noticeable causes. Butteries of this type of heat exchangers are connected in series-parallel or series in arrangements in order to obtain grater area of surface for heat transfer. The working fluids that are transmitting heat energy from one fluid to another fluid depending up on our requirement in the inner and outer pipes. The increase of heating and cooling systems in a factories or industrial aspects will create a saving the energy, reducing the process-time, raising the temperature and increasing the life of apparatus. The improvement of high operation of thermal processes for augmentation of heat transfer will become trendy now-a-days. There are

Various methods to develop the efficiency heat transfer by use of extended surfaces that are Passive methods and aspect of vibration to the heat transfer parts that are Active methods etc. Efficiency of heat transfer can be developed by raising the thermal conductivity of the base fluids. Generally water, ethylene glycol, and engine oil etc., are having low thermal conductivity and used as base fluids, when compared to solid particles. To raise the thermal conductivity of these fluids, solid particles, generally having higher thermal conductivity, are used to mix with these fluids with a certain concentrations.
These are having following drawbacks represented below:

A. The particles are settled down rapidly and form a small layer on the surface and dropping the heat transfer rate.

B. Whenever rate of circulation increases, sedimentation is diminished, but increasing the erosion rapidly of the heat exchanger parts such as pipe walls, etc.

C. Particles are of large size tends to block the flow loops.

D. The pressure drop increases hastily in the fluid.

E. Finally, development of conductivity based on particle-concentration is reached. That is the higher the particle volume-fraction is, higher the improvement and having major problems.

II OBJECTIVE AND METHODOLOGY

Several research works have been done in the tube flow recently on heat transfer aspects. Convective heat transfer improvement with different types of Nano fluid in a plain tube is clarified by several researchers.
A closer observation at experi0mental and numerical results reveals that most of the convective heat transfer studies in the tube flow have been done with Al_2O_3, CuO, SiC, CNT and Fe_3O_4 etc., Nano fluids itself. So in the present work, TiO2/Ethylene Glycol is considered as a Nano fluid because of the advantage with this, there is a possibility of separation of magnetic Nanoparticles (Fe_3O_4)

from the base fluid, isis not achievable with non-magnetic (Al_2O_3, CuO and TiO_2) type nanoparticles.

In order to complete a project successfully, the objectives for the project must be determined and the objectives of this project includes:

A. To investigate numerically the behavior of Nano fluid (TiO2/Ethylene Glycol) at different Reynolds numbers and volume concentrations (0.03%, 0.1%, 0.2%, 0.3%, 0.4%) during the forced convection heat transfer using ANSYS FLUENT.

B .To compare the results obtained from the numerical simulation software with the Analytical results by using the several correlations given by different authors, who have researched on this work and study the enhancement of the heat transfer in comparison with that of water.

No. of elements	Coldwater outlet temperature (°C)	Hot water outlet temperature (°C)
876874	31.458	53.970
895812	31.652	53.625
856253	30.256	54.325

III CFD ANALYSIS OF DOUBLE PIPE HEAT EXCHANGER AND SIMULATION

This chapter deals with the computational fluid dynamics (CFD) analysis of the behaviour of the turbulent flow through a 2 pass double pipe heat exchanger using ANSYS FLUENT 16 software.

Geometry and Modelling Specifications of Geometry and Boundary *conditions*

The analysis is performed on a 2-pass double pipe heat exchanger with the inner diameter of inner pipe is 0.019 m & outer diameter of inner pipe is 0.025 m, similarly for annulus pipe, the inner diameter of outer pipe is 0.05 m & outer diameter of outer pipe is 0.056 m and the total length of heat exchanger is 2.36 m (2-pass).

A. Meshing of Geometry

Structured meshing method in ANSYS WORKBENCH was used for the geometry. The element for meshing considered is hexahedral shape with number of elements of 876874 to 1240000 as shown in Fig.1.Naming selections were also done at required places.

TABLE 5.2: Properties of Water and Fe_3O_4 Nanoparticles

S.No	Boundary type	Annulus Pipe	Inside Pipe
1	Mass flow rate at Inlets	0.134 kg/s	0.134 to 0.267 kg/s
2	Temperatures	333 K	300 K
3	Constant heat flux at pipe wall (Insulation)	0 W/m^2	---

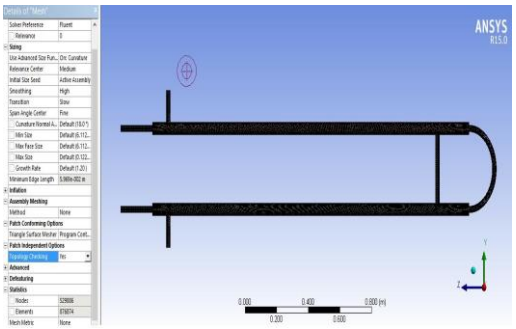

Fig. 1. Meshing of 2 pass double pipe heat exchanger in ANSYS Workbench

B. Grid Independence Test

Grid independence test was conducted at 8 lpm hot water and 10 lpm cold water flow rates in ANSYS-FLUENT, by decreasing and increasing the size of the elements. The gained results are tabulated in Table 5.1, for outlet temperatures of cold water and hot water of 2-pass double pipe heat exchanger.

TABLE 5.1 Grid Test Results

Finally, I selected as final mesh elements of 876874 for further simulation purpose.

C.Physical Models

The standard k-ϵ (k-epsilon) model is used for single phase turbulent flow in circular pipe channel. Based on the Reynolds number, ρVd/μ either viscous laminar or standard k-ϵ model is used for laminar and turbulent flow respectively. The choice of the model is shown in Table 5.2. Where, d is the diameter of the pipe, ρ is are the density and μ is viscosity of the fluid.

E.Material Properties

Pure water is used as base fluid, steel is used for pipes and TiO2/Ethylene Glycol used as cold fluid, the properties are shown in Table 5.3.

TABLE 5.2: Properties of Water and Fe_3O_4 Nanoparticles

TABLE 5.3: Boundary Conditions

S. no	m	dia	Den	K	SG	KV
1	Ethylene Glycol	--	1220	0.258	2360	8.32 E-07
2	TiO2	50-100	3970	11.8	683	-----

D.Boundary Conditions

A Velocity inlet, uniform mass flow inlets and a constant inlet temperature were assigned at the channel inlet. At the exit, pressure was specified. The boundary conditions assigned as shown in Figure.2.

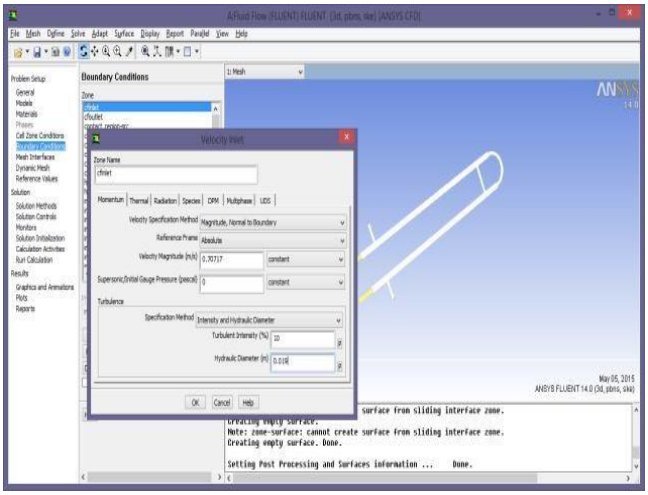

Fig. 2: Boundary conditions given in Problem setup in ANSYS-FLUENT

E.Method of Solution

The CFD method follows the use of commercial software ANSYS FLUENT 15.0 to solving the problem. The solver in ANSYSFLUENT used a pressure correction based SIMPLE algorithm with 2nd order upwind scheme for discretizing the convective transport terms. The criteria for convergence dependent variables are specified as 0.001.

In the present analysis, the analytical values of heat transfer coefficients are calculated. The heat transfer coefficients are also obtained using CFD methods and compared with analytical values.

The Flow diagram of 2 pass Double Pipe Heat Exchanger as shows in Figure below

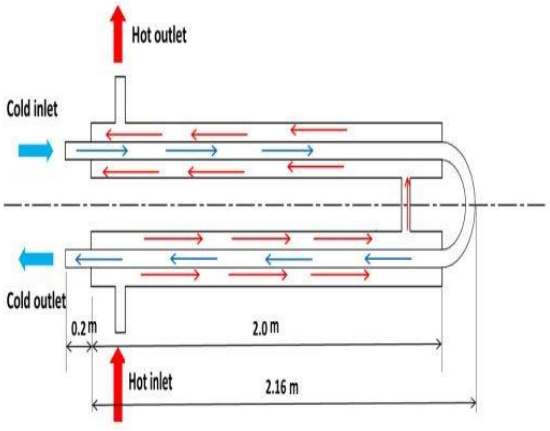

Fig.3: Flow diagram of double pipe heat exchanger

The CFD method follows the use of commercial software ANSYS FLUENT 15.0 to solving the problem. The solver in ANSYSFLUENT used a pressure correction based SIMPLE algorithm with 2nd order upwind scheme for discretizing the convective transport terms. The criteria for convergence dependent variables are specified as 0.001.

In the present analysis, the analytical values of heat transfer coefficients are calculated. The heat transfer coefficients are also obtained using CFD methods and compared with analytical values.

Model Calculations

Model calculations were taken at 0.03% Nano fluid at 8 lpm hot fluid and 12 lpm cold fluid:

IV.RESULTS AND DISCUSSION

A.Validation of Numerical Results

Effect of Nusselt number on Reynolds number. Here Analytical relation taken by **Sunder and Sharma [22]** equation.

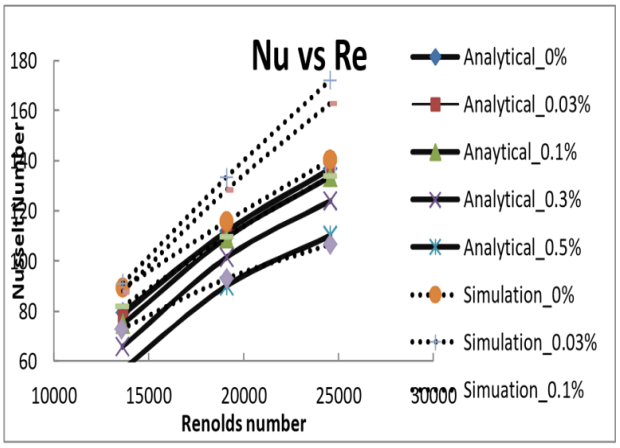

Fig 4:Effect of friction factor on Reynolds number.

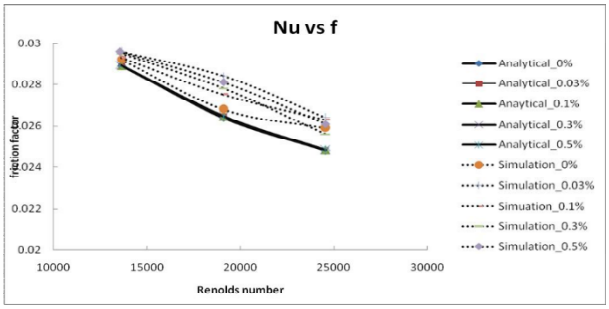

Fig.5: shows that comparison of Numerical friction factor with Blasius correlation for pure water.

From this illustration, it was observed that there is a closer agreement for simulation results with Analytical data is achieved. The figure shows comparison of friction factor values of Analytical and Simulation results at corresponding Reynolds numbers. It was observed that the friction factor values are closer to the values obtained by correlation by Sunder and Sharma.

CONCLUSION

In this work the hydrodynamics and thermal behavior of Double pipe 2 pass heat exchanger were studied. Pure water and its Nano

fluids (TiO2/Ethylene Glycol) were considered in pipe channel. A steady state computational fluid dynamics (CFD) models was simulated by ANSYS FLUENT 15.0.

Conclusion of the present work can be summarized as follows.

The heat transfer enhancement is observed that better in the turbulent region compared to that in the laminar region for all volume fractions considered in the analysis.

There is a good agreement between the results gained from the simulation and analytical data. The maximum error was found that 10.56%.

It is observed that according to simulation results there is a 34.93% enhancement in heat transfer coefficient at 0.4% volume concentration of Nano fluid when compared to water at Reynolds number range of 9000 to 22,000.

It is observed that there is a maximum friction-factor found that 1.34 times at 0.3% volume-concentration of TiO2/Ethylene Glycol Nano fluid at Reynolds number of 10,833 when compared to water.

The friction-factor is increased with the increase of volume concentration but it is observed that the friction-factor enhancement is less compared to the enhancement to the heat transfer for volume fraction considered in the analysis.

REFERENCES

[1] MoravejiM.K. and MajidHejazian, "Modelling of turbulent forced-convective heat transfer and friction factor in a tube for Fe_3O_4 magnetic Nano fluid with computational fluid dynamics" in International communications in Heat and Mass transfer, 2012, vol. 39, pp. 1293-1296.

[2] Dalkilic A.S., SomchaiWongwises, Ali Celen, Kayaci N., Alican Cebi and Hakan Demir, "Numerical investigation for the calculation of TiO_2/water Nano fluids' pressure drop and enhanced pipes" in International communications in Heat and Mass Transfer, 2014, vol. 53, pp. 98-108.

[3] Adnan M. Hussein, Sharma K.V., Bakar R.A. and Kadirgama k., "The Effect of Nano fluid volume concentration on Heat Transfer and Friction factor inside a horizontal tube", Journal of Nanomaterials, Hindawi Publishing corporation, 2013, vol. 2013.

[4] Jongwook Choi and Yuwen Zhang, "Numerical simulation of laminar forced convection heat transfer of Al2O3-water Nano fluid in a pipe with return bend", International journal of Thermal Sciences, 2012, vol. 55, pp. 90-102.

[5] Chandra Sekhara Reddy M., Vasudeva Rao V., NarasingaRao T., and SyamSundar L., "Enhancement of Convective Heat Transfer coefficient with TiO2Nano fluid in a Double pipe Heat Exchanger" in International Journal of Nanotechnology and Applications, 2011, vol. 5, pp. 59-68.

[6] SyamSundar L., ManojK.Singh and Antonial C. M. Sousa, "Investigation of thermal conductivity and viscosity of Fe3O4Nano fluid for heat transfer applications" in International Communications in Heat Mass Transfer, 2013, vol. 44, pp. 7-14.

[7] SyamSundar L., Manoj K. Singh and Antonial C. M. Sousa, "Thermal conductivity of ethylene glycol and water mixture based Fe3O4Nano fluid" in International Communications in Heat and Mass Transfer, 2013, vol. 49, pp. 17-24.

[8] Hamilton R.L., and Crosser O.K., "Thermal conductivity of heterogeneous tow component systems", Industrial Engineering Chemical Fundamentals, 1962, vol. 1(3), pp. 187-191.

[9] Vajjha R.S., and Das D.K., "Experimental determination of thermal conductivity of three Nano fluids and development of new correlations", International Journal of Heat Mass Transfer, 2009, vol. 52, pp. 4675-4682.

[10] Pak B.C., and Cho Y.I., "Hydrodynamic and heat transfer study of dispersed fluids with submicron metallic oxide nanoparticles", Experimental Heat transfer, 1998, vol. 11, pp. 15-170.

 ISBN: 978-93-91420-02-4

Simulation and Optimization of Extrusion Process Parameters of Aluminum 2A12T4 Alloy

K. Anupama Francy [1] and Dr.Ch SrinivasaRao [2]
[1] Department of Mechanical Engineering, Vishnu Institute of Technology, Bhimavarm, AP, India,
[2] Department of Mechanical Engineering, Andhra University College of Engineering, Visakhapatnam AP, India,

Abstract – **The present paper deals with input process parameter optimization in an extrusion process using DEFORM-3D software and Taguchi approach. Selection of process parameters in an extrusion process is a trivial task in order to minimize the power consumption as an objective function by using Aluminum alloy 2A12T4. The present research focuses on input process parameters including the shape of the work piece; half die angle, coefficient of friction, logarithmic strain, ram velocity and die length. The simulations are done by DFORM-3D software used for expecting minimum force attained in cold forward extrusion process. The results attained from DFORM-3D software has been comparing with analytical results. The results reveal that effective parameters have the significant influence on decreasing the minimum extrusion force.**

Keywords: DEFORM-3D, Taguchi, coefficient friction, effective stress, extrusion force.

1. INTRODUCTION

The extrusion is a metal forming process is considered by various important variables including cross-sectional area, half die angle, ram speed, frictional conditions, extrusion ratio, and material properties of the work piece. This process is an attractive production method in industry for its ability to achieve energy, material saving, quality improvement and development of homogeneous properties throughout component [1].Many industrial applications requires excellent capability from area of cross-section, aluminum is find an ideal material, because it has ability to extrude any shape. Aluminium and its alloys makes high strength-to-weight ratio better than other materials. Now-a-days, in the manufacturing process the use of computer aided design gives more accuracy, reduces design time, improves tolerance and also decreases each stage of the process [2].

In general for the curved sections, the conical extrusion dies have been preferred because it can be manufactured very easily. Noorni [3] found the effects of die profile on the cold extrusion of aluminum by experimentally and numerically. The deformation load was reduced, the metallurgical properties of the product and die life was improved by considering optimum die profile. The optimum die geometry was found by means of incremental slab method. The two types of optimized extrusion dies, namely curved and conical dies were used and compared.

Through conical converging dies Zimerman [4] analyzed the plastic zone in radial flow. The assumed boundaries have been generalized and the actual solution has been approached by selecting lowest possible upper bound and highest possible lower bound. The exact energy was obtained by selection of flow pattern through conical dies. A kinematically admissible velocity field has been built up for the process of extrusion through a wedge shaped die. This velocity field satisfies the asymptotic behavior of the real velocity field in the vicinity of maximum frictional surfaces [5].

A new slab method was applied to three-dimensional problems in metal forming by Ghoschi [6]. In this analysis a parametric slab has considered and free balance on the slab was carried out to obtain equilibrium equations. The geometry of the final extruded shape, the die and the material flow region assumed in the formulation has been correlated with the parameters. The effect of reduction of area, frictional conditions and other process parameters on the extrusion pressure has been analyzed. Both experimental and theoretical results obtained have been validated.

The capabilities of the DEFORM system for the automatic mesh generation and re-meshing which is an essential feature for Industrial applications. The design of the complex cold forging process has been mainly achieved based on experience of trial and error. Development of the process simulation technology enables a designer to study and even optimize the cold forging process on a computer before actual tryout which reduces process design cost and time [7].

3D FEM simulations are performed on Aluminum extrusion in order to determine state of stress, strain and the temperature of a commercial aluminum alloy sent through square and round dies. From the simulations, under the process conditions, the state of stress in the aluminum alloy extruded through round dies is more favorable than square die especially at reduction ratios. [8]. In addition to 3D FEM simulations of the extrusion die pocket on metal flow to yield two chevron profiles with unequal thicknesses through two hole dies. The predicted values of extrusion through various designs of pocket dies have been validated with the extrusion experiments. 3D FEM simulations were proven to be an efficient tool in optimizing the die design and decreasing the number of trial runs.

The present research work is concerned with the effect of input process parameters on the extrusion force. Selection of input process parameters such as half die angle, extrusion ratio, length of the work piece, geometry of the cross- section, coefficient of friction, ram speed can significant load and energy saving, when this manufacturing process is employed. Taguchi technique was used to determine minimum extrusion force, deform-3D software were used for simulations.

 ISBN: 978-93-91420-02-4

2. FORCE PREDICTION MODEL

In the present paper the solid forward extrusion process was consider to analyse the forces because the direction of the flow of metal is in the same direction of the direction of punch. The samples of
Aluminum alloy 2A12T4 ingot taken as a billet material whose chemical composition is presented in table1.

Table.1.Chemical composition of aluminum alloy 2A12T4

Element	Composition (wt %)
Si	0.45
Mg	0.50
Fe	0.22
Cu	0.03
Mn	0.03
Ti	0.02
Cr	0.03
Al	98.72

The material of the billet was Aluminum modeled as a Von Mises elastic-plastic material with isotropic hardening.

According to Holloman, based on compression test the data for the flow stress curve has the following form [10].

$$\sigma = C.\emptyset^{n}$$

Where σ is the flow stress, C is constant, and n is strain hardening coefficient. The following equation was taken from the reference [12] for mean flow stress.

$$\sigma = (570.558).\emptyset^{0.16}$$

For the total forward extrusion force based on the literature known mathematical model.

$$F_{tot} = A_o\sigma_f\left[\frac{2}{3}\alpha + \left(1+\frac{2\mu}{\sin^2\alpha}\right)\phi_{\max}\right] + \pi d_0 l.\mu.\sigma_f \quad --(1)$$

3. MODELING AND SIMULATION OF COLD FORWARD EXTRUSION.

The die geometry, work piece and punch tool were designed in CATIA software. Figure 1. Shows assemble component of billet, die and punch having the billet diameter of 15mm and length 20mm with meshing before deformation. The die and punch were considered as a rigid material whereas the material of the billet was considered as plastic. Three die angles such as 30°, 45°, 60°; extrusion ratio 1.2, 1.5,2 and coefficient of friction as 0.066, 0.7 were considered as input process parameters. The initial cross section of the billet was round. The billet, punch and die of varying dimensions were generated in CATIA and then transferred in the STL format to Deform-3D. A four node tetrahedral element with the Lagrangian increment was applied. A finite element mesh is done automatically with number of nodes 1412, elements 5851 and surface polygons 1556. The billet is permitted only finished conical converging die for different reductions and friction with constant die length. The material properties were selected from software data base for simulation. The Newton-Raphson method was used for the solution of the non-linear simulation equations. The flow stress ($\bar{\sigma}$)was a function of effective strain ($\bar{\epsilon}$), effective strain rate,($\dot{\bar{\epsilon}}$)and temperature(T) in the isotropic rigid plastic model.

$$\bar{\sigma} = \sigma(\bar{\epsilon}, \dot{\bar{\epsilon}}\mathrm{T}) \text{ ---------- (2)}$$

Figure 1. shows the initial geometry of the billet, punch and container/die also the billet with meshing.

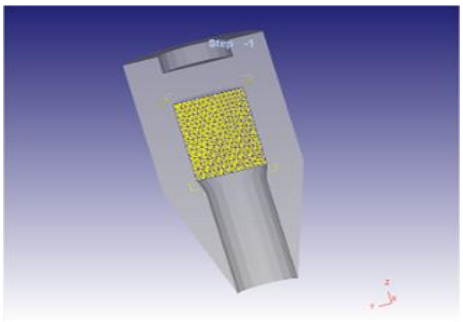

Fig.1. Initial geometry with billet, punch and container

4. TAGUCHI APPROACH

To achieve more efficiency, Taguchi optimization method is used in the present. The results obtained by using DEFORM-3D software are set by the Taguchi approach. The key set up in the Taguchi optimization approach is the parameters design and to increase the more quality of the product without increasing the cost. The appropriate Taguchi three factorial with three level orthogonal array L_{18} with notations is designed for the experimental set up. In this approach, the simulation results are transformed into S/N ratios. The S/N ratio is calculated by the following equation:

$$\frac{S}{N} = \eta = -10\log_{10}\left[\frac{1}{n}\sum_{i=1}^{n} y_i^2\right] \text{------ (3)}$$

Where η is called signal to-noise ratio. i.e. is (S/N), 'n' is called number of repetitions of the experiment, and y_i is the measured value of quality characteristic. Therefore, it is a minimization problem, the (S/N) ratio is calculated smaller is better which means minimization of the extrusion force.

Figure 2 shows the change of S/N ratios of control parameters is changed from one value to another. By the response graphs presented, the setting of control parameters with best quality can be achieved. The determination of optimal design process parameters, estimation of quality characteristics and prediction of optimal design parameters can be achieved by Taguchi approach [11].

 ISBN: 978-93-91420-02-4

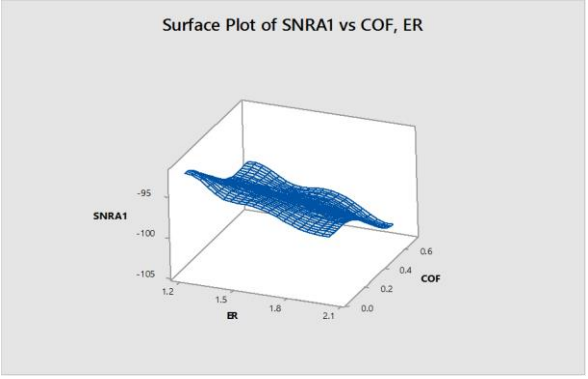

Fig 3.The response surface graph for μ=0.066.

5. RESULTS AND DISCUSSION

Figure 4 and 5 shows post processor result analysis with a load stroke plot for run 340 and 240 run with extrusion ratio 1.2, coefficient of friction 0.066 and die angle 30º,having die length 20mm and billet diameter 15mm combinational set. The figure also shows the maximum principal stress and velocity distribution across the billet at the various stages of extrusion process is presented.

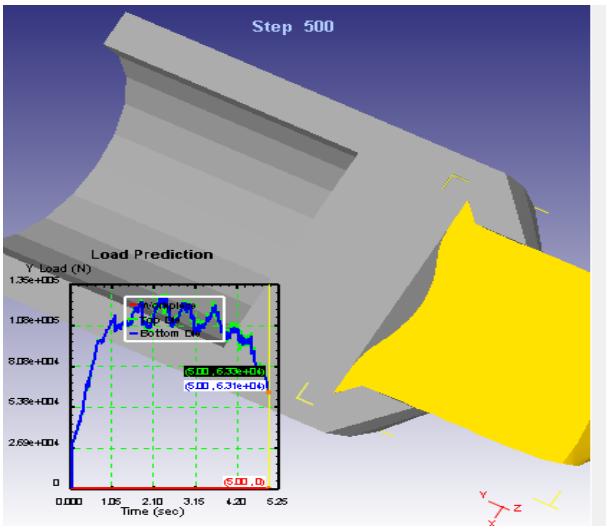

Fig 4. Prediction of load-stroke plot and effective stress distribution from the post –processor analysis

Table.2. 18 set of combination of parameters with output and also comparison

COF	ER	DA(°)	Force (Deform-3D)	Slab Analysis
0.066	1.2	30	55100	51200
0.066	1.2	45	63100	61147
0.066	1.2	60	78400	76048
0.066	1.5	30	90500	74551
0.066	1.5	45	105000	89754
0.066	1.5	60	145000	106450
0.066	2	30	167000	111200
0.066	2	45	192000	126740
0.066	2	60	205000	145020
0.7	1.2	30	89230	69197
0.7	1.2	45	91600	80510
0.7	1.2	60	104000	98437
0.7	1.5	30	185000	128740
0.7	1.5	45	191000	136670
0.7	1.5	60	205000	160640
0.7	2	30	295000	209520
0.7	2	45	305000	211880
0.7	2	60	345600	243330

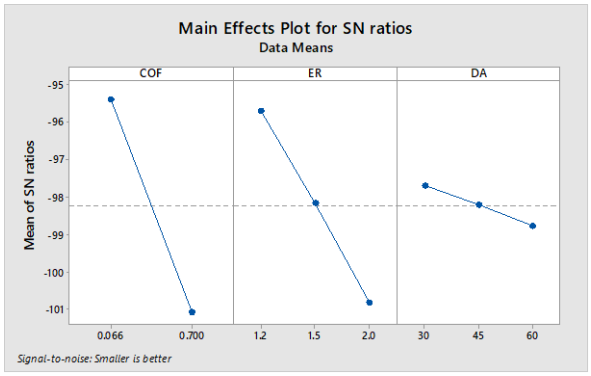

Fig 2.S/N graphs for control parameters

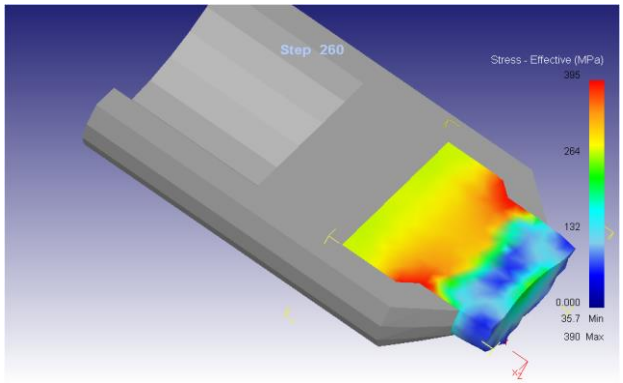

Fig 5. Effective stress distribution from the post processor analysis

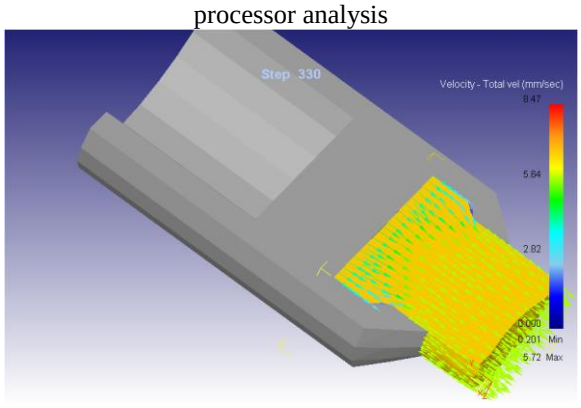

Fig.6.The velocity distribution across the die profile

From figure 6, it is clearly observed that there is no dead metal zone formation by using the conical die profile. Therefore, when there is no dead metal zone means there is no extra energy

consumption to overcome redundant work which only minimizing the minimum extrusion load requirement.

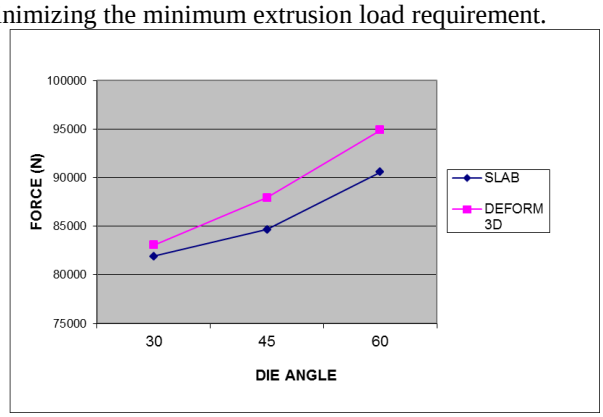

Fig 7.Comparision of analytical and simulation results

Figure 7 shows the comparison among the analytical method and simulation. It is observed that, deform results are well matched with analytical method. When the die angle increases, the extrusion pressure also increases because large area of contact.

6. CONCLUSION

Extrusion force is one of the most important specifications in extrusion process. Therefore, the study of this parameter is of utmost importance. This work addresses the selection of process parameters in an extrusion process to minimize the power consumption. Aluminum alloy 2A12T4 of extrusion has been used to evaluate the effect of various parameter settings. The results obtained from DFORM-3D software compared with analytical results. The parameters extrusion ratio, coefficient of friction and die angle have the maximum significance in reducing the extrusion force.

In the next case, Taguchi is used to determine the optimal values of input process parameters to achieve the minimum extrusion force. The optimal process parameters for extrusion force are die angle 45^{o}, extrusion ratio 1.2 and coefficient of friction 0.066.

REFERENCES

1. K. Karayel; Simulation of direct extrusion process and optimal design of technology parameters using FEM and artificial neural networks, key engineering materials. 2008.367:185-192.
2. UK Aluminum Industry Fact Sheet 9: Aluminum Extrusions. www.alfed.org.uk.
3. Noorani-Azad, M.Bakshi- Jooybari, M. Hosseinipou, S.J. Gorji, A Experimental and numerical study of optimal die profile in cold forward rod extrusion of aluminum , Journal of Material Processing Technology 2005, 164-165,1572-1577.
4. Zimerman, B.Avitzar, Metal flow through conical converging dies- A lower and Upper Bound Approach using Generalized Boundaries of the Plastic zone ,Journal of Engineering for Industry 1970,(119-129)
5. Sergei Alexandrov, Yusof Mustafa, Yeong-Maw-Hwang and Elena Lyanima, An accurate Upper Bound solution for strain Extrusion through a Wedge –Shaped Die. The Scientific World Journal Volume 2014, Article ID 189070.
6. A. Samadi Ghoshchi, S.M.Bazargani and S.Emani, Slab method of Analysis for three Dimensional Forward Extrusion of Squared End Section , 10th Biennai Conference on Engineering Systems Design and Analysis ,ASME 2010, Volume 4(491-495)
7. S.I. Oh,W.T.Wu and J.P.Tang, Simulations of cold forging processes by the Deform system,Journal of Materials Processing Technology 1992,Volume 35(357-370).
8. T.Chandra.J.Zhou. J.Duszczyk, FEM Analysis of Aluminum extrusion through square and round dies, Materials and Design 2000, Volume 21(323-335).
9. G.Fang, J.Zhou and J. Duszczyk. FEM Simulation of Aluminum extrusion through two hole Multi-Step pocket dies, Journal of Materials Processing Technology 2008, Volume 209,(1891-1900).
10. Lange, K. Handbook of metal forming, 1985, McGraw-Hill, New York.
11. W.H.Yang; Tang Y.S. Design optimation of cutting parameters for turning operations based on the Taguchi method, Journal of Materials Processing Technology 1998, vol 84, 122-129.
12. A. Hosseini, Kh. Farhangdoost, M. Manoochehri Modelling of extrusion process and application of Taguchi method and ANOVA analysis for optimization the parameters. ISSN 1392 - 1207. MECHANIKA. 2012 Volume 18(3): 301-305.

 ISBN: 978-93-91420-02-4

Importance of Ice Jet machining - A Review

Penugonda Sundara Krishna and Mrs. I.Sri Phani Sushma
Departement of Mechanical Engineering, University College of Engineering JNTUK Narasaraopet, Andhra Pradesh, India

***Abstract*— Ice jet technology also known as Ice Abrasive Water Jet (IAWJ) machining is one of the machining process for removal of work piece material and is a prototype technology currently under development. In IAWJ technology ice particles made from water are used instead of mineral abrasive. The aim is to increase the productivity of pure water jet (WJ) while keeping its advantages, producing no other waste product but water. Although the use of Abrasive Water Jet (AWJ) technology in cutting, cleaning, machining and surface processing is a very successful industrial process, a considerable amount of secondary particle waste and contamination impingement by abrasive materials has been an important issue in AWJ process and this was overcoming by this process. This review paper mainly focusses on generation of ice particle, advantages, disadvantages, applications of this process**

Keywords*— *IAWJ machining; Ice Jet; Ice abrasive; Ice particles.

I. INTRODUCTION

Actually, there are several limitations for traditional machining process, because of which it is very difficult to machining some materials. Here this Ice jet machining process is a type of unconventional machining process which uses ice as abrasive particles for machining. Abrasive water jet (AWJ) machining process uses a high-speed water jet for acceleration of very hard abrasive grains, enabling the removal of work piece material. The high-speed waterjet is generated by pushing the water under high pressure, up to 600 MPa, through the water nozzle of a small diameter (from 0.08 mm to 0.4 mm) where the potential energy is transformed to kinetic energy, achieving supersonic speeds of the formed water jet. The process is universal as it is possible to machine almost any kind of material regardless of its composition, structure, hardness or other physical properties. This makes it possible to machine different materials that cannot be machined by traditional machining processes. AWJ machining technology has received considerable attention from several domains of production industry due to this competitive advantage.

In AWJ machining, the quantity of waste abrasive material produced is huge compared to the quantity of removed workpiece material. Handling of this sludge is usually not critical since abrasive material is non-toxic, but in e.g., disintegration of nuclear power plants the quantity of sludge plays an important role. Ice abrasive water jet (IAWJ) technology, also named Ice Jet, uses ice grains that melt away after the machining instead of mineral abrasive. The technology also has a great potential in both food and medical industries for applications. It is expected that the machining capability of IAWJ technology will be between pure WJ and AWJ technology [1]

In abrasive water jet cutting the water jet contains abrasive particles such as silicon carbide (SiC) or aluminium oxide (Al2O3) to increase the material removal rate when compared to water jet machining. By using this technique, hard brittle materials such as ceramics, metals and glass and also soft materials such as foam and rubbers can be cut. But, the major disadvantages of this method are high capital cost and high noise levels during operation. [2]. Another advantage of the water jet is the ability to cut material without interfering with its inherent structure, as there is no heat-affected zone (HAZ). Minimizing the effects of heat allows metals to be cut without harming or changing intrinsic properties [3, 4]

II. HISTORY OF ICE JET MACHINING PROCESS

The first experimental researching done on Ice Jet technology dates back to 1982, when the first ice particles were created by mechanical crushing of bigger ice particles. Galecki and Vickers performed surface cleaning and abrading with an ice-blasting technique. The ice particles were produced by refrigeration of 3 cm blocks, which were then transferred to a container of liquid nitrogen where the ice cubes were further cooled, and finally transferred to a mechanical crusher where those were crushed and subsequently entrained into a nozzle.

Also in 1982, Krzysztof et al. showed that one of the most promising applications for ice particles is the cleaning technology. Water ice is readily available, inexpensive material, which can be used as a green manufacturing tool. Only water, electricity and refrigerant are needed for the fabrication of this tool, which can be produced just in time. The use of ice tools might practically prevent pollution and eliminate work piece contamination.

Since then, several researchers have developed equipment for producing ice particles, mainly for cleaning polishing and surface decontaminating purposes. Newer research works and show that ice particles can be used for water jet applications such as cleaning, degreasing and cutting. Anyway, the process productivity is less than when using mineral abrasive particles [5]. Generally, ice is even preferred for other super finishing process such as dry ice deburring process, dry ice blasting process

Dry Ice Deburring Process

- Removal of burrs from edges and holes.
- Where burrs could not be removed with any other means like filing or grinding.

Dry Ice blasting process

- Used for cleaning purpose
- Cleaning of engine block can be done with ice blasting process effectively

III. GENERATION OF ICE PARTICLES

There are two approaches to generate ice particles [1]

1. Generating the ice in a generator before mixing it to the water jet.
2. Forming ice particles during water jet formation by introducing a cooling gas like liquid nitrogen

3.1 Using Ice Generator:

 ISBN: 978-93-91420-02-4

This figure shows ice generation by introducing the liquid nitrogen to the atomized water droplets.

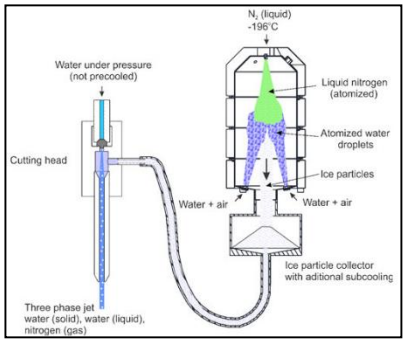

Fig-1 ice generation system using ice generator [6]

Here in fig-1 ice particles are generated in a separate collector and temperature of the liquid nitrogen is -196 C. Here liquid nitrogen (N2) is a cryogenic liquid as the water comes into contact with liquid nitrogen it is converted into ice particles. It is collected into the storage tank and additionally cooled. When it is required, this is sent to jetting head where it is supplied under pressurized water to get material be machined

3.2 By introducing cryogenic gas to water jet:

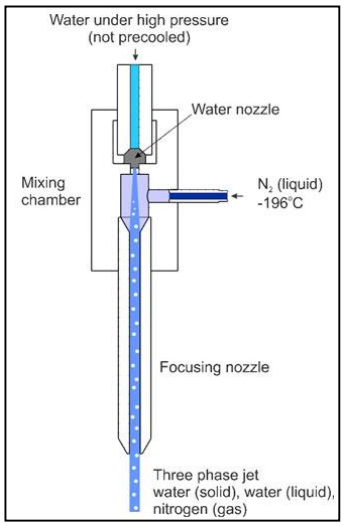

Fig-2 Ice formation directly on jetting head [6]

Here in the fig- 2 cryogenic gas i.e., liquid Nitrogen is directly introduced to the jet of the ice. Due to low temperature of the LN, ice particles are formed into the jet of ice. But compressor, nozzle, atomizer is same in both process.

IV. REQUIRED SPECIFICATIONS

- Water Pressure: 50 to 700 MPa (for harder materials: 700 MPa & for softer materials: 50 MPa
- The ultrasonic atomizer used in the ice particle generator can produce uniform water droplets of 45 to 90 microns and 2 ltr/hr to 12 ltr/hr.
- Water nozzle diameter:0.1mm to 0.3mm
- Speed of water jet:500 to 900 m/s
- No heat affected zones.
- Treatment of all kind of materials.

V. COST ANALYSIS FOR AWJ, WJ AND IJM

Cost source	AWJ	WJ	IJM
Depreciation	2040		
Maintenance	510		
Abrasive	749.7	0	0
N2	0	0	906.78
Replacement of wearing parts	197.88	30.6	153
Electric power	414.12	37.74	225.42
HP pipe cooling	0	0	131.58
Water consumption	12.24	1.224	32.64
TOTAL	**3923.94**	**2619.564**	**3999.42**

Table-1 comparison of costs of various process

Here table-1 provides the detailed analysis of ice jet machining (IJM) with abrasive water jet machining and water jet machining. There is no abrasive cost in IJM as water is natural resource. There would be additional cost for liquid nitrogen (N2) - cryogenic liquid compared with remaining processes. Remaining factors are same for all process. Compared with remaining processes this process (IWJ) is high

VI. ADVANTAGES AND DISADVANTAGES OF ICE JET MACHINING PROCESS

6.1 Advantages:

- As the hardness of ice is less than that of the abrasives used in conventional AWJ, IJ may not be as highly productive as AWJ. However, cost reduction and elimination of the negative environmental effects could overweigh the reduction in productivity [7].
- We can reuse the water as it is free from contaminations
- Ice Jet process is an environmentally friendly process which makes worth its value.
- Uses natural resources
- It has 40% more MRR compared with water jet manufacturing
- Also, solid waste is produced in the AWJ technology and it pollutes the environment [8].
- Heat affected zone (HAZ) is generally with metals where the cutting process will generate enough heat to change the mechanical properties of the metal, essentially locally heat treating the material at and nearby the cutting area. Water jet does not get near hot enough to create a heat affected zone [9]

6.2 Disadvantages

- Injection of ice particles in to the water jet it is not a complicated task but it requires continuous monitoring of the process to control the temperatures in order to avoid clogging and melting

 ISBN: 978-93-91420-02-4

of the ice particles. However, this can be automated [10]

- Cost of this process is very high compared with other process
- We should safe with liquid nitrogen (N_2)

VII. APPLICATIONS OF ICE JET MACHINING PROCESS

7.1 Food industry:

To cut meat this process is widely used as contamination is very negligible.

7.2 Medical industry:

Surgical device handles and stents, maintaining product quality and clean manufacturing equipment is important, keeping micro-cavities clean, as well as cleaning the small, deep, and complex geometry of micro-tools, is a critical concern when manufacturing very high tolerance medical device parts.

VIII. CONCLUSIONS

This ice jet machining process is an unconventional process which was used as a machining and as a super finishing process. The feasibility of the use of ice particles as a pollution free machining tool was demonstrated. It might therefore be applicable in the primary cutting of carcasses (meat and bone) in abattoirs. The process might also have use in the cutting of frozen and soft foods. These enhanced hygienically beneficial effects can be achieved at far lower water pressures than are required in the cutting of common engineering materials. Soft food products should be undamaged by ice-jet cutting. The cutting of human and other tissues by non-traditional abrasives included in water-jet processes also becomes relevant.

This emerging technology includes precision cleaning of highly delicate and complex mechanical, electronic and biomedical components. A low cost of ice-air cleaning will enable us to use it for processing large surfaces at a high rate. Still another application involves cleaning of sensitive facilities such as lining of pharmaceutical or food processing reactors, aircraft skin, etc. Cleaning of discarded parts for reuse or recycling constitutes another potential application [10]

A disadvantage of WJC is the high capital cost of the equipment. The highest cost is that of an intensifier pump with high power requirements. Whether lower pressures needed for softer biomaterials reduce this cost and it is still has to be established [11]

REFERENCES

1. Marko Jerman, Izidor Sabotin, Andrej Lebar, Andrej Lebar "Ice jet technology" Article in MM Science Journal, June, 2018, DOI: 10.17973/MMSJ.2018_06_201772
2. M. Sagar, Experimental investigation and optimization of process parameters in abrasive water jet machine, international research journal of engineering and technology (irjet), volume: 05 issue: 03 | mar-2018
3. https://en.wikipedia.org/wiki/Water_jet_cutter
4. Rushabh B. Joshi, Dr. A. A. Shaikh, Brijesh K. Gotawala, A Review on Abrasive Water Jet Machining on Different Material, 2016 IJEDR | Volume 4, Issue 2 | ISSN: 2321-9939
5. https://en.wikipedia.org/wiki/CryoJet
6. https://www.interempresas.net/MetalMecanica/Articulos/57531-empresa-Iamcut-Tecnalia-participan-proyecto-corte-chorro-agua-particulas-hielo.html
7. Radovan Kovacevic, Ram Mohan, Mohamed Hashish, M. Ramulu "State of the Art of Research and Development in Abrasive Waterjet Machining" Article in Journal of Manufacturing Science and Engineering · November 1997 DOI: 10.1115/1.2836824
8. Dinesh Kumar Shanmugam Industrial Research Institute Swinburne, Faculty of Engineering and Industrial Sciences, Swinburne University of Technology, June, 2005 "Development of Ice Particle Production System for Ice Jet Process"
9. https://engineering.stackexchange.com/questions/18365/why-is-there-no-heat-affected-zone-with-water-jet-cutting
10. Dmitri V. Shishkin "Development of Ice jet Machining Technology"
11. J A McGeough 18th CIRP Conference on Electro Physical and Chemical Machining (ISEM XVIII) "Cutting of Food Products by Ice-particles in a Water-jet" ScienceDirect Procedia CIRP 42 (2016)

 ISBN: 978-93-91420-02-4

Performance Investigation of a Battery Powered Peltier Cooler

Srinivasa Reddy Y, Jabihulla Shariff Md

Department of Mechanical Engineering, PACE Institute of Technology and Sciences, Ongole, AP, India

***Abstract*— Now a days, Thermoelectric cooling systems are used in more applications due to their advantages over conventional cooling devices, such as compact in size, light in weight, high reliability, no mechanical moving parts and no working fluid. Thermoelectric (TE) technology is regarded as alternative and environmentally friendly technology for harvesting and recovering heat which is directly converted into electrical energy using thermoelectric generators (TEG). Conversely, Peltier coolers and heaters are utilized to convert electrical energy into heat energy for cooling and heating purposes. A thermoelectric (TE) cooler, sometimes called a thermoelectric module or Peltier cooler, is a semiconductor-based electronic component that functions as a small heat pump. By applying a low voltage DC power source to a TE module, heat will be moved through the module from one side to the other. One module face, therefore, will be cooled while the opposite face simultaneously is heated.**

In this work, we did investigation on performance of Thermoelectric cooler by installing it in a Industrial Helmet.

Keywords*— *Peltier effect, Thermoelectric Module, Industrial Helmet

I. INTRODUCTION

Thermoelectric coolers (TEC), also known as Peltier Coolers are solid state heat pumps that utilize the Peltier effect to move heat. The principle of thermoelectric cooling dates back to the discovery of the Peltier effect by Jean Peltier in 1834. Peltier observed that when electric current passes across the two junctions of two dissimilar conductors (a thermocouple) there was a heating effect that could not be explained by Joule heating alone. Infect, the direction of current decides the cooling effect or heating effect. This effect can be harnessed to transfer heat, creating a heater or cooler. Peltier could not realize the importance of this phenomenon and the other scientists also could not utilize this phenomenon till late 20th century. Thermoelectric technology, as one entirely solid state energy conversion way, can directly transform thermal energy in to electricity and vice-versa by using thermoelectric transformation materials. A thermoelectric TEC has no moving parts, and is compact, quiet, highly reliable and environment friendly. Due to these merits, this technology is presently becoming a noticeable research direction.

There are three types of thermoelectric effects: The Seebeck effect, the Peltier effect, the Thomson effect. From these three effects, Peltier cooler works on the Peltier effect; which states that when voltage is applied across two junctions of dissimilar electrical conductors, heat is absorbed from one junction and heat is rejected at another junction.

LITERATURE REVIEW

A. Performance Investigation

The novel concept of thermoelectric self-cooling introduced as a cooling and temperature control of a device using thermoelectric technology without electricity consumption was studied by Martínez et al., 2011. Various theoretical and experimental studies have been reported to evaluate and enhance the utility of thermoelectric coolers. The performance of a thermoelectric air cooling module for electronic device was studied by Chang et al., 2009. It was shown that at a specific heat load, the thermoelectric cooling module reaches the best cooling performance at an optimum input current. An experimental investigation using a Peltier thermoelectric cooler to cool down a cryoprobe for cryosurgery was performed by Putra et al., 2010. Two prototypes of cryosurgery devices consisting of 5 to 6 stages of TEC modules were analyzed using a variety of electrical voltages. A model of thermoelectric generator driven thermoelectric refrigerator with external heat transfer was probed. The influence of the external and internal irreversibilities of the thermoelectric refrigeration device on the performance of the system was analyzed (Chen et al., 2011, Pan et al., 2007).

B. Recent Developments in Thermoelectrics

Thermal resistance models extensively adopted in the previous two stage thermoelectric cooler studies could not predict the two-stage thermoelectric cooler performance accurately because they assume the one-dimensional temperature distribution and constant material properties. The results also show that the thermoelectric element number on the hot stage should be larger than that on the cold stage for improving the cooling capacity and COP. It was also reported that the performance can be improved by applying the different amount of current in two stages. Wang et al (2014). Geometric design of an integrated thermoelectric generation-cooling system was performed numerically by Chen et al. (2014) using a finite element method. In the system, a thermoelectric cooler (TEC) was powered directly by a thermoelectric generator (TEG). Two different boundary conditions in association with the effects of contact resistance and heat convection on system performance were taken into account.

II. THEORY

The thermoelectric effect is the direct conversion of temperature differences to electric voltage and vice versa. A thermoelectric device creates voltage when there is a different temperature on each side. Conversely, when a voltage is applied to it, it creates a temperature difference. At the atomic scale, an applied temperature gradient causes charge carriers in the material to diffuse from the hot side to the cold side. The term "thermoelectric effect" encompasses three separately identified effects: Seebeck effect, Peltier effect, and Thomson effect.

 ISBN: 978-93-91420-02-4

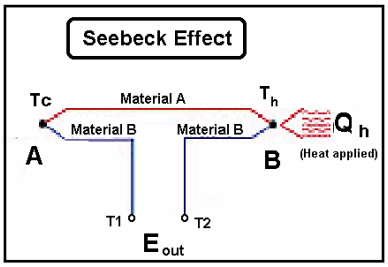

A. Seebeck Effect

The Seebeck effect is the conversion of heat directly into electricity at the junction of dissimilar electrical conductors. It is named for the Baltic German physicist Thomas Johann Seebeck.

The Seebeck EMF, can be expressed as

$$E_{out}=\alpha\ (T_h-T_c)$$

B. Peltier Effect

Peltier found there was an opposite phenomenon to the Seebeck Effect, whereby thermal energy could be absorbed at one dissimilar metal junction and discharged at the other junction when an electric current flowed within the closed circuit.

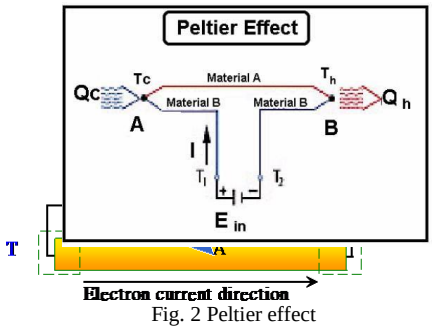

Fig. 2 Peltier effect

The Peltier effect can be expressed mathematically as

$$Q_C \text{ or } Q_{H = \beta\ X\ I = (\alpha\ T)\ X\ I}$$

C. Thomson Effect

As per the Thomson effect, when an electric current is passed through a conductor having a temperature gradient over its length, heat will be either absorbed by or expelled from the conductor. Whether heat is absorbed or expelled depends on the direction of both the electric current and temperature gradient. This phenomenon is known as the Thomson Effect.

Choosing materials

The best thermoelectric materials currently available, compounds of doped Bi_2Te_3, have ZT≈1 at room temperature and attain maximum temperature differential of

≈82K. Some of the commonly used conventional thermoelectric materials are as follows:

- Bi_2Te_3, Bi_2Se_3 and Sb_2Te_3 ; ZnSb, PbTe and PbSe Bi_2Te_3, this compound has been extensively used in the construction of thermoelectric modules. The performance of these modules has steadily improved, since the original observations, due to a number of factors. The thermoelectric figure of merit has increased from the order of 0.5 to values significantly greater than one.

III. WORKING AND FABRICATION

The Peltier effect occurs whenever electrical current flows through two dissimilar conductors; depending on the direction of current flow, the junction of the two conductors will either absorb or release heat. In the world of thermoelectric technology, semiconductors (usually Bismuth Telluride) are the material of choice for producing the Peltier effect because they can be more easily optimized for pumping heat. Using this type of material, a Peltier device (i.e., thermoelectric module) can be constructed in its simplest form around a single semiconductor "pellet" which is soldered to electrically-conductive material on each end (usually plated copper). In this configuration, the second dissimilar material required for the Peltier effect, is actually the copper connection paths to the power supply. [10] It is important to note that the heat will be moved in the direction of charge carrier movement throughout the circuit (actually, it is the charge carriers that transfer the heat).

When the two ends of two dissimilar conductors are connected to a battery, electrons flow out of one in which the electrons are loosely bound to the one in which the electrons are tightly bound. This occurs due to the deference in the Fermi level between the conductors. The Fermi level represents the demarcation in energy within the conduction band of a metal, between the energy level occupied and unoccupied energy levels. When the two different conductors are joined which have different Fermi levels, electron start flowing from the conductor with higher level to the other one. This flow continues till the electrostatic potential bridges this gap and the two Fermi levels come at the same value. Current passing across the junction results in either a forward or a reverse bias, resulting in temperature gradient. If the temperature of the hotter junction is kept low by removing the heat, the temperature of the cold plate can be cooled by tens of degrees.

A. Fabrication of Peltier cooler

As we have seen in previous section, for producing thermoelectric effect couples of P and N type semiconductors are connected in series by metal plates. By doing this it absorbs the heat from one side and releases the heat to another side.

So, when solid state P-N materials are connected electrically in series and thermally in parallel it makes one thermoelectric unit as shown in Figure 4.

A typical TEC module comprises of two highly thermally conductive substrates ($A1_2O_3$, AlN, BeO) that serve as Hot/Cold plates. An array of p-type and n-type semiconductor ($B_{i2}Te_3$, Sb_2Te_3, Bi_2Se_3, PbTe, Si-Ge) pellets are connected electrically in series sandwiched between the substrates. The device is normally attached to the cold side of the TEC module, and a heat sink which is required for enhanced heat dissipation is attached to the hot side. Solder is normally used to connect the TEC elements onto the conducting pads of the substrates, the component will run as per the efficiency of the thermoelectric module.

D. Governing Equations and performance parameters

1) Cooling power:

The cooling capacity Q_1 results from the energy balance at the cold side of the thermoelectric refrigerator.

The expression for cooling power is

$$Q_1= (\alpha_p-\alpha_n)\ IT1-(T_2-T_1)*(K_p+K_n)-[I^2(R_p+R_n)/2]$$

2) Power consumed:

The electrical power consumption W in the thermo element is the Joule resistance heating plus the power used to create the temperature difference ΔT by applying Peltier voltage

B. Components and Their Specifications

A complete thermoelectric cooling system comprises the Peltier element and heat sink assembly, temperature sensors to monitor the hot and cold plates and a controller unit to ensure the correct current is supplied to maintain the desired temperature difference across the module. The specifications of Peltier module used are

- Model: TEC1-12706
- Voltage: 12V
- U max (V): 15V
- Max Current (A): 4-4.6A
- Cooling Power: Q_c max 50-60W
- Resistance: 2.1-2.4Ω
- Δ T max(Q_c=0): up to 67^0C
- Operates Temperature: -55^0C to 83^0C
- Dimensions: 40mm x 40mm x 3.75mm (L*W*T)

C. Procedure of assembling parts

We all know an industrial helmet and its design; we have to select the area to mount the thermoelectric cooler on the helmet. Mark the top of the helmet and cut the marked part of the helmet.

The thermoelectric module components should be ensure whether it worked correctly or not and the module requires two heat sink and two fans and one thermoelectric cooler. All the components should be arranged in the format, the cool side of the thermoelectric cooler is faced to the bottom and heat side is faced to the top side. The design structure of the thermoelectric cooler is placed inside the helmet and giving the connection of battery $W= (\alpha_p-\alpha_n).I.(T_2-T_1)+I^2.(R_p+R_n)$

3) Coefficient of performance (COP):

The coefficient of performance COP is the ratio between the cooling capacity Q_1 and the electrical power consumption W,

$$COP=Q_1/W$$

4) Maximum cooling power:

Referring equation for cooling power,

$$Q_1= (\alpha_p-\alpha_n)\ IT1-(T_2-T_1)*(K_p+K_n)-[I^2(R_p+R_n)/2]$$

As the current is increased, the Peltier cooling rises linearly but the Joule heating depends on I^2. Thus, a plot of cooling power against current has the parabolic form shown in Figure 6.The cooling power is negative until the Peltier effect is great enough to counteract both heat conduction and Joule heating. As the current increased, Peltier effect increases and after some value Peltier effect will be more that sum of heat conduction and joule heating. So, cooling power will become positive at a certain value of the current. However, as the current is increased further, there will come a point at which the difference between the Peltier cooling and the Joule heating begins to diminish. In other words, there is a particular current at which the cooling power reaches its maximum value. To find the maximum cooling power, differentiating Q_1, with respect to I and equating it to 0,

$$dQ_1/dI =0$$

Value of maximum cooling power, corresponding to I_{max},

$$Q_{max}= [(\alpha^2*T_1^2)/2R]-K*(T_2-T_1)$$

5) Figure of merit

We can see from the above equations of Q_{max} and COP_{max} that, it solely depend on Z and the temperatures of the source and sink. So, Z is known as the figure of merit for thermocouple. Z has the dimensions of inverse temperature and it is more usual nowadays to specify the dimensionless figure of merit, which is equal to ZT_m at a mean temperature T_m.

$$Z = \alpha^2/R.K \quad \text{and} \quad ZT_{mean}= (\alpha^2.T_{mean})/R.K$$

Here, R is the electrical resistance.

In practice, ZT represents the efficiency of the N-type and P-type materials which compose a thermo element. A thermoelectric material having a higher figure of merit ZT is more convenient, as it can carry out higher cooling power.

V RESULTS AND DISCUSSION

The variation of temperatures at the hot side and cold side of the heat exchanger as well as the room temperature over operating period of 8 hours, it is worth observing that the temperature drops from 34^0C to 28.2^0C only after 15 minutes. The ambient temperature attains its stable value till the end of operating hours. The achievement of ambient temperature of 24^0C is most probably controlled by the surrounding condition like air conditioning system, good building envelope of the laboratory, and the location of the laboratory which minimizes the exposure of the experiment room to the sunlight. On the other hand, the cold side temperature drops drastically from 25^0C to 23.28^0C in 480 minutes. It maintains nearly constant till the end of operating hour. By contrast, the temperature of the hot side of heat exchanger is found to be decreased from 32.3^0C to 26.7^0C, its lowest temperature after operating in 480 minutes. Its temperature will be then increased slightly and fluctuates between 29^0C and 30^0C. The relatively high temperature of the hot side location is due to the heat released by the heat exchanger. This is because the heat exchanger of thermoelectric refrigerator acts as a solid-state active heat pump which transfers heat from the cabinet (cold side) to its hot side against the temperature gradient with consumption of electrical energy. This working mechanism is called as thermoelectric effect.

VICONCLUSION

With near exhaustion of fossil fuel resources coupled with desire to reduce global warming, it has become increasingly necessary to exploit alternative and renewable energy sources to diversify the energy supply. Thermoelectric (TE) devices are regarded as alternative and environmental friendly technology for harvesting and recovering heat which is directly converted into electrical energy. A notable use of TEG/TEC devices to recover heat energy from, geothermal, biomass, infra-red radiation have been observed in addition to the primary use of TE devices for waste heat recovery. Nevertheless, the main challenge remains in de- signing and optimizing advanced TE

 ISBN: 978-93-91420-02-4

materials with appropriate values of ZT and power factor, calling for more research work into TE technology.

REFERENCES

[1] H. Julian Goldsmid, Bismuth Telluride and Its Alloys as Materials for Thermoelectric Generation, Materials 2014, 7, 2577-2592.

[2] S. Stackhouse, L. Stixrude, Theoretical Methods for Calculating the Lattice Thermal Conductivity of Minerals, Mineralogy & Geochemistry Vol. 71 pp. 253-269, 2010.

[3] Melcor homepage http://www.melcor.com (assessed on October, 2015)

[4] S. Riffat, S.A. Omer, Xiaoli Ma, A novel thermoelectric refrigeration system employing heat pipes and a phase change, Renewable Energy 23 (2001) 313–323

[5] R. Chein, Y. Chen, "Performances of thermoelectric cooler integrated with microchannel heat sinks", International Journal of Refrigeration 28 (2005) 828–839

[6] S. Riffat, X. ma, Improving the coefficient of performance of thermoelectric cooling systems, international journal of energy research Int. J. Energy Res. 2004; 28:753–768

[7] C. Hermes, J. Barbosa, "Thermodynamic comparison of Peltier, Stirling, and vapor compression portable coolers", Applied Energy 91 (2012) 51–58

[8] J. Vian, D. Astrain, "Development of a heat exchanger for the cold side of a thermoelectric module", Applied Thermal Engineering 28 (2008) 1514–1521

[9] Kaseb S., El-hairy G, *Electronics Cooling*, Mechanical Power Engineering Department, Faculty of Engineering, Cairo University, Egypt

[10] Thermoelectric cooling FAQ, Tellurex Corporation

[11] Marc H., *Thermoelectric Modules: Principles and Research*, InterPACK july 6-8, 2011, Portland

[12] Kaseb S., El-hairy G, *Electronics Cooling*, Mechanical Power Engineering Department, Faculty of Engineering, Cairo University, Egypt

[13] Enescu D, Virjoghe EO, *A review on thermoelectric cooling parameters and performance*, Renewable and Sustainable Energy Reviews , 2014, 38:903–916

[14] Goldsmith, H.J., *Introduction to thermoelectricity*, Springer-Verlag Berlin Heidelberg 20

 ISBN: 978-93-91420-02-4

Analysis of Disc Brake Rotor using ANSYS Workbench

Sai Durga Kiran Pulletikurthi, Satish Kona and Balaji Naik Mudavath
Department of Mechanical Engineering,UCEN-JNTUK, Narasaraopet, Guntur Dist, AP,India.

***Abstract*— Braking system represents one of the most fundamental safety critical components in modern vehicles.Brake absorbs kinetic energy of the rotating parts (wheels) and the energy is dissipated in the form of heat energy to the surrounding atmosphere. Disc (Rotor) brakes are exposed to large stresses during routine braking and extraordinary thermal stresses during hard braking. The aim of the project is to model a disc. Modeling is done using ANSYS design modeler. Structural and Thermal analysis is to be done on the disc brakes using three materials i.e. cast iron, aluminum alloy and carbon fiber. Structural analysis is done on the disc brake to validate the strength of the disc brake and thermal analysis is done to analyze the thermal properties. Comparison can be done for deformation, stresses, temperature from the three materials to check which material is best. ANSYS is general-purpose finite element analysis (FEA) software package. Finite Element Analysis is a numerical method of deconstructing a complex system into very small pieces called elements.**

Keywords*— *Disc brake, ANSYS, FEA (Finite element analysis

I. INTRODUCTION (*HEADING 1*)

DISC BRAKE:

A disc brake consists of a cast iron disc bolted to the wheel hub and a stationary housing called calliper. The calliper is connected to some stationary part of the vehicle like the axle casing or the stub axle as is cast in two parts each part containing a piston. In between each piston and the disc there is a friction pad held in position by retaining pins, spring plates etc. passages are drilled in the calliper for the fluid to enter or leave each housing. The passages are also connected to another one for bleeding. Each cylinder contains rubber-sealing ring between the cylinder and piston. A schematic diagram is shown in the figure 1.1. The main components of the disc brake are: The Brake Pads The Calliper which contains the piston The Rotor, which is mounted to the hub When the brakes are applied, hydraulically actuated pistons move the friction pads in to contact with the rotating disc, applying equal and opposite forces on the disc. Due to the friction in between disc and pad surfaces, the kinetic energy of the rotating wheel is converted into heat, by which vehicle is to stop after a certain distance. On releasing the brakes the brakes the rubber-sealing ring acts as return spring and retract the pistons and the friction.

During the braking action, the kinetic energy developed at the wheel is translated into heat energy, which doesn't break up fast profusion into the air stream from the brake to the brake disk, as a result, the thermal conductivity plays a significant role in handling such heat generated.

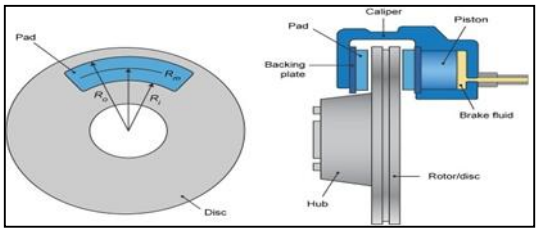

II. MATERIAL PROPERTIES

Disc brakes are made up of various materials. The materials used for this analysis are Cast Iron, Aluminium Alloy and Carbon Fiber. Their properties are shown below.

Properties	Cast Iron	Aluminum Alloy	Carbon Fiber
Density	7100 kg/m^3	2770 kg/m3	1800 kg/m3
Young's modulus	125 Gpa	71 Gpa	395 Gpa
Thermal Conductivity	54.5 W/m k	150W/m k	25W/mk
Specific Heat	586 J/kg C^o		
Compressive Strength	820 Mpa	280 Mpa	869Mpa
Poisons Ratio	0.28	0.33	0.2

III. DESIGN AND CALCULATIONS

Automobile model: Maruti Suzuki Swift

ITEM	**VALUE**
Disc diameter	250 mm
Disc Thickness	20 mm
Weight of Automobile	1335 kg
Top Speed	165 km/h
Tyre Radius	15 inches
Effective Radius Of Rotor	100 mm
Mass of Disc	3.87 kg
Angular Velocity	60 rad/sec
Specific Heat	554 J/kg C^o

 ISBN: 978-93-91420-02-4

IV. METHODOLOGY

A. Modelling of disc ANSYS

The modelling of disc is done is ANSYS design modeller as per the dimensions of the disc rotor of Maruti Suzuki swift. The modelled disc is shown below:

- Poly-line
- Revolve
- Extrude
- Pattern
- Face split
- Circle
- Rectangle etc

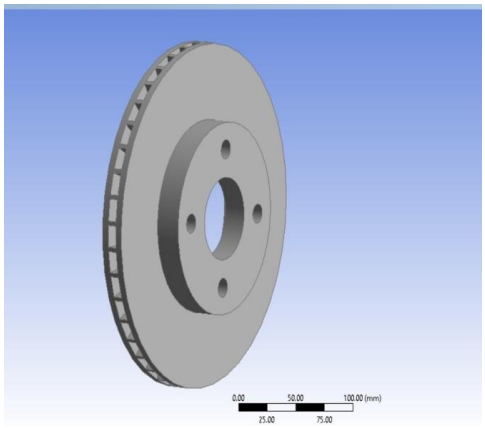

B. Meshing:

The disc is meshed with the 6 node tetrahedral element as shown below for both structural and thermal analysis.For meshing select the geometry and click on generate mesh with required element.The number of elements used for the mesh are 5021 and the number of nodes are 2572.

C. Loading and boundary conditions

For thermal analysis a temperature of 66 degrees is applied on the face of the disc and air convection is applied on the other faces. For structural analysis a force of 12203N is applied on the disc.

The following commands are used for modelling of disc face and fixed support is given at the bolt holes. Along with this a rotational velocity of 60 rad /sec is also applied on the disc. The applied boundary conditions and loading are shown below

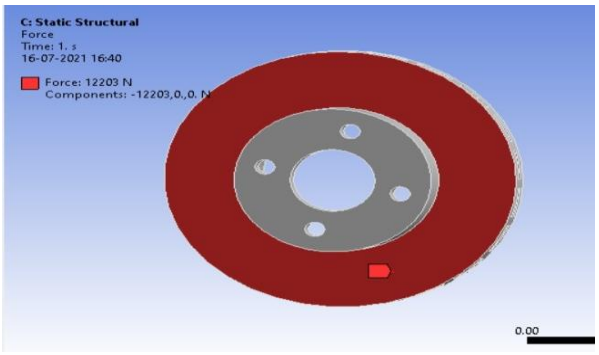

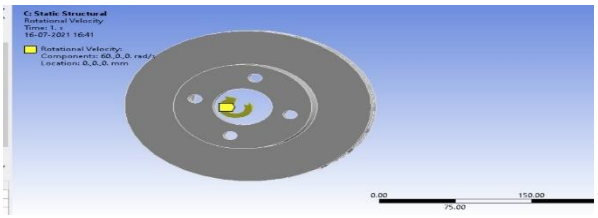

V. RESULTS AND ANALYSIS:

CAST IRON

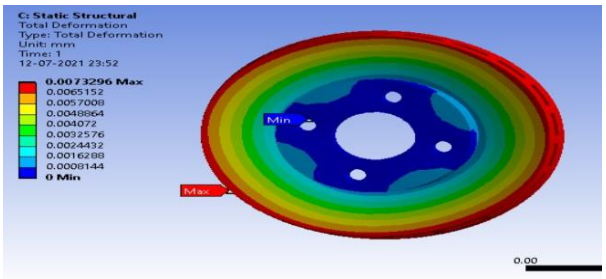

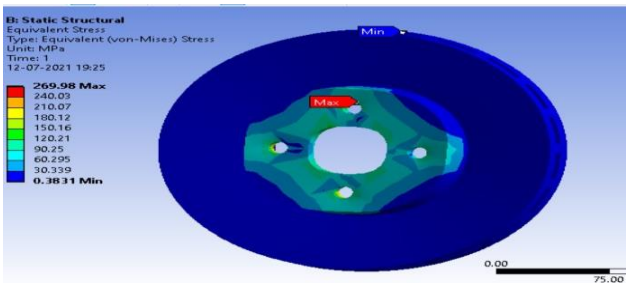

 ISBN: 978-93-91420-02-4

CARBON FIBER

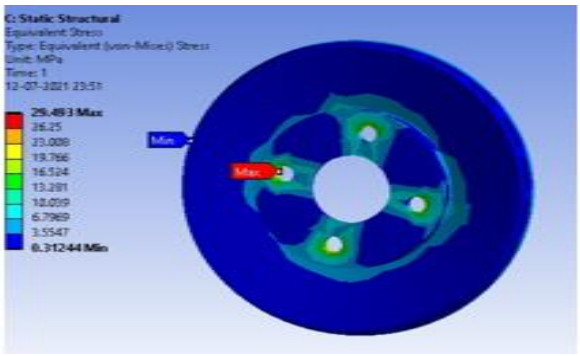

VI. CONCLUSION

It can be observed that from the above results the deformation and stresses are less in carbon fiber material. So carbon fiber material will be best suited as disc brake material.

NOMENCLATURE

E =Energy of the vehicle
M =Mass of Vehicle
m =Mass of rotor
I =Moment of inertia
W =Angular velocity
μ =Coefficient of friction
Rf =Effective radius of the disc
F =Force on the disc
P =Pressure on the disc
C =Specific heat of material

VII. REFERENCES

[1] Machine design by V B Bhandari and R S Khurmi
[2] Finate Element Analysis by Saeed Moaveni
[3] V. Chengal Reddy, M. Gunasekhar Reddy, Dr. G. Harinath Gowd, Modeling and Analysis of FSAE Car Disc Brake Using FEM, ISSN 2250-2459, 3(9), September 2013.
[4] Praveena S, Lava Kumar M, Sreekanth Reddy S, Modeling and Structural Analysis of Disc Brake, ISSN: 2319-8753, 3(10) October 2014.
[5] V. Chengal Reddy, M. Gunasekhar Reddy, Dr. G. Harinath Gowd, Modeling and Analysis of FSAE Car Disc Brake Using FEM, ISSN 2250-2459, Volume 3, Issue 9, September 2013.
[6] S. Lee and T. Yeo, Temperature and coning analysis of brake rotor using an axisymmetric finite element technique, Proc. 4th Korea-Russia Int. Symp. on Science & Technology, Vol.3, pp.17-22, 2000.
[7] Ali. Belhocine, Abd. Rahim Abu Bakar , Mostefa Bouchetara, Structural and contact analysis of disc brake assembly during single stop braking event, American Journal of Mechanics and Applications.
[8] Limpert, R. Brake design and safety (Second Edition), Society of Automotive Engineers, 1999.
[9] Komanduri, R, Hou, Z. B., Analysis of heat partition and temperature distribution in sliding systems, Wear 251 (1-12) (2001) 925-938.
[10] Ozturk, B., Arslan, F., Ozturk, S., Effects of different kinds of fibres on mechanical and tribological properties of brake friction materials, Tribology Transactions 56 (4) (2013) 536-545
[11] Jang, Y.H., Ahn, S. H, Frictionally-excited thermo elastic instability in functionally graded material, Wear 262 (2007) 1102- 1112
[12] Jang, Y.H., Ahn, S. H, Frictionally-excited thermo elastic instability in functionally graded material, Wear 262 (2007) 1102- 1112
[13] G. Ranjith Kumar, S. Thriveni, M. Rajasekhar Reddy, Dr. G. Harinath Gowd, Design Analysis & Optimization of an Automotive Disc Brake, International Journal of Advanced Engineering Research and Science
[14] Haider Hussain and Dr. A.I. Khandwawala. Application of Transient Thermal Analysis For Three Feeder Design Optimization For Sand Casting, International Journal of Mechanical Engineering and Technology, 4(6), 2013, pp. 241-248.
[15] P. Dufr´enoy and D. Weichert. A thermo mechanical model for the analysis of disc brake fracture mechanisms. Journal of Thermal Stresses, 26(8):815–828, 2003.

 ISBN: 978-93-91420-02-4

Modelling and Optimization of Two Wheeler Disk Brake Using ANSYS –Review

Kadru John Babu and Kiran Chand Kopila
Department of Mechanical Engineering, Narasaraopeta Engineering College (Autonomous), Narasaraopet, India.

Abstract— Each single system has been studied and developed in order to meet safety requirement. Instead of having air bag, good suspension systems, good handling and safe cornering, there is one most critical system in the vehicle which is brake systems. Without brake system in the vehicle will put a passenger in unsafe position. Therefore, it is must for all vehicles to have proper brake system. In this paper carbon ceramic matrix disc brake material use for calculating normal force, shear force and piston force. And also calculating the brake distance of disc brake. The standard disc brake two wheelers model using in Ansys and done the Thermal analysis and Modal analysis also calculate the deflection and Heat flux, Temperature of disc brake model. This is important to understand action force and friction force on the disc brake new material, how disc brake works more efficiently, which can help to reduce the accident that may happen in each day.

Keywords— Disc Brake, Thermal Analysis, Modal Analysis, Ansys

I. INTRODUCTION

The disc brake is a wheel brake which slows rotation of the wheel by the friction caused by pushing brake pads against a brake disc with a set of callipers. The brake disc (or rotor in American English) is usually made of cast iron, but may in some cases be made of composites such as reinforced carbon– carbon or ceramic matrix composites. This is connected to the wheel and/or the axle. To stop the wheel, friction material in the form of brake pads, mounted on a device called a brake calliper, is forced mechanically, hydraulically, pneumatically or electromagnetically against both sides of the disc. Friction causes the disc and attached wheel to slow or stop. Brakes convert motion to heat, and if the brakes get too hot, they become less effective, a phenomenon known as brake fade.

Disc-style brakes development and use began in England in the 1890s. The first calliper-type automobile disc brake was patented by Frederick William Lanchester in his Birmingham, UK factory in 1902 and used successfully on Lanchester cars. Compared to drum brakes, disc brakes offer better stopping performance, because the disc is more readily cooled. A disc brake consists of a cast iron disc bolted to the wheel hub and a stationary housing called calliper. The calliper is connected to some stationary part of the vehicle like the axle casing or the stub axle as is cast in two parts each part containing a piston. In between each piston and the disc there is a friction pad held in position by retaining pins, spring plates etc. passages are drilled in the calliper for the fluid to enter or leave each housing. The passages are also connected to another one for bleeding. Each cylinder contains rubber-sealing ring between

The cylinder and piston. A schematic diagram is shown in the figure 1

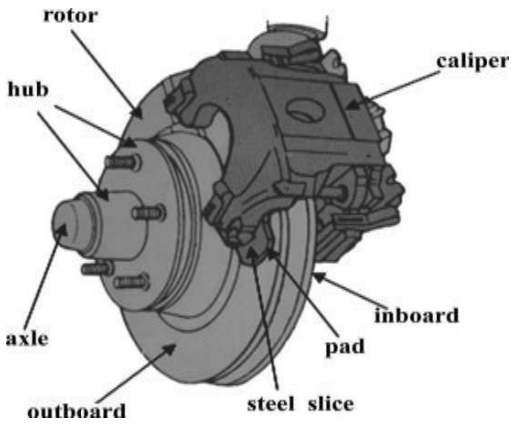

Fig 1 Disc Brake

II. PROBLEM OCCURRED IN DISC BRAKE

Discs are made up mainly gray cast iron, so discs are damaged in one of three ways: scarring, cracking, warping or excessive rusting. Service shops will sometimes respond to any disc problem by changing out the discs entirely. This is done mainly where the cost of a new disc may actually be lower than the cost of workers to resurface the original disc. Mechanically this is unnecessary unless the discs have reached manufacturer's minimum recommended thickness, which would make it unsafe to use them, or vane rusting. Severe (ventilated discs only). Most leading vehicle manufacturers recommend brake disc skimming (US: turning) as a solution for lateral run-out, vibration issues and brake noises.

The machining process is performed in a brake lathe, which removes a very thin layer off the disc surface to clean off minor damage and restore uniform thickness. Machining the disc as necessary will maximize the mileage out of the current discs on the vehicle. Braking systems rely on friction to bring the vehicle to a halt – hydraulic pressure pushes brake pads against a cast iron disc or brake shoes against the inside of a cast iron drum. When a vehicle is decelerated, load is transferred to the front wheels – this means that the front

Brakes do most of the work in stopping the vehicle. Scarring can occur if brake pads are not changed promptly when they reach the end of their service life and are considered worn out.

Cracking is limited mostly to drilled discs, which may develop small cracks around edges of holes drilled near the edge of the disc due to the disc's uneven rate of expansion in severe duty environments. The discs are commonly made from cast iron and a certain amount of what is known as "surface rust" is normal. Sometimes a loud noise or high pitched squeal occurs when the brakes are applied. Most brake squeal is produced by vibration (resonance instability) of the brake

 ISBN: 978-93-91420-02-4

components, especially the pads and discs (known as force-coupled excitation). This type of squeal should not negatively affect brake stopping performance.

III. CALCULATION OF DISC BRAKE

The forces acting on the inner and outer rotor faces due to contact with brake pads are shown in Figure 2

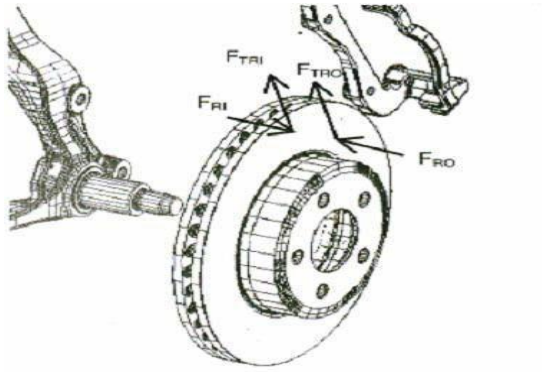

Fig 2 Forces Acting On Rotor Due To Contact with Brake Pads

Disc Brake Standard

Rotor disc dimension = 240mm. (240×10^{-3} m)
Rotor disc material = Carbon Ceramic Matrix
Pad brake area = 2000 mm^2 (2000×10^{-6} m)
Pad brake material = Asbestos
Coefficient of friction (Wet) = 0.07-0.13
Coefficient of friction (Dry) = 0.3-0.5
Maximum temperature = 350 ºC
Maximum pressure = 1MPa (106 Pa)

3.1 Tangential force between pad and rotor (Inner face), FTRI

FTRI = µ1.FRI
Where, FTRI = Normal force between pad brake
And Rotor (Inner)
µ1 = Coefficient of friction = 0.5
FRI = P max / 2 × A pad brake area
So, FTRI = µ1.FRI
FTRI = (0.5)(0.5)(1×106 N/m2) (2000×106 m2)
FTRI = 500 N.

Tangential force between pad and rotor (outer face), FTRO. In this FTRO equal FTRI because same normal force and same material

3.2 Brake Torque (TB) –

With the assumption of equal coefficients of friction and normal forces FR on the inner and outer faces:

TB = FT.R
Where TB = Brake torque
µ = Coefficient of friction
FT = Total normal forces on disc brake,
= FTRI + FTRO
FT = 1000 N.
R = Radius of rotor disc.
So, TB = (1000) (120×10-3)
TB = 120 Nm

3.3 Brake Distance (x) –

We know that tangential braking force acting at the point of contact of the brake, and
Work done = FT. x..... (Equation 1)
Where FT = FTRI + FTRO

X = Distance travelled (in meter) by the vehicle before it come to rest.

We know kinetic energy of the vehicle.
Kinetic energy = $(mv^2) / 2$..... (Equation 2)
Where m = Mass of vehicle
v = Velocity of vehicle

In order to bring the vehicle to rest, the work done against friction must be equal to kinetic energy of the vehicle. Therefore equating (Equation 1) and (Equation 2)
FT. x = $(mv^2) / 2$
Assumption v = 100 kg/h = 27.77 m/s
M = 132 kg. (Dry weight of Vehicle) (mv2) / 2 FT
So we get x =
x = (132×27.772) / (2×1000) m.
x = 50.89 m

Heat Generated (Q) = M .Cp. ΔT J/S
Flux (q) = Q/A W/m^2
Thermal Gradient (K) = q / k K / m

Carbon Ceramic Matrix –

Heat generated Q= m*cp*ΔT
Mass of disc = 0.5 kg
Specific Heat Capacity = 800 J/kg 0 c Time taken Stopping the Vehicle = 5sec Developed Temperature difference = 15 0 c Q = 0.5 * 800 * 15= 6000 J

Area of Disc = Π * (R2 – r2) = Π * (0.120 2 – 0.055 2) = 0.03573 m ^{2}

Heat Flux = Heat Generated /Second /area = 6000 /5 / 0.0357 = 33.585 kw/m 2
Thermal Gradient = Heat Flux / Thermal Conductivity
= 33.582*10 3 / 40
= 839.63 k/m

IV. FEM USING ANSYS

Ansys is one of the useful software for design analysis in mechanical engineering. This software is based on the Finite Element Method (FEM) to simulate the working conditions of your designs and predict their behaviour. FEM requires the

 ISBN: 978-93-91420-02-4

solution of larges systems of equations. Powered by fast solvers, Ansys makes it possible for designers to quickly check the integrity of their designs and search for the optimum solution.

A product development cycle typically includes the following steps:

- Build your model in the Pro-Engineer system.
- Prototype the design.
- Test the prototype in the field.
- Evaluate the results of the field tests.
- Modify the design based on the field test results.

4.1 Model of Disc Brake

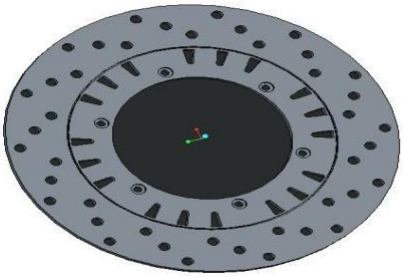

Fig 3 Model of Disc Brake

4.2 Thermal Analysis of Disc Brake

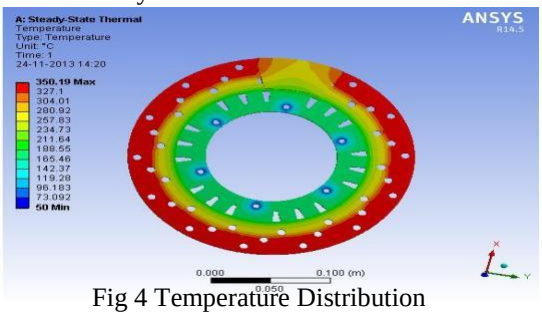

Fig 4 Temperature Distribution

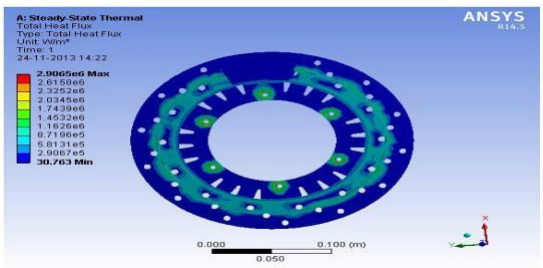

Fig 5 Total Heat Flux

4.2 Modal Analysis of Disc Brake

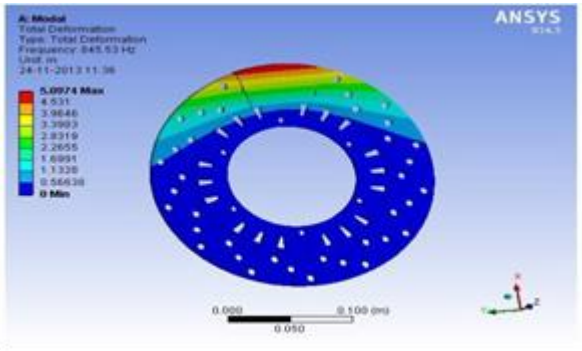

Fig 6 Frequency and Total Deformation of Disc Brake

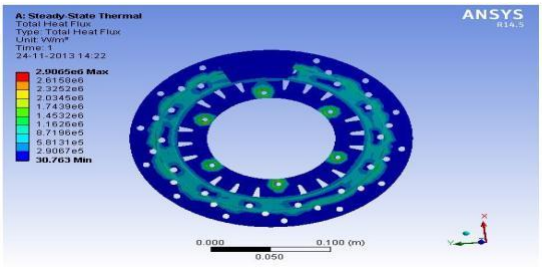

V. CONCLUSIONS

Using carbon ceramic matrix disc brake material calculating normal force, shear force and piston force and also calculating the brake distance of disc brake. The standard disc brake two wheelers model using in Ansys, done the Thermal and Modal Analysis calculate the deflection, total heat flux, Frequency and temperature of disc brake model. This is important to understand action force and friction force on the disc brake new material, which use disc brake works more efficiently, which can help to reduce the accident that may happen in each day.

ACKNOWLEDGMENT

The authors are thankful to all friends and Professors to help the paper and would like to thank the anonymous reviewers for their comments which were very helpful in improving the quality and presentation of this paper.

 ISBN: 978-93-91420-02-4

REFERENCES

[1]Dr. Ramesha, Santhosh Kumar and Bharath Shekar, "Temperature Distribution Analysis of Aluminum Composite and Cast Iron Brake Drum Using Ansys", 'International Journal of Emerging trends in Engineering and Development', 2012, Vol. 3, Issn 2249-6149, pp 281-292.

[2]Ameer Shaik and Lakshmi Srinivas,"Structural and Thermal Analysisof Disc Brake Without Cross-drilled Rotor Of Race Car 2012 , Vol. I, Issn 2249-8974, pp 39-43

[3] Chogdu Cho and Sooick Ahn, "Thermo-Elastic Analysis for Chattering Phenomenon of Automotive Disk Brake", 'KSME International Journal', 2001, Vol-15, pp 569-579.

[4] Guru Murthy Nathi, K. Gowtham and Satish Reddy, "Coupled Structual / Thermal Analysis of Disc Brake", IJRET 2012, Vol.1, pp.539-553.

[5] V. M. Thilak , R. Krishnara Deepan & R.Palani ,"Transient Thermal and Structural Analysis of the Rotor Disc of Disc Brake ", International Journal of Scientific & Engineering Research Volume 2, Issue 8, August-2011 Issn 2229-551.

 ISBN: 978-93-91420-02-4

Fabrication of Sewage Waste Cleaner

Wasima Banu Shaik, Balaji Naik Mudavath, Jagadeesh Tammineni and Anusha Jyothirmai,
Department of Mechanical Engineering, UCEN-JNTUK, Guntur Dist, AP, India.

***Abstract*— Still today, drainage cleaning is a tensed and risky task for sanitary workers. The problem of water clogging arises due to presence of plastic bottles, polythene covers etc., n sewage, which affects the marine life, pest growth, and human health. Our proposed machine finds a solution for all these drainage problems and prevents the humans from getting affected by various diseases. In this project, an attempt has been made to fabricate a sewage waste cleaner for reducing the human work, for minimizing the cleaning time, to combat the increasing pollution problems.**

Keywords*— *Water clogging, Sewage waste cleaner, pollution problems, marine life, human health

I. INTRODUCTION (*HEADING 1*)

Sewage will be formed by the wastes which are coming from the industries, houses, hotels and other chemical factories and by throwing unwanted materials like bottles, polythene covers etc. This contamination makes reuse of waste water very difficult. During rainy seasons and floods the wastes will block the flow of water which leads to more land pollution.

Sewage waste cleaner is a machine which collects all the floating debris present in sewage. This machine is used to clean the drainage canals, gutters, rivers, ponds, and other sewage resources. This cleaner prevents the sanitary workers from cleaning drainages with aid of their hands. One of the best merits of this cleaner is replacing the manual work in drainage cleaning.

II. LITERATURE REVIEW

Machine and Authors	**Outcome**	**Drawbacks**
Automatic Drainage Cleaning System using Solar Panel, (Abhishek Anil Batavale)	Collects solid wastes and filters it from stage to stage.	This machine cannot be used in presence of electricity.
Smart Drainage Cleaning System, (Prof. Amay Tipayale)	By using this, workers can manage their reports through their own mobile phone.	This system needs human attention to check the message and reports in mobile phone.
Automatic Gutter Cleaning System, (S. Navaneetha Krishnan)	Manages the disposal of wastages and with regular filtration.	Needs skill, training and knowledge over automation.

III. PROBLEM STATEMENT

A. Pollution created from plastic bags

It takes 100s of years for plastic bags to completely decompose. Globally we use trillions of bags a year that is approximately 10 million every 5 minutes. In 2002, around 50 to 80, 000, 000 bags ended up as litter in our environment. This accumulation causes harmful effects on aquatic and terrestrial animals.

B. Green house gases

Bio degradable plastic bags take about 3 years to breakdown. The process of breaking down these petrol based bags causes carbon to meeting which is a greenhouse gas.

C. Water Pollution

Water pollution is a major global problem. It affects the entire biosphere. The water pollution is the worldwide cause of death and diseases and for the deaths of more than 14,000 people daily.

IV. MOTIVATION AND OBJECTIVES

Drainage cleaning results in very dangerous diseases and sometimes results in loss of lives due to getting into the drainages and cleaning them .The problem of water clogging occurs due to plastics, bottles, polythene covers, metals etc., which in turn affects the pest growth. Hence, these problems motivated us to fabricate this sewage waste cleaning machine.

Objectives

1. To fabricate and design a portable machine.
2. To provide a flexible frame.
3. To minimize the risk of labour from getting affected by infections, diseases due to chemicals, wastes in sewage.
4. To reduce the labour involvement.
5. To avoid water blockage caused due to garbage.
6. To combat the increasing pollution problems.

To construct the light weight and compact machine

V. METHODOLOGY

METHODOLOGY

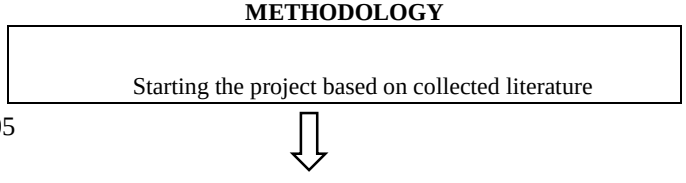

 ISBN: 978-93-91420-02-4

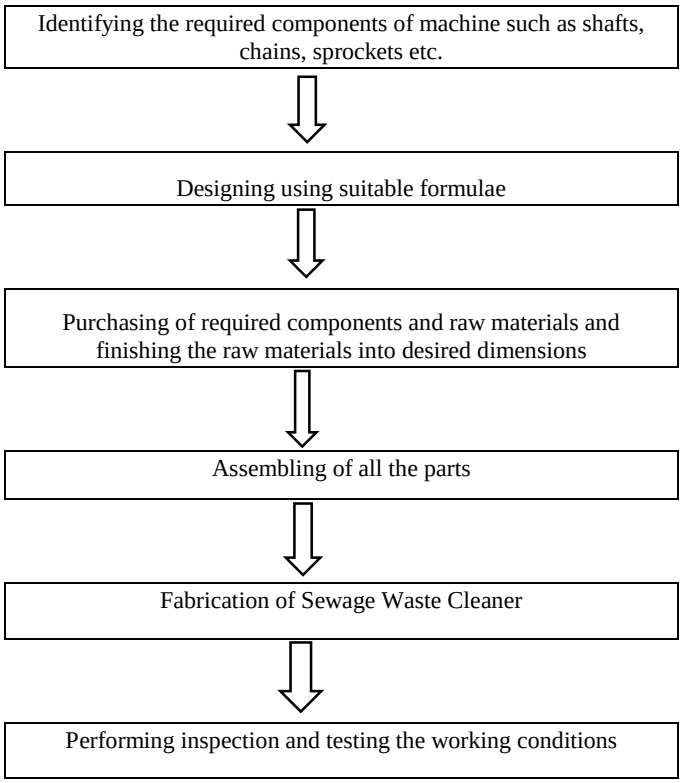

VI. COMPONENTS AND MATERIALS USED

6.1 Sprocket

Material Used: Stainless Steel

Sprocket or sprocket wheel is a profile deals with teeth fixed to the shafts and meshed with the chain drive in this sewage waste cleaner.

6.2 Shaft

Material Used: Mild Steel

Shaft is a rotating machine element usually circular in cross section which is used to transmit power from one part to another, to which motor is connected.7.1

6.3 Bearings

Type: Deep Groove Ball Bearing

Bearing is a machine element that constrains relative motion to only the desired motion and reduce friction between moving parts. These are mounted on shafts in this respective machine.

6.4 Chain

Material Used: Stainless Steel

Chain drive is a way of transmitting mechanical power from one place to another. Most often the power is conveyed by a roller chain. This sewage waste cleaner works on this chain drive mechanism.

6.5 Fasteners

Nut

A nut is a type of fastener with a threaded hole. Nuts are almost always used opposite a mating bolt parts together. The two partners are kept together by a combination of threads friction, a slight stretch of the bolt and compression of parts.

Screw or bolt

A screw or bolt is a type of fastener characteristic by a helical ridge known as external thread wrapped around a cylinder.

6.6 Battery

Battery used is a rechargeable battery, storage battery, secondary cell or accumulator is a type of electrical battery which can be discharged, charged into a load and recharge many times as opposed to disposable or primary battery.

6.7 D.C Motor

D.C motor is designed to convert electrical power into mechanical power.

6.8 Lifting mounts

Material used: Galvanized Iron Sheet

Lifting equipment also as lifting bin is a general term for the machine we used to lift the loads.

VII. DESIGN RULES

7.1Design calculations of motor

7.1.1Workdone to lift garbage upwards

W=F×s=mgsinϴ × $\frac{h}{sin\theta}$=mgh

W= 9× 9.81 × 1 =88.29J

7.1.2Torque of the motor

T=F× $r = mgsin\theta \times 0.025$

$= 9\times 9.81 \times \sin 45° \times 0.025 = 1.56N - m$

$T_{max} = 1.56 \times F.O.S$

($Since\ F.O.S$ is taken as 2)

$=1.56\times 2 = 3.12N - m$

7.1.3 Power of the motor

P=$T_{max} \times \frac{2\pi N}{60}$ =3.12× $\frac{2\times\pi\times50}{60}$=16. 33Watt

$P=16.33\times 2 = 32.66watt$

7.2Design calculations for lifting capacity

$\emptyset = \frac{s}{r} = \frac{h}{rsin\theta}$=56.56rad=9 rev

It takes 9 rev to lift 6kg of garbage once.

As the speed of motor is 50rpm, the chain circulates 5 times to lift the garbage in 1 min

Lifting capacity of garbage = 5 × 6 = 30kg per min

7.3Design of chain drive

(Reference text book: Design of Machine Elements by V.B. Bhandari)

7.3.1 Determination of power rating of chain

Power (KW) rating of chain (p_c)

$$= \frac{Power\ to\ be\ transmitted\ \times Ks}{K1 \times K2}$$

$=\frac{32.66\times10^{-3}\times1}{1\times1}$=0.032KW

Selection of dimensions of roller chains

Pitch of roller chain (p) =9.525mm

Roller diameter (d1) =6.35mm

Width between inner plates (b1) =5.72mm

Breaking load = 8900N

7.3.2 Determination of chain drive velocity ratio

$i = \frac{n1}{n2} = \frac{z2}{z1} = \frac{17}{17}$=1

7.3.3 Determination of average velocity of chain

V=$\frac{\pi DN}{60} = 0.13085m/sec$

7.3.4 Determination of length of the chain

L=Ln× p

Ln=2 $\left(\frac{a}{p}\right) + \left(\frac{Z1+Z2}{2}\right) + (\frac{Z2-Z1}{2\pi})^2 \times (\frac{p}{a})$

Since z1=z2, Ln=2 $\left(\frac{a}{p}\right) + (\frac{Z1+z2}{2})$

 ISBN: 978-93-91420-02-4

L=3m

7.3.5 Determination of tensions in chain

T=2(T1-T2)× r

Tension in slack side (T2)=k× $mg \times a = 5.687N$

Tension in tight side (T1) is calculated as

T= 2(T1-T2)× r

3.12=2(T1-5.687)× 0.025

T1=68.087N

7.4Design of Sprocket

D=$\frac{p}{sin(\frac{180}{z})}$=0.05m

Hence assumed diameter of sprocket is correct.

7.5 Design of shaft

7.5.1 Determination of length of shaft

Length of shaft is considered as 0.6m

7.5.2 Determination of diameter of shaft

Horizontal Plane:

Identification of forces and loads acting on shaft is done according to machine conditions.

Horizontal plane shear force:

Load (P_{hp}) = (T1+T2)cosϴ = (68.087+5.687)cos 45= 52.16 N

R1=R2= (T1+T2)cosθ

R1=R2=52.16N

Horizontal plane bending moment:

Bending moment (M_{hp}) = 52.16× 0.05 = 2.608 Nm

With the values obtained above Horizontal shear force and bending moment diagrams.

Vertical plane :

Taking all the forces acting on shafts into consideration.

Vertical plane shear force:

Load(Pvp)=mg+(T1+T2)sinϴ =(0.15× 9.81)+52.16

= 53.63N

Vertical plane bending moment :

Bending moment(Mhp)= 53.63× 0.05 = 2.6815Nm

Resultant bending moment(M)= $\sqrt{Mhp^2 + Mvp^2}$=3.14 Nm

Diameter of shaft (d) is calculated as

$\tau_{max} = \frac{16Te}{\pi d^3} = \frac{16}{\pi d^3}\sqrt{(Kb \times M)^2 + (Kt \times T)^2} (since\ \tau max = 62.5N/mm^2)$

d= 8.53mm< 10mm

Hence design is safe.

VIII. FABRICATION AND WORKING PROCEDURE

Firstly the base frame was prepared according to the dimensions by drilling the square metal rods using drilling machine. Net layer is bolted to square rods. Sprockets are mounted on the shafts using welding. Bearings are fitted to the shafts. Chains are connected to the sprockets so that they mesh with the teeth of sprockets accordingly,to which the lifters are connected. The motor which is used to run the machine is connected to shaft. Collecting is placed behind the frame of the machine.

Working procedure:

All the parts will be connected together according to the requirement using suitable fabrication processes.

The DC gear motor which is battery operated starts running when the power supply is given.The chain which is attached to the sprocket is driven by motor.When the motor runs , the chain starts to circulate making the spoke lifters to lift up the waste floating materials.The waste materials caught by spoke lifters are further collected in waste storage bin and it can be removed to unload the waste

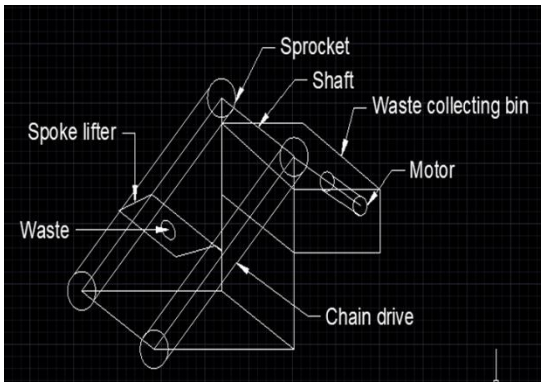

Sewage waste cleaner

IX. FABRICATION PROCESSES

The processes involved in fabrication of sewage waste cleaner are: Welding, Drilling ,Metal Cutting .

X. ATTACHMENT

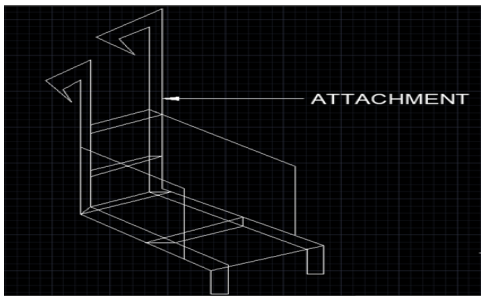

Till now, various sewage cleaners are fabricated but no such cleaners can be used in real time world. No solution has found to use this machine in real time.So, we thought of making an attachment to overcome this problem. This attachment holds the sewage waste cleaner for collecting the wastes in sewage. Because of this attachment, the sewage waste cleaner can be used in low, medium and heavy depth sewage resources such as rivers, ponds , canals etc.

XI. MERITS, DEMERITS, APPLICATIONS AND FUTURE SCOPE

Merits

Simple in construction, maintenance, .Low capital cost, maintenance cost, Easy availability of components,Portable, Skilled labour is not required.

Demerits

Continous power supply is needed, Waste collecting bin needs to be cleaned time to time.

XII. APPLICATIONS

Used by Municipal Authority, in sewage treatment, in controlling the disposal of wastes, in cleaning drainages of small and larger depth.

Future Scope

.By using more techniques, technology, automations with sensors, these machines can be modified and developed according to the real time applications so that they can be used more widely everywhere.

XIII. CONCLUSION

Hence, our intension is to fabricate and design this cleaning machine using suitable calculations which can also be used effectively during rainy seasons and thus avoids the overflow of waste water and sewage waste. Fabricating in order to reduce the time of cleaning and can be used in deep depths sewage resources too.

REFERENCES

[1]Abhishek Anil Batavale, Santosh Dhebe, Durgesh Chinchkar, Omkar Gaurav, Prof. Sachin Solanke, Dept. of Mechanical Engineering. "Automatic Drainage Cleaning System Using Solar Panel" (IJSER) Volume-10, Issue-05, May-2019.

[2] Prof. Amay Tipayle, Kunal Jadhav, Sanket Deshmukhe, Harshal Nisal, Yogesh Naragude "Smart Drainage Cleaning System" (IJSRD) Volume-5, Issue 02, 2017.

[3] S. Navaneetha Krishnan, J. Manivannan, S. Karthikeyan, K.Ganesh Ram, R. Indrajith, K. Kavinprakash, C.Lakshman "Automatic Drainage or Gutter Cleaner"(IJAR)2021.

[4] Design of Machine Elements textbook by V.B. Bhandari.

[5]S. Jayasree, P.G Research Scholar, Advanced Manufacturing System, "Fabrication of Automatic Sewage Cleaning System", designed to control the disposal of waste in efficient manner (IJREAM) Volume-04,Issue-06,Sep2018.

[6]P. Ramesh, Jaboz shiyan Varghese, Akhil Jose Manavaln, Akhil P.R, Adarsh V.V. Asst Professor, Department of Mechanical Engineering, P.P.G Institute of Technology. "Design and fabrication of automatic trash removal machine using in automobile service stations". Designed to replace the manual work in drainage cleaning by automated system in automobile service stations (IRJAT) 2018.

[7] M. Bhavani, S. Kalaiselvan, S. Jagan, S. Gopinath, asst professor, department of mechanical engineering, sri bhavani college of engineering and technology. "semi-automated wireless beach bearing robot vehicle. International journal of recent technology & engineering. Volume8,issue152, may 2019.

[8]Prashant D. Chaudari, Gaurav S. Gajare, Department of mechanical engineering, Dr. Vithalrao patel college of engineering. "design and fabrication of semi-automated drainage cleaning system". IJERT volume9 issue04, april 2020.

[9] Ganesh S.Patil, Rahul A.Pawar, Manish D.Borole, Shubham G.Ahire, Ajay L.Krishnani, Amit H.Karwande. "Review paper on drainage water cleaner machine" (IRJET) Volume 05, Issue: 01, Jan-2018

[10] B.babu, P.Raju, A.Anand Jayakumar Department of mechanical engineering. "Design & Development, Automatic sewage cleaning machine" Journal of Huaztong university of science and Technology Vol.50, Issue 01, Feb 2021.

[11]Viki sahebrao bagul Yogesh Dilip Yadav, automatic drainage cleaning system, international journal of science & technology.

[12] R.Sathiyakala, "smart sewage cleaning system" international journal of innovative research in computer and communication engineering.

[13] Ganesh UL Vinod V rampur assistant professor, mechanical department, PESITM, Shimoga Karnataka, semi-automatic drain for sewage water treatment of floating materials, India international referenced journal of engineering and science (IRJEC) Vol no.5, July 2016.

[14] Dr. k. kumarensanetal, "automatic sewage cleaning equipment", international conference on explorations and innovations in engineering and technology, 2006.

[15] Theory of machines - SS rattan department of mechanical engineering college Kurukshetra (2004). Publication: Tata mc grow hill publishing company limited.

 ISBN: 978-93-91420-02-4

MANUFACTURING OF HYPERBOLOIDAL GEAR MODEL USING ULTIMAKER S5 3D PRINTING MACHINE

Bachali.Rambabu
Deaprtment of Mechanical Engineering, Narasaraopeta Engineering College(A), Narasaraopet, AP,India.

***Abstract*- Hyperboloidal gears are extensively used in power transmission. The manufacturing of the gear components with complex geometry involves a tedious procedure. Additive manufacturing/Rapid prototyping is a technique used for producing complex geometry. 3D printing is one of the techniques of RPP. Present work focus on the manufacturing of hyperboloidal gear of given dimension in an Ultimaker S5 3D printing Machine. The gear components were initially prepared using CURA software which is followed by Slicing methods in order to facilitate the smooth addition of the molten material. The total gear assembly is of seven parts which are made separately to form a set of hyperboloidal gear. The total time required for the components is 30 hours.**

I. INTRODUCTION TO MANUFACTURING OF HYPERBOLIODAL GEAR MODEL

3-D printing is an additive manufacturing (am) technique for fabricating a wide range of structures and complex geometries from three dimensional (3d) model data. the process consists of printing successive layers of materials that are formed on top of each other. this technology has been developed by charles hull in 1986 in a process known as stereolithography (sla), which was followed by subsequent developments such as powder bed fusion, fused deposition modelling (fdm), inkjet printing and contour crafting (cc). 3d-printing,which involves various methods, materials and equipment, has evolved over the years and has the ability to transform manufacturing and logistics processes. additive manufacturing has been widely applied in different industries, including construction, prototyping and biomechanical. the uptake of 3d printing in the construction industry, in particular, was very slow and limited despite the advantages e.g. less waste, freedom of design and automation.

A. Objective of HGM

New applications are emerging as novel materials and AM methods are continuously being developed. One of the main drivers for this technology to become more accessible is attributed to the expiry of earlier patents, which has given manufacturers the ability to develop new 3D printing devices. Recent developments have reduced the cost of 3D printers, thereby expanding its applications in schools, homes, libraries and laboratories. Initially, 3D printing has been extensively used by architects and designers to produce aesthetic and functional prototypes due to its rapid and cost-effective prototyping capability.the situation, it is important that the objective criteria for system success are clearly identified at the start of the project, because different requirements need different design considerations.

B.Components of HGM

The component of HGM system are shown in below figure:

Program for Optimization Geometric and Technological Synthesis of Spired Gears upon a Pitch Contact Point This program includes solving of the following tasks: ¬ Synthesis of geometric pitch circles. ¬ Synthesis of the active tooth surfaces of the spired pinion and of the cutting tool for generation of the Spiroid crown (Spiroid hob). Verification if that the accepted quality criteria of the gear drive are fulfilled. From the formulation of the defined tasks, it can be seen that the algorithm of this program corresponds to the approach to mathematical modeling for synthesis upon a pitch contact point. In this sense, when designing the spired gears, it is of particular importance to select the location of the pitch contact point in the fixed space. The placement of the pitch contact point (as a common point of the pitch circles and conjugated active tooth surfaces) effects on one hand on the common geometry of the designed gear system (overall dimensions of the gear pair) and on the other- on the geometry and proportions of the gears teeth, as well as on the gears quality (through the geometric, kinematic and strength characteristics of the conjugated gear pair)

C. Software Program for a Preliminary Synthesis

The aim of the preliminary synthesis is to be calculated the main geometric parameters of the special case of Spiroid gear, when the angle, at which the rotations axes are crossed, is 90o, and pinion is of cylindrical form. With other words, the preliminary synthesis of the Spiroid gears is essentially oriented to the geometric dimensioning (without an optimization) of hyperboloid drive of type Helicon. The

 ISBN: 978-93-91420-02-4

mathematical model upon a pitch contact point is in the basis of the program for a preliminary synthesis. It is assumed that this point is placed on the outside cylinder of the Helicon pinion. The input data of the computer program are: gear (velocity) Ratio. - number of teeth of the pinion depending on the degree of accuracy and the conjugation type of the tooth surfaces; a standard pinion tooth deflection (thinning) - ; set of standard axle modules; coefficients and etc. In the commented program, the possibility of defining the following geometric technological requirements is taken into consideration when choosing the outer diameter of the gear.

II.GEOMETRICA AND TECHNOLOGICAL SYNTHESIS OF SPIROID GEARS

The shown considerations for designing of software programs, applicable to the synthesis of hyperboloid mechanisms are also realized in connection with constructing three types' software products for the design of Spired gears, which functional relations are shown in Fig. 1. Each one of the illustrated three main directions, has its own importance. It means that the user can restrict himself to use the results of only one program; to analyse and interpret these results and then after an adequate assessment, to go through the entire process shown in the figure. Further below, each of the directions, that includes the whole process of synthesis and design of Spired gears, will be considered.

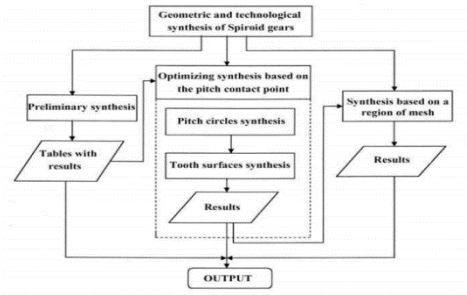

The process of optimization synthesis, in this case, is realized by applying the method of direct search. This method provides an opportunity to reduce the number of calculated gear pairs, which compose the synthesized gear mechanism. It will be reminded, that the essence of this method is as follows

The process of optimization synthesis and design of the third type of software is based on adequate iterative procedures, by which the desired solution is found by variation of certain parameters.

A. Basic Principles and Approaches of the Mathematical Modelling for Synthesis and Design

When profiling the kinematically conjugated surfaces, by means of which the rotations transformation between crossed axes is realized, the basic observed principles are the principles of T Olivier. Here, it will be summarized only that part of them, which is directly related to the construction of the concrete computer programs.

B. Principles of Organizing the Design Process

The following principles are obvious and have been commented by various authors. Here, the focus will BE PUon those which are determining for the construction of the computer programs for synthesis of gears type Spired and Helicon.

C. Determination of the groups of independent and variable input parameters

To the group of independent input parameters a set of standardization modules should be included, that determines the technological capabilities of the hobbling machines; coefficients that define the tooth geometry as a function of the modules; coefficients of frictions between the different pairs of materials applicable for producing of the tooting of the conjugated gear pairs; coefficients, linear and angular values associated with the design of the instrumental equipment and etc. To the input data parameters, among which the variable ones are chosen, as a rule are included those which define the overall geometry of the calculated gear system. Here belongs the parameters determining the dimensions of the gear structure: the offset, distances from the offset to the planes in which the pitch circles lie; the angles defining the orientation of the above said planes relative to the pitch normal and etc. The variable input data include also those, from which the geometry of the conjugated active tooth surfaces depends: the independent coordinates of the tooth surfaces; their helical parameters; parameters which determine face width of the teeth, etc.

D. Introducing the main analytical relations, which are based on the chosen approach to the mechano-mathematical modelling

Here are included solutions of the fundamental tasks of the synthesis upon a pitch contact point and upon a mesh region with the application of the adequate geometric interpretations of the basic equation of meshing, namely the task for the synthesis of pitch circles; the task for the defining the geometry of the active tooth surfaces by their linear and angular characteristics in the pitch contact point; the task for defining the singularity in the pitch contact point (without describing the analytical type of the tooth surfaces); the task for analytically defining of the entire mesh region; formulations of relations, which are used to determine the optimal dimensions and placement of the region of mesh on the active surface and etc. This principle of organizing the computer design includes also the introduction of geometric and kinematic relations, intended for the reduction of the input parameter sets.

 ISBN: 978-93-91420-02-4

E. Constructing the complex process for synthesis and design of hyperboloid gear drives

This is realized by defining the separate sub-stages of the synthesis and design in their sequence and interconnection. This principle, applied in the design of each computer program, is directly dependent on the type of functioning, in the elaborated algorithm, complex of criteria. Those criteria determine the preliminary defined quality characteristics of the gear mechanism in dependence of the accepted approach to the mathematical modelling. A distinctive characteristic of the accepted principle for construction of the complex process for synthesis and design is the chosen approach for the estimation of the calculated option of gear drive.

III. ASPECTS OF COMPUTER DESIGN

The wide variety of gear mechanisms used in industry and transport, as well as the permanent pursuit of researchers to create new and improved gears drives on one hand and on the other- the different and changing approaches to the mathematical modeling for synthesis and design, make it difficult to realize universal CAD systems. In connection to all said above, it specially should be noted the note the extremely dynamic development of modern technical computing tools and software programs. This often requires a reassessment not only of the way in which computer programs are organized, but also leads to informal changes of applied mathematical models. In order to realize these researches into the field of theory gearing, as well as to provide an adequate scientific support for this type of production, the computer design has evolved, forming three types of software.

1. First Type
2. Second Type
3. Third Type

- Input parameters are defined, as well as those that will not be changed throughout the whole synthesis process
- The variables parameters are determined as well the way of their variation, respectively;
- The process of variation the defined variable input parameters compared to their initially given value continues, until the preliminary defined optimization criteria are fulfilled;
- From the calculated pairs of conjugated gear sets, a final variant is chosen for which, there is the best fulfilment of the additional conditions (restrictions) introduced in the mathematical model.

IV. COMPONENTS PRODUCED USING ULTI MAKER 3D PRINTER

Hyper Base: After slicing
Time(minutes): 07 hour 16minutes
Material(grams) : 66grams

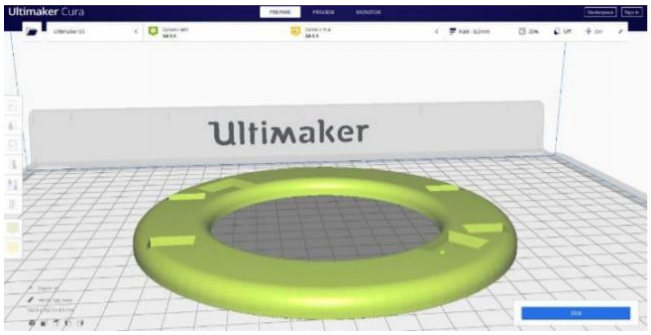

Hyper Gear: After slicing
Time(minutes): 12hour 45minutes
Material(grams) : 45grams

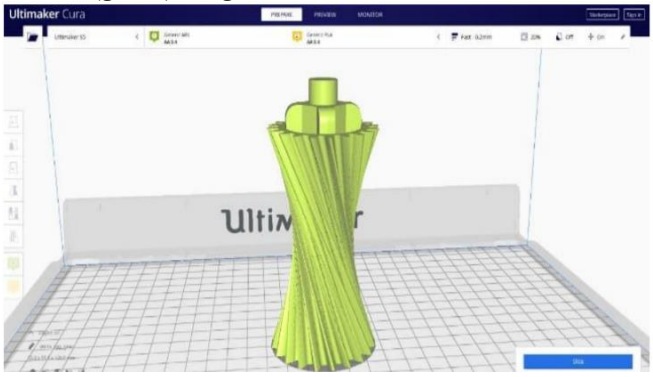

*Hyper Gear End***:** After slicing
Time(minutes): 47minutes
Material(grams) : 07 grams

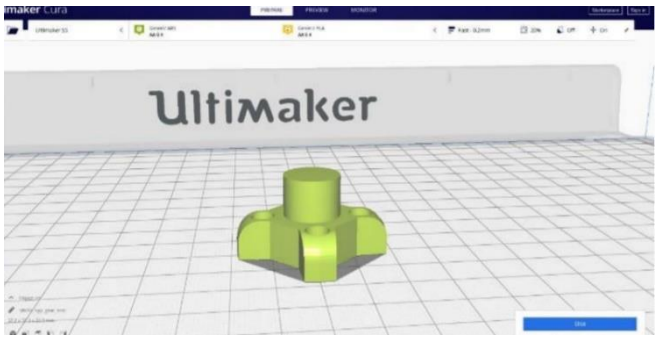

*Hyper Gear End Long***:** After slicing
Time(minutes): 55minutes
Material(grams) : 08 grams

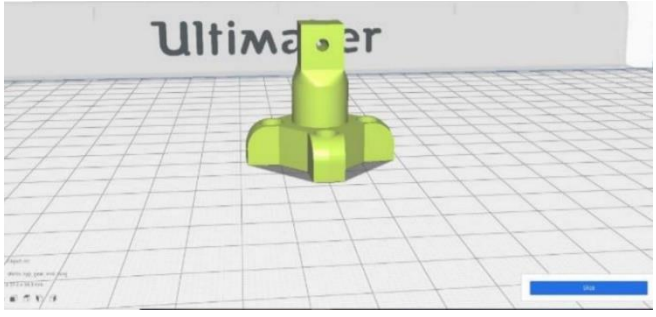

 ISBN: 978-93-91420-02-4

Hyper Handle: After slicing
Time(minutes): 1 hour 44minutes
Material(grams) : 13 grams

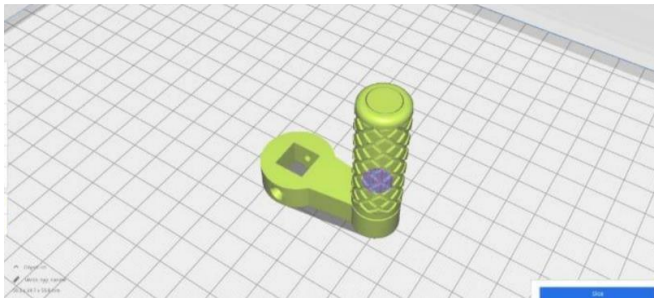

Hyper Stand Lower: after slicing
Time(minutes): 58minutes
Material(grams) : 09 grams

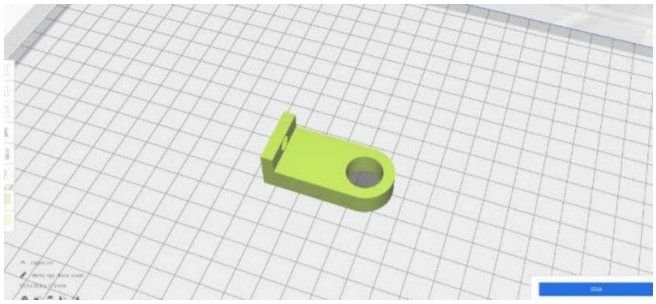

*Hyper Stand Upper***:** After slicing
Time(minutes):103minutes
Material(grams) : 15 grams

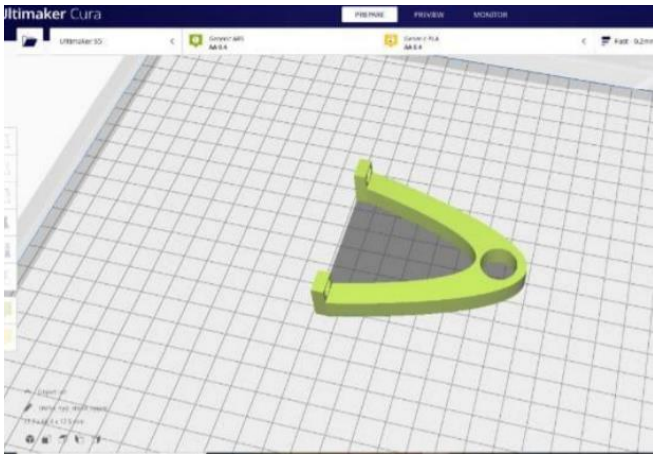

REFERENCES

1. Abadjiev, V. Gearing Theory and Technical Applications of Hyperboloid Mechanisms, Sc. D. Thesis, Institute of Mechanics, Bulgarian Academy of Sciences, Sofia, 2007, 309p (In Bulgarian).
2. Goldfarb, V. Aspects of Gears and Reduction Drives Automated Design. Gearing and Transmissions, Izhevsk, Assoc. Engineers, 1991, No 1, 20-24 (in Russian).
3. Bulgarian Standard 17108 (CT na CIV 5744 - 86). Cylindrical Involute Gears with Externally Meshing. Standardization Strength Calculation of the Gear's Teeth, G-15, 1999, Sofia, p. 124, (in Bulgarian).
4. Gear Engineering Standard. Bending, Stresses in Bevel Gear Teeth. Gleason Works, Rochester, N.Y., Copyright 1955, 1960, 1965, 28 p
5. Anchev, A., K. Minkov, D. Petrova, Og. Kumchev. Synthesis and Analysis of Bevel Gears with Spiral Teeth, Publishing House of the Bulgarian Academy of Sciences, Sofia, 1980, p. 160
6. Giznbrug, E., N. Golovanov, N. Firun, N. Hlebskiy. Gears Handbook of Mechanical Engineering. Leningrad, 1980, 416 p., (in Russian).
7. Dudley, D., J. Sprengers, D. Schroder, H. Yamashina. Gear Motor Handbook, Springer – Verlag, Berlin Heidelberg, 1995, 607

 ISBN: 978-93-91420-02-4

ARC WELDING PROCESS SELECTION THROUGH QUALITY AND COST ANALYSIS

[1] Priyanka Bodda, [2] Balaji Naik Mudavath and Himaraka Sony
[1,3] Student, Department of Mechanical Engineering, UCEN-JNTUK, Guntur Dist., AP, India
[2] Balaji Naik Mudavath, Assistant Professor, Department of Mechanical Engineering, UCEN-JNTUK, Guntur Dist.

***Abstract*— Welding is the most feasible fabrication process for complex designs and intricate shapes. There are many types of welding processes which are used in the modern day fabrication operations. It is challenging when it comes to the selection of most economical process for a given application. This project presents a methodology to compare three welding processes, namely SMAW (Shield Metal Arc Welding), GTAW (Gas Tungsten Arc Welding), and SMAW & GTAW (Hybrid Welding) to select the best one for a given application. The present work is evaluating and proposing the best arc welding process for the fabrication Ship Deck plate based on quality, cost and time criteria. The three welding process were performed on the plates and were then tested by Dye penetrant test, Magnetic particle test, Radiography test and Tensile test. The best process for given application is then found out by analyzing and interpreting the quality obtained and cost incurred.**

Keywords*— SMAW, GTAW, Hybrid welding.

I. INTRODUCTION

Welding is the process of joining together two pieces of metal so that bonding takes place at their original boundary surfaces. Two parts to be joined are melted, together, heat or pressure or both is applied and with or without added metal for formation of metallic bond.

Shield Metal Arc Welding

The weld quality is primarily dependent on the skill of the welder. For our analysis, SMAW is done on mild steel in 1G position .When an arc struck between the coated electrode and the work piece, both surfaces melt to form a weld pool.

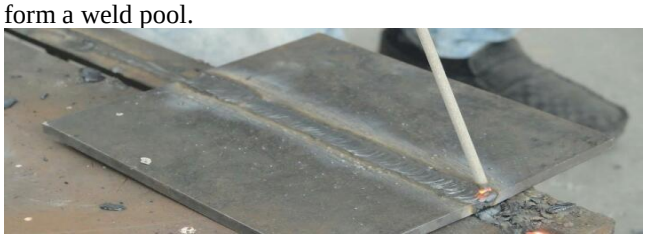

The flux forms gas and slag which protect the weld pool from oxygen and nitrogen in the surrounding atmosphere. The molten slag solidifies, cools and must be chipped off the weld bead once the weld run is complete (or before the next weld pass is deposited).

Gas Tungsten Arc Welding

Gas Tungsten arc welding process is also called as TIG welding. Melting is produced by heating with an arc struck between a non-consumable tungsten electrode and the work piece. An inert gas shields the electrode and weld zone to prevent oxidation of the tungsten electrode and atmospheric contamination of the weld and hot filler wire.

Hybrid Welding

In SMAW, flux covered consumable electrode is used whereas in GTAW non consumable Tungsten electrode is used and consumable filler wire is supplied externally. In case of GTAW and SMAW hybrid welding both processes are used to complete the complete the weld, such that root pass is done by GTAW process and subsequent passes are made by SMAW process. The objective of hybrid welding is to aggregate advantage of both processes in enhancing productivity and work quality.

Visual Inspection Process

Visual inspection is a common method of quality control, data analysis. Visual Inspection, used in maintenance of facilities, mean inspection of equipment and structures using either or all of raw human senses. The most common welding discontinuities found during visual inspection are conditions such as undersized welds, undercut, overlap, surface cracking, and surface porosity, under fill, incomplete root penetration, excessive root penetration, burn through, and excessive reinforcement.

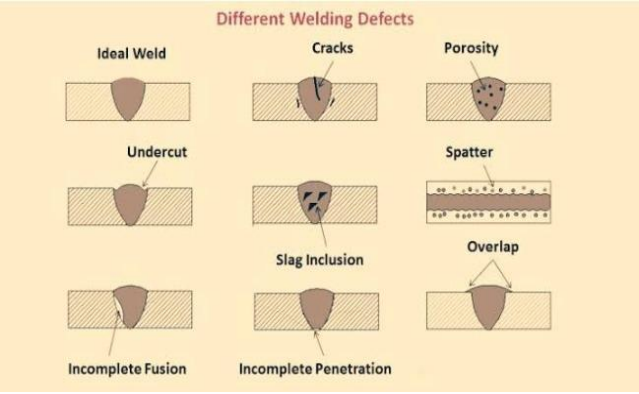

Dye penetrant test

Penetrant to be drawn into a “clean” surface breaking flaw by capillary action.after dwell excess surface penetrant is removed and developer applied it drawn out the penetrant from the flaw by blotter action.

 ISBN: 978-93-91420-02-4

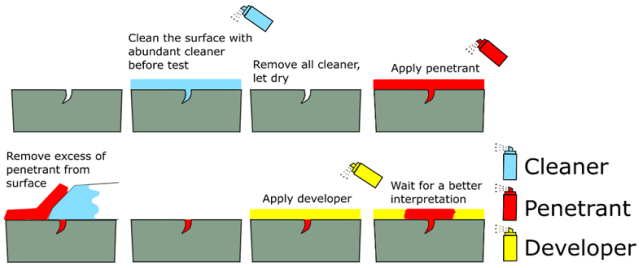

Magnetic Particle test:

Magnetic particle test is used for checking cracks mainly in weld joints which are not visible to the naked eye. The leakage fields attract magnetic particles to themselves leading to the formation of an indication.

Radiography test:

This method of weld testing makes use of X-rays, produced by an X-ray tube, or gamma rays, produced by a radioactive isotope. Penetrating radiation is passed through a solid object that is in a weld joint, onto a photographic film, resulting in an image of the object's internal structure being deposited on the film. All discontinuities are detected by viewing shape and variation in density of the processed film.

This testing method is usually suited to having access to both sides of the welded joint.

S. No	Type of welding	Dr (kg/h)	S (kg/h)	SI %	De %	F_{elect} (kg/h)
1	SMAW	2.07	0.1215	5.85	94.5	2.1955
2	GTAW	1.1088	0.0512	4.62	95.6	1.16
3	Hybrid	1.644	0.089	5.413	94.9	1.738

II. METHODOLOGY

SMAW and GTAW are common arc welding processes in which heat required to melt parent and filler material is generated by an arc established between an electrode and the work piece. In SMAW, flux covered consumable electrode is used where as in GTAW non consumable Tungsten electrode is used and consumable filler wire is supplied externally. In case of GTAW and SMAW hybrid welding both processes are used to complete the weld, such that root pass is done by GTAW process and subsequent passes are made by SMAW process. The welds are carried out in Dry Penetration Test, Magnetic Particle Test and Radiographic Test for Quality analysis and geometrical aspects of the beads .For cost analysis, welding parameters and consumable prices are considered. Quantitative indices were proposed and evaluated. After that, evaluation of both quality and costs calculated, it possible to select the most suitable welding process to a specific application, taking into account the market conditions.

Tensile Testing Results of Non heat treated welded specimens

Welding Type	Tensile Strength in N/mm^2	Yield strength N/mm^2	Modulus of Elasticity ,GPa	% age of Elongation	% age of reduction in area
SMAW	495.6	390	186	20.514	28.17
GTAW	530	419.12	186.5	21.366	31.45
Hybrid	520.3	406.05	186.2	20.932	30.02

III. RESULTS AND DISCUSSION

Welding Quality Analysis:

Not all manufacturing processes are perfect and have an associated non-conformance rate. Manufacturers seeking to achieve higher quality of conformance have a wide range of options to choose from. These can be divided into two categories; improving produced quality of conformance via defect prevention and improving quality of conformance delivered to the customer via inspection.

Welding quality is determined by these terms

Formula for determination of welding quality

s.no	Welding Quality	formula
1	Deposition rate	$Dr = 3.6 \times (M_{fcp} - M_{icp}) / tarc$
2	Fusion rate electrode	Electrode consumption / time
3	Fusion rate of wire	Wire consumption / time
4	Deposition efficiency	$De = Dr / (F_{elect} \text{ or } F_{wire}) \times 100$ [%]
5	Spattering rate	$S = (F_{elect} \text{ or } F_{wire}) - Dr$
6	Spattering index	$SI = (S / Dr) \times 100$ [%]

Quality Calculation:

 ISBN: 978-93-91420-02-4

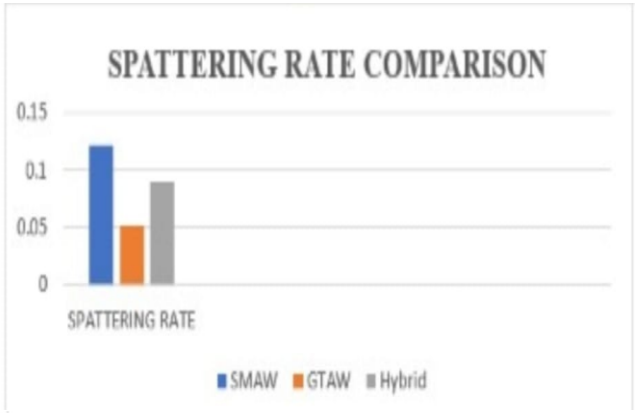

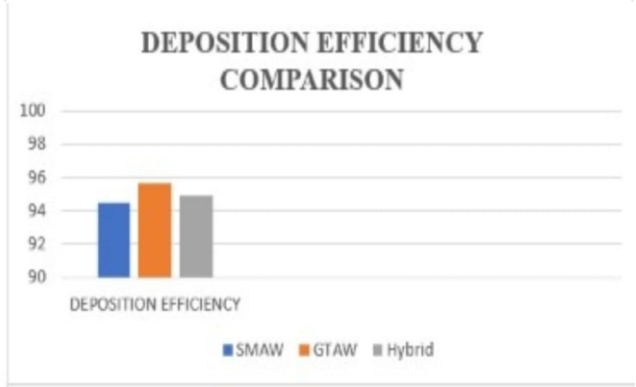

Welding Costs Calculations:

Cost analysis is an important tool for product design and material selection. Efficient and effective cost estimation tool is necessary for early design evaluations. Each cost component has been closely analysed and the major cost components have been included in the cost calculation. In the present case, Costs will be used as a balancing parameter during selection of the most suitable welding process.

The composition of costs takes into account materials, electricity, labour and equipment. Indirect costs will not be considered, since they are approximately the same in terms of comparison. Total welding cost (TWC) is a composition of equipment, materials and labour costs. Indirect costs are approximately the same in terms of comparison. With respect

$$TWC=EC+MC+LC$$

Equations used for determining each term of the costs

1	Material cost(MC)	Cost determining Equations
1.1	SAW wire (CSw)	$Csw = P_w \times (Dr \times 100/De)/(t_{speed} \times 60/100)$
1.2	MIG wire (CMw)	$Cmw = P_w \times (Dr \times 100/De)/(t_{speed} \times 60/100)$
1.3	SMAW electrode (Ce)	$Ce = P_e \times (Dr \times 100/De)/(t_{speed} \times 60/100)$
1.4	Flux (Cf)	$Cf = P_f \times Rf \times 100/t_{speed}$
1.5	Gas(Cg)	$Cg = P_g \times R_g \times 100/t_{speed}$
2	Labor cost(LC)	$LC = S_w/(t_{speed} \times 60/100 \times f_{op}/100)$
3	Investment (Ci)	$Ci = V_e \times (Ir/100) \times D_r/(P_m \times t_{speed} \times 60/100)$
4	Depreciation(Cd)	$Cd = V_e \times D_r/(T_d \times P_m \times t_{speed} \times 60/100)$
5	Maintenance (Cm)	$Cm = E_m \times Dr/(P_m \times t_{speed} \times 60/100)$
6	Electrical power (EPC)	$EPC= (I_m \times V_m \times P_{el})/(1000 \times (ee/100) \times t_{speed} \times 60/100)$

Total cost/m for three different welding with respect to deposition rate, operating factor, labor cost, depreciation cost etc.,

Type of welding	SMAW	GTAW	Hybrid Welding
Weight of deposit per meter (Kg/m)	1.152	1.232	1.187
Deposition efficiency (%)	94.6	95.6	94.9
Deposition rate (Kg/hr)	2.074	1.108	1.644
Welding current (amps)	135	145	140
Welding voltage (volts)	70	80	70
Operating factor (%)	60	60	35
Labour + Overhead cost (Rs/hr)	400	580	540
Power source efficiency (%)	60	60	60
Depreciation cost (C_d)[Rs/m]	0.44	0.4760	0.5946
Labour + Overhead Cost/meter of weld (ETB/m)	634.798	1074.8	650
Electrode cost/ Meter of weld (ETB/m)	296.22	1589.682	515.77
Total [ETB/m)	931.018	2664.482	1165.77

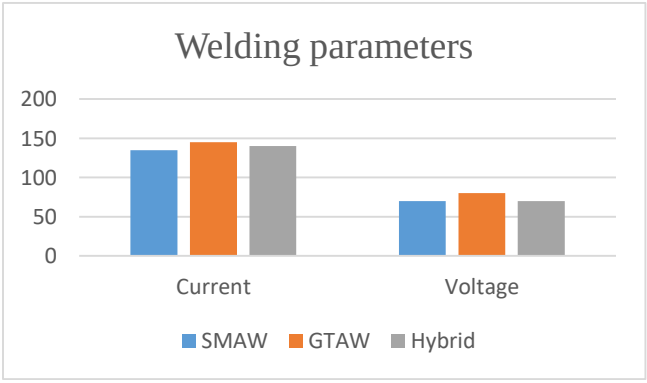

 ISBN: 978-93-91420-02-4

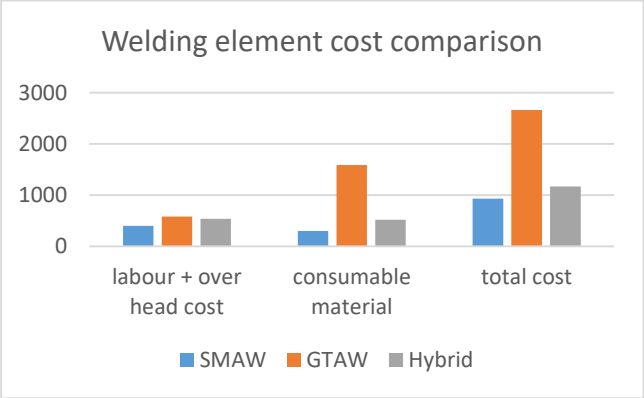

IV. CONCLUSION

From the above observations and results, it is observed that

- GTAW possess more deposition efficiency but consumes more cost.
- SMAW takes lesser time but is of inferior quality in terms of tensile strength and deposition efficiency.
- Hybrid welding consumes lesser cost and time than GTAW and possess a tensile strength superior than SMAW.
- From our work, it can be concluded that, Hybrid welding is the most suitable for the fabrication of ship deck plate.

REFERENCES

[1] Cary HB and Helzer S. Modern welding technology. Upper Saddle River, NJ: Prentice Hall, 2004.
[2] Serope K and Steven S. Manufacturing engineering and Technology. Upper Saddle River, NJ: Prentice Hall, 2001.
[3] Klas W. Welding processes handbook. New York: CRC Press, 2003.
[4] Rosenthal D. The theory of moving sources of heat and Its application to metal treatments. Trans ASME 1946; 68: 849–865.
[5] Bellet M, Hamide M, Pequet C, et al. New numerical Technologies for the simulation of arc welding processes.

 ISBN: 978-93-91420-02-4

Li-Br H_2O VAR System Analysis by Applying Magnetic Field to Liquid Line

Shaik Bajan
Department of Mechanical Engineering, Narasaraopeta Engineering College (A), Narasaraopet, AP, India.

***Abstract* - Process of industries and automobile vehicles, there is usually a great amount of waste heat available at different temperatures and at the same time, there are cooling or refrigeration demands at different temperatures. In this work, a single effect vapour absorption refrigeration system is to be fabricated. And to perform the optimal matches between heat source temperatures and refrigeration levels of the vapour absorption refrigeration cycle are determined in terms of two indicators, coefficient of performance (COP) and efficiency of the cycle**

The results shows that the theoretical COP of an VAR system is maximum for the system operated with two pairs of magnets.

Keywords: Fabrication of Vapour absorption Refrigeration System, VAR, LiBr-H2O absorption refrigerator, waste heat VAR system.

I. Introduction

In the early years of the twentieth century, the vapour absorption cycle using water-ammonia systems was popular and widely used. After the development of the vapour compression cycle, the vapour absorption cycle lost much of its importance because of its low coefficient of performance (about one fifth of that of the vapour compression cycle). Today, the vapour absorption cycle is used mainly where fuel for heating is available but electricity is not, such as in recreational vehicles that carry LP gas. It is also used in industrial environments where plentiful waste heat overcomes it's inefficiency. The absorption cycle is similar to the compression cycle, except for the method of raising the pressure of the refrigerant vapour. In the absorption system, the compressor is replaced by an absorber which dissolves the refrigerant in a suitable liquid, a liquid Pump which raises the pressure and a generator which, on heat addition, drives off the refrigerant vapour from the high-pressure liquid. Some work is needed by the liquid pump but, for a given quantity of refrigerant, it is much smaller than needed by the compressor in the vapour compression cycle. Side = 0.625 inches. Each column measures 3.5 inches wide, with a 0.25-inch gap between the two columns.

In an absorption refrigerator, a suitable combination of refrigerant and absorbent is used. The existing review works on heat transformers confirm that water-lithium bromide the most investigated couple for heat transformers. Despite that, they also report many studies researching alternative fluids, due to the high corrosiveness, viscosity and crystallization risk in some operating ranges of the water-lithium bromide pair. Improvements can be achieved by adding additives as ethylene glycol or using mixtures of various salts rather than (Li-Br) alone, but none of the proposed alternatives succeeded in solving all the drawbacks.

METHADOLOGY

In this experiment the exhaust pipe of the engine is connected to the generator shell by using a pipe. Inside this generator shell a generator tank is placed. This generator tank is made up of copper. The generator tank is connected to the condenser.

The condenser is of air flow type condenser. The air is supplied by the fan which is powered by a motor. The condenser is connected to an expansion valve, this expansion valve is connected to evaporator by using copper wire and copper L-bend connectors. The evaporator is bent and wound in a spiral around an eternal sheet. The outlet of the eternal pipe is connected to the absorber tank.

Fig.1

Fig.1: Generator is connected to engine exhaust manifold pipe

One outlet of the absorber is connected to evaporator outlet, another is connected to a pump, and last outlet is connected to the generator which is connected to the heat exchanger. There is a pipe connecting the generator and pump. Generator second outlet pipe is connected to the heat exchanger which is in connection to a regulating valve which connects the absorber tank. This total equipment is fixed on a frame. A pipe is welded to the absorber for adding absorber Absorber and the refrigerant is filled into the absorber tank in the ratio of 25% (refrigerant) and 75 %(absorber). The engine exhaust pipe is mounted on the generator shell. When the engine is started and run for a while the hot exhaust gases of temperature above 1500C enters the generator shell. The heat from the exhaust gases is absorbed by the generator tank. Inside the generator tank water which is the refrigerant absorbs this heat. The refrigerant evaporates and enters the condenser in the form of vapor

 ISBN: 978-93-91420-02-4

Fig.2: Experimental setup on VAR system is connected to the diesel engine

This vapor condenses by using air from the fan. The heat removed by the fan from the refrigerant in the condenser. In the condenser the refrigerant changes its phase from vapor to liquid due to the heat lost in the condenser. The liquid refrigerant enters the expansion valve where the temperature and pressure reduces due to the narrow space of the copper pipe (capillary). This cold refrigerant enters the evaporator. This cold refrigerant absorbs the heat from the surroundings of the evaporator creating a cooling effect. This heat absorbed refrigerant then flows into the absorber tank and mixes with lithium bromide forming a weak solution. This weak solution is pumped to the generator tank while passing through a heat exchanger. Simultaneously the lithium bromide separates and falls down into the heat exchanger where it exchanges it's heat with the weak solution and falls down into the absorber tank whereas the water vapor to the condenser there by starting the cycle again. The exhaust gases exchanges its heat given to the generator tank and passed away to the atmosphere

EXPERIMENTAL CALCULATIONS

A. Calculations for 25%Li Br 75% H2O

1) Heat Rejection from Condenser(Qr)Condenser temperature at the inlet (T1) = 41+273 =314 K Condenser temperature at the outlet (T2) = 30.5+273 = 303.5 K Mass flow rate of air (m) = 1.2 Kg/min

Specific heat of air (C p) = 1.005 Kj/Kg-k

$$QR = m \times C_p \times (T1-T2)$$

$$= 1.2 \times 1.005 \times (314 - 303.5) = 12.663 \text{ KW}$$

2) Heat Extract from Evaporator(Qe)Evaporator temperature at the inlet (T2) =16.2+273 =289.2 K Evaporator temperature at the outlet (T1) = 21.1+273 =294.1 K Mass flow rate of refrigerant (Water) (m) = 1.2Kg/min Specific heat of refrigerant (Water) (C p) = 4.187kJ/Kg-k

$$QE = m \times C_p \times (T1-T2)$$

$$=1.2 \times 4.187 \times (294.1 - 289.2) =24.61 \text{ KW}$$

1) Heat given to Generator(Qg)Generator temperature at the inlet (T2) =118+273 =391k Generator temperature at the outlet (T1) = 87.8+273 =360.8 k Mass flow rate of exhaust gases (m) = 1.2Kg

Specific heat of exhaust gases (C p) = 1.063 Kj/Kg-k

$$QG = m \times Cp \times (T2-T1)$$

$$=1.2 \times 1.063 \times (391 - 360.8)$$

$$=36.45 \text{ KW}$$

Coefficient of Performance (COP) Actual

$$\text{(COP) actual} = \frac{\text{Amount of heat extracted from the evaporator}}{\text{Amount of heat given to the generator}}$$

$$\frac{36.45}{}$$

Maximum Coefficient of Performance (COP)

$$COP = \frac{(Tg - Tc)}{(Tc - Te)} \times \frac{Te}{}$$

$$\frac{393}{} \quad \frac{289.2}{}$$

$$COP = \frac{(393 - 314)}{(314 - 289.2)} \times$$

$$COP = 2.344$$

Observation and Result of VARSystem

Table 1: Experimental observation for VAR System with 25%Li-Br 75% H2O, Using Water (Refrigerant) and Li-Bromide (Absorber) is Working Fluid

S.N0	Mixture 25% LI-BR and 75% of water	Volume (liters)	Tg °C	Tg °C	Tg °C	Qe kW	Qe kW	COP
1		1.5	118	16	41	24	36.	0.65

Temperature at evaporator Te =16.2 0C+273=289.2k
Temperature at condenser Tc =410C+273=314k
Temperature at generator Tg = 118 0C+273=393k

The reading as in above the tabular form is taken from the performance and experimental values of the vapour absorber refrigeration. And observe the COP of the vapour absorption refrigeration (VAR) system by using a working fluid as water and lithium bromide.

RESULTS AND DISCUSSIONS

The results obtained from the absorption refrigeration system using the engine exhaust gas as energy source and widely varying engine speed. The refrigerator average internal temperature at the engine operational conditions. In the first 30–45 min it is observed that the average refrigerator temperature increases with time.

The distinct behaviors of the absorption refrigeration cycle as a function of its generator temperature.

 ISBN: 978-93-91420-02-4

When the heat input is too low (t_g=100oC) the evaporator is not effectively cooled and the temperature inside the refrigerator is lowered by only approximately 20oC. At 120oC, rapid cooling is achieved at first, but after the temperature reaches approximately a 15oC minimum, a continuous increase is then observed for 180oC, no refrigeration actually occurs due to the overheating of the water and lithium bromide or ammonia and water solution. for tg=120oC the temperature initially drops because the water and lithium bromide or ammonia and water solution going through the generator is not yet overheated at the start of the process.

When the water and lithium bromide or ammonia and water solution eventually becomes overheated at the generator (which happens for t g=120^{o}C after 4 min and for tg=180oC from the start), the refrigerant is not condensed at the condenser of the absorption cycle and is unable to extract heat From the evaporator. The only condition which produced a steady decrease in temperature throughout the entire duration of the experiments wastg=110^{o}C

The results agree with the predictions of previous works, which stated that excessive exhaust gas heat (produced by high engine speeds/torque) lead to poor refrigeration performance justifying the implementation of the control scheme proposed In the present study.

The experiments whose results are present in process will be recorded in the experimental table. Were such the extended periods of time because their objective is to determine the reference values for the generator temperature which was capable of causing the refrigerator to cooling efficiently.

CONCLUSION

Performance of vapour absorption system using exhaust waste energy from diesel engine has been carried out in this experiment. It is marked that COP strongly depends on working conditions such as generator, absorber, condenser and evaporating temperature.

The vapour absorption automobile air conditioner is an economically attractive concept for utilizing exhaust waste heat because most of the energy input comes from the heat available in the exhaust gases, with only small electric power used to operate the pump.

For 25% Li-Br 75%H2O the theoretical efficiency of a vapour absorption refrigeration system is 0.675 and it is 0.609 for 30% Li-Br 80%H2O, from this we conclude that VAR with 25% Li-Br 75%H2O gives the best efficiency In the second stage tests were conducted with the 25% Li-Br 75%H2O and Magnets are connected in liquid line of the refrigerator, here we use anlico (Aluminium Nickel Cobalt alloy) magnets are used for the experimental study.

The COP of an Li-Br H2O vapour absorption refrigeration system is 0.872 for 25% Li-Br 75%H2O with one pair of magnet, 1.2 with two pairs of magnets and 1.01 for three pairs of magnets. So the maximum COP is 1.2 obtained for 25% Li-Br 75%H2O with two pairs of magnetic pairs.

The engine exhaust gas was confirmed as a potential power source for absorption automobile air conditioner system. In other words, the absorption refrigeration system may be able to take advantage of the exhaust gas power availability and provide the cooling capacity required for automotive air-conditioning.

Water and lithium bromide, should be considered as a viable alternative to mechanical vapour compression cycle. Appreciable cooling load reduction can be realized by modification on the automobile body and the door and windows design.

With flexibility in operation, absence of compressor noise, very low maintenance and high reliability. The waste heat energy available in exhaust gas is directly proportional to the engine speed and exhaust gas flow rates.

REFERENCES

1. Marcos, J. D., Izquierdo, M., and Palacios, E., 2011, “New Method for COP Optimization in Water- and Air-Cooled Single and Double Effect LiBr–Water Absorption Machines,” Int. J. Refrig., 34(6), pp.1348–1359.
2. Ganguly, A., Talukdar, K., and Basu, D. N., 2013, “Modeling and Analysis of a Solar Photovoltaic Assisted Absorption Refrigeration System,” Proceedings of the 4th International Conference on Advances in Energy Research, Mumbai, India, Dec. 10–12, Paper No. 57, pp.260–266.
3. Pongtornkulpanicha, A., Thepa, S., Amornkitbamrung, M., and Butcher, C., 2008, “Experience With Fully Operational Solar-Driven 10-ton LiBr/H2O Single- Effect Absorption Cooling System in Thailand,” Renewable Energy, 33(5), pp.943–949.
4. Said, S. A. M., El-Shaarawi, M. A. I., and Siddiqui, M. U., 2012, “Alternative Designs for a 24-h Operating Solar-Powered Absorption Refrigeration Technology,” Int. J. Refrig., 35(7), pp.1967–1977.
5. Das, K., and Mani, A., 1996, “Comparative Study of Cycle Performance for a Two Stage Intermittent Solar Refrigerator Working With R22-Absorbent Combinations,” Energy Convers. Manage., 37, pp.87–93.
6. Fan, Y., Luo, L., and Souyri, B., 2007, “Review of Solar Sorption Refrigeration Technologies: Development and Applications,” Renewable Sustainable Energy Rev., 11, pp. 1758–1775.
7. Agrawal, B., and Karimi, M., 2012, “Thermodynamic Performance Assessment of a Novel Waste Heat Based Triple Effect Refrigeration Cycle,” Int. J. Refrig., 35(6), pp.1647–1656.Pandya, B., Kumar, V., Patel, J., andMatawala, V. K., 2018, “Optimum Heat Source Temperature and Performance

 ISBN: 978-93-91420-02-4

Comparison of LiCl-H2O and LiBr-H2O Type Solar Cooling System," ASME J. Energy Resour. Technol., 140(5), p.051204.
8. Ministry of Energy and Mineral Resources Annual Report; 2009: Amman, Jordan.
9. Frank F, Nekola, Trenton F. Heat generator for use with an absorption air conditioning system for Automobiles 1990; United State Patent, 5: 49-82. 476Khaled
10. S. AlQdah / Energy Procedia 6 (2011) 467–476.
11. Al-Aqeeli N, Gandhidasan P. The use of an open cycle absorption system in automobile as an alternative to CFC. The 6th Saudi Engineering Conference, KFUPM, Dhahran, December 2002;

 ISBN: 978-93-91420-02-4

Heat Transfer Enhancement on Shell and Coil Type of Heat Exchanger Using SiO_2 and CuO Nano-Fluids

[1] G. Sreenivasulu Reddy, [2] Dr.R.Kalaivanan, [3] Dr.R.Uday Kumar
[1,3] Department of Mechanical Engineering, Mahatma Gandhi Institute of Technology Gandipet, Hyderabad
[2] Dr.R.Kalaivanan, Department of Mechanical Engineering, Annamalai University, Annamalai Nagar, Tamilnaadu

***Abstract*— This work presents the effect of changes in inlet temperature of coil side of the heat exchanger while the shell side of inlet fluid temperature is remains constant. The aim of this work is to study for the influence of Sio_2 and Cuo Nano-fluids with constant concentration of 2.5% along the shell side of the heat exchanger. To capture the flow dynamics and the heat transfer characteristics the *k-ε* model is employed for the turbulent flow regime. The numerical simulation is carried out with use of software Ansys Fluent 14.0. The three different inlet hot fluid temperature of coil side of heat exchanger is varied (i.e., 333 °K, 343 °K and 353 °K) and also three different mass flow rate of 0.03 kg/s, 0.05 kg/s and 0.07 kg/s are varied. The results showed that the convection heat transfer coefficient increases with increasing the inlet hot fluid temperature of coil side of heat exchanger. Consequently, the base fluid and Sio_2 Nano-fluid showed similar performance while Cuo nan-fluid showed moderate improvement of heat dissipation rate for variation in temperature as well as mass flow rate of the fluid. In addition, by adding concentration of Nano fluid in the base fluid leads to increase in the pumping power with increasing mass flow rate of the fluids.**

Keywords—convective heat transfer coefficient, mass flow rate, pressure drop, Nano fluids, shell and coil type heat exchanger.

INTRODUCTION

In the present scenario the shell and tube heat exchanger is the most prominent and commonly used heat exchanger in oil refinery industry and other chemical processes, because it suits high pressure applications. The natural law of physics always allows the driving force in a system to flow until the system is reached to equilibrium. In general, the heat energy leaves from the hottest fluid or warmer body there is exits a temperature gradient or the temperature difference, and it allows to transfer to a cold body or cold fluid. The heat exchanger adopts this principle in it's to attempt to reach equalization. Hence, the most well-known kind of heat exchangers to be experienced in the warm applications is shell-and-cylinder heat exchangers [1]. These are accessible in an assortment of setups with various development highlights and with varying materials for explicit applications. The enhancement of heat dissipation through the shell and tube heat exchanger quite taking more attention by the researchers. Abd et al. [2] explored the parametric study on the performance of shell and tube type of heat exchanger. The study investigated in account of the effect of parameters like tube length and shell diameter on convection coefficient and pressure loss in alteration of square and triangular pitches on shell side of heat exchanger. Son and Shin [3] extended the study on the enhancement of heat transfer through shell and tube heat exchanger by providing spiral baffles fins inside the tube. The spiral baffles fins create more turbulence inside the shell leads to increase in efficiency of the heat exchanger. De et al. [4] carried out the numerical investigation on the enhancement of heat dissipation for shell and tube heat exchanger by designing helical baffles plates inside the tube. The helical baffles are designed in such way that the angle of helix is varying from 0° to 30° and with these obtained numerical results is compared with straight baffles. The results revealed that, the convection coefficient improves with increasing the inlet fluid velocity. The results of pressure drop decreases on shell side compared to straight conventional baffles heat exchanger. However, with increasing the angle of helix up-to 12° the pressure drop increases significantly and it lowers helix angle larger than 12°. The optimum helix angle is found to 10° for better enhancement of heat transfer and similar kind of study is carried out by Elias et al. [5]. Swetha et al. [6] carried out experimental study on shell and tube heat exchanger for various concentration of Al_2O_3 nano-fluid. They reported that by varying the concentration of nano-fluid the thermal conductivity of the fluid increases sharply until a certain limit. Surana et al. [7] carried out numerical investigation on augment of heat transfer through shell and tube heat exchanger in consideration of Al_2O_3 nano-fluid. This study explored the effect of tube diameter and unequal baffles are located inside the heat exchanger. The study concludes that, the overall heat transfer coefficient of the heat exchanger increases up-to the certain concentration of nanoparticle and thereafter it decreases significantly. Furthermore, with insertion of unequal baffles the convection coefficient increases, and pressure drop decreases.

The augment in heat transfer can be accomplished by providing the spiral/coil type of heat exchanger through which hot inlet fluid flows while cold fluid flow from shell of the heat exchanger. The spiral/coil type heat exchanger takes more attention because fluid swirls or proper mixing of fluid inside the coil leads to increase heat transfer coefficient leads to advance in heat dissipation rate. Though the more study are available on shell and coil type of heat exchanger. But, for the present study the authors motivated to work variation in inlet temperature of hot fluid of coil side of heat exchanger while shell side cold fluid at inlet is kept constant.

METHODOLOGY

- *Geometry modelling*

The geometry is modelled using Creo 2.0 software. Creo 2.0 is a fundamental, ascendible stage that gives an entire arrangement of style, investigation and creating abilities. Later the geometry is meshed and simulated using commercially available software Ansys Fluent 14.0. Details the dimensions of shell and coiled heat exchanger which is shown in the Fig. 1(a) and (b).

 ISBN: 978-93-91420-02-4

- *Numerical domain*

The computational domain is meshed using software Ansys Fluent 14.0. For the current study tetra-hydral element is considered for the numerical simulation which is revealed in Fig. 2(a). For the present study finite volume method (FVM) is adopted for numerical simulation. The inlet hot fluid flows from coil side varying three different temperatures and shell side of the cold fluid is kept constant with varying mass flow rate of base fluid as well as Nano-fluids. The direction of the hot and cold fluid are presented in Fig. 2(b).

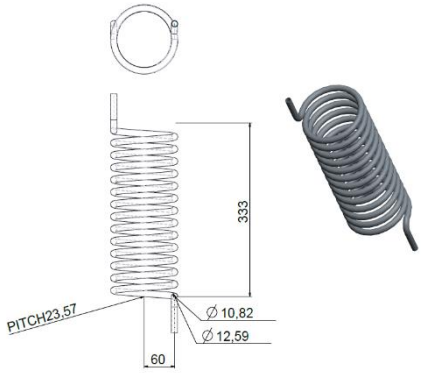

(a)

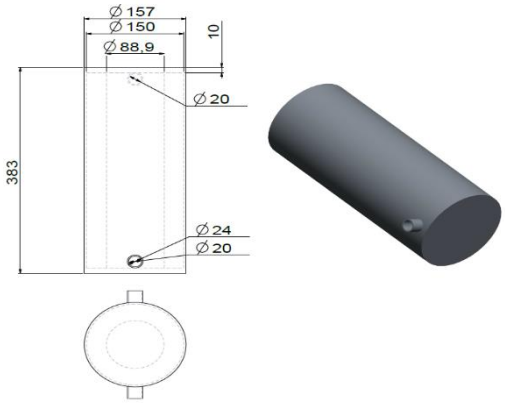

(b)

Fig. 1 Geometry modeling and dimensions of heat exchanger

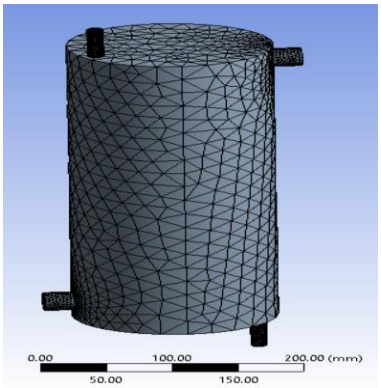

(a)

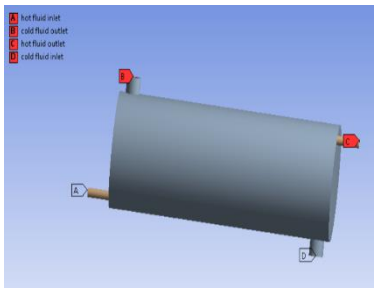

(b)

Fig. 2 computational domain considered for numerical simulation.

- *Boundary conditions*

The coil side heat exchanger of the hot fluid is varying various temperatures of 333 °K, 343 °K and 353 °K respectively and shell side of cold fluid temperature is kept constant of 300 °K. Further, the three different mass flow rate of the cold fluid is varying at inlet shell side of heat exchanger. The properties of nano-fluid are computed using the relation as per [1]. The zero-gauge pressure is maintained at outlet of coil and shell heat exchanger. The no-slip boundary condition is adopted for all surfaces. The details of the boundary conditions incorporated for the present numerical simulation is depicted in Table 1.

Table.1

Parameter	***Coil side***	***Shell side***
Inlet temperature	333 °K, 343 °K and 353 °K	300 °K
Mass flow rate	0.03, 0.05 and 0.07 kg/s	0.03, 0.05 and 0.07 kg/s
Outlet	Zero-gauge pressure	Zero-gauge pressure
Fluid	Hot water	Cold water, Cold water + concentration of 2.5% of Sio_2, and cold water + 2.5% of Cuo nano-fluids
Material	aluminium	aluminium

- RESULTS AND DISCUSSION

The numerical analysis of this research work has been carried out for the following various cases of inlet hot fluid temperature of coil side heat exchanger and also various mass flow rates of hot and cold fluids and studied the convection heat transfer coefficient and pressure drop.

- *Heat transfer coefficient*

Case – I:
Coil side region: Hot Fluid- water (temperature: 333k)
Shell side region: Cold fluid: Cuo (temperature: 300k)

The results of case-1 as shown in fig. 3. Fig 3(a) presents the heat transfer coefficient versus mass flow rate of the fluid for base fluid water and constant volume of fraction of 2.5% Sio_2 and Cuo of nano-fluids blended with water. From the Fig. 3(a), it is observed that the convection coefficient increases with increasing the mass flow rate of the fluid. It is also observed that the base fluid of water and concertation of Sio_2 performs the similar results with increasing the mass flow rate of the fluid. However, the concentration of Cuo blended with water showed the significant improvement in the convection coefficient at mass flow rate of 0.05 kg/s. Fig.

 ISBN: 978-93-91420-02-4

3(b), (c) and (d) presents the temperature contour plots of coil and shell type of heat exchanger at constant mass flow rate of 0.03 kg/s.

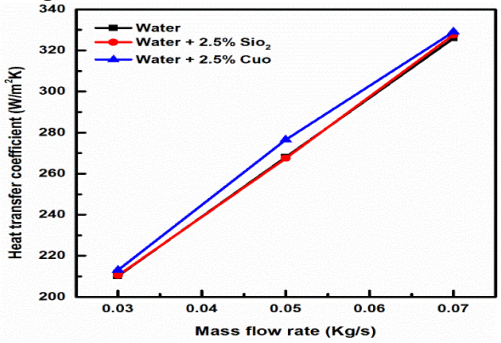

(a)

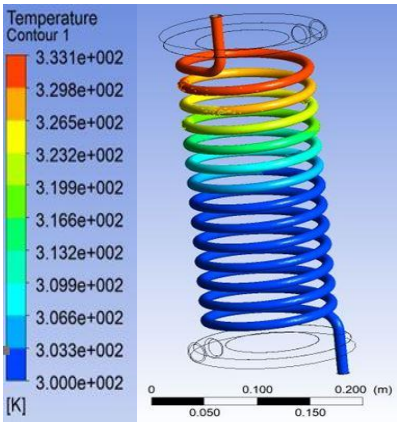

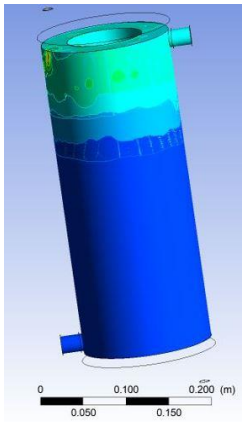

(b)

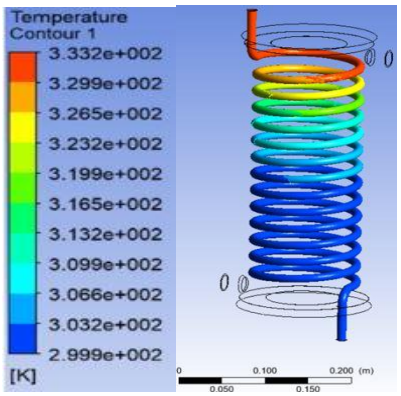

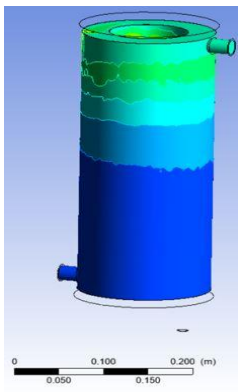

(c)

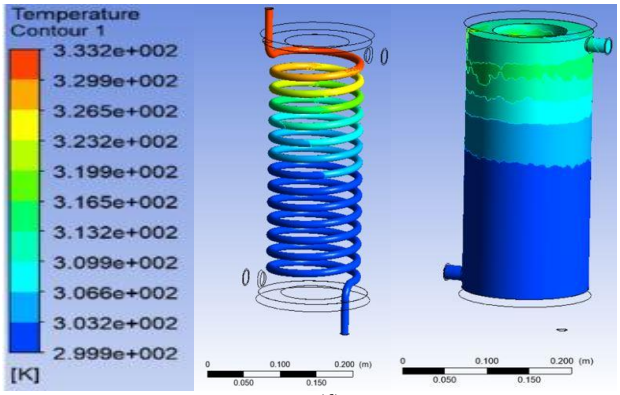

(d)

Fig. 3 (a) Heat transfer coefficient vs. mass flow rate, temperature contour plots for, (b) water, (c) water + 2.5% Sio2 and (d) water + 2.5% Cuo, at constant mass flow rate of 0.03 kg/s.

Case – II:

Coil side region: Hot Fluid- water (temperature: 343k)

Shell side region: Cold fluid: Cuo (temperature: 300k)

The results of case-2 as shown in fig. 4. Fig 4(a) presents the heat transfer coefficient versus mass flow rate of the base fluid and concentration of nano-fluid. From the Fig. 4(a), it is understood that, the base fluid of water and concertation of Sio_2 blended with water shown the similar kind of results. This is may be due to the thermal conductivity of water and blended Sio_2 in water has almost equal. However, Cuo nano-fluid blended with water has shown advancement in heat transfer coefficient compared to water and Sio_2 blended with water. This is because Cuo nano-fluid blended with water tends to improve the thermal conductivity of fluid and it leads to gain more heat from coil side heat exchanger of hot

 ISBN: 978-93-91420-02-4

fluid. It is also seen that, the concentration of Cuo blended with water showed the considerable improvement in the convection coefficient for all mass flow rate of fluid is considered for numerical simulation. Fig. 4(b), (c) and (d) presents the temperature contour plots of coil and shell type of heat exchanger for water and concentration of nano-fluids mixed with water at constant mass flow rate of 0.03 kg/s. From the temperature contour plots it is clearly observed that as the hot fluid flow from the coil side the shell side cold fluid gains heat is almost equal for water and water with Sio_2 nano-fluid. Consequently, shell side of Cuo nano-fluid absorb more heat at half the length of heat exchanger from coil side of hot fluid as the fluid progress towards the exit of coil heat exchanger.

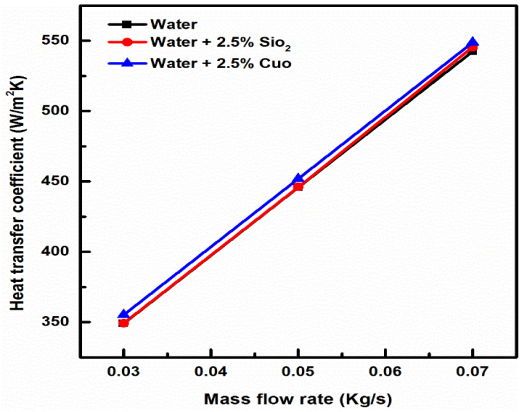

(a)

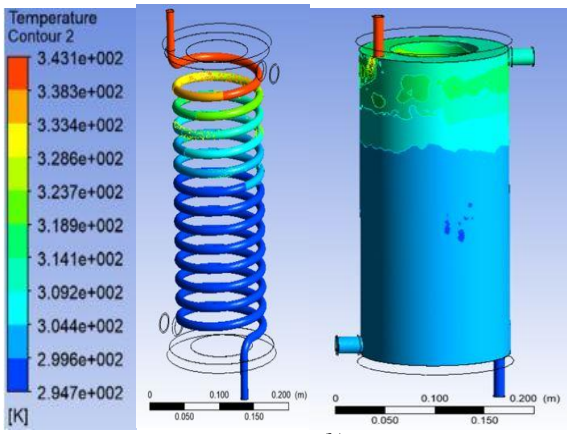

(b)

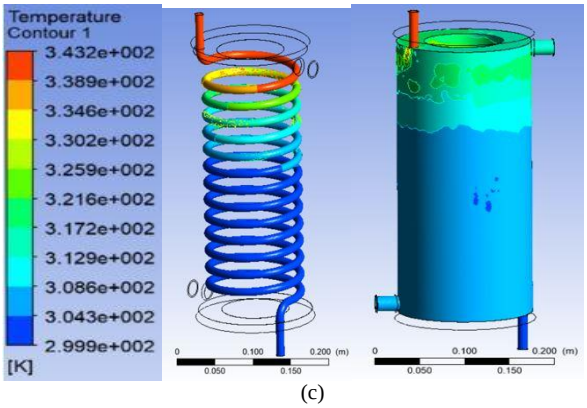

(c)

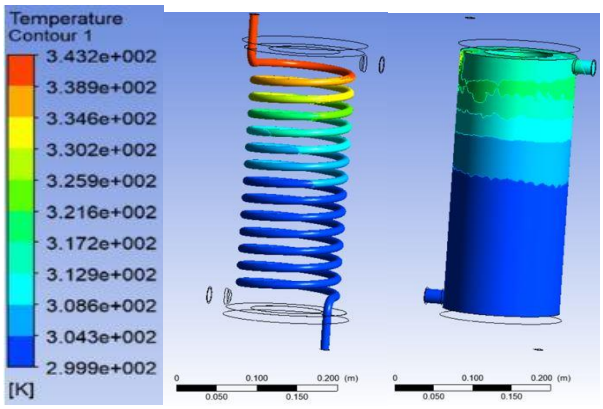

(d)

Fig. 4 (a) Heat transfer coefficient vs. mass flow rate, temperature contour plots for, (b) water, (c) water + 2.5% Sio2 and (d) water + 2.5% Cuo, at constant mass flow rate of 0.03 kg/s.

Case – III:

Coil side region: Hot Fluid- water (temperature: 353k)

Shell side region: Cold fluid: Cuo (temperature: 300k)

The results of case-3 as shown in fig. 5. Fig. 5(a) presents the heat transfer coefficient versus mass flow rate of the base fluid and concentration of Nano-fluid. In this case also, the convection coefficient is showed very similar kind of results for water and water with Sio_2 Nano-fluid with respect to mass flow rate of fluid. Moreover, the Cuo Nano-fluid mixed with water has augment in convection coefficient with progressively increasing mass flow rate of the fluid. But, this increase in convection coefficient improved marginally for different mass flow rate of the fluid is considered for study. Fig. 5(b), (c) and (d) presents the temperature contour plots of coil and shell type of heat exchanger for water and concentration of Nano-fluids mixed with water at constant mass flow rate of 0.03 kg/s. The temperature contour plots showed very similar for the base fluid and nano-fluids considered for the simulation.

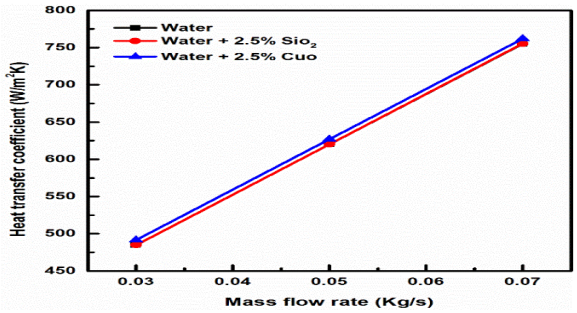

(a)

 ISBN: 978-93-91420-02-4

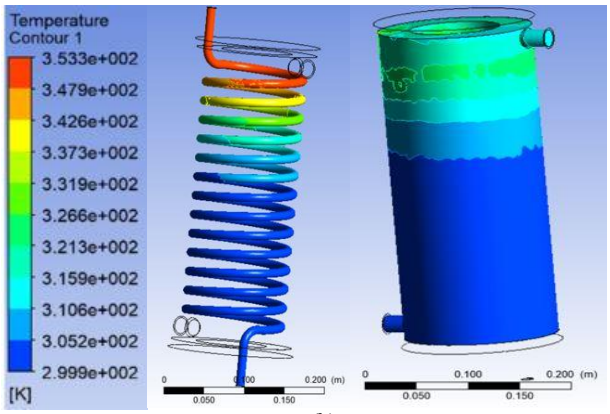

(b)

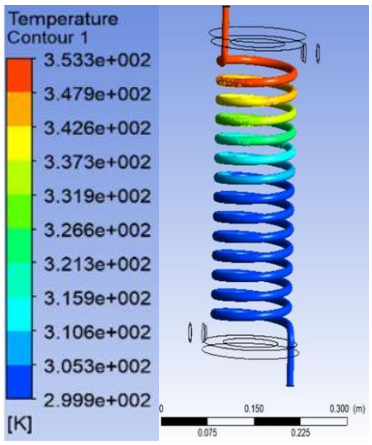

Fig. 5 Heat transfer coefficient vs. mass flow rate, temperature contour plots

Pressure drop variation with mass flow rate of fluids as shown in fig. 6. From the figure it revealed that the pressure drop increases with increasing the mass flow rates of the fluids. However, base water with Cuo Nano fluid presents the highest pressure drop than the base fluid and base fluid with Sio_2 nanofluid. This may be due to that the concentration of Cuo has higher in dense require more pumping power to lift the fluid. In addition, the base fluid with Sio_2 nanofluid has more pressure drop for all flow rates of fluid is considered compared to the base fluid.

CONCLUSIONS

Based on the present study of shell and coil type heat exchanger the important points are drawn below.

- The results of convection heat transfer coefficient and total heat dissipation rate showed the similar performance for base fluid as well as Sio_2 Nano-fluid. Henceforth, the Sio_2 Nano-fluid with concentration of 2.5% is not significant effect on the performance of the heat exchanger.
- The Cuo Nano-fluid showed moderate enhancement in heat transfer compared to base fluid and Sio_2 Nano-fluid.

With increasing inlet temperature of hot fluid of coil side of heat exchanger and with increasing the mass flow rate of fluid, the convection heat transfer coefficient as well as total heat transfer rate increases for base fluid and even for Nano-fluids also.

The pressure drops increases for all flow rates of fluid. The Cuo Nano fluid shows the highest pressure drop and Sio_2 showed in between Cuo Nano fluid and base fluid. It is important to note that the Sio_2 Nano fluid showed the highest pressure drop compared to base fluid with similar heat transfer enhancement.

References

1. B. Farajollahi, S.G. Etemad, M. Hojjat, International Journal of Heat and Mass Transfer Heat transfer of nanofluids in a shell and tube heat exchanger, International Journal of Heat and Mass Transfer. 53(2010)12–17.
2. A. Ali, M. Qasim, S. Zaki, Case Studies in Thermal Engineering Performance analysis of shell and tube heat exchanger: Parametric study, Case Studies in Thermal Engineering. 12 (2018) 563–568.
3. Y. Son, J. Shin, Performance of a Shell-and-Tube Heat Exchanger with Spiral Baffle Plates v, 15 (2001) 1555–1562.
4. D. De, T.K. Pal, S. Bandyopadhyay, A publication of IIETA Helical baffle design in shell and tube type heat exchanger with CFD analysis, 35 (2017) 378–383.
5. M. Elias, I.M. Shahrul, I.M. Mahbubul, R. Saidur, N.A. Rahim, International Journal of Heat and Mass Transfer Effect of different nanoparticle shapes on shell and tube heat exchanger using different baffle angles and operated with nanofluid, International Journal of Heat and Mass Transfer. 70 (2014) 289–297.
6. D. Swetha, K.S. Chalapathi, P. Saritha, Performance Analysis of Shell and Tube Heat Exchanger using Nano Fluid, 5 (2016) 320–325
7. A.K. Surana, K.J. Samuel, S. Harshit, U. Kumar, R.T.K. Raj, Numerical investigation of shell and tube heat exchanger using Al2O3 nanofluid Numerical Investigation of Shell and TubeHeat Exchanger Using Al2O3 Nanofluid, (2017).

 ISBN: 978-93-91420-02-4

Study of Rheological Characteristics of Nano Suspensions

Vidya Chaparala[1] and Venkaiah Mandula[2]
[1]Department of Mechanical Engineering, P.V.P.Siddhartha Institute of Technology, Vijayawada,India,
[2]Department of Mechanical Engineering, Narasaraopeta Engineering College,Narasaraopet,India.

***Abstract*— Nano suspensions serve as best candidate in variety of industrial and engineering applications. One such sector is heat transfer agent. Nano fluids enhance the heat transfer rate by many folds than conventional cooling media while making the system compact. Present study aims to explore the role of PH on rheological behavior of SiO2 nano fluids. Present investigation reports a drop in viscosity of fluid by around 9% for a volume concentration of 0.07% with surfactant concentration of 0.05%.**

Keywords— rheology, dynamic viscosity, PH value, nano fluid

INTRODUCTION

Nano materials are tiny particles of which at least one dimension is in the order of nm which contributes to surprising enhancement in thermo physical properties of the same [1,2]. Evaluation and control of dispersion stability by the way of electrostatic and electrostatic modification is of major concern from various scientific applications [3]. Stirred media milling technique can be adopted to produce various popular nano particles in which PH value can be controlled easily to promote stability of suspension [4].

The rheology of CaP suspensions is used to predict the inject ability of this generation of biomaterial. In 1965, one of the first studies related to CaP suspension rheology investigated the viscosity of dicalcium phosphate suspensions (Bujake, 1965). Results demonstrated appreciable shear thinning behavior and suggested significant particle–particle interaction in these suspensions. Over most regions of the shear rate ($\gamma^{\cdot}$), the empirical power-law equation $\tau = K\gamma^{\cdot}n$ was proposed to describe flow curve of CaP suspensions, where τ is the shear stress, K is the consistency factor and n is the flow index. Rao and Kannan examined the yield stress and viscosity of hydroxyapatite suspensions (Rao and Kannan, 2001).

For all suspensions, the researchers observed a yield stress and a shear-thinning followed by shear-thickening behavior. Generally, shear thickening appears to occur at high particle loading (Knowles *et al*., 2000). Friberg *et al.* (2001) measured the viscosity of βTCP suspension by varying the liquid-to-powder ratio (LPR), employing powders of two medium particle sizes, and adding three different modifiers. More recently, Baroud *et al.* (2005) have studied the rheological properties of concentrated aqueous βTCP suspensions. This study has reported measurements of the yield stress and the viscosity as a function of LPR and milling time of the powder.

The LPR clearly affected the rheological properties of CaP suspensions. Increasing LPR results in a more dilute solution with less particle–particle interaction, and hence lower viscosity and yield stress. The effect of milling time was significant, viscosity and yield stress increased as a function of the milling time (Bujake, 1965; Knowles *et al*., 2000). Liu *et al.* (2006) studied rheological properties of concentrated aqueous injectable CaP cement. Their investigations showed that CaP cement presented visco plasticity and thixotropy. Results of this study confirmed the dependence of the technological parameters such as LPR, temperature and particles size on the rheological behavior of CPC (Liu *et al*., 2006).

Nanoparticles with their unique and unpredictable properties have recently attracted much attention in several branches of the petroleum industry. This paper is aimed at studying hydrophilic silica-alumina and slightly hydrophobic silica nanoparticle behaviors to see if they have enough feasibility to be used as an appropriate agent in enhanced oil recovery, especially polymer flooding. The main focus is on the rheological behavior of these nanomaterials in aqueous and polymeric media. Viscosity measurements showed that both nanoparticles had a great ability in rheology modification of aqueous solution.

The solution viscosity was studied as a function of nanoparticle concentration and shear rate. The stability improvement of nanoparticle suspensions was also investigated by dissolving fixed amounts of hydrolyzed and sulfonated polyacrylamides. The stability of slightly hydrophobic silica suspensions was significantly improved by low molecular weight polymers. Instead, nanoparticles considerably enhanced polymer solution viscosity. Finally, sand-pack flow experiments, conducted in optimum conditions, revealed how nanoparticles may uniquely enhance polymer flooding performance.

Methodolgy of sample preperation

In the present investigation nano suspension samples prepared by dispersing SiO2 nano particles in distilled water. SiO2 nano particles of average diameter 20nm was purchased from Sisco Research Laboratories, India. Nano particles were used as received without any further processing. Various nano fluids samples were prepared with different surfactants in order to understand the compatibility of surfactant with the chosen nano material. Experimental trails revealed C-TAB as best compatible one as compared to other surfactants. Hence, C-TAB was used as surfactant in the present experimentation. Nano fluid samples were prepared by two step method. Initially surfactant dispersed in to distilled water and stirred with magnetic stirrer. After ensuring the surfactant particles dispersed uniformly in the base fluid then nano particles

 ISBN: 978-93-91420-02-4

added to it and continued stirring. REMI make 5MLH stirrer used for the mixing

Figure 1: Magnetic stirrer

Then the stirred suspension was loaded into ATHENA make Ultrasonic probe sonicator with 20 Khz frequency and sonicated by setting run program to six. In this particular program the probe run time is for 15 seconds and idle time for 15 seconds.

Figure 2: Ultrasonic probe sonicator

All prepared samples were collected into glass tube sample bottles and preserved for stability observation. Thermo physical properties of the coolant play a key role in improving the heat transfer rate and convective heat exchange coefficient. In the present investigation an attempt made to study the rheological properties of nano fluid with adjusting the PH value. In this work, we used the method of changing suspension pH value to generate strong repulsive forces and to reduce the coagulation of nanoparticles to obtain low viscosity (well-dispersed) suspension. In order to alter the PH value, the samples were added 0.1M concentration NaOH solution and HCL acid drop wise using micro pipette and stirred thoroughly.

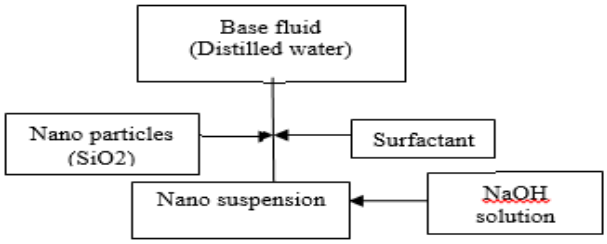

FIGURE 3: NANO SUSPENSION PREPERATION FLOW CHART

TABLEI. PROPERTIES OF SUSPENSION CONTITUENTS

Constituent of suspension	***dimension***	***density***
Water	-	997.5Kg/m^3
SiO_2 Nano particle	20nm average diameter	2220Kg/m^3

Dynamic viscosity of the samples was tested using LMDV60 digital rotational viscometer with different rotations of the spindle ranging between 0.3RPM to 60RPM and considered average value of all different observations. For ensuring accuracy of the results every observed was conducted for thrice repeatedly for same sample.

Figure 4: Viscosity measuring unit

RESULTS AND DISCUSSION

Figures 5,6 presents the variation plots of dynamic viscosity and PH value of suspension for different volume concentrations. From the experimental results it is concluded that the temperature plays prominent influence on dynamic viscosity for the same volume concentration of nano particles. As the temperature increases the viscosity changes inversely due to shear thinning nature of the suspension. From figure 6, it is reported that the concentration of surfactant is playing vital role in adjusting the PH value of the suspension which leads to better dispersion stability of the nano suspension.

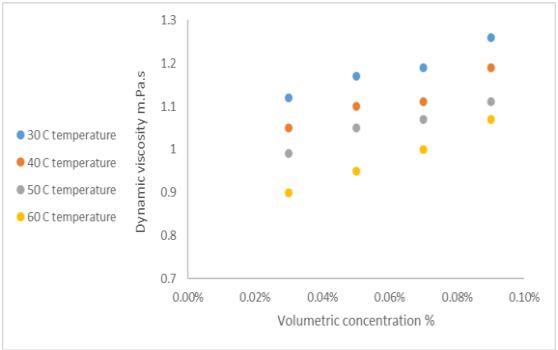

Figure 5: Dynamic viscosity of nano fluid against volume concentration at different temperatures.

 ISBN: 978-93-91420-02-4

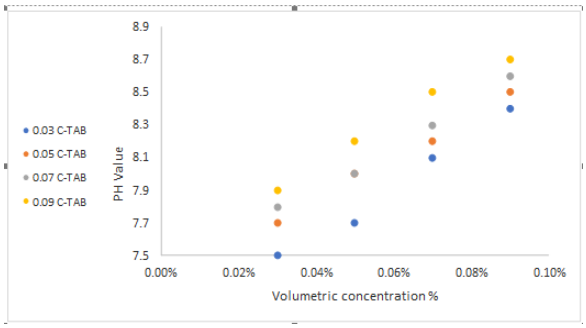

Figure 6: PH value of nano fluid against volume Concentration at different temperatures

CONCLUSIONS

Effects of particle concentration and surfactant concentration towards the variation of dynamic viscosity as well as PH value of the nano fluid were investigated. As rheological properties reflect on the energy dissipation by the way of inertia to free flow of fluids it has become major concern of this investigation. Present study reports the role of PH on rheological behavior of SiO2 nano fluids. Present investigation reports a drop in viscosity of fluid by around 9% for a volume concentration of 0.07% with surfactant concentration of 0.05%.

REFERENCES

[1] Prasher R 2005 Phys. Rev. Lett. 94 025901

[2] Timofeeva E V, Gavrilov A N, McCloskey J M and Tolmachev

[3] Moayedi, H., B. B. K. Huat, S. Kazemian, and T. A. Mohammad. 2012. Effect of stabilizer reagents on zeta potential of kaolinite and its relevance to electrokinetic treatment. *Journal of Dispersion Science and Technology* 33(1):103-110.

[4] Sakthivel, S., V.V. Krishnan, and B. Pitchumani. 2008. Influence of suspension stability on wet grinding for production of mineral nanoparticles. *Particuology* 6(2):120–124.

[5] P. Keblinski, J. A. Eastman, and D. G. Cahill, Mater. Today **8**, 36 (2005). https://doi.org/10.1016/S1369-7021(05)70936-62.J. Eapen, W. C. Williams, J. Buongiorno, L. Hu, S. Yip, R. Rusconi, and R. Piazza, Phys. Rev. Lett. **99**, 095901 (2007).

[6] V. Timofeeva, A. N. Gavrilov, J. M. McCloskey, and Y. V. Tolmachev, Phys. Rev. E **76**, 061203 (2007). https://doi.org/10.1103/PhysRevE.76.061203, 4.J. Buongiorno, ASME J. Heat Transfer **128**, 240 (2006

[7] U. S. Choi, Z. G. Zhang, W. Yu, F. E. Lockwood, and E. A. Grulke, Appl. Phys. Lett. **79**, 2252 (2001).

[8] Nanda, C. Maranville, S. C. Bollin, D. Sawall, H. Ohtani, J. T. Remillard, and J. M. Ginder, J. Phys. Chem. C **112**, 654 (2008).

[9] C. Maxwell, A Treatise on Electricity and Magnetism, 2nd ed. (Clarendon, Oxford, 1881).

[10] J. Philip, P. D. Shima, and B. Raj, Appl. Phys. Lett. **91**, 203108 (2007). https://doi.org/10.1063/1.2812699

[11] U. Rea, T. Mckrell, L. Hu, and J. Buongiorno, Int. J. Heat Mass Transfer **52**, 2042 (2009).

[12] R. Prasher, D. Song, J. Wang, and P. Phelan, Appl. Phys. Lett. **89**, 133108 (2006). https://doi.org/10.1063/1.2356113

[13] R. Prasher, W. Evans, P. Meakin, J. Fish, P. Phelan, and P. Keblinski, Appl. Phys. Lett. **89**, 143119 (2006).

[14] W. Evans, J. Fish, and P. Keblinski, Appl. Phys. Lett. **88**, 093116 (2006).

[15] K. B. Anoop, T. Sundararajan, and S. K. Das, Int. J. Heat Mass Transfer **52**, 2189 (2009

[16] J.Jung and J. Y. Yoo, Int. J. Heat Mass Transfer **52**, 525 (2009).

[17] 15.X. F. Zhou and L. Gao, J. Appl. Phys. **103**, 083503 (2008).

[18] 16.M. P. Beck, Y. Yuan, P. Warrier, and A. S. Teja "The effect of particle size on the thermal conductivity of alumina nanofluids," J. Nanopart. Res. (in press).

[19] K. C. Fang, C. Weng, and S. P. Ju, Nanotechnology **17**, 3909 (2006).

 ISBN: 978-93-91420-02-4

Design and Fabrication of Loop Wheel System

Akshay C. Hatagale, Vinay C. Yadav, Yash P. Edakhe and Anand Babu Kotta
Depart of Mechanical Engineering, G.H Raisoni College of Engineering, Nagpur, Maharashtra, India

***Abstract*— In today's world, bicycles are the most popular choice when it comes to health, pollution and other things. A lot of research has been done to make the journey more comfortable. Different types of wheels designed for travelers for a variety of applications such as cycling, mountain biking and bike racing. This paper introduces a loop wheel designed for the suspension system, which extends inside the wheel excellent performance and good comfort. Loop wheels give you a smooth ride. Loop wheel spring is available it is usually made of composite materials carefully crafted to provide good compression and lateral strength and strength and endurance. The three loops on all wheels act as a self-repair system. This spring system between the hub and the wheel of the wheel provides a continuous adjustment arrangement in unequal places stopping passengers from an unknown wheel on the road. Spring configuration allows torque to occur transmits smoothly between hub and the rim. This cycle is made using C20 material.**

Keywords: Loop wheel, integrated suspension system, Triangular hub.

I. INTRODUCTION

Loop wheel is a wheel with an important suspension, designed for better performance of surprise and great improvement. Loop wheels give you a smooth ride. They are more comfortable than regular wheels. The springs produce boring vibrations, as well as bumps and shock. They are designed for everyday use and are durable and long lasting. The bicycle loop wheels help people cross uneven roads, rough tracks and paved roads, with minimal effort, and springs give you more power to get up or down the road. They reduce vibration, compared to a talking wheel. In our project the concept of suspension wheel suspension represents a new approach to the external road by taking advantage of current high-power power components. The concept of a loop wheel has been found to be very useful in a world that reduces aging and cracking. The Loop wheel wheels in the spring are made of synthetic carbon material, carefully developed and tested to provide lateral stability, as well as strength and durability. Carefully developed and tested for this specific application. All loop wheels within the product category have a certain degree of compression.

II. METHODOLOGY

The main target is to achieve the desired deflection in the suspension for a particular weight of rider means driver. Considering the use of application of mild steel material is selected for the loop wheel. The wheel is designed to considering the impact forces coming from ground and lateral forces while Cornering. Also a custom hub is used to design to accommodate the entire loop with the help of nut and bolt.

Project identification: Finally after reading a separate research paper, we decided that work would be done on System suspension. The concept of loop wheels is a suspension system built into circles or disabled vehicles. The standard bicycle have a different suspension system that gets more space and not stuff too Weight but still unable to maintain the sudden effects we think which system can be changed will do just that and increase the design process. Realizing the problem with suspension, we decided to work on the suspension process.

Composition phase: In this section we plan to design a waiting wheel suspension by calculating the width, length and thickness also includes its bending strength and load retention capacity. The most important thing in this project with material selection will be decided by who can support the highest and most flexible load.

System drawing: The calculated values are used to draw a realistic drawing that provides an easy way to do it build your mind.

Procurement: The specified parts is purchased from the market according to our requirement and. A special design rim will also be purchased at the market at all things must be right.

Production Phase: It covers all the purchased items of our design, including a welding process, grinding cut, turning, balance.

Testing: In testing we are evaluating deflection of the loop wheel on the basis of different road level.

III. OBJECTIVE

(1) To provide better shock-absorbing performance.
(2) To give smoother ride.
(3) To increase load bearing capacity

IV. COMPONENTS USED

Tires: The tire is a circular wheel that measures the rim of the tires to protect it and allow for better motor performance by providing a flexible cushion that holds the shock while keeping the tire very close to the ground.

Wheel Rim: A rim is usually made of metal to form a loop, or it may be a carbon fiber composite structure. Bicycle tires are usually designed to fit the frame and fork using scrap, and to hold bicycle tires.

Loop Spring: Spring loop is a simple spring method commonly used for suspension in wheeled vehicles.

Wheel Hub**:** The hub is the central part of a bicycle wheel. It contains an axle, bear and a harp shell. The harp is the center of the wheel.

V. DESIGN AND CALCULATION

WE KNOW THAT,

$$R_A+R_B=90 \text{ KG}$$
$$90*9.81=882.9N$$

TAKING MOMENT ABOUT A

$$MA=0$$
$$W*X-R_B*Y=0$$
$$882.9*750-R_B*1080=0$$

- RB=613.125N (REAR WHEEL FORCE)
- RA=882.9-RB
- =882.9-613.125
- =269.775N (FRONT WHEEL FORCE)

FROM ABOVE CALCULATION WE HAVE CONCLUDE THAT,

1. *30 % load acting on front wheel*

IE. (269.775 N)

2. 70 % LOAD ACTING ON REAL WHEEL

IE. (613.125 N)

AVERAGE MASS OF RIDER = 75KG.

AND AVERAGE WEIGHT OF CYCLE = 15KG

TOTAL AVERAGE WEIGHT OF CYCLE INCLUDING RIDER

M = 90KG, F = 882.9N

NOW CALCULATION OF FOR TOTAL LOAD ON EACH WHEEL.

- LOAD ACTING ON FRONT WHEEL.

  =269.775N
- LOAD ACTING ON REAR WHEEL.

  =613.125N

SO, MAXIMUM LOAD ACTS ON REAR WHEEL SIDE.

NOW, LEAF SPRING WILL BE DESIGNED FOR MAXIMUM LOADING CONDITION. (I.E. FOR REAR WHEEL.)

F MAX = F = 613.125N

WE USED C-20 MATERIAL,

- TENSILE STRENGTH = 560N/MM^2
- YIELD STRENGTH = TENSILE STRENGTH / F.O.S

  = 560/2
- YIELD STRENGTH = 280N/MM^2.

DIMENSION OF CROSS SECTION OF THE LEAF IS TO BE DETERMINED.

FOR, F = 613.125

FOR DETERMINING THE THICKNESS OF THE LEAF, LET US CONSIDER

- MAJOR AXIS LOOP (L) =300MM (12INCH)
- MINOR AXIS LOOP (H) =195MM (7.8INCH)
- WIDTH OF SPRING (B) =25MM (1INCH)
- E=200 MPA

WE KNOW THAT MAXIMUM PRINCIPLE STRESS

ΣMAX = 3FL/2NBT^2

560=3*613.125*300/2*1*25* T^2

T=4.439MM ~5MM.

THICKNESS OF THE SPRING T = 5MM.

1. CALCULATION OF MAXIMUM PRINCIPAL STRESS

ΣMAX = 3FL/2NBT^2

= 3*613.125*300/2*3*25*5^2

= 147.15 N/MM2 < 280 N/MM^2

HENCE, DESIGN IS SAFE.

2. CALCULATION OF MAXIMUM DEFLECTION

ΔMAX = 3FL^3/8NBT^3E

=3*613.125*300^3/8*3*25*5^3*2*10^5

= 3.3108 N ~ 4 MM.

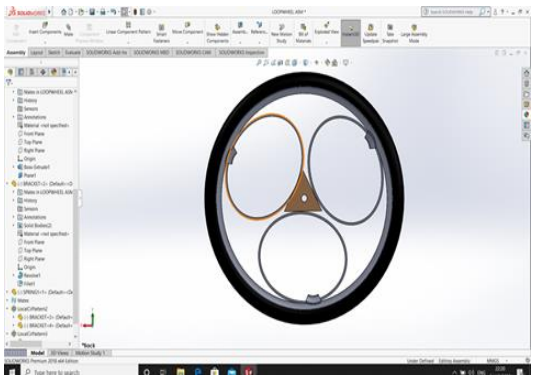

FIG -1:- 3D Model of Loop Wheel

A. Advantages

1) Better shock-absorbing performance.
2) Greater comfort.
3) Smoother ride.
4) More comfortable than standard wheels.
5) They are extremely strong.

CONCLUSION

This project is to increase shock - better absorption and suspension of the bicycle wheel. the loop wheel is designed to help you navigate uneven roads, grass cliffs, grass, difficult tracks and rocky terrain with minimal effort. Combined rubber bands give you extra strength to get up or down the road.

REFERENCES

[1] PankajSaini, AshishGoel, Dushyant Kumar, “Design and Analysis of Composite Leaf Spring for LightVehicles”, International Journal of Innovative Research in Science, Engineering and Technology, ISSN: 2319-8753, Vol. 2, Issue 5, May 2013, PP 1-10.

[2] Baviskar A. C., Bhamre V. G. andSarode S. S., “Design and Analysis of a Leaf Spring for automobilesuspension system- A Review”, International Journal of Emerging Technology and Advanced Engineering, ISSN2250-2459, Volume 3, Issue 6, June 2013, PP 406-410.

[3] Mr. Tharigonda Niranjan Babu, Mr P. Bhaskar and Mr. S. Moulali, “Design and Analysis of Leaf Spring with Composite materials”, INTERNATIONAL JOURNAL OF ENGINEERING SCIENCES & RESEARCHTECHNOLOGY, ISSN: 2277-9655, Babu, 3 (8): August, 2014, PP 759-756.

[4] HolfgangTrauthein, “Loop-wheel suspension system development status”, Engineering Consultant, D-7758 Meersburg, Federal Republic of Germany, Formarly of Lokeeed Research and Engineering center, Huntsville, Al. USA.

[5] Mechanics of Materials I, Third Edition, E. J. Hearn, University of Warwick, United Kingdom, Chapter 1, Page No. 1-8.

[6] Mechanical Vibrations, Thammaiah Gowda, Jagadeesha T, D. V. Girish, Tata Mcgraw Hill Education Private Limited, Page No. 44, Topic – Spring Element.

[7] Strength of Materials, S. Ramamrutham, R. Narayanan, Dhanpat Rai Publication Company, Page No. 116-118.

 ISBN: 978-93-91420-02-4

Performance of Solar Vapour Absorption System And Its Dependence on Generator Temperature

J. SidharthaYadav[1], R.S.M Swaroop Sharma[2], Ch. ManikanteswarRao[3] and Y.Karun Kumar[4]
[1]Raghu Engineering College (Autonomous), , Visakhapatnam
[2]Narayana Polytechnic College, Srikakulam
[3,4]Raghu Engineering College (Autonomous),Visakhapatnam

***Abstract*— As the saying goes, "There is no energy crisis, only a crisis of ignorance". With the minds of research along with scientific investigation, a pathway has led to deep dive into renewable energy sources. In the era of energy crisis renewable energy is seen as a farsighted option with great capability and endurance. This paper deals with application of solar thermal energy with vapor absorption system. In vapor absorption, system heat energy is taken as source of input energy unlike mechanical energy in vapor compression refrigeration system. The performance characteristics and evaluation depends on heat energy supplied and pump work used in the refrigeration system .Hence, here idea of experimental setup developed from this thought that if the heat energy required for the process is extracted from the solar energy and supplied to the generator then energy requirement to the generator can be reduced. Hence, our project novelty is based on the running a vapour absorption refrigeration system using the heat energy extracted from solar energy by using a parabolic solar heat collector. This heat is used to supply the heat required in the generator for the system. Hence, our result of experiment would aim for generation where the input work of electrical energy is given only through pump and other sources of input work are removed. Air-conditioner and refrigerator uses 70% of domestic energy utilized. This work provides a solution for this high energy consuming machines. We hope to take a small step in this direction for future development and establishment of new advancements in this regard.**

Keywords - Renewable Energy, Vapor Absorption, Heat Energy, Parabolic Solar Heat Collector, Solar thermal energy, pump work

INTRODUCTION

Per capita energy consumption of the people of a particular country plays a major role in the country's development. It is said that more the energy consumption more prosperous is the country, small changes are done in the same case by utilizing clean energy which is environmental friendly. According to Martin Rees, he stated that "we do not understand the consequences of rising population and increasing energy consumption on the interwoven fabric of atmosphere, fabric and life." There is an increased need of using the clean energy and specially dealing with the refrigerants causing the depletion of ozone layer. So, the need has been arrived to utilize the renewable sources of energy to find the solution in this path of literature surveys like Sorawitkaewpradub[1] et al found a way to utilize waste engine heat from the exhaust of the automobiles in generating refrigerating effect. Piyush mahendru[2] et al studied about the analysis of lithium bromide, water vapor absorption refrigeration system using the mole concentration concept. Pongsidsrikhirin[3] et al studied about various vapor absorption refrigeration systems present and the working fluids which may be used to achieve various outputs. Arturo Gonzalez Gils[4] studied about solar air cooling on single and double effect lithium bromide vapor absorption refrigeration system. Benjamin Bronsema[5] identified the problems faced in hybrid ventilation systems and provided certain solution to them. T.O Ahamdu[6] studied about a lithium bromide chiller, which gave a maximum cop of 0.42. The source utilized was waste heat in the experiment. Mr. Aniket Gandhi & Dr. R.Arakerimath[7] studied about solar vapor absorption cooling system utilizing parabolic solar dish collector where the cop was obtained to be 0.72 for the cycle.JoydeepChakraborty[8] et al studied about lithium bromide vapor absorption system using solar energy. Anan Pongtornkulpanich[9]studied about a new pair of absorbent and refrigeration in vapor absorption refrigeration system using activated carbon and methanol providing the required heat through solar energy. Soteris Kalogirou[10] studied about designing a lithium bromide vapor absorption refrigerator providing the necessary design conditions for heat exchangers.

GAPS IDENTIFIED FROM LITERATURE SURVEY

Although vapor absorption refrigeration outstands vapor compression system in many aspects like using non- harmful refrigerants, using clean energy and reducing carbon emissions indirectly most of the literature work has been done on lithium bromide refrigeration system. Very little work is done in the recent times on ammonia water vapor absorption system. Since ammonia has the freezing point of -77c which is very less compared to lithium bromide which is better option considering the application in the field of refrigeration? Hence, based on literature survey it is decided to conduct an experimental analysis on ammonia water based vapor absorption refrigeration system aiming for obtaining better results compared to lithium bromide refrigeration system. The novelty of the paper is the utilization of solar heat energy applications for producing refrigerating effect using ammonia water as the working pair. In the vapor absorption system, we require heat energy for the separation of refrigerant and absorbent. The heat source required for this is supplied with the help of solar heat supplied from the parabolic solar collector. Once the connections are made, coefficient of performance is calculated and the results are analyzed.

Renewable energy sources make the future path for saving energy and the solutions to energy consumption. The concept of setting an interlink for obtaining refrigerating effect with solar heat generated from parabolic

 ISBN: 978-93-91420-02-4

solar trough not only overcomes the deficiency of energy consumption but also deals with overcoming the high-end solution for ozone layer depletion which is the problem at alarming stage in the present days.

WORKING PRINCIPLE OF ABSORPTION SYSTEM

In a vapor absorption system, two fluids are used which are the absorbent and refrigerant. Absorbent is a substance which absorbs the refrigerant causing the pressure to reduce. As a refrigerant vapor gets absorbed the temperature of the refrigerant gets reduced due to vaporization of the refrigerant. This basic process causes the refrigerating effect. As this occurs the absorbent becomes more and more diluted due to refrigerant getting absorbed into it and hence to separate this again heating is used to bring the absorber back to its normal state. Hence, by the process of supplying heat energy the refrigerating effect is produced in a cyclic process.

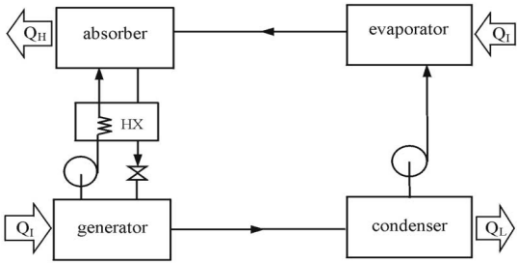

Fig-1.Working of vapor absorption system.

EXPERIMENTAL SET UP

SOLAR PARABOLIC TROUGH COLLECTOR:

A parabolic shaped solar collector is used to obtain maximum concentration of solar radiation. The fabricated solar trough collector is made up of materials like aluminum plates and ply wood was used. The ply wood was set up as the initial layer on which aluminum sheets are placed and pasted. A pipe situated at the focus on the parabola so that the solar radiation on the collector will be concentered on it and the refrigerant flowing inside the pipes gets heated up. Here this works as a generator for separating the refrigerant and absorbent.

Fig-2. Fabrication of solar parabolic trough collector

Fig-3. Condenser, absorber and evaporator unit.

Table -1: COMPONENTS USED IN THE EXPERIMENT:

S.No	Component	Material	Specification	Size	Units
1	Parabolic collector	Aluminum	1 tube	1	meter
2	Condenser	Copper	16 Windings	0.4	meter
3	Expansion valve	Copper	40 Windings	1.5	meter
4	Absorber	Iron	1	0.15 x 0.20	$Meter^2$
5	Pump	Plastic	1	4	Watt
6	Thermocouples	Digital	4		Celsiu, Kelvin

The experiment was made by using the above listed materials and connected in an order based on working principle. The refrigerant was filled into the condenser after all the necessary connections are made under the supervision of a technician. The fabricated parabolic solar collector was connected to the refrigeration system. The experiment is conducted and the values of different temperatures are noted using digital thermocouples at the various connections like condenser, generator, & evaporator, based on the values of temperature readings we found the coefficient of performance at various timings of the day according to the availability of solar energy in the day time. On completion of it we collected the values of temperatures for a week and the average instantaneous coefficient of performance was found.

THE EXPERIMENT WAS MADE ON THE FOLLOWING ASSUMPTIONS:

- The flow is considered as steady and renewable
- Pure refrigerant is flowing in the condenser, expansion valve and evaporator.

There is no pressure loss in the system

- Changes in kinetic and potential energy are negligible in the system

CALCULATIONS

T_g- Generator Temperature T_c- condenser temperature

T_e- evaporator temperature

Sl. No.	Readings for Day	GeneratorTemperature (T_g)	C.O.P	Remarks
1	DAY -1	345	0.354	
2		353	0.305	
3		339	0.353	
4	DAY -2	342	0.228	
5		360	0.356	
6		335	0.212	
7	DAY -3	349	0.228	

 ISBN: 978-93-91420-02-4

8		362	0.356	
9		348	0.212	
10	DAY -4	357	0.400	
11		361	0.542	
12		346	0.318	
13	DAY -5	362	0.308	
14		358	0.351	
15		348	0.165	LOWEST C.O.P
16	DAY -6	340	0.271	
17		356	0.278	
18		360	0.640	HIGHEST C.O.P
19	DAY -7	360	0.266	
20		362	0.211	
21		358	0.278	

Coefficient of performance =

$$\left[\frac{\text{Refrigerating effect in the evaporator}}{\text{Heat supplied in the generator}}\right]$$

$$\text{CO.P}=\left[\frac{T_g-T_c}{T_g}\right]*\left[\frac{T_e}{T_c-T_e}\right]$$

$$\text{Average C.O.P} = \left[\frac{COP1+COP2+COP3}{3}\right]$$

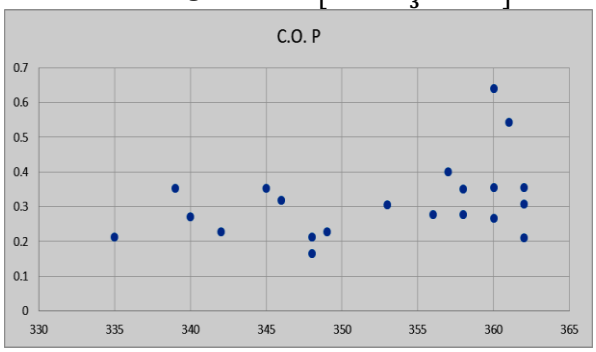

CONCLUSION

In the present generation, the main aim of development is “first & fast” rather than “slow & steady”. So, here we used solar heat energy as an input to the generator. Harnessing solar energy to the panels is a technological stuff giving an overall output of maximum 8% only but when we use solar heat from collectors, we could generate a great cause and effect in producing refrigerating effect. In this paper, we have made a keen study and compared the generator temperature to the coefficient of performance, although the temperature differences obtained here is low range (8-13) degrees maximum. An improvisation in the temperature difference can be obtained by changing the concentration levels of absorbent and refrigerant pairs or by considering other design factors of evaporators, condensers, length between the evaporator and parabolic solar trough etc. hence, this may be a pathway for the future scope of development in this direction.

Furthermore utilizing this device in the application of air conditioning has futuristic approach rather than refrigeration. Hence, with the present generation facing the crisis of energy generation, consumption and utilization this method forms a pathway in finding small steps towards a mighty development in the field of energy saving design of appliances. Reconsidering the designs in a proper way would lead to utilization in every domestic household refrigeration and air conditioning appliances connected through solar energy, which is safe, clean and simple technology. As the saying goes “ Nature satisfies everyone’s need not greed” so this is a definite and promising solution for overcoming the problems of ozone depletion, high energy consumption & global warming by utilizing nature’s greatest, brightest and everlasting source. “The SUN”.

REFERENCES

[1] Sorawit Kaewpradub et al “Absorption refrigeration system using engine exhaust gas as an energy source”, Case Studies in Thermal Engineering 12 (2018) 797–804

[2] Piyush Mahendru et al, “Steady State Analysis of Vapor Absorption Refrigeration System using li-br-h2o as a Refrigerant”, International Journal of Emerging Technology and Advanced Engineering(ISSN 2250-2459, Volume 2, Issue 9, September 2012)

[3] Pongsid Srikhirin et al, “A review of absorption refrigeration technologies”, Renewable and Sustainable Energy Reviews5 (2001) 343–372

[4] Arturo González Gil, “Novel single–double-effect LiBr/H2Oabsorption prototype with a highly efficient direct air-cooled adiabatic absorber”.

[5] Benjamin Bronsema et al. “Hybrid Ventilation: Our First Choice!”, 7th REHVA World Congress, CLIMA 2000 NAPOLI 2001.

[6] T. O. Ahmadu, “Experimental Evaluation of A 3 Kw Absorption Chiller Prototype”, Nigerian Journal of Technology (NIJOTECH)Vol. 38, No. 2, April 2019, pp. 337 – 344

[7] Aniket Gandhi et al, “Solar Vapor Absorption Cooling System Using parabolic dish Collector”, IOSR Journal of Mechanical and Civil Engineering (IOSR-JMCE) e-ISSN: 2278-1684,p-ISSN: 2320-334X, Volume 13, Issue 2 Ver. II (Mar. - Apr. 2016), PP 09-13

[8] Joydeep Chakraborty et al, “A Review Paper On Solar Energy Opearted Vapour Absorption System UsingLibr-H2o”, International Journal of Engineering Research & Technology (IJERT), ISSN: 2278-0181.

[9] Anan Pongtorn kulpanich, “Dynamic Simulation of Solid Adsorption Solar Refrigerator System with AC/CH3OHas a Working Pair”, Energy and Power Engineering, 2014, 6, 459-465.

[10] Soteris Kalogirou et al, “Design and Construction of a Lithium Bromide Water Absorption Refrigerator”, CLIMA 2000/Napoli 2001 World Congress – Napoli (I), 15-18 September 2001

 ISBN: 978-93-91420-02-4

Design and Analysis of Handicapped Steering Tricycle

Dakshay R. Pratapwar, Dhananjay D. Dhoke, Manoj Parate, Madhusudhan Mujumdar and Hitesh Gotmare
Department of Mechanical Engineering, Institute of G.H.Raisoni College Of Engineering, Nagpur, India

Abstract: **Conventional tricycles for handicapped require a lot of human effort to operate. They generally come with separate arrangements for providing motion and giving direction to the vehicle. These separate arrangements cause asymmetric use of hands and this results in discomfort of the rider. To alleviate this discomfort, a new arrangement which is mechanically more efficient than the conventional handicapped tricycle has been introduced, contains a single unit for providing motion and giving direction to the tricycle. Push and Pull motion of the steering results in forward and backward motion of the chair, while rotational motion of the same gives direction to the chair. In this paper, structural analysis is performed on the handicapped steering tricycle. Modelling is done on catiav5**

Keywords- **Lever-propelled wheelchair, Handicapped Steering Tricycle, Structural Analysis, and Design optimization.**

INTRODUCTION

About 1.85% of the total world's population that is 7.1billion, 130 million need wheelchairs or handicapped tricycles. Out of these 130 million, nearly 120 million population live in developing countries. Developed countries easily fulfill the demands of handicapped vehicles because of better technology and strong economy. On the other hand, in developing countries, due to limited resources in terms of economy and technology, the handicapped vehicles are required to be made cheaper, durable, comfortable, and efficient. There are cheaper materials available which are durable too, but the main area of concerns comfort ability and efficiency. Conventional handicapped tricycles are tedious because of their asymmetrical mechanisms and inefficient drive systems. Handicapped steering tricycle is a better substitute because of its better motion and steering unit and drive system.

B. Handicapped Steering Tricycle

Handicapped Steering Tricycle uses a crank-lever mechanism for its forward and backward motion. It is equipped with a small diameter steering wheel which can provide both: direction and motion to the tricycle. By pushing and pulling this steering, the rider can move the tricycle and by rotating the steering the rider can direct the tricycle. A braking lever is provided just beneath the steering wheel to apply the brakes.

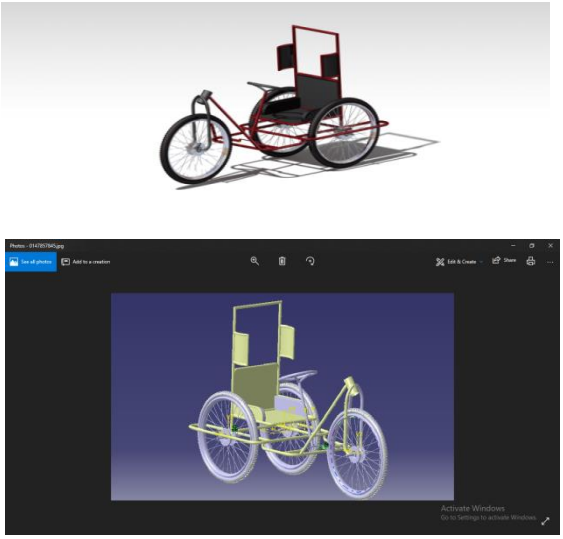

Fig -1: Handicapped steering tricycle

C. Materials Used and Dimensions

Due to their higher strength to weight ratios, better Machine ability, low cost and durability, metals are used for manufacturing these tricycles. They are easily available and they can be used specifically for a desired mechanical or physical property.

The metal used to assign to all the parts except chassis is: Stainless Steel 304. Material properties are given in Table-1.

Chassis is made by assigning the material: Structural Steel. It is a very common material, used for constructing frames of automobiles. Foam is used for seat. Material properties of SS-304 are given in Table-2.

TABLE 1 MATERIAL PROPERTIES OF STAINLESS STEEL (SS-304)

Sr.	Material Properties	Value
1.	Density	8000kg/m3
2.	Young's Modulus	193Gpa
3.	Poisson's ratio	0.27
4.	Yield Strength	500Mpa
5.	Coefficient of Thermal expansion	17×10-6/ oC

TABLE 2 MATERIAL PROPERTIES OF STRUCTURAL STEEL

Sr.	Material Properties	Value
1.	Density	8000kg/m3

2.	Young's Modulus	193Gpa
3.	Poisson's ratio	0.27
4.	Yield Strength	500Mpa
5.	Coefficient of Thermal expansion	17×10-6/ oC

Dimensions of Handicapped Steering cycle are given in Table-3.

TABLE 3 DIMENSIONS OF HANDICAPPED STEERING CYCLE

S.No	DETAILS	Dim (mm)
1.	Distance between center of front wheel and rear wheel	72cm
2.	Length of steering rod	55cm
3.	Height of steering from footpad	67cm
4.	Diameter of steering wheel	32cm
5.	Distance between center of front wheel and steering rod	67cm
6.	Height of seat from footpad	37cm
7.	Height of footpad from ground	33cm

D. Catiav5 Model

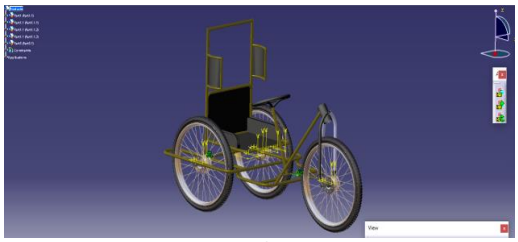

Fig -1: **Catiav5model of handicapped tricycle**

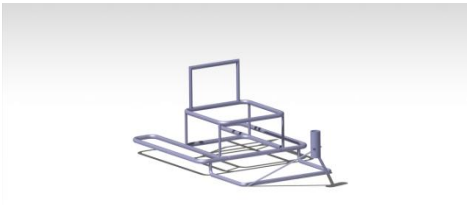

Fig -2: **Handicapped tricycle frame without seat.**

ANSYS RESULTS

ANSYS Workbench 15 is one of best Finite Element Analysis software in the simulation industry. Structural analysis is performed on the tricycle. To make the problem easier, analysis is done only on the chassis rather than the whole cycle. The chassis is fixed at point A, assuming the wheels to be fixed, and a load of 1000 N is applied in downward direction from the bottom of the seat. 1000 N is approximately 100 kgs i.e.; weight of rider and the cycle. ANSYS results are shown in Figures 4, and 5.

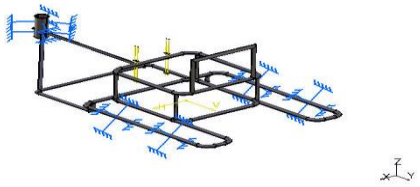

Fig -3: **Support and Traction**

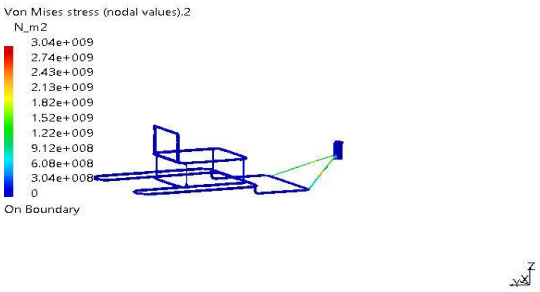

Fig -4: Equivalent stress in tricycle at load 1000 N. Equivalent stress at the load 1000 N, in tricycle is found to be nearly 50 MPa. Tensile Yield strength of Structural Steel is 210 MPa, so the chassis is safe.

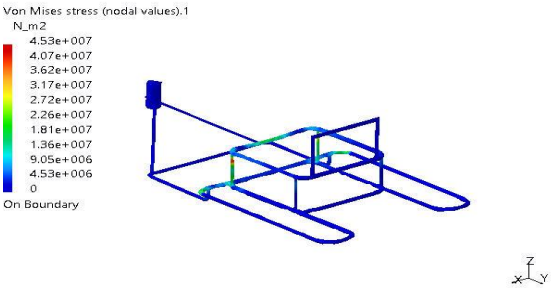

Fig -5: Total deformation in tricycle at load 1000 N. Total deformation in the chassis is found to be 1.15 mm. It is mostly concentrated near the seat.

CONCLUSION

Results from structural analysis of this handicapped steering cycle shows that the stress and deformation is within the limits. If it is compared with conventional handicapped cycles then it is found to be easy to maneuver, control, and move. It is driven with subtle and periodic motion of hands, and less power is required by the rider to drive it. It can be said that it is more comfortable and efficient than the conventional handicapped steering cycles.

REFERENCES

1. Khurmi, R. S., and J. K. Gupta. Machine design. S.Chand, 2005.
2. Bhandari, V. B. Design of machine elements. Tata McGraw-Hill Education, 2010.
3. Khurmi, R. S., and J. K. Gupta. Theory of machines. S. Chand, 200

 ISBN: 978-93-91420-02-4

Machining Characteristics and Micro-biological Growth of Stir Casted A356-SiC MMCs and Pure Metals

Suneel Donthamsetty and Penugonda Suresh Babu
Department of Mechanical Engineering, Narasaraopeta Engineering College (Autonomous), Narasaraopet, India

Abstract-- Because of the good properties like light weight, durability, high strength, corrosion resistance etc. the need of Metal Matrix Composites (MMCs) are increasing day by day. In the present work A356 is taken as main base material due to due to proximity with reference to density. Meanwhile silicon carbide (SiC) and A356 are close in terms of density, SiC is chosen as reinforcement material. Machining by changing machining parameters with cutting fluids is done with and without cutting oil by using automatic feed lathe machine by varying the speed and depth of cuts to find out the cutting forces, cutting tool temperatures and surface roughness. It is found that these values are gradually increased in many cases. Microbiological check also done and found that the colony count is gradually increased from fresh oil usage to used cutting oil after machining. These tests also done on MMCs, pure brass and pure aluminium and compared the results with MMCs.

***Keywords*-- A356; SiC; Machining; Composites; Bacterial Count**

1. INTRODUCTION

A metal matrix composite (MMC) is a composite in which two or more reinforced materials are added to the metal matrix in order to improve the properties of the composite. MMCs are made by scattering a reinforced material into a base material or matrix which is a monolithic material and is completely continuous [1].

The composites strength, stiffness and density is depends on its constituent materials properties, the reinforced material's size, shape, quantity & distribution and the bond between base and reinforced material. [2]. The composite materials are classified into Metal Matrix Composites of metals based, Ceramic Matrix Composites of ceramic materials based and Polymer Matrix Composites of plastic materials based [3].

Al-MMCs have much importance for aerospace, automobile, agriculture farm machinery industries etc., due to their good properties such as high strength, low density, good wear resistance compared to any other metal [4]. The cutting fluids reduces the cutting temperature by minimizing the friction between work piece and cutting tool, [5].

In the current work the silicon carbide is used as reinforcing material and Al 356 as base material synthesized by using stir casting machine.

2. MATERIALS

2.1 A356 Alloy

A356 alloy is used as a matrix for obtaining composites, which have an enhanced wear resistance, favourable mechanical properties at room temperature and enhanced mechanical properties at elevated temperatures. This is used in the field of application in the automotive and avionics industries [6] and selected as matrix material owing to good and readily castable [7, 8]. The chemical composition of Al 356 alloy is given in Table 1 [6].

Table 1. Chemical composition of Al 356 Alloy

Element	Si	Cu	Mg	Mn	Fe	Zn	Ni	Ti	Al
Wt. (%)	7.20	0.02	0.29	0.01	0.18	0.01	0.02	0.11	Balance

2.2 Fortifying material (Silicon carbide)

Recently lot of research is being done in to incorporate the silicon carbide on aluminum and its alloys to improve their mechanical and tribological properties. Silicon carbide particulates have proven to increase mechanical strength of aluminum and its alloys with increasing content and reduced particle size [9].

2.3 Cutting fluid

The advantages of cutting fluids includes cooling, lubrication, flushing away the chips, reduce the wear, extended tool life etc. The water based cutting oils are fully contaminated with the microorganisms, which deteriorate the cutting fluids properties, causes corrosion of work pieces, choking of fluid flow lines etc. And also chances of getting skin deceases and health issues to the workers who are exposed to these contaminated oil [10]. Emulsions can be prepared at water-to-oil ratios ranging from 5:1 to 100:1 [11]. In this work, taken this ratio as 20:1 and used for machining.

After machining, the used oils were taken and stored in sterilized bottles and tested to study the microbial contamination.

3. EQUIPMENT

3.1 Surface Roughness Tester

The Surf test SJ-210 Portable Surface Roughness Tester shown in Figure 1, is used for testing the surface roughness of the work pieces in microns (µm) after machining on the lathe machine.

 ISBN: 978-93-91420-02-4

Fig 1. Surface Roughness Tester with work piece

3.2 Automatic feed lathe machine with Coolant Pump Facility

The machining process is done by using Banka 35 Automatic feed lathe machine, shown in Figure 2, along with a coolant pump of 40 LPM capacity with 2900 rpm used to circulate the coolant oil.

Fig 2. Automatic feed lathe machine with coolant

3.3 Tool dynamometer

Electronic machine tool dynamometer of IEICOS (India) make, shown in Fig 3, used to find out the cutting forces while machining the MMC bar samples on the lathe machine.

Figure 3. Tool dynamometer set up

3.4 Microbial Growth

Cutting fluid samples are collected in the sterilized bottles shown in Fig 4 after machining Al- silicon carbide MMC bars, Pure Al and Pure Brass each with 5 hours machining per day to find the microbial growth.

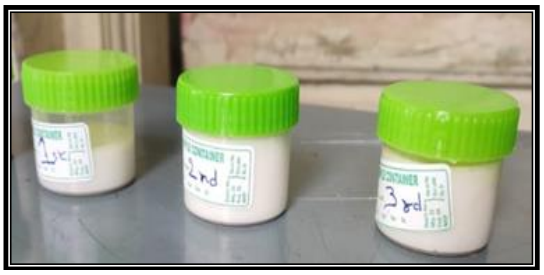

Fig 4. Sterilized bottles to collect oil for microbial growth

3.5 Petri Plates

A Petri dish or petri plate (fig.5) is a transparent lidded dish used to find bacteria, fungi or small mosses. It is the most common type of culture plate [12, 13]. Standard plate count which is conventional method for monitoring microbial levels in Cutting fluids is used. In the present work, Petri plates duly sterilized were taken and filled with nutrient Agar which is liquid and the temperature is above 45°C. Upon on cooling of this to the room temperature, it will be dried and hardened like a gel.

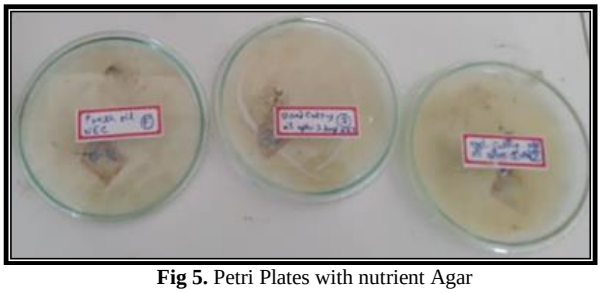

Fig 5. Petri Plates with nutrient Agar

3.6 Incubation

An incubator shown in Fig 6 is a device used to grow and maintain microbiological cultures or cell cultures. The incubator maintains optimal temperature, humidity and other conditions such as the CO_2 and oxygen content of the atmosphere inside. As both agar media and fluids are easily attacked by the bacteria present in the air, in order to prevent the contamination, the Laminar Air Flow chamber is used to transfer the fluid samples to the Petri plates in the presence of blue flame.

Fig 6. Incubator

The samples were then kept in the Incubator (incubation kept at 37°C for 24 hours, the bacteria formed is known as colonies shown in Fig7. These colonies (figure naked eye and counted).

 ISBN: 978-93-91420-02-4

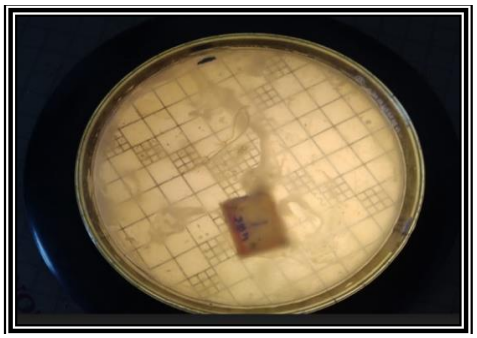

Fig 7. Bacteria developed in the petri Plates

4. EXPERIMENTATION

The MMCs are formed with the A356 as base, SiC of 50 microns size as reinforcing material and stir casting route for melting purpose. Chosen the Bottom Pouring Type Stir Casting Machine (Make: M/s. Swam Equip, Chennai, India) to melt the both the raw materials. Initially, dropped the pieces of A356 material into the furnace. After melting the same, poured the preheated silicon carbide powder of 5% by weight into the furnace through the feeder and use the stirrer for even mixing of both the A356 and silicon carbide powder. After that poured the liquid material into the die and allowed for solidification. Those solidified bars are taken for all tests.

5. RESULTS AND DISCUSSIONS

The results of various testing's are tabulated in the following tables

5.1 Forces in X, Y & Z Directions with & without coolant, Temperature and Surface roughness studies

5.1.1. Al 356 / Silicon carbide *MMC with variable D.O.C and at Fixed speed*

The Table 2 gives the tested values of forces in X, Y & Z directions, cutting tool temperature and roughness values of Al 356 / Silicon carbide MMC with variable D.O.C and at fixed speed and found that all the parameters of cutting Forces, cutting tool temperatures and surface roughness values are gradually increased.

Table 2 Al 356-Silicon carbide MMC with variable D.O.C and at Fixed speed

Variable D.O.C (mm)	Fixed speed in RPM	F_x (N)		F_y (N)		F_z (N)		Temperature °C		Surface Roughness in Micro Meters	
		Without Coolant	With Coolant	Without Coolant	With Coolant	Without Coolant	With Coolant	Without Coolant	With Coolant	Without Coolant Avg. value	With Coolant Avg. value
1.5	685	6	14	7	17	9	20	41	33	4.32	5.31
2	685	8	19	9	20	11	23	48	39	6.34	6.19
2.5	685	9	23	8	22	12	25	60	45	6.82	7.06

5.1.2. Al 356 / Silicon carbide *MMC with variable speed and at Fixed D.O.C*

Table 3 Al356-Silicon carbide MMC with variable speed and at Fixed D.O.C

Variable Speed (RPM)	Fixed D.O.C (mm)	F_x (N)		F_y (N)		F_z (N)		Temperature °C		Surface Roughness in Micro Meters	
		Without Coolant	With Coolant	Without Coolant	With Coolant	Without Coolant	With Coolant	Without Coolant	With Coolant	Without Coolant Avg. value	With Coolant Avg. value
1025	1.5	11	17	13	22	18	32	42	34	5.23	8.75
685	1.5	14	19	17	29	21	33	40	37	4.25	8.23
303	1.5	17	25	22	26	22	35	44	41	3.62	4.97

The Table 3 gives the tested values of forces in X, Y & Z directions, cutting tool temperature and roughness values of Al 356 / Silicon carbide MMC with variable speed and at fixed D.O.C and found that parameters of cutting Forces of Fx and cutting tool temperatures are gradually increased, Fy & Fz are varied and surface roughness values are gradually decreased.

5.1.3. Pure Al with variable D.O.C and at fixed speed

Table 4 Pure Al with variable D.O.C and at fixed speed

Variable D.O.C (mm)	Fixed speed in RPM	F_x (N)		F_y (N)		F_z (N)		Temperature °C		Surface Roughness in Micro Meters	
		Without Coolant	With Coolant	Without Coolant	With Coolant	Without Coolant	With Coolant	Without Coolant	With Coolant	Without Coolant Avg. value	With Coolant Avg. value
1.8	303	4	5	5	6	25	17	34	33	4.71	23.29
2	303	5	11	9	14	29	20	41	38	4.54	22.45
2.8	303	7	14	11	16	31	22	49	44	3.94	25.53

The Table 4 gives the tested values of forces in X, Y & Z directions, cutting tool temperature and roughness values of Pure Al with variable D.O.C and at fixed speed and found that the parameters of cutting Forces of Fx & Fy, cutting tool temperatures and surface roughness values with coolant are gradually increased. But, Fz and surface roughness values without coolant are varied.

 ISBN: 978-93-91420-02-4

4.1.4. Pure Al with variable speed and at Fixed D.O.C

Table 5. Pure Al with variable speed and at Fixed D.O.C

Variable Speed (RPM)	Fixed D.O.C (mm)	F_x (N)		F_y (N)		F_z (N)		Temperature °C		Surface Roughness in Micro Meters	
		Without Coolant	With Coolant	Without Coolant	With Coolant	Without Coolant	With Coolant	Without Coolant	With Coolant	Without Coolant Avg. value	With Coolant Avg. value
1025	2	3	3	5	5	4	4	36	36	7.43	40.46
685	2	5	5	7	5	18	11	40	42	2.65	24.71
303	2	7	8	10	42	25	21	43	45	3.57	15.31

The Table 5 gives the tested values of forces in X, Y & Z directions, cutting tool temperature and roughness values of Pure Al with variable speed and at fixed D.O.C and found that the parameters of cutting Forces of Fx & Fy, cutting tool temperatures and surface roughness values with coolant are gradually increased. But, Fz and surface roughness values without coolant are varied.

5.1.5. Pure Brass with variable D.O.C and at fixed speed

The Table 6 gives the tested values of forces in X, Y & Z directions, cutting tool temperature and roughness values of Pure Brass with variable D.O.C and at fixed speed and found that all the parameters of cutting Forces, cutting tool temperatures and surface roughness values are gradually increased.

Table 6 Pure Brass with variable D.O.C and at fixed speed

Variable D.O.C (mm)	Fixed speed in RPM	F_x (N)		F_y (N)		F_z (N)		Temperature °C		Surface Roughness in Micro Meters	
		Without Coolant	With Coolant	Without Coolant	With Coolant	Without Coolant	With Coolant	Without Coolant	With Coolant	Without Coolant Avg. value	With Coolant Avg. value
1.5	303	1	7	4	5	5	4	35	30	5.59	10.54
2	303	3	11	3	9	8	7	37	32	7.52	12.98
2.5	303	4	16	4	11	12	11	49	39	10.69	15.24

5.1.6. Pure Brass with variable speed and at Fixed D.O.C

The Table 7 gives the tested values of forces in X, Y & Z directions, cutting tool temperature and roughness values of Pure Brass with variable speed and at fixed D.O.C and found that the parameters of cutting Forces of Fx & Fy, cutting tool temperatures are gradually increased. But, Fz and surface roughness values are varied.

Table 7 Pure Brass with variable speed and at fixed D.O.C

Variable Speed (RPM)	Fixed D.O.C (m)	F_x (N)		F_y (N)		F_z (N)		Temperature °C		Surface Roughness in Micro Meters	
		Without Coolant	With Coolant	Without Coolant	With Coolant	Without Coolant	With Coolant	Without Coolant	With Coolant	Without Coolant Avg. value	With Coolant Avg. value
1025	2	4	4	1	7	10	5	32	31	2.74	7.81
685	2	4	7	3	12	14	9	34	32	6.05	7.34
303	2	5	10	5	16	10	13	33	31	4.41	6.10

5.1.7 Bacterial Count:

After using for 5 hrs. of machining and waited for 24 hrs., each cutting Fluid was tested for Bacterial Count and results are tabulated in Table 8 and Fig 8 It is found that the colony count is gradually increased from fresh oil to Cutting Oil after machining Al 356 + Silicon carbide MMC bar, Pure Al bar and Pure Brass bars.

Table 8 Bacterial Count

Sl. No.	Cutting Fluid Details	Colony Count
1	Fresh Cutting Oil	10
2	Cutting Oil after machining Al 356 + SiC MMC	19
3	Cutting Oil after machining Pure Al	28
4	Cutting Oil after machining Pure Brass	43

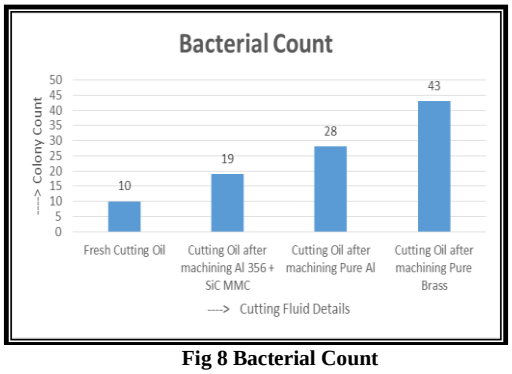

Fig 8 Bacterial Count

CONCLUSIONS

The following are the conclusions after various testings were done on Al 356- Silicon carbide Metal Matrix Composite, Pure Al & pure Brass.

- All the parameters of cutting Forces of Fx, Fy & Fz, Cutting tool temperatures and Surface roughness values are gradually increased in majority of cases
- The colony count is gradually increased from fresh oil to used Cutting Oil after machining. Found colony count of 10 in fresh oil, 19 in Cutting Oil after machining Al 356 + SiC MMC, 28 in Cutting Oil after machining Pure Al and 43 in Cutting Oil after machining Pure Brass.

ACKNOWLEDGMENT

Present work is an outcome of an undergraduate project and authors are acknowledging efforts of students for their commendable work.

REFERENCES

[1] Rohit Sharma, Saurabh Jha P, Khushboo Kakkar, Kushal Kamboj and Pardeep Sharma 2017 A Review of the Aluminium Metal Matrix Composite and its Properties *International Research Journal of Engineering and Technology (IRJET) Volume: **04** Issue: 02*

[2] https://www.asminternational.org/documents/10192/1942084/composite.pdf/0eb5cca8-4613-482c-811c-993c58b42e92https://www.substech.com/dokuwiki/doku.php?id=classification_of_composites

[3] Suneel Donthamsetty, Penugonda Suresh Babu "Studies on Machining Characteristics and Microbiological Growth over Stir Casted A356-Graphite Metal Matrix Composites (A Comparison between Pure Metals and Composite)", in IOP Conference Series: Materials Science and Engineering, ISSN: 1757-899X, Vol. 1112 (2021) 012004, PP 1-12

[4] Pei Yan, Yiming Rong and Gang Wang 2015 The effect of cutting fluids applied in metal cutting process *Proc IMechE Part B:J Engineering Manufacture 1–19, DOI: 10.1177/0954405415590993*

[5] Z. Mišković, I. Bobić, S. Tripković, A. Rac and A. Vencl 2006 The Structure and Mechanical Properties of an Aluminium A356 Alloy Base Composite With Al_2O_3 Particle Additions *Tribology in industry, Volume **28**, No. 3&4*

[6] Suneel Donthamsetty 2013 Investigations on mechanical properties of A356 nano composites reinforced with high energy ball milled SiC nanoparticles with ultrasonic assisted cavitation (with a comparison of micro composite) *International Journal of Nanoparticles (IJNP), Inderscience Publishers, Vol.**6**, No.1, pp.38-49*

[7] Suneel Donthamsetty and Penugonda Suresh Babu 2017 Experiments on the wear characteristics of A356 MMNCs fabricated using ultrasonic cavitation *International Journal of Automotive and Mechanical Engineering, Volume **14**, Issue 4 pp. 4589-4602*

[8] Ali Dad Chandio, Muhammad Basit Ansari, Shahid Hussain, Muhammad Ali Siddiqui, Silicon Carbide Effect as Reinforcement on Aluminium Metal Matrix Composite, J.Chem.Soc.Pak., Vol. 41, No. 04, 2019

[9] Prasad M.M.S and Srikant R.R 2014 Evaluation of Microbial Contamination of Cutting Fluids with Nano Graphite Inclusions *Research Journal of Engineering Sciences, Vol. **3(2)**, 12-16*

[10] https://www.princessauto.com/en/detail/cutting-oil-coolant/A-p8034012e

[11] Frederick J. Passman 1988 Microbial problems in metalworking fluid *Tribology and Lubrication Technology*

[12] Marc Veillette, Peter S. Thorne, Terry Gordon and Caroline Duchaine 2004 Six Month Tracking of Microbial Growth in a Metalworking Fluid After System Cleaning and Recharging *Ann. occup. Hyg., Vol. **48**, No. 6, pp. 541–546*

 ISBN: 978-93-91420-02-4

Design and Analysis of Connecting Rod

K. Krishna kishore,T. Manoah Daniel, P. Sai kumar and P. Chandra kanth
Gudlvalleru Engineering college,Gudlavalleru, Andhra pradesh, India

***Abstract*- The connecting rod is the intermediate part between piston and Crank shaft. The function of the connecting rod is to convert the reciprocating motion into rotational motion. In this Mini project we describe the Design and analysis of connecting rod. The drafting is done from a reference diagram (taken from TVS website) and dimensions are scaled in the ratio 1:4. The parametric modelling of connecting rod is done in Fusion 360 and model analysis is carried in Ansys 2020 R2 software.**

The connecting rod is subjected to forces generated by Mass itself. This phenomenon occurs as a result of repeated cycles to which the connecting rod is subjected. Combination of parameters like Equivalent (Von-mises) stress, Equivalent (Von-mises) strain, Total deformation, directional deformation, fatigue stress. Connecting rod processing surface for the two materials structural steel and cast iron are used in analysis. The obtained results are helpful in determining various stress, strain and Equivalent (Von-mises) stress, Equivalent (Von-mises) strain located at different points. In this Mini project the analyzed model in Ansys is compared with the result of existing model from reference model.

Keywords— connecting rod, Fusion 360, Ansys 2020 r2 workbench, Structural steel, Cast iron

I. INTRODUCTION

A connecting rod, also called a con rod, is the part of a piston engine which connects the piston to the crankshaft. Together with the crank, the connecting rod converts the reciprocating motion of the piston into the rotation of the crankshaft. The connecting rod is required to transmit the compressive and tensile forces from the piston, and rotate at both ends. The predecessor to the connecting rod is a mechanic linkage used by water mills to convert rotating motion of the water wheel into reciprocating motion. A connecting rod can rotate at both ends, so that the angle between the connecting rod and the piston can change as the rod moves up and down and rotates around the crankshaft. As in fig the Connecting rods are designed to withstand dynamic stresses from combustion and piston movement. The small end of the connecting rod connects to the piston with a piston pin. The piston pin, or wrist pin, provides a pivot point between the piston and connecting rod. Spring clips, or piston pin locks, are used to hold the piston pin in place. The big end of the connecting rod connects to the crankpin journal to provide a pivot point on the crankshaft. Connecting rods are produces as one piece or two-piece components. A rod cap is the removable section of a two-piece connecting rod that provides a bearing surface for the crankpin journal. The rod cap is attached to the connecting rod with two cap screws for installation and removal from the crankshaft. The most common usage of connecting rods is in internal combustion engines or on steam engines.

II. MATERIALS USED FOR MANUFACTURING

Connecting rods are commonly made from cast aluminum alloy, steel Titanium, cast iron. In mass-produced automotive engines, the connecting rods are most usually made of steel. In high performance applications, "billet" connecting rods can be used, which are machined out of a solid billet of metal.

For high performance and high-speed engine Titanium. Racing engines may utilize titanium alloys such as Ti-6Al-4V for connecting rods in order to achieve a high ratio of strength to mass of the part. A connecting rod with a tension load is made of forged steel, cast steel, or fabricated steel. Rods with a compression loading are cast nodular steel or aluminum alloy.

Materials for connecting rods have included powder metallurgy steels, which are formed into an initial shape then forged to near final dimension, as well as medium carbon steels, which develop superior strength either through separate heat treating processes or by controlled cooling following the forging step. Composite materials are also used for manufacturing. Generally connecting rods are manufactured using carbon steel and in recent days aluminum alloys are finding its application in connecting rod. In this work connecting rod is replaced by aluminum based composite material reinforced with silicon carbide and fly ash Connecting rod. Aluminum alloy (which is already existing) made of 42crmo4, aluminum based composite material reinforced with Boron carbide (Al6061+B4C).

III. MODELLING AND ANALYSIS

Modelling

1) ***Software used:***

Autodesk Fusion 360 is a cloud-based CAD/CAM tool for collaborative product development. It combines organic shapes modelling, mechanical design and manufacturing in one comprehensive package. It's the first 3D CAD, CAM, and CAE tool of its kind, connecting your entire product development process into one cloud-based platform. It is functionally similar to other 3D software's like Solid works, Siemens NX,

Catia, Solid edge. The parametric modelling, program tool path for CNC machine is also performed in this software. These features are not available in any other software's. Other than modelling you can also perform CNC milling, CNC lathe, computer Aided manufacturing.

The connecting rod is modelled according to 1:4 scale from the reference diagram taken in the Fusion 360 software.

Name	Original dimensions	Scaled dimensions
Length (from small circle to big circle)	585mm	140mm
Big circle internal diameter	230 mm	50mm
Small circle internal diameter	65 mm	18mm
Thickness	150mm	20mm

Table 3.1: Shows the dimensions of the connecting rod.

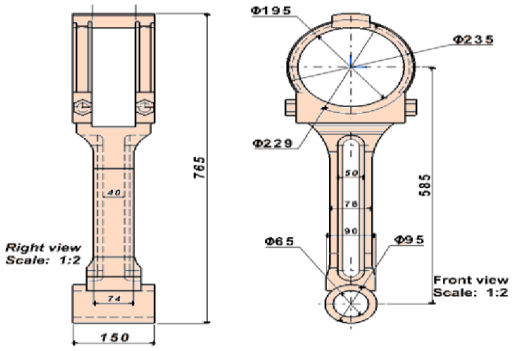

Fig 1 Shows the Refernce model

Fig 2 Connecting rod modelled in fusion 360.

Analysis

1. *software used:*

Ansys develops and markets Multi physics engineering simulation software for product design, testing and operation and offers its products and services to customers worldwide. Ansys made numerous acquisitions of other engineering design companies, acquiring additional technology for fluid dynamics, electronics design, and other physics analysis. Ansys develops and markets engineering simulation software for use across the product life cycle. Ansys Mechanical finite element analysis software is used to simulate computer models of structures, electronics, or machine components for analyzing strength, toughness, elasticity, temperature distribution, electromagnetism, fluid flow, and other attributes.

IV. MATERIALS AND MATERIAL PROPERTIES USED FOR ANALYSIS

Structural steel		Cast iron	
Young's modulus	2E+11 Pa	Young's modulus	8.944E+11Pa
Density	7850kgm^-3	Density	6999 kg m^-3
Poisson's ratio	0.3	Poisson's ratio	0.26
Yield's strength	2.5E+8 Pa	Yield's strength	7.981E+7 Pa
Shear modulus	7.6923E+10 Pa	Shear modulus	3.5492E+10 Pa

Table 2.2: Shows the materials and material properties.

1.1 JOINTS IN ASSEMBLY

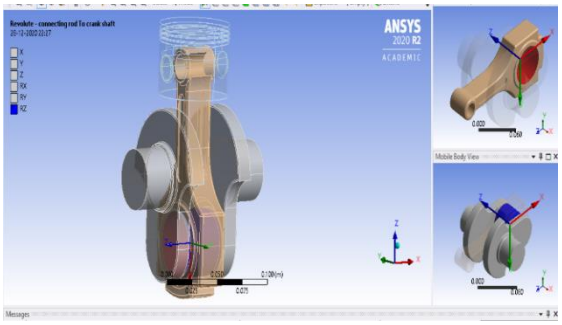

Fig 3 Shows the joint between connecting rod and crank shaft

RESULTS

Material: Structural steel

1. Total deformation:

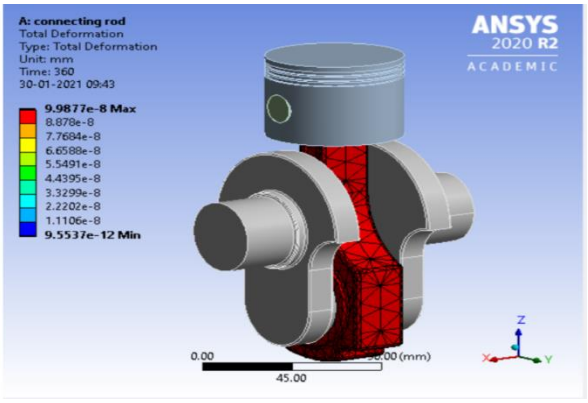

Fig 4 Total deformation Structural steel

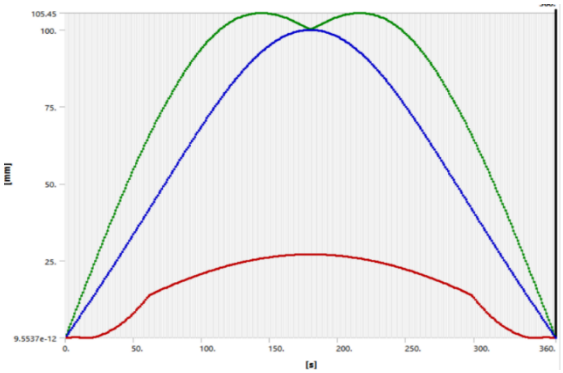

Fig 5 Graph generated for Total deformation

2. Equivalent (von-mises) stress:

 ISBN: 978-93-91420-02-4

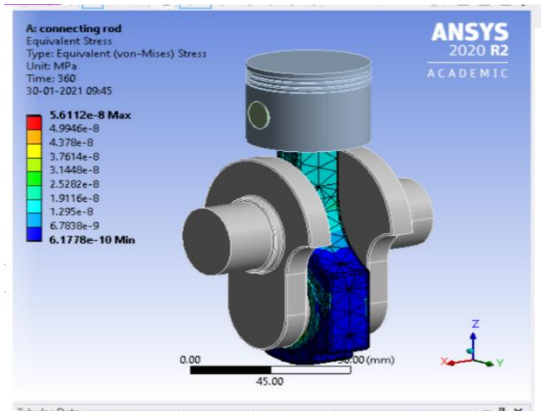

Fig 5 Equivalent (von-mises) stress of Structural steel

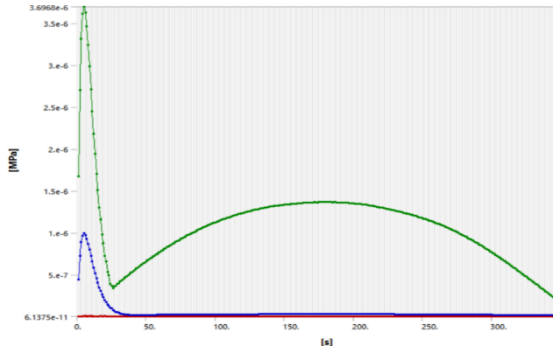

Fig 6 Graph generated for Equivalent (von-mises) stress

3. Equivalent elastic strain:

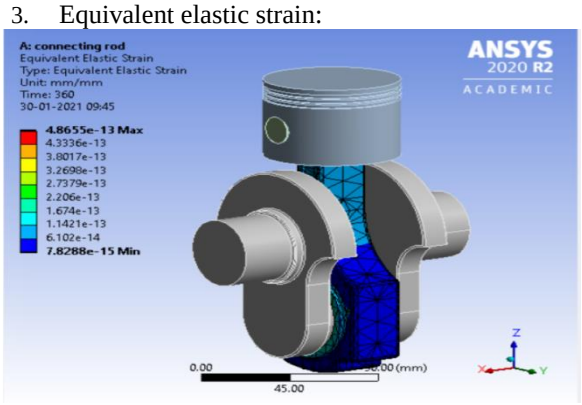

Fig 7 Equivalent elastic strain of structural steel

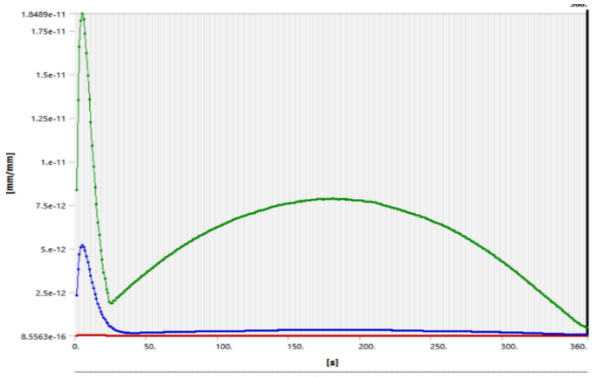

Fig 8 Graph generated for equivalent elastic strain

Material: Cast iron

1. Total deformation:

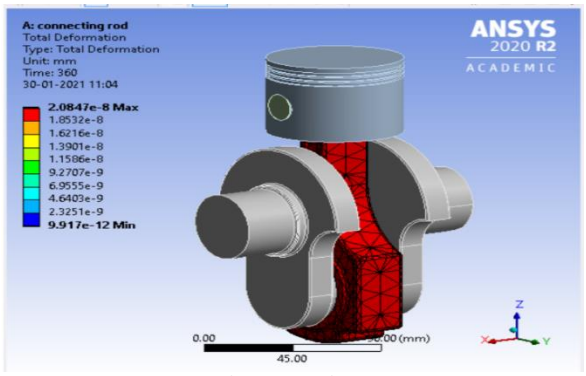

Fig 9 Total deformation of cast iron

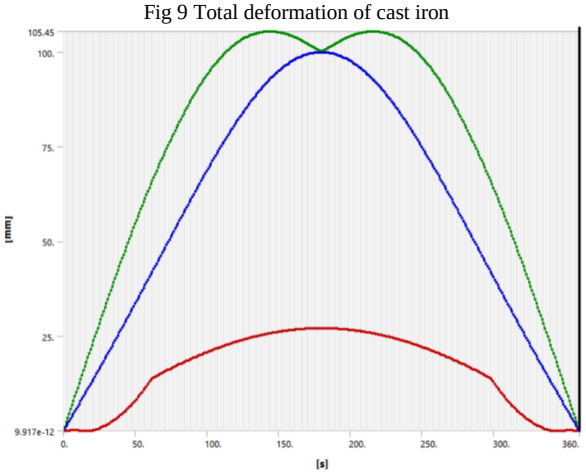

Fig 10 Graph generated for Total deformation

2. Equivalent (von-mises) stress:

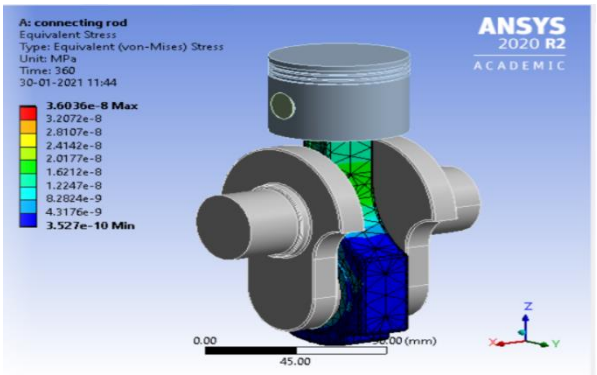

Fig 10 Equivalent (von-mises) stress of cast iron

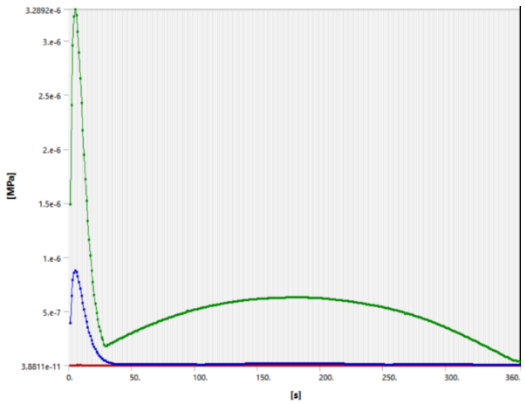

Fig 11 Graph generated for Equivalent(von-mises) stress

3. Equivalent elastic strain:

 ISBN: 978-93-91420-02-4

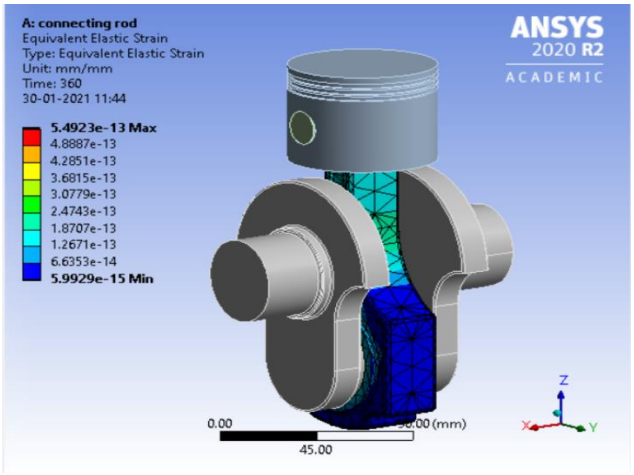

Fig 12 Equivalent elastic stain of cast iron

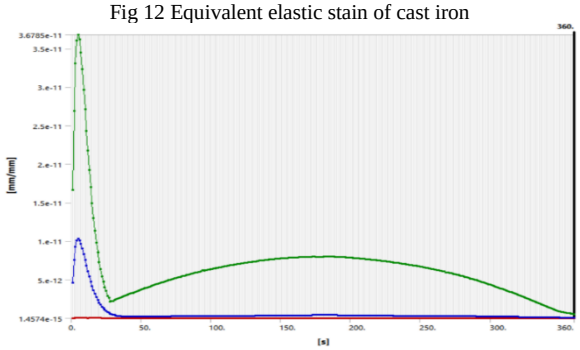

Fig 13graph generated for Equivalent elastic strain

CONCLUSION

The model of a connecting rod was generated, discretizes, analyzed and the results are tabulated and presented above. The alternating forces to which the connecting rod is subjected, determining the aging of the material by the appearance. This overview research report studies the possibilities of connecting rod made of structural steel and cast iron we designed obtained its stress distribution on application of the force from the results of the study, following conclusions can be made.

- It was observed that connecting rod designed and analyzed can be used for normal engines, for high performance and low performance engines also.
- As per the results received from the Transient structural analysis we done. We got the results nearer to the reference model analysis taken.

REFERENCES

1. "Design and Analysis of Connecting Rod for Weight and Stress Reduction" 1.Dr. B S N Murthy, 2. K. Adarsh Kumar, 3. Mohammed Abdul Shafeeq, 4. S. Sai Sundara Praveen 1. Associate Professor, 2. Assistant Professor, 3,4- Student, 1,2,3,4 Dept. of Mechanical Engineering.
2. Fatigue analysis of the connecting rod in internal combustion engines" M Frătița, F Popescu, K Uzuneanu, V Mereuta, I Ion, Department of Thermal Systems and Environmental Protection, Mechanical Engineering Department.
3. "BUCKLING ANALYSIS OF CONNECTING ROD" Nagaraju K L, Chandan R, Department of Mechanical Engineering.
4. "Design And Analysis of Connecting Rod Using Forged steel" Leela Krishna Vegi , Venu Gopal Vegi Department of Mechanical Engineering.
5. "Design and Analysis of Connecting Rod" Sebastian Antony, Arjun A., Shinos T. K Mechanical Department, Anoop P. Mechanical Engineering Department.
6. "Comparison Of Manufacturing Methods and Analysis of Connecting Rod for Reducing Cost" Ankit B. Sidhpara, Vashim I. Kureshi, Prof. Pinank A. Patel Department of Mechanical Engineering.
7. "Finite Element Analysis of I.C Engine Connecting Rod", Mukesh Kumar, Veerendra Kumar Department of Mechanical Engineering.
8. "DESIGN & ANALYSIS OF CONNECTING ROD BY COMPOSITE MATERIALS" A.Prem kumar, Department of Mechanical Engineering.
9. "Modern Optimized Design Analysis of Connecting Rod of an Engine", Naman Gupta, Manas Purohit, Kartik Choubey, Department of Mechanical Engineering.
10. Compartive study on Different materials for Connecting rod. Ashish somani, Department of mechanical Engineering.

 ISBN: 978-93-91420-02-4

Pressure Vessel Optimum Design Using Particle Swarm Optimization

P Ravi Kumar[1], T Nancharaiah[2], D Sameer Kumar[3], S Radhika[4] and Sreedevi E[5]
[1,2,3] Department of Mechanical Engineering, ANU, Bapatla Engineering College, Bapatla, AP, India
[4] Department of Mechanical Engineering, ANU, R V R & J C College of Engineering, Guntur, AP, India
[5] Department of Computer Science and Engineering, Koneru Laxmaiah Education Foundation, Vaddeswaram, AP, India

***Abstract*— Particle Swarm Optimization is one of the leading optimization algorithms among the very complex design problems. Particularly in the area of mechanical engineering design, the problems are complex and involve lot of design variables that significantly alter the design process. Optimum design is desirable for the effective use of resources. Particle Swarm Optimization proved to be very efficient in dealing with NP – hard problems. Therefore this paper confers to the application of PSO to the standard bench marks problem of pressure vessel. The results obtained are compared with Ant Colony Optimization results to find the efficacy of the algorithm for the proposed problem**

***Index Terms*—Particle Swarm Optimization, Pressure vessel Design, PSO**

I. INTRODUCTION

Optimization is the act of obtaining the best result under given circumstances. Optimization problems are of high importance both for the industrial as well as for the scientific world. Examples of the practical optimization problems include Travelling Salesman Problems, Scheduling Problems, and Design Optimization….etc. [1]. Swarm intelligence techniques are developed based on the natural behavior of self-organizing agents. The cooperation between these agents are studied and formulated to apply in many fields. Since the application of these algorithms is stochastic in nature, these require more computational time. On the other hand mechanical Engineering problems have lot of parameters and require more and more operations in reaching the stability of the solution. So the application of Swarm Intelligence techniques to Mechanical Engineering Problems is a challenging task for the researchers. However with the advent of computer technology, the application of these methods is become simple and vigorous research has been undergone in all the diversified fields of mechanical Engineering [2].

Popular Techniques of Swarm Intelligence Techniques include Ant Colony Optimization and Particle Swarm Optimization. Ant Colony Optimization uses the behavior of ants for finding the optimum design whereas Particle Swarm Optimization (PSO) deals with the natural behavior of birds. Venter [3] has successfully reviewed the potentials of PSO in many fields. Kulkarni [4] and Ben [5] demonstrated the various applications of PSO in Mechanical and allied domains. The

applications of PSO optimization in many Engineering design fields are emerging and researchers are trying to put their efforts to find the best even from minimum resources.

Pressure vessel problems are of great importance in Mechanical design. These problems typically involve lot of parameters and cost is the main criterion in design. Wrong selection of parameters lead to huge cost and also product failure.

The present work deals with the standard bench mark optimum design of Pressure vessel with the help of MATLAB coding. Section 2 deals with the principles of PSO and Section 3 focus on Problem formulation while results and discussions are included in Section 4 followed by conclusions.

II. PARTICLE SWARM OPTIMIZATION (PSO)

During 1990s, several studies related to the behavior of animal groups were reported. These results showed that few animals particularly as a group, i.e. birds and fishes, are able to share information called stigmergy among their group, and such capability confers these animals a great survival advantage. Inspired by these works, Kennedy and Eberhart proposed in 1995 the PSO algorithm [1], a metaheuristic algorithm that is appropriate to optimize nonlinear continuous functions.

Particle swarm intelligence was basically developed through simulation of bird flocking in two-dimensional space. The observation leads to the assumption that every information is shared inside flocking. The position of each agent is represented by xy-axis position and the velocity expressed by Vx and Vy. Modification of agent position is realized by using the position and the velocity information. A Flock of agents optimizes a certain objective function. Each agent knows its best value so far (pbest) and its xy position. The information corresponds to the personal experiences of each agent. Moreover each agent knows the best value so far in the group (gbest) among the pbest. Then each agent try to modify its position using pbest and gbest. The general representation of PSO methodology is depicted in the following Fig. 1.

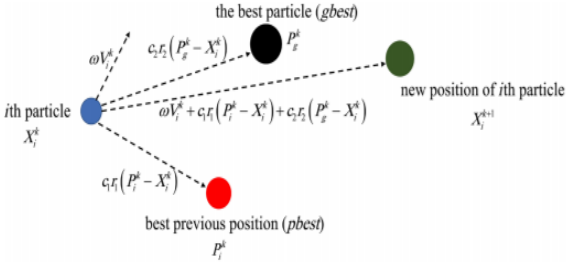

Fig. 1 Methodology of PSO [6]

 ISBN: 978-93-91420-02-4

A standard pseudo Code of PSO Algorithm [7] is as follows

{

For each Particle

Initialize Particle

End

Do

For each particle

Calculate Fitness value

If the fitness value is best (pbest) save it in history and compare with the next fitness values

End

Choose best as all particles best fitness value

For each particle

Calculate Particle Velocity using the Equation

Update the Particle Position using the Equation

End

Repeat the process till maximum iterations or minimum error criteria satisfied.

}

III. Problem Formulation

A. Mathematical Modeling

The main aim of the current work is to design an air storage tank with a working pressure of 3000 psi and a minimum volume of 750 ft^3.The pressure vessel is capped at both the ends by hemispherical heads. Using the rolled steel plate, the shell is to be made in two halves that are joined by two longitudinal welds to form a cylinder each head is forged and then welded to the shell. The design variables be denoted by the vector X = [x1 x2 x3 x4] T , where x1 is the Spherical head thickness , x2 is the shell thickness , x3 and x4 are radius and length of the shell respectively. This is the standard benchmark problem for the design of pressure vessel. The detailed diagram indicating all the components of pressure vessel are mentioned in Fig. 2

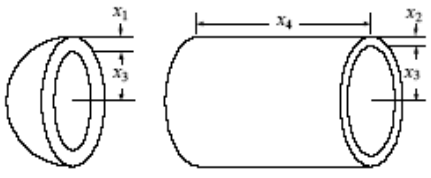

Fig. 2 Pressure Vessel

The main objective of this problem is to minimize the manufacturing cost of the pressure vessels. The Manufacturing cost is a combination of material cost, welding cost and forming cost. The mathematical model of the problem is

Minimize

$$f(x) = 0.6224x1x2x3x4 + 1.7781x2x32 + 3.1661x12x4 + 19.84x12x3 \quad (1)$$

Subjected to

$$G1(x) = 0.0193\ x3 - x1 \leq 0 \text{ (Stress Constraint)} \quad (2)$$

$$G2(x) = 0.00954\ x3 - x2 \leq 0 \text{ (Stress Constraint)} \quad (3)$$

$$G3(x) = 750*1728 - 3.1415\ x32\ x4 - 4/3 * 3.1415\ x33 \leq 0 \text{ (Volume Constraint)} \quad (4)$$

$$G4(x) = x4 - 240 \leq 0 \text{ (Width Constraint)} \quad (5)$$

The upper bounds and lower bounds of design variables are as follows

$0 \leq x1 \leq 99$

$0 \leq x2 \leq 99$

$10 \leq x3 \leq 200$

$10 \leq x4 \leq 200$

Where the design variables x3, x4 are continuous, while x1 and x2 are discrete values and integer multiples of 0.0625 inch respectively, in accordance with the available thickness of rolled steel plates

B. Material

A typical input data required to use a mathematical model for pressure vessel design is as follows

Pressure vessel Material is SAE J2340 – 830R, Where R = High Strength Recovery Annealed. The material has multiple behaviors at different rolling conditions. However, the typical properties of the material [8] is

1. Modulus of elasticity (E) = 200x109 N/mm2
2. Yield Strength = 960 MPa
3. Factor of safety = 1.78
4. Allowable Yield Strength = 540 MPa
5. Applied Pressure = 6.80272 N/mm2 (1000 PSi)

IV. Results and Discussions

MATLAB program has been written for the objective value i.e. minimization of cost of the pressure vessel corresponding to the global optimum solution of this problem. The Results obtained by employing PSO (Particle Swarm Optimization) algorithm is listed in Table 1. While the convergence is shown in the Fig. 3

TABLE I
RESULTS OF PSO FOR THE DESIGN OPTIMIZATION OF PRESSURE VESSEL

Symbol	Parameters	Results
X_1	Thickness of main cylinder	0.8125
X_2	Thickness of heads	0.4325
X_3	Radius of main cylinder	42.094

X_4	Length of the main cylinder	176.6376
	Constraints	Results
g_1	Constraints of hoop stress	-2.01E-03
g_2	Constraints of longitudinal stress	-3.58E-02
g_3	Constraints of volumes	-24.7593
g_4	Constraints of lengths	-63.3523
	f(x) Objective function Value	6.1398e+03

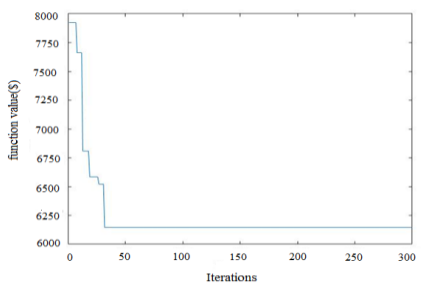

Fig. 3 Convergence of PSO algorithm

From Figure 3, it has been observed that the objective value has been found to be decreasing iteration by iteration and reaching the convergence. From the iteration approximately 40 onwards, there is no change in the output that means the value is converged. The objective function value is found to be 6139$. The following Table 2 provides the comparison of the proposed method with the other Meta heuristic techniques for the cost optimization of Pressure vessel problem.

An advantage of PSO is its ability to handle optimization problems with multiple local optima reasonably well and its simplicity of implementation – especially in comparison to related strategies like genetic algorithms (GA) [14]. A particle calculates its next position based on a combination of its last movement vector, the individual and global memories, and a random component. Therefore, with in the less time and with less updation of parameters the results are obtained. Some researchers reported that it is impracticable to say that the result obtained by an optimization method such as PSO is the global maximum or minimum, so some authors call the results as the most likely optimal global [15]. Thus, some strategies can be employed in order to verify the validity of the optimal results obtained. One of the strategies is to compare with the results obtained by other optimization algorithms, as used in the present work. From Table 3, It has been observed that PSO has proposed the best value by considering the other algorithms with in the given conditions considered.

V. CONCLUSIONS

The following conclusions have been drawn from the present investigation

- In the present work, parameters such as thickness of the shell, and dish end, length and radius of the pressure vessel are optimized by making use of
- PSO, a powerful non- traditional optimization method.
- It can be concluded that by applying Particle Swarm Optimization, the optimal design parameters for the pressure vessel are obtained and the objective of minimization of cost by reducing weight of Pressure vessel is achieved.
- It is found that the results obtained from PSO are better as its search is for global optimum as against the local optimum in traditional search methods.
- The results of the PSO have been compared with other Optimization Methods, and it is found that PSO yielded best results among the techniques compared with in the given assumptions and considered conditions.

VI. FUTURE SCOPE OF WORK

The same work can be extended further by using hybrid optimization techniques (combining ACO , GA , ABC and many other techniques with PSO) to achieve the further yielding , if possible . The same technique can be applied to Multi objective optimization problems also to solve the complex problems in less time with acceptable consistency.

TABLE 2
COMPARISON OF PSO OVER OTHER METHODS FOR THE STANDARD PRESSURE VESSEL PROBLEM [9]

Algorithm Name	Optimum Value				Objective Function Value
	X_1	X_2	X_3	X_4	
Branch-bound [10]	1.1250	0.6250	47.7000	117.7010	8129.1036
Lagrangian Multiplier [11]	1.1250	0.6250	58.2910	43.6900	7198.0428
GA [12]	0.9375	0.5000	48.3290	112.6790	6410.3811
GA [13]	0.8125	0.4345	40.3239	200.0000	6288.7445
PSO	0.8125	0.4325	42.0984	176.6376	6139.8002

 ISBN: 978-93-91420-02-4

REFERENCES

[1] S S Rao , “Engineering Optimization - Theory and Practice” , New Age International , 2000

[2] Handbook of Swarm Intelligence edited by Bijaya Ketan Panigrahi ,Yuhui Shi , Meng-Hiot Lim , Springer-Verlag Berlin Heidelberg 2011.

[3] Venter, Gerhard, and Jaroslaw Sobieszczanski-Sobieski. "Particle swarm optimization." AIAA journal 41.8 (2003): 1583-1589.

[4] Kulkarni, Mr Ninad K., et al. "Particle swarm optimization applications to mechanical engineering-a review." Materials Today: Proceedings 2.4-5 (2015): 2631-2639.

[5] N. Ben. Guedria, Improved Accelerated PSO Algorithm for Mechanical Engineering Optimization Problems, Applied Soft Compu

[6] Mashayekhi, Mohammadreza, Mojtaba Harati, and Homayoon E. Estekanchi. "Development of an alternative PSO-based algorithm for simulation of endurance time excitation functions." Engineering Reports 1.3 (2019): e12048.

[7] Hudaib, Amjad A., and A. K. A. L. Hwaitat. "Movement Particle Swarm Optimization Algorithm." Modern Applied Science 12.1 (2017): 148.

[8] Information from https://www.a-sp.org/wp-content/uploads/2020/08/High_Strength_Steel_Stamping_Design_Manual.pdf

[9] S. Mirjalili, Moth-Flame Optimization Algorithm: A Novel Nature-inspired Heuristic Paradigm, Knowledge-Based Systems (2015), doi: http://dx.doi.org/10.1016/j.knosys.2015.07.006

[10] E. Sandgren, "Nonlinear integer and discrete programming in mechanical design," 1988, pp. 95- 105

[11] B. Kannan and S. N. Kramer, "An augmented Lagrange multiplier based method for mixed integer discrete continuous optimization and its applications to mechanical design," Journal of mechanical design, vol. 116, p. 405, 1994.

[12] K. Deb and A. S. Gene, "A robust optimal design technique for mechanical component design," presented at the D. Dasgupta, Z. Michalewicz (Eds.), Evolutionary Algorithms in Engineering Applications, Berlin, 1997.

[13] C. A. Coello Coello, "Use of a self-adaptive penalty approach for engineering optimization problems," Computers in Industry, vol. 41, pp. 113-127, 2000.

[14] Meissner, M., Schmuker, M. & Schneider, G. Optimized Particle Swarm Optimization (OPSO) and its application to artificial neural network training. BMC Bioinformatics 7, 125 (2006),https://doi.org/10.1186/1471-2105-7-125

[15] Bruno Seixas Gomes de Almeida and Victor Coppo Leite (December 3rd 2019). Particle Swarm Optimization: A Powerful Technique for Solving Engineering Problems, Swarm Intelligence - Recent Advances, New Perspectives and Applications, Javier Del Ser, Esther Villar and Eneko Osaba, Intech Open, DOI: 10.5772/intechopen.89633.

 ISBN: 978-93-91420-02-4

Design and Analysis of Wheel Rim on Radial Loads

Kiran Chand Kopila[1], Kandru John Babu[2]
Narasaraopeta engineering College (Autonomous), Andhra Pradesh, Guntur, India

***Abstract*—Wheels are one of the important components in the vehicle. The two-wheeler, there are two types of wheels used. One is alloy wheel and another one is spokes wheel. Mostly alloy materials are used for fabricate the wheel rim. The main reason used for the alloy material is increase the efficiency of the two-wheeler by reducing the weight.**

In this study a tire of car wheel rim belonging to the disc wheel category is considered. Design in an important industrial activity which influences the quality of the product. The wheel rim is designed by using modelling software CATIAv5R19. ANSYS software used for simulating the different forces, pressure acting on the component and also for calculating and viewing the results. In the present work a detailed static analysis - displacement, maximum and minimum von-misses stresses and fatigue analysis of wheel rim under radial loads has been done. The application of finite element method for analyzing stress distribution and fatigue life of wheel rim was summarized.

Keywords—Wheel rim, static analysis, fatigue analysis of wheel rim

I. INTRODUCTION

Archaeologists and historians of today see the introduction of the wheel as the real genesis of any old civilization. The wheel is perhaps the most important discovery of old times. This discovery capitulated commerce to heights unknown before. The wheel has developed from nothing more than an oversize bearing to a fully integral part of any modern transportation vehicle. The modern vehicle is also seen today a fashion item to complement people's individual tastes. Motor vehicles are produced according to very strict rules to ensure the safety of the passengers. Every component is therefore designed according to the criticality of the component. Wheels are classified as a safety critical component and international cods and criteria are used to design a wheel.

II. FUNCTIONS OF A WHEEL RIM.

In its basic form a wheel rim is a transfer element between the tyre and the vehicle. The following are the main functions of a wheel rim:

- ✓ Transfers torque (braking and acceleration).
- ✓ Support mass
- ✓ Adds mass (damped mass for driving comfort).
- ✓ Dissipates heat (from braking).
- ✓ Adds value.
- ✓ Absorbs impact (road hazards).
- ✓ Conserves energy

III. CLASSIFICATION OF CAR WHEELS

Car wheels are divided in to two main categories, steel wheels and alloy wheels. Alloy wheels are often fitted standard during the manufacturing of modern vehicles.

Steel Wheels:

All steel wheels consist of two pressed Components, the rim and the wheel disc, which are welded together. The rim is the part on which tyre is mounted. Its dimensions shape and condition must suitable to satisfactorily accommodate the particular tyre required for the vehicle. The wheel disc is the supporting member between the vehicles hub and the rim. Its dimensions shape and location in the rim must be suited to the design of the wheel hub and the suspension geometry of the vehicle to which it has to be mounted. The purpose of the rim is to provide a firm base on which to fit the tire. Four vital dimensions are involved. The different parts developed in the PART module of CATIA are assembled in the ASSEMBLY module of CATIA. The components developed are assembled using the placement constraints available from the list in the component placement dialogue box. On to the rim, it would be impossible for the inside diameter of the tire to pass over the large diameter of the tire rim without causing damage to the beads. Forcing the tire bead into the rim well opposite to the fitting head of the machine tire bead. Steel disc

Alloy Wheels:

Alloy wheels are often incorrectly referred to as magnesium or "Mag" wheels. Magnesium is used in alloys. However, they are almost found only in racing rims meant for the track. Its brittle and highly flammable qualities make it unsuited as a road rim. Low pressure, die-casted aluminum alloy wheels are used and offer certain benefits over steel wheels. It is possible to design alloy wheels that alloy for the better air flow over the brakes and that are also slightly lighter and visually more appealing than steel wheels. Because alloy is lighter than steel, wider rims can be used without sacrificing unsprang weight.

Fig 1: Aluminum alloy wheel

IV. STEPS INVOLVED IN PROJECT WORK

Gathering all relative data for the design of wheel rim.

Generation of model using CATIAV5. Importing the generated model to ANSYS for analysis work Static analysis is carried out on the wheel rim to evaluate the performance. Modal analysis is carried out on the wheel rim.

 ISBN: 978-93-91420-02-4

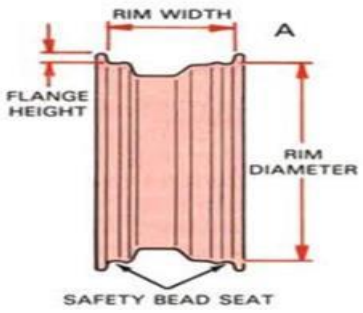

Fig 2: Wheel Rim

V. MODELLING USING CATIA

Modules of CATIA:

Sketcher:

A feature is able building block that describes the design, like a key way on a shaft. Each feature indicates how to add material (like a rib) or remove a portion of material. Feature adjusts automatically to changes in the design there by Interface guides you through the design process. After you choose an object an action, CATIA interpret he current modelling context and presents requirements and optional attempts to complete the task. This information is displayed in a non-obstructive user interface called the dashboard that enhances your ability to directly work with your models by assessing your action and guiding you through the design process.

Assembly:

Geometric Modelling:

Computer representation of the geometry of component using software is called a geometrical model. There are three types of geometric modelling.
Those are
i. Wire-framing modelling
ii. Surface modelling
iii. Solid modelling

Solid modelling:

This is most advanced geometric modelling in Three dimensions. This typically uses solid geometry shapes called picture to construct the object. Another feature of the CATIA system is color graphics capability. By means of color, it is possible to display more information on the graphics screen colored images help to clarify components is an assembly or highlight dimensions or host of other purposes.

VI. STEPS INVOLVED IN DESIGN

1. Draw the profile diagram of the wheel rim solid modelling software the designer can create a feature in two basic ways. One is to sketch of the shape to be added and then extrude, revolve or sweep it to create the shape. This are called sketched features. Another type of the features is the pick and place feature. In this feature engineering operation such as placing a hole, chamfering, or rounding a set of edges, or shelling out the model is done.

allowing the capture of design intent. This also saves times when design changes are made. Because features have the ability to intelligently reference other features, the change made will navigate through design updating the 3D model in all affected areas. In typical Part CATIA part enables you to design models as solids in progressive 3D solids modelling environment. Solid models are geometric models that offer mass properties such as volume, surface area and inertia. If you manipulate any model, a 3D model remains solid. CATIA provides a progressive environment in which you create and change your models through direct graphical manipulation. You drive the design process for your project by selecting an object (geometry) and then choose a tool to invoke an action on that object. This object- action work flow provides greater control over the design of your models while allowing you to express your creativity. The user interface provides further support for this design process. With this model, the context sensitive us

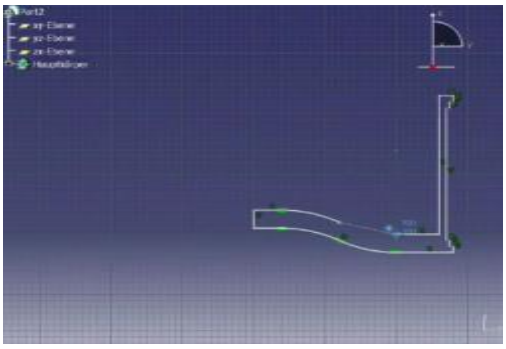
Fig 3: wheel rim profile

2. Now revolve the profile body with respect to y-axis. Then we obtain the wheel rim body as

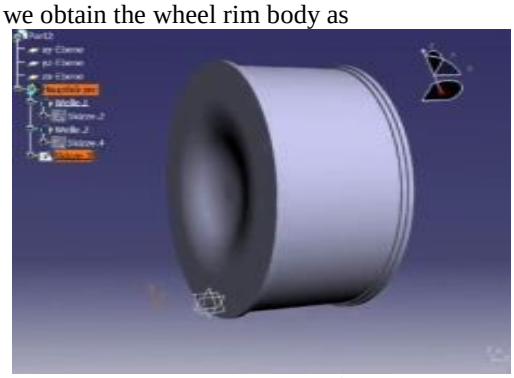
Fig 4: wheel rim profile

3. By selecting the face of wheel, the required design is Drawn on the surface is removed by using POCKET Operation

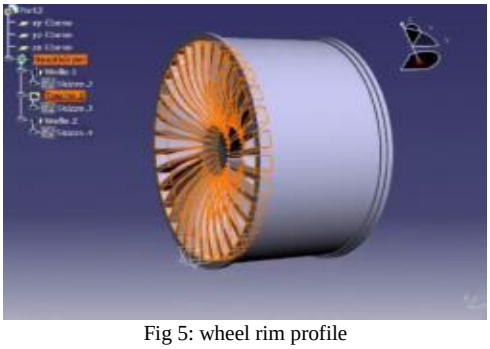
Fig 5: wheel rim profile

 ISBN: 978-93-91420-02-4

4. by using circular pattern the specific design is obtained all over the rim
5. Once again selecting the face draw the circle for and rotate them using circular pattern.
6. Form holes using POCKET option.
7. And finally using the EDGE FILLET option the side edges are made filleted for final finishing.

VIEWS OF WHEEL RIM

(a) Top View

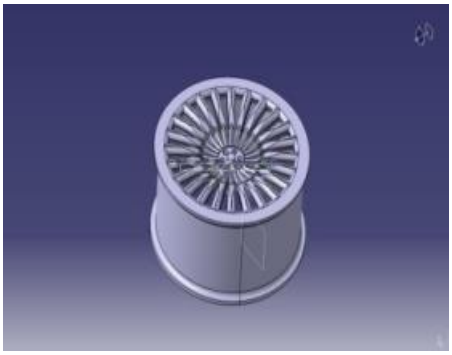

Fig 6: wheel rim profile

(b) Side View

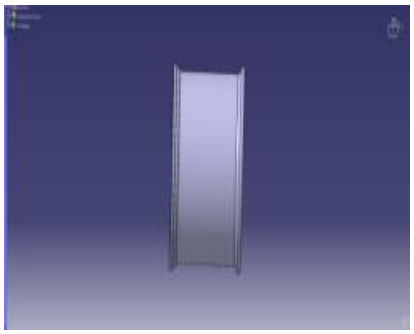

Fig 7: wheel rim profile

Drafting is a process of making dimensions to a model in various views. Some of the drafted views of the wheel rim are as follows:

Finite Element Method (FEM):
FEM is the most popular numerical method.
Applications- Linear, Nonlinear, Buckling, Thermal, Dynamic & Fatigue analysis. FEM will be discussed in Detail at later stage.

Software Based FEM:

For using any commercial software there are 3 steps -
1) Preprocessing- Consumes most the out of the three Steps.
2) Processing (or solution) - just click on “Solve"& it's the software's turn to do the job
3) Post processing- Result viewing & interpretation

Step 1 - Pre processing:

a) CAD data
b) Meshing
C) Boundary conditions
In early stage of industrial applications of Finite Element Analysis, CAD, meshing & analysis al1 used to be carried out b**y** a single engineer only. Soon it was realized that separation of the jobs &forming dedicated subgroups i.e. CAD group, Meshing group & Analysis or calculation group is necessary for optimum output and efficiency. CAD & Meshing -There are specialized software’s for CAD, Meshing & Analysis. CAD & meshing consumes most of the time For example - Typical time for a single person to mode1 (CAD) 4cylinder engine block is 6 weeks & for brick meshing 7 weeks (For tetra mesh about 2 weeks). Boundary Conditions -Consumes least time but it is the most Important step (typically applying load cases is about 1 day job). 3 months hard work of meshing & CAD data preparation of engine block would be undone in just 1 day if boundary conditions are not applied properly. After completion of preprocessing i.e., CAD, Meshing and Boundary conditions, software internally forms
Mathematical equations of the form $[F] = [K] [\delta]$

Step 2 - Processing or Solution:

During preprocessing user has to work hard while solution step is the turn of computer to do the job. User has to just click on solve icon & enjoy a cup of tea! Internally software carries out matrix formations, inversion, multiplication & solution for unknown e.g. displacement & then find strain stress for static analysis. Today we are using FEA just because of availability of computers. FEM has been known to Mathematicians & engineers right from late 50's but since solving so many equations manually was not possible, in true sense FEA got recognition only after emergence of high capacity Computers.

Step 3 - Post processing:

Post processing is viewing results, verifications, and conclusions & thinking about what steps could be taken to improve the design. Consider a simple example which involves al1 the above Steps Probably at the moment you are sitting on a chair or stool & reading this book. In this example we will analyses the stool itself for stress & displacement for a load of 200 **kg** (assuming it could be used for sitting as well as supporting any object up to max. 200 kg wt.)

Static analysis:

A static analysis calculates the effects of study loading conditions on a structure, which ignoring inertia and damping effects such as those caused by time varying loads. A static analysis can, however, includes study inertia loads (such as gravity and rotational velocity), and time varying loads that can be approximated as static equivalent loads (such as the static equivalent wind and seismic loads common defined in many building codes). Static analysis is used to determine the displacements, stresses, strain, and forces in structures or components caused by loads that do not induce significant inertia and damping effects. Study loading and resonance conditions are assumed; that is, the loads and the structures response are assumed to vary slowly with respect to time moment is equal to reaction forces and moments

VII. SPECIFICATIONS

a. Tire diameter (approx.) =560mm
b. Wheel size=14 inches

c. Length =86mm
d. Flange shape=J
e. Rim width=5 inches
f. Wheel type= disc wheel
g. Flange height= 0.68inches
h. Tyre type = radial
i. Aspect ratio=65 Off set=80.54

VIII. ANALYSIS USING ANSYS

After preparing the model in CATIA it is imported to ANSYS. The file is imported from CATIA by File>Import>IGES 2. The imported model is meshed by using TETRA mesh. The meshed model is as follows:

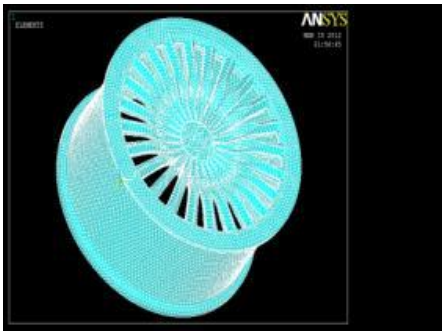

Fig 8: wheel rim-meshing

3. Later this meshed model is defined with two different materials namely ALUMINIUM and FORGED STEEL and subjected to static analysis.

Discretization of the Mathematical Model:

The ANSYS workbench uses a finite element method to discretize the model into finite elements. Finer mesh size was used; a mesh size of 10mm (0.01m). SOLID 187 10 node tetrahedral is the element used for the analysis. The Element is defined by 10 nodes having three degrees of freedom at each node: translations in the nodal x, y, and z directions. In meshing the rim, a smooth transition inflation option is used, with transition ratio of 0.272 and growth rate of 1.2. A total of nodes and elements are created for this mesh. A patch conforming method is also used. Figure shows a discretized rim from the ANSYS Workbench.

Boundary Conditions:

In the experimental set-up used in the industry that is been mimicked by this simulation, two boundary conditions were applied. These initial boundary conditions are the number of degree of freedom (DOF) at the holes where the

RESULT AND DISCUSSION

From the finite element software, the result of the Von Misses stress distribution obtained from the static stress analysis is as shown in Figure. It shows that the maximum Von Misses stress occurred at the wheel forks.

RESULTS OF AL356:

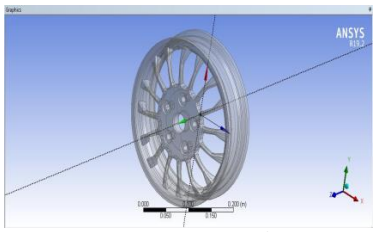

Fig 9: wheel rim profile

IX. AT PRE-PROCESSOR STAGE

Input data for ALUMINIUM:
Young's modulus =0.71e5 N/mm²
Poisson ratio =0.33
Density =2800 kg/m³
Circumferential pressure =200 kpa
Input data for FORGED STEEL:
Young's modulus =2.1e5 N/mm²
Poisson ratio =0.3
Density =7600 kg/m³
Circumferential pressure =200 kpa
After this meshed model is constrained at holes by all DOF where the bolts has to be placed.
After constraining the meshed model, the model is subjected to a circumferential load of 200 Kpa.
Later the results were obtained in the SOLVER module.
In the similar way MODAL (VIBRATION) ANALYSIS is carried out. In modal analysis only all
DOF is given, beyond that no external force is applied.
Later in the SOLVER module, analysis type is
Changed from static command to modal command
And solution in done in solution window.
Next solution results such as Stress, Displacement,
Von mises stress, ultimate strength etc.., can be
Observed in GENERAL POST-PROCESSOR.

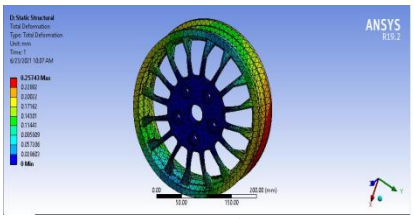

Fig10: Total Deformation

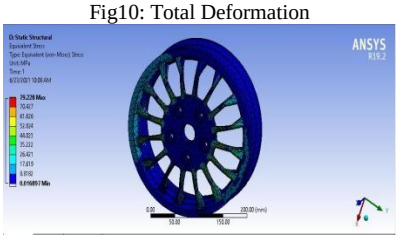

Fig11: Von Misses Stress

RESULTS OF AZ91E:

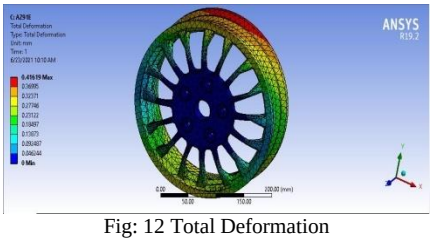

Fig: 12 Total Deformation

 ISBN: 978-93-91420-02-4

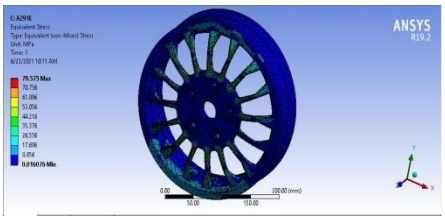

Fig 13: Equivalent Stress

Fatigue Study:

During the static analysis of the steel wheel, it was discovered that the maximum stress concentration occurred at the spokes and ventilation hole of the rim under loads Fr and *pi*. This point of maximum stress concentration was found to be identical with that of actual practical test results. The wheel rotating at a speed of 950 rpm under the stated loads, fatigue crack propagation at the point of

Maximum stress concentration is observed as demonstrated in Figure

Fatigue results of AZ91E:

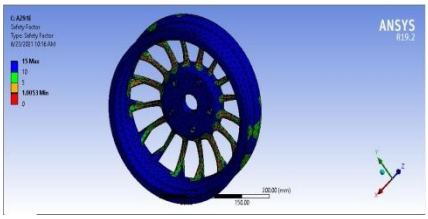

Fig 14: Factor of Safety

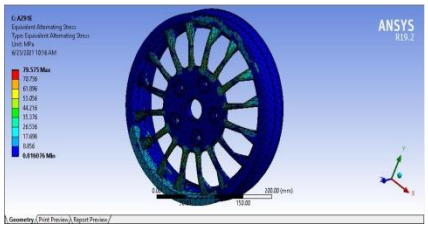

Fig 15: Equivalent Stress

RESULTS OF AL356:

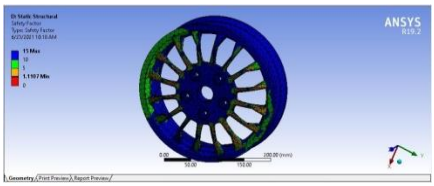

Fig 16: Safety Factor

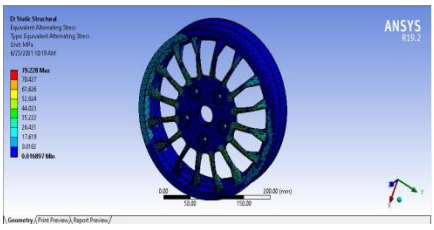

Fig 17: Equivalent Stress

CONCLUSION

The finite element based approach, using ANSYS, is an effective method of predicting the failure mode of an automobile wheel during the wheel design stage. Finite element-based stress analysis and fatigue life prediction obtained from the ANSYS software showed that the fatigue crack initiation regions on the wheel are subjected to stress concentration. Fatigue crack initiation occurs at the most stress concentrated regions of the wheel spokes and air ventilation holes which are the critical regions of the wheel. The predicted failure locations are identical to the actual crack initiation regions and are consistent with order reports.

REFERENCE

1. Courtney, T.H. (2005), Mechanical behavior of materials. Long Grove, IL: Waveland Press, Inc Callister, J.R. (2008), Fundamentals of materials science and engineering: an integrated approach, Hoboken NJ: Waveland Press, Inc
2. Kocabicak, U. and Firat, M.(2001) Numerical analysis of wheel cornering Fatigue tests, Engineering Failure Analysis 8, pp339-354
3. Lu, S., Wei, W., Yu, L., Jiang, Y., Tan, J. and HongQiang, R. (2011), Fatigue life analysis of Aluminum HS6061-T6 rims using finite element method," Remote Sensing, Environment and Transportation Engineering (RSETE), International Conference on , vol., no., pp.5970,5973,doi: 10.1109/RSETE.2011.5965715
4. Wang, L., Chen, Y., Wang, C. and Wang, Q. (2011), Fatigue Life Analysis of Aluminum Wheels by Simulation of Rotary Fatigue Test, Journal of Mechanical Engineering 571, pp 31-39, DOI:10.5545/sv-jme.2009.046
5. Topaç, M. M., Günal H, and Kuralay N.S. (2009), Fatigue failure prediction of a rear axle housing Prototype by using finite element analysis, Engineering Failure Analysis 16 (5),pp1474-1482
6. Torgal, S. and Mishra, S. (2012), Stress Analysis of wheel rim, International Journal of Mechanical Engineering and Research, Vol. 1, pp34-37.
7. Association of European Wheel Manufacturers (2006), Biaxial Test requirements for Truck steel wheels, EUWA standards.

 ISBN: 978-93-91420-02-4

COP Enhancement of VCR System Using Diffusers

P. Srinivasarao[1] and G. Nagaraju[2]
Department of Mechanical Engineering, Narasaraopeta Engineering College (A), Narasaraopet, India
Department of Mechanical Engineering, VITAP, Amaravathi, India

Abstract: In This paper the performance of the vapor compression refrigeration system with diffusers at compressor inlet was studied by using R134a refrigerant. Initially to making the four diffusers with the divergence angles of 10°,12°,14°,16°. The experiment is carried to testing of diffusers at inlet of the compressor. When diffuser placed at compressor inlet the outlet tube diameter of evaporator is equal to inlet diameter of the diffuser and outlet tube diameter of the diffuser is equal to the suction tube diameter of the compressor. The system performance is analyze by using of thermodynamic first and second law, to calculate the coefficient of performance.

Key Words: Diffuser, Refrigerating effect, cop.

I. INTRODUCTION

In vapour compression system, mainly the refrigerant under goes phase changes from vapor to liquid state and then liquid to vapor state. In the refrigeration system reject the heat in condenser and heat will be absorbed in evaporator. The cop is the ratio of the heat transfer rate in the evaporator to work of the compressor. The system performance is mainly increases by increasing the refrigeration effect or by decreasing the work of the compressor. Different type of techniques are find on the way to improve the cop of the system, as reported in literature.

M. Yohanet al., [1] to study the use of diffuser in refrigeration system at condenser inlet. The performance can be enhanced by reducing the compressor work by using of diffuser. The system cop was increased by 6% and work of the compressor was reduced by 6.10%.

P. Pranitha et al., [2] in this study to analysis the performance of vcr system by placing the nozzle and diffuser. Nozzle is incorporated at inlet of the evaporator and diffuser is incorporated at inlet of the condenser.

B.Sandhya Rani et al.,[4] In this paper study the experiment was successfully completed by incorporate the nozzle in the cycle at outlet of the condenser. The exta pressure droped in the nozzle, these additional help to achieve the more performance of the refrigeration system. The convergent angle of nozzle is increases from 10° to 14°. The 14° convergent angle of nozzle is got the better cop of the system.

K.Jaya Sudheer Kumar et al.,[5] to study this paper to evaluate the performance of the vcr system without and with nozzle at inlet of the expansion valve. By using the nozzle in the system again decreasing of refrigerant pressure before entering the evaporator. It improve the refrigeration effect and increase the cop of the system increases.

From the above literature survey I can understand the use of diffuser. None of the literature survey studied the effect of the diffuser in VCR system, it will rise the same amount of pressure before entering the compressor of the refrigerant. It will reduce the work of compressor. Due to these reduction, the system performance will increase.

II. EXPERIMENTAL SETUP AND METHODOLOGY

Manufacturing of Diffusers:

The flow of the refrigerant in the VCR system is subsonic. The diffuser is increases the pressure of the refrigerant without any work input. The diffusers are shown in figure2.

Diffuser length (L) = 10 mm
Outlet diameter of diffuser inlet (d_1) = 11 mm
Inner diameter of diffuser inlet (d_2) = 6 mm
Outlet diameter of diffuser outlet (D_1) = 15 mm
Inner diameter of diffuser outlet (D_2) = 10 mm
Divergence angles (θ) =10°, 12°, 14° and 16°.

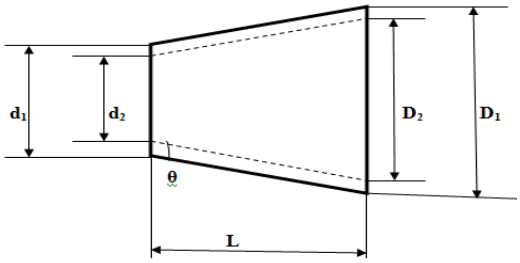

Fig.1 line diagram

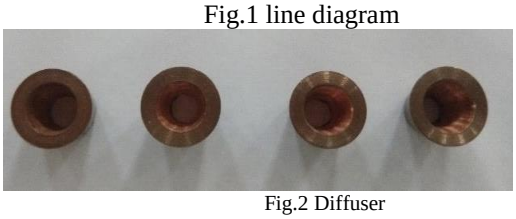

Fig.2 Diffuser

III. EXPERIMENTAL SETUP

It mainly consists of the main loop of system. The main loop is consists of a compressor, condenser, capillary tube valve (expansion valve) and evaporator. The compressor used in this one is hermetically sealed reciprocating type compressor and capacity is 1/8th TOR. The condenser and evaporator both are the coppered single tube. In this single flow tube condenser, inner side refrigerant flows and air is flows out side of the tube. The refrigerant then flows in to the evaporator through expansion valve. The capillary tube is used to control the flow rate of the refrigerant in to the evaporator coil and also to set the difference pressure. In the one flow tube evaporator, the refrigerant flow through the inner side of the tube and water is in storage tank outside of the tubes. To minimize the heat losses, the tube is insulated. The four

 ISBN: 978-93-91420-02-4

diffusers were tested at compressor inlet by changing one by one diffuser.

The readings were taken with changing the diffuser at compressor inlet. By using the five pressure gauges, these gauges are incorporated in the system to note down the pressure at various points (diffuser inlet, outlet, compressor outlet, condenser outlet and inlet of evaporator). By using the temperature sensors, to measure the temperatures at various points in the system like as pressure gauges. The voltage and the current in the system are measured by using the voltmeter and ammeter. Power consumption of the system is constant that is 230wats.

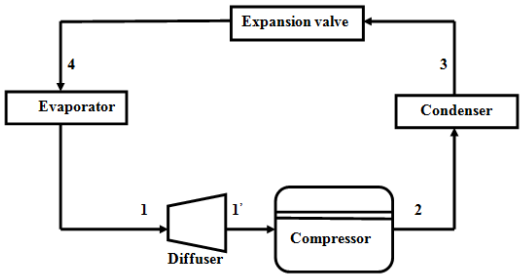

Fig.3 Experimental set up line diagram

Fig.4 Experimental set up

IV. RESULTS AND DISCUSSIONS

A. Experimental set up readings

Table 1 shows the experimental readings of pressure

State points	Position	Pressure (psi)				
		Without diffuser	With diffuser			
			10°	12°	14°	16°
1	Compressor inlet	6	6	8	10	7
2	Condenser inlet	170	170	170	170	170
3	Condenser outlet	170	170	170	170	170
4	Evaporator inlet	5	5	5	5	5

Table 2 shows the experimental readings of temperature

State points	Position	Temperature(c^0)				
		Without diffuser	With diffuser			
			10^0	12°	14°	16°
1	Compressor inlet	31	31	32	33	31.5
2	Condenser inlet	41	41	41	41	41
3	Condenser outlet	38	38	38	38	38
4	Evaporator inlet	-4	-4	-4	-4	-4

B. Calculations.

From the **p-h** chart of **R-134a** refrigerant

h_1 = 433 kj/kg

h_1' = 438 kj/kg

h_2 = 520 kj/kg

$h_3 = h_4 = h_{f3}$ = 250 kj/kg

Compressor work (c.w) = $h_2 - h_1$ = 520 – 433 = 87 kj/kg

Refrigeration effect = $h_1 – h_4$ = 433 - 250 =183 kj/kg

Diffuser work = $h_1' - h_1$ = 438 - 433 = 5 kj/kg

Reduction in compressor work = $(h_2 - h_1) - (h_1' - h_1)$

=87- 5= 82 kj/kg

$COP_{\text{without diffuser}}$ = 183 / 87 = 2.10

$COP_{\text{with diffuser}}$ = 183 /82 = 2.23

Parameters		Refrigeration effect	Reduction in compressor work	COP
Without diffuser		183	87	2.10
With diffuser	10°	183	87	2.10
	12°	183	85	2.15
	14°	183	82	2.23
	16°	183	86	2.12

C. Variation of pressure with respect to the diffuser divergence angles

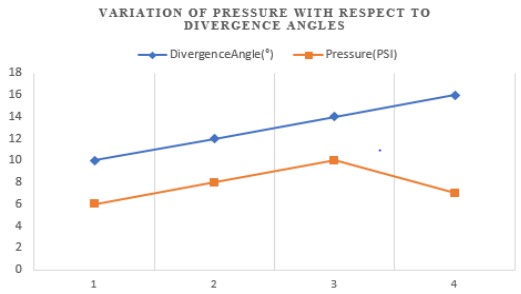

Fig.5 Variation of pressure with diffuser diverging angle

 ISBN: 978-93-91420-02-4

Figure 5 shows the variation of pressure with respect to the diffuser divergence angles. It was observed that, initially the pressure at 6 PSI when experiment without diffuser. Using 10° angle of diffuser pressure is same as 6 PSI and increases 8 PSI by using 12° angle of diffuser and increased to 10 PSI when using the 14° divergence angle of diffuser. The pressure is decreases up to 7 PSI when using the 16° diffuser. At 14° angle of diffuser get the maximum pressure.

D. Variation of temperature with respect to the diffuser angles:

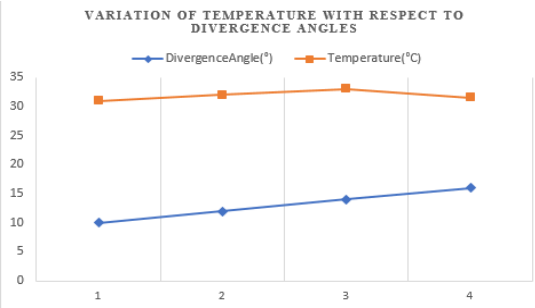

Fig.6 Variation of temperature with diffuser divergence angles

Figure.6 shows the variation of temperature with respect to the diffuser angles. Initially temperature at 31°C without diffuser. When using diffusers, the temperature increases to 33°C up to 14° angler of diffuser and then decreased 31.5°C when using the 16° angle of diffuser. This is the maximum temperature is get when using 14° angle of diffuser.

E. Variation of cop with respect to the diffuser divergence angles:

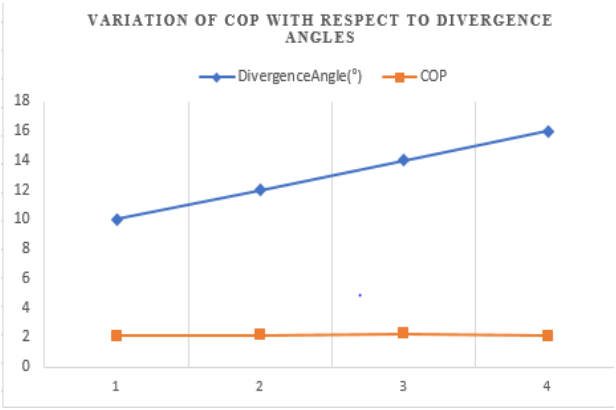

Fig.7 Variation of cop with diffuser divergence angles

Figure 7. Shows the variation of cop when using the diffusers in the refrigeration system. It was noted that the maximum percentage of reduction in compressor work and maximum obtained COP are at diffuser with divergence angle 14º at suction pressure 10 psi. By applying the first law of thermodynamics to the diffuser, it was observed that the increase in enthalpy is proportional to the kinetic energy of refrigerant. The rise in enthalpy is without any power consumption. Net compressor work was reduced for constant refrigerating effect.

CONCLUSION

The experimental investigation was carried out to study the effect of diffusers at compressor inlet of vapour compression refrigeration system. The four diffusers are tested in the system.In this investigation, diffuser with angle of 14° is given by the maximum cop (2.23) to compare to other diffusers. The pressure of the refrigerant increased from 6 to 10 psi and the work of the compressor is reduced by 6.19%. The COP is increased approximately 6.19%. This is most helpful to improve the cop of the system to provide the diffuser at compressor inlet in VCR system.

REFERENCES

1. M. Yohan and G. kiran Kumar, Proc. of International Conference on Advances in Mechanical Engineering, June 06-08, 2011 S.V. National Institute of Technology, Surat – 395 007, Gujarat, India.
2. P. Pranitha, International Journal of Technical Innovation in Modern Engineering & Science (IJTIMES) Impact Factor: 3.45 (SJIF-2015), e-ISSN: 2455-2585 Volume 3, Issue 10, October-2017
3. Bala Kartheek, International Journal of Recent Technology and Engineering (IJRTE) ISSN: 2277-3878, Volume-8 Issue-2, July 2019.
4. B. Sandhya Rani, International Journal of Mechanical Engineering and Technology.Volume 7, Issue 6, November–December 2016, pp.642–659, Article ID: IJMET_07_06_064 ISSN Print: 0976-6340 and ISSN Online: 0976-6359.
5. K. Jaya Sudheer Kumar, International Journal of Technical Innovation in Modern Engineering & Science. (SJIF-2017), e-ISSN: 2455-2585 Volume 4, Issue 12, December-2018.

 ISBN: 978-93-91420-02-4

Design and Fabrication of Radiant Cooling System

Kasukurthi Prakash babu[1], Kukkala Haribalakrishna[2] and Venkannababu Mendi[3]
[1,2] Department of Mechanical Engineering Azad College of Engineering and Technology, Hyderabad, India
[3] Department of Mechanical EngineeringNarasaraopeta Engineering College (A),Narasaraopeta, India

***Abstract*: A radiant cooling system refers to a temperature-controlled surface that cools indoor temperatures by removing sensible heat and where more than half of heat transfer occurs through thermal radiation. This project includes the fabrication of air conditioning (HVAC) systems for commercial building by using radiant cooling systems. The two main benefits of radiant cooling systems include the potential to save energy and improvement of indoor thermal comfort. The radiant cooling panels can work more efficiently especially when proper control strategies are employed to avoid condensation. In this project we are studying about two primary types of radiant cooling systems. The first type is systems that deliver cooling through the building structure, usually slabs, these systems are also named thermally activated building systems (TABS).The second type is systems that deliver cooling through specialized panels. We are fabricating the working model of radiant cooling system and its pipe system.Radiant cooling panels are generally attached to ceilings, but can be attached to walls also. They are usually suspended from the ceiling, but can also be directly integrated with continuous dropped ceilings. Radiant cooling cools a floor or ceiling by absorbing the heat radiated from the rest of the room. When the floor is cooled, it is often referred to as radiant floor cooling; cooling the ceiling is usually done in homes with radiant panels.**

1. INTRODUCTION

1.1 RADIANT COOLING: Radiant cooling systems are generally chilled ceiling beams or panels, to take advantage of convective air cooling as well as mean radiant temperature. Because cool air sinks, a chilled ceiling beam will cool air that will sink and distribute itself through the space. Convection is more important for radiant ceiling panels and beams because, unlike radiant floors, no one will touch these surfaces. Because of this, they are sometimes simply called "chilled beams". However, radiant cooling systems can be located in floors as well.

1.2 ADVANTAGES OF RADIANT COOLING SYSTEMS: There are several good reasons designers should consider including radiant cooling systems in new buildings in any climate zones. Commercial buildings primarily cooled by radiant means are more comfortable than buildings cooled by traditional HVAC systems. The first costs for radiant systems are comparable with those for traditional variable-air-volume (VAV) systems, but their lifetime energy savings over VAV systems are routinely 25% or even more. With radiant systems, people are cooled by radiant heat transfer from their bodies to adjacent surfaces ceilings, walls, or floors whose temperatures are held a few degrees cooler than ambient.

Space conditioning energy is usually moved from chillers or boilers to radiant panels or concrete slab using water as a medium. This produces impressive savings, since water has roughly 3,500 times the energy transport capacity of air. Even accounting for the pressure drop involved in pumping water throughout a building, a hydronic system can transport a given amount of cooling with less than 5% of the energy required to deliver cool air with fans.

1.3 TYPES OF RADIANT COOLING SYSTEMS:

CHILLED SLABS: These deliver cooling through the building structure, usually slabs, and is also known as thermally activated building systems (TABS). Radiant cooling from a slab can be delivered to a space from the floor or ceiling. Floor cooling is similar to floor heating that has been used in Europe since last few decades.

CEILING PANELS: These deliver cooling through specialized panels. Systems using concrete slabs are generally cheaper than panel systems and offer the advantage of thermal mass while panel systems offer faster temperature control and flexibility.

2. LITERATURE SURVEY

2.1 LITERATURE SURVEY: Numerous specialists talked about the thermal comfort with in surfaces with a brilliant radiant cooling some of them are: Kulpmann in 1993 exhibited his analyzed result about the radiant cooling system with a decent thermal comfort and an air superiority in a zone where this system present. Kulpmann utilized some heat gain for showing the condition surface. Loveday in 2003 talked about the estimations done by him on thermal comfort on human related in a working space with brilliant radiant cooling with no modifications the thermal comfort by the radiant cooling is conceivable. In 2002 Mariel has built up a specific model with simulation application TRNSYS, utilizing the analyzed study, the execution of thermal comfort and energy utilization comes about for verification.

In fact, instead of using boilers or chillers that consume high-grade fossil fuels and electricity for low-grade needs (space heating and cooling), a more dramatic reduction in loss in terms of exergy would be the use of alternative low-grade cooling/heating sources. Examples are night cooling with ventilation, solar heating/cooling, evaporative processes, and ground heat exchange (Floride set al. 2002,

Gao et al. 2008, Wei and Zmeureanu 2009, Sakulpipatsin et al. 2010, Hang et al. 2011).

The purpose of HVAC systems is for maintaining better thermal comfort and indoor air quality. Two main parameters for providing acceptable thermal conditions are air temperature and mean radiant temperature. The combined influence of these two temperatures is expressed as the operative temperature. For low air velocities (< 0.2 m/s), the operative temperature can be approximated with the simple average of air and mean radiant temperature. This means that air temperature and mean radiant temperature are equally important for the level of thermal comfort in a space (ASHRAE 2010). As air-based systems condition a space only by convection heat transfer, it can only directly manipulate air temperature, and mean radiant temperature cannot be controlled effectively. Therefore, it is a challenge for the air-based system to maintain thermal comfort in spaces where mean radiant temperature deviates largely from air temperature.

3. FUNDAMENTALS

3.1 PRINCIPLES OF RADIANT COOLING AND THERMAL COMFORT: Whenever there is a temperature difference between two objects, both objects will attempt to equalize the temperature. The energy transfer required to approach equivalent temperatures occurs through radiation, conduction and convection. Radiant energy is infrared energy that travels from "hot" to "cold" through a space, without heating the space itself. Humans are exothermic heat generators. Heat emission from the human body occurs via four modes of heat transfer: Radiation (~45%), Convection (~30%), Evaporation (~20%), and Conduction (~ 5%)

3.2 MEAN RADIANT TEMPERATURE (MRT): According to ASHRAE (American Society of Heating Refrigerating and Air - Conditioning Engineers) Standard 55-2010 defines six factors that affect thermal human comfort. They are Air temperature, Radiant temperature, Humidity, Air velocity, Clothing and metabolism.

3.3 CHILLED SLABS: These deliver cooling through the building structure, usually slabs, and is known as thermally activated building systems (TABS). Radiant cooling from a slab can be delivered to a space from the floor or ceiling. Floor cooling is similar to floor heating that has been used in Europe since last few decades. Radiant cooling systems are generally chilled ceiling beams or panels, to take advantage of convective air cooling as well as mean radiant temperature. Because cool air sinks, a chilled ceiling beam will cool air that will sink and distribute itself through the space. However, delivering cooling from the ceiling has several advantages: It is easier to leave ceilings exposed to a room than floors, increasing the effectiveness of thermal mass.

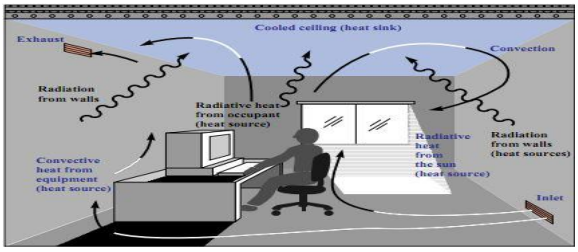

Figure 3.1 - Radiant Cooling from Ceiling

Radiant cooling systems typically use chilled water running in pipes in thermal contact with the surface. The circulating water only needs to be 2-4°C below the desired indoor air temperature. Heat is removed by the water flowing in the hydronic circuit once the heat from different sources in the space is absorbed by the actively cooled surface – ceiling, floor or walls.

Figure 3.2: Laying of PEX pipes in Slab

Majority of the cooling process results from removing sensible heat through radiant exchange with people and objects and not air, occupant thermal comfort can be achieved with warmer interior air temperatures than with air based cooling systems. Combined with higher cooling capacity of water than air, and having a cooled surface close to the desired indoor air temperature, radiant cooling systems offer significant reductions in cooling energy consumption.

3.4 CEILING PANELS: Radiant cooling panels are generally attached to ceilings, but can also be attached to walls. They are usually suspended from the ceiling, but can also be directly integrated with continuous dropped ceilings. Modular construction offers increased flexibility in terms of placement and integration with lighting or other electrical systems. Lower thermal mass compared to chilled slabs means they can't easily take advantage of passive cooling from thermal storage, but controls in panels can more quickly adjust to changes in outdoor temperature. Chilled panels are also better suited to buildings with spaces that have a greater variance in cooling loads. Chilled ceiling panels can be more easily integrated with ventilation supplied from the ceiling. Panels tend to cost more per unit of surface area than chilled slabs. Cooling the ceiling is usually done in homes with radiant panels.

 ISBN: 978-93-91420-02-4

Figure 3.3: Radiant cooling panel attached to ceiling

4. SYSTEM DESIGN & FABRICATION OF RADIANT COOLING SYSTEM

4.1 BASIC ON RADIANT COOLING SYSTEM UTILIZING BORE WELLS: To keep up slab temperature and soil temperature equal with an association comprises of two bore wells from which one is associated with radiant slab and water is pumped through it and another drag well is linked with the heated water that leaves the radiant slab. During the time the temperature of earth beneath 12ft is consistent which is a mean temperature of particular geographical limitation is. The underneath figure demonstrates recorded room temperature. Utilizing stack impact ventilation framework, the way is likewise ventilated.

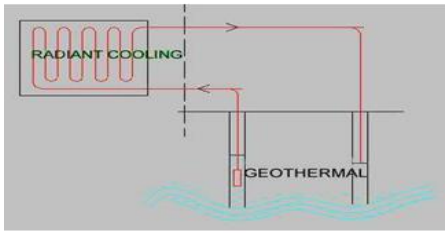

Figure 4.1-Radiant cooling system utilizing bore well

4.2 RADIANT COOLING SYSTEMS UTILIZING COOLED WATER: In this plan, the chiller creates the cool water by which the slab is chilled. The dew point temperature of breeze is progressively more when contrasted with the cool water temperature which was provided to a radiant slab. But the natural air climatically outline development can accomplish 24^0 C in space with no air dealing with unit by this systems. At the point when natural air is pumped it limits to 20% of power required for air taking care of units.

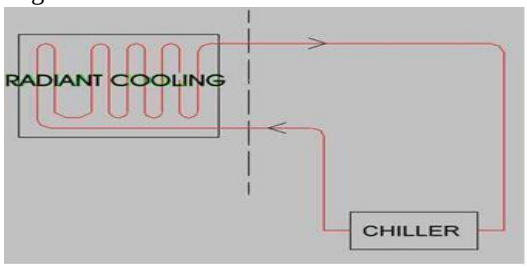

Figure 4.2: Radiant cooling system utilizing cool water

4.3 BASIC SECTION RADIANT COOLING SYSTEM UTILIZING COOLING TOWER: To keep up the slab temperature close to wet globule temperature otherwise called wet knob approach, the slab of radiant cooling is connected to a cooling tower. The dry globule and wet knob temperature very change in hot and dry atmospheres so this plan cools the space well impressively. The high measure of warmth is emanated from sun to largest amount of structures to possess space is overwhelmed by utilizing this framework.

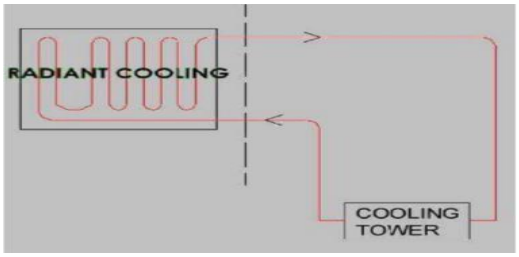

Figure 4.3: Radiant cooling system utilizing cooling tower

4.4 RADIANT COOLING THROUGH CEILING PANELS: Radiant cooling boards are associated with ceiling and walls. They are generally ousted from the rooftop, yet can correspondingly be specifically integrated with constantly drop ceiling. Secluded developments article most elevated adaptability in conditions like situating and coordination with electrical system or lighting. From warm capacity the advantage of placing passive cooling cannot be effortlessly taken by bring down warm mass when co-related to chilled slabs, however constraint in panel scan quickly adjust to changes in outside temperature. Chilled panels are proper or space structures with spaces that includes a higher change in cooling loads.

Chilled ceiling panels or Chilled roof panels can be easily joined with ventilation given from the rooftop. Chilled sections cost less per unit than juries. Ceiling is cooled ordinarily in houses with radiant ceiling boards. In spite of possibly appropriable for broadcast atmosphere, families I high sultry atmospheres radiant cooling is questionable. In North America brilliant cooling home apparatuses depend on ceiling boards suspended from the rooftop by which chilled water is dispersed.

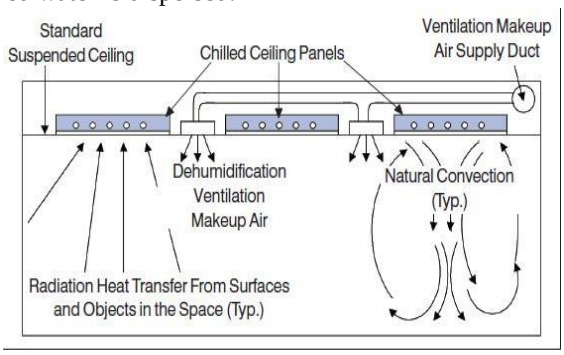

4.4 – figure radiant cooling panels working

4.5 COMPRESSOR: The refrigerator compressor is both a motor and a pump that move the refrigerant through the system. Temperature sensors signal the compressor to start when the temperature inside the refrigerator rises above its set point. No refrigerator is completely airtight; cold air leaks out, and warmer air leaks in, causing the temperature to rise above its set point.

 ISBN: 978-93-91420-02-4

Figure- 4.5: Compressor used for fabrication

COMPRESSOR SPECIFICATIONS:

Capacity	0.10 ton (or) 3.5 kw
Suction pressure	100 psi
Discharge pressure	180 psi
Standing pressure	70 psi
Standing pressure during leak test	60 psi
Running pressure during leak test	8-10 psi

4.6 CONDERSER: In systems involving heat transfer, a condenser is a device or unit used to condense a substance from its gaseous to its liquid state, by cooling it. In so doing, the latent heat is given up by the substance and transferred to the surrounding environment.

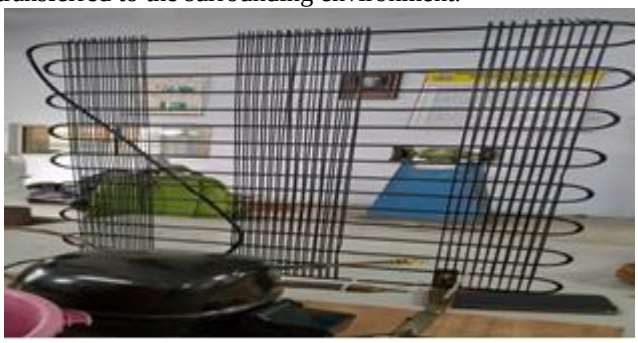

Figure 4.6: condenser used for fabrication

4..7 CAPILLARY TUBE: Capillary tube is one of the most commonly used throttling devices in the refrigeration and the air conditioning systems. The capillary tube is a copper tube of very small internal diameter. It is of very long length and it is coiled to several turns so that it would occupy less space. The internal diameter of the capillary tube used for the refrigeration and air conditioning applications varies from 0.5 to 2.28 mm (0.020 to 0.09 inches). Capillary tube used as the throttling device in the domestic refrigerators, deep freezers, water coolers and air conditioner.

Fig 4.7 Capillary tube used in fabrication

4.8 EVAPORATOR: An evaporator is a device in a process used to turn the liquid form of a chemical substance such as water into its gaseous-form/vapor. The liquid is evaporated, or vaporized, into a gas form of the targeted substance in that process

Fig 4.8 Evaporator for fabrication

The solution containing the desired product is fed into the evaporator and passes across a heat source. The applied heat converts the water in the solution into vapor. The vapor is removed from the rest of the solution and is condensed while the now-concentrated solution is either fed into a second evaporator or is removed. The evaporator, as a machine, generally consists of four sections. The heating section contains the heating medium, which can vary. Steam is fed into this section. The most common medium consists of parallel tubes but others have plates or coils typically made from copper or aluminum. The concentrating and separating section removes the vapor being produced from the solution. The condenser condenses the separated vapor, then the vacuum or pump provides pressure to increase circulation.

4.9 REFRIGRANT: R134a is also known as Tetra fluoro ethane (CF3CH2F) from the family of HFC refrigerant. With the discovery of the damaging effect of CFCs and HCFCs refrigerants to the ozone layer, the HFC family of refrigerant has been widely used as their replacement. It is now being used as a replacement for R-12 CFC refrigerant in the area of centrifugal, rotary screw, scroll and reciprocating compressors. It is safe for normal handling as it is non-toxic, non-flammable and non-corrosive. Currently it is also being widely used in the air conditioning system in newer automotive vehicles. The manufacturing industry use it in plastic foam blowing. Pharmaceuticals industry use it as a propellant. It exists in gas form when expose to the environment as the boiling temperature is -14.9°F or -26.1°C. This refrigerant is not 100% compatible with the lubricants and mineral-based refrigerant currently used in R-12. Design changes to the condenser and evaporator need to be done to use this refrigerant. The use of smaller hoses and 30% increase in control pressure regulations also have to be done to the system.

Table 4.1: Properties of R-134a:

S. No	Properties	R-134a
1	Boiling Point	-14.9°F or -26.1°C
2	Auto-Ignition Temperature	1418°F or 770°C

 ISBN: 978-93-91420-02-4

3	Ozone Depletion Level	0
4	Solubility In Water	0.11% by weight at 77°F or 25°C
5	Critical Temperature	252°F or 122°C
6	Cylinder Color Code	Light Blue
7	Global Warming Potential (GWP)	1200

5. PROJECT EXPENDITURE

COMPONENT	COST In Rs
COMPRESSOR	2500
CONDENSOR	260
COPPER PIPES	1200
WOOD AND THERMOCOOL	850
WIRING AND MOTOR	220
WELDING GAS AND R-134A (REFRIGERENT)	750
TECHNICAIN CHARGES	500

6. CONCLUSION

The desired working model of radiant cooling through chilled slabs is successfully fabricated. It is also successfully tested for working. The model gives the best results. The radiant cooling panels can work more efficiently especially when proper control strategies are employed to avoid condensation. Radiant cooling cools a floor or ceiling by absorbing the heat radiated from the rest of the room. When the floor is cooled, it is often referred to as radiant floor cooling; cooling the ceiling is usually done in homes with radiant panels.

7. REFRENCES

1. Refrigeration and air conditioning by domkundwar, aurora.
2. Lehmann, B.M gwerder, V. dorer and F. renggli (2011) thermally activated building system.
3. ISHRAE handbook 2007
4. ASHRAE handbook 2001
5. Engineering design guidelines fluid flow hydraulics sizing selection http://kolmetz.com
6. Chapter 37: Compressors. ASHRAE Handbook: HVAC Systems and Equipment. Altanta,GA, American Society of Heating, Refrigerating and Air Conditioning Engineers Inc.
7. Advantages of radiant cooling system by Robert cubic june 2016
8. Abellon, D. (2011). "Blueprint for America's energy future-Radiant slab system highlights first-of-its-kind green office building." PME.
9. Achermann, M. and G. Zweifel (2003). RADTEST – Radiant Heating and Cooling Test Cases. IEA Task 22, Subtask C, International Energy Agency.
10. ANSI/ASHRAE (2010). "ANSI/ASHRAE 62.1-2010: Ventilation for acceptable indoor air quality." American Society of Heating, Refrigerating and Air-Conditioning Engineers, Atlanta (Journal Article).
11. ASHRAE (2002). ASHRAE Guideline 14-2002: Measurement of Energy and Demand Savings. Altanta,GA, American Society of Heating, Refrigerating and Air Conditioning Engineers .Inc.

 ISBN: 978-93-91420-02-4

Comparative Performance Analysis of Engine Fuelled with Diesel Biodiesel Iron Oxide Nano Particles

Donepudi Jagadish, Ch. Sekhar, P. Srinivasa Rao, Sk Bajan
Department of Mechanical Engineering, Narasaraopet Engineering College (A), Narasaraopet, Guntur, A.P, India.

Abstract: Energy demand is the hot topic of all developing and developed countries. Energy demand has been increasing day by day at a high rate. So, it is necessary to find an alternative solution that is eco-friendly. Biodiesel can be the alternative solution for this problem. The main purpose of this paper is to test the engine performance and emission parameters of a diesel engine using animal fat biodiesel (fatty acid methyl esters) with diesel and using iron oxide Nano particles as additive. The parameters measured are volumetric efficiency, brake thermal efficiency, specific fuel consumption, mass fuel consumption and emission parameters are CO2, CO, NOx, and O2andHC.

I.INTRODUCTION

The need of diesel fuel is increasing in the current situations from several industries and vehicles. Simultaneously, because of its high compression ratio it increases the pollution to the environment. The demand for petroleum products and the cost is increasing day by day, so considering into current and future requirements for the usage of petroleum products there is a need of alternative fuels. The addition of biodiesel to diesel fuel improves the performance and emission characteristics of the diesel engine. The optimized biodiesel mix can Reduce some important portion of fuel dependency and surroundings from pollution with none modification to the diesel engine. The oxygen content presence in biodiesel reduces the carbon monoxide and hydrocarbons emissions and it increases the NOx formation at the exhaust. It leads to incomplete combustion due to poor atomization and to reduce the viscosity, pouring point and increasing the calorific value of biodiesel many researches have been carried out by researchers on different types of additives. The additives, metal and platinum based blended biodiesel improve the diesel engine performance and emission characteristics, but increases the size of the particles and accumulate less. Iron oxide has high level of purity in water and release hydrogen which provides more surface area helps in the combustion process. The optimum fuel with iron oxide brake thermal efficiency (Bth%) increased and specific fuel consumption minimized as related to neat diesel. The emissions carbon monoxide (CO) and hydrocarbons (HC) reduced respectively however increase in NOX were observed. Improved hydrocarbon and carbon monoxide with addition of nanoparticles blended biodiesel compared to biodiesel. Reduced NOx with iron oxide nanoparticles due to sufficient fuel accumulation made early combustion and reduced ignition delay. Increase in brake thermal efficiency for biodiesel-ethanol blend was observed due to better mixing abilities of nanoparticles in the presence of oxygen and significant reduction in unburnt hydrocarbon sand carbon monoxide as compared to diesel at 1/4th and 1/2nd percentage load. Brake thermal efficiency increased as compared to biodiesel and exhaust emissions hydrocarbons, carbon monoxide and NOx were reduced with nanoparticles compared to biodiesel. The higher dosage of alumina nanoparticles to diesel increased brake thermal efficiency compared to diesel and reduced carbon monoxide, hydrocarbons and NOx with iron oxide nanoparticles in comparison with diesel. The addition of Fe2O3 nano particles to biodiesel (B20) in compression ignition engine were improved performance and reduced emissions hydrocarbon, carbon monoxide and NOx with nano additives in diesel engine as compared to biodiesel.

The nanoparticles by mass fraction 50ppm, 100ppm and 150 ppm were added to diesel fuel and compared the results with diesel. Observed that average brake thermal efficiency increased with nanoparticle dosages compared to diesel fuel. Exhaust emissions were decreased after 25% of the load than the diesel fuel. Bio-diesel with iron metal oxide nanoparticles added on the diesel engine with various dosages of nanoparticles resulted in lower BTE, BSFC and exhaust emissions compared to diesel. However, increase in NOx was noted with nanoparticles Investigations from researchers were carried out on iron oxide nanoparticles to see the effect of additions on performance and emission characteristics of the diesel engine. In the literature review most of the researchers established the addition of varying dosages of iron oxide nanoparticles in biodiesel blends and in diesel increases the calorific value of the fuel and found improvement in specific fuel consumption and brake thermal efficiency. Results also showed iron oxide nanoparticles to diesel and biodiesel. Also, with lower dosage levels of iron nano particle as additive in B10 and B20, the BTE, BSFC and emissions characteristics were comparable with the diesel. The objectives of the present paper are to see the influence of addition of iron oxide nanoparticles blended with animal fat-based biodiesel on the CI engine for understanding the performance and emissions characteristics. The outcome of this study is improvement in the engine performance and exhaust emissions

MATERIALS AND METHODS

Some of the paper mentioned here are the works done on implementation of biodiesel in the present engines. Most of the results are in favour of biodiesel showing improvement in performance and emissions.

D. Jagadish et al. [1] mentioned that usage of biofuels received much attention in the current situation of depleting fossil-fuel reserves and in-creased emission legislation. Many ideas have been implemented upon usage of biofuels for energy production to achieve low-emission levels. Internal combustion engines are the basic prime movers for power generation as well as for transportation purpose, which are basically run on fossil petroleum.

 ISBN: 978-93-91420-02-4

Usage of eco-friendly fuels like ethanol and biodiesel as alter-Nate fuels in engines attracted the attention of researchers. The present work envisages the effects of ester addition to the ethanol-diesel blendslikeE10, E20andE30. The performance and emissions nature of ethanol-diesel blended fuel was observed using a single -cylinder, direct injection, constant speed diesel engine. Exhaust gas recirculation was adopted to control NOx emissions. Engine performance in terms of brake specific fuel consumption, and brake thermal efficiency is compared. The results showed that, the engine performance has been improved with an addition of ester to ethanol -diesel blend. Considerable reductions in emissions also been observed with the addition of ester, and using the EGR option reduction of NOx emissions was observed.

K Ramarao et al [2] obtained the results of engine performance and emissions of a single cylinder Direct Injection (DI) diesel engine using diesel-biodiesel blends with Nano additive. Method: Blends of diesel-biodiesel of different proportions are prepared, to which Nano additive Cerium Oxide (CeO2) is added. Properties like Flash point, Fire point, Calorific values are established for these blends. This fuel is used in single cylinder Direct Injection (DI) 4-strokdiesel engine and performance of the engine is recorded along with emission details. Finding: In this present investigation cotton seed oil is taken as base oil (biodiesel) and Cerium Oxide (CeO2) as Nano additive. by using different blends of cotton seed oil methyl esters for which Cerium Oxide (CeO2) Nano additives of size 30-50 nm is added in different proportions with neat diesel fuel.

The experiments were conducted on a single cylinder Direct Injection (DI) 4-stroke diesel engine, and observed the variation of Specific Fuel Consumption (SFC), Brake Thermal Efficiency, Air-Fuel ratio, Exhaust Gas Temperature (EGT), NOx emissions, Carbon Monoxide (CO), and Hydro Carbons (HC) emissions. Conclusion: The results have shown lower fuel consumption, better performance, and lower emissions of Carbon Monoxide (CO), Hydro Carbons (HC) but higher emissions of (NOx), in comparison to neat diesel fuel.

Meshack Hawietal[3] Observed the effects of iron-doped cerium oxide(FeCeO2) nano particles as a fuel additive was experimentally investigated with waste cooking oil methyl ester (WCOME) in a four-stroke, single cylinder, direct injection diesel engine. The study aimed at the reduction of harmful emissions of diesel engines including oxides of nitrogen (NOx) and soot. Two types of nanoparticles were used: cerium oxide doped with10% iron and cerium oxide doped with 20% iron, to further investigate the influence of the doping level on the nanoparticle activity. The nanoparticles were dispersed in the tested fuels at a dosage of 90 ppm with the aid of an ultrasonic homogenizer. Tests were conducted at a constant engine speed of 2000 rpm and varying loads (from 0 to 12 Nm.) with neat diesel (D100) and biodiesel–dieselblendsof30%WCOMEand70% diesel by volume(B30).The engine combustion, performance, and emission characteristics for the fuel blends with nanoparticles were compared with neat diesel as the base fuel. The test results showed improvement in the peak cylinder pressure by approximately 3.5% with addition of nano particles to the fuel. A reduction in NOx emissions by up to 15.7% were recorded, while there was no noticeable change in unburned hydrocarbon (HC) emissions.

2.0. EXPERIMENTAL SETUP

The present experiments are conducted on a 5HP Vertical Cylinder single cylinder, water cooled engine of Kirloskar make. The compression ratio of engine is 16:1. Various Thermocouples are arranged at their respective positions to read the values of Exhaust gas temperature, Exhaust water temperature, water inlet temperatures. The amount of air inducted is measured by manometer connected to air box. The time taken for 10cc fuel consumption measured by stopwatch. The proportions of exhaust gases are measured by inserting the probe into adjustment made in the exhaust manifold. The schematics of the engine are shown below.

3.0 RESULTS and DISCUSSION

Experiments have been performed, experimental data have been obtained, investigated and analyzed for a single cylinder 4-stroke, 5HP diesel engine using Animal fat, diesel and Animal fat oil at different blends. Calculations of engine performance are derived in order to obtain the statistical differences between Animal fat oil, diesel and Animal fat oil by using different blends. Most of the discussions emphasize on the comparison of engine performance for Animal fat oil, diesel and Animal fat oil by using different blends at minimum and maximum load condition at average speed (rpm) of the engine. During continuous running of a single cylinder 4-stroke, 5HP diesel engine for given time period, the mass flow rate of fuel, airflow rate for lambda (for getting engine performance), speed and oil temperature of engine, are studied and through overall performance of the engine has been shown. The variation of results appeared is according to load operations and type of fuel used. The variation of Indicated Thermal Efficiency with load for different fuels and blends is presented in Fig. It can see from graph that Indicated Thermal Efficiency is higher than that of B20Animalfatoilatmaximumloadtocompareother fuels and different blends.

MEASUREDPARAMETERS:

1. Break Thermal Efficiency (Bth%)
2. Volumetric Efficiency (Vol%)
3. Mass Fuel Consumption (Mfc)
4. Specific Fuel Consumption (Sfc)

ENGINEPERFORMANCE

Brake thermal **Efficiency**

Fig.6shows the variation of Brake thermal efficiency with variation of loads. It can be seen from graph that Brake thermal efficiency in all cases it increased with increased in load. The maximum Brake thermal efficiency was obtained at B20animalfat oil.

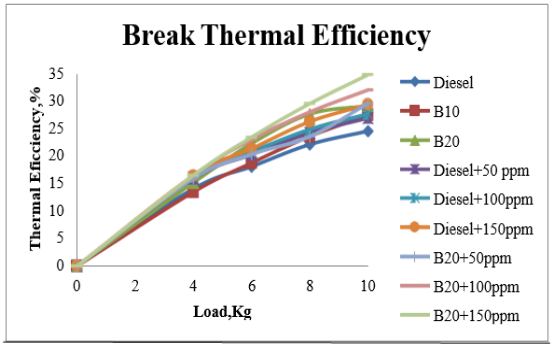

Fig.6Brakethermalefficiency vs load

ISBN: 978-93-91420-02-4

Volumetric Efficiency:

Volumetric efficiency (VE) in internal combustion engine engineering is defined as the ratio of the mass density of the air-fuel mixture drawn into the cylinder at atmospheric pressure to the mass density of the same volume of air in the intake manifold.

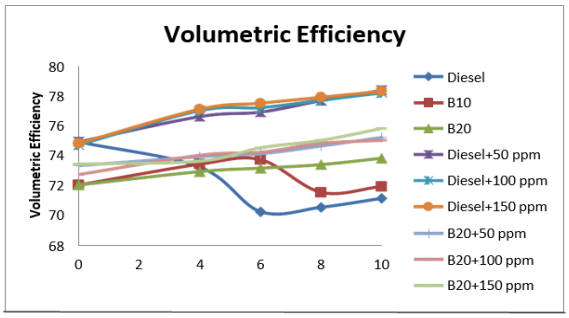

Fig.7 Volumetric Efficiency Vs Load

Mass of fuel consumption:

Specific fuel consumption is the amount of fuel consumed by a vehicle for each unit of power output. A vehicle's specific fuel consumption is more or less independent from its nitrogen oxide emissions per kilometre. The specific fuel consumption of an engine is the rate of fuel burnt to produce a unit of thrust

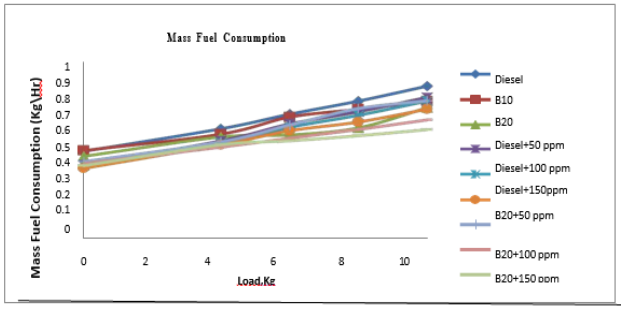

Fig.8 Mfc vs load

Specific fuel consumption:

Specific fuel consumption is the amount of fuel consumed by a vehicle for each unit of power output. A vehicle's specific fuel consumption is more or less in dependent from its nitrogen oxide emissions per kilometre. The specific fuel consumption of an engine is the rate of fuel burnt to produce a unit of thrust.

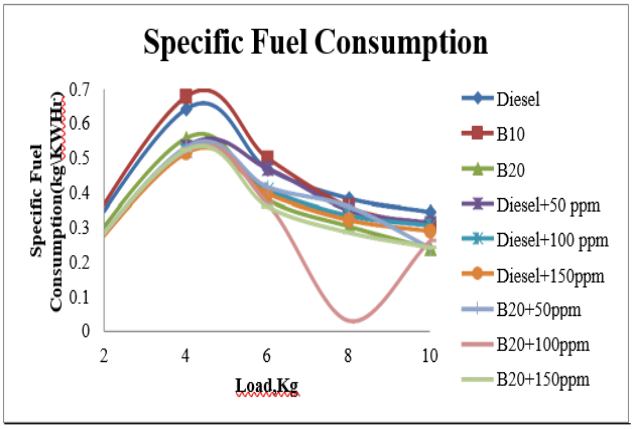

Fig.9 Sfc vs load

Exhaust Emissions:

An exhaust system is used to guide reaction exhaust gases away from a controlled combustion inside an engine.

NOx Emissions:

Fig.11 shows the parts per million (ppm) variations of the NOx emissions of the test engine for cotton seed oil and its different blends with reference to diesel fuel. It is seen that the cotton seed oil and its different blends operations usually it is evident from plot that NOx emissions are less with samples B20 + (50,100,150) ppm Fe2O3 and B10 + (50,100,150) ppmFe2O3compared to diesel fuel. NOx emissions with other samples are higher compared to diesel fuel. The maximum increase in NOx emissionswereobtainedinthecaseofB20blend.

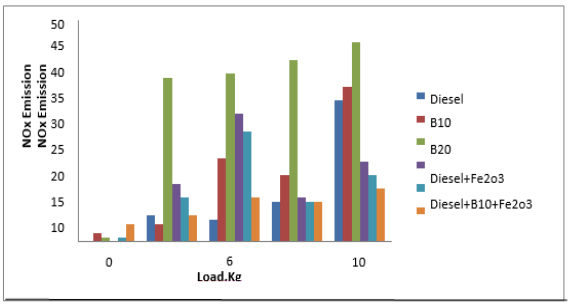

Fig.10 NOx vs load

CO Emissions:

CO emissions are plotted for diesel and diesel-biodiesel-Nano additive fuels as shown in Figure 12. Due to incomplete combustion of fuel, CO is formed in the combustion process. With sufficient air supply, it can be converted to CO2. CO will also be formed due to low gastemperature.CO emissions high with rich-fuel mixture compared to lean mixture. CO emission is less for diesel-biodiesel-Nano additive fuel compared to that of diesel. Because of biodiesel's enhanced oxygen content CO emission is reduced which is converted into CO2. To increase the load the CO emissions will decrease compared to diesel fuel.

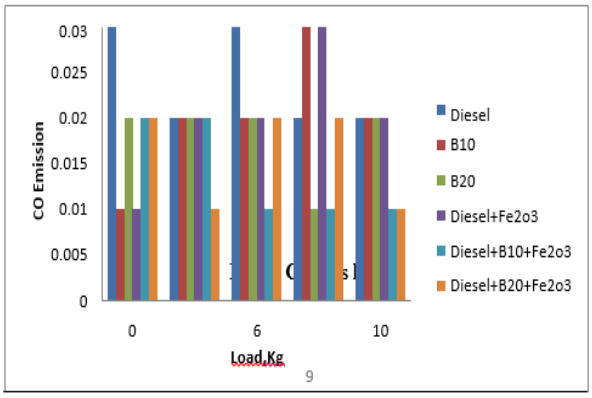

Fig co emissions vs load

 ISBN: 978-93-91420-02-4

HC Emissions:

HC is an important parameter for determining the emission behavior of the engines. It is observed from Figure 13 the HC emissions are decreased as compared to diesel fuel. The reason is similar to that about CO emissions

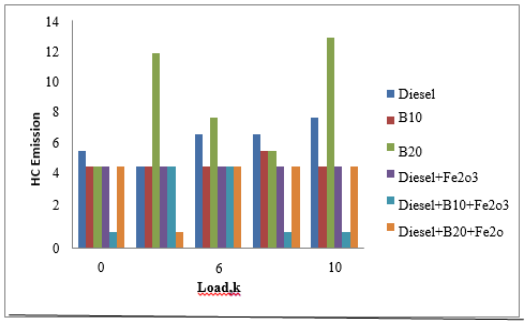

Fig.12 HC vs Load

CONCLUSIONS:

The performance, and the emission characteristics of cotton seed oil and it's all blended fuels have been done in a single-cylinder, constant speed, direct-injection diesel engine. Based on experimental data, the following conclusions have been drawn: The BTE of the engine increases with increasing load for diesel and bio diesel and its blends with the addition of Nano additive (Iron Oxide (Fe2O3)).

At lighter loads specific fuel consumption is less in case of diesel-biodiesel blend with nano additive compared to that of diesel, but with an increase in load there is little variation.

The Air-Fuel ratio of the engine decreases with increasing load for diesel and biodiesel and its blends with the addition of Nano additive (Iron Oxide (Fe2O3).

The EGT of the engine decreases with increasing load for diesel and biodiesel and its blends with the addition of Nano additive (Iron Oxide(Fe2O3).The NOx emissions with their different blend accepts B10 + (50,100,150) ppm andB20 + (50,100,150) ppm iron oxide with addition of Nano additive decrease as compared to diesel fuel.

CO emissions are less at lower loads for all blends compared to diesel fuel, but CO emissions are nearly equal with that of diesel fuel at higher loads. HC emissions are less for all the blends at all loads, compared to that of diesel fuel. In this experimental observation the NOx emissions of the fuel blends are higher with increase of load compared with diesel fuel emission. These emissions are reduced with various other emission controlling techniques.

REFERENCES

[1] Farobie O, Leow ZYM, Samanmulya T, Matsumura Y. In-depth study of continuous production of biodiesel lusing super critical1-butanol.Energy Convers Manag 2017;132:410–7.doi:10.1016/j.enconman.2016.09.042.

[2] Yahya NY, Ngadi N, Jusoh M, Halim NAA. Characterisation and parametric study of mesoporous calcium titanate catalyst for transesterification of waste cooking oil into biodiesel.Energy ConversManag2016;129:27583.doi:10.1016/j.enconman.2016.10.037.

[3] Dharma S, Ong HC, Masjuki HH, Sebayang AH, Silitonga AS. An overview of engine durability and compatibility using biodiesel–bioethanol–diesel blends in compression-ignition engines

[4] Aydogan H. Performance, emission and combustion characteristics of bioethanol-biodiesel-diesel fuel blends used in a common rail diesel engine

[5]SayinC.Dieselengineemissionsimprovementsbytheuseofsunflowermethylester/dieselblends.JThermSciTechnol2013;33:83–8.

[6]Imdadul HK, Masjuki HH, Kalam MA, Zulkifli NWM, Alabdulkarem A, Rashed MM,et al. Influences of ignition improver additive on a ternary(diesel-biodiesel higher alcohol)blends thermal stability and diesel engine performance.Energy Convers Manag 2016; 123:252–64.doi:10.1016/j.enconman.2016.06.040.

[7]Celik M. examining combustion and emission characteristics of cotton methyl ester to which manganese additive material was added. J Mech Sci Technol 2017;31:6041–50.doi:10.1007/s12206-017-1148-3.

[8]Çelik M, ÖnderÖzgören Y. The determination of effects of soybean and hazevl nut methyl ester addition to the diesel fuel on the engine performance and exhaust emissions. Appl ThermEng2017;124:124–35.doi:10.1016/j.applthermaleng.2017.06.008.

[9]Müller, TE. Biodiesel Production Systems: Reactor Technologies,2019, p. 15–25.doi:10.1007/978-3-030-00985-4_2.

[10]Rouhany M, Montgomery H. Global Biodiesel Production: The State of the Art andImpactonClimateChange,2019,p.1–14.doi:10.1007/978-3-030-00985-4_1.

[11]DemirbaşA.Biodieselfromvegetableoilsviatransesterificationinsupercriticalmethanol.EnergyConversManag2002;43:2349–56.doi:10.1016/S0196-8904(01)00170-4.

[12]DemirbasA.Biodiesel:Arealisticfuelalternativefordieselengines.SpringerLondon;2008.doi:10.1007/978-1-84628-995-8.

[13]Biodiesel. Biodiesel, London: Springer London; 2008, p. 111–9. doi:10.1007/978-1-84628-995-8_4.

[14]KnotheG.Biodiesel:Currenttrendsandproperties.TopCatal2010;53:714–20.doi:10.1007/s11244-010-9457-0.

[15]Celik M, Yucesu HS, Guru M. Investigation of the effects of organic-based manganese addition to biodiesel on combustion and exhaust emissions.FuelProcessTechnol2016;152:8392.doi:10.1016/j.fuproc.2016.06.004.

[16]Abinandan S, Subash chandra bose S R,Cole N, Dharmarajan R,Venkateswarlu K, Megharaj M. Sustainable production of biomass and biodiesel by acclamation of non-acidophilic micro algaeto acidic conditions.Bio resour Technol2019;271:316–24.doi:10.1016/j.biortech.2018.09.140.

 ISBN: 978-93-91420-02-4

Performance Analysis of a CI Engine Fueled With Olive Oil and Soybean Oil Mixture as Biofuels

Nagul Meeravali Shai and Bajan Shaik,
Department of Mechanical Engineering, Narasaraopet Engineering College (A), Narasaraopet, Guntur, A.P, India.

***Abstract*—The aim of this research is to evaluate the performance of a CI diesel engine at various loads when it is fueled with a combination of olive oil and soybean biodiesel. All of the tests were conducted on a constant speed. Olive oil and soyabean oil mixtures are used as fuel in the diesel engine.in this research we use a combination two biofuels as a single fuel. When the engine was run with DSO-I, DSO -II, and DSO-III blends at full load, the engine generated brake thermal efficiency of 33.54%, 32.06% and 30.4% respectively, and the conventional fuel efficiency is 34.25%. NOx emissions were reduced greatly in DSO-II blend comparatively diesel and we observe slightly decrease in CO emissions in all blends. Based on the plots DSO-II biofuel is suitable for the fuel in diesel engine without any engine modifications.**

Keywords— pollution, Bio diesels, IC Engines, Brake Thermal Efficiency.

I. Introduction

India is the most important changeover and developing economy on the planet. India's utilization growth of non-renewable energy sources will be most elevated by 2035. The rapid development in economy means expanding air pollution and energy consumption. India energy consumption increases 4% per year. There is a link between the transport industry and the country's economic growth, which directly affects the demand for portable energy sources. The tremendous growth of vehicular pollution and industrialization of the world has led to steep rise in the demand for petroleum products. This has given rise to frequent disturbance and uncertainties and uncertainties in the supply of petroleum and its prices. This situation is likely in the long run a lead to diesel scarcity and ultimately its depletion. The rapid depletion of petroleum fuels and their ever increasing costs have led to an intensive search for alternative fuels. Also there was need to reduce consumption of conventional fuels in the developing countries. Urban air quality management continues to pitch through the development of two wheelers and light engine passenger cars on road transport. Newly licensed cars in India contribute 70-80% of domestic emissions of carbon dioxide and oxides of nitrogen. Abnormal automotive traffic circumstances contributed 31% to 57% of oxides of nitrogen and carbon dioxide respectively [1]. It is estimated that the contribution of the transport industry to carbon dioxide air pollution increases by 4-6% per year, leading to approximately seven times by 2050 [2]. Blends of Karanja and castor biodiesel with standard diesel in an unmodified single-cylinder DI diesel engine have been researched in multiple ratios directly in lowering emissions, whereas slight decreases in thermal efficiency have been observed and the concentration of blends rises the Brake specific fuel consumption, as well as the increased concentration of castor biodiesel, has resulted in increased HC, soot emissions, particulate matter NOX has been discovered to boost for all biodiesel mixtures [3]. Results acquired from light-duty diesel engine provided with used cooking sunflower oil and new sunflower oil biodiesel blends under steady speed and variable load conditions showed decreased emissions except NOX were higher than diesel at lower load circumstances. Waste cooking oil is suggested from the results [4]. Research on diesel engines with Jatropha and fish waste biodiesel mixtures resulted in lower carbon monoxide, HC and soot emissions, but exhaust gas temperatures and NOX were higher than diesel fuel [5]. The analytical validation of various biofuel blends in which average emissions were reduced by 4%, 15.6%, 43.3%, 3% and 37% for soya bean, jojoba curcas, veal oil, grease oil and pentanol respectively [6]. A single cylinder four-stroke DI diesel engine powered by Jatropha as alternative fuel delivered smooth performance with mildly enhanced BTE and decreased carbon oxides [7]. Adding Jamun seed powder and Jackfruit seed powder directly injected into a four-stroke single-cylinder computerized water-cooled diesel engine has resulted in enhanced efficiency up to certain limits and reduced oxides of nitrogen levels [8]. The combined impact of the injection timing and EGR method on a single cylinder four-stroke diesel engine possessively affected by a 10% reduction in NOX emissions from the motor operating waste plastic based oil and elevated performance compared to diesel fuel [9]. Black solder fly is used as alternative fuel in DI diesel engine to analyse the exhaust emissions it increases the oxides of nitrogen emissions as an alternative fuel. Higher oxides of nitrogen recorded in blends under 10% and 20% comparative to diesel [10]. Tyre pyrolitic oil used in a CRDI diesel engine of different proportions as an alternative fuel. From the outcomes it was concluded that the formation of carbon deposits was discovered, which also showed an enhanced Brake Thermal Efficiency of 30% [11]. Animal fat is used in alternative fuel in a single cylinder diesel engine have given remarkable reductions in emissions except oxides of nitrogen [12]. Common single-cylinder rail direct injection DI diesel engine running at higher fuel injection pressures and higher fuel injection times showed enhanced BTE with lower HC and NOX [13]. Mahua methyl esters used as biodiesel on CRDI engines at higher FIP have revealed improved combustion characteristics resulting in enhanced brake thermal efficiency with reduced oxides of carbon, oxides of nitrogen and unburnt hydrocarbons [14]. Honge biodiesel as an alternative fuel on Common rail diesel injection is coupled with Exhaust gas recirculation setup operating with multi injection at 900 bar and 15% EGR has resulted in higher Brake thermal efficiency and decreased CO, CO2, particulate matter, unburnt hydrocarbons and nitrogen oxides [15]. Lemon peel oil is used as a biodiesel in common rail diesel injection system couples with exhaust gas recirculation. The EGR mass flow rate were 10% shows the decreases in SFC and reduction in soot emissions, oxides of carbon and oxides of nitrogen [16]. Higher Exhaust gas recirculation flow rates shown adverse effects on Brake thermal efficiency of light duty diesel engine whereas 5%

ISBN: 978-93-91420-02-4

and 10% of exhaust gas recirculation have enhanced combustion characteristics [17]. Higher EGR flow rates show the decreases the combustion diffusion, improved premixed combustion and load increases cylinder gas temperature increases due to fuel quantity [18]. Soybean derived biodiesel fuel shows the premixing combustion increase at all loads. Maximum HRR and Maximum in-cylinder pressure expanding with the combined effects of biodiesel fuel addition and EGR application [19]. Higher cylinder pressure, faster burning rate and longer ignition delay at Bu40 in a heavy duty diesel engine. By adding EGR, maximum cylinder pressure decreases, maximum HRR increases because all the combustion process is delayed to expansion stroke [20]. The thorough review of the literature highlights the suitability and insufficiency of other sources, which will be mostly addressed by further enhancements and testing. As a result, the focus of this study is on fossil fuel substitution as well as hazardous cocktail control.

II. Experimental Setup

Investigations are carried out on computerized single cylinder CI engine Detailed specification of setup is provided in table 1. Performance readings captured and tabulated with the help of "enginesoft" software. Emission ranges are collected from AVL 437C smoke meter and AVL DIGAS 444N exhaust analyzer.

TABLE I. Engine Setup Specifications

Parameter	Specification
Make	Kirloskar
No of cylinders / strokes	One / 4
Power / Speed / Compression ratio	3.5 kW / 1500 RPM / 17.5
Stroke length / Cylinder bore / Swept volume	110 mm /87.5 mm /661.45 cc
Coolant	Water
Dynamometer	Eddy current
ECU	Model Nira i7r with programmable ECU software and calibration cable

Fig. 1: Engine Setup

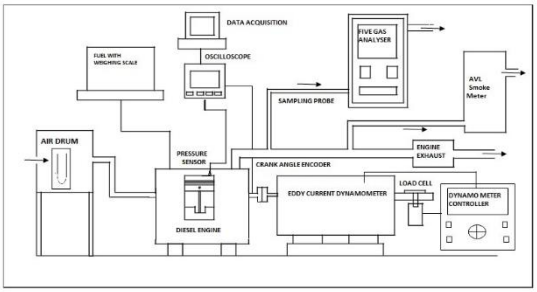

Fig. 2: Schematic of Experimental setup

III. RESULTS *AND DISCUSSIONS*

With a computerized diesel test rig, the engine performance was tested on a single cylinder, four-stroke, naturally aspirated, direct injection, water cooled, 3.7 kW output power engine. The engine was directly linked to a swinging field dynamometer, and the parameters of the engine are listed in the engine specs. The fuel line was cleansed of leftover fuel after each fuel change. To stabilize on new fuel circumstances, the engine is made to operate at maximum load for at least 2 hours. Performance characteristics and exhaust parameters are at stable speed and various load conditions. Some of the important performance parameters and emission plots are glanced briefly.

A. Brake Thermal Efficiency

The brake thermal efficiency deviation with brake power is shown by a figure that obviously shows that brake thermal efficiency is expanding with brake power. From the graph, it is noted that at all loads diesel has more brake thermal efficiency, which is the calorific value function. Since diesel has a greater calorific value compared to the remaining biofuels, the thermal efficiency of the brake has been directly affected. At maximum load, brake thermal efficiencies are 34.25%, 33.54%, 32.06% and 30.4% respectively for Diesel, DSO-I, DSO-II and DSO-III blends.

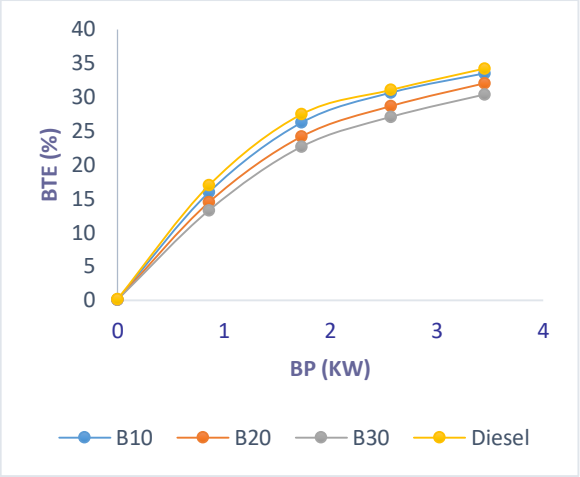

Fig. 3: variation of BTE with BP

B. Specific Fuel Consumption

Specific fuel consumption is a significant parameter that directly affects engine efficiency and defines fuel economy engine capacity. Figure shows the fuel consumption level at different charges. From the outcomes acquired, it is noted that diesel and sample fuels consumed more fuel without any load, and this gradually reduces with load increases. From the plots it is observed that DSO-III biofuel consumes less fuel compared with conventional fuel and all other blends it is 8.7% greater than the diesel at the rated load.

C. Oxides of Nitrogen

At higher temperatures, air and biodiesel oxygen forms an appropriate environment for the formation of nitrogen oxides. From the plots it is observed that biodiesel 20% mixture that means DSO –II less NO_X comparatively other blends it reduces oxides of nitrogen by 7% and all the blends produces less NO_X exhausts than the conventional fuel

ISBN: 978-93-91420-02-4

because biofuels have high latent heat of vaporization which causes lower combustion temperatures.

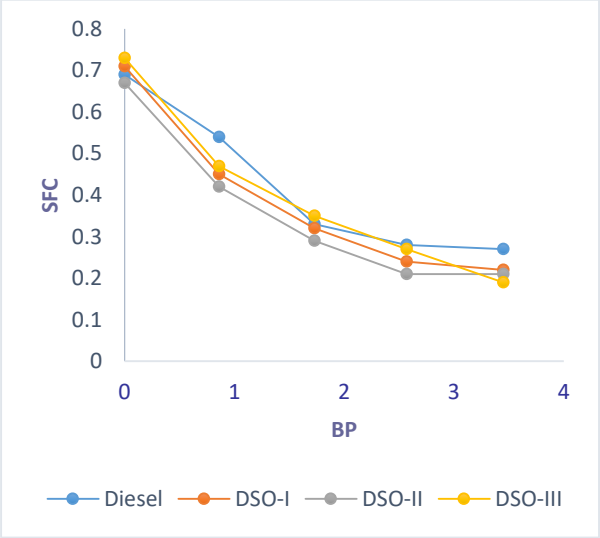

Fig. 4: variation specific fuel consumption with BP

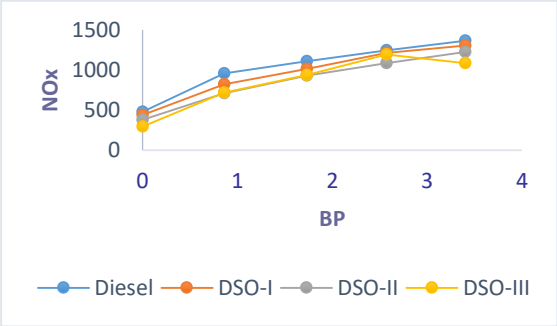

Fig. 5: variation of oxides of nitrogen with brake power

D. Carbon Monoxide

CO is formed during combustion of fuel-rich mixtures due to less oxygen. Oxidation reactions involving intermediate species such as smaller molecules of hydrocarbons, aldehydes, ketones, etc. Exhaust consists of low concentrated carbon monoxide, which increases gradually with load. Capricious distribution of charge and lack of time at peak load influence the emission of CO. From the plots it is observed that at the peak loads all biodiesels produces less emissions compared to the diesel but the DSO-II biofuel mixture reduces by CO exhausts by 22% which is a greater amount of emissions are reduced by DSO-II fuel.

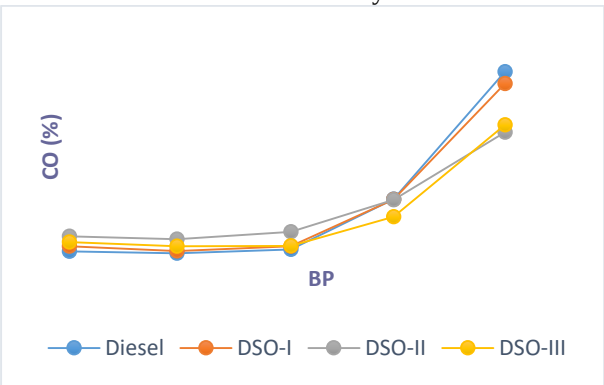

Fig. 6: variation of CO with BP

IV. CONCLUSIONS

From graphs and data it is summarised that the brake thermal efficiencies obtained by blended fuel samples are less than that obtained by diesel fuel. Sample DSO-I has shown optimistic outcomes whereas DSO-II and DSO-III outstripped at peak load. Fuel economy of samples DSO-I and DSO-II found same, which is 8% more than that of diesel at rated load.

Shaft power for particular fuel consumption is more for sample DSO-I, which has higher conversion percentage at all loads. Percentage of energy transmission from source to end is almost equal with diesel at rated load. Energy interaction through exhaust gases is more for diesel and almost equal for both the samples at peak load which enhances quality of availability.

At no load CO emissions are more compared to diesel which is reversed at full load. Increase in percentage of biodiesel decreased the percentage of CO emissions.

From the above discussion, it is concluded that performance parameters of samples are in margin with each other and less than that of diesel. Sample blend DSO –II has given optimistic values in emissions and it is preferable sample for Diesel engine.

V. Nomenclature:

DSO–I: Mixture of 90% Diesel, 5% soyabean biodiesel and 5% olive oil.
DSO-II: Mixture of 80% Diesel, 10% soyabean biodiesel and 10% olive oil.
DSO-II: Mixture of 70% Diesel, 15% soyabean biodiesel and 15% olive oil.

REFERENCES

[1] Jai Prakash, Gazala Habib. A technology-based mass emission factors of gases and aerosol precursor and spatial distribution of emissions from on road transport sector in India. J. Clerk Maxwell, A Treatise on Electricity and Magnetism, 3rd ed., vol. 2. Oxford: Clarendon, 1892, pp.68–73.

[2] Anantha Lakshmi Paladugula, Nazar Kholod, Vaibhav Chaturvedi, Probal Pratap Gosh, Sarbojit Pal, Leon Clarke, Meredydd Evans, Page Kyle, Poonam Nagar Koti, Kirit Parikh, Sharif Qamar, Sangeetha Ann Wilson. A multi-model assessment of energy and emissions for India's transportation sector through 2050. Energy Policy 116, 10-18, 2018.

[3] Kahkashan Khan, Gitesh Kumar, Amit Kumar Sharma, P. Suresh Kumar, Chandan mandal and V. Chintala. Performance and emission characteristics of a diesel engine using complementary blending of castor and Karanja biodiesel. Biofuels,2018.

[4] Abin Mathew and K. Anand. Comparison of engine characteristics with biodiesels produced from fresh and waste cooking oils. Biofuels, 2018.

[5] Bhaskar Kathirevelu, Sendivelu Subramanian, Nagarajan Govindan, Sampath Santhanam. Emission characteristics of biodiesel obtained from Jatropha seeds and fish wastes in a diesel engine. Sustainable Environmental Research, 2017.

[6] Upendra Rajak, Tikendra Nath Verma.Effect of emission from ethylic biodiesel of edible and non-edible vegetable oil, Animal fats, Waste oil and Alcohol in CI engine. Energy Conversion Management 166, 704-718, 2018.

[7] Y. V. Hanumantha Rao, Ram Sudheer Voleti, V. S. Hariharan, P. Nageswara Reddy and A. V. Sita Rama Raju. Performance and emission characteristics of diesel engine with methyl ester Jatropha oil and its Blends. Energy and Environment, Vol. 20, No. 8 and Vol. 21, No.1., 2009,2010.

[8] Nitin. D. Kamitkar, Akula Sivasai Jiran, Batna Santosh, Anisetti Srinivas and Nasina Rajesh. Performance Investigation and exhaust analysis of CI Engine Fuelled by Diesel mixed with Jamun seed powder and Jack fruit seed powder. International Journal of Mechanical and production Engineering Research and Development. Vol.8, pp. 339-350, 2018.

[9] D. Damodharan, A. P. Sathiyagnanam, D. Rana, B. Rajesh Kumar, S. Saravanan. Combined influence of injection timing and EGR

combustion, performance and emissions of DI diesel engine fuelled with neat Waste plastic oil. Energy Conversion Management 161, 294-305, 2018.

[10] Kashif ur Rehman, Xiu Liu, Hui Wang, Lougyu Zheng, Rashid ur Rehman, Xiaobei Cheng, Qing Li, Wu Li, Minmin Cai, Jibin Zhang, Ziniu Yu. Effects of black solider fly biodiesel blended with diesel fuel on combustion, performance and emission characteristics of diesel engine. Energy Conversion management 173, 489-498, 2018.

[11] V. K. Shahir, C. P. Jawahar, V. Vinod, P. R. Suresh. Experimental investigations on the performance and emission characteristics of a common rail direct injection engine using tyre Pyrolytic Biofuel. Journal of King Saud University- Engineering sciences, 2018.

[12] Kamil Duda, Shawomir Wierzbicki, Michal Smieja and Maciej Mikulski. Comparison of performance and emissions of a CRDI Diesel Engine fuelled with biodiesel of different origin. Fuel 212, 202-222, 2018.

[13] D. Babu, R. Karvembu, R. Anand. Impact of split injection strategy on combustion, performance and emissions characteristics of biodiesel fuelled common rail direct injection assisted diesel engine. Energy, 2018.

[14] B. Prem Anand, S. Prasanna Raj Yadav, B. Aasthiya, G. Akshaya and K. Arulmozhi. Effect of fuel injection strategies on the performance of common rail direct injection (CRDI) powered by Biofuel, International Journal of Ambient Energy, 2018.

[15] S. V. Khandal, N. R. Banapuramth, V. N. Gaittude. Effect of exhaust gas recirculation, fuel injection pressure and injection timing on the performance of common rail direct injection engine powered with Honge Biodiesel (BHO), Energy,2017.

[16] B. Ashok, K. Nanthagopal,a B. Saravanan, P. Somasundaram, C. Jegadheesan, Bhaskar Chaturvedi, Shivam Sharma, Gaurang Rathi. A novel study on the effect lemon peel oil as a fuel in CRDI engine at various injection strategies, Energy Conversion and Management 172, 517-528,2018.

[17] Gautam Edara, Y. V. V Satyanarayana Murthy, Paleti Srinivas, Jayashri Nayar, Merigala Ramesh. Effect of cooled EGR on modified light duty diesel engine for combustion, performance and emissions under high pressure split injection strategies. Case studies in Thermal Engineering 12, 188-202, 2018.

[18] Gautam Edara, Y.V.V. Satyanarayana Murthy, Jayashri Nayar, Merigala Ramesh, Paleti Srinivas. Combustion analysis of modified light duty diesel engine under high pressure split injections with cooled EGR. Engineering Science and Technology, an International Journal. 2016.

[19] Ozer Can, Erkan Ozturk, Hamit Solmaz, Fatih Aksoy, Can Cinar, H. Serdar Yucesu. Combined effects of soybean biodiesel fuel addition and EGR application on the combustion and exhaust emissions in a diesel engine. Applied thermal engineering. Vol.95, 115-124,2016.

[20] Zheng Chen, Jingping Liu, Zhenkuo Wu, Chiafon Lee. Effects of port fuel injection (PFI) of n-butanol and EGR on combustion and emissions of a direct injection diesel engine. Energy conversion management, vol.76. pp. 725-731,2013.

 ISBN: 978-93-91420-02-4

Design and Analysis of Landing Gear

[1]Banavathu.Gopala Krishna Naik and [2]Bachali Rambabu
[1]Central Institute of Tool Design, Hyderabad, India
[2] Department of Mechanical Engineering, Narasaraopet Engineering College (A), Narasaraopet, Guntur, A.P, India.

***Abstract*- Landing gear is a vital structural unit of an aircraft which enables to take off and land safely main landing gear units. Even during a normal landing operation heavy loads (equal to the weight of an aircraft) are to be absorbed by the landing gear. In turn joints are to be provided such that heavy concentrated loads are first received by the airframe and subsequently diffused to the surrounding areas. Normally heavy concentrated loads are received through a lug joint. Therefore design of a lug joint against failure under static and fatigue loading conditions assumes importance in the development of an aircraft structure**.

Keywords- Landing Gear types and Arrangement.

I. Introduction

Aircraft is machine that is able to fly from one place to another place. Many researches were made to fly the machine since from mythology, many had lost their life during their experiments, and many failed to fly their machine. But finally in 1910 Wright Brothers build machine which is able to fly for 59 seconds, which is very short duration but it is first milestone for development of aviation. Further many researches were made to transport the goods and passengers. Then it is brought into business for transportation. And also used in military for air support, thus many fighter planes are developed. An aircraft is a machine that is able to fly by gaining support from the air, or, in general, the atmosphere of a planet. It counters the force of gravity by using either static lift or by using the dynamic lift of an aerofoil, or in a few cases the downward thrust from jet engines. The human activity that surrounds aircraft is called aviation. Landing gear is one of the critical subsystem of an aircraft and is often configured along with aircraft structure.

II. TYPES OF LANDING GEAR

A. Tail wheel-type Landing Gear

Tail wheel-type landing gear is also known as conventional gear because many early aircraft use this type of arrangement. The main gear are located forward of the centre of gravity, causing the tail to require support from a third wheel assembly. A few early aircraft designs use a skid rather than a tail wheel. This helps slow the aircraft upon landing and provides directional stability. The resulting angle of the aircraft fuselage, when fitted with conventional gear, allows the use of a long propeller that compensates for older, underpowered engine design. The increased clearance of the forward fuselage offered by tail wheel-type landing gear is also advantageous when operating in and out of non-paved runways. Today, aircraft are manufactured with conventional gear for this reason and for the weight savings accompanying the relatively light tail wheel assembly. The proliferation of hard surface runways has rendered the tail skid obsolete in favor of the tail wheel. Directional control is maintained through differential braking until the speed of the aircraft enables control with the rudder. A steerable tail wheel, connected by cables to the rudder or rudder pedals, is also a common design.

B.Tandem Landing Gear

Few aircraft are designed with tandem landing gear. As the name implies, this type of landing gear has the main gear and tail gear aligned on the longitudinal axis of the aircraft. Sailplanes commonly use tandem gear, although many only have one actual gear forward on the fuselage with a skid under the tail. A few military bombers, such as the B-47 and the B-52, have tandem gear, as does the U2 spy plane. The VTOL Harrier has tandem gear but uses small outrigger gear under the wings for support. Generally, placing the gear only under the fuselage facilitates the use of very flexible wings. The tail wheel aircraft also sits with its nose higher than tricycle gear airplane, lowering forward visibility for the pilot during ground operations. It's more difficult to taxi without being able to see directly in front of you, which is why you'll often see pilots of tail wheel aircraft do S-turns while taxiing. And steering a tail wheel aircraft is different than steering a nose wheel aircraft since steering is accomplished from behind the pilot instead of in front. There are certainly benefits to a tail dragger, as well. The nose-high attitude on the ground means that the propellers on tail wheel aircraft often have more clearance from the ground, making them better suited for grass or dirt runways. And they're often designed and configured for slow flight, making them easier to land on short runways. Many are high-design and are better suited for backcountry flying than nose wheel aircraft are. Tail wheel airplanes are without a doubt the favorite airplane among bush pilots.

C. Tri-Cycle Type Landing Gear

ISBN: 978-93-91420-02-4

The most commonly used landing gear arrangement is the tricycle-type landing gear. It is comprised of main gear and nose gear. In this type of Gears the main gears are mounted below the wings. COG is exactly in between the nose wheel nose Gear and main Gear. Tricycle-type landing gear is used on large and small aircraft with the following benefits: 1. Allows more forceful application of the brakes without nosing over when braking, which enables higher landing speeds. 2. Provides better visibility from the flight deck, especially during landing and ground manoeuvring. 3. Prevents ground-looping of the aircraft. Since the aircraft centre of gravity is forward of the main gear, forces acting on the centre of gravity tend to keep the aircraft moving forward rather than looping, such as with a tail wheel type landing gears. The nose gear of a few aircraft with tricycle-type landing gear is not controllable. It simply casters as steering is accomplished with differential braking during taxi. However, nearly all aircraft have steerable nose gear. On light aircraft, the nose gear is directed through mechanical linkage to the rudder pedals. Heavy aircraft typically utilize hydraulic power to steer the nose gear. Control is achieved through an independent tiller in the flight deck. The main gear on a tricycle-type landing gear arrangement is attached to reinforced wing structure or fuselage structure. The number and location of wheels on the main gear vary. Many main gear have two or more wheels. Multiple wheels spread the weight of the aircraft over a larger area. They also provide a safety margin should one tire fail. Heavy aircraft may use four or more wheel assemblies on each main gear. When more than two wheels are attached to a landing gear strut, the attaching mechanism is known as a bogie.

D. Fixed and Retractable Landing Gear

Further classification of aircraft landing gear can be made into two categories: fixed and retractable. Many small, single engine light aircraft have fixed landing gear, as do a few light twins. This means the gear is attached to the airframe and remains exposed to the slipstream as the aircraft is flown. As discussed in Chapter 2 of this handbook, as the speed of an aircraft increases, so does parasite drag. Mechanisms to retract and stow the landing gear to eliminate parasite drag add weight to the aircraft.

II. SOFTWARE USED IN THE PROJECT

Solid Works:

Solid works is a suite of design software supporting product design developed by Dassault systems. It consists of apps, each with a distinct set of capabilities for a user role within product development. It runs on MS-Windows and provides apps for 2D design. 3D CAD feature modelling, 3D direct modelling, finite Element Analysis and simulation, schematic design, technical illustrations, and viewing and visualization.

This app of the solid works software package consists of different modules based on the area of software usage and are as follows:

- Sketch
- Part
- Assembly
- Drawing
- Simulation
- Flow simulation
- Sheet metal
- Mold tools
- Surface
- Mechanism

III. 3D MODELLING OF EXCAVATOR LOG LOADER

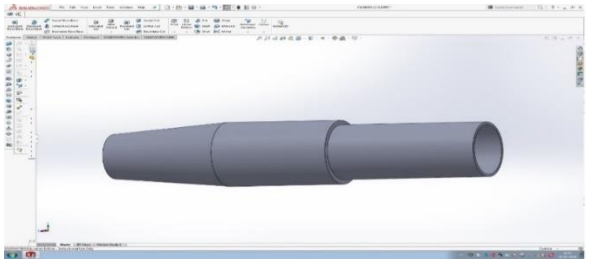

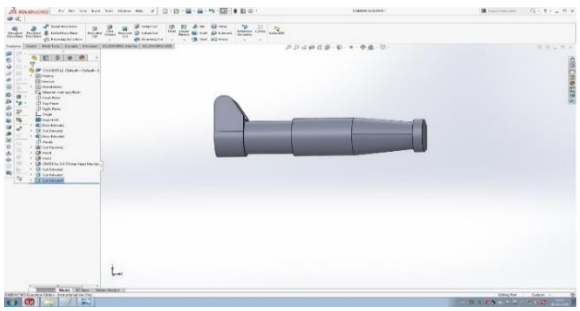

A. Computer Aided Engineering (CAE)

Computer-aided engineering (CAE) is the broad usage of computer software to aid in engineering analysis tasks. It includes Finite Element Analysis (FEA), Computational Fluid Dynamics (CFD), Multi body dynamics (MBD), and optimization.

Software tools that have been developed to support these activities are considered CAE tools. CAE tools are being used, for example, to analyze the robustness and performance of components and assemblies. The term encompasses simulation, validation, and optimization of products and manufacturing tools. In the future, CAE systems will be major providers of information to help support design teams in decision making.

In regard to information networks, CAE systems are individually considered a single node on a total information network and each node may interact with other nodes on the network.

CAE systems can provide support to businesses. This is achieved by the use of reference architectures and their ability to place information views on the business process. Reference architecture is the basis from which

 ISBN: 978-93-91420-02-4

information model, especially product and manufacturing models.

The term CAE has also been used by some in the past to describe the use of computer technology within engineering in a broader sense than just engineering analysis. It was in this context that the term was coined by Jason Lemon, founder of SDRC in the late 1970s. This definition is however better known today by the terms CAX and PLM.

REFERENCES

[1] Anil Kumar, G.Vijay Kumar, “Design optimisation of Landing Gears Legs for unmanned aerial Vehicle’’. 4 August, 2012. 2) Amit Ghoyal, Dr.H.V.Lakshminarayan “Design, Analysis and simulation of a composite main Landing Gear for light Aircraft”. Coventry university postgraduate study centre MSRSAS, Bangalore.

[2] http://gizmodo.com/the-worlds-largest-cargo-plane-can-swallow-a-737-whole-511093454 6) Canada Aviation and Space Museum (n.d.). "Messerschmitt Me 163B-1a Komet". Retrieved 13 May 2012. 7) "Aerostories: Arado 234, July - August 1944: no ordinary missions." Aerostories. Retrieved: 16 March 2016.

[3] Manuale tecnico catalogo nomenclatore illustrato delle parti di ricambio VELIVOLO F-104S. Psang Dain Lin and Jung-Fa Hsieh (2007): A new method to analyze spatial binary mechanisms with spherical pairs. – Journal of Mechanical Design, vol.129, pp.455-458. Reimpell J. and Betzler J. (2004): Car chassis. Basics of structures. – Warsaw: WKiŁ. Shigley J.E. and Uicker J.J. (1995).

 ISBN: 978-93-91420-02-4

A Review on Parameters of Composite Materials

A.Pavan Kumar and Shaik Chand Mabhu Subhani
Department of Mechanical Engineering, Narasaraopet Engineering College (A), Narasaraopet, Guntur, A.P, India.

***Abstract*— In the present work Taguchi method is used to optimize tensile strength and hardness of the stir casted LM 26 Al/RHA/RM hybrid composites. Taguchi's L_9 orthogonal array is used for experimental design. Overall performance of the stir casting method is improved significantly by combining the experimental and analytical concepts and the most important parameter is determined on the result response. Hybrid composites are prepared by stir casting technique using three different parameters, stirring time, stirring speed, and weight fraction of the reinforcement particles. Better parameters for highest tensile strength and hardness to the castings are predicted by Taguchi technique and then composites are prepared at these parameters. The experimental and analytical results proved that the Taguchi method was successful in predicting the parameters that give the highest properties. From analysis of variance (ANOVA) test weight fraction is the most influential parameter on the tensile strength and hardness results of castings.**

Keywords: LM 26 Al/RHA/RM hybrid Composites; Taguchi method; ANOVA; Tensile strength; Hardness.

I. INTRODUCTION

Aluminium-based composite exhibit many attractive material properties such as increased stiffness, wear resistance, specific strength and vibration damping and decreased coefficient of thermal expansion compared with the conventional aluminium alloys [Donnell and Looney (2001)]. Al–Si alloys are widely used for various automobile applications owing to their high corrosion resistance, good castability and low density [Hemanth (2005)]. Taguchi technique is a powerful tool for the design of high quality systems [Luangvaranunt *et al.* (2010); Siva Prasad and Rama Krishna (2011)].It provides a simple efficient and systematic approach to optimize design for performance, quality and cost. The methodology is valuable when design parameters are qualitative and discrete. Taguchi parameter design can optimize the performance characteristic through the setting of design parameters and reduce the sensitivity of the system performance to source of variation [Taguchi and Konishi (1997)]. Dingal *et al.* [2004] used Taguchi method to find out the significant factors influencing density, porosity and hardness on selective laser sintering of iron powder. Guharaja *et al.* [2006] made an attempt to obtain optimal settings of green sand casting parameters using Taguchi method. Rama Rao and padmanabhan [2012] used Taguchi method and ANOVA in optimization of process parameters for material removal rate in electrochemical machining of Al/5% SiC composites. Nataraj *et al.* [2005] used risk analysis Taguchi method to find optimum conditions of design parameters. Barua *et al.* [1997] used the Taguchi Method to optimize the mechanical properties of V (Vacuum) casting process. In this paper they consider the effects of the selected process parameters on the mechanical properties of alloy casting and subsequent optimal settings of the parameters, which are accomplished using Taguchi's Parameter Design Approach.

In the present study, the Taguchi method is used to obtain optimum tensile strength and hardness in the casting process of LM 26 Al/RHA/RM hybrid Composites. Finally, ANOVA and confirmation test have been conducted to validate the test result.

II. MATERIALS AND METHODS

A. Experimental work

Fabrication of LM 26 Al, rice husk ash and red mud (LM 26 Al/RHA/RM) hybrid composites were carried out by stir casting equipment as shown in Fig. 1. In the present work red mud was maintained constant at 5 wt% and rice husk ash was varied at 5, 10 and 15 wt% while preparing the hybrid composites.

Fig.1. Stir casting equipment

Based on the literature available, the experimental conditions shown in Table 1 are selected as input casting parameters to study the influence of theses parameters on tensile strength and hardness of the fabricated composites. A measured amount of LM 26 aluminium alloy was taken into a graphite crucible and melted in an electric furnace. A measured amount of RHA and RM powder was preheated at 150^0C for 20 minutes and then added to the melt. After that, the melt was stirred inside the furnace at different speed and times to make a vortex in order to disperse the particles in the melt. The melt temperature was controlled around 700^0C and poured into an EN8 steel die. The dimensions of the resulted castings are 30 mm diameter and 120mm length cylindrical rod. The fabricated composites were observed with scanning electron microscope (SEM). The SEM picture shows the uniform distribution of the RHA and RM particles in the LM 26 Al alloy as shown in Fig. 2. Tensile specimens of hybrid composites were prepared according to ASTM E-8 specification. The tensile test was performed at room temperature on a Universal Testing Machine of 10T (model Dak UTB9103). The hardness of each specimen is measured by using Vickers hardness apparatus type Zwick & Co., Germany.

TABLE I. CONTROL FACTORS AND LEVELS

ISBN: 978-93-91420-02-4

Symbol	Control factor	Level	Level	Level
A	Stirring time	6	9	12
B	Stirring speed	100	200	300
C	Weight fraction	5	10	15

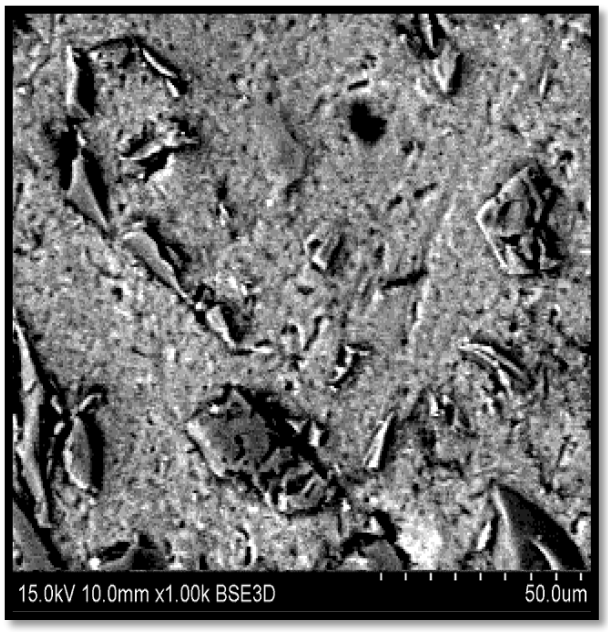

Fig. 2. SEM Picture of Hybrid AMMC

B. Methodology

In engineering analysis Taguchi methods have been utilizing for a long time for planning and conducting the experiments with the objective of acquiring data in a controlled way. The main advantage of Taguchi method is the saving of experimental time, reducing the cost, saving of effort in conducting experiments and discovering significant factors quickly. Taguchi's robust design method is a powerful tool for the design of a high-quality system. In addition to the S/N ratio, a statistical analysis of variance (ANOVA) can be employed to indicate the impact of input process parameters on output response values. The steps applied for Taguchi optimization in this study are as follows.

- Select noise and control factors
- Select Taguchi orthogonal array
- Conduct Experiments
- Measurement of responses
- Analyze results (Signal-to-noise ratio and ANOVA)
- Predict optimum performance
- Confirmation experiment

Taguchi method stresses the importance of studying the response variation using the signal – to – noise (S/N) ratio, resulting in minimization of quality characteristic variation due to uncontrollable parameter. The responses considered as the quality characteristic with the concept of "the larger-the-better". The S/N ratio used for this type response is given as:

S/N = −10×log (mean square deviation)

$$S/N = -10\log_{10}\left[\frac{1}{n}\sum\frac{1}{y^2}\right] \quad (1)$$

ANOVA is a statistically based, objective decision-making tool for detecting any differences in the average performance of groups of items tested. ANOVA helps in formally testing the significance of all main factors and their interactions by comparing the mean square against an estimate of the experimental errors at specific confidence levels. First, the total sum of squared deviations SS_T from the total mean S/N ratio n_m can be calculated as [Lindman (1992)]:

$$SS_T = \sum_{i=1}^{n}(n_i - n_m)^2 \quad (2)$$

Where n is the number of experiments in the orthogonal array and n_i is the mean S/N ratio for the i^{th} experiment. The percentage contribution P can be calculated as:

$$P = \frac{SS_d}{SS_T} \quad (3)$$

where SS_d is the sum of the squared deviations.

III. RESULTS AND DISCUSSIONS

A. S/N ratio analysis

The design matrix, tensile strength and Vickers hardness values of the LM 26 Al/RHA/RM hybrid composites prepared with different stirring speeds, stirring times and weight fraction are given in Table 2. The S/N ratio values for tensile strength and Vickers hardness are calculated by taking into consideration "Eq. 1" and presented in Table 2. The measured responses were analyzed by using a standard commercial statistical software package MINITAB 14.

TABLE II. DESIGN MATRIX AND EXPERIMENTAL OBSERVATIONS

Exp. No.	A	B	C	TS (MPa)	S/N ratio	HV (N/mm^2)	S/N ratio
1	1	50	5	158	43.97	78	37.84
2	1	150	10	175	44.86	86	38.69
3	1	250	15	185	45.34	92	39.28
4	2	50	15	188	45.48	86	38.69
5	2	150	5	199	45.98	93	39.37
6	2	250	10	164	44.30	80	38.06
7	3	50	10	211	46.49	95	39.55
8	3	150	15	168	44.51	82	38.28
9	3	250	5	182	45.20	87	38.79

The tensile strength response table for the stirring time, stirring speed and weight fraction was created in the integrated manner and the results are given in Table 3. Regardless of the category of the performance characteristics, a greater S/N value corresponds to a better performance. Therefore, the optimal level of the casting parameters is the level with the greatest S/N value. Based on the analysis of the S/N ratio, the optimal casting parameters for maximizing the tensile strength was obtained at 12 min stirring time (level 3), 100 rpm stirring speed (level 1) and 15 % weight fraction of reinforcement (level 3).

ISBN: 978-93-91420-02-4

TABLE III. S/N RATIOS OF TENSILE STRENGTH AND VICKERS HARDNESS VALUES

	Tensile strength			Vickers hardness		
Level	A	B	C	A	B	C
1	44.73	45.31	44.26	38.60	38.70	38.06
2	45.25	45.11	45.18	38.71	38.78	38.72
3	45.40	44.95	45.94	38.87	38.71	39.40
Delta	0.67	0.37	1.68	0.27	0.08	1.34
Rank	2	3	1	2	3	1

Fig. 3 shows the effect of the casting parameters on the tensile strength values. From Fig. 3 it is observed that the tensile strength of the composites increases with increase in stirring time and weight fraction of reinforced particles and decreases with increase in stirring speed.

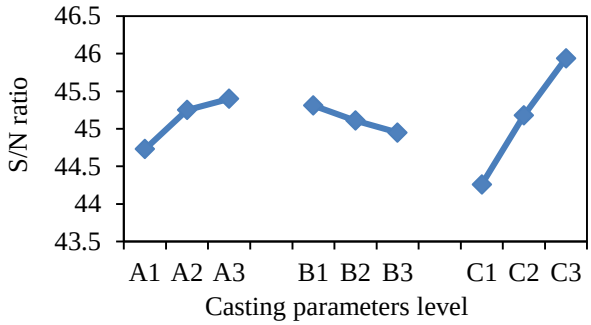

Fig. 3. Effect of casting parameters on Tensile Strength

The Vickers hardness response table for the stirring time, stirring speed and weight fraction was created in the integrated manner and the results are also given in Table 3. Based on the analysis of the S/N ratio, the optimal casting parameters for maximizing the hardness values was obtained at 12 min stirring time (level 3), 200 rpm stirring speed (level 2) and 15 % weight fraction of reinforcement (level 3). Fig. 4 shows the effect of the casting parameters on the tensile strength values.

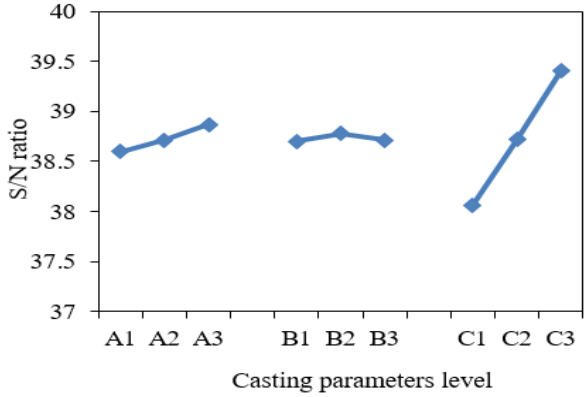

Fig. 4. Effect of casting parameters on Hardness Values

IV. ANALYSIS OF VARIANCE

ANOVA results for tensile strength are given in Table 4. The predicted R^2 of 0.99 is in reasonable agreement with the adjusted R^2 of 0.96. It can observed from Table 4 that the stirring time (A), stirring speed (B) and weight fraction of reinforced particles (C) affect the tensile strength by 14.6%, 4.9% and 79.5% in stir casting of LM 26 Al/RHA/RM hybrid composites.

TABLE IV. ANOVA RESULTS FOR TENSILE STRENGTH

Source	**DF**	**Seq SS**	**Adj SS**	**Adj MS**	**F-value**	**P-value**	**Percentage (%)**
A	2	337.56	337.56	168.78	14.75	0.064	14.6
B	2	113.56	113.56	56.78	4.96	0.168	4.9
C	2	1838.89	1838.89	919.44	80.34	0.012	79.5
Error	2	22.89	22.89	11.44			
Total	8	2312.89					

ANOVA results for Vickers hardness values are given in Table 5. The predicted R^2 of 0.9944 is in reasonable agreement with the adjusted R^2 of 0.9778. It can observed from Table 5 that the stirring time (A), stirring speed (B) and weight fraction of reinforced particles (C) affect the hardness value by 3.9%, 0.3% and 95.24% in stir casting of LM 26 Al/RHA/RM hybrid composites.

TABLE V. ANOVA RESULTS FOR VICKERS HARDNESS VALUES

Source	**DF**	**Seq SS**	**Adj SS**	**Adj MS**	**F-value**	**P-value**	**Percentage (%)**
A	2	10.889	10.889	5.444	7.00	0.125	3.9
B	2	0.889	0.889	0.444	0.57	0.636	0.3
C	2	266.889	266.889	133.444	171.57	0.006	95.24
Error	2	1.556	1.556	0.778			
Total	8	280.222					

A. Confirmation test

In Taguchi's design approach experimental confirmation test is the final step to verify the results. The optimal conditions are set for the significant factors (the insignificant factors are set at economic levels) and a selected number of experiments are run under specified cutting conditions. The confirmation experiment is a crucial step and is highly recommended by Taguchi to verify the experimental results [Ross (1996)]. In this study, a confirmation experiment was conducted by utilizing the levels of the optimal casting parameters A3B1C3 for tensile strength and A3B2C3 for hardness value in the casting of LM 26 Al/RHA/RM hybrid composites. The confirmation experiments results are given in Table 6. From Table 6 it is observed that the error between the prediction confirmation values of tensile strength and Vickers hardness is very.

TABLE VI. RESULTS OF CONFIRMATION TESTS FOR TENSILE STRENGTH AND HARDNESS VALUE

Optimal casting parameters			
Tensile strength		Hardness value	
Prediction	Confirmation	Prediction	Confirmation
A3B1C3	A3B1C3	A3B2C3	A3B2C3

ISBN: 978-93-91420-02-4

218	220	82	82

V. CONCLUSION

This work has discussed the application of the Taguchi method for investigating the effects of casting parameters on mechanical properties of LM 26 /RHA/RM hybrid composites prepared by stir casting technique. From the analysis of the results in the casting process using the conceptual signal-to-noise (S/N) ratio approach, analysis of variance (ANOVA), and Taguchi's optimization method, the following can be concluded from the present study:

- The optimum level of casting parameters to obtain good tensile strength for stir casting of L26 /RHA/RM hybrid composites are 15% weight fraction of particles, 12 min stirring time, and 100 rpm stirring speed.
- The optimum level of casting parameters to obtain good hardness for stir casting of L26 /RHA/RM hybrid composites are 15% weight fraction of particles, 12 min stirring time, 200 rpm stirring speed for hardness.
- Weight fraction of reinforced particles has the major effect on the mechanical properties of L26 /RHA/RM hybrid composites.
- Taguchi method has proved its success in prediction the optimum casting parameters to reach the best properties.

REFERENCES

[1] Barua, P.B.; Kumar, P.; Gaindhar, J.L. (1997): Optimization of mechanical properties of V-Process castings by Taguchi method. Indian Foundry Journal, 18(3), pp. 17–25.

[2] Dingal, S.; Pradhan, T.R.; Sundar, S,; Roy C.A.; Roy S.K. (2004): Experimental investigation of selective laser sintering of iron powder by application of Taguchi method. In: Proceedings of the Laser Assisted Net Shape Engineering conference LANE, Erlangen, Germany, pp. 445–456.

[3] Donnell, G.O.; Looney, L. (2001): Production of aluminium matrix composite components using conventional PM technology. Material Science Engineering A,303, pp. 292–301.

[4] Guharaja, S.; Noorulhaq, A. (2006): Optimization of green sand casting process parameters by using Taguchi's method. International Journal of Advanced Manufacturing Technology, 30(11), pp. 1040–1048.

[5] Hemanth, J. (2005): Tribological behavior of cryogenically treated B4Cp/Al-12%Si composites. Wear, 258, pp. 1732–1744.

[6] Lindman, H. (1992): Analysis of variance in experimental design, Springer-Verlag, New York.

[7] Luangvaranunt, T.; Dhadsanadhep, C.; Umeda, J.; Nisaratanaporn, E.; Kondoh, K. (2010): Aluminum-4 mass%Copper/Alumina Composites Produced from Aluminum Copper and Rice Husk Ash Silica Powders by Powder Forging. Materials Transactions, 51(4), pp. 756-761.

[8] Nataraj, M.; Arunachalam, V.P. (2005): Using risk analysis and Taguchi's method to find optimal conditions of design parameters: a case study. . International Journal of Advanced Manufacturing Technology, 27(5), pp. 445–454.

[9] Rama Rao, S.; and Padmanabhan, G. (2012): Application of Taguchi methods and ANOVA in optimization of process parameters for metal removal rate in electrochemical machining of Al/5%SiC composites, International Journal of Engineering Research and Applications, 2(3), pp. 192-197.

[10] Ross, P.J. (1996): Taguchi techniques for quality engineering, McGraw-Hill International Editions, Singapore.

[11] Siva Prasad, D.; Rama Krishna, A. (2011): Production and Mechanical Properties of A356.2 /RHA Composites. International Journal of Advanced Science and Technology, 33, pp. 51-58.

[12] Taguchi, G.; Konishi, S. (1997): Taguchi methods, orthogonal arrays and linear graphs, tools for quality engineering, Dearborn, MI: American Supplier Institute, pp. 35 – 38.

 ISBN: 978-93-91420-02-4

Optimization in WEDM of HCHCR Steel Using Taughi Method

[1]P Gopalakrishnaiah and [2]Mandula Venkaiah
[1]Department of Mechanical Engineering, PVP Siddhartha institute of Technology, Vijayawada, India,
[2]Department of Mechanical Engineering, Narasaraopet Engineering College (A), Narasaraopet, Guntur, A.P, India.

Abstract—The purpose of this study aims to obtain excellent products, consistent investigation and manufacturing process control which are the preconditions that organizations have to consider In this paper, process capability analysis was applied during wire electrical discharge machining (WEDM) to study the process performance within specific limits. The purpose of the experimentation is to identify the factors which have strong effects on the machining performance. From mean of S/N ratios for MRR, it is found that pulse-on time has highest rank '1'. Therefore, it has most significant effect on MRR. The wire feed has least effect on MRR. The order of other influencing parameters for MRR: pulse-off time, upper flush, lower flush and wire tension.

Keywords- WEDM, MRR, S/N ratios, pulse-off time, upper flush, lower flush and wire tension

I. INTRODUCTION

1.1 Evolution of EDM Process

Electrical Discharge Machining (EDM) is one of the most extensively used non-conventional material removal processes. The basis of EDM can be traced back to 1770, when English chemist Joseph Priestly discovered the erosive effect of chemical discharges or sparks. However, it was only in 1943 at Moscow University where Lazarenko and Lazarenko exploited for constructive use. They developed a controlled process for machining difficult-to-machine metals by vaporizing materials from the Surface of metal. The Lazarenko EDM system used resistance – capacitance type of power supply, which was used by EDM machine in 1950s and later served as a model for successive development in EDM.In 1980s the advent of Computer Numerical Control (CNC) in EDM brought about tremendous advances in improving the efficiency of the machining operation. CNC has facilitated total EDM, which implied an automatic and unattended machining from inserting the electrodes in the tool changer to a finished polished cavity or cavities. These growing merits of EDM have since then been intensively sought by the manufacturing industries yielding enormous benefits and generating research interests.

1.2 About Alloys and Super Alloys:

Alloys are metallic materials consisting of two or more elements combined in metals used are in the form of alloys. Such a way that they cannot be readily separated by physical means. More than 90% of family of engineering. Materials that provide a wide range of products with useful properties.

Stainless steel alloys are a combination of iron, chromium and nickel frequently modified by the presence of other elements. This family of alloys is particularly resistant to corrosion, in contrast to the rusting phenomenon that consumes ordinary steel.

Super alloys of nickel and cobalt are used in aircraft engines due to their corrosion- and heat-resistance.

Super alloys are heat-resisting alloys based on nickel, nickel-iron, or chromium that exhibit a combination of mechanical strength and resistance to surface degradation. Alloys and Super Alloys used in Aircrafts, Power Plants, Nuclear Plants, Gas turbines, Space Vehicles.

II. LITERATURE REVIEW

[1] Ms. Shalaka Kulkarni and Manik Rodge , Process Parameters Optimization In WEDM of HCHCR Steel Using Taughi Method and Utility Concept Research Scholar, Associate Professor Production Engineering Dept., SGGSIE&T, Nanded (India) international journal of mechanical engineering and technology (ijmet)

[2] Kashid D.V., S.G. Bhatwadekar ,S.B. Sangale , P.R. Kubade Investigations of Effect of Process Parameters on Material Removal Rate in Wire-cut Electrical Discharge Machining of Steel Grade EN 9.

[3] P. Abinesh1, Dr. K. Varatharajan, Dr. G. Satheesh Kumar Research Scholar, Velammal Engineering College, Chennai Optimization of Process Parameters Influencing MRR, Surface Roughness and Electrode Wear During Machining of Titanium Alloys by WEDM

III. Wire EDM Set-Up and Working

3.1 Construction of Wired:

The wire-cut EDM is a discharge machine that uses CNC movement to produce the desired contour or shape. It does not require a special shaped electrode; instead it uses a continuous-travelling vertical wire under tension as the electrode. The electrode in wire-cut EDM is about as thick as a small diameter needle whose path is controlled by the machine computer to produce the shape required.

Wire Electric Discharge Machine at Experimentation

Fig:3.1:Electric Discharge Machine

1) In wire electrical discharge machining (WEDM), also known as wire-cut EDM and wire cutting thin single-strand metal wire, usually brass, is fed through the work piece, submerged in a tank of dielectric fluid, typically de ionised water.

2) Wire-cut EDM is typically used to cut plates as thick as 300mm and to make punches, tools, and dies from hard metals that are difficult to machine with other methods. The wire, which is constantly fed from a spool, is held between upper and lower diamond guides.

 ISBN: 978-93-91420-02-4

3) The upper and lower diamond guides are usually accurate to 0.004 mm, and can have a cutting path or kerfs as small as 0.021 mm using Ø 0.02 mm wire, though the average cutting kerfs that achieves the best economic cost and machining time is 0.335 mm using Ø 0.25 brass wire.

4) The wire-cut process uses water as its dielectric fluid, controlling its resistivity and other electrical properties with filters and de-ionizer the water flushes the cut debris away from the cutting zone. Flushing is an important factor in determining the maximum feed rate for a given material thickness. Units.

5) Wire-cutting EDM is commonly used when low residual stresses are desired, because it does not require high cutting forces for removal of material.

3.2 Components in Wire EDM:

3.2.1 Dielectric Fluid	-	Di Ionized Water
3.2.2 Electrode Material	-	Tool electrode(Cathode) Work Piece (Anode)
3.2.3 Wire	-	Brass
3.2.4 Power Supply	-	Direct Power Supply
Range	-	20,000HZ - 30,000HZ

3.3 Working Principle Of Wired

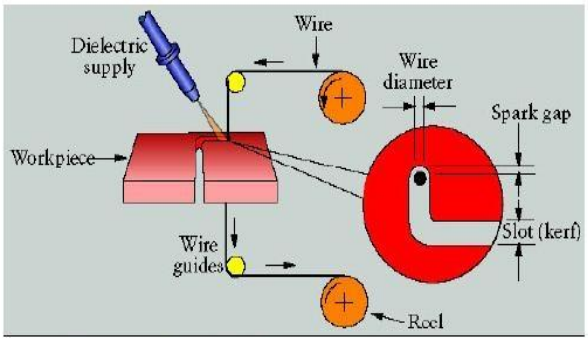

Fig:3.2:**Working Principle Of Wired**

Wire EDM machining (also known as "spark EDM") works by creating an electrical discharge between the wire or electrode and the work piece. As the spark jumps across the gap, material is removed from both the work piece and the electrode. To stop the sparking .Process from shorting out, a non-conductive fluid or dielectric is also applied. The waste material is removed by the dielectric, and the process continues. The wire-cut process uses de-ionized water as its dielectric fluid, controlling its resistivity and other electrical properties with filters and de-ionizer units. The water flushes the cut debris away from the cutting zone.

Wire EDM Set-Up at Experimentation

Flushing is an important factor in determining the maximum feed rate for a given material thickness. Wire-cutting EDM is commonly used when low residual stresses are desired, because it does not require high cutting forces for removal of material. If the energy/power per pulse is relatively low (as in finishing operations), little change in the mechanical properties of a material is expected due to these low residual stresses, although material that hasn't been stress-relieved can distort in the machining process.

3.4 Part Programming

Fig:3.3:**Part Programming**

Wire EDM Programming Set-up at Experimentation

The geometry of the profile and the motion of wire electrode tool along the profile is fed to the part programming system through key board, in terms of various definitions of points, lines and circles as the tool path element, in a totally menu driven, conversational mode. The wire compensation and taper gradient can be

Specified for each path element separately. After the profile is fed to the computer, all the numerical information about the path is calculated automatically and its printout is generated. The entered profile can be verified on the graphic display screen. After successful profile definition, it is recorded by the computer which is then put in the generator for execution of the program.

The wire, which is constantly fed from a spool, is held between upper and lower diamond guides. The guides, usually CNC-controlled, **move in the x–y plane**.

On most machines, the upper guide can also **move independently in the z–u–v axis,** giving rise to the ability to cut tapered and transitioning shapes.

The upper guide can **control axis movements in x–y–u–v–i–j–k–l–.** This allows the wire-cut EDM to be programmed to cut very intricate and delicate shapes.

In Above Figure

X - Represents movements in X- axis
Y - Represents movement in Y –axis
U - Taper Along X- axis
V - Taper along Y-axis

Voltage and Current readings are set by using adjustments available at Board of Wire EDM

X-axis and Y-axis and Taper Angles are set by using adjustments provided at keyboard

3.5 The Set-up by Set-up Wired Process

ISBN: 978-93-91420-02-4

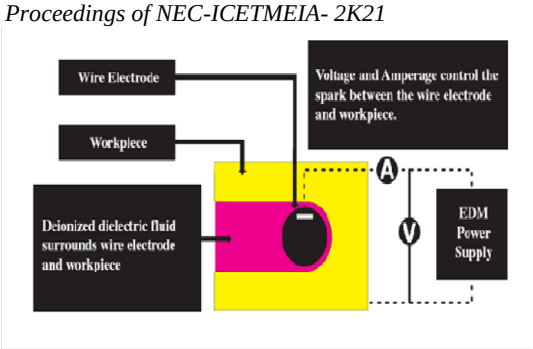

Fig:3.4:The Set-up by Set-up Wired Process

During one time controlled spark erodes material:
the demonized water surrounding the wire electrode as the power supply generates volts and amps to produce the spark. the process during pulse on time where the spark erodes the material by melting and vaporizing it.

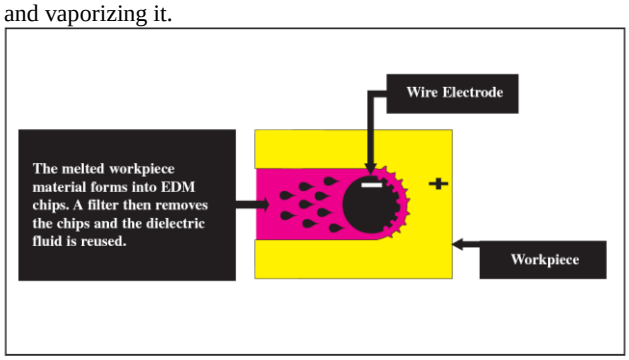

Fig:3.5: **spark erodes material**

3.6 Process Parameters Of Wired

3.6.1 Dielectric pressure

Flushing is important in the process to achieve a stable machining condition. The pressure with which the coolant strikes the inter-electrode gap is determined in two levels- high and low. The flushing pressure is determined according to the material. For machining High Carbon High Chromium, high flushing pressure is recommended

3.6.2 Pulse time On (Ton)

Pulse on time is the period for which the voltage is applied across the gap. It is denoted by TON. The range of pulse on time is **1 to 10**, in steps of 1. Higher the TON setting larger is the pulse on period. The single pulse discharge energy increases with increasing TON period, resulting in higher cutting rate and poor surface finish. Higher Value discharge leads to Wire Breakage.

3.6.2 Pulse time Off (T off)

Pulse off time is the period for which voltage across the gap is absent. It is denoted by TOFF. The range of pulse off time is **1 to 10**, in steps of 1. Higher the TOFF setting larger is the pulse off period. This results in better surface finish.

3.6.3 Wire Tension

Wire tension is a gram-equivalent load with which the continuously fed wire is kept under tension so that it remains straight between the wire guides. Wire tension can be adjusted by the wheel provided on machine
Column. While the wire is being fed continuously, appropriate wire tension prevents the undesirable wire deflection from its straight path. The wire deflection is caused due to spark induced reaction forces and water pressure brass wire of 0.25mm diameter can be applied with a maximum tension of 1000gm. Optimum wire tension results in high MRR and low surface roughness

3.6.4 Wire Feed Rate:

Wire Feed is the rate Wire electrode travel along the wire guide path and it is fed continuously for Sparking. The wire feed range available for the present Wired is **1-10m/min,** it is always set the maximum wire feed rate this will be result less wire breakage and good machinability.

3.6.5 Gap Voltage:

Gap voltage is the potential difference across the work piece and wire electrode. It is read directly on the voltmeter. Gap voltage depends on the set values of gap potentiometer and sensitivity potentiometer. High gap voltage gives poor finish.
Ranges are **0-120V**

3.6.6 Average Gap Current:

Gap current is the actual current consumed by the machining process. Its value is read on the ammeter directly. The values of average machining current given in the guidelines charts are indicative and differ with machines. Normally the wire can pass current of **4-6Amps** in water. Since air bubbles are mixed in water only75% of the value may be achievable. High gap currents results in high MRR and vivo for Ra

3.6.8 Metal Removal Rate (MRR)

Maximum of MRR is an important indicator of the efficiency and cost effectiveness of the WEDM process, however increasing MRR is not always desirable for all applications since this may scarify the surface integrity of the work piece. A rough surface finish is the outcome of fast removal rates.

3.6.9 Uses and Applications Of Wired

EDM can easily machine parts with very thin walls, complex geometry, narrow slots, small corner radii, very small features, etc. with virtually no mechanical stress.
EDM can cut hardened steel, titanium, Income and other difficult materials without the limitations of traditional machining.
EDM can achieve an excellent surface finish with no burrs right out of the machine.
EDM can reduce production costs with stacked parts machining using wire EDM as well as multi-up featuring for wire, sinker and hole pop EDM.
Use EDM over broaching for better precision, accuracy and finish, no need to make a custom broach, and no risk of introducing unwanted debris into the finished part.
Wire EDM is Used for Modern Tooling Applications. Advance Ceramic Materials, Modern Composite Materials

IV. WORK PIECE MATERIAL

"HIGH CARBON HIGH CHROMIUM-D3 STEEL"

4.1 HCHCR-D3 STEEL

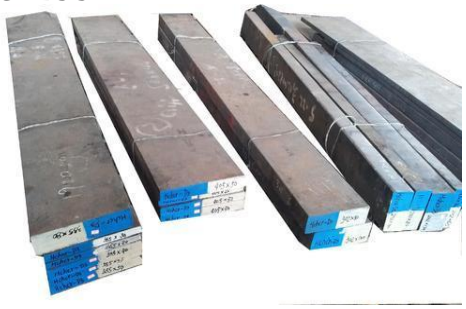

Fig:3.6: HIGH CARBON HIGH CHROMIUM-D3 STEEL

ISBN: 978-93-91420-02-4

4.1 HCHCR-D3 STEEL:

Tool steel refers to a variety of carbon and alloy steels that are particularly well-suited to be made into tools. Their suitability comes from their distinctive hardness, resistance to abrasion and deformation and their ability to hold a cutting edge at elevated temperatures. As a result, tool steels are suited for their use in the shaping of other materials. With carbon content between 0.5% and 1.5%, tool steels are manufactured under carefully controlled conditions to produce the required quality. The presence of carbides in their matrix plays the dominant role in the qualities of tool steel. The four major alloying elements in tool steel that form carbides are: tungsten, chromium, vanadium and molybdenum. The rate of dissolution of the different carbides into the austenite form of the iron determines the high temperature performance of steel (slower is better, making for a heat resistant steel). Proper heat treatment of these steels is important for adequate performance.[1] The manganese content is often kept low to minimize the possibility of cracking during water quenching.

4.2 Size and Dimension

Table1.1: Specimen: 1

Specimen specification: - **80*70*20 (mm)**

Thickness :-**20mm**

L=length=80mm, B=Breadth=70mm, T=thickness=20mm

Specimen: 2

Specimen specification: - **80*70*15 (mm)**

Thickness :-**15mm**

L=length=80mm,B=Breadth=70mm, T=thickness=15mm

4.3 Composition of HCHCR-D3 Steel:

Cold-work tool steels which include D2, D3, D4, D5, and D7 steels are high-carbon, high-chromium steels. Apart from D3 steel all group D steels have 1% Mo and are air hardened. Type D3 steel is oil-quenched; though small sections can be gas quenched after austenitization using vacuum. As a result, tools made with type D3 steel tend to be brittle during hardening. Type D2 steel is the most commonly used steel among the group D steels. The D3 steels contain 1.5 to 2.35% of carbon and 12% of chromium.

Table1.2: Chemical Composition:

ELEMENT	PERSENTAGE
Carbon, (C)	**2.0**
Manganese , (Man)	**0.3**
Silicon ,(Si)	**0.3**
Nickel ,(Ni)	**0.3**
Molybdenum ,(Mo)	**1.0**
Chromium, (Cr)	**12**
Iron	**84.1**

4.3 Properties of HCHCR-D3 Steel:

Table1.3:Properties of HCHCR-D3 Steel

Properties	Metric	Imperial
Density	**7.7 × 1000 kg/m3**	**0.278 lb/ inch3**
Melting Point	**1421 .C**	**2590 .F**

4.3.2 Chemical Properties

Tempering:

The D3 tool steel should be cooled to room temperature and should be tempered immediately. The parts should be placed in the tempering furnace and increased slowly to the desired tempering temperature. Tempering for 1 hour per inch of thickness is required

.C	150	200	250	300	350	400
HRC	**64/63**	**63/ 61**	**62/ 60**	**61/ 60**	**60/ 59**	**59/58**

V. EXPERIMENTATION

5.1 Signal to Noise

Traditionally a designed experiment can be used to estimate or test the significance of certain factors on the basis of a measurable response over a set of experimental conditions. Taguchi emphasized that in addition to this, the variation of the experimental data needs to be studied. In order to facilitate this study he used the concept of a signal-to-noise ratio. The simplest form of signal-to-noise ratio (S/N) is the ratio of the mean (signal) to the standard deviation (noise).

Properties	Metric	Imperial
Poisson's Ratio	**0.27 - 0.3**	**0.27 - 0.3**
Elastic modulus	**190-210 Gap**	**27557-30457 ski**
IPod impact unmatched	**28.0 J**	**20.7 ft-lb**
Thermal expansion	**12 x 10-6/°C 20-100**	**----------**
Hardness	**58-64 HRC**	**58-64 HRC**
Stress	**Max:3.4837 N/m2**	**Min:598.23 N/m2**
Tensile Strength	**950 N/mm²**	**----------**
Yield Stress	**650 N/mm²**	**----------**

$$\text{Type 1 : } S/N_{LB} = -10 \log_{10}[\sum Y_{ij}^2/n]$$

$$\text{Type 2 : } S/N_{HB} = -10 \log_{10}[(1/n)\,(\sum 1/ Y_{ij}^2)]$$

Where

Yak is the value of the response 'j' in the it experiment condition, with I=1, 2, 3, n; j = 1, 2…k.

5.2 Taguchi Method

Gnocchi Taguchi, an international consultant in the field of total quality control and assurance formulated both a philosophy and a methodology for the process of quality improvement that depends on statistical concepts, especially statistically designed experiments. Taguchi defined quality as the loss imparted to the society from the time a product is shipped to the market. The primary goals of the tag chi methodology

Can be described as:

1. A reduction in the variation of a product design to improve quality and lower the loss Imparted to society.

ISBN: 978-93-91420-02-4

2. A proper product or process implementation strategy which can further reduce the level of variation.

5.3 Orthogonal Array

Orthogonal arrays are highly fractional orthogonal designs proposed by Dr. Gnocchi Taguchi, a Japanese industrialist. These designs can be used to not only applicable to two level factorial experiments.

It can investigate main effects when factors have more than two levels. Designs are also available to investigate main effects for certain mixed level experiments where the factors included do not have the same number of levels

5.4 Total Experiments and values

Expand	Voltage (volts)	Ton (µs)	Toff (µs)	M/C Speed (mm/min)	Time taken (min)
1	58	4	7	0.90	26
2	58	5	6	0.60	26
3	58	6	5	0.85	24
4	59	4	6	0.82	24
5	59	5	7	0.70	23
6	59	6	5	0.83	25
7	60	4	5	0.70	22
8	60	5	7	0.70	20
9	60	6	6	0.90	18

Specimen: 1- 20mm (t)

Experiment No: 1 for (20 mm thickness :)
Specimen specification: - **80*70*20 (mm)**
Thickness :-**20mm**
Shape of cut: -L shape in 10*10 (mm)
Type of cut : - **Rough Cut**
Machining parameters and their levels
Total 9 experimental values for specimen: 1(20 mm t)
OA with assigned values of control Factors

	Parameter	Unit	Level-1	Level -2	Level-3
A	Voltage	Volts	58	59	60
B	Pulse time On	µs	4	5	6
C	Pulse time Off	µs	5	6	7
D	Peak Current	Amps	2	2	2

Voltage	58 Volts
Current	2 Amps
M/C speed	0.75 mm/min
Ton	4
Tuff	5
Tuff 1	5
Spool Wire Pass Speed	1
Wire Tension	1000
Time taken to cut the L-shape(10*10)	26 minutes
Weight of Specimen before cutting	890 grams
Weight of Specimen after cutting	735.9 grams

Total 9 experimental values for specimen: 1(20 mm t)
OA with assigned values of control Factors

Expand	Voltage (volts)	Ton (µs)	Toff (µs)	M/C Speed (mm/min)	Time taken (min)
1	58	4	7	0.90	26
2	58	5	6	0.60	26
3	58	6	5	0.85	24
4	59	4	6	0.82	24
5	59	5	7	0.70	23
6	59	6	5	0.83	25
7	60	4	5	0.70	22
8	60	5	7	0.70	20
9	60	6	6	0.90	18

Exp	Code	Ton	Toff
1	1	1	3
2	1	2	2
3	1	3	1
4	2	1	2
5	2	2	1
6	2	3	3
7	3	1	1
8	3	2	3
9	3	3	2

Specimen: 2- 15mm (t)
Experiment No: 2 for (15 mm thickness :)
Specimen specification: - **80*70*15 (mm)**
Thickness :-**15mm**
Shape of cut: -L shape in 10*10 (mm)
Type of cut : - **Rough Cut**
Reference Orthogonal Array
Machining parameters and their levels

Total 9 experimental values for specimen: 2 (15 mm t) OA with assigned values of control Facto

NO	Voltage (volts)	Ton (µs)	T0ff (µs)	M/C Speed (mm/min)	Time taken (min)
1	58	4	7	0.60	26
2	58	5	6	0.66	25
3	58	6	5	0.71	24
4	59	4	6	0.74	24
5	59	5	7	0.79	23
6	59	6	5	0.83	21
7	60	4	5	0.85	22
8	60	5	7	0.79	20
9	60	6	6	0.80	20

Voltage	59 Volts
Current	2 Amps
M/C speed	0.85 mm/min
Ton	6
Tuff	6
Tuff 1	6
Spool Wire Pass Speed	1
Wire Tension	1000
Time taken to cut the L-shape(10*10)	21 minutes
Weight of Specimen before cutting	680 grams
Weight of Specimen after cutting	668.9 grams

ISBN: 978-93-91420-02-4

SL.No	Voltage (volts)	Ton (µs)	T0ff (µs)	M/C Speed (mm/min)	Time taken (min)
1	58	4	7	0.60	26
2	58	5	6	0.66	25
3	58	6	5	0.71	24
4	59	4	6	0.74	24
5	59	5	7	0.79	23
6	59	6	5	0.83	21
7	60	4	5	0.85	22
8	60	5	7	0.79	20
9	60	6	6	0.80	20

VI. RESULTS AND DISCUSSION

6.1 Calculation MRR for Experiments

Specimen No: 1 for (20 mm thickness :)

Weight of the Specimen **before** cutting--------**890 grams**

Weight of the Specimen **after** cutting----------**753.3 grams**

MRR =

$$\frac{\textit{Weight Of The Material Before Cutting} - \textit{Weight Of Material After Cutting}}{\textit{Time taken To utting}}$$

Exp:1, :MRR = $\frac{890-874.9}{26}$ = 0.580 g/min

Exp:2 :MRR = $\frac{874.9-859.7}{26}$ = 0.584 g/min

Exp:3 :MRR = $\frac{859.7-844.5}{24}$ = 0.633 g/min

Exp:4 :MRR = $\frac{844.5-829.4}{24}$ = 0.629 g/min

Exp:5 :MRR = $\frac{829.4-814.1}{23}$ = 0.665 g/min

Exp:6 :MRR = $\frac{814.1-798.7}{25}$ = 0.616 g/min

Exp:7 :MRR = $\frac{798.7-783.6}{22}$ = 0.686 g/min

Exp:8 :MRR = $\frac{783.6-768.4}{20}$ = 0.760 g/min

Exp:9 :MRR = $\frac{768.4-753.3}{18}$ = 0.838 g/min

Orthogonal Array with Response

Exp	Voltage (volts)	Ton (µs)	Toff (µs)	MRR (g/min)
1	58	4	7	0.580
2	58	5	6	0.584
3	58	6	5	0.633
4	59	4	6	0.629
5	59	5	7	0.665
6	59	6	5	0.616
7	60	4	5	0.686
8	60	5	7	0.760
9	60	6	6	0.838

ANOVA

General Linear Model: MRR (grm/min versus VOLTAGE (VOL, Ton (Micro S, ...

Factor	Type	Levels	Values
VOLTAGE (VOLTS)	fixed	3	1, 2, 3
Ton (Micro Seconds)	fixed	3	1, 2, 3
Toff (Micro Seconds)	fixed	3	1, 2, 3

Source	DF	Seq SS	Adj SS	Adj MS	F	P
VOLTAGE	2	0.043915	0.043915	0.021957	7.05	0.124
Ton	2	0.006158	0.006158	0.003079	0.99	0.503
Toff	2	0.001698	0.001698	0.000848	0.27	0.786
Error	2	0.006230	0.006230	0.003115		
Total	8	0.058000				

S = 0.0558102 R-Sq = 89.26% R-Sq(adj) = 57.04%

Mathematical model using multiple regression analysis Fitted line flot

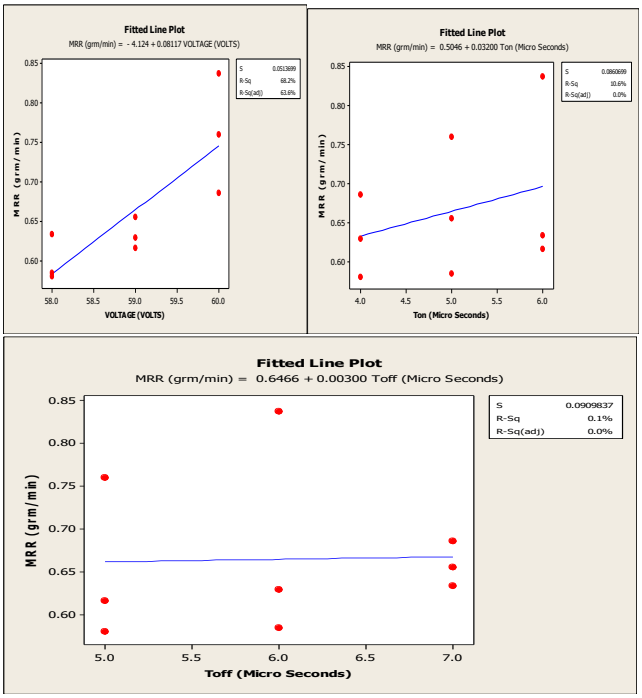

$$MRR = A*(X)^{a}*(Y)^{b}*(Z)^{c}$$

$$\log(MRR) = \log(A) + a\log(X) + b*\log(Y) + c*\log(Z)$$

VII. CONCLUSION

The purpose of the experimentation is to identify the factors which have strong effects on the machining performance. From mean of S/N ratios (Table 5) for MRR, it is found that pulse-on time has highest rank '1'. Therefore, it has most significant effect on MRR. The wire feed has least effect on MRR. The order of other influencing parameters for MRR: pulse-off time, upper flush, lower flush and wire tension.

Optimum Voltage: volts when voltage range between 58-60

Optimum Ton: 6 microseconds when ton range between 4-6

Optimum Toff: 6 microseconds when toff range between 4-6

Obtained highest MRR:" 0.838 g/min at voltage-60volts, ton-6 microseconds, toff -6 microseconds,"

Signal –To- Noice Ratio: Larger Is Better

 ISBN: 978-93-91420-02-4

Current: 2Amps

At Above Ranges we get the Optimum Metal Removal Rate for High Carbon High Chromium D3- Steel

REFERENCES

[1] R.Nagaraja, K.Chandrasekaran, S.Shenbhgaraj Assistant Professor, Department of Mechanical Engineering, Nadar Saraswathi College of Engineering and Technology, Theni, Tamilnadu, India. International journal of engineering sciences & research technology optimization of parameter for metal matrix composite in wire edm

[2] Kaladhar M., Subbaiah K. V., Ch. SrinivasaRao and NarayanaRao K., 'Application of Taguchi approach and Utility Concept in solving the Multi-objective Problem when turning AISI 202 Austenitic Stainless Steel', Journal of Engineering Science and Technology Review 4 (1) (2011) 55-61

[3] Ms. Shalaka Kulkarni and ManikRodge , Process Parameters Optimisation In WEDM of HCHCR Steel Using Taughi Method and Utility Concept Research Scholar, Associate Professor Production Engineering Dept., SGGSIE&T, Nanded (India) international journal of mechanical engineering and technology (ijmet)

[4] Manoj Malik, Rakesh Kumar Yadav, Nitesh Kumar, Deepak Sharma, Manoj, 'Optimization of process parameters of wire EDM using zinc-coated brass wire', International Journal of Advanced Technology.

 ISBN: 978-93-91420-02-4

Automated Pneumatic Sheet Metal Cutting Machine

Venkateswarlu Sampathi, Kiran Chand Kopila and Kadru John Babu
Department of Mechanical Engineering., SKN Sinhgad Institute of Technology & Science (SKNSITS)
Savitribai pune university, pune, India
[2]Department of Mechanical Engineering, Narasaraopet Engineering College (A), Narasaraopet, Guntur, A.P, India.

***Abstract*—One of the major challenges in innovating manufacturing process is to make an equipment or system affordable and as well as compatible for small industries and large scale businesses. Already existing traditional machinery is bulky and expensive which small scale industries can neither accommodate and nor can afford. Traditional machinery requires large capital investment and work force. This machineries have some basic flaws like to increase the production you either need more machines or skilled work force (or both). In this paper, we propose a small but efficient pneumatic metal cutting machines that can be automated using simple microcontrollers. Our machines uses simple fabrication and easily available but good quality parts which makes or machinery efficient and easily affordable for small industries or home based businesses.**

Keywords—Automated, Pneumatic, Sheet metal cutting machine.

I.INTRODUCTION

Today is world is more practical and thinks more of cost reduction, so the punching process for sheet-metal has to be done in economical way of operation, easier implementation for mass- production, as well as greater control on the other technical parameters. In most of the sheet metal operations punching is the main operation in the process sequence. Automating this operation results in reduced time and also can reduce human effort. Automation is a process in which combination of mechanical work, electronic work is carried out. Automation systems to operate and control production with help of computer and commanding software. The reason for automating this process may be to reduce manufacturing lead time, to increase labor productivity or to improve the worker safe. In these unit high-pressure air is used to move piston with required pressure and piston consist of punch with modified design to punch sheet metal into required shape and size. Thin and flat pieces of sheet metal are then obtained. It is one of the fundamental forms used in metal working and can be cut and bent into variety of different shapes. Sheet metals are available in flat pieces or as a coiled strip. Sheet metals has wide range of applications in car bodies, airplane wings, medical tables, roofs of buildings and many other things.

PROBLEM STATEMENT

In traditional pneumatic punching machine all operation is controlled manually and due to this the production rate is reduced and due to this the accuracy of the product may be reduced. In traditional pneumatic punching machine, the lot of time is wasted in to change the setting of the machine for new pitch distance. To overcome the above problem then the solution is to use the CNC Punching machine but the cost of the CNC Punching is high and the small-scale industries cannot afford the cost of the CNC Machine

II.LITERATURE REVIEW

A lot of researchers have worked on pneumatic sys-tems as well as on sheet metal experiments. The work done by various authors are explained below.Pneumatics was first documented by Hero of Alexan-dria in 60 A.D., but the concept had existed before then .Vallance and Matlock (1992) studied the friction be-havior of zinc-based coated sheet steels and laboratory scale friction analysis techniques that involve sheet sliding over cylindrical dies.Sanchez et al. (1999) has focused on systematic analy-sis of testing equipment as a measurement system of the friction phenomenon on sheet metal under plain strain. It has also provided experimental reference in order to optimize the usage of sheet metal and lubricants. Mutoh et al. proposed that the exhaust pressure of the cylinder hold middle level is 0.2-0.5 MPa. If the ex-haust flow is used effectively, losses can be reduced in pneumatic systems. If the exhaust pressure is set near 0.2 MPa, it reduces the losses by 15% of total con-sumption .

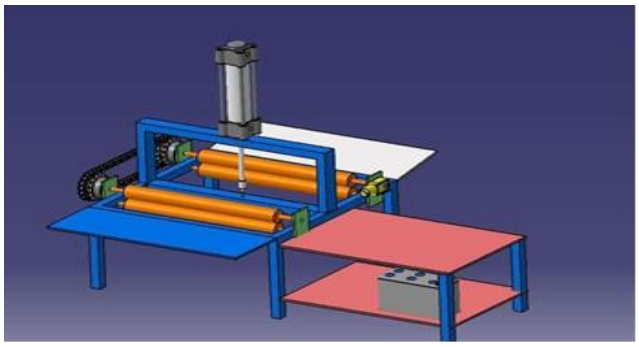

A. WORKING PRINCIPLE:

The sheet metal will be fed through feed rollers. The gear arrangement on the rollers is meshed with the DC motor, which feeds the sheet. The inductive proximity switch/sensor will be used, it detects the metal sheet and also records the sheet length as the sheet passes over it. After detection, these information are sent as a input to the microcontroller circuit containing series of relays. The microcontroller carries out the computations according to the coding done on it.

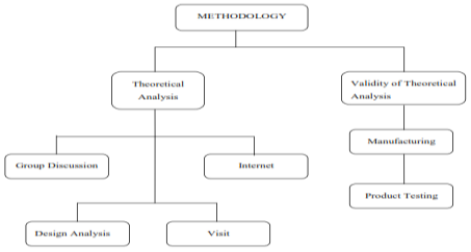

Fig 1: Flowchart of methodology

ISBN: 978-93-91420-02-4

III.DESIGN OF MACHINE

In our attempt to design a special purpose machine we have adopted a very careful approach, the total design work has been divided into two parts mainly;

- System design
- Mechanical design

System design mainly concerns with the various physical constraints and ergonomics, space requirements, arrangement of various components on the main frame of machine no of controls position of these controls ease of maintenance scope of further improvement; height of m/c from ground etc.

In Mechanical design the components are categories in two parts.

1. Design parts
2. Parts to be purchased.

For design parts detail design is done and dimensions thus obtained are compared to next highest dimension which are readily available in market this simplifies the assembly as well as post production servicing work. The various tolerances on work pieces are specified in the manufacturing drawings. The process charts are prepared & passed on to the manufacturing stage .The parts are to be purchased directly are specified &selected from standard catalogues. Methodology can properly refer to the theoretical analysis of the methods appropriate to a field of study or to the body of methods and principles particular to a branch of knowledge. In this chapter, it talks about the methods used to gather information in order to finish the research. It was involve the process flow of every step in archive the objective of this project. There are many methods use in this project such as internet references, interviewing lecturers and technicians and the most important is group discussion.

IV. Material selection & methodology

The proper selection of material for the different part of a machine is the main objective. In the fabrication of machine. For a design engineer it is must that he be familiar with the effect, which the manufacturing process and heat treatment have on the properties of materials. The Choice of material for engineering purposes depends upon the following factors:

1. Availability of the materials.
2. Suitability of materials for the working condition in service.
3. The cost of materials.
4. Physical and chemical properties of material.
5. Mechanical properties of material

Selection of the material depends upon factor of safety, which in turn depends upon the following factors.

1. Reliabilities of properties
2. Reliability of applied load
3. The certainty as to exact mode of failure
4. The extent of simplifying assumptions
5. The extent of initial stresses set up during manufacturing
6. The extent loss of life if failure occurs

Methodology of Design & Analysis:

A parameter study is done to evaluate the most crucial parameters for FE analysis of axial ball bearings. The parameters that are evaluated are mesh density, contact stiffness, osculation, load level, geometrical nonlinearity and material nonlinearity. The studies are performed by means of the FE software Ansys. The accuracy of finite element analysis depends on different parameters such as element type, boundary condition and how the loads are applied etc. Therefore the FE model is nothing else but an approximate realization of the reality. The parameter study can be

Done by physical tests. However it will increase the cost, time and resources consumed and therefore FE analysis is more suitable choice, at least for parameter evaluation

Selection of Bearing

Spindle bearing will be subjected to purely medium radial loads; hence we shall use ball bearings for our application.

I S I No.	Bearing B No.	d	D1	D	D2
20 BC02	6000z	10	10	26	24

$P = X F + Y F a$

For our application $F a = o$

$P = X F r$

Where $F r = 204.5$ N

As; $F r < e \rightarrow X = 1$

$P = F r$

Max radial load = $F r = 204.5$ N

$P = 204.5$ N

Calculation dynamic load capacity of bearing

$L = (C) p$ where $p = 3$ for ball bearings

When P for ball Bearing

For m/c used for eight hr of service per day;

$L h = 12000- 20000$ hr

But; $L = 60 n L h$

$L = 600$ mrev

Now; $600 = (C) 3$

$= (204.5)3$

$C = 1724.8$ N

As the required dynamic capacity of bearing is less than the rated dynamic capacity of bearing;

Bearing is safe.

A. PART NAME: MAIN SHAFT

Part weight – 1.5 kg

Part material – C30

Part quantity – 1

Part size – 30 x 16x 320 mm.

Sr. No.	Operation	Machine	Tool	Time
1	Cutting the material as per our required size.	Power Hacksaw	Hacksaw Blade	10 min
2	Turning both side and make dia14mm	Lathe machine	turning tool	10 min
3	Drilling at center 10mm hole	Lathe machine	Drilling Bit 10mm	10

ISBN: 978-93-91420-02-4

DESIGN CALCULATIONS

Press force = cutting force + stripping force
Sample Calculation for Aluminum Sheet
Here is a sample calculation to calculate the punching force required for different thickness of aluminum sheet.
• Perimeter, L =31.41 mm. (For D = 10mm)
• If Sheet thickness, t = 1mm.
• Maximum tensile strength of aluminum, Tmax = 180 N/mm2
• Total cutting force = L x t x Tmax
= 31.41 × 1 × 180
= 5654.86 N
• Stripping force = 15% of the cutting force
= 848.229 N
• Press force = Cutting force + Stripping force
= 5654.86 N + 1350 N
= 6503 N

REDUCED PUNCH FORCE CALCULATIONS

Force required is reduced which can be seen by the formula,
F=Fmax.K.tK.t+1
Where,
F= Reduced force after providing shear in Newton (N)
Fmax= Maximum force required to punch the sheet of thickness t in Newton (N)
K= Percentage Penetration
t= Thickness of sheet in mm
I= Amount of shear given to the tool (in terms of t) in mm
Aluminum Sheet
1) For I=t/5 & K=0.6 F=0.75Fmax
2) For I=t/4 & K=0.6 F=0.705Fmax
3) For I=t/3 & K=0.6 F=0.643Fmax
4) For I=t/2 & K=0.6 F=0.545Fmax
5) For I=t/1 & K=0.6 F=0.375Fmax
We are taking selecting empirical relation as,
F=0.375Fmax
Therefore, I = t/1 and K = 0.6 and F= 0.375Fmax
Therefore, F = 0.375 X 6503 N
F = 2500 N
Therefore reduced force after giving shear to the punch is 2500 N.
We are selecting the punching force range from 2000N – 2500N.
2.2.3 Pneumatic Cylinder Calculations
• For Double Acting Cylinder
• For Extension Stroke (Working Stroke)
• F = P x A
Where, F = Punching Force
P = Working Pressure
A = Area of the cylinder
Therefore, 2500 = (12 x 10^5) x (π/4 x D^2)
D = 25mm

V CONCLUSION

1. By using modified die and punch we reduced punching force.
2. By automation using micro-controller we reduce the time required for setup of pitch distance.
3. Due to automation we successfully increase accuracy and productivity of machine by reducing time required to process metal sheet from 1-1.5 min to 10 sec.
4. By our this project we successfully made a machine which is affordable as well as compatible for small scale businesses under 10 to 12 thousands.

REFERENCES

[1] Aniruddha Kulkarni, Mangesh Pawar, “Sheet Metal Bending Machine”, International Journal of Engineering Re-search and Technology, Vol. 2, March 2015.
[2] Adithya Polapragada A.S, K.Srivarsha, “Pneumatic Auto Feed Punching, Cutting and Riveting machine”, International Journal of Engineering Research and Technology, Vol.1, Sep-tember 2012.
[3] Dinesh Lamse, Akash Navghane, Rahul Chavhan, Ajay Ma-hawadiwar, “Design and Fabrication of Pneumatic Sheet Metal Cutting and Sheet Metal Bending Machine”, International Research Journal of Engineering and Technology, Vol. 4, March 2017.
[4] Paul.Degarmo .E, “Shearing in metal cutting”, Materials and Processes in Manufacturing, Eight edition, 2003, p. 518-528.
[5] Karthikumar K , K.V.S.S. Saikiran, Jakkoju Satish, “Pneumatic Sheet Metal Cutting Machine”, International Journal and Magazine of Engineering and Technology, Management, Research”, Vol. 3, March 2016

 ISBN: 978-93-91420-02-4

Cylindrical Panel's Numerical and Analytical Investigations Subjected to Different Loads

KLN Murthy and L.Vijay
Department of Mechanical Engineering, Eswar College of engineering, Narasaraopet, Andhra Pradesh.

Abstract: **The weight reduction of the cylindrical panel can have a certain role in the general weight reduction of the vehicle and is a highly desirable goal. Substituting composite structures for conventional metallic structures has many advantages because of higher specific stiffness and strength of composite materials. The materials used for these analyses are composite materials. Static & linear layer analysis to determine the deformation, stress of the cylindrical panel, modal analysis to determine the natural frequency and deformation for mode shapes. And we are using layer stacking method for 3, 5 and 7 layers for analysis of steel, E-glass polyester and glass fiber reinforced plastic material.**
3D modelled by using the software CREO and analysis done in ANSYS software.

Keywords: panel and cylindrical panel, CREO, ANSYS.

1. INTRODUCTION
CYLINDRICAL PANEL

The eigen frequencies and eigen modes of a skinny isotropic cylindrical panel are calculated. The purpose of the analysis is to study the performance of the MITC shell elements mixed to factor mass factors (PMASS).

The panel is supported with four springs connected to the corners of the plate. Thus, the panel isn't always completely restrained and a shift of one. Zero must be applied with a view to be capable of clear up the eigenvalue problem. Curved panel model: Mesh includes 10 by 14 Q4 factors or five by means of 7 Q8/Q9 factors.

A Composite fabric (additionally called a composition fabric or shortened to composite, that's the commonplace call) is a cloth crafted from two or extra constituent substances with considerably one of a kind physical or chemical houses that, whilst mixed, produce a material with characteristics extraordinary from the person components. The man or woman components stay separate and wonderful in the completed shape. The new material can be desired for lots motives: not unusual examples encompass substances which might be stronger, lighter, or much less highly-priced whilst in comparison to standard substances. More recently, researchers have additionally all started to actively include sensing, actuation, computation and verbal exchange into composites, which might be referred to as Robotic Materials.

Typical engineered composite substances consist of:

•mortars, concrete
•Reinforced plastics, together with fiber-reinforced polymer
•Metal composites
•Ceramic composites (composite ceramic and metallic matrices)

Composite substances are typically used for buildings, bridges, and structures inclusive of boat hulls, swimming pool panels, race vehicle bodies, bathe stalls, bathtubs, storage tanks, imitation granite and cultured marble sinks and countertops. The maximum advanced examples carry out mechanically on spacecraft and aircraft in worrying environments.

1.1 HISTORY

The earliest guy-made composite materials were straw and dust mixed to form bricks for building production. Ancient brick-making was documented through Egyptian tomb art work.

Wattle and daub is one of the oldest man-made composite substances, at over 6000 years antique.[2] Concrete is also a composite cloth, and is used more than any other guy-made fabric within the international. As of 2006, about 7.Five billion cubic metres of concrete are made every year multiple cubic metre for every person on Earth.

II. LITERATURE SURVEY

Vibration Analysis of Cylindrical Sandwich Aluminum Shell with Viscoelastic Damping Treatment

This paper has implemented the constrained viscoelastic layer damping remedies to a cylindrical aluminum shell the usage of layer wise displacement theory. The transverse shear, the everyday lines, and the curved geometry are precisely taken under consideration in the gift layer wise shell version, that could depict the zig-zag in-aircraft and out-of-aircraft displacements. The damped natural frequencies, modal loss factors, and frequency response functions of cylindrical viscoelastic aluminum shells are as compared with those of the base thick aluminum panel without a viscoelastic layer. The thickness and damping ratio of the viscoelastic damping layer, the curvature of proposed cylindrical aluminum structure, and placement of damping layer of the aluminum panel have been investigated using frequency reaction characteristic. The provided outcomes show that the sandwiched viscoelastic damping layer can efficaciously suppress vibration of cylindrical aluminum shape.

Three-Dimensional Exact Free Vibration Analysis of Spherical, Cylindrical, and Flat One-Layered Panels

The paper proposes a three-dimensional elastic analysis of the free vibration hassle of 1-layered round, cylindrical, and flat panels. The precise solution is evolved for the differential equations of equilibrium written in orthogonal curvilinear coordinates for the free vibrations of clearly supported systems. These equations consider an genuine geometry for shells without simplifications. The important novelty is the possibility of a preferred formulation for unique geometries. The equations written in popular orthogonal curvilinear coordinates permit the analysis of spherical shell panels and that they mechanically degenerate into cylindrical shell panel, cylindrical closed shell, and plate instances. Results are proposed for isotropic and orthotropic systems. An exhaustive

ISBN: 978-93-91420-02-4

evaluate is given of the vibration modes for a number of thickness ratios, imposed wave numbers, geometries, embedded materials, and angles of orthotropy. These results can also be used as reference solutions to validate - dimensional models for plates and shells in both analytical and numerical form (e.G., closed solutions, finite detail method, differential quadrature technique, and worldwide collocation technique).

2.1 INTRODUCTION TO CAD

Computer-aided design (CAD) is using laptop structures (or workstations) to aid within the advent, change, analysis, or optimization of a layout. CAD software is used to increase the productiveness of the clothier, improve the great of layout, improve communications via documentation, and to create a database for production. CAD output is frequently within the form of digital documents for print, machining, or other manufacturing operations. The term CADD (for Computer Aided Design and Drafting) is also used.

2.2 INTRODUCTION TO CREO

PTC CREO, formerly referred to as Pro/ENGINEER, is 3D modeling software used in mechanical engineering, design, manufacturing, and in CAD drafting carrier firms. It turned into one of the first 3-d CAD modeling programs that used a rule-primarily based parametric device. Using parameters, dimensions and functions to capture the behavior of the product, it is able to optimize the development product in addition to the design itself.

The name become changed in 2010 from Pro/ENGINEER Wildfire to CREO. It was introduced through the organization who developed it, Parametric Technology Company (PTC), all through the release of its suite of design products that includes programs which includes assembly modeling, 2D orthographic views for technical drawing, finite detail analysis and greater.

3D MODEL

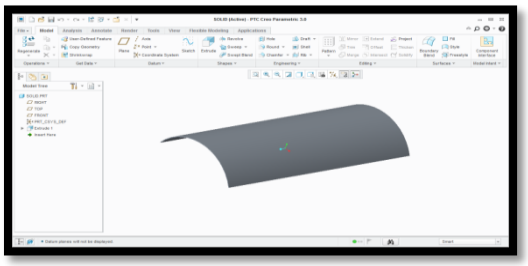

2D MODEL

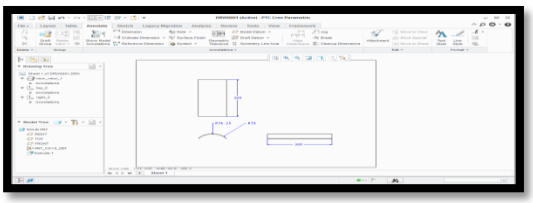

III. INTRODUCTION TO FEA

Finite element evaluation is a technique of solving, normally approximately, certain problems in engineering and science. It is used specially for troubles for which no precise solution, expressible in a few mathematical shape, is available. As such, it is a numerical in preference to an analytical technique. Methods of this type are wanted due to the fact analytical strategies cannot cope with the real, complicated troubles which can be met with in engineering. For instance, engineering electricity of substances or the mathematical principle of elasticity may be used to calculate analytically the stresses and lines in a bent beam, but neither will be very successful in locating out what's going on in a part of a car suspension device for the duration of cornering.

IV. INTRODUCTION ANSYS

ANSYS is well known-reason finite detail evaluation (FEA) software bundle. Finite Element Analysis is a numerical method of deconstructing a complicated system into very small pieces (of person-exact length) called factors. The software implements equations that govern the behavior of these factors and solves all of them; creating a comprehensive clarification of ways the machine acts as a whole. These outcomes then can be offered in tabulated, or graphical forms. This kind of analysis is typically used for the layout and optimization of a machine some distance too complex to analyze by hand. Systems that may match into this category are too complicated due to their geometry, scale, or governing equations.

4.1 STATIC ANALYSIS

Save Creo Model as .iges format

→→Ansys → Workbench→ Select analysis system → static structural → double click

→→Select geometry → right click → import geometry → select browse →open part → ok

→→ Select mesh on work bench → right click →edit

Double click on geometry → select MSBR → edit material →

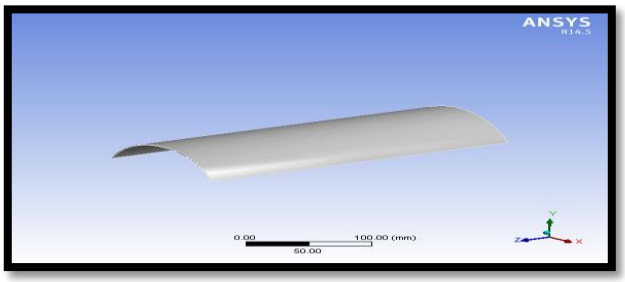

Select mesh on left side part tree → right click → generate mesh →

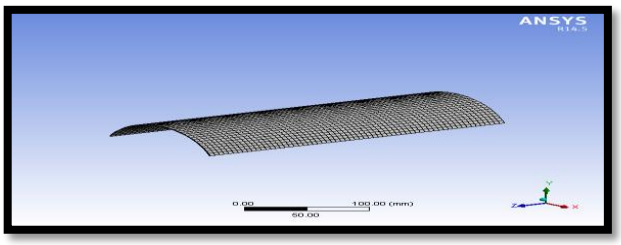

Select static structural right click → insert → select rotational velocity and fixed support → Select displacement → select required area → click on apply → put X,Y,Z component zero →

 ISBN: 978-93-91420-02-4

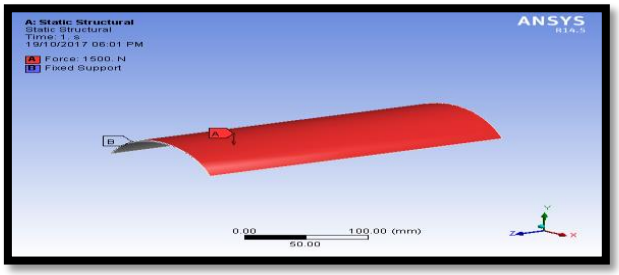

Select force → select required area → click on apply → enter rotational velocity
Select solution right click → solve →
Solution right click → insert → deformation → total →
Solution right click → insert → strain → equivalent (von-mises) →
Solution right click → insert → stress → equivalent (von-mises) →
Right click on deformation → evaluate all result

MATERIAL – POLYESTER
Deformation

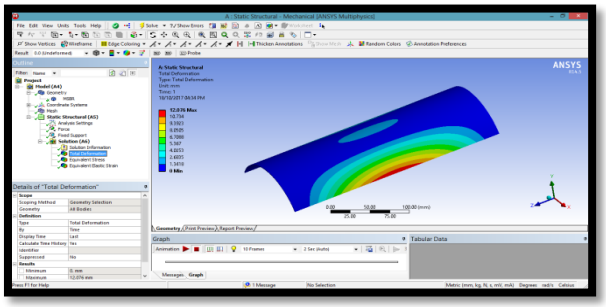

Stress

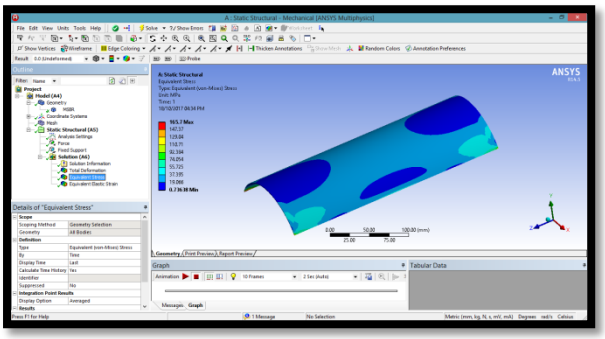

Strain

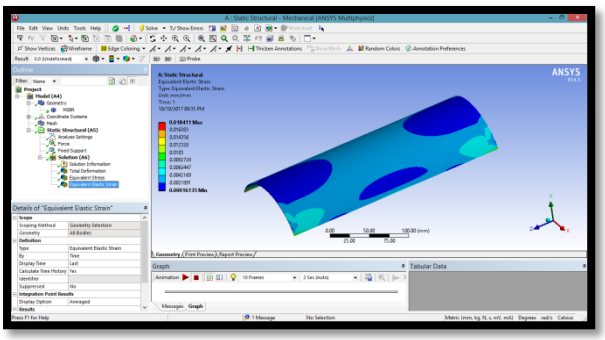

MATERIAL – E-GLASS
Deformation

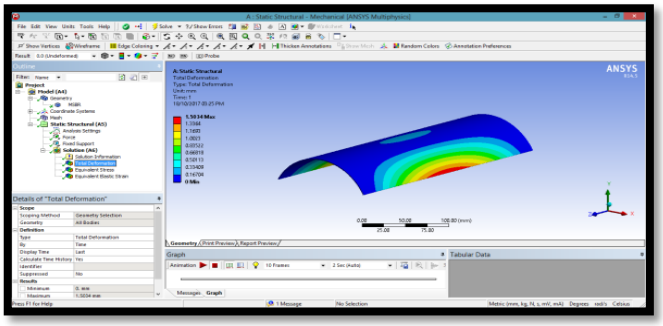

Stress

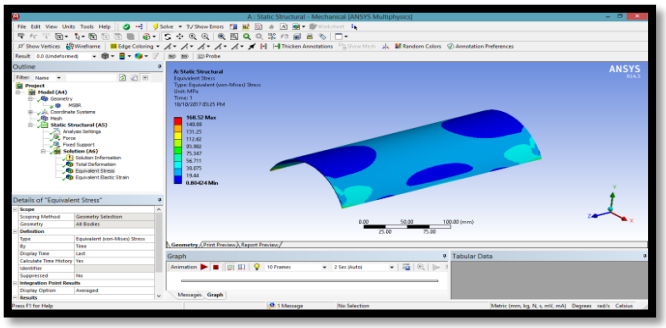

Strain

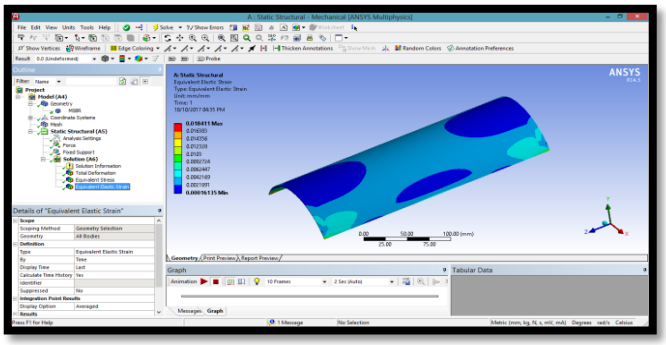

MODAL ANALYSIS

MATERIAL – POLYESTER

MODE SHAPE 1

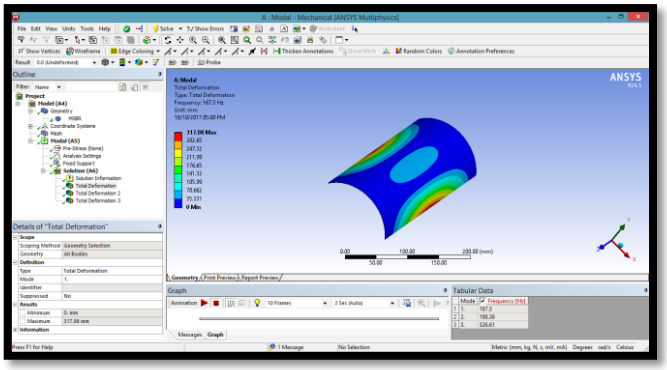

MODE SHAPE 2

ISBN: 978-93-91420-02-4

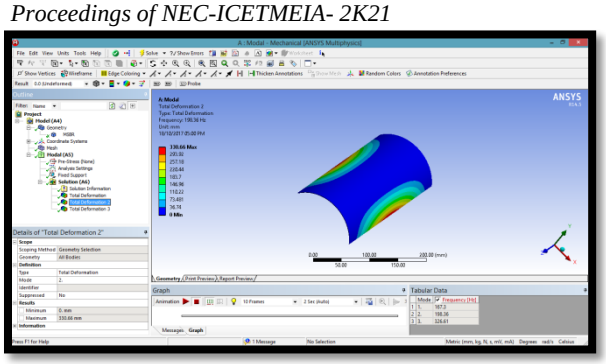

MODE SHAPE 3

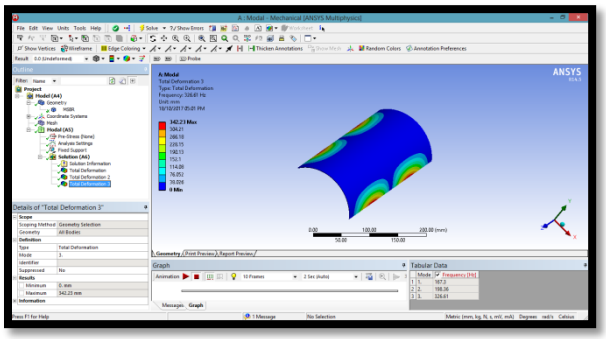

LINEAR LAYER STATIC ANALYSIS FOR 7 LAYERS DEFORMATION

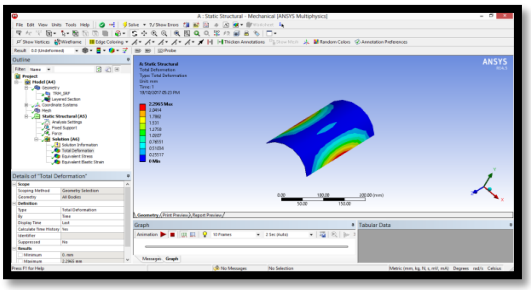

STRESS

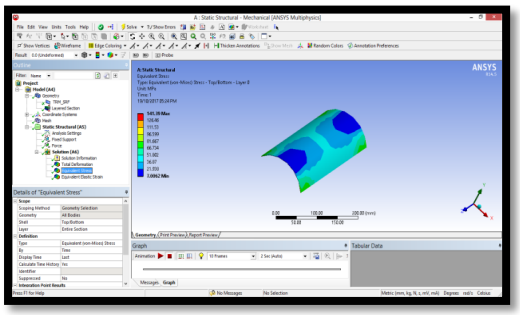

STRAIN

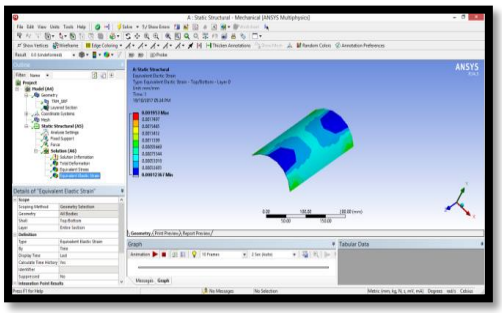

V.RESULTS AND DISCUSSIONS

5.1 STRUCTURAL ANALYSIS

Loads (N)	Materials	Deformation(mm)	Stress (N/mm2)	strain
1500	E-glass	1.5034	168.52	0.0023277
	polyester	12.076	165.7	0.018411
	GFRP	2.1697	170.89	0.0034306
1200	E-glass	1.2027	134.82	0.0018621
	polyester	9.6606	132.56	0.014729
	GFRP	1.7358	136.71	0.0027228

5.2 MODAL ANALYSIS RESULTS TABLE

Material	Mode shapes	Deformation (mm)	Frequency (Hz)
E-glass	1	164.48	245.35
	2	171.22	290.84
	3	177.02	479.76
polyester	1	317.98	167.3
	2	330.66	198.36
	3	342.23	326.61
GFRP	1	317.68	394.49
	2	330.91	467.53
	3	341.82	772.43

LINEAR LAYER STATIC ANALYSIS

Layer stacking	Deformation(mm)	Stress (N/mm2)	strain
3	2.362398	142.831	0.0019728
5	2.9728	166.78	0.002306
7	2.29665	141.39	0.001953

CONCLUSION

The materials used for those analyses are composite substances. Static & linear layer analysis to decide the deformation, stress of the cylindrical panel, modal analysis to decide the herbal frequency and deformation for mode shapes. And we are the use of layer stacking technique for 3, 5 and 7 layers for evaluation of metal, E-glass polyester and glass fiber strengthened plastic cloth.

By gazing the static evaluation the deformation, pressure and strain values are increases by way of growing the masses. The stress values are much less for polyester cloth while we compare the E-Glass and glass fiber strengthened plastic fabric.

By gazing the modal analysis the deformation values are greater for polyester fabric while we evaluate the E-Glass and glass fiber bolstered plastic cloth.

Through staring at the linear layer analysis the strain values are less for 7 layers.

REFERENCES

[1] Volmir, A. S.: Stability of deformable systems, Izd. Nauka, Fiz–Mat–Lit, Moskwa, 1967.

[2] Staat, M.: Local and international fall apart pressure of longitudinally wrong pipes and cylindrical vessels, International Journal of Pressure Vessels and Piping, Vol. 82, 217–225, 2005.

[3] Aghajari, S., Abedi, K. And Showkati, H.: Buckling and put up-buckling conduct of skinny–walled cylindrical steel shells with various thickness subjected to uniform external strain, Thin–Walled Structures, Vol. Forty four, 904–909, 2006.

[4] Ahn, S. H., Nam, K. W., Takahashi, K. And Ando, K.: Comparison of experimental and finite detail analytical outcomes for the strength and the deformation of pipes with neighborhood wall thinning subjected to

 ISBN: 978-93-91420-02-4

bending moment, Nuclear Engineering and Design, Vol. 236, one hundred forty–one hundred fifty five, 2006.
[5] Jullien, J. F. And Limam, A.: Effects of openings of the buckling of cylindrical shells subjected to axial compression, Thin–Walled Structures, Vol. 31, 187–202, 1998. 176 Stasiewicz, P.
[6] Vaziri, A. And Estekanchi, H. E.: Buckling of cracked cylindrical skinny shells underneath combined inner pressure and axial compression, Thin–Walled Structures, Vol. Forty four, 141–151, 2006.
[7] Schenk, C. A. And Schueller, G. I.: Buckling analysis of cylindrical shells with cutouts including random boundary and geometric imperfections, Comput. Methods Appl. Mech. Engrg, Vol. 196, 3424–3434, 2007.
[8] Meng–Kao, Y., Ming–Chyuan, L. And Wen–Tsang, W.: Bending buckling of an elastoplastic cylindrical shell with a cutout, Engineering Structures, Vol. 21, 996–1005, 1999.
[9] Alashti, R. A., Rahimi, G. H. And Poursaeidi, E.: Plastic restrict load of cylindrical shells with cutouts difficulty to natural bending moment, International Journal of Pressure Vessels and Piping, Vol. Eighty five, 498–506, 2008.
[10] Wilde, R., Zawodny, P. And Magnucki, K.: Critical nation of an axially compressed cylindrical panel with 3 edges virtually supported and one facet free, Thin– Walled Structures, Vol. 45, 955–959, 2007.
[11] Timoshenko, S. And Goodier, J. N.: Theory of Elasticity, McGraw–Hill Book Company, New York, Toronto, London, 1951.

 ISBN: 978-93-91420-02-4

Application of a Thermoplastic Polyurethane/Polylactic Acid Composite Filament for 3d-Printed Personalized Orthosis

[1]V.Vana Kiran Kumar and [2]T.Ashok Kumar
[1]Department of Mechanical Engineering, Sree Rama Engineering College Tirupathi, Andha Pradesh, India.
[2]Department of Mechanical Engineering, Narasaraopeta Engineering College (A), Andha Pradesh, India.

Abstract:
For designing and fabricating personalized, cost-effective and bio-degradable orthoses, a finger orthosis was chosen as an example to explore a suitable material, personalized design method, and fabrication with a fuse-deposition-modeling (FDM) open-source 3D printer. Thermoplastic polyurethane (TPU)/polylactic acid (PLA) composite filaments were explored for 3D printing. The polymer composite compositions were TPU/PLA: 0 %/100 % (TP0), 25 %/75 % (TP25), and 50 %/50 % (TP50) by weight, respectively. The mechanical performance, thermal properties, and structure of the TPU/PLA composite filaments were assessed by tensile tests, thermal gravimetric analysis (TGA), differential scanning calorimetry (DSC), and powder X-ray diffraction (XRD) measurements. Compared to the neat PLA, the TP25 specimens exhibited almost the same tensile strength, but its higher elongation at the break indicates that TP25 is more suitable for the material of orthoses. However, a further increase of the TPU ratio to 50 % resulted in a sharp decrease of the tensile strength. The addition of TPU had little effect on the starting thermal decomposition temperature, glass-transition temperature, and melting temperature of the composites. The com- posite filaments can be printed through the normal 3D printing procedure. 3D scanning and open-source 3D printers can be used to complete the design and fabrication of personalized orthoses.

Keywords: 3D printing, 3D scanning; orthosis, thermoplastic polyurethane, polylactic acid

I.INTRODUCTION

In the medical field, orthoses are used for many purposes. Depending on the patient's impairment, they might be used as braces for the rehabilitation of peripheral nerves' dysfunctions, the improvement of gait performance for people with an impaired lower-limb function, or the optimization of the support of a limb used in rheumatology, traumatology, or other articulations inflammatory processes. 3D printing (3DP), also known as additive manufacturing (AM) technology, can be defined as a technique for creating three-dimensional objects in a layer-by-layer manner. Over the past few years, 3DP has extended to areas of aerospace, auto-motive, architecture, medical, education, and fashion. Nowadays, 3DP is spreading in the orthosis field. Given its low-cost and continuous materials evolution, its diffusion is expected to rapidly increase in the near future.3

Fused deposition modelling (FDM) is one of the most commonly used techniques in 3DP. The expiration of early FDM patents has led to the growth of relatively low-cost, open-source 3D printers. In essence, an FDM printer consists of an engine, gear wheels, an extrusion nozzle, and a building plate. The filament with a well- defined and consistent diameter is loaded and pushed towards the extrusion nozzle (Which is set at an elevated temperature) to be melted and deposited onto a building plate. Dictated by the slicing software, the extrusion nozzle can be moved in different XY directions. Once each individual cross-section of the desired object is completed, the building plate can be moved down (Z direction) to deposit different layers.4

Polylactic acid (PLA) filaments are widely used as bio-based feedstock for FDM. Although PLA filaments are degradable and exhibit outstanding properties, its brittleness restricts their suitability for orthosis applications. Preparing PLA composites by mixing PLA with an elastomer offers a solution for ameliorating the tough- ness of PLA.5 Thermoplastic polyurethane (TPU) elastomers are excellent biocompatible materials for many applications in the medical field, such as blood bags and surgical gloves, catheters, synthetic veins, and wound dressings.6 Based on the chemical structure of PLA and TPU, it is possible to achieve better compatibility between both polymers. PLA is compatible with the soft polyester segments of TPU and can form hydrogen bonds with the carbonates from hard segments of TPU.7, 83DP's most distinguishing feature is its ability to construct complex spatial objects rapidly from a digital model file. The design and production of personalized products in the pharmaceutical field, such as medicines, oral dosage forms, and medical devices, has benefitted from the advantages of 3DP.9,10 Computer-aided design (CAD) and 3D scanning technology are commonly used to generate 3D models. For personalized orthoses, 3D scanning technology offers an ideal technique for obtaining patient-specific 3D models.

In this paper, a finger orthosis was chosen as an example to explore the design and fabrication of a personalized orthosis. The TPU/PLA composite filaments were developed for FDM 3DP. The properties of the TPU/PLA composite were investigated. The feasibility of making personalized orthoses using 3D scanning and an open-source 3D printer was explored.

II.EXPERIMENTAL PART

Preparation Of TPU/PLA Polymer Composite Filaments:

Virgin PLA (4032D) pellets were purchased from Nature Works LLC, USA. The density is 1.24 g cm–3 and the melting temperature is about 160 °C. TPU (1170A Elastonllan) pellets were obtained from the BASF Company, Germany. This is a polyether TPU with high toughness and elongation at the break, and a density of 1.08 g cm–3.The PLA and TPU pellets were initially dehydrated (103 °C) for 4 hours to eliminate the moisture. After drying, the TPU and PLA pellets were then blended with different ratios of TPU/PLA (0 %/100 %(TP0), 25 %/75 % (TP25), and 50 %/50 % (TP50) by weight and extruded using a single screw extruder (C2 model, Well zoom

 ISBN: 978-93-91420-02-4

LLC, Shenzhen, China) for fabricating neat PLA and TPU/PLA polymer composite filaments. The extruder has separate temperature (maximum 320 °C) controls for the mixture and the extrusion parts, which offers a maximum extrusion speed of 2 m•min–1. The extruded TPU/PLA filament was cut into smaller particles and extruded again for three times to obtain a well-mixed TPU/PLA composite filament with different TPU blend proportions. During fabrication, 1.75 mm filaments were used, the processing temperatures were set at 180 °C (extrusion part) and 185 °C (mixture part), with a filament yield (extrusion) speed of 1 m•min–1.

Property Measurements Of TPU/PLA Composite Filaments:

The tensile properties of the specimens were measured with a universal testing machine (Changchun Kexin instruments Co. Changchun, China). The specimens were designed according to ASTM D638. Three replicates were printed from each TPU/PLA ratio composite filament for a mean value calculation. The typical stress-strain curves and elasticity modulus were obtained. Thermal gravimetric analyses (TGA) and differential scanning calorimetry (DSC) analyses of the specimens were performed in a TA analyzer (Q 50, TA Instruments, USA) and DSC analyzer (Q 20, TA Instruments, USA). The samples were heated from 25 °C to 400 °C for the TGA and to 300 °C for the DSC with an increase rate of 10 °C min–1 to observe their thermal degradation behaviors. Throughout the whole procedure, the N2 flow rate was 30 mL•min–1. Powder X-ray diffraction (XRD) measurements were recorded using a D/max 220 analyzer (Rigaku, Japan). The samples were scanned under conditions of a voltage of 40 kV, a current of 30 mA, a starting angle of 5°, a termination angle of 40°, and a step width of 0.02°.

3D Scanning And Printing:

A Sense 3D Scanner (3D Systems, Inc. USA) was used to scan the finger to create a digital finger model of an orthosis. As shown in Figure 1a, the lens of the scanner faced and slowly rotated around the finger until the digital finger model was generated in the computer. Geomagic Studio software (developed by Geomagic Company) was used to edit the digital finger model, such as deleting misplaced polygons, etc. Then the Boolean operation of the 3DS MAX software (developed by Autodesk) was used to design the matching orthosis model. The finger orthosis model was saved in STL (Stereolithographic) format and transferred to the 3D printer.

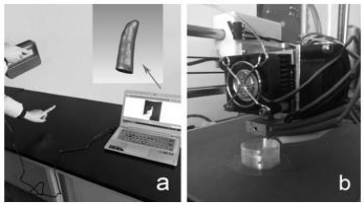

Figure 1: 3D scanning and printing: a) the finger was scanned using a 3D scanner to obtain the digital finger model, b) the finger orthosis was printed using an open-source 3D printer with FDM technology

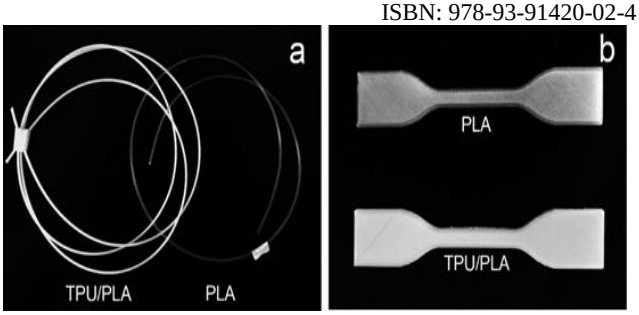

Figure 2: Filaments and test specimens: a) neat PLA and TPU/PLA composite filament, b) specimens for tensile property measurements

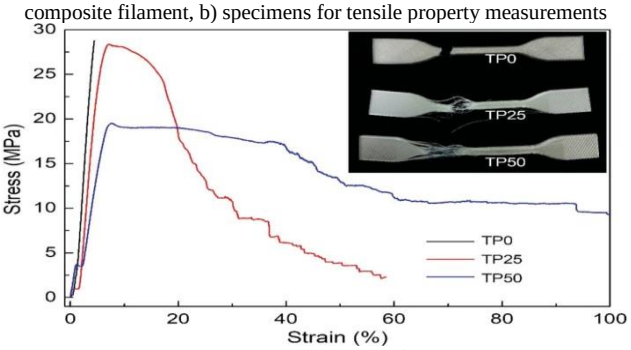

Figure 3: Typical tensile stress-strain curves of the TP0, TP25, and TP50 specimens as well as the fracture morphology of the specimens

The specimens for the tensile properties and the finger orthosis were printed with TP0, TP25, and TP50 filaments using an open-source 3D printer (605S model, Shenzhen Aurora Technology Co, Shenzhen, China). The nozzle diameter of the printer was 0.4 mm. The CURA software (15.04 version, developed by Ultimaker) was used to set the printing parameters. The printing layer height was set to 0.3 mm, the shell thickness to 1.2 mm, the top and bottom thickness to 1.2 mm, the filling density to 10 %, the printing speed to 30 mm s–1, the printing temperature to 200 °C, the hot-bed temperature to 60 °C, and the wire material flow rate to 100 %. The printing process of the finger orthosis is shown in Figure 1b.

III.RESULTS AND DISCUSSION

Filaments and test specimens:

The neat PLA and TPU/PLA composite filaments were manufactured successfully by the extruder with a diameter of 1.75 mm, as shown in Figure 2a. The TPU/PLA composite filaments showed a smooth surface and a uniform diameter. Compared to the neat PLA, the transparency of the TPU/PLA composite decreased. The printed specimens of neat PLA and TPU/PLA composite for the tensile property tests are shown in Figure 2b. Through experimentation and observation, the TPU/PLA composite filaments were determined to be suitable for FDM printing.

Tensile properties:

In Figure 3, the tensile stress-strain curves show that the TP0 specimen has almost no plastic deformation after the tensile yield point, and the neat PLA part under- goes brittle fracture. Nevertheless, the TP25 and TP50 specimens exhibit plastic deformation and ductile fracture after the tensile yield point. The fracture morphology of the specimens shows that TP0 suffers breakage without elongation. While the TP25 specimens can be broken after the plastic deformation, and the fibers of the TP50 specimen were stretched with no fracture.

The failure characteristics of the specimens revealed that a higher TPU content results in a greater tensile toughness.

Table 1: Tensile properties of the specimens

Specimens	Tensile modulus(MPa)	Tensile strength(MPa)	Elongation at break(%)
TP0	666.3	28.8	4.4
TP25	569.2	28.4	58.5
TP50	371.4	19.5	>100

Table 1 shows that the tensile modulus of the specimens decreases gradually with the increase of the TPU content, and while the tensile strength of the TP25 specimens undergoes insignificant changes, the elongation at break increases over tenfold. However, the tensile modulus and tensile strength of the TP50 specimens are greatly reduced and the elongation at break is more than 100 %. The alternating hard and soft segments of its molecular chain endow the TPU with the unique properties of flexibility and elasticity. When blended with the brittle PLA, the TPU could contribute to the composite's flexibility. Furthermore, the hydrogen bond formed between the PLA and TPU molecules guarantees that at an optimized TPU addition ratio, the tensile strength of the composite will be no less than that of the neat PLA. The elongation determines the maximum deformation of a material without breakage, which is especially important from a manufacturing standpoint. Therefore, to obtain optimal performance, it is necessary to prepare PLA/TPU composites with tailored strength, modulus, and elongation.11

DSC analysis:

As shown in Figure 4 and Table 2, the neat PLA can be characterized with a Tg at 57.9 °C, a cold crystallization temperature (Tc) around 113.1 °C and a melting temperature of (Tm) 153.9 °C. Compared with the neat PLA, the Tg of the two TPU/PLA composites slightly decreased, which means that the TPU and PLA were partially miscible. The compatibility of polymer blends can be assessed by observing the shift in the Tg of the phases in comparison with their original values.12 The Tc of the polymer composite decreased with an increase of the TPU content, indicating that the TPU affected the cold crystallization of the PLA. These phenomena can be attributed to the added TPU, which acts as a crystallization nucleation agent by providing nucleation spots. Among the three filaments, both the cold crystallization peak and the melting peak decreased with an increase of the TPU content.13 The melting temperatures of TP0, TP25, and TP50 are about 153 °C. Therefore, the printing temperature of TP25 and TP50 can equal that of the neat PLA.

Table 2: Thermal properties of neat PLA and TPU/PLA composite filaments

Specimens	T_g(°C)	T_c(°C)	T_m(°C)
TP0	57.9	113.1	153.9
TP25	57.5	96.2	153.2
TP50	57.0	91.1	152.6

Thermal gravimetric analysis:

As shown in Figure 5 and Table 3, the addition of TPU has little effect on the initial decomposition temperature (Ti) of the polymer composite. Compared to the neat PLA, when the weight loss was 10 % (T10) of TP25 and TP50, the decomposition temperatures decreased less than 5 °C. The fast decomposition temperature of the polymer composites shifted obviously to lower temperature ranges, and the TPU/PLA composites exhibited two fast decomposition peaks. The increase of the TPU content had almost no effect on the fast decomposition temperature. Compared to the neat PLA, the heat stability of the polymer composite was reduced; the initial decomposition temperatures of the TPU/PLA composites were around 190 °C. The fast decomposition temperature range was 270–280 °C, which can fully meet the requirements of FDM 3D printing.

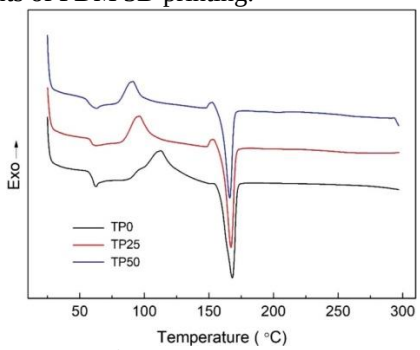

Figure 4: DSC curves of neat PLA and TPU/PLA composite filaments

Table 3: Decomposition temperature of the neat PLA and TPU/PLA composite filaments

Specimens	T_i(°C)	T_{10}(°C)	T_f(°C)
TP0	188.2	250.4	292.6
TP25	187.9	245.6	273.1,331.3
TP50	187.7	247.2	272.8,331.1

X-ray diffraction spectra:

In Figure 6, the XRD peak shape of the TPU/PLA composite is similar to that of the neat PLA. The neat PLA showed a broad amorphous halo at 2θ = 16.9°, which is the characteristic diffraction peak of the PLA crystallization. However, compared with the neat PLA, due to the contribution of the TPU, the broad halo of the diffraction peak 2θ = 20.2°. The addition of TPU to PLA has a heterogeneous nucleation effect on the crystallization of PLA. After 25 % TPU mixing, the peak intensity decreases slightly, and the diffraction peak of 2θ increases, indicating that the interplanar distance decreases. When 50 % TPU is added, the peak width decreases, as a result of the larger grain size.

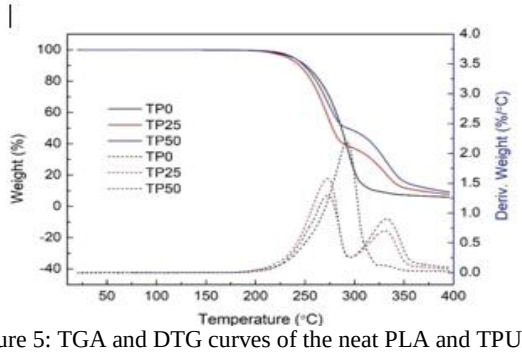

Figure 5: TGA and DTG curves of the neat PLA and TPU/PLA composite filaments

 ISBN: 978-93-91420-02-4

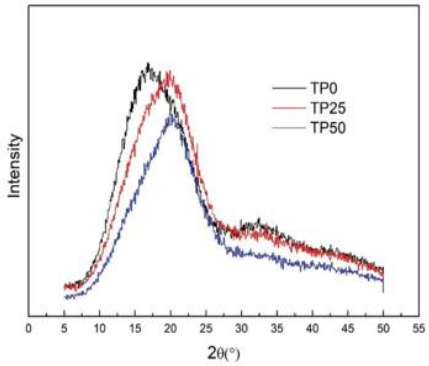

Figure 6: XRD spectra of the neat PLA and TPU/PLA composite filaments

Printed orthosis:

The TP25 has more toughness than the neat PLA, but a similar tensile strength and printing temperature with the neat PLA. Therefore, it was chosen to print the orthosis. The TP25 filament can be successively printed through FDM 3D printing, and the finger orthosis designed and printed can be a good fit, as shown in Figure 7. This indicates that the TPU/PLA composite filament is feasible for 3D printing orthoses.

IV.CONCLUSIONS

The TPU/PLA composite filaments were prepared and the potential of the composites for an application in orthosis fabrication was evaluated. The research demonstrated that the TPU/PLA composite filament is compatible with the FDM process. Compared with the neat PLA, the addition of TPU has little effect on the starting thermal decomposition temperature, the glass- transition temperature, and the melting temperature. Without sacrificing any tensile strength, the composite with 25 % TPU exhibited better toughness than the neat PLA and can be printed smoothly, just like the PLA. The results revealed that the TPU/PLA composite filament is more suitable for the design of orthoses than the neat PLA. 3D scanning and open-source 3D printers can be used to complete the design and fabrication of per- sonalized orthosis.

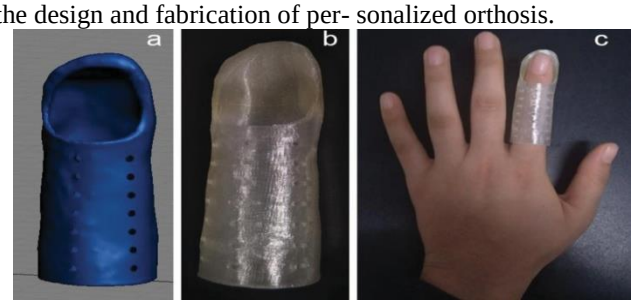

Figure 7: a) the finger orthosis model, b) printed finger orthosis and c) wearing the finger orthosis

ACKNOWLEDGMENT

This project was supported by the Program for New Century Excellent Talents in University of China (NCET-13-0711). The authors would like to thank Zelong Li for his help and advice.

REFERENCES

[1] M. C. Faustini, R. R. Neptune, R. H. Crawford, S. J. Stanhope, Manufacture of passive dynamic ankle–foot using selective laser sintering, IEEE T. Bio-med. Eng., 55 (2008) 2, 784–790

[2] R. Miclaus, A. Repanovici, N. Roman, Biomaterials: Polylactic acid and 3D printing processes for orthosis and prosthesis, Mater. Plast., 54 (2017) 1, 98–102

[3] G. Baronio, S. Harran, A. Signoroni, A critical analysis of a hand orthosis reverse engineering and 3D printing process, Appl. Bionics Biomech., (2016), 8347478

[4] G. Verstraete, A. Samaro, W. Grymonpré, V. Vanhoorne, B.Van Snick, M. N. Boone, T. Hellemans, L. Van Hoorebeke, J. P. Remon,

[5] C. Vervaet, 3D printing of high drug loaded dosage forms using thermoplastic polyurethanes, Int. J. Pharmaceut, (2018), 318–325

[6] V. Ja{o, M. Cvetinov, S. Raki}, Z. S. Petrovi}, Bio-plastics and elastomers from polylactic acid/thermoplastic polyurethane blends, J. Appl. Polym. Sci., 131 (2014), 41104

[7] 6 S. H. Ajili, N. G. Ebrahimi, M. T. Khorasani, Study on thermoplastic polyurethane/polypropylene (TPU/PP) blend as a blood bag material, J. Appl. Polym. Sci. 89 (2003) 9, 2496–2501

[8] V. Ja{o, M. V. Rodi}, Z. S. Petrovi}, Biocompatible fibers from thermoplastic polyurethane reinforced with polylactic acid microfibers, Eur. Polym. J., 63 (2015), 20–28

[9] J. Han, H. Huang, Preparation and characterization of biodegradable polylactide/thermoplastic polyurethane elastomer blends, J. Appl. Polym. Sci., 120 (2011), 3217–3223

[10] 9 C. L. Ventola, Medical applications for 3D printing: current and projected uses, Pharmacol. Ther., 39 (2014), 704–711.

[11] Goyanes, U. Det-Amornrat, J. Wang, A. W. Basit, S. Gaisford, 3D scanning and 3D printing as innovative technologies for fabricating personalized topical drug delivery systems, J. Control Release, 234 (2016), 41–48

[12] 11 I. S. S. Sharifah, M. D. A. Adnan, M. K. Nor Khairusshima, N. M. Shaffiar, Y. F. Buys, Effect of thermoplastic polyurethane (TPU) on the thermal and mechanical properties of polylactic acid (PLA)/ curcumin blends, IOP Conf. Series: Materials Science and Engineering, 290 (2017), 012081

[13] S. K. Dogan, S. Boyacioglu, M. Kodal, O. Gokce, G. Ozkoc, Ther- mally induced shape memory behavior, enzymatic degradation and biocompatibility of PLA/TPU blends: Effects of compatibilization, J. Mech. Behav. Biomed., 71 (2017), 349–361

[14] H. Mi, M. R. Salick, X. Jing, B. R. Jacques, W. C. Crone, X. Peng, L. Turng, Characterization of thermoplastic polyurethane/polylactic acid (TPU/PLA) tissue engineering scaffolds fabricated by micro- cellular injection molding, Mat. Sci. Eng. C, 33 (2013), 4767–4776

 ISBN: 978-93-91420-02-4

Design and Analysis of a Connecting Rod

[1]G. Raju and [2]T. Ashok Kumar,
[1]Department Of Mechanical Engineering, JNTUN, Narasaraopet, Andha Pradesh, Guntur District
[2]Department of Mechanical Engineering, Narasaraopeta Engineering College (A), Narasaraopeta
Andha Pradesh, India.

Abstract: The main function of a connecting rod is to convert linear motion of piston to rotary motion of crank. It is the main component of an internal combustion (IC) engine and is the most heavily stressed part in the engine. During its operation various stresses are acting on connecting rod. The influence of compressive stress is more in connecting rod due to gas pressure and whipping stress. The objective of this study is to carry out a FEA analysis of a connecting rod and obtain its stress distribution on application of the force. Geometry of connecting rod used for FEA, its generation, simplifications and accuracy is done by using CATIA. Mesh generation, the load application, particularly the distribution at the contact area, factors that decide application of the restraints and validation of the FEA model are also discussed. FEM was used to determine structural behavior under static load condition (static FEA).
Keywords: Connecting Rod, Catia, Ansys, FEA

I. INTRODUCTION

In modern automotive internal combustion engines, the connecting rods are most usually made of steel for production engines, but can be made of aluminium (for lightness and the ability to absorb high impact at the expense of durability) or titanium (for a combination of strength and lightness at the expense of affordability) for high performance engines. They are not rigidly fixed at either end, hence the angle between the connecting rod and the piston changes as the rod moves up and down and rotates around the crankshaft. Connecting rods are manufactured by means of forging. Being one of the most integral parts in an engine's design, the connecting rod must be able to withstand tremendous loads and transmit a great deal of power. In a reciprocating piston engines, connecting rod connects the piston to the crank or crankshaft. Together with the crank, they form a simple mechanism that converts reciprocating motion into rotating motion. As the connecting rod is rigid, it may transmit either a push or a pull and so the rod may rotate the crank through both halves of a revolution, i.e., piston pushing and piston pulling. The small end is attached to the piston pin and the big end connects to the bearing journal on the crank. Typically, there is a pinhole bored through the bearing and the big end of the connecting rod so that pressurized lubricating motor oil squirts out onto the thrust side of the cylinder wall to lubricate the travel of the pistons and piston rings.

II.FINITEELEMENTANALYSIS

Design

The connecting rod is designed using CATIA V5 6R 2014accordingtothespecificationsgivenbelow.

Parameter	Value
Length of connecting rod	150
Outer diameter of big end	56
Inner diameter of big end	48
Outer diameter of small end	32
Inner diameter of small end	24

Table1: Dimensions of Connecting Rod

Meshing

The connecting rod model is imported to the ANSYS(mechanical APDL 14.5) by converting the Catia file into .anf extension file format. The element type selected is solid185.After successful import of model material property is defined. The materials and their properties used and necessary for the analysis is given in table2.

Material	Young's modulus(GPa)	Poisson's ratio	Density(Kg/mm3)
Steel	200	.303	8050
Aluminium	69	.334	2700

Table2:Material Properties

After defining the element type and material property, meshing is done. Meshing is probably the most important part in analysis. Meshing means to create a mesh of some grid-points called 'nodes'. It's done with a variety of tools & options available in the software. The results are calculated by solving the relevant governing equations numerically at each of the nodes of the mesh. For the design under consideration, finite element mesh is generated using tetrahedral mesh type taking fine size to 1mm and minimum edge length as 0.1mm with 50730 nodes

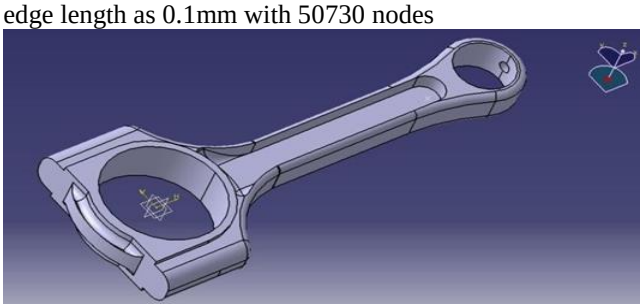

Fig1: CatiaModelofConnectingRod

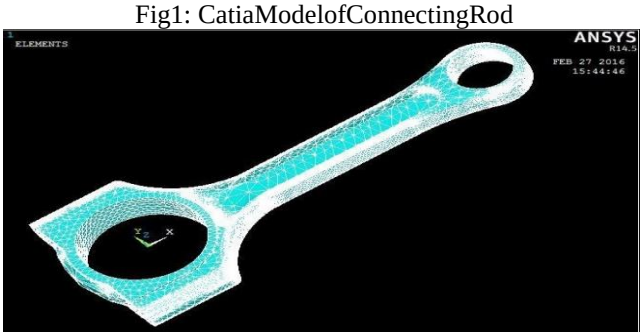

Load Analysis
Compressive Loading:
Crank End: p = 37.66 MPa Piston pin End: p=69.98MPa

Tensile Loading:
Crank End: p = 41.5 MPa Piston pin End: p=77.17MPa

Since the analysis is linear and elastic, for static analysis the stress, displacement and strain are proportional to the magnitude of the load. Therefore, the result obtained from FEA is applied to several elastic load carries in a proportional manner.

ISBN: 978-93-91420-02-4

Compression at Bigger end

For the analysis of connecting rod, a compressive force of magnitude 37.66MPa is applied on the bigger end, keeping the smaller end fixed.

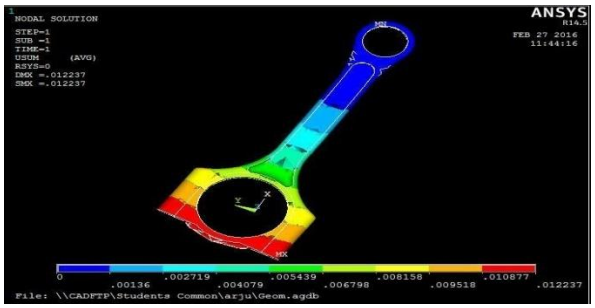

Fig.3: Total Deformation of Steel

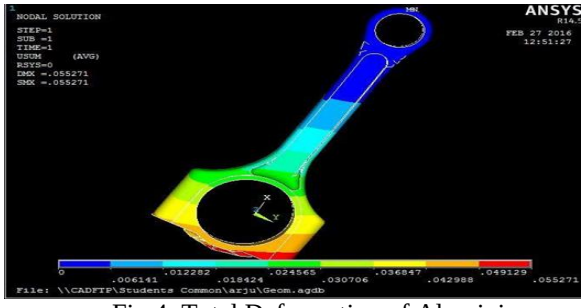

Fig.4: Total Deformation of Aluminium

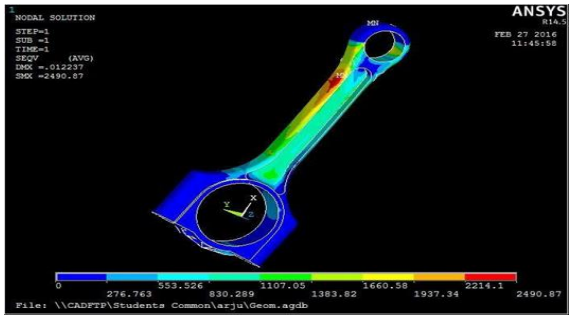

Fig.5: Von-Mises Stress of Steel

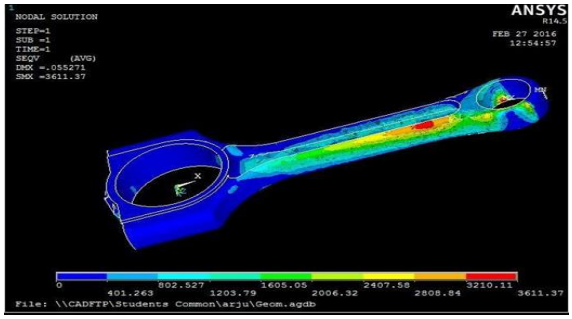

Fig.6: VonMises Stress of Aluminium

Tension at bigger end

A tensile forceofmagnitude41.15M Pa is applied at the bigger end while keeping the smaller end remain fixed.

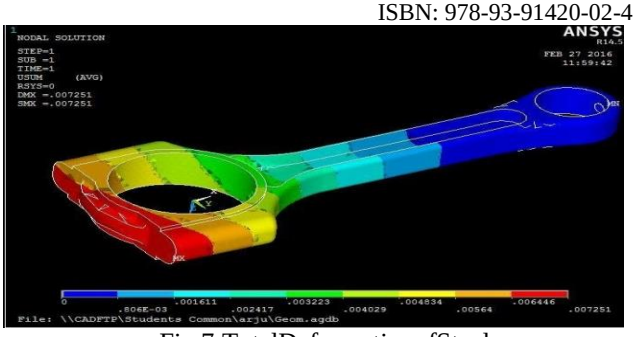

Fig.7:TotalDeformationofSteel

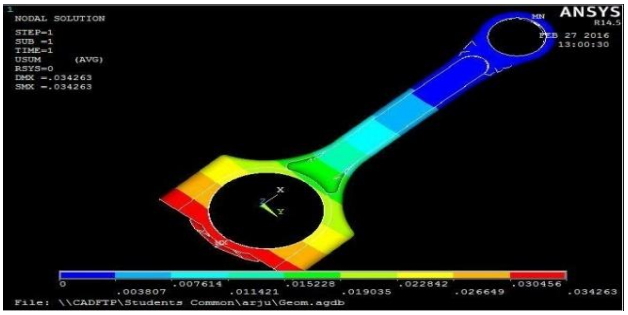

Fig.8: Total Deformation of Aluminium

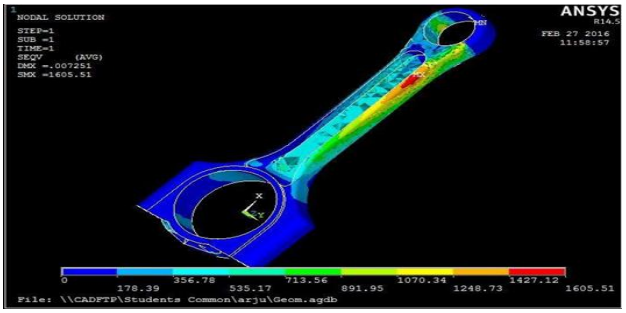

Fig.9: Von-Mises Stress of Steel

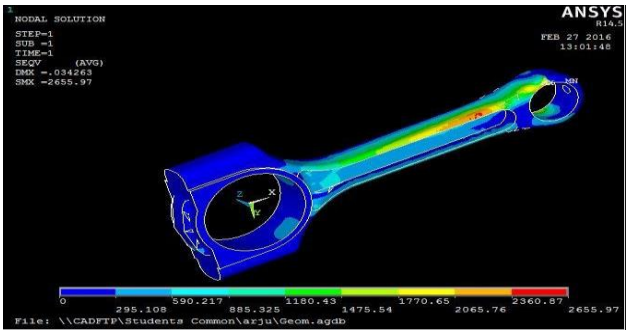

Fig.10: Von Mises Stress of Aluminium

Compression in Smaller End

Acompressiveloadofmagnitude69.98MPaisappliedatthesmaller end keeping the bigger end fixed.

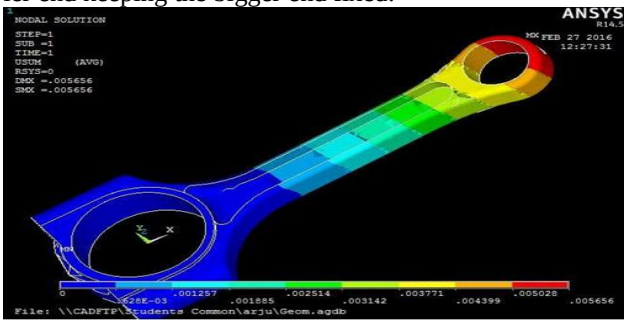

Fig.11:Total Deformation of Steel

 ISBN: 978-93-91420-02-4

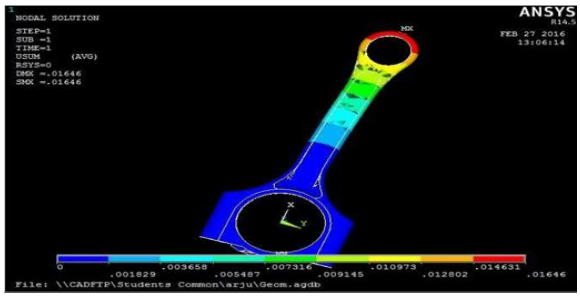

Fig.12:Total Deformation of Aluminium

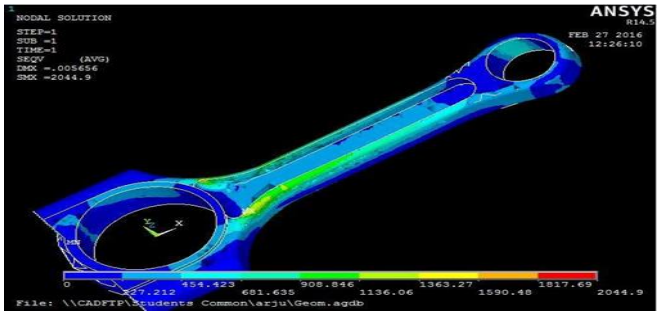

Fig.13: Von-Mises Stress of Steel

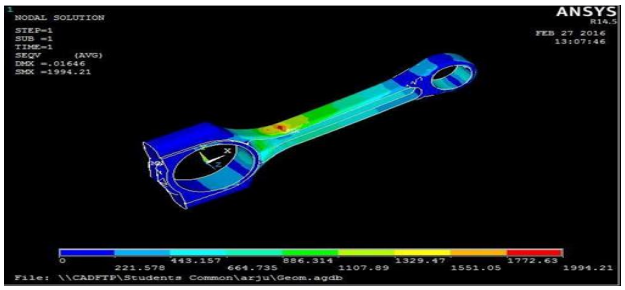

Fig.14:Von-Mises Stress of Aluminium

Tension in Smaller End

A tensile force of 77.17MPa is applied at the smaller end while keeping the bigger end remains fixed.

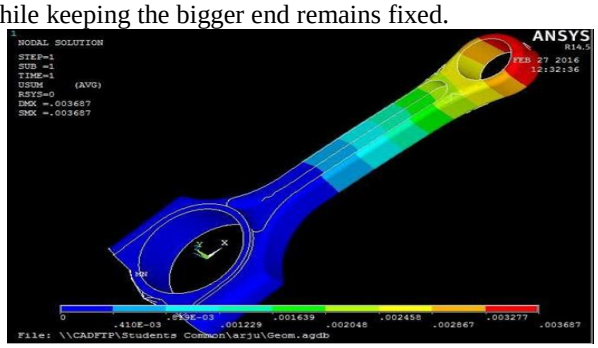

Fig.15:TotalDeformationofSteel

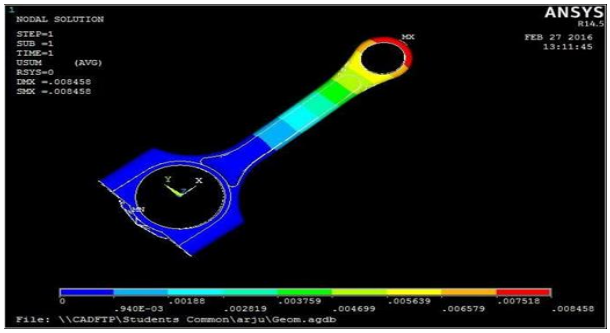

Fig.16:Total Deformation of Aluminium

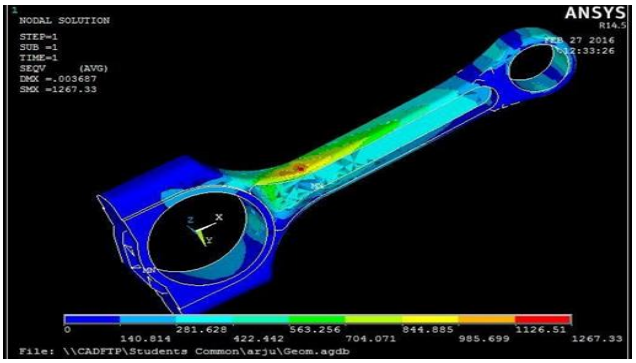

Fig.17: Von-Mises Stress of Steel

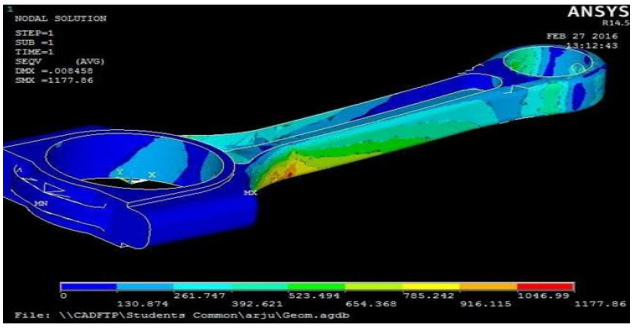

Fig.18:Von Mises Stress of Aluminium

III.RESULTS AND DISCUSSIONS

Material: Steel

Method of loading	Load applied(MPa)	Maximum displacement(mm)	Maximum stress(N/mm^2)
Compressive at bigger end	41.15	0.012	2490.87
Tensile at bigger end	37.66	0.007	1605.51
Compressive at small end	77.17	0.005	2044.90
Tensile at smaller end	69.98	0.003	1267.33

Material: Aluminium

Method of loading	Load applied(MPa)	Maximum displacement(mm)	Maximum stress(N/mm^2)
Compressive at bigger end	41.15	0.055	3611.37
Tensile at bigger end	37.66	0.034	2655.57
Compressive at small end	77.17	0.016	1999.21
Tensile at smaller end	69.98	0.008	1177.86

Comparison of von mises stress variation for the two materials are as shown below:

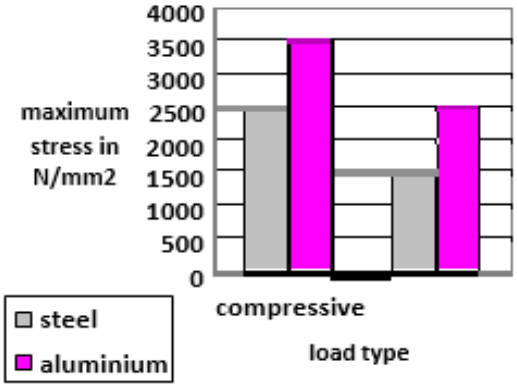

Graph 1: Load applied at The Bigger End

ISBN: 978-93-91420-02-4

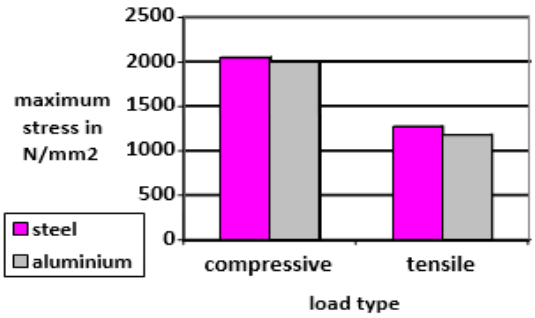

Graph 2: Load applied at smaller End

Buckling and bending stresses, non – symmetric shape of connecting rod, Flash and bolt holes was eliminated while analysis. We could conclude that the influence of compressive stress is more in connecting rod due to gas pressure and whipping stress as shown. The piston region suffers tensile stress due to inertia loads. The more stressed part of the rod is being shown using von misses stress plot.

IV.CONCLUSION

It was observed that connecting Rod made up of Aluminum has higher intensity of stress induced as compared to connecting Rod made up of Steel. Also, there is a great opportunity to improve the design. Hence steel is a better choice for connecting rods.

REFERENCES

[1] Hippoliti R., 1993,"FEM method for design and optimization of connecting rods for small two-stroke engines," SmallEngineTechnologyConference,pp.217-231.

[2] Serag, S., Sevien, L., Sheha, G., and El-Beshtawi, I., 1989, "Optimal design of the connecting-rod", Modelling, Simulation and Control, B, AMSE Press, Vol.24,No.3, pp.49-63.

[3] Mukesh Kumar, Veerendra Kumar" Finite Element Analysis of I.C Engine Connecting Rod: A Review", International Journal of EngineeringSciences&ResearchTechnologyJuly,2014

[4] Kuldeep B, Arun L.R, Mohammed Faheem "Analysis and optimization of Connecting rod using Alfasic Composites", International Journal of Innovative Research in Science, Engineering and Technology; Vol.2, Issue 6, June2013

[5] Abhinav gautam, K Priya Ajit "Static Stress Analysis of Connecting Rod Using FEA Approach", Journal of Mechanical and Civil Engineering(IOSR-JMCE)Volume10,Issue1(Nov.-Dec.2013)

 ISBN: 978-93-91420-02-4

A Study and Synthesis of 8 Bar one Degree of Freedom Walking Mechanism

D. Samson and B.Venkata Siva
Department of Mechanical Engineering, Narasaraopeta Engineering College (A), Narasaraopet, India.

***Abstract*—With the advent of robotics the researchers are thriving to achieve animal like walking creatures for obvious advantages but all the walking like robots have their own disadvantages, use of multiple actuators and coordination between these actuators among these research. Theo Jansen [6] proposed a mechanism which has single degree of freedom varying a single actuator can produce walking like mechanisms without the use of complex coding required in above said mechanisms.**

Present study is to analyze the Theo Jansen walking mechanism and study its advantages and disadvantages and second part of thesis a new mechanism is synthesis using random sampling and basic mechanisms, which would be more stable and efficient over the existing mechanisms.

Keywords— Walking Robot, Mechanisms, Kinematic analysis, SolidWorks.

I. INTRODUCTION

Many animals in nature have adopted legs for various environmental conditions. Centipedes, spiders, cockroaches, cats, camels, kangaroos, and human are among those, either with different number of legs or with different kind of walking. It is understandable that people turned their attention to those walking animals, after it was recognized that the human invented wheeled and tracked systems did not satisfy all the needs. In this sense, legged systems have a peculiarity of imitating the nature.

It introduces more flexibility and terrain adaptability at the cost of low speed and increased control complexity. In order to develop dynamic model and control algorithm of legged robots, it is important to have good models describing the kinematic behavior of the complex multi-legged robotic mechanism as walking machines are increasingly gaining importance in space for planetary exploration, where the terrain is rugged thus reducing the expensive and dangerous extra vehicular Activities by Astronauts. Walking machines find wide range of applications like in military logistic support where there are no highways.

Legged locomotion is a proper solution for movements on loose-rough-uneven terrains. This advantage of legged locomotion is mostly due to the fact that legged systems use isolated footholds. Wheeled and tracked systems follow the surface in a continuous manner; therefore their performance is limited by the worst parts on the terrain. A legged system, on the other hand, can choose the best places for foot placement. These footholds are isolated from the remaining parts; hence the performance of the legged system is limited by the best footholds. Besides using isolated footholds, the legged system can provide active suspension, which does not exist in wheeled or tracked systems. This means that the system can have control on the force distribution through the foothold points. In this way an efficient utilization of the footholds provides further improvement of the vehicle-ground interaction. A legged system is well adaptive to uneven terrains, namely the legs can be arranged (lengthened and shortened according to the level changes, and they can jump over obstacles or holes. Therefore, the body can be moved in a desired orientation.

The sensible control of swimming [Tan et al.2011], muscle-driven biped recreation [Geijtenbeek et al.2013], step revelation for quadrupeds [Lee et al.2013], or learning bike stunts [Tan et al. 2014].Translating virtual walk recreations into this present reality is non-insignificant. For people and creatures, many muscles need to act as one by means of a focal sensory system for steady and productive walks. In a robot, the arrangement of actuators as muscles requires numerous sensors and a mind boggling controller. In this setting it is hard to manufacture as, regardless of whether one could discover physical actuators and joints for every single virtual engine, the subsequent cost would surpass what is satisfactory for most applications, and particularly for the basic automata that we consider: for toy and instructive utilize, they have one engine for each appendage, no sensors, and no abnormal state controller; yet, they can walk effectively once created.

Strolling Motions Control in Animation and Robotics An assortment of cutting edge control techniques have been proposed for human physically-mimicked people [Geijtenbeek et al.2013; Lee et al 2010] and creatures [Wampler and Popovic 2009; Coros et al 2011].Such strategies have been connected to modern legged robots to produce controllers [Gehring et al 2013], or to build the dexterity of headway controllers [Gehring et al 2014]. Nonetheless, complex control techniques require muddled mechanics, sensors, and actuators, and the StarlETH robot is well past the intricacy and cost of our objective of automata as toys, in their plans are essentially more straightforward in nature, yet are as yet ready to perform strolling movements. As such, the work is substantially nearer to late work in computational outline than to the general field of mechanical technology.

Computational Design and Fabrication This field lessens the trouble of plan and assembling issues by making devices which forego or decrease the requirement for master space information. For example, late works display specially formed articles that can fly [Umetani et al 2014], remain without anyone else [Prevost et al.2013],or turn steadily [Bacher et al.2014]. A few techniques intend to convey virtual characters to this present reality, and it is currently conceivable to make 3D printable portrayals of virtual characters with joints [Bacher et al 2012; Calı et al.2012], to plan mechanical toys fit for intriguing (non-strolling) movements [Coros et al.2013; Ceylan et al.2013; Thomaszewski et al.2014], or to produce physical characters utilizing flexible materials with the end goal that their twisting affected by outer powers can be controlled.

Coros et al. [2013] take note of that regardless of whether the movement of a mechanical character at first look takes after strolling, this does not imply that the robot would really walk if manufactured. In beginning tests, they were not ready to make any automata along these lines that were fit for strolling steadily, unless we utilized an expansive number of legs (i.e., hexapod). This features the requirement for mechanized techniques. As far as anyone is concerned, work is first to

 ISBN: 978-93-91420-02-4

research the test of planning programmed robot that can walk steadily

II. MODELLING

A. Conceptual Design of the walking mechanism in CAD

Solid works is one of the best CAD Solid modeling software, Solid works is also known as "DSS Solid works". DSS means the Dassault Systems, the developer of this CAD Software. This is CAD Software, which helps to create 2D or 3D Solid models without any complexity, faster and in the cost effective way. The main advantage of the solid works is that very easy to use, simple graphics user interface and much more friendly, as compared with other CAD Solid modeling software's it contains solid modeling, motion, simulation, toolbox, tool analyst, circuit works etc..

The Solid Works software enables you to design models quickly and precisely based on two methods: Defined by 3D design, Based on components

B. Design intent

Design intent determines how you want your model to react as a result of any changes you need to make to the model. Design intent is primarily about planning. Deciding how to create the model determines how changes affect the model. The closer your design implementation is to your design intent, the greater the integrity of the model. Various factors contribute to the design process, including current needs. Understand the purpose of the model to design it efficiently. Future considerations. Anticipate potential requirements to minimize redesign efforts when changing the model.

C. Design Method

After the conceptualization of the model sketching, applying features, and finally assembling is the process of the design model development. Fig.1

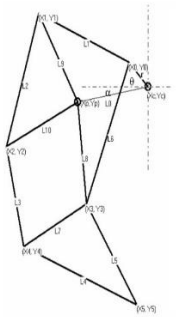

Fig.1 Theo Jansen Mechanism

III. SIMULATION

A. FOOT POINT TRAJECTORIES FOR WALKING

The Path followed by the foot of a walking machine is of crucial importance to the machine's correct functioning. There is a relationship between the trajectory provided by the mechanism and the overall design and format of the walking machine. The general idea of the project is to develop a walking mechanism from Jansen's work which states that the foot should follow a triangular path as shown in the figure below.

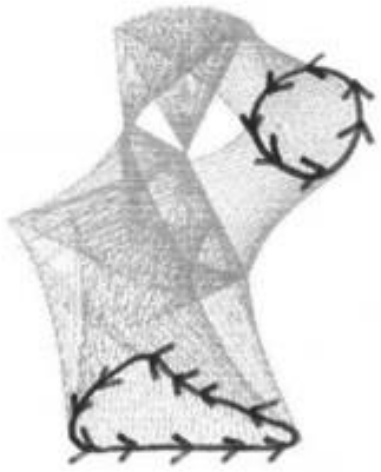

Fig.2 Walking stride

The foot trajectory shown in Figure is not necessarily the optimum trajectory shape. The problem with this specific trajectory is the curve between points 2 and 5, the walking portion of the cycle. The vehicle body, being connected to the foot by a rigid leg, would experience a motion inverse to this foot curve. Vehicle occupants would feel the vehicle rising and falling. A better foot trajectory would have this portion of the curve as near to a horizontal straight line as possible, keeping the body horizontal on a horizontal walking surface. Note that flatter lower portion in Jansen's trajectory in the above case.

The flatness of the walking curve can be determined by obtaining a straight line fit to the trajectory points using a least squares linear regression. The correlation coefficient of the regression is taken as a measure of the flatness. The future work can be varied to quantify flatness.

B. Duty Cycle

The duty cycle of a leg mechanism is the proportion of the total cycle time that the leg is touching the ground, making it capable of bearing weight. Mathematically this can be expressed as

$$DC = \frac{T_1}{T_t} \text{ ----------} \quad \text{Equation 19}$$

Where

DC = Duty cycle
T_1 = Loaded time
T_t = Total leg cycle time

Initial look out into the properties of the Jansen mechanism were to see if mechanisms with 75% duty could be found, such a mechanism would allow the design of a statically balanced quadruped machine layout. Unfortunately, no such mechanism was found, using a simple exhaustive search algorithm. Later searches all implicitly accept mechanisms with a 50% duty cycle.

C. Mechanism size

Clearly, the smaller the mechanism the better performance. Smaller mechanism will be lighter, have stiffer

 ISBN: 978-93-91420-02-4

links and have lower inertial loads. The size of the mechanism can be represented by the sum of the length of the links as.

$$L_l = \sum_{i=1}^{10} l_i \qquad \text{---------- Equation 20}$$

Where

L_l = Total link length

l_i = Length of link i

IV. RESULTS AND DISCUSSION

The part design ,assembly and motion study modules of solid works were used to justify the path traced by each point of the mechanism an also compare the proposed mechanism with Theo Jansen mechanism.

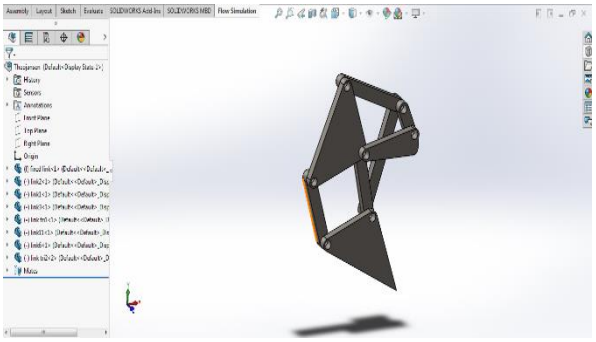

Fig 3: Assembly of Theo Jansen Mechanism in Solid Works

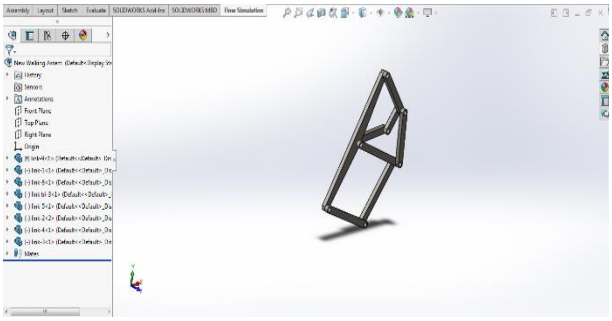

Fig 4: Assembly of Proposed Mechanism in Solid Works

Links of both synthesized and Theo Jansen mechanisms were drafted in part design module and were assembled according to the constraints and were simulated to generate the below discussed results.

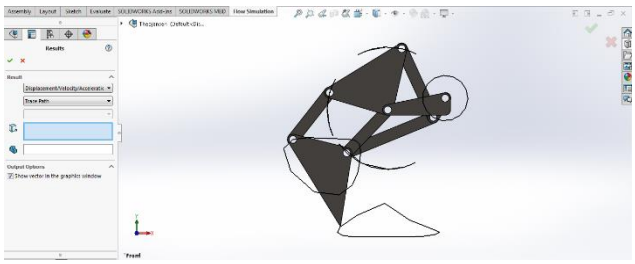

Fig 5: Path Traced by links of Theo Jansen Mechanism in Solid Works

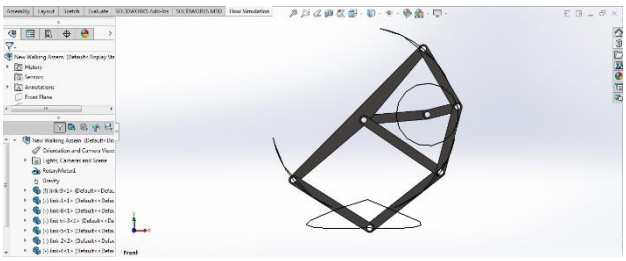

Fig 6: Path Traced by the Proposed Mechanism in Solid Works

From the above figure, we can see that the required path as planned is produced by the newly developed mechanism compared to the Theo Jansen mechanism the mechanism has less number of innings and the more distributed walking path the trajectory followed is as produced by the combined effect of lambert Lambda mechanism and inverting mechanism combined.

The other features like the displacement acceleration and velocity analysis were also done on both the mechanisms and the results are displayed as follows.

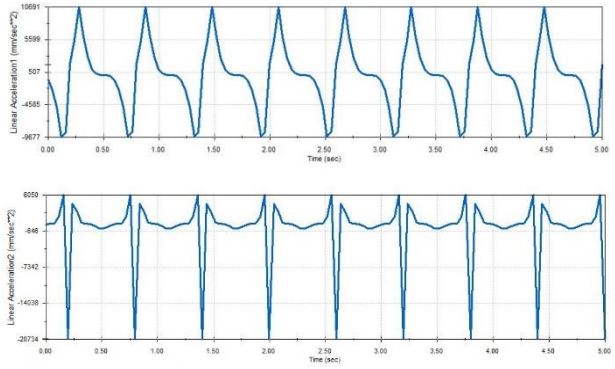

Fig. 7: Plots for acceleration in X and Y direction for Proposed mechanism

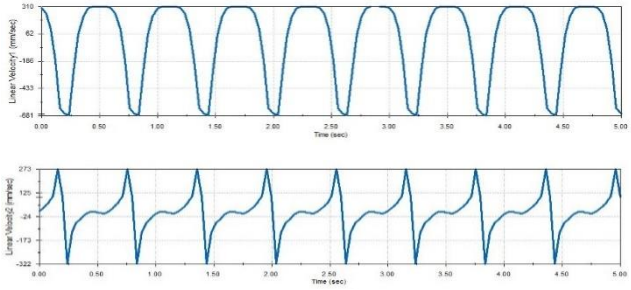

Fig. 8: Plots for velocity in X and Y direction for proposed mechanism

The above plot shows the different velocity and acceleration plot traced by the newly development mechanism and when compared to the Theo Jansen plots shows that the velocity develop in the newly developed mechanism is superior to the velocity develop in case of Theo Jansen mechanism.

The following observation was made after the comparison of displacement, velocity and acceleration diagrams in solid works as shown in the table 1.

 ISBN: 978-93-91420-02-4

	Theo Jansen Mechanism	Proposed Mechanism
Normalized Stride Length	1	1
Normalized Step Height	0.33	0.2491
Normalized Standard Deviation of y position	0.0070	0.0030
Normalized Mean x velocity	0.0020	0.01871
Normalized Standard Deviation of x velocity	0.0036	0.0018
Normalized Crank radius	0.22	0.2682
Normalized CM Y deviation (One leg)	0.14	0.079
Normalized CM X deviation (One leg)	0.36	0.071
Normalized CM Y deviation (Leg Pair)	0.064	0.053
Normalized CM X deviation (Leg Pair)	0.31	0.035
Normalized CM Y deviation (three leg pairs)	0.031	0.0041
Normalized CM Y deviation (three leg pairs)	0.018	0.011

Table 1 Comparison between the Proposed Mechanism and the Theo Jansen Mechanism

V. CONCLUSIONS

From the above result we can conclude that the newly developed mechanism has:

- Lower center of gravity that is the system is more stable than that Theo Jansen mechanism.
- The new mechanism is simpler in case of number of links and joints.

It has shortened links compared to the other mechanism. Require less torque compared to the other mechanism. Table 2 gives the comparison of existing mechanism with the proposed mechanism.

Theo Jansen Mechanism Advantages	Proposed Mechanism Advantages
• Step height 33% higher • 4% faster Stride • Pair of legs may occur same plane	• Standard deviation of stride height is 50% lower • Standard deviation of stride x velocity is 50% lower • Locus is symmetric across the y axis • 85% less CM movement during locomotion

Table 2: Summary of comparison

REFERENCES

[1] Aan, A. &Heinloo, M. 2012. Computer based comparison analysis of single and double connecting-rod slider-crank linkages. Agronomy Research 10, 3–10.

[2] Aan, A., Heinloo, M., Aarend, E. &Mikita, V., 2012. Analysis of four-stroke cycle internal combustion V-engine in Mathcad environment. 8th International DAAAM Baltic Conference 'Industrial Engineering', Tallinn, TTU Press, 389–394.

[3] Aan., A. 2014. Jansen linkage. Available at: http://www.youtube.com/watch?v=B_dR2_O3ujc(30.01.2014)

[4] Artobolevski, I.I. 1961. Theory of mechanism and machines (in Estonian). Tallinn, 743 p.

[5] Moldovan, F., Dolga, V., Ciontos, O. & Pop, C. 2011. Cad design and analytical model of a twelve bar walking mechanism. Scientific Bulletin, Series D, 73(2).

[6] Jansen, T. 2007. Theo Jansen: The Great Pretender. Rotterdam, 010 Publisher, 240 p.

[7] Komoda, K. & Wagatsuma, H. 2011. A study of availability and extensibility of Theo Jansen mechanism toward climbing over pumps. The 21st Annual Conference of the Japanese

 ISBN: 978-93-91420-02-4

Mechanical Properties and Machining of Al 7075-SiC Composites

S. Rama Rao [1] , M. Ravi Kumar[2], V. Rama Koteswara Rao [3]
[1]Department of Mechanical EngineeringTirumala Engineering College, Narasaraopet, India.
[2] Department. of Mechanical Engineering, MANIT Bhopal, Bhopal, India.
[3]Department of Mechanical Engineering, R.V.R & J.C College of Engineering, Guntur, India,

***Abstract*—Al 7075 has potential applications in space, aircraft, marine and automobile industries. So, the strength and wear resistance of the Al 7075 should be improved. Moreover, the strength and wear resistance can be improved by adding of various ceramic particles which are known as composites. Therefore, in the current research work the reinforcements silicon carbide (SiC) ceramic particles with different wt. %(2, 4 and 6) are added with the matrix Al7075. Later on, the mechanical properties like tensile strength and hardness of the fabricated composites are investigated. In addition to, the machinability (turning) characteristics of the fabricated Al7075-SiC composites are examined. Second order regression models are developed using response surface methodology and statistical validity of the models is checked by conducting ANOVA.**

Keywords*—*Al 7075 alloy, ANOVA, material removal rate, SiC, surface roughness

I. INTRODUCTION

Manufacturing of aluminium metal matrix composites (AMMCs) with improved mechanical and tribological properties has been one of the foremost requirements in the area of aircraft, marine and space industries. Aluminium 7075 alloy reinforced with Silicon Carbide (SiC) is using instead of aluminium oxide (Al_2O_3)-aluminium composites due to their elevated creep and wear resistances properties [1]. The distinguished properties of Al-SiC composites are less weight, high tensile strength, modulus of elasticity, hardness and fatigue strength. The impact strength, tensile strength and hardness of Al-SiC composites increases with increase in wt. % of SiC in composites [2]. Machinability of AMMCs is entirely different from single-phase metals or alloys due to high abrasive nature of the reinforce element and leads to high tool wear [3].Conventional materials are replacing rapidly by AMMCs in the industries like automobile and aerospace [4]. Amongst other fabrication techniques stir casting is one of the best liquid metallurgy techniques which is used to produce the metal matrix composites. This process is trouble-free, flexible and economical and can be used in mass production of composites [5]. Carbon dioxide sand molding process was used to produce LM6 alloy-quartz-silicon dioxide metal matrix composites and observed that tensile strength decreases while adding of quartz particle to LM6 alloy [6].Stir casting rout is used by many researcher to produce metal matrix composites (MMCs) [7, 8 and 9]. The tool wear and material removal rate (multi-responses) were optimized in turning of Al7075 with 15 wt. % SiC micro composites using regression models [10]. Moreover, the response surface methodology (RSM) was implemented in various applications like, for designing the experiments in turning of Al-SiC nano-composites [11], for parametric study of Al6061/Al2O3/SiC hybrid composites with improved hydrophobicity [12], for tuning a machine learning algorithm's hyper parameters [13], to develop the regression models in grinding of silicon [14], etc.

The tensile strength and hardness of the composites varies by varying the weight percentage of reinforcement which ultimately effects on the machining quality of the composites like SR, MRR and tool wear rate (TWR) etc. Therefore, in the present research work percentage of reinforcement is also considered as one of the machining parameter along with feed, cutting speed and depth of cut. Moreover, in this research paper a comparative study for the multiple responses, i.e. SR and MRR, while turning the Al-SiC composites was also discussed.

II. MATERIALS AND METHODS

In this work Al 7075 alloy is used as the matrix material and silicon carbide (SiC) is used as a reinforcement. The chemical composition of Al7075 alloy is shown in Table 1. Due to the high strength, high resistance to stress and strain and light weight of Al7075 aluminum alloy makes it highly useful in aircraft, marine, automobile and space applications.

TABLE I. CHEMICAL COMPOSITION OF AL 7075

Element	Al	Zn	Mg	Cu	Cr	Others
Wt %	90	5.6	2.5	1.6	0.23	0.07

Response Surface Methodology (RSM): It is a group of statistical and mathematical techniques useful for solving the problems in which numerous input (independent) factors influence a output (dependent) factor or response, and the objective is to optimize this output factor [15]. Central composite design in RSM is considered in present work with 18 factorial points, 6 axial points and 3 central points (total 27 runs) for the experimentation. Moreover, the development of regression models to various responses of machining process, a quadratic response surface has been anticipated as:

$$P = \beta_0 + \sum_{i=1}^{k} \beta_i q_i + \sum_{i=1}^{k} \beta_{ii} q_i^2 + \sum \sum_{i<j} \beta_{ij} q_i q_j + \varepsilon \quad (1)$$

In (1), q_1, q_2 and q_k are linear terms, q_1^2, q_2^2 and $q_k^2$are squared terms, q_1q_2, q_1q_3, … $q_{k-1}q_k$are interaction terms and β is the regression coefficient.

III. FABRICATION AND MECHANICAL PROPERTIES OF COMPOSITES

A. Fabrication of Composites

Fabrication of Al 7075-SiC composites with varying weight percentages of SiC particles (2, 4 and 6) are carried out by stir casting setup which is shown in Fig. 1. Moreover, the SiC particles surface is oxidized by preheating them at 800^0C for 2 hrs. and Al 7075 alloy slabs are melted in muffle furnace. Further, the molten metal is cooled to below the melting point temperature and the slurry is maintained at semi-solid state.

 ISBN: 978-93-91420-02-4

The preheated SiC particles are added in to the slurry and mixed manually. Then the slurry with SiC particles is reheated to liquid state and mixing mechanically for 20 min at a mixing speed of 350 to 400 rpm. Finally, the temperature of composite slurry is controlled around 750^0C and after continues stirring, and then it is poured into circular moulds of 20 mm diameter and cooled to obtain cast rods.

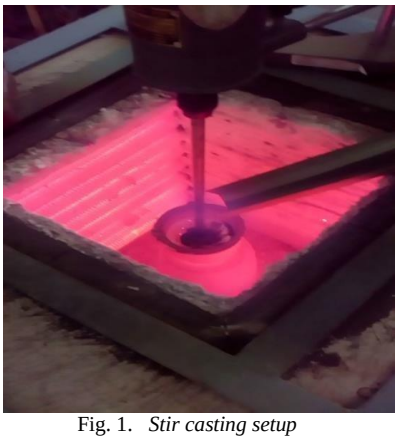

Fig. 1. *Stir casting setup*

B. Mechanical Properties of Composites

The hardness values of the developed composites are tested using brinnel hardness testing machine and are given in Table 2. The ultimate tensile strength of the composites are also tested using universal testing machine (UTM) and the values are given in Table 2 and observed that both hardness and tensile strength of the Al-SiC composites are increased by the addition of SiC ceramic particles.

TABLE II. MECHANICAL PROPERTIES OF COMPOSITES

Composition	Hardness (BHN)	Ultimate Tensile Strength(N/mm^2)
Al 7075	90.0	300.20
Al7075+2%SiC	97.5	304.12
Al7075+4%SiC	108.0	309.85
Al7075+6%SiC	120.0	315.00

IV. EXPERIMENTAL RESULTS AND ANALYSIS

A. Machining of the Composites

The strength and hardness of the composites are changing with wt% of reinforcement in composites. As the hardness increases MRR decreases, in this paper percentage of reinforcement (wt%) is also taken as one of the variable along with feed, speed and depth of cut while turning the composites. The variables and their levels are considered in the present study are shown in Table 3.

Experiments are conducted on CNC lathe by varying the predominant machining parameters such as, cutting speed, feed rate, depth of cut and wt% of reinforcement and the observations are recorded. Moreover, while conducting the experimentation the machining time is kept constant as 25 s. The SR is measured with the help of Mitutoyo Talysurf tester. The output response MRR is the ratio of weight loss of the work piece in machining and the machining time. Therefore, the value of MRR is measured using (2) and the experimental results are shown in Table 4.

$$MRR = (W_{bm}-W_{am})/T \quad (2)$$

where W_{bm}= Weight of workpiece before machining,W_{am}= Weight of workpiece after machining and T = Time taken for machining.

TABLE III. PROCESS PARAMETERS AND THEIR LEVELS

Parameters	Code	L1	L2	L3
Cutting Speed(m/min)	A	1200	1350	1500
Feed Rate(mm/rev.)	B	0.2	0.15	0.18
Depth of Cut(mm)	C	0.8	0.9	1.0
% of Reinforcement (wt%)	D	2	4	6

TABLE IV. EXPERIMENTAL RESULTS

EXP. NO.	SPEED (RPM)	FEED (MM/REV.)	DEPTH OF CUT (MM)	% OF SIC	MRR (G/S)	SR (µM)
1	1200	0.15	0.8	2	7.713	2.42
2	1500	0.15	0.8	2	11.096	2.35
3	1200	0.20	0.8	2	7.563	1.79
4	1500	0.20	0.8	2	10.345	2.78
5	1200	0.15	1.0	2	8.345	2.45
6	1500	0.15	1.0	2	11.638	2.91
7	1200	0.20	1.0	2	10.035	2.59
8	1500	0.20	1.0	2	12.256	4.02
9	1200	0.15	0.8	6	8.562	2.69
10	1500	0.15	0.8	6	9.937	2.46
11	1200	0.20	0.8	6	8.320	2.51
12	1500	0.20	0.8	6	8.789	2.70
13	1200	0.15	1.0	6	8.894	2.61
14	1500	0.15	1.0	6	9.874	2.46
15	1200	0.20	1.0	6	10.259	3.31
16	1500	0.20	1.0	6	10.392	3.91
17	1200	0.175	0.9	4	7.116	1.83
18	1500	0.175	0.9	4	9.002	1.98
19	1350	0.15	0.9	4	8.123	2.36
20	1350	0.20	0.9	4	8.250	2.46
21	1350	0.175	0.8	4	7.793	2.31
22	1350	0.175	1.0	4	8.898	2.96
23	1350	0.175	0.9	2	8.123	2.75
24	1350	0.175	0.9	6	7.535	2.53
25	1350	0.175	0.9	4	7.579	2.25
26	1350	0.175	0.9	4	7.695	2.32
27	1350	0.175	0.9	4	7.723	2.31

B. Regression Models

A non-linear regression equation correlating dependent response with independent variables is obtained through response surface.

Experimental data in the Table 4 is utilized to establish the non-linear regression model for response material removal rate. Response equation (1) in the coded form of the parameters is given as:

$$MRR=7.63+0.9179A+0.1126B+0.5818C-0.2529D-0.2141AB-0.864AC-0.5451AD+0.4051BC-0.0571BD-0.1091CD+0.4535A^2+0.581B^2+0.74C^2+0.2235D^2 \quad (5)$$

Non-linear regression model for surface roughness in coded form is also developed by using data in Table 4 is given as:

$$SR=2.29+0.1871A+0.1868B+0.2894C+0.0621C+0.0621D+0.2002AB+0.0915AC-0.15AD+0.2211BC+0.0726BD-0.0436CD-0.3767A^2+0.1248B^2+0.3548C^2+0.3588D^2 \quad (6)$$

C. Analysis of Variance (ANOVA)

Once the non-linear regression equations are developed, statistical validity of the equations is checked by conducting

 ISBN: 978-93-91420-02-4

ANOVA test and by verifying coefficient of correlation of the model. Table 5 and 6 show the ANOVA results for MRR and SR, respectively. Results of ANOVA show that all the factors have significant contribution on the objectives MRR and SR with 95% confidence level. Further, coefficient of correlation for MRR and SR are found to be equal to 0.99 and 0.96 respectively. It provides a good relationship between process parameters and responses. From Table 5 and 6 it is observed that the model is significant and lack of fit is insignificant.

TABLE V. ANOVA FOR MRR

SOURCE	SUM OF SQUARES	DOF	MEAN SQUARE	F-VALUE	P-VALUE	
Model	**49.36**	**14**	**3.53**	**687.12**	**< 0.0001**	**significant**
A-A	15.16	1	15.16	2955.2	< 0.0001	
B-B	0.2282	1	0.2282	44.48	< 0.0001	
C-C	6.09	1	6.09	1187.5	< 0.0001	
D-D	1.15	1	1.15	224.29	< 0.0001	
AB	0.7336	1	0.7336	142.96	< 0.0001	
AC	0.1194	1	0.1194	23.26	0.0004	
AD	4.75	1	4.75	926.46	< 0.0001	
BC	2.63	1	2.63	511.78	< 0.0001	
BD	0.0522	1	0.0522	10.17	0.0078	
CD	0.1906	1	0.1906	37.13	< 0.0001	
A^2	0.5289	1	0.5289	103.06	< 0.0001	
B^2	0.8681	1	0.8681	169.16	< 0.0001	
C^2	1.41	1	1.41	274.41	< 0.0001	
D^2	0.1285	1	0.1285	25.03	0.0003	
Residual	**0.0616**	**12**	**0.0051**			
Lack of Fit	0.0499	10	0.0050	0.8564	0.6499	insignificant
Pure Error	0.0117	2	0.0058			
Total	49.43	26				

TABLE VI. ANOVA FOR SR

SOURCE	SUM OF SQUARES	DOF	MEAN SQUARE	F-VALUE	P-VALUE	
Model	49.36	14	3.53	687.12	< 0.0001	significant
A-A	15.16	1	15.16	2955.2	< 0.0001	
B-B	0.2282	1	0.2282	44.48	< 0.0001	
C-C	6.09	1	6.09	1187.5	< 0.0001	
D-D	1.15	1	1.15	224.29	< 0.0001	
AB	0.7336	1	0.7336	142.96	< 0.0001	
AC	0.1194	1	0.1194	23.26	0.0004	
AD	4.75	1	4.75	926.46	< 0.0001	
BC	2.63	1	2.63	511.78	< 0.0001	
BD	0.0522	1	0.0522	10.17	0.0078	
CD	0.1906	1	0.1906	37.13	< 0.0001	
A^2	0.5289	1	0.5289	103.06	< 0.0001	
B^2	0.8681	1	0.8681	169.16	< 0.0001	
C^2	1.41	1	1.41	274.41	< 0.0001	
D^2	0.1285	1	0.1285	25.03	0.0003	
Residual	0.0616	12	0.0051			
Lack of Fit	0.0499	10	0.0050	0.8564	0.6499	insignificant
Pure Error	0.0117	2	0.0058			
Total	49.43	26				

Figures 2 and 3 show the diagnostics of the responses MRR and SR, respectively. The normal probability plot indicates whether the residuals follow a normal distribution or not. Normal probability plot of the residuals for MRR and SR are shown in Figs. 2(a) and 3(a) respectively. From the Figs. 2(a) and 3(a) it is observed the graph is a straight line. Hence for all responses, the residual distribution is normal

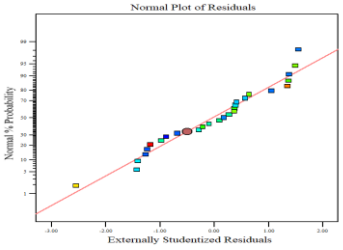

(a)

(a)

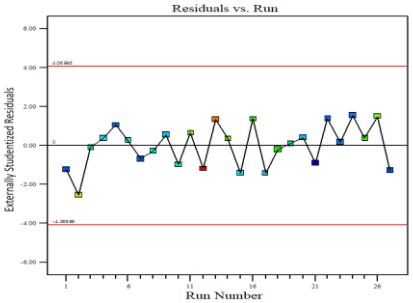

(b)

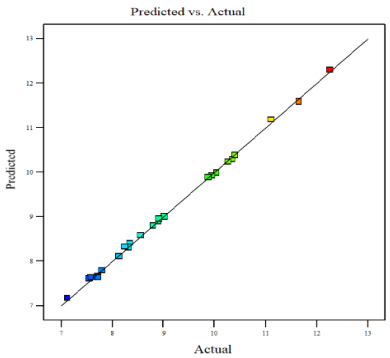

(c)

Fig. 2. *Diagnostics plots of MRR (a) Normal probability curve(b)Residual vs. Run and (c) Predicted vs. Actual*

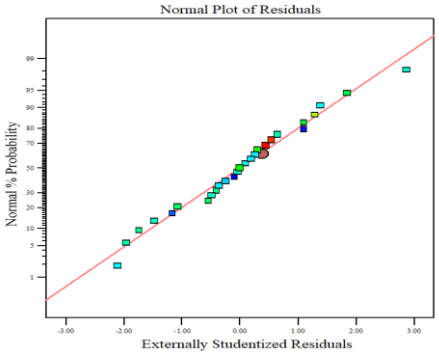

(a)

 ISBN: 978-93-91420-02-4

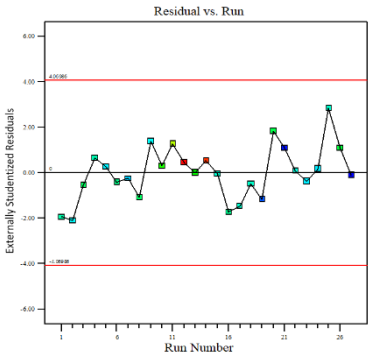

(b)

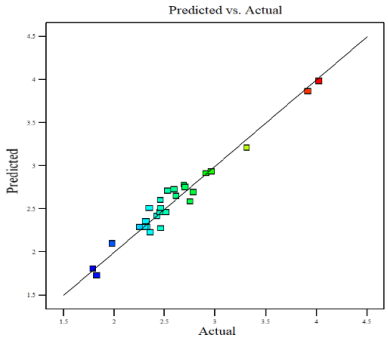

(c)

Fig. 3. *Diagnostics plots of SR (a) Normal probability curve(b)Residual vs. Run and (c) Predicted vs. Actual*

Figures 2(b) and 3(b) show residual values versus the experimental run order for MRR and SR, respectively. This checks the lurking parameters that may have influenced the response during the experiment and the graph should indicate a random scatter. From Figs. 2(b) and 3(b) it is observed the residuals are well distributed above and below the mean and there is no blocking. This implies that the proposed model is adequate. The graph between actual values versus predicted values developed by regression equation is shown in Figs. 2(c) and 3(c). From the Figures it is revealed that actual and predicted values are very near and the error is minimum. So, the developed regression models are adequate.

V. CONCLUSIONS

In the present work Al7075-SiC composites with 2%, 4% and 6% of SiC are fabricated with stir casting equipment and machined on a CNC lathe and finally observed the following:

- Hardness and strength of the fabricated composites increases with increase in wt% of SiC in composites.
- Cutting speed and depth of cut are the significant variables that effect both on MRR and SR in turning of the Al7075-SiC composites.
- With the addition of SiC ceramic particles to aluminium the MRR of the composites decreases and SR increases.
- Regression models for MRR and SR are developed and validated by ANOVA results.

REFERENCES

[1] V.Balaji, N.Sateesh and M. ManzoorHussain, "Manufacture of Aluminium Metal Matrix Composite (Al7075-SiC) by Stir Casting Technique," Materialstoday: proceedings, Vol. 2(4–5), 2015, Pp. 3403-3408

[2] K. L. Meena, A. Manna, S. S. Banwait , Dr. Jaswanti, "An Analysis of Mechanical Properties of the Developed Al/SiC-MMC's," American Journal of Mechanical Engineering, Vol. 1(1), 2013, Pp.14-19

[3] T. Ozben, E. Kilickap and O. Cakir, "Investigation of mechanical and machinability properties of SiC particle reinforced Al-MMC", Journal of materials processing technology, Vol.108, 2008, Pp.220-225.

[4] J.E. Allison, and G.S.Cole, "Metal Matrix Composite in Automotive Industry: Opportunities and Challenges," Journal of Mechanical Science, Vol. 45(19-24). 1993., Pp. 19-24

[5] M.K. Surappa, "Microstructure Evolution during Solidification of DRMMCs: State of the Art," Journal of Materials Processing Technology, Vol. 63(1-3), 1997, Pp. 325-333.

[6] S. Sulaiman, M.Sayuti, and R. Samin, "Mechanical Properties of the As-Cast Quartz Particulate Reinforced LM6 Alloy Matrix Composites," Journal of Material Processing Technology, Vol. 201, 2008, Pp.731-735.

[7] S. Rama Rao, G Padmanabhan and PV Chandra Shekar Rao, "Fabrication and tribological properties of Al-Si/B4C metal matrix composites," International Journal of Surface Engineering and Interdisciplinary Materials Science, 2(1), 2014, Pp. 74-84.

[8] D. Siva Prasad and Ch. Shoba, "Experimental evaluation onto the damping behavior of Al/SiC/RHA hybrid composites, Journal of Materials Research and Technology,"Vol. 5(2), 2016, Pp. 123-130.

[9] Ch. Shoba,D. Siva Prasad andP. Raju, "Investigations on the Machinability of Al/SiC/RHA Hybrid Metal Matrix Composites,"Silicon, Vol. 11(1), 2019, Pp. 2907–2918.

[10] P. Garga,A. Jamwal, D.Kumar, K.K. Sadasivuni, C. M. Hussain, and P. Gupta, "Advance research progresses in aluminium matrix composites: manufacturing & applications," Journal of Materials Research and Technology, Vol. 8(5), 2019, Pp. 4924-4939.

[11] J. Hemanth, "Tribological behavior of cryogenically treated B_4Cp/Al-12%Si composites." Wear, Vol. 258, 2005, Pp. 1732–1744.

[12] B. Acherjee, "Laser transmission welding of dissimilar plastics: analyses of parametric effects and process optimization using grey-based Taguchi method,"Modern Manufacturing Processes, Woodhead Publishing Reviews: Mechanical Engineering Series, 2020, Pp. 131-144.

[13] G. Taguchi and S. Konishi, "Taguchi methods, orthogonal arrays and linear graphs, tools for quality engineering," Dearborn, MI: American Supplier Institute, 1997, Pp.35–38.

[14] A. P. Kumar , B. J. Naik, Ch. Venkatarao and S. Rama Rao, "Optimization of casting parameters for casting of Al/RHA/RM hybrid composites using taguchi method," International Journal of Engineering Trends and Technology, Vol. 4(8), 2013, Pp. 3284-3288,

[15] G. Eason, B. Noble, and I. N. Sneddon, "On certain integrals of Lipschitz-Hankel type involving products of Bessel functions," Phil. Trans. Roy. Soc. A mathamatical, Physcical and Engineering Sciences, vol. 247, 1955, Pp. 529–551,

 ISBN: 978-93-91420-02-4

Characterization of Tungsten carbide reinforced Al7075 matrix Composites

Dr. D Venkata Rao, Y. Ravi Kishore and G. Raju [3]
Department of Mechanical Engineering,, Kallam Haranadhareddy Institute of Technology, Guntur, Andhra Pradesh, India.
,

***Abstract*—Metal matrix composites are exhibit extremely good thermal stability associated with high strength, ductility and toughness at higher temperature. These characteristic features of MMCs are most desirable for design applications The Purpose of this work is to study about the microstructures and mechanical properties of as cast tungsten carbide (wc) reinforced aluminum matrix composites. Aluminum matrix composite of varying WC content (1.5, 3, 4.5 and 6 wt. %) were prepared by stir casting process. Microstructures, hardness, tensile strength and impact strength are were analyzed for prepared composites. The results showed that adding wc reinforcements in aluminum (Al) matrix increased hardness, tensile strength at 6wt%WC and Decreased Impact strength. .Microstructure observation revealed clustering and non-homogeneous distribution of wc particles in the Al matrix. Porosities were observed in microstructures.**

I. INTRODUCTION

The primary matrix materials are being used in the manufacture of MMCs such as aluminum, magnesium, copper, titanium and super alloys. The matrix is a continuous phase which provides a binding support for the reinforcement .MMCs exhibit extremely good thermal stability associated with high strength, ductility and toughness at higher temperature. These characteristic features of MMCs are most desirable for design applications. Rule of mixtures provide an approximation of the desired properties of the composites such as thermal conductivity, thermal expansion and density in certain cases. Mechanical properties such as strength, stiffness, toughness, ductility and wear resistance cannot be easily predicted. The presence of reinforcements produces changes in the microstructure of the matrix and corresponding changes in the contribution of the matrix to the overall properties of the metal matrix composites (MMCs).Most metals and alloys could be used as matrices and they requ5ire reinforcement materials which need to be stable over a range of temperatures and also non-reactive. However, the choices for low temperature applications are not many. Only light metals, with their low density prove to be advantageous. Aluminum, Titanium and Magnesium are the popular matrix metals. The Metal Matrix Composites (MMCs) have to offer high strength, and hence they require high modulus reinforcements. The strength to weight ratio of resulting composites can be higher than most alloys. The melting point, physical and mechanical properties of the composite at various temperatures determine the service temperature of composites. Metal Matrix Composites (MMCs) exhibit extremely good thermal stability associated with high strength, ductility and toughness at higher temperatures. . The primary requirement of a material, for such an arduous operation, is to maintain desired strength and stiffness without failing and deforming excessively. Metal Matrix Composites are preferred engineering materials for automobile, aerospace and mineral processing and mining industries, for various high performing components that are being used for varieties of applications, owing to their high elastic modulus, hardness, tensile strength at room and elevated temperatures, excellent thermal conductivity, wear resistance combined with significant weight savings and improved corrosion resistance over conventional alloys [1-2].

The common metals used as matrix materials are Aluminum, Magnesium, Titanium, and their alloys. The reinforcements are being used in the form of fibers, whiskers and particulates. The advantages of particle-reinforced composites over others are their formability with cost advantage and improved abrasion resistance [3]hence they find applications as cylinder blocks, bearings, disk brakes, calipers, connecting rods, and space structures The elastic properties of MMCs are strongly influenced by micro structural parameters of the reinforcement such as shape, size, orientation, distribution and volume fraction [4].

AMCs can be manufactured by liquid state processing (stir casting, infiltration, squeeze casting etc.), semisolid processing and powder metallurgical route. Usually nonmetallic and ceramic particles like silicon carbide (SiC), Tungstone carbide (wc) alumina (Al2O3), boron carbide (B4C), graphite etc. are used as reinforcements in AMCs.

The aim of this study is to observe the effect of WC reinforcements in Al matrix composites on micro structural aspects, hardness, tensile strength and impact test

II. EXPERIMENTAL

A. Materials

Aluminum 7075

The material used in the present study is Al 7075 whose chemical composition is listed in Table 1. It therefore has a low melting point 660°C. The molten metal has high fluidity and solidifies at constant temperature. It possess excellent mechanical properties, such as good corrosion resistance, good deformation behaviour, high specific modulus, tensile strength, hardness, good wear resistance and low coefficient of thermal expansion.

TABLE I: chemical Composition of AL7075 matrix used the present study.

Chemical Composition	Cu	Mg	Si	Fe	Mn	Zn	Cr	al
Al7075	1.16	1.92	0.119	0.13	0.003	4.5	0.005	Bal

B. Tungustun crabide

Tungsten carbide (WC) is commonly known as carbide. It is an inorganic compound having Tungsten and carbon atoms in equal amount Fig. 1 which is colloquially called carbide. In its most basic form it is a fine gray power. In the present investigation WC of 5 microns size is used as reinforcement in preparing the MMCs. The wt% of WC was varied from 1.5 to 6 wt% in steps of 1.5 wt%. Tungsten

 ISBN: 978-93-91420-02-4

Carbide (WC) is having very high hardness, density, tensile strength and modulus of 1630 Mohr's scale, 14.9 g/cc, 5000 MPa and 629 GPa respectively. It is widely used in industrial machinery, tools, abrasive and also in high hardness. It is basically used in the manufacture of friction pads and liner tubes in furnace etc. The Tungsten carbide is approximately three times stiffer than steel, and much denser than steel.

Fig. 1: Tungsten carbide (WC) particulates

C. Preperation of Al7075- WC composits:

In the present study, stir casting method is used for the preparation of metal matrix composite. In this process Al 7075 bars are cut into small ingots. These ingots are placed in Graphite crucible in which it is kept in induction furnace. The ingots are melted at a temperature of 800^0C, after effective degassing predetermined mass of preheated WC of 1.5wt%, 3wt%, 4.5wt%, 6 wt% at suitable intervals of 1.5wt% in steps of 4 is added into the alloy and stirred continuously in order to achieve uniform distribution of particles in the matrix. After the mixing of the reinforcements (WC) with the base matrix, the crucible is taken out from the furnace and the molten metal is poured into the mould die and allowed to solidify. After the solidification, the casted specimen is removed from the mould and machined as per ASTM standards for testing.

Fig. 2:Stir Casting Set-up used for fabrication of Composite Plates (Al 7075/WC

Fig. 3: Metal Matrix composite plates (Varying of WC content)

D. Experimental Testing

Microstructures of the composites were observed to reveal the distribution of WC particles in Al matrix. Samples were polished on emery papers of different grades and then cloth polished with fine alumina powder on revolving wheel. Microstructures were seen in un etched condition using optical microscope at 500X magnification. Indenter was impressed on material at a load of 5 kg for 10 seconds. To avoid the segregation effect of the reinforcements in the matrix, four readings were taken for each sample. Vickers hardness of the samples was determined using Future Tech - FV 800 Vickers hardness testing machine. Samples were mounted with Bakelite so that samples could not move when the load was applied. A diamond indenter was impressed on material at a load of 5 kg for 10 seconds. To avoid the segregation effect of the reinforcements in the matrix, four readings were taken for each sample.

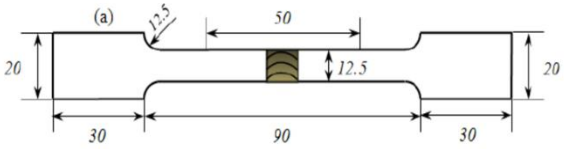

Fig.4: Dimensions of tensile test specimen

Tensile test was performed using computerized Instron tensile testing machine. The test was conducted using strain rate of 2mm/min at room temperatures. As cast Al and composite tensile test specimens were prepared using lathe machine and shaper machine according to the dimensions as shown in Fig. 4.

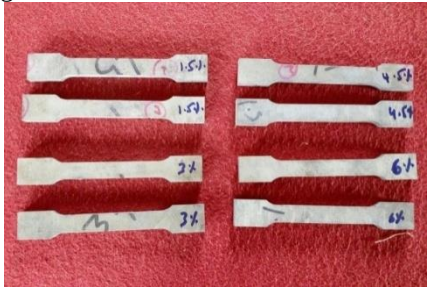

Fig. 5: Tensile test samples

 ISBN: 978-93-91420-02-4

III. RESULTS AND DISCUSSION

A. Microstructures

The properties of composites depend on the microstructure and interface characteristics between reinforcements and matrix. Fig. 4, Fig 5 and Fig.6 show the optical microstructures of 1.5, 3,4.5 and 6 wt. % WC reinforced AMCs respectively. From micro structural analysis, clustering and non-homogeneous distribution of WC particles in Al matrix were observed. This was due to the variation of contact time between WC particles and molten Al during composites processing, high surface tension and poor wetting behavior of WC particles in the liquid Al [6]. No homogenization of WC particles in Al matrix can be observed in the microstructure of 6 wt. % WC reinforced AMC as shown in Fig. 6. Some places in Al matrix can be identified without WC reinforcing particles. Porosities were observed in all microstructures. This was because when WC particles were added in the melt during casting, it introduced air in the melt entrapped between the particles. Therefore increasing wt. % of WC particles increased entrapped air resulted in higher amount of porosity [4].

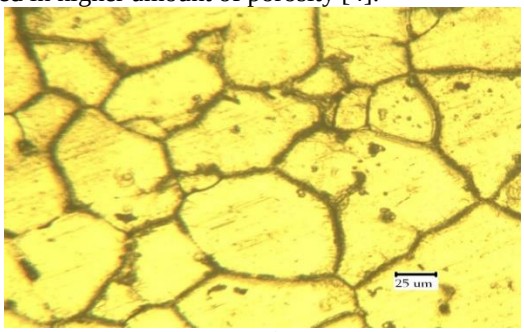

Fig. 5: Microstructure of Base Metal Al -7075

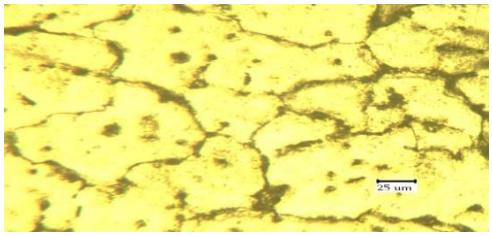

Fig. 6:.Microstructure of 1.5 wt. % WC reinforced AMC

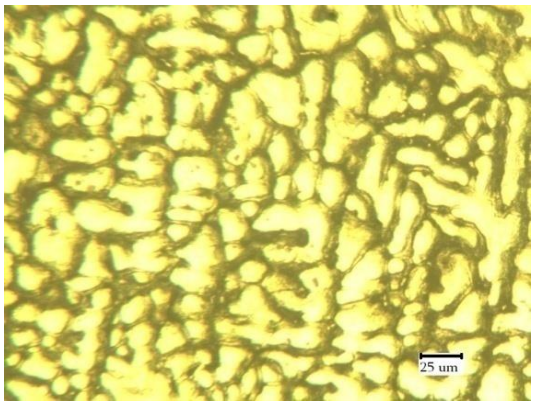

Fig. 7: Microstructure of 3wt. % WC reinforced AMC

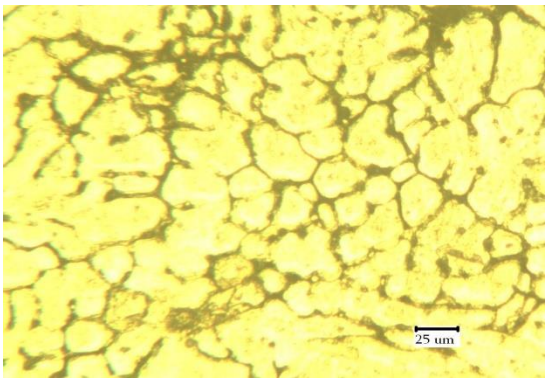

Fig..8: Microstructure of 4.5. % WC reinforced

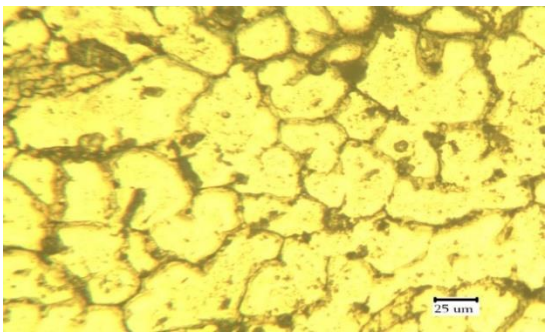

Fig. 9: Microstructure of 6 wt. % WC reinforced

B. Hardness

The hardness consequences of the Al 7075/WC composites are proven in figure.5 .The hardness cost is elevated by way of growing the wt% of WC reinforcement debris in the composites, as the presence of hard reinforcement debris on the floor resists the plastic deformation of the material. The energy of the grain obstacles increases to most degree and dislocation of atoms is decreased by means of increasing the wt% of reinforcement, which offers power to the matrix and thereby hardness of the composite gets improved. The same phenomenon is determined [11]

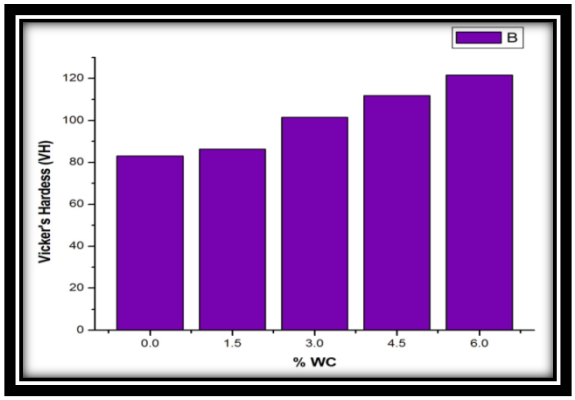

.

C. Tenstile strength

The tensile strength outcomes of the Al 7075/WC composites are proven in Figure 4.it is observed that final tensile Strength is elevated by means of growing the percentage of the WC particles inside the composite. that is because of higher interfacial bonding among the matrix and the reinforcement which transfers and distributes the load

 ISBN: 978-93-91420-02-4

from the matrix to the reinforcement. Therefore the reinforcement particle has a tendency to bear the whole load that has been acted upon the matrix [10.]

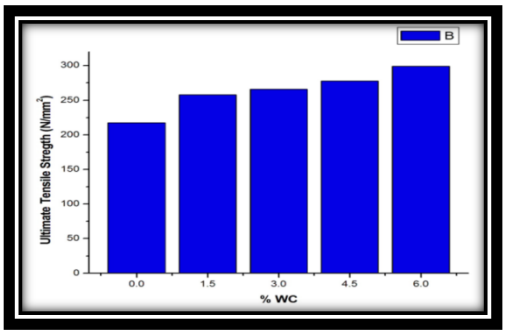

D. Impact Test

The impact strength of the Al 7075/WC composites are shown in Fig 6. It is observed that the toughness is decreased by increasing the weight percentage of the WC particles in the composite. This is due to the addition of WC in various percentages with aluminum, the brittleness of the material also increased. Because of high brittleness, the impact strength of the material is decreased.

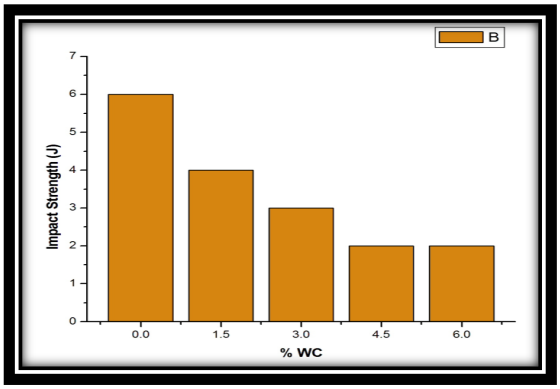

IV.

ONCLUSION

The Al 7075/WC composites were produced by stir cast route with different weight percentage of Microstructural Mechanical properties was evaluated. From this study, the following conclusions are derived.

In this Al 7075 with WC Metal matrix composite successfully completed. The micro hardness of the composites was Enhancing from 83 HV to 121 HV with increasing weight percentage of WC particles. The WC reinforcement has enhanced the tensile strength of Aluminum Matrix Composites (AMCs) from 217 MPa to 298 MPa.The Wt% Of WC reinforcement has Increased the impact strength of Aluminum Matrix Composites (AMCs) Reduced from 6 J to 2 J.

REFERENCES

[1] Gilbert Kaufman, (2002), "Properties of Aluminum Alloys; Tensile, Creep, and Fatigue Data at High and Low Temperatures", ASM International.

[2] T. Miyajima, Y. Iwai, (2003), "Effects of reinforcements on sliding wear behavior of aluminum matrix composites", Wear, Vol. 255, pp. 606–616.

[3] M K Surappa, Aluminium matrix composites: challenges and opportunities, Sadhana 28 (2003) 319-334.

[4] K.M. Shorowordi, T. Laoui, A.S.M.A. Haseeb, J.P. Celis, L. Froyen, Microstructure interface characteristics of B4C, SiC and Al2O3 reinforced Al matrix composites: a comparative study, J. Mater. Process. Technol. 142 (2003) 738–743.

[5] Dunia Abdul Saheb, Aluminum silicon carbide and aluminum graphite particulate omposites, ARPN J. Eng. Appl. Sci. 6 (2011) 41-46.

[6] C.Neelima Devi, N.Selvaraj, V.Mahesh, Micro structural aspects of aluminium silicon carbide metal matrix composites, Int. J. Appl. Sci. Eng. Res. 1 (2012) 250-254.

[7] S Jerry Andrews Fabian, B. Selvam, "Densification behaviour of Aluminium reinforced with Tungsten Carbide particulate Metal Matrix Composite processed by P/M", IOSR Journal of Mechanical and Civil Engineering (IOSR-JMCE), PP 24-29.

[8] Amarnath.G, K.V. Sharma, "Microstructure and tribological properties of nanoparticulate WC/Al metal matrix composites", International journal of mechanical engineering and technology (ijmet), Volume 4,Issue 2, pp. 178-188 March - April 2013.

[9] Hari Prasada Rao Pydi, Balamurugan Adhithan, A.Syed Bava Bakrudeen ,"Microstructure Exploration of the Aluminum-Tungsten Carbide Composite with different Manufacturing circumstances", International Journal of Soft Computing and Engineering (IJSCE) ISSN: 2231-2307, Volume-2, Issue-6, January 2013.

[10] K. Kalaiselvan, N. Murugan and Siva Parameswaran, "Production and characterization of AA6061-B_4C stir cast composite", Materials and Design, Vol. 32, 4004-4009, 2011.

[11]] Toptan F, Kilicarslan A, Cigdem M, Kerti I. "Processing and micro structural characterization of AA1070 and AA6063 matrix B_4C_p reinforced composites". Materials and Design 2010; 31: 987-91.

 ISBN: 978-93-91420-02-4

3D Printing of Prototype through Image Processing Using Autodesk Recap Photo Software

Chandra Bose Boyapati, M. Sreenivasa Kumar and B.Venkata Siva
Department of Mechanical Engineering (Student), Narasaraopeta Engineering College, Guntur, Andhra Pradesh, India.

***Abstract*— Autodesk Recap Pro 3D scanning software to transform the physical world into a digital asset. With reality capture data you can better understand and verify existing and as-built conditions to gain insights and make better decisions. Recap Photo, a cloud-based service of Recap Pro, processes drone, camera photography to create digital representations of current conditions. These representations can be used to create 3D conception models based on real-world context. 3D printing, or additive manufacturing, is the construction of a three-dimensional object from a CAD model or a digital 3D model. The term "3D printing" can refer to a variety of processes in which material is deposited, joined and solidified under computer control to create a three-dimensional object, with material being added together (such as plastics, liquids or powder grains being fused together), typically layer by layer. The part file should be in. STL format.**

Keywords—component, formatting, style, styling, insert (*key words****)***

I. INTRODUCTION

A. *Autodesk Recap Photo*

Autodesk Recap Photo processes photographs that are taken from drones, camera to create 3D representations of current conditions of sites, objects, and more. In this process we collect the photos with different angles of the same object and upload in the software and follow the steps regarding to the steps for creation of object.

B. *Photography Tips*

- The following tips will help you take quality photos for photogrammetry:
- If you can, take photos in a location where lighting is consistent and doesn't cast shadows.
- Try to keep your own shadow out of the picture.
- Make sure that there are no moving objects in the background when you take the photos.
- If the camera that you're using has a high dynamic range (HDR) setting, turn the feature off, and try not to adjust the exposure of your photographs while you capture images.
- Take pictures about one meter apart while you circle the object.
- If you can, maintain a perpendicular location relative to the object while you take photos.
- If the object is large, move in a lateral motion from one end of the object to the other. Change the height at each pass until you've captured all surfaces.

With the impact of digital technology development and the continuous expansion of its application direction, there are a lot of applications be employed in the heritage protection area. It has become a development direction. This article explores the potential of digital technology in heritage protection in the context of increasingly sophisticated digital methods. The primary goal is to design a digital restoration plan for the rooster-shaped statue of Notre Dame damaged in the fire [1]. This plan includes steps of data acquisition and processing, digital modelling and surface repairing, and digital demonstration. In this paper, a large number of successful cases from digital project cases and literature references in recent years were collected. Similarly there are selected potential cases and technical means to analyze their reference to the virtual restoration of the target sample (Rooster-shaped statue of Notre Dame Cathedral). Through the analysis and comparison of digital technology, the virtual restoration plan most suitable for the restoration of rooster-shaped statues is obtained. The plan is not fixed and has reference significance for the protection and restoration of other statues, buildings, and various cultural heritages [2]. It can provide sustainable and promising concrete methods for protecting cultural heritage. A research paper submitted to the University of Dublin, in partial fulfilment of the requirements for the degree of Master of Science Interactive Digital Media.

II. EXPERIMENTAL WORK

A. *Methodology: Image Processing Using Autodrsk Recap Photo*

Open Autodesk Recap Photo. When you first open Autodesk Recap Photo, you'll see the dashboard. On the dashboard, you can select either Aerial or Object to create a new 3D project. This tutorial covers the Object workflow.

Under Create 3D, select Object.

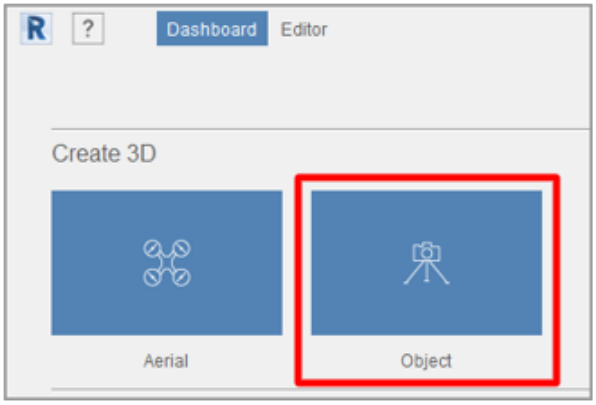

Click anywhere on the page that appears, according to the prompt, and then add the photos that you want to use to create your 3D model. After you've finished importing the photos, select Create.

 ISBN: 978-93-91420-02-4

- After the 3D model has been processed, it appears in the My Cloud Drive section of the dashboard. Select the Download this project from the cloud (down arrow) button to download your 3D model.

- Select a location to save the model, and then select Folder.

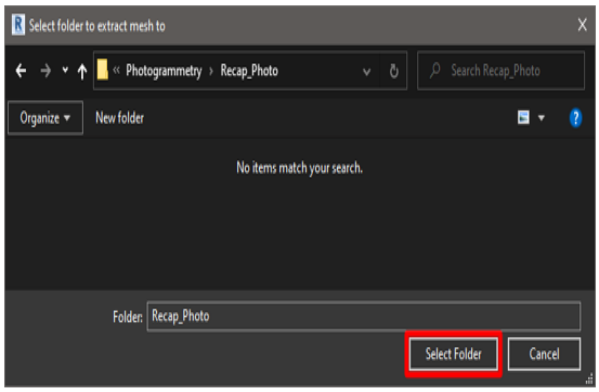

- You'll see a new 3D model that has the name that you entered. Select the model to open it in the editor.The saved 3D model is loaded on the editor page

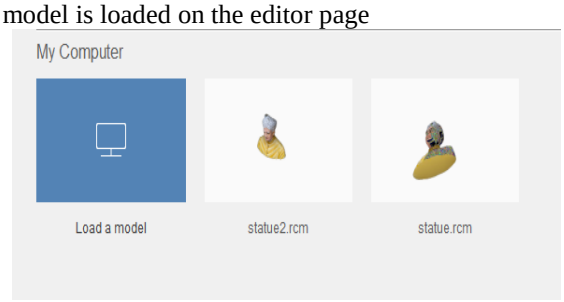

B. Edit The 3D Model:

Several tools are available on the left side and at the bottom of the editor page. You can use these tools to clean up the 3D model. Experiment with these tools to clean up the parts of 3D model that you don't want to keep. This tutorial shows how to remove the floor from the model. At the bottom of the editor page, select the **Lasso/Fence** tool.

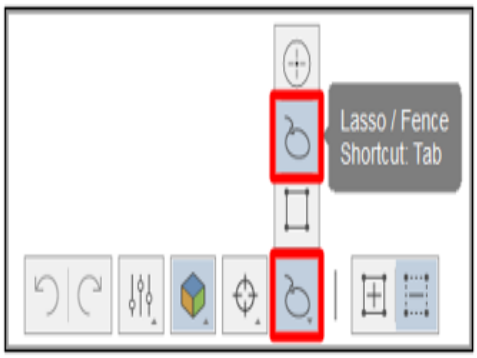

- Press Enter, and then press Delete. Repeat these steps a few times to remove most of the floor. Select the Slice tool to remove the rest of the floor. This tool creates a slicing plane that can use to cut away geometry below a specific point. The following settings are available in the Slice dialog box.

Fill: Select this option to close the model, based on the boundary of the open area of the model. In some cases, filling might not be easy.
No fill: Select this option to leave the model as an open model.
Transform plane: Select this check box to align the plane so that the floor isn't visible.

When the model looks the way that you want it to, select Apply. The rest of the floor is removed from your 3D model and the mesh on the bottom is filled.

C. Export 3D Model as an STL File

Before you can use the 3D model in Dynamics 365 Guides or Power Apps, it must be in the STL file format. In this step,

you'll export the model as an STL file that can then be converted to a STL file.

- On the left side of the editor page, Select the **Export** button, and then select the **Export model** button to open the export settings.

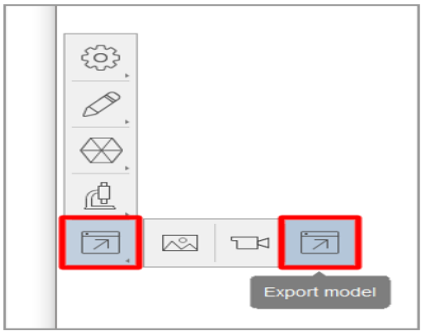

- In the **Export model** dialog box, in the **Exports** field, select **STL** as the export file type, when you've finished, select **Export** and Select a location to save your file to, and then select Folder.

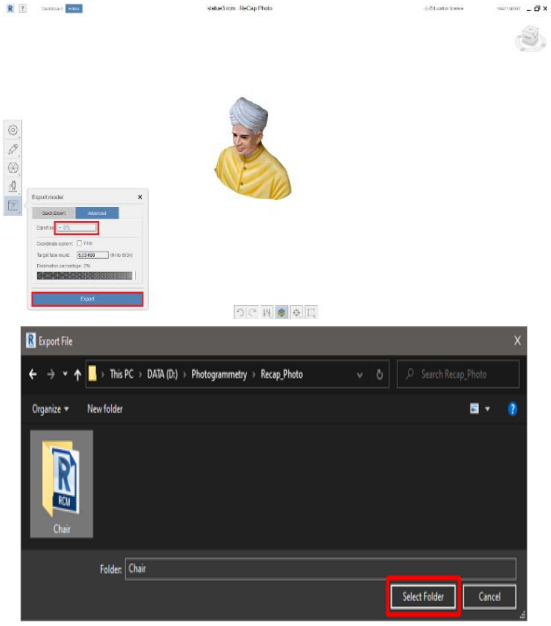

The 3D model is exported to the folder.

III. PRINT OBJECTY ON 3D PRINTER

A. *Introduction to 3Dprinting*

The 3D printing process was devised in the 1980s and originally known as 'rapid prototyping'. It enabled companies to develop prototypes quickly and more accurately than with other methods. After over 30 years of innovation, its uses are far more diverse today. Manufacturers, engineers, designers, educators, medics, and hobbyists alike use the technology for a huge range of applications.

How does 3D printing work?

We know in the earlier, the 3D printing process involves building up layer upon layer of molten plastic to create an object. As each layer sets, the next layer is printed on top and the object is built up. To make a 3D print, a digital file is needed that tells the 3D printer where to print the material. The most common file format to this is the G-code files. This file essentially contains 'coordinates' to guide the printer's movements, both horizontally and vertically – also known as the X, Y, and Z axes. 3D printers can print these layers at different thicknesses, known as layer height. A bit like pixels on a screen, more layers in a print will give a higher 'resolution'. This will give a better-looking result, but take longer to print.

B. Models to Expalin concepts

As well as designing and making products, 3D printing is also a useful tool for visualizing concepts in 3D. Benefit of 3D printing in education is that students get involved with using the technology, developing essential STEAM skills such as 3D design, and understanding material properties and manufacturing processes.

C. Material Selection

ABS provides favorable mechanical properties such as impact resistance, toughness, and rigidity when compared with other common polymers. A variety of modifications can be made to improve impact resistance, toughness, and heat resistance.

D. The characterstics of fillment in 3D printing

Available in the form of filaments with a diameter of 1.75 mm or 2.85 mm and in several colors, ABS has interesting properties for many industries that want to 3D print functional parts or prototypes. Although it is more difficult to print than PLA, ABS remains a very popular material for 3D printing professionals due to its resistance to impact and high temperature (between -20°C and 80°C). It is opaque, offers smooth and shiny surfaces and can be welded by chemical processes using acetone. ABS has a melting temperature of around 200°C, it is therefore recommended that the extrusion temperature be between 230 and 260°C. The use of a heating plate (between 80 and 130°C) is mandatory: it is a plastic that shrinks on contact with air, causing the part to shrink (or warp) and thus detaching itself from the plate. For large parts, it is even advisable to use a special adhesive such as Kapton or an adhesive lacquer. Finally, a 3D printer with a closed enclosure is preferable because ABS plastic emits particles that can be dangerous for the user

E. Preparing Print with Ultimaker Cura

Interface After you have added the Ultimaker S5 in Ultimaker Cura, the main interface will become visible. Here is an overview of the user interface (UI):

- Open the file and select the file.
- The object will visible on the bed, and make it as center to the bed.
- Now, select the print settings and make the setting regarding to the purpose.
- If there is a need of supporting click the generate support options.
- After the completion of settings now slice the object.
- After the slicing the object save the file, the file format is in g-files format.
- Save the file and move to SD-card and the place the SD card in the 3d printer.
- Load the material in 3d printer, follow in the manual.
- Select the file which you want to print and click on conform button.

TABLE I: ***The following settings made for print***

 ISBN: 978-93-91420-02-4

S.NO	PARAMETER		VALUE
1	QUALITY	layer height	0.1mm
2	WALLS	Wall thickness	1.3mm
		count	4
3	TOP/BOTTOM	Top Thickness	1.2mm
		Top Layers	12
		Bottom Thickness	1.2mm
		Bottom Layers	12
4	INFILL	Infill Density	20%
		Infill Pattern	Cubic subdivision
5	MATERIAL	Printing Temperature	240c
		Build Plate Temperature	85c
6	SPEED	Print speed	55mm/sec

Time period for printing=1 hour32 minutes
Material consumption=4g, 0.64miters

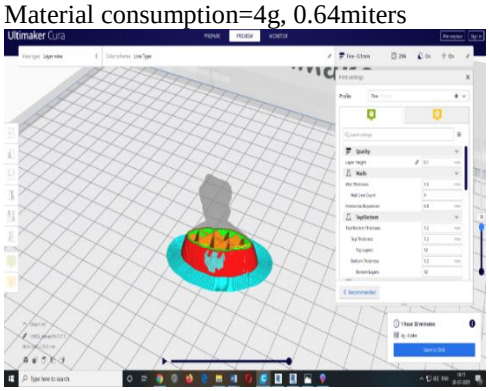

IV. CONCLUSION

It is one of advance technology, we can scan and print any complicated structures with in short time and decrease man power.

- At first I captured around 55 images at different angles on the Sarvepalli Radhakrishnan statue.
- Next go the Autodesk Recap photo and select Create 3D object and upload the photos.
- The cloud starts creating the object, after the completion of object open it.
- There is an edit tools if any editing is needed can follow the tools.
- Finally export the file in the .STL format for the 3D printing.
- Insert the file in 3d printing software (Cura) and set the print settings.
- Completion of setting slices the file and saves to SD card.
- Select the file in the printer and prints start.
- Finally the output comes (Sarvepalli Radhakrishnan) statue.

FUCTURE SCOPE

In the future generation the work time must be decrease and for any conferences we want to submit prototypes and this techniques is useful. We can generate any structures without dimensions by using photo processing. This process is used for only prototypes or physical structure, we can't generate accurate dimensions of the body.

REFERENCES

[1] https://www.autodesk.in/products/recap/overview All over details about Autodesk Recap Photo Software.

[2] https://docs.microsoft.com/en-us/dynamics365/mixed reality/guides/3d-content-guidelines/Autodesk-recap-photo

[3] Process or steps to follow the run the Autodesk recap photo software.

[4] https://ultimaker.com/software/ultimaker-cura Machine used for printing the statue

[5] https://en.wikipedia.org/wiki/Acrylonitrile_styrene_acrylate

 ISBN: 978-93-91420-02-4

Fabrication and Testing Mechanical Behavior of Hemp Fiber, Chopped E Glass and Hybrid with Nano Particle

Mr. Srinivasulu.Dorasila , Mr.K.Srinivasa Reddy and Mr.V.Mahendra Reddy
Department of MechanicalEngineering, Kallam Haranatha Reddy Institute of Technlogy, Guntur,India

***Abstract*- A composite material is made from two or more constituent materials; having better properties compared to both two parent materials. The composite is stronger, lighter, and less expensive compared with the traditional materials. In current years composites have considerable importance as a potential operational material. Low cost, light weights, high specific modulus, renewability and biodegradability are the most basic and common attractive features of composites that make them useful for industrial applications. With low cost, high specific mechanical properties natural fiber signifies a worthy renewable and biodegradable composite. Among those hemp, chopped e glass and its hybrid fibers. The present work has been done with an objective to explore the use of hemp fiber, chopped e glass fiber and its combinations (hybrid) are used as a reinforcement material in epoxy base, final find out the mechanical properties like tensile, hardness, impact of hemp fiber, chopped e glass fiber its combination (hybrid) composites and hybrid with nanoparticles.**

Keywords: Silicon carbide, Copper, Graphite, hemp, chopped e glass, tensile test, hardness test, Impact test.

I. NTRODUCTION

A "Composite" can be defined as where two ormoredifferentmaterialsarephysicallycombinedtogether.Twoconstituentmaterialswhicharehavingdifferent mechanical, physical and chemical propertiesarebondedwillproduceamaterialwithdifferentcharacteristics from the individual material is called a composite material. The two constituents are reinforcement and matrix .The reinforcement and matrix are the main load carrying elements in a composite material. This matrix can maintain the alignment of fiber, shape and from environmental fortify here enforcement can improve the strength of the material. The properties of composite material are exhaustion life ,electrical

protection, wear resistance ,warm protection quality, light weight, solidness, warm conductivity, fire resistance, temperature-subordinate conduct, and warm protection. The utilization of composite materials is very long.These composite materials are renewable biodegradable. Composite materials have good fatigue resistance compared to other metals. Low radar visibility and Moulding to complex forms of composites are easy compared to other materials. The wide use of composite materials in surface transportation is because of their huge size. The strength-weight ratio is higher than other materials which results in the effectiveuseofcompositematerialsinsurfacetransportation.Resilience and good productivity are the basic required qualities of a good composite material. Composite materials can be classified in different ways. Classification based on the geometry of are presentative unit of reinforcement is convenient since it is the geometry of the reinforcement which is responsible for the mechanical properties and high performance of the composites.

II. COMPOSITE SPECIMENS

The two broad classes of composites are

(1) Particulate composites

(2) Fibrous composites.

A. Fabrication of Composite Specimens:

Hand lay-up technique is the simple and cheapest method of composite processing. The infrastructural need for this technique is also minimal. The standard test procedure for Mechanical properties of fiber-resin composites; ASTM-D790M-86 is utilized to according to the measurements. The mold is prepared on smooth clear film with 2-way tape to the required measurement..

B. Maintaining the Integrity of the Specifications

After fabrication specimens are cut form sheets according to the ASME statndards165mm long, 12.5mm in width and 4mm in thick are fabricated for tensile testing. 100mm long, 25mm width and 4mm in thick are fabricated for flexural testing. 63.5mm long, 12.36mm width and 6mm thick are fabricated for impact testing.

III. ALKALI TREATMENT

Chopped E fiber and Hemp fibers were soaked in 5 and 5 (wt.)% of NaOH solutions at 23°C for 4 h, maintaining a liquor ratio of 1:14. The fibers were washed for several times with distilled water to remove any alkali solution sticking on their surface.

The polymer is uniformly spread with the help of brush. Then second layer of fiber is placed on the polymer surface and another layer of polymer is applied after this is closed with another thin plastic sheet after squeezer is moved with a gentle pressure on the thin plastic sheet to remove air.

The consequential mould is cured for 24 hours at room temperature. Cu, Si, Graphite powder is mixed with epoxy resign and stirred uniformly half an hour and same process is follow to produce Cu, Si, graphite composites.

IV. MECHANICAL CHARACTERISTICS OF COMPOSITES

The properties of the hemp & pineapple grass fib reinforced epoxy hybrid composites with of fiber under this investigation are presented in below Tables &figures respectively. Details of processing of these composites and the tests conducted on them. The results of various characterization tests are reported here. This includes evaluation of tensile strength, flexural strength, impact strength. Has been studied and discussed.

 ISBN: 978-93-91420-02-4

Graphs:

A. *Hemp Fiber***:** The graph shows the hemp fiber composite of tensile strength when load is applied in 310N and Elongation is 0.5mm as shown below graph.

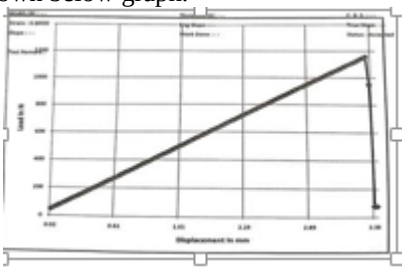

Tensile strength graph of hemp fiber

B .Chopped E Glass Fiber

The graph shows the chopped e glass fiber composite materials of tensile strength when load is applied in 2640N and Elongation is 2.8mm as shown below graph.

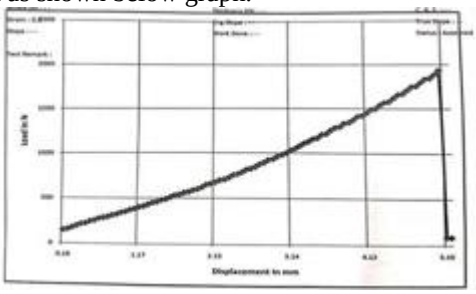

Tensile strength graph of chopped e glass fiber

C. Hybrid Composite Material

The graph shows the Hybrid fibre composite material of tensile strength when load is applied in 1200N and Elongation is 1.0mm as shown below graph.

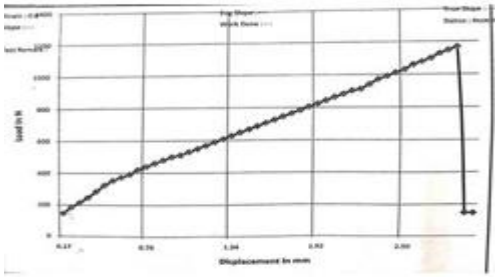

Tensile strength graph of hybrid composite material

D. Hybridfibre With 10% Cu Composte Material

The graph shows the PINE APPLE fiber composite material of Flexural strength when load is applied in 280N and Elongation is 4.6mm as shown below graph.

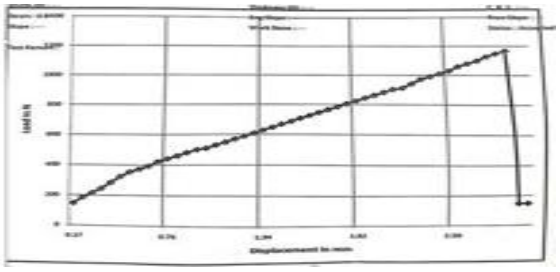

Tensile strength graph of hybrid composite with 10% CU material

E. *Hybrid With 10%Graphite Fiber Composite Material*

The graph shows the hybrid composite material of Flexural strength when load is applied in 180N and Elongation is 3.1mm as shown below graph.

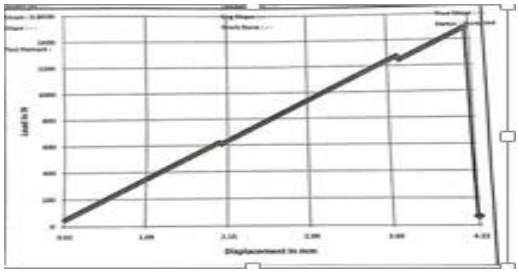

Tensile strength graph of Hybrid with 10%GRAPHITE composite material

F. Hybrid Fiber With 10% Sic Composite Material

The graph shows the Hemp composite material of Flexural strength when load is applied in 300N and Elongation is 2.8mm as shown below graph.

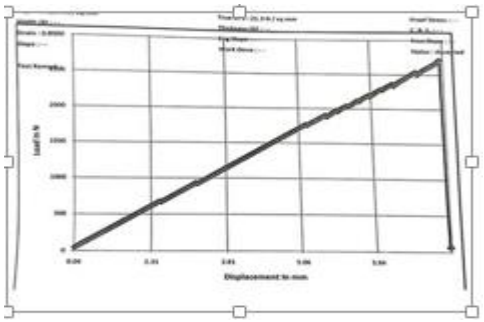

Tensile strength graph of hybrid with 10% SIC composite material.

REFERENCES

1. Belgacem, M. N., & Gandini, A. (2005). The surface modification of cellulose fibers for use as reinforcing elements in composite materials. Composite Interfaces, 12,41–75.

2. Munikenche Gouda, T., Naidu, A. C. B., & Chaya, R. (1999). Some mechanical properties of untreated jute fabric-reinforced polyester composites.

3. M. Ramesh, K. Palanikumar, K.Hemachandra Reddy. (2012). Mechanical property evaluation of sisal–jute–glass fiber reinforced polyester composites.

4. John, M. J., & Thomas, S. (2008). Biofibres and bio composites. Carbohydrate Polymers, 71(3), 343–364.

5. Jones, F. R. (1994). Handbook of polymer composites. England: Longman Scientific and Technical.

6. Koradiya, S. B., Patel, J. P., & Parsania, P. H. (2010). The preparation and Physicochemical study of glass, jute and hybrid glass–jute bisphenol-C-based Epoxy resin composites. Polymer-Plastics Technology and Engineering,49(14),1445–1449.

 ISBN: 978-93-91420-02-4

Optical characterization of V_2O_5 doped Na_2O-SiO_2-ZrO_2 glasses

K. Neeraja, K. Ephraim Babu and G.S.John
Department of Physics, Narasaraopeta Engineering College (A), Narasaraopet, Guntur, India

Abstract: Vanadium doped Na_2O-SiO_2-ZrO_2 glass system by means of optical properties has been carried out as a function of the concentration of vanadium ions. These glasses were characterized using X-ray diffraction, Optical absorption and Photoluminescence spectra. Various physical parameters can be calculated like density, refractive index, electronic polaraisability etc. Many of these parameters vary non-linearly exhibiting a minima or maxima with increasing alkali concentration, indicating the mixed alkali effect. From the optical absorption spectra of VO(II) ions in these glasses show two bands corresponding to the transitions corresponding to $^2B_2 \rightarrow {}^2B_g$ and $^2B_2 \rightarrow {}^2E_g$ transitions in the order of decreasing energy respectively. The overall measured parameters from the structural and/or positron annihilation spectra indicated that the majority of the vanadium ions in the range 0–0.5 mole% of V_2O_5 are in the V^{5+} valence state which act as a glass former. The majority of the vanadium ions are in the range 0.7–2 mole% of V_2O_5 are the V^{3+} and V^{4+} states acting as a glass modifier.

I. INTRODUCTION

Among the transition metal ions like vanadium, the electrical conductivity consists of mixed electronic and ionic, pure electronic or pure ionic conduction depending on the composition of the glass constituents. It considered as effective and useful tool owing to the fact that exists not only in different valence states but also in different coordinates within the glass network. Further, V_2O_5 glasses find various applications in the development of new tunable solid state lasers, luminescent solar energy concentrators and fiber optic communication devices. Usually, vanadium ions exhibit four common oxidation states i.e. V^{5+}, V^{4+}, V^{3+} and V^{2+} [1-3]. When alkali oxide like sodium is present in the glass network it produces non-bridging oxygen atoms and it easily enters into the glass network interstitially forming a new environment. This leads to the change in the structure of the studied glass samples. Hence, the molar volume will decrease and the glass transition temperature is lowered due to the reduced degree of cross-linkage.

When alkali oxide like sodium is present in the glass network it produces non-bridging oxygen atoms and it easily enters into the glass network interstitially forming a new environment. This leads to the change in the structure of the studied glass samples. Hence, the molar volume will decrease and the glass transition temperature is lowered due to the reduced degree of cross-linkage. Due to this, the glasses are suitable for fabrication of optical wave guide devices [4-6]. The glass forming oxide silica is added to the alkali oxide then it changes the glass network leading to the formation of non-bridging oxygen atoms and having applications in different areas [7-9].

The addition of Zirconium into the sodium silicate glasses is expected to increase the electrical resistivity and chemical inertness, high alkaline resistance and alkali durability of the glasses, in the view of these qualities ZrO_2 containing glasses find variety of applications such as optical fibers, thermal barrier coating, laser mirrors and practically as fibers reinforcing cements. [10-12].

The aim of the present study is to examine the structural changes that take place due to varied oxidation state of vanadium ions in Na_2O-SiO_2-ZrO_2 glass network using XRD, Optical Absorption, Photoluminescence Spectra, EPR, FT-IR and Raman. These studies have yielded valuable information regarding the structural transformations that are taking place in these glasses.

II. EXPERIMENTAL TECHNIQUE

The usual way of obtaining a glass is by quenching a melt obtained by fusion of one or more substances. When the rate of cooling is sufficiently fast to bypass crystallization, the disordered state of the liquid is retained in the solid state. All the chemicals used for the present work were procured of analytical grade with 99.99 % purity. Table 1 presents the molar composition of the glasses of present study which were prepared by the standard melt quenching technique. About 10 g of the batch composition was thoroughly crushed in an agate mortar and the homogeneous mixture was heated in a silica crucible inside an electric furnace. The duration of melt and melt temperature is dependent on the glass composition. The melting temperature ranges from 1350-1450^{o}C and the melting duration is 60 min. The melt is then air quenched by pouring it onto a thick polished brass plate and pressed with another polished brass plate. The glasses were annealed at a temperature slightly less than the glass transition temperature (T_g) i.e. at 450^{o}C to remove thermal strains. The samples were found to be stable at ambient conditions and were well polished before measuring their optical properties.

Table 1: Composition of the studied glasses (batch mol %)

S.No.	Glass code	Na_2O (mol %)	SiO_2 (mol %)	ZrO_2 (mol %)	V_2O_5 (mol %)
1	Pure	40	55	5	-
2	V1	40	55	4.8	0.2
3	V2	40	55	4.6	0.4
4	V3	40	55	4.4	0.6
5	V4	40	55	4.2	0.8
6	V5	40	55	4	1.0

III. RESULTS

3.1. Physical Properties

To understand the physical properties of these glasses, the measured values of density (d) and refractive index along with other physical parameters [13-15] such as vanadium ion concentration (N_i), mean ionic separation (r_i), polaron radius (r_p), field strength (F_i), electronic polaraizability (α), reflection loss, molar refractivity (R_M) and optical dielectric constant (ε) are evaluated and are presented in the Table 2. The variation of density and refractive index as a function of glass samples is as shown in Fig 1. The variation of molar volume and refractivity as a function of glass samples is as shown in Fig 2.

 ISBN: 978-93-91420-02-4

Physical Parameters	Pure	V1	V2	V3	V4	V5
Density d (g/cm³) (±0.004)	2.679	2.676	2.658	2.645	2.646	2.648
Average molecular weight (M)	63.99	63.91	63.83	63.74	63.66	63.58
Ion concentration N_i (10^{20}ions/cm³) (±0.005)	-	0.504	1.003	1.499	2.002	2.508
Interionic distance r_i (Å)(±0.005)	-	27.06	21.52	18.82	17.09	15.85
Polaron radius r_p (Å) (±0.005)	-	10.90	8.67	7.58	6.88	6.38
Field strength F. (10^{15}cm⁻²) (±0.005)	-	2.52	3.98	5.21	6.32	7.34
Refractive index n (±0.0001)	1.674	1.652	1.654	1.655	1.657	1.659
Reflection loss	0.0336	0.0319	0.0320	0.0321	0.0323	0.0324
Molar reflectivity R_M (cm⁻³) (±0.005)	8.969	8.736	8.808	8.848	8.859	8.855
Electronic polaraizability (α_e) (10^{-23} ions/cm³)(±0.005)	-	17.324	8.733	5.848	4.391	3.511
Optical dielectric constant(ε_∞) (±0.005)	2.803	2.730	2.738	2.741	2.748	2.752

Table-2 Various physical properties of Na_2O-SiO_2-ZrO_2: V_2O_5 doped glasses

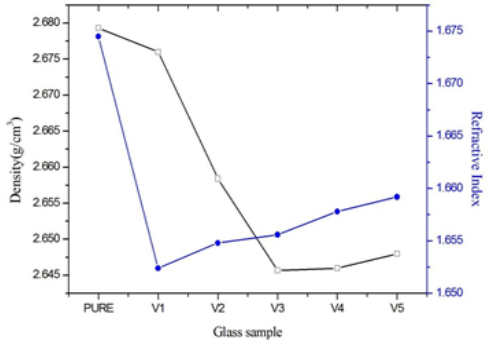

Fig.1 Variation of density and refractive index with glass sample of Na_2O-SiO_2-ZrO_2: V_2O_5 doped glasses

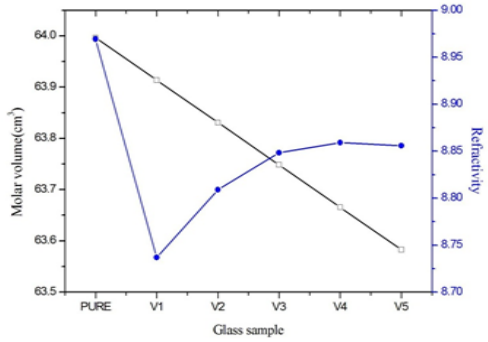

Fig.2 Variation of molar volume and refractivity with glass sample of Na_2O-SiO_2-ZrO_2: V_2O_5 doped glasses

3.2. X-ray diffraction spectra

X-ray diffraction patterns of several compositions of the prepared samples are shown in Fig 3. No peak corresponding to V_2O_5 has completely entered in the glass matrix. The overall features of these XRD pattern confirms the amorphous nature of the present glasses.

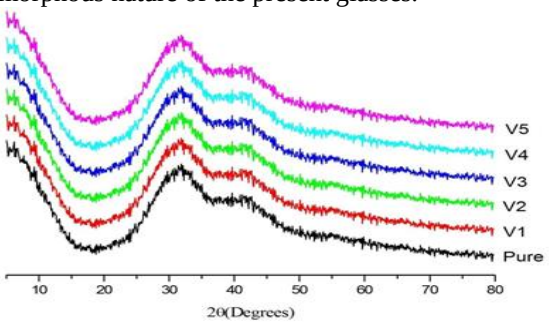

Fig.3 XRD spectra of Na_2O-SiO_2-ZrO_2: V_2O_5 doped glasses

3.3. Optical absorption spectra

The absorption spectra of Na_2O-SiO_2-ZrO_2:V_2O_5 glasses are recorded at room temperature in the wavelength region 400-1200 nm is as shown in Fig 4. The spectrum of undoped glasses does not exhibit any bands. With the introduction of V_2O_5, the spectrum of the glass samples exhibited two broad absorption bands at 666 and 1052 nm corresponding to $^2B_2 \rightarrow {}^2B_g$ and $^2B_2 \rightarrow {}^2E_g$ transitions of VO^{2+} ions [16]. With gradual increase in the concentration of V_2O_5 , the half width and peak height of these bands are observed to increase in the glass network as a result they have all possible transitions takes place (direct and indirect transitions) between valency band and conduction band under the influence of external field.

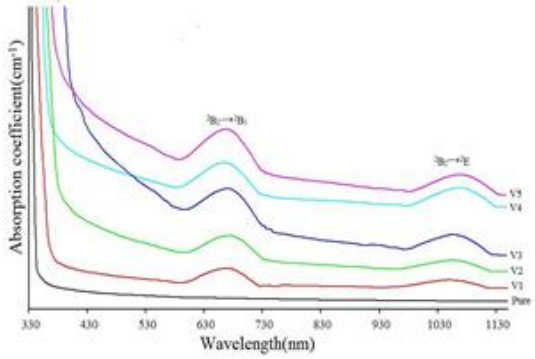

Fig.4 Optical absorption spectra of Na_2O-SiO_2-ZrO_2: V_2O_5 doped glasses

3.4. Photoluminescence spectra

The Photoluminescence spectra of Na_2O-SiO_2-ZrO_2:V_2O_5 glasses are recorded at room temperature in the wavelength region 400 nm. The spectrum of glass samples exhibited a broad emission band in the region 750-850 nm. This band is identified due to $^2E \rightarrow {}^2T_2$ transition of vanadyl ion [17-18]. Fig 5 shows the luminescence spectra of Na_2O-SiO_2-ZrO_2:V_2O_5 glasses.

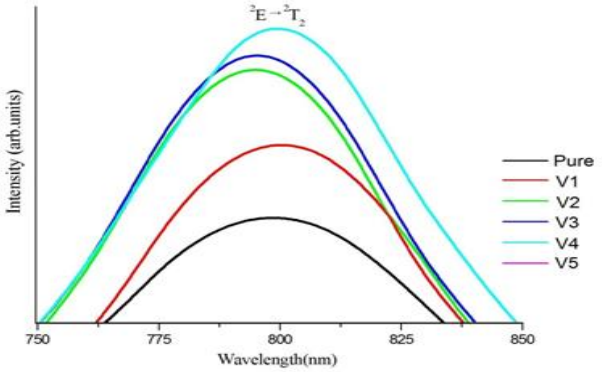

Fig.5 Luminescence spectra of Na_2O-SiO_2-ZrO_2: V_2O_5 doped glasses

IV. DISCUSSIONS

Various physical parameters density is found to decrease with the addition of V_2O_5 in all the glasses. Basically, when V_2O_5 enters into the glass network in two forms, they act as network modifier at low content in addition to high content, then it acts as network forming group. Due to this, non bridging oxygen content further increases. Fig 1 shows the observed parameters density and refractive indexes of the glasses varying non- linearly with increasing vanadium concentration in x mol%. Fig 2 shows the molar volume and refractivity of the glasses also varying non- linearly with increasing vanadium concentration.

The absorption spectrum of Na_2O-SiO_2-ZrO_2: V_2O_5 glasses, exhibited two broad absorption bands at 666 and 1052 nm corresponding to $^2B_2 \rightarrow {}^2B_g$ and $^2B_2 \rightarrow {}^2E_g$ transitions of VO^{2+} ions. The VO^{2+} ion has a single d electron which gives rise to the free ion term ^2D. In a crystal field of octahedral symmetry, this electron occupies the T_{2g} orbital and gives rise to ground state term $^2T_{2g}$. when the electron absorbs energy, it excited to the E_g orbital and accordingly in octahedral geometry only one band corresponding to the transition $^2T_{2g} \rightarrow {}^2E_g$. Because of the non symmetrical alignment of the V=0 bond along the axis, the site symmetry, in general, is lowered to tetragonal (C_{4v}) in general of rhombic (C_{2v}) symmetry. In C_{4v} symmetry, $^2T_{2g}$ splits into $^2B_{2g}$ and ^2E_g, where as ^2E_g splits into $^2B_{1g}$, $^2A_{1g}$. This yields the energy levels of the VO^{2+} ion in the order: $^2B_{2g}$ (ground state) $< {}^2E_g < {}^2B_{1g} < {}^2A_{1g}$ [19-20]. Thus the optical absorption spectrum one can expect three bands corresponding to the d-d transitions $^2B_{2g} \rightarrow {}^2B_{1g}$ and $^2B_{2g} \rightarrow {}^2E_g$ and $^2B_{2g} \rightarrow {}^2A_{1g}$. In the present glass system exhibit only first two bands is observed that indicating the presence of the concentration of VO^{2+} ions in these glasses.

The Photoluminescence spectra of Na_2O-SiO_2-ZrO_2:V_2O_5 glasses with wavelength correspond to $^2B_{2g} \rightarrow {}^2B_{1g}$, resulted a broad emission band. Since the wavelength of the band is maximum of the band $^2B_{2g} \rightarrow {}^2E$, this is attributed to $^2E \rightarrow {}^2T_2$ transitions of V^{4+} ions. The emission band is relatively broad. With increase in the concentration of V_2O_5, the intensity of the peak is observed to increase. Hence, the increase in the band intensity with increasing the V_2O_5 suggests that the increasing presence of vanadyl ions in the glass samples.

V. CONCLUSIONS

Na_2O-SiO_2-ZrO_2 glasses mixed with different concentrations of V_2O_5 were prepared by using melt quenching method. The calculated and measured physical parameters of the glasses vary non-linearly with X mol% of dopant. The XRD has indicated that the glasses samples contain well defined and randomly distributed grains are present for the prepared glass samples. From the Optical absorption and Photoluminescence spectra of the glass samples indicate that a considerable proportion of vanadium ions do exist in V^{4+} state in addition of V^{5+} state with the increasing the dopant of V_2O_5.

REFERENCES

[1] I. Nicula, E. Culea, I. Lupsa, J. Non-Cryst. Solids 79 (1986) 325-332.
[2] C. Mereier, G. Palavit, L. Montage, C. Follet, C. R. Acad. Sci. Paris 5 (2003) 683-693.
[3] H.R. Panchal, D.K. Kanchan, Solid state phys. symp. (Mumbai), 39c, 1996, pp. 218-220.
[4] H.A.Schaeer, J. Mecha, J. Steinmann, J. Am.Ceram.Soc.62 (1979)343-352.
[5] C.A. Maynell, G.A. Saunders, S. Scholes, J. Non-Cryst. Solids 12 (1973) 271-282.
[6] M. Williams, G. Scott, Glass Technol. 11 (1970) 76-84.
[7] H.A.Schaeer, Phys.Status Solidi (a) 22(1974)281-292.
[8] I. Fanderlik, Silica Glass and its Applications, Elsevier, Amsterdam, 11(1991) 95.
[9] K.V. Arun, Fundamentals of Inorganic Glasses, Academic Press, New York, 1995. p. 2, 4.
[10] H. Yang, S. Wu, J. Hu, Z. Wang, R. Wang, H. He, Mater. Des. 32 (2011) 1590-1593.
[11] S. Banijamali, H.R. Rezaie, V.K. Marghussian, Thermochim. Acta 488 (2009) 60-65.
[12] E.M.M. Ewais, M.A.A. Attia, R.K. Bordia, Ceram. Int.36 (2010) 1327-1338.
[13] B. Bendow, P.K. Benerjee, J. Lucas, J. Am. Ceram. Soc. 65 (1985) C 92-102.
[14] Y. Ohishi, S. Mitachi, T. Kanamori, T. Manabe, Phys. Chem. Glasses 24 (1983)135140.
[15] J.E. Shelby, J. Ruller, Phys. Chem. Glasses 28 (1987) 262-268.
[16] J. Ballhausen, H.B. Gray, Inorg. Chem. 1 (1962) 111-122.
[17] J. Ballhausen, H.B. Gray, Inorg. Chem. 1 (1962) 111-121.
[18] S.F. Fang, H.Bihui, Jin. Sizho Bopuxue Zazhi .v.10 (1993) 9.
[19] F.E. Salman,J. Phys. Chem. Solids 63 (2002)1957-1966.
[20] Ortolano T R, Selbin J and McGlynn S P 1964 J. Chem. Phys.41 262-268.

 ISBN: 978-93-91420-02-4

Determination of Efficient Location of Split Air Conditioner Using CFD

Venkannababu Mendi [1] ,Kasukurthi Prakash Babu[2] and Kukkala Haribalakrishna[3]
[1]*Associate Professor, Department of Mechanical EngineeringNarasaraopeta Engineering College (Autonomous),* Andhra Pradesh
[2,3]*Associate Professor, Department of Mechanical Engineering, Azad College of Engineering and Technology*,Hyderabad, Telangana

***Abstract*: Air conditioning deals with conditioning of air for maintaining specific conditions of temperature, relative humidity and air movement inside an enclosed space. The working performance and efficiency of the air conditioner mainly depends on the location inside the room where it was installed. If the air conditioner was installed correctly, it will perform efficiently and economically. Proper distribution of air in a ventilated room is important in order to achieve satisfactory temperature and air velocity. The inlet location and the conditions of air at the inlet can affect the airflow pattern significantly. Experimentally determining the efficient location for air conditioner is very difficult and tedious. The technique of Computational Fluid Dynamics (CFD) with the help of computers is used for solving fluid problems and spans a wide range of non - industrial and industrial application areas. This technique was applied for the present analysis. In room air conditioning, temperature of the air in human comfort region is the main parameter. This parameter depends on the input parameters such as inlet temperature of the air, wall temperature and velocity of the inlet air. In the above analysis, the efficient location of air conditioner for good performance was found out to be 2.1 m above the floor. Keeping the inlet location at this efficient location, simulation was carried out with in the range of input parameters.**

I. INTRODUCTION

Human beings feel comfort and work efficiently with in a restricted set of physical conditions of temperature, humidity, draught and fresh air requirements. Fresh air is generally required to dilute the pollution levels and CO2 levels. Lack of environmental control in buildings may affect the health of human beings apart from reduction in efficiency and comfort level. In excessively hot climates. It is necessary to reduce temperature and humidity of supply air and in excessively cold climates it is necessary to increase them. Energy efficient buildings with good thermal insulation require low volume flow rates of supply air. This may lead to non-uniform velocity and temperature distribution apart from stagnation zones and accumulation of pollutants and odour due to poor recirculation. Architects and air conditioning engineers have to consider all these facts apart from providing better ambience and aesthetics. The velocity and temperature distribution in the room plays a vital role from this point of view. The need of precise determination of air flow pattern and temperature distribution in room was realized first by air-conditioning engineers so as to provide comfort throughout the occupied zone. The cooling load of an office air condition have increase significantly because of an increase in various types of heat sources such as electric machinery. In particular, the increased no. of personal computers, engineering work stations, main frames etc., generates a large amount of heat, cause serious air conducting problems. In room air conditioning, temperature of the air in human comfort region is the main parameter. This parameter depends on the input parameters such as inlet temperature of the air, wall temperature and velocity of the inlet air. In the above analysis, an attempt was made to find the efficient location of the air conditioner. Considering this model as basis, simulation is done within the range of input parameters.

II. LITERATURE SURVEY

In 1963, a new long-range study on human comfort was initiated by the American society of heating, refrigerating, and air-conditioning engineers (ASHRAE) [1], which was conducted by the institute for environmental Research at Kansas State University under contract to ASHRAE. On the basis of results obtained from that research, a New Effective Temperature scale has been developed. Its comfort Envelope (ABCD) is depicted in Fig. 2.8, which is adapted from data provided in ASHRAE standard 55-74, thermal environment conditions for Human Occupancy, published in 1974, and from ASHRAE handbook, 1977 Fundamentals [1]. It is evident that the comfort envelope has on its lower boundary a line that approximates the 20% RH line. Along this boundary, the “comfort” condition lies between about 72 0F DBT. The upper boundary of the comfort envelope straddles the 65 percent RH line, and here “comfort” exists between about 70 0F DBT and 77 0F DBT.

Mr. Kwok [2] examined the comfort criteria of ASHRAE standard 55-1992 for their applicability in typical classrooms. A file study conducted in Hawaii used a variety of methods to collect the data; survey questionnaires, physical measurements, interviews and behavioral observations. A total of 3,544 students and teachers completed questionnaires in 29 naturally ventilated air-conditioned classrooms in six schools during two seasons. The majority of classrooms failed to meet the physical specification of the standard 55 comfort zone. Thermal neutrality, preference and acceptability votes by occupants of both naturally ventilated and air- conditioned classrooms exceeded the standard’s 805 acceptability criteria, regardless of whether physical conditions were in or out of the comfort zone. Responses from these two school populations suggested not only a basis for separate comfort standard but also energy conservation opportunities through raising thermostat set points.

The National Appliance Energy Conservation act (NAECA) of 1987 established minimum energy-efficiency standards for room air-conditioners, which became effective on January 1, 1990 [3]. The 1990 minimum energy-efficiency ratios (EER) range from 8.0 to 9.0 (Btu/h)/W (2.34 to 2.64 W/W). As required by NAECA, the department of energy (DOE) must also consider amending the room air conditioner standards and affected it in 1990. As a result, the DOE issued a notice of proposed rulemaking (NOPR) in March 1994 proposing new energy-efficiency standards for several

products including room air standards that were proposed. A reanalysis was conducted incorporating the comments, resulting in revised estimates of the cost and increased efficiency for more efficiency room air conditioner designs. This paper describes the cost-efficiency standards that were proposed for room air conditioners in March 1994. the analysis shows that for the most popular classes of room air conditioners (classes without reverse cycle, with lowered sides, and with capacities ranging from less than 6000 to 20,000 Btu/Hr) EER of approximately 10 Btu/Hr/Watt (2.93 W/W) can be achieved by incorporating commonly used technologies, such as high frequency rotary compressors, grooved refrigerant tubing, sub coolers and permanent split capacitor fan motors. Even grater increase in efficiency can realized with brushless permanent magnet fan motors, enlarged heat exchanger coils and variable speed compressors.

III. CFD ANALYSIS OF AIR DISTRIBUTION INSIDE A ROOM

3.1 Introduction: Proper distribution of air in a ventilated room is important in order to achieve satisfactory temperature and air quality. A uniform cooling and freshness of the room are difficult to obtain in residential or office cooling rooms because of uneven distribution of airflow. The airflow distribution depends on the cooling medium, the geometry and characteristics of the cooling room. The velocity distribution of air can be determined based on the mass and momentum conservation equations. An analytical solution can be found only in simple cases. The variables can be examined experimentally, but is tedious, costly, time-consuming method and furthermore, it is only applicable to existing rooms. It can, hence, not be used to optimize the storage room in an early phase of the design. With the increasing availability and power of computers together with efficient solution algorithms and processing facilities, the governing fluid flow equations can be solved numerically. The technique of computational fluid dynamics (CFD), which uses computers for solving fluid problems is very powerful and spans a wide range of non-industrial and industrial application areas. Several user-friendly software packages such as PHOENICS, CFX, STAR-CD AND FLUENT/FIDAP are available. Numerical analysis of air temperature and velocity distribution for a 4m x 4m x 3m room fitted with split air conditioner was carried out. The main aim was to find the ventilation efficiency of air conditioner for various inlet locations (top, middle and bottom) by keeping wall temperature 400 C, cold inlet temperature 150C and air inlet velocity of 2.07 m/s. Air flow inside a room was investigated using computational fluid dynamics.

3.2 Problem Statement and Assumptions**:** The exact problem under investigation and formulation of the model for CFD analysis are presented below. The split air conditioners available in the market are at 1.0, 1.5 and 2.0 Ton capacities. The size of split air conditioner available in the market was surveyed. It was found to be almost 80 cm x 16 cm x 36 cm in size. Those air conditioners have 80 cm x 12 cm area for inlet into the room and 80 cm x 12 cm area for air outlet from the room. In those air conditioners, air enters the room at 300 with horizontal which makes the air flow and the temperature distribution patterns totally different from the other cases. The physical layout of the room under investigation is shown in Fig.3.1.a In the figure, the faces F1, F2, F3 and F4 represents the wall of the room, F6 represents the ceiling of the room and F5 represents the floor of the room. Along the walls and floor air velocities are zero. Heat entering into the room is modeled by specifying constant wall temperatures. The cold air enters into the room at a specified velocity (V) and specified temperature (IT) through inlet and the hot air exits from the room through the outlet that is above the inlet as shown in Fig.3.1.b Normally there will be a blower to suck the air from room and pass it over the evaporator coils and then to force the cold air into the room.

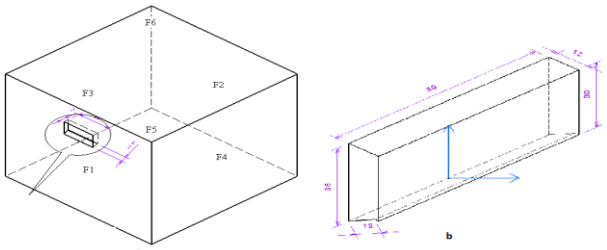

Fig. 3.1: Physical Layout of the Room

3.3 Pre Processing**:** Preprocessing consists of input of a flow problem to a CFD program by means of an operator friendly interface and the subsequent transformation of this input into a suitable form which can be solved by solver module.

3.4 Material Properties**:**

Air properties**:** Density (ρ) = 1.25 kg/m3
Viscosity (μ) = 1.7894e-05 kg/m-s
Thermal conductivity (k) = 0.0242 W/m- K
Specific heat (Cp) = 1006.43 j/kg- K
Molecular weight (M) = 28 kg/kg-mol
Wall properties: Density (ρ) = 2719 kg/m3
Thermal conductivity (k) = 202.4 w/m- oK
Specific heat (Cp) = 871 j/kg- oK

3.5 Operating conditions:

Operating pressure = 101325 Pascal
Operating Temperature = 288.16 0K
Gravity = 9.81 m/s2

a. Boundary conditions:

The condition of air, which enters the room through the evaporator, is:
Velocity = 2.07 m/s
Temperature = 288 0K
The air leaving the room is taken as:
Pressure outlet = 1 atm
Temperature = 298 0K
The temperature of walls and roof of the room is 303 0K
Floor temperature = 303 0K

IV. RESULTS AND DISCUSSIONS

The temperature and velocity distribution inside the room obtained for various locations from the CFD model (bottom, middle, and top) are shown in Fig. 4.1-4.3.As the air enters through the inlet, it mixes with room air and carries it in its stream. The air coming through the inlet is termed as primary air and the room air that mixes with it is called secondary air or induced air.The temperature of air is lowest at the inlet and as the air travels, while the velocity is reducing; its temperature is gradually increasing since the secondary room air is mixed with the primary stream. During this process the air is

 ISBN: 978-93-91420-02-4

absorbing the heat from the space to be cooled. The human breathing region stays in a region of 1 m to 1.8 m height. People feel comfortable when the air velocity and temperature inside the human breathing region are within limits. The recommended velocities in this region are 0.1 m/s to 0.2 m/s (25 fpm to 50 fpm) for an office rooms and residences. People complaint below 0.2 m/s velocity is stagnant and above 0.3 m/s velocity is uncomfortable. The temperature and velocity distribution inside the room obtained from the air conditioner, which is fitted at the bottom of the room, are shown in Fig. 4.1 a and b. The Fig. 4.1 c and d indicates the velocity and temperature distribution graphs in Human comfort region respectively. Here the velocities of air in human breathing are in some regions above 0.3m/s and in some regions less than 0.1 m/s. this shows that the velocities in this region are not in uniform and temperature distribution also not in uniform

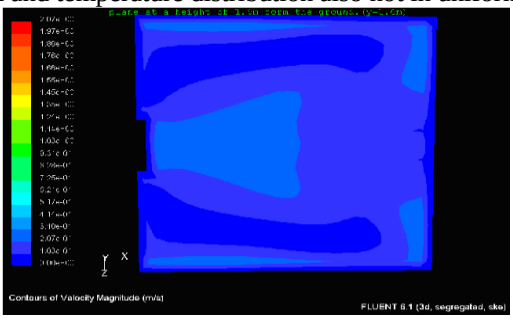

Fig. 4.1a Velocity Distribution inside the room for air conditioner fitted at the Bottom of the Room

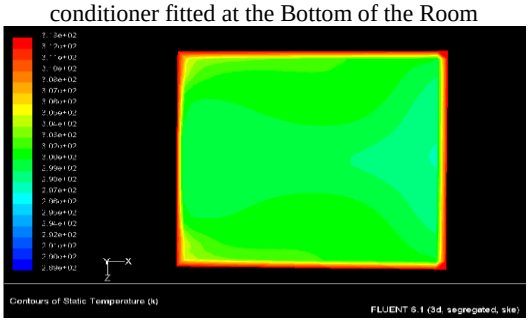

Fig. 4.1b Temperature Distribution inside the room for air conditioner fitted at the Bottom of the room

.

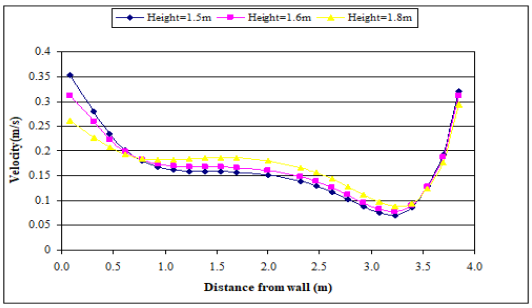

Fig. 4.1c Velocity Distribution Graph in Human Breathing Region for the Air-Conditioner Fitted at the Bottom of the Room.

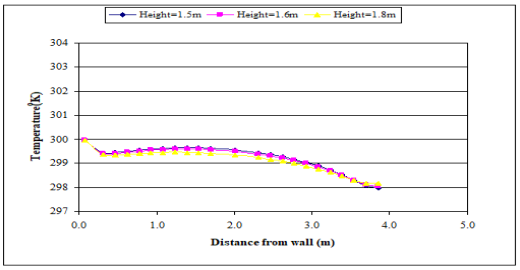

Fig. 4.1d Temperature Distribution Graph in Human Breathing Region for the Air-Conditioner Fitted at the Bottom of the Room.

The temperature and velocity distribution inside the room obtained from air conditioner, which is fitted at the middle of the room, are shown in Fig. 4.2 a and b. The Fig. 4.2 c and d indicates the velocity and temperature distribution graphs in Human comfort region respectively. The figure shows that the velocity in first half of the distance is nearer to 0.3 m/s and in second half of the distance is 0.1 m/s. the temperature in this is varying from 299 0K to 301 0K.

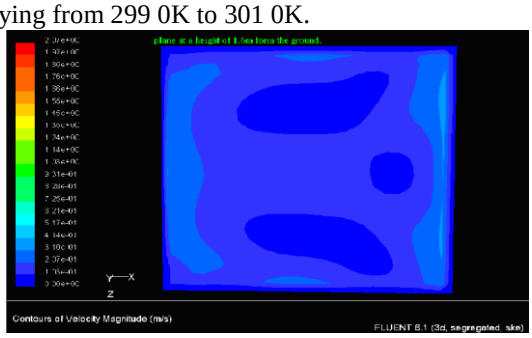

Fig. 4.2a Velocity Distribution inside the room for air conditioner fitted at the Middle of the Room

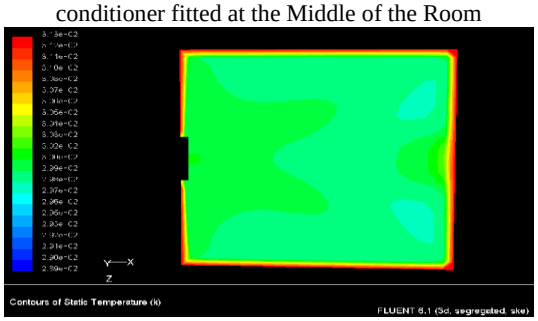

Fig. 4.2b Temperature Distribution inside the room for air conditioner fitted at the Middle of the Room

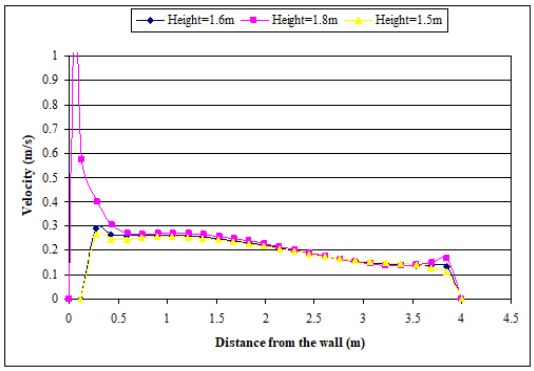

Fig. 4.2c Velocity Distribution Graph in Human Breathing Region for the Air-Conditioner Fitted at the Middle of the Room.

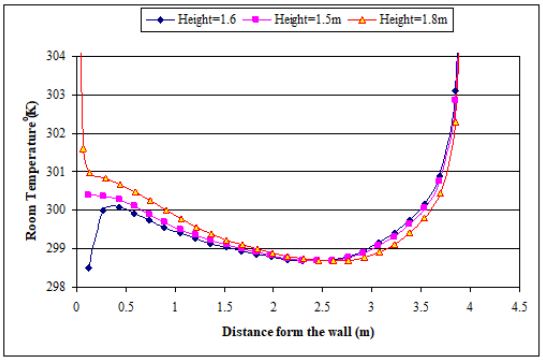

 ISBN: 978-93-91420-02-4

Fig. 4.2d Temperature Distribution Graph in Human Breathing Region for the Air-Conditioner Fitted at the Middle of the Room

The temperature and velocity distribution inside the room obtained from air conditioner, which is fitted top of the room, are shown in Fig. 4.3 a and b.Fig. 4.3 c and d indicates the velocity and temperature distribution graphs in Human comfort region. Here, the velocity versus position of the room graph shows the velocities of air in human breathing region are in between 0.2 m/s to 0.1 m/s which is showing uniform air distribution and pleasant for the occupants. The temperature in this region gives by our air-conditioner shows that 300 0K, which is better than the other arrangements.

In these three locations, the results reveal that fitting the air conditioner at the top of the room is better than middle and bottom arrangements of the room.

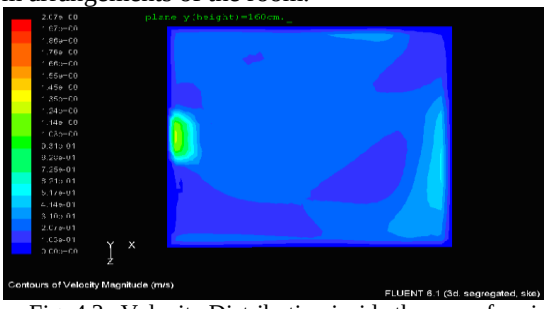

Fig: 4.3a Velocity Distribution inside the room for air conditioner fitted at the Top of the Room.

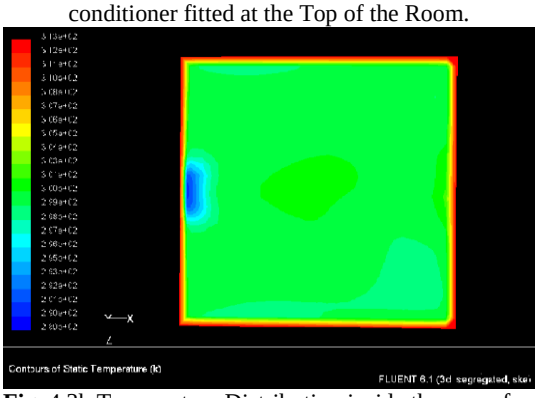

Fig. 4.3b Temperature Distribution inside the room for air conditioner fitted at the Top of the Room

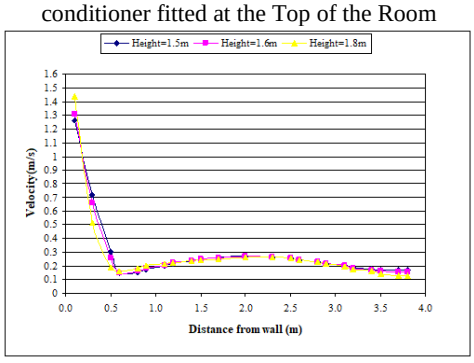

Fig. 4.3c Velocity Distribution Graph in Human Breathing Region for the Air-Conditioner Fitted at the Top of the Room.

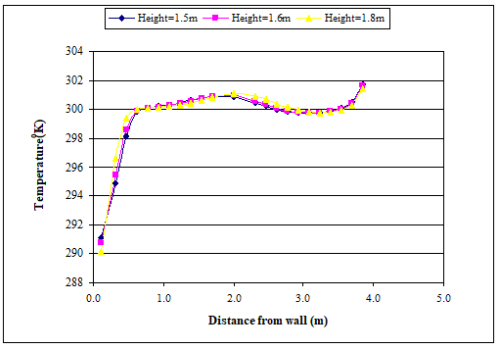

Fig. 4.3d Temperature Distribution Graph in Human Breathing Region for the Air-Conditioner Fitted at the Top of the Room.

V. CONCLUSIONS

In recent years Split Air Conditioner have become very popular due to various advantages such as it occupancy less space; low maintenance cost; remote condenser etc. The 1.5 TR capacity air conditioner exactly suits for many applications such as Residential Rooms, Offices and Laboratories.

The working performance and efficiency of the split air conditioner is not only depends on the sound design but, also location inside the room where it was installed. Experimentally it is very difficult and also tedious to find the efficient location for it. In this thesis, a rigorous simulation was done using FLUNET package to determine the efficient location of the Split Air Conditioner in a 4m x 4m x3m room. The analysis was done for three different locations (top, middle and bottom) and it was found that fitting this air conditioner at a height of 2.1m from the floor gave better performance.

REFERENCES

1. ASHRAE 1974. “Thermal environmental conditions for human occupancy”, ASHRAE Standard 1955-74
2. Mr. Kwok, “HVAC Computational Fluid Dynamics”, ASHRAE Hand Book standard 1955-92, pp16.1-16.3.
3. Mr.Rosenquist, “Minimum energy efficiency standards for room air conditioners”, NAECA (National Appliance Energy Conservation Act) standard 1987-90.
4. Mr.M.L.HOANG, “CFD analysis of air distribution in HVAC systems”, standard 2000
5. MANOHAR PRASAD, refrigeration and air conditioning, Second Edition, New Age International Publishers, 2002.
6. ROY J.DOSSAT, Principles of Refrigeration, fourth edition, Pearson Education Publishers, 1997.
7. C.P.ARORA, Refrigeration and Air Conditioning, Second Edition, Tata Mc Graw Hill Publishing Company Limited, New Delhi, 1998.
8. STOCKER.W.F, Refrigeration and Air Conditioning, Mc Graw-Hill Book Company, 1982.
9. BALLANEY.P.L, Refrigeration and Air conditioning, Khanna Publishers, 2000.
10. ANDERSON, JOHN DAVID, computational fluid dynamics (the basis with applications), Mc Graw-Hill Book Company, 1995.
11. P.S.Ghoshdastidar, computer simulation of flow and heat transfer, Tata Mc Graw-Hill publishing company, New Delhi, 1998.
12. FLUENT USER MANUAL, Fluent Inc.

 ISBN: 978-93-91420-02-4

Frictionless Electromagnetic Braking System

PWDS Milton, G Suresh Babu, S.Dass
Department of Mechanical Engineering, Kallam HaranadhaReddy Institute of Technology, Guntur, India

***Abstract* -There are various types of conventional braking system such as Mechanical brakes (Drum brake, Disc brake), Hydraulic brake etc. Most of Braking system run on the principle of friction and that release of kinetic energy to the heat energy. These braking systems produce higher amount of friction which produce heat wear and tear of braking parts. The frictionless magnetic braking system is proposed using eddy current phenomenon. This phenomenon is governed by faraday law of electromagnetic induction and lenz law. Eddy current is created by relative motion between the magnet and metal conductor. The current induce magnetic field in conductor which oppose the actual magnetic field of magnet and result in deceleration of motion.**

Key Words: Braking System 1, Kinetic Energy , Heat Energy, Eddy Current, Metal Conductor.

I. INTRODUCTION

An Electromagnetic Braking system uses Magnetic force to engage the brake, but the power required for braking is transmitted manually. The disc is connected to a shaft and the electromagnet is mounted on the frame. When electricity is applied to the coil a magnetic field is developed across the armature because of the current flowing across the coil and causes armature to get attracted towards the coil. As a result it develops a torque and eventually the vehicle comes to rest. In this project the advantage of using the electromagnetic braking system in automobile is studied. These brakes can be incorporated in heavy vehicles as an auxiliary brake. The electromagnetic brakes can be used in commercial vehicles by controlling the current supplied to produce the magnetic flux. Making some improvements in the brakes it can be used in automobiles in future.

1.1 PROBLEM STATEMENT

A brake is a device which inhibits motion. Its opposite component is a clutch. Most commonly brakes use friction to convert kinetic energy into heat, though other methods of energy conversion may be employed. For example regenerative braking converts much of the energy to electrical energy, which may be stored for later use.

1.2 PROJECT OBJECTIVE

Electromagnetic brakes operate electrically, but transmit torque mechanically. This is why they used to be referred to as electro-mechanical brakes. Over the years, EM brakes became known as electromagnetic, referring to their actuation method. The variety of applications and brake designs has increased dramatically, but the basic operation remains the same. All the devices such as AC Motor, Electromagnet, Inducting motor, Electronic piston, spring, Brake shoes.

II. INTRODUCTION OF ELECTRO MAGNETIC BRAKES

Electromagnetic brakes operate electrically, but transmit torque mechanically. This is why they used to be referred to as electro-mechanical brakes. Over the years, EM brakes became known as electromagnetic, referring to their actuation method. The variety of applications and brake designs has increased dramatically, but the basic operation remains the same. Single face electromagnetic brakes make up approximately 80% of all of the power applied brake applications.

III. ELECTROMAGNETISM

Electromagnetism is one of the four fundamental interactions in nature. The other three are the strong interaction, the weak interaction and Gravitation. Electromagnetism is the force that causes the interaction between electrically charged particles; the areas in which this happens are called electromagnetic fields.

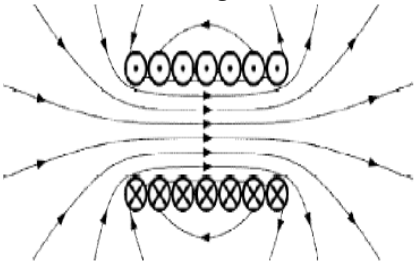

Figure: Magnetic Field Lines

IV. TYPES OF ELECTROMAGNETIC BRAKES

4.1ELECTROMAGNETIC POWER OFF BRAKE

Power off brakes stop or hold a load when electrical power is either accidentally lost or intentionally disconnected. In the past, some companies have referred to these as "fail safe" brakes. These brakes are typically used on or near an electric motor. Typical applications include robotics, holding brakes for Z axis ball screws and servo motor brakes. Brakes are available in multiple voltages and can have either standard backlash or zero backlash hubs. Multiple disks can also be used to increase brake torque, without increasing brake diameter. There are 2 main types of holding brakes. The first is spring applied brakes. The second is permanent magnet brakes.

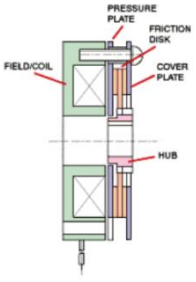

4.2 ELECTROMAGNETIC PARTICLE BRAKE

 ISBN: 978-93-91420-02-4

Magnetic particle brakes are unique in their design from other electromechanical brakes because of the wide operating torque range available. Like an electromechanical brake, torque to voltage is almost linear; However, in a magnetic particle brake, torque can be controlled very accurately (within the operating RPM range of the unit). This makes these units ideally suited for tension control applications, such as wire winding, foil, film, and tape tension control. Because of their fast response, they can also be used in high cycle applications, such as magnetic card readers, sorting machines and labeling equipment.

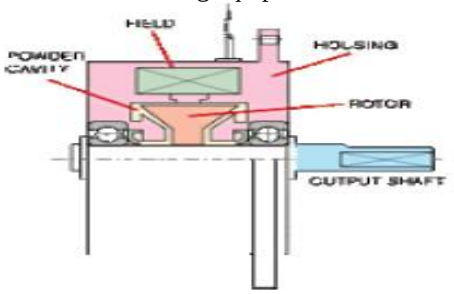

4.3ELECTROMAGNETIC HYSTERESIS POWER BRAKE

Electrical hysteresis units have an extremely wide torque range. Since these units can be controlled remotely, they are ideal for test stand applications where varying torque is required. Since drag torque is minimal, these units offer the widest available torque range of any of the hysteresis products. Most applications involving powered hysteresis units are in test stand requirements.

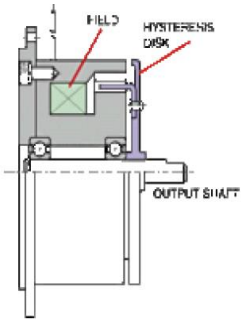

4.4 MULTIPLE DISK BRAKES

Multiple disk brakes are used to deliver extremely high torque within a small space. These brakes can be used either wet or dry, which makes them ideal to run in multi speed gear box applications, machine tool applications, or in off road equipment.

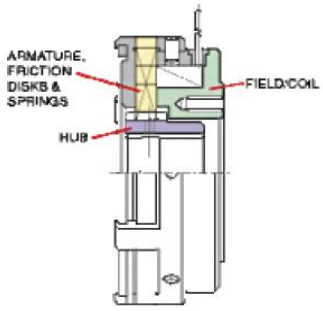

V. DESIGN CALCULATIONS

Centre distance between the pulleys= 24 Cm
Diameter of the driving pulley = 0.085 m=d
Diameter of the driven pulley = 0.05 m=D
Speed of the driving pulley = 1800 rpm=N1
Material of the belt = fabric
Material of the pulley = plastic

A. Determination of speed of the driven pulley

n1d=n2D

$$i = \frac{n1}{n2} = \frac{D}{d}$$

$$N2 = \frac{D}{d} * N1$$

$$N2 = \frac{.085}{.05} * 1800$$

= 3060 rpm

B. Checking for centre distance:

"The Centre distance between the two pulleys must be greater than the average value of the diameters of both the pulleys."

$C \geq \frac{D+d}{2}$

$\frac{D+d}{2} = \frac{.085+.05}{2} = .07m$

C= .24 m

Therefore $C \geq \frac{D+d}{2}$

C. Arc of Contact:

Arc of contact $= 180^0 - \frac{D-d}{C} X\ 60^0$

$= 180^0 - \frac{.085-.05}{.24} X\ 60^0$

$= 172^0$

C. Arc of Contact:

$$L_o = 2C + \frac{\pi}{2}(D+d) + \frac{(D-d)^2}{4C} \text{ (opendrive }$$

$$= 2 * .24 + \frac{\pi}{2}(.085 + .05) + \frac{(.085 - .05)^2}{4 * .24}$$

=.6933 m/s

D. Length of the Belt:

$$L_o = 2C + \frac{\pi}{2}(D+d) + \frac{(D-d)^2}{4C} \text{ (opendrive)}$$

$$= 2 * .24 + \frac{\pi}{2}(.085 + .05) + \frac{(.085 - .05)^2}{4 * .24}$$

=.6933 m/s

E. Actual Length of the Belt:

= L – [1% of L]

= .6933 – [.01*.6933] =.6240 m.

VI. APPLICATIONS

1. This brake system used in two wheeler.
2. Electromagnetic breaking system can be used as a modern technology of braking in automobile.
3. Electromagnetic breaking system used in all types of light motor like car and heavy motor vehicle.

VII. ADVANTAGES

1. In electromagnetic breaking system maintenance is less.

2. Electromagnetic breaking system work is done fast, because of electronic component.
3. Flowing of current is very fast.
4. Very less effort is required to apply the break.
5. It is reasonable as compare to other brakes.
6. The electromagnetic brakes have excellent heat dissipation efficiency owing to the high temperature of the surface of the disc which is being cooled.
7. Electromagnetic brake systems will reduce maintenance cost
8. The problem of brake fluid vaporization and freezing is eliminated

VIII. DISADVANTAGES

1. Dependence on battery power to energize the brake system drains down the battery much faster.
2. Due to residual magnetism present in electromagnets, the brake shoe takes time to come back to its original position.
3. A special spring mechanism needs to be provided for the quick return of the brake shoe.

IX. CONCLUSIONS AND FUTURE ENHANCEMENT

CONCLUSION

With all the advantages of electromagnetic brakes over friction brakes, they have been widely used on heavy vehicles where the 'brake fading' problem exists. The same concept is being developed for application on lighter vehicles. The concept designed by us is just a
Prototype and needs to be developed more because of the above mentioned disadvantages. These electromagnetic brakes can be used as an auxiliary braking system along with the friction braking system to avoid overheating and brake failure. ABS usage can be neglected by simply using a micro controlled electromagnetic disk brake system .These find vast applications in heavy vehicles where high heat dissipation is required.

9.2 FUTURE ENHANCEMENT

When these brakes are combined it increases the life of brake and act like fully loaded brakes. These electromagnetic brakes can be used in wet conditions which eliminate the anti-skidding equipment, and cost of these brake are cheaper than the other types. Hence the braking force produced in this is less than the disc brakes if can be used as a secondary or emergency braking system in the automobiles.

X. PHOTOGRAPHY

REFERENCES

[1] H.Van Oostveen and R. Siezen, "ErfahrungenmitPermanentmag-net- Schienenbremsen", GlasersAnnalen, Nr 12, S. 613-617, 1997.
[2] Gagarin, G., Kroger, U. and Saunweber, E., ''Eddy-current magnetic track brakes for high-speed trains,'' Joint ASME/IEEE/AAR Railroad Conference, pp. 95–99, 1987.
[3] Ohyma, T., ''Adhesion at higher speeds, its basic characteristic, its improvement and some related problem,'' Japanese Railway Engineering, Vol. 108, 1988.
[4] McConnell, H.M., ''Eddy-current phenomena in ferromagnetic material,'' AIEE Transactions, Vol. 73, part I, pp. 226–234, July, 1954.
[5] Kesavamurthy, N., ''Eddy-current in solid iron due to alternating magnetic flux,'' The Institution of Engineers Monograph, No. 339U, pp. 207–213, June, 1959,
[6] Biro, O. and Preis, K., ''Finite element analysis of 3-D eddy current,'' IEEE Transactions on Magnetics, Vol. 26, No. 2, pp. 418–423, Mar, 1990.
[7] Heald, M.A., ''Magnetic braking: improved theory,'' American Journal of Physics, Vol. 56, No. 6, pp. 521–522, 1988.

 ISBN: 978-93-91420-02-4

Performance evaluation of Vegetable oils as Cutting fluid under MQL condition in Turning

Rajesh Mikkili, Putta Nageswara Rao, Ajith Athota and N.S. Prameela
Dept. of Mechanical Engineering, Jntuk, Vasiredddy Venkatadri Institute of Technology, Guntur, AP, India

***ABSTRACT*—In the metal cutting process, the tool performs the cutting action by overcoming the shear strength of the work piece material. This generates a large amount of heat in the work piece resulting in a highly localized thermo mechanically coupled deformation in the shear zone. Therefore, to reduce the generated heat and achieve favourable machining performance, usage of proper cutting fluid is the main factor. Metalworking fluids are considered to be primary and most of these fluids increase productivity and the quality of manufacturing operations through cooling and lubrication during metal cutting process. Despite their widespread use, they pose significant health and environmental hazards throughout their life cycle. To reduce these negative effects, various vegetable oil-based lubricants are widely being used because of their high lubrication performance and less toxic, eco-friendly and non-hazardous nature. Hence, we selected cutting fluids that are not dangerous or problematic to the environment or hazardous to workers. The following are used in the process: rice bran oil, soybean oil, sesame oil, coconut oil, neem oil. And the performance was checked to find out the better one. A technique called minimal quantity lubrication (MQL) is used. In this work the performance of pure vegetable oils were evaluated in turning AISI 304 austenitic stainless steel using Carbide tool under MQL by measurements of Surface roughness, maximum temperature generated at specified location and observation of chip formation. In the work done by us among the five oils Soybean oil gave the best results. All measured parameters confirmed that vegetable oils produce good surface finish, low temperature generated at specified location and better chip formation. It is suggested that considerable cost reduction by using vegetable oils as compared to commercial oils.**

***Keywords*—Thermomechanical, Metalworking fluids, Chip formation, MQL.**

I. INTRODUCTION

Machining is a manufacturing term encompassing a broad range of technologies and techniques. It can be roughly defined as the process of removing material from a work piece using power-driven machine tools to shape it into an intended design. Most metal components require some form of machining during the manufacturing process which leads to developing heat in the cutting zone. The amount of generated heat depends upon the hardness of the work piece material as well as the amount of material removed and the removal rate. A major portion of the generated heat is carried away by the chips, while the remaining heat is dissipated into the work piece and cutting tool.

II. LITERATURE SURVEY

- *KishoreKumarGajrani, M.RaviShankarth is* paper is focused on review of composition, physico-chemical properties, advantages, applications and practical use of individual vegetable oils as metal working fluid in environmental conscious machining to make the process environmentally friendly and less toxic for operators, the study gave best results proving vegetable oils are ecofriendly and they are the fluids which have to be developed in future.
- *MSusmitha, PSharan and P N Jyothi* should that friction between work piece-cutting tool-chips generates heat in the machining zone. The heat generated reduces the tool life, increases surface roughness and decreases the dimensional sensitiveness of work material. This can be overcome by using cutting fluids during machining which has led to reducing the tool wear and formation of continuous chips.

III. SOURCES OF HEAT GENERATION

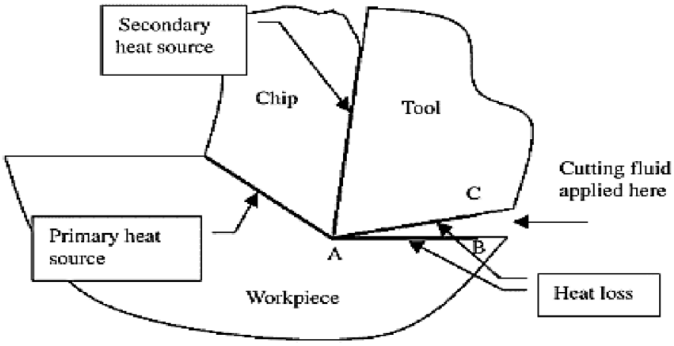

Heat is generated at the cutting point from three sources. Those sources and causes of development of cutting temperature are:

• Primary shear zone - where the major part of the energy is converted into heat.

• Secondary deformation zone - at the chip – tool interface where further heat is generated due to rubbing or shear.

• At the flanks - due to rubbing between the tool and the finished surfaces.

Generated heat leads to accelerated tool failure and thermal damage of the work piece. Thermal damage leads to bad surface finish, induction of residual stresses, micro cracks, and corrosion. Further, the elevated temperature in the cutting zone significantly promotes the formation of built-up edge (BUE) on the tool tip. BUE leads to inconsistent cutting forces and poor surface finish of the product which indirectly effects the machining performance.

IV. EFFECT OF HIGH CUTTING TEMPERATURE

The effects of the high cutting temperature, particularly when it is high, are mostly detrimental to both the tool and the job. The major portion of the heat is taken away by the chips. But it does not matter because chips are thrown out. So attempts should be made such that the chips takeaway more and more amount of the heat leaving a small amount of heat to harm the tool and the work piece.

Effect of heat generated on cutting tool:

 ISBN: 978-93-91420-02-4

- Heat generated during machining results in tool wear eventually leading to high surface roughness of the work piece.
- Thermal cracking which is due to the expansion and cracking caused by thermal stresses is another way the cutting tool can fail.
- After some time, the cutting tool experiences a reduction in weight due to the wear (flank and crater) at the face.

The possible detrimental effects of cutting temperature on the machined work piece are:

- Dimensional inaccuracy of the job due to thermal distortion and expansion-contraction during and after machining.
- Surface damage by oxidation, rapid corrosion, burning etc.
- Induction of tensile residual stresses and micro cracks at the surface and sub surfaces.

V. MACHINING CONDITIONS

5.1. DRYMACHINIG:

This is a machining condition where no lubricant or metal cutting fluid is used instead of the usual traditional coolant and oil for cooling. It is mainly used for milling operation and not advisable for drilling operation as already stated earlier. It could be used in turning operation if hard cutting technology is present in the industry. Dry machining requires no coolants hence the working environment is cleaner and more comfortable eliminating the possibility of slippage during machining. It is cheaper as there is no consumption of water and oil for cooling nor cost incurred for used coolant disposal. However, during dry machining, cutting tool life is short; this results from high temperature generated due to absence of coolant. The absence of coolant to lubricate during cutting results in high energy consumption.

5.2. WET MACHINING:

Here, both the tool and the work piece require the right quantity of coolant. Under wet machining, the heat generated and chip removal rates occur at the same time. Tools utilized here are either externally or internally cooled, depending on the machining process and the work piece material. Cooling fluid fed by the pump also carries away chips produced during the cutting process. The application of coolant during machining reduces friction between the two surfaces thereby improving machinability, preserving tool life and improving surface finish.

VI. TYPES OF METAL WORKING FLUIDS

Metalworking fluids basically fall into four basic categories based on their composition which are straight oils (often called cutting oils), soluble oils, synthetic and semi-synthetic oils.

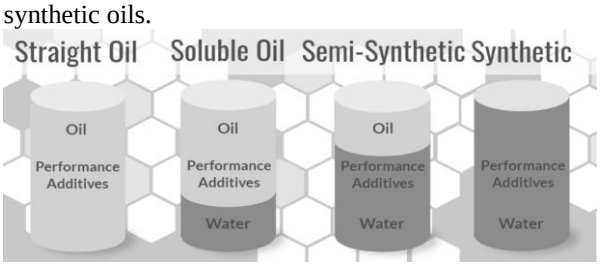

.

6.1. STRAIGHT OILS:

Straight oils are mineral based oils containing no water. Generally straight oils are preferred in low-speed applications for machining of stainless steels and other poorly machinable metals due to their excellent lubrication, good corrosion protection and easy maintenance. However, poor heat removal, formation of toxic mist, easily flammable and high cost are the major obstacles for their excessive usage.

6.2. SOLUBLE OILS:

Soluble oils are also referred to as emulsifiable oils, these oils are mineral oil based and contain emulsifiers, extreme pressure (EP) and other additives. Emulsifiers reduce interfacial tension between oil droplets and water, providing stable and finely dispersed oil emulsion in water. Emulsifiable oils are mixed with water in a concentration range between 2-10%. Emulsion provides good lubrication, good cooling capability, and high corrosion protection, in addition it is of low cost and nonflammable. But the generation of bacteria and fungi during their usage is found to be harmful.

6.3. SYNTHETIC OILS:

Synthetic metalworking oils are water-based solutions which are a combination of soaps, other wetting agents, corrosion inhibitors, water softeners, extreme pressure, anti-bacteria additives (biocides), glycols and other additives. Synthetic oils are prepared in the form of concentrates which are mixed with water before use. Synthetic oils have several advantages such as good cooling capability, excellent lubrication properties, and good stability in hard water, corrosion protection, formation of low mist, easy handling, cleaning and maintenance. However, because of their toxic nature they easily pollute and are of relatively high cost. Because of these negative reasons tribologists got inclined towards development of semi-synthetic oils.

6.4. SEMI-SYNTHETIC OILS:

Semi-synthetic oils are a water-based mixture (solution and emulsion) of synthetic lubricants, additives, emulsifiers and some amount (2-30%) of mineral oil. Semi-synthetic oils combine the advantages of mineral oil emulsions and synthetic oils. They possess better corrosion protection than synthetic oils, better cooling and wetting capabilities, easier to handle and maintain than mineral emulsions. Creation of mist, poor stability in hard water and partial toxic nature are the major disadvantages associated with semi-synthetic oils.

VII. USAGE OF LUBRICANTS

In general, apart from improving the machining performance, a successful development of cutting fluid should fulfil a number of requirements such as non-toxic in nature, non-harmful to health of operators, non-fire hazard, and non-smoke or fog inductor and also should be of less cost. To overcome these challenges, various alternatives to petroleum-based MWFs are currently being explored by scientists and tribologists. Such alternatives include synthetic lubricants, solid lubricants and vegetable-based lubricants. In general, vegetable oils are highly attractive substitutes for petroleum-based oils because they are environmental friendly, renewable, less toxic and readily biodegradable. Currently, vegetable-based oils are more potential candidates for the use in industry as lubricants. Many investigations are in progress to develop many bio based cutting fluids based on various vegetable oils available around the world which differ from

various metalworking fluids. Based on the comparison of properties it is concluded that vegetable oils possess relative advantages compared to Metal working fluids such as less polluting effect on the environment, less toxicity, high flash point, low volatility, high viscosity index which are very much necessary in the machining environment.

VIII. BACKGROUND OF VEGETABLE OILS

Vegetable oils consist of primarily triglycerides i.e., tri-esters of long chain carboxylic acids (fatty acids) combined with glycerol. A fatty acid is a long-chain of carboxylic acid that may be saturated or unsaturated.

To the saturated acids no more hydrogen atoms could be bonded to the carbon atoms present in the basic structure and these compounds contain only C-C single bonds. Whereas unsaturated acids are potential for hydrogen atoms to get bonded to the carbon atoms through further chemical reactions. It is due to these fatty acids containing C=C double bonds that can be chemically converted to C-C single bonds during hydrogen atoms bonded. Soybean oil has been used in China since before historical records [citation needed]. It arrived in the USA in the 1930s. Soybeans are protein-rich, and the medium viscosity oil rendered from them was high in polyunsaturated. Henry Ford established a soybean research laboratory, developed soybean plastics and a soy-based synthetic wool, and built a car "almost entirely" out of soybeans.

Most of these oils contain at least four and sometimes as many as twelve different fatty acids. The proportion of each fatty acid depends not only on the type of the plant, but also on the geo-climate and the weather available. The triglyceride structure of the vegetable oils provides desirable qualities of boundary lubrication, a high natural viscosity, viscosity index (the strong intermolecular interactions are resilient to temperature changes) and structural stability over reasonably operating temperature ranges. The flash point of vegetable oils is high which correlates to a very low vapor pressure and volatility, thereby eliminating potential hazards during use. The long and polar fatty acid chains produce oriented molecular films that interact strongly with the metallic surfaces, reducing both friction and wear.

Properties	Soybean	Sunflower	Rapeseed	Jojoba	Jatrophacurcas	Neem	Castor	Coconut
Kinematic viscosity at 40°c(cst)	32.93	40.05	45.60	24.90	47.48	68.03	220.6	36.2
Kinematic viscosity at 100°c(cst)	08.08	08.65	10.07	06.43	08.04	10.14	19.72	6.76
Viscosity index	219	206	216	233	208	10.14	220	130
Saponification value (mgKOHg-1)	189	-	180	94.69	196.80	166	180	248-265
Total acid value (mgKOHg-1)	00.61	-	1.40	01.10	03.20	23.00	01.40	-
Iodine value (mgl g-1)	144	-	104	98.00	97.00	66.00	87.00	6-8
Pour point (0°c)	-09.00	-12.00	-12.00	09.00	0.00	09.00	-27.00	20
Flash point (0°c)	240	252	240	-	240	-	250	240

IX. VEGETABLE OILS

Being a tropical country, India is rich in forest resources having a wide range of trees, which yield a significant quantity of oilseeds. India is importing crude petroleum & petroleum products from Gulf countries. Indian scientists searched for an alternative to petroleum-based lubricant to preserve the global environment and to withstand the economic crisis. Some Non-Edible Vegetable Oils Available in India.

9.1. APPLICATIONS OF VEGETABLE OILS:

1. Turning process
2. Drilling process
3. Grinding process
4. Milling process

9.2. LIMITATIONS OF VEGETABLE BASED MWF'S:

There are typical examples where metalworking fluids application whether it is vegetable or mineral based harms the process and therefore, it must not be used. Example is when machining with ceramic tools, it must be performed without fluid, because it may promote thermal shocks and eventually, cause tool breakage. Some ceramic tools, mainly those based on Si3N4 and the "whiskers" which have higher toughness and thermal shock resistance can avoid this kind of failure and so cutting fluid can be applied. When machining magnesium, more serious problems may occur when water based fluids are applied because water reacts with the chips, releasing hydrogen, which may cause ignition and fire hazards. It is highly recommended that dry machining be adopted when machining with ceramic tool and straight oil can be used in the case of magnesium as a metalworking fluid.

X. MINIMUM QUALITY LUBRICATION

This is also called near- dry machining condition; it is an alternative to conventional fluids like water and oil. It implies the use of a minimal amount of quality lubricant directly on the surface of the cutting tool. It is almost like the opposite of the use of conventional coolants. For drilling operation, when using the fluid as coolant the application is done externally to cool the tool surface but for MQL, lubricant is applied on the surface of the cutting tool which means that cooling is done internally. Major advantages of MQL include reduction in health risk and energy consumption. It is cheaper because of limited use of coolant. However, MQL technology is much more technical and could pose challenges for machinists and chip evacuation in MQL is poorer compared to those of wet machining.

The concept of MQL is fundamentally different from that of flood coolant and this can be a large stumbling block to machinists who are new to MQL. The use of flood coolant is incredibly basic. As long as relatively clean coolant 'floods' the interface of the cutting tool and work piece, the heat generated by machining operations is kept at bay. This process works (another reason it is widely accepted!), but has some significant consequences. One of the main downsides to the use of coolant, is that it adds extra equipment into the equation. Equipment to recirculate, filter, test, and treat

 ISBN: 978-93-91420-02-4

coolant to keep it viable is required. Contamination from bacteria, tramp oil, and swarf are major concerns as is the disposal of spent coolant. Spent coolant is typically classified as toxic waste and its disposal is regulated.

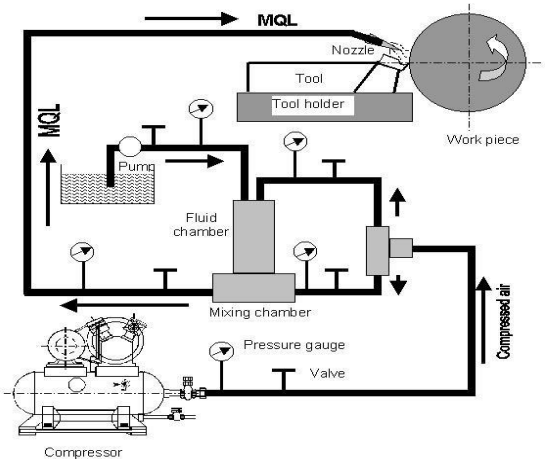

Line diagram of MQL process

Users of flood coolant must factor the cost of its disposal into their machining costs. Another consequence of coolant is that it's messy. Despite containment methods, coolant invariably winds up covering more than just the cutting tool and work. Machines, floors, and finished parts are often left wet from coolant, causing potential slip hazards and often requiring part cleaning before secondary operations can take place.

Repeated exposure too many coolants can have real consequences for the humans involved as well. Some coolants have been shown to cause dermatitis and to be carcinogenic with long-term exposure to coolant vapour. Studies have shown that the cumulative cost of coolants/MWFs can equal as high as 15% of the total cost to produce a part. In a nutshell, MQL makes use of a lubricant, not a coolant, and does so in 'minimum quantities' (like its name!).

Where coolants flood the interface in an attempt to cool things down, MQL coats the interface with a thin film of lubricant and prevents heat buildup through friction reduction. The excellent lubricity of a good MQL lubricant means that the majority of the heat from friction is transmitted to the chip and exits the interface as chips are expelled.

This lubrication and transfer of heat keeps the cutting tool much cooler and reduces tool wear. It is not uncommon for machinists to experience twice the tool life after adopting MQL. MQL lubricants are mostly consumed in the cutting process. The friction and heat in the interface vaporizes the small amount of lubricant and leaves cutting tools, parts, equipment, and floors dry and clean.

The swarf or chips from cutting with MQL are virtually dry and can be recycled without cleaning and for greater profit. With MQL, parts often do not require any cleaning before secondary operations take place. Because the lubricant is consumed, there is no disposal required and no extra equipment is necessary for fluid reclamation. Many MQL lubricants are essentially highly refined bio-based (plant) oils and are completely safe for skin contact as well as having the extra benefit of coming from renewable, environmentally-friendly material.

XI. PROBLEM STATEMENT

Metalworking fluids are used to reduce the generation of heat and friction at the tool work piece interfaces during the machining process. The widespread use of metalworking fluids caused significant health and environmental hazards through their life cycle. To overcome these problems, various alternatives to petroleum-based lubricant have currently been explored by researchers which include the developments of synthetic oils, vegetable based-oil and nano fluids. The growing demand for biodegradable materials opened an opportunity for using vegetable oil as a replacement to petroleum-based oils.

Therefore, Metal working fluids made of vegetable oils are favourable as a sustainable alternative to the conventional Metal working fluids. Metal working fluids from vegetable oils served as an antiwear and anti-friction medium due to strong interactions with the lubricant at the contact surfaces.

Moreover, vegetable oils can be increased for long term usage by further improvement of thermo physical properties by various modification methods such as blending of vegetable oils, adding of nano particles which can influence the machining performances by reducing friction and wear. Therefore, the present work focuses on development of vegetable oil-based cutting fluid for long term sustainable machining.

XII. PREPARATION METHODS

12.1. SELECTION OF VEGETABLE OILS

As a lubricant in machining applications vegetable oils are used widely from the 21st century due to their environmental friendliness and good machining response. However, there are a wide variety of oils available in nature consisting of a wide variety of fluid properties, therefore selection of proper oil as a lubricant for the particular machining application has always been a confusing task. Selection of good cutting fluid depends on its Viscosity, Flash and Fire Points and Adhesiveness. The cutting fluid should possess high flash and fire points, as it should not catch fire at high temperatures.

An incorrect selection of lubricant contributes to very high cost as well as undesirable machining performance. Hence among the variety of vegetable oils selection of proper oil for the particular application leading to generation of minimum temperature and surface roughness during machining is of

primary importance. Various researchers have proved the worth of edible vegetable oils viz., coconut oil, palm oil, soya bean oil, canola oil to be used as eco-friendly fluid in recent past.

Therefore within the present work selection of best vegetable oil as a lubricant among the wide variety of oils available and also with respect to various manufacturing conditions as well as environment has been done through a highly promising approach known as Multi Attribute Decision Making (MADM) for arriving at effective decision- making.

Being a tropical country, India is rich in forest resources having a wide range of trees, which yield a significant quantity of oilseeds. India is importing crude petroleum & petroleum products from Gulf countries. Indian scientists searched for an alternate to petroleum based lubricant to preserve global environment and to withstand economic crisis. Some Non-Edible Vegetable Oils Available in India.

Thermo-physical properties are taken from extensive literature and output responses are measured in terms of surface roughness and maximum temperature generated. The best vegetable oil as a lubricant was selected using a highly promising approach known as Multi Attribute Decision Making (MADM). The results showed that Soybean oil gave best performance among 11 Vegetable oils and consequently the Coconut oil, Cotton seed, Sesame, Rice bran led to better.

Ranking							
S.No.	Vegetable Oil	SAW	WPM	AHP	Multiplicative AHP	TOPSIS	Modified TOPSIS
1	Palm oil	9	9	9	9	9	10
2	Cotton seed	3	3	3	3	3	6
3	Castor	11	11	11	11	11	11
4	Sesame	4	4	4	4	4	2
5	Soybean	1	1	1	1	1	1
6	Canola (Rapeseed)	10	10	10	10	10	7
7	Neem	6	6	6	6	5	9

Table 12.1 Ranking of each alternate based on performance score with different MADM methods

However, among other alternatives Soybean oil is found to be superior to the other vegetable oil considered and ranked one in all conditions discussed. Based on the rankings of the vegetable oils through MADM methods the oils that were selected are as follows:

12.2. SETTING UP VEGETABLE OILS

The vegetable oils are taken and poured into the bottles. Each bottle should be properly mentioned with the oil name on it. Names of the oils in the photograph

1 - Rice bran Oil

2 - Soybean Oil

3 - Sesame Oil

4 - Coconut Oil

5 - Neem Oil

XIII. PERFORMANCE EVALUATION OF SELECTED VEGETABLE OILS

After selecting vegetable oils their performance was evaluated in machining (turning) through MQL. Performance evaluation of oils in machining was carried out considering the factors such as generated cutting temperature at 4mm away from the tool tip, surface roughness and chip formation in turning of AISI-304 steel with carbide insert cutting tool at different speed-depth of cut combinations. The parameters are compared and the results are obtained in MQL

13.1. EXPERIMENTAL DETAILS FOR MACHINING

During the experimentation the selected AISI-304 steel work piece chemical composition and properties are shown in the Table-13.1 and 13.2.Table 13.1 Chemical composition of AISI 304 steel.

Element	Weight [%]
Iron (Fe)	66.345–74
Chromium (Cr)	17.50-19.50
Nickel (Ni)	8–10.5
Manganese(Mn)	Max. 2
Silicon (Si)	Max. 1
Carbon (C)	Max. 0.07
Sulphur (S)	Max. 0.015
Phosphorus (P)	Max. 0.045

Table 13.2 Properties of AISI 304 steel.

Property	Value
Density	8 g/cm3
Thermal conductivity	16.2 W/m.K
Specific heat capacity	0.5 J/g.°C
Tensile strength (ultimate)	720 MPa

The machining under MQL Environment is considered from various literatures as a rigorous solution in achieving sustainable machining. Therefore, experimental testing has been carried out by turning of work piece (AISI 304 steel) with 100 mm length on a conventional lathe by a standard carbide insert.

For the measurement of temperature a hole of 1.6 mm diameter is made through the insert holder nearer to the insert rake face (~0.3mm below rake face) it is diagonally 4 mm away from the tip of the tool. In this hole, one end of the K-type thermocouple probe of 1.5 mm diameter is fitted, the other is a connected temperature digital display unit. Proper precautions are taken to avoid entry of air into the hole for the accurate measurement. The hole was made through the electro discharge machine.

For the performance evaluation of selected vegetable oils tests have been carried out with the following Low and high cutting conditions, which are shown in Table 13.3. All these parameters are selected based on Lathe specifications for machining of AISI 304 steel with carbide insert.

Table 13.3 Experimental conditions.

 ISBN: 978-93-91420-02-4

Machine tool	:	Conventional Lathe Machine		
Work materials	:	AISI 304 Steel, Diameter 30mm*100mmLength		
Cutting tool	:	Carbide Insert		
Cutting Conditions	:	Speed (rpm)	Feed rate (mm/rev)	Depth of cut (mm)
Low	:	350	0.1	0.5
High	:	800	0.3	1.5
MQL	:	Nozzle distance -25mm Flow rate:180ml/h Pressure :60kg/cm^2		

The experimental set-up under dry and MQL environments photographic views is shown in Figure 13.1. A cylindrical bar of AISI 304 steel of 30 mm diameter was selected for straight turning the cutting insert is fixed with a thermocouple sensor at 4 mm away from the tip, during machining the generated maximum temperature is recorded by the thermocouple sensor. After conducting experiments, the machined specimen's surface roughness was measured by a Taly surf using a sampling lengthof 4 mm for 3 trails and average value was taken and finally the chip morphology studies were carried out under all cutting conditions for the selected vegetable oils.

XIV. RESULTS AND DISCUSSION

To observe the performance of five vegetable oils under different cutting conditions in MQL environment. The obtained results are discussed in following sections.

14.1 CUTTING TEMPERATURE

Machining with high speed, feed rate and depth of cut inherently generates more heat as well as high cutting zone temperature. The magnitude of this cutting temperature increases, though in different degrees, with the increase of speed, feed rate and depth of cut, as a result, production levels are constrained by rise in temperature. In the present work, the maximum temperature generated during machining at 4mm away from the tool tip was measured under dry and MQL with the help of a thermocouple sensor.

In this research work, a tool-work thermocouple with proper calibration was used to determine the maximum generated temperature at 4 mm away from the tool tip during turning of AISI 304 steel at various cutting conditions. The obtained results were tabulated with digital photographs and the results are plotted against different cutting conditions in MQL for the vegetable oils.

Table 14.1 Generated maximum temperature (0C) from 4 mm away of tool tip.

S.No	VEGETABLE OILS	Digital Photograph of Generated Temperature at 4mm away from the Tool tip along the rake face diagonal T^{0}c	
		Low	High
1	Rice bran oil	91	245
2	Soybean oil	67	91
3	Sesame oil	98	137
4	Coconut oil	91	129
5	Neem oil	102	134
6	Dry condition	171	210

Figure 14.1 Generated maximum temperature (0C) from 4 mmaway of tool tip vs Speeds (rpm) under different Depth of cuts.

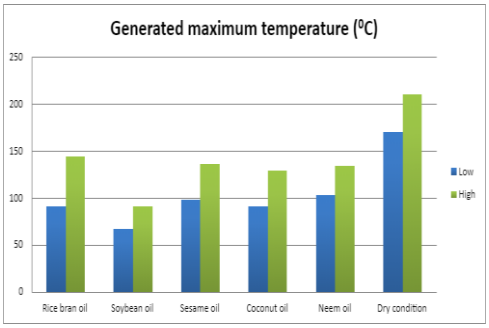

The maximum generated temperature at 4 mm away from the tool tip along the rake face is evaluated at different cutting conditions for the five selected vegetable oils under MQL.

Figure 4.5 clearly shows that the maximum generated temperature for soybean oil is very less compared to all other oils for all cutting conditions. With the increase in cutting conditions, maximum generated temperature has been increased as usual, due to increase in energy input generated temperature increases with the increase in specific energy consumption and material removal rate i.e., with the increase of cutting speed, feed rate and depth of cuts. The maximum generated temperature at specified distance i.e., 4mm away from the tool tip for the soybean oil is found to be very less and at Low cutting condition is 67°C and at high cutting condition is 91°C. This is due to impinging of fine droplets of mist into the region of chip-tool interface which dissipates the heat effectively and it provides better lubrication between chip–tool interfaces in turn avoids formation of Build-up edge even at higher cutting conditions.

 ISBN: 978-93-91420-02-4

14.2 SURFACE ROUGHNESS

Surface roughness is a widely used index of product quality and in most cases a technical requirement for mechanical products. In this work after machining surface roughness has been measured by a Taly surf, taking the average of 3 Trails for each work piece as shown in below table.

Variation of surface roughness at different Cutting conditions (Low and High) has been plotted shown in Figure 14.2

Table 14.2 Surface roughness of selected vegetable oils

S.No	VEGETABLE OILS	Digital Photograph of Surface Roughness					
		CODE	Cutting condition	Trail 1 (µInch)	Trail 2 (µInch)	Trail 3 (µInch)	Average R_A (µm)
1	Rice bran oil	A1	Low				5.867739
2		A2	High	208.85	215.58	238.09	5.609336
3	Soybean oil	B1	Low	212.26	181.98	213.46	5.402495
4		B2	High	159..95	241.72	191.85	4.747641
5	Sesame oil	C1	Low	235.85	241.72	239.26	6.069161
6		C2	High	203.82	207.2	209.36	5.252551
7	Coconut oil	D1	Low	215.58	215.58	238.09	5.666317
8		D2	High	190.67	192.89	193.12	4.882557
9	Neem oil	E1	Low	233.08	237.44	239.26	6.009471
10		E2	High	214.57	214.57	218.73	5.533729
11	Dry condition	F1	Low	258.95	253.1	256.93	6.510697
12	Dry condition	F2	High	263.95	262.1	265.93	6.705431

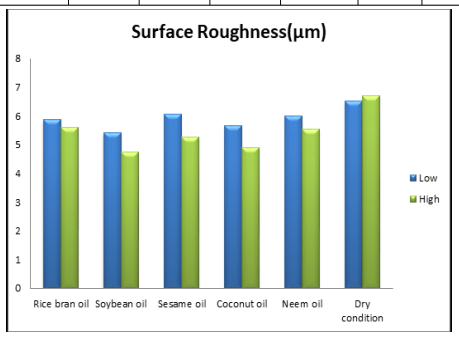

Figure 14.2 Surface roughness of Vegetable oils

Variation of surface roughness at different Cutting conditions (Low and High) has been plotted shown in figure it was observed that the Soybean oil is having less surface roughness compared to other oils for all cutting conditions, accomplished by the lubricating effect of the MQL jet.

The MQL jet with its velocity was able to reach the tool tip where it performed its lubricating and cooling effects and minimized friction to a remarkable amount. It is also observed that at higher cutting conditions as the machining process continues, the sprayed cutting fluid on the work piece forms a thin layer which reduces further rise of temperature causing good surface finish. This improvement might be due to reduction in wear and also due to the fact of prevention of built- up-edge formation.

14.3 CHIP FORMATION

From the table it was observed that chips produced for the soybean oil at low cutting condition is very long ribbon coiled chips (continuous chips) due to continuous plastic deformation and it was observed inside part of the chip shows steps due to intermittent slip and outside is smooth, for higher cutting conditions Serrated Chips (semi-continuous) are generated which possess a saw tooth profile due to the alternating high shear strain followed by a low shear strain. It is clearly observed that the effectiveness of MQL is suitable for the Soybean oil. The chip formation for other selected oils is unfavourable at low and high cutting conditions as shown in table which are similar to dry cutting condition due to the fact that others are having less heat carrying capacity as compared to the Soybean oil. During Machining, chip formation usually depends on type of metal being machined i.e. weather ductile or brittle and temperature at the machining zone. This temperature is due to friction that exists between drill bit and the work piece. Chip may break due to chattering of work piece and due to overheating of work surface during the cutting process. The chatter in the material is avoided by strong work holding work element. Due to excessive heat produced during the machining, surface of work piece material gets converted from ductile to brittle and the chip becomes discontinuous.

Table 14.3 Chip formation under different cutting conditions for vegetable oils.

S.No	VEGETABLE OILS	Digital Photograph of Chips Formation	
		Low	High
1	Rice bran oil		
2	Soybean oil		
3	Sesame oil		
4	Coconut oil		
5	Neem oil		
6	Dry condition		

XV. CONCLUSION AND FUTURE SCOPE

15.1 CONCLUSION

In this work the effect of selected vegetable oils under minimum quantity lubrication (MQL) on machining performance in turning of AISI 304 steel is investigated in terms of maximum generated temperature, surface finish and chip morphology has been examined at low and high cutting conditions.

1. The maximum generated temperature at specified distance i.e. 4mm away from the tooltip for the Soybean Oil is found to be very less in both the conditions i.e. for low cutting condition it is 67°C and for high is 91°C.
2. It was observed that for Soybean Oil there is a good surface finish as compared to other oils in all cutting conditions due to the increase in the Conventional heat transfer.
3. Chips produced for the Soybean oil at low cutting condition is a very long continuous chip whereas for higher cutting conditions short ribbon type chips are produced.
4. MQL provides proper lubrication that minimizes the friction resulting in retention of tool sharpness for a longer period.
5. The other oils neem, coconut are not effective under MQL condition may be due to the poor thermo-physical properties.

15.2 FUTURE SCOPE

1. We can develop blended vegetable oils in different ratios by making these variations we can acquire more data which helps for evaluating data accurately.
2. Performance need to be evaluated at other cutting conditions also.
3. By mixing various Nano-particles we can also improve the properties of vegetable oils.

REFERENCES

[1] *thomasnet*.com/articles

[2] Salman Pervaiz"*Investigation Cooling and Lubrication Strategies for Sustainable Machining of Titanium Alloys*",2014.

[3] Palanikumar, K. (2008). "*Application of Taguchi and response surface methodologies for surface roughness in machining glass fibre reinforced plastics by PCD tooling"*. TheInternational Journal of Advanced Manufacturing Technology, 36(1-2), 19-27.

[4] B.udak, E. and Ozturk, E. (2010). "*Analytical methods for increased productivity in 5-axis ball-end milling*". Int. J. Mechatron. Manuf. Syst. Adv. Multi- Axis Mach. Mach. Tool Control 4, 238– 265, Special issue

[5] Ogedengbe T.S., Abdulkareem S. and Aweda J.O. (2018). "*Effect of Coolant Temperature on Machining Characteristics of High Carbon Steel*". Covenant Journal of Engineering Technology. Volume 1.73-86.

[6] Songmene V., Zaghbani I. and Kientz G. (2018), "*Machining and Machinability of Tool Steels: Effects of Lubrication and Machining Conditions on Tool Wear and Tool Life Data*", Procedia CIRP 77 (2018) 505– 508, doi: 10.1016/j.procir.2018.08.252.

[7] Shokrani A., Dhokia V. and Newman S.T. (2012). "*Environmentally conscious machining of difficult-to-machine materials with regard to cutting fluids*". International Journal of Machine Tools and Manufacture, 57, 83-101.

[8] Mia M., Kumar Gupta M., Singh G., Królczyk G., Pimenov D.Y. (2018), "*An Approach to Cleaner Production for Machining Hardened Steel Using Different Cooling-Lubrication Condition*s", Journal of Cleaner Production doi: 10.1016/j.jclepro.2018.03.279.

[9] Marksberry, P. W. (2007). "*Micro-flood (MF) technology for sustainable manufacturing operations that are coolant less and occupationally friendly*". Journal of Cleaner Production,15(10), 958-971.

[10] Gauthier, S. L. (2003). "*Metalworking fluids: oil mist and beyond*". Applied occupational and environmental hygiene, 18(11), 818-824.

[11] Bennett. "Water based cutting fluids and human health", Tribology International, Volume 16, Issue 3, pp. 133-136, 1983.

[12] VaibhavKoushik, Narendra Shetty and Ramprasad. *"Vegetable oil-based metalworking fluids-A review",* International Journal on Theoretical and Applied Research in Mechanical Engineering, Volume-1, Issue-1, pp.95-101, 2012.

[13] Gunstone. "*Vegetable oils in food technology - composition, properties and uses",* Oxford, UK: Blackwell Publishing, 2002.

[14] Madiwale and Bhojwani. "*An overview on production, properties, performance and emission analysis of blends of biodiesel*", Procedia Technology, Volume 25, pp.963 - 973, 2016.

 ISBN: 978-93-91420-02-4

A Novel Hybrid Fuzzy AHP And VIKOR Methodology For Reclaimer Selection In GSCM

Dr.Karuna Kumar .G[1], Ratna Kumar Gotru[2] , Dr.Seelam Krugon[3] , Ramakanth K[4]
[1,2,4]Mechanical Engineering, Gudlavalleru Engineering College, Gudlavalleru, India
[3]Mechanical Engineering, Bapatla Engineering College, Bapatla, A.P, India

***Abstract*—In typical green supply chain management, distributors collect used goods (oil, plastics, metals, etc.) and ship the goods to recycling processing centers and then collect recycled items from recycling centers. Recycled / recycled goods are sold in secondary markets. In this current paper, the proposed effective strategy for selecting an eligible contender for the recycling industry is similar to the selection problem, the study aims to select a contender in the green supply chain using a comprehensive Fuzzy AHP and VIKOR Method.**

In this paper, four criteria and four criteria such as cost, quality, technical satisfaction, and environmental efficiency are considered and relative weights are generated as the criterion weights by Fuzzy Analytic Hierarchy Process (FAHP). Then, for the ideal solution, the VIKOR method is applied for the best recall selection. A case study was carried out in the oil recovery industry to demonstrate the proposed methodology.

Keywords— Fuzzy AHP, VIKOR, Reclaimer, Green Supply Chain Management.

I. INTRODUCTION

Reclamation selection plays an important role in maintaining green schedules for oil recycling. The characteristics of recapture are that selection is a multi-criteria decision problem (MCDM), influenced by several conflicting factors. Consequently, the purchasing manager must evaluate compensation between different criteria. MCDM methods assist decision makers (DMs) in evaluating a set of options. Depending on the purchase condition, standards may have different importance and weight [7].

The claim selection process is one of the most important variables that have a direct impact on the performance of the organization. As the company becomes more dependent on its suppliers, the direct and indirect consequences of poor decision making become more complex. The nature of this decision is usually complex and structured. On the other hand, the problem in supplier selection decision trade is between multiple criteria with quantitative and qualitative factors, which is also contradictory [8].

Recycling is the process of converting waste into new materials and materials. It is an alternative to "traditional" waste disposal, which saves material and helps reduce greenhouse gas emissions. Recycling can reduce wastage of useful materials and reduce the consumption of fresh raw materials, reducing energy consumption, air pollution (from infusion) and water pollution (from landfill) [9].

Recycling is an important part of modern waste reduction and the third part of the waste hierarchy is "Reducing, Recycling and Recycling". Therefore, recycling aims at environmental sustainability by diversifying raw material exchanges and isolating waste reserves outside the economy [10]. Recycling prevents the depletion of waste land resources [11].

II. LITERATURE REVIEW

The use of comparisons between AHP and its peers has led to the creation of several other decision-making methods. In addition to its widespread acceptance, it has also drawn some criticism; For theoretical and practical reasons. From the early days it was clear how peer was being compared with some issues and how AHP was evaluating alternatives. AHP is the most widely accepted method and is considered by many to be the MCDM method. Multi-criteria decision making process (MCDM) for supplier selection based on 2000 to 2008 journal articles. A blurred method of multi-level decision making is proposed to overcome supplier selection problems. And use TOPSIS to determine the ranking order of all providers). Gray-based approach PROMETHEE (a method of evaluating suppliers for strategic sourcing, in which suppliers are evaluated against supplier co-design capabilities and categorized based on overall performance. (Ghodipur and O'Brien, 2001 (3)) non-linear programming model) designed by Hwang, CL and Yoon, K., (1981), who have studied many features of decision-making processes and applications.

The VIKOR method was mainly established by Jeleni and later advocated by Aprikovic and Teng (Adhikari et al, 2015). This method helps solve multi-level decision-making problems with conflicting and non-initiating criteria when the decision-maker wants a solution that is close to the ideal solution, assuming that an agreement Conflict resolution is acceptable. And from the negative ideal solution, and with respect to all established criteria, alternatives can be assessed. It focuses on classifying and selecting the best option from a set of conflicting criteria and proposing a compromise solution (one or more). A compromise solution is a possible solution, close to an ideal solution, and a compromise is a compromise between mutual subsidies (Rao, 2007). In the VIKOR method, the best option is preferred by increasing the utility group and decreasing the sadness group. This method calculates the ratio of positive to negative ideal solutions. In fact, the TOPSIS and VIKOR methods provide a ranking list. The best ranked option by VIKOR is close to the ideal solution. However, TOPSIS is the best ranked option in terms of rating, which does not always mean that it is a near-perfect solution. In addition to classification, the VIKOR method proposes a compromise solution with a gain rate (Teng and Huang, 2011).

III. BRIEF ON VARIOUS TECHNIQUES USED

Fuzzy AHP

Fuzzy analytic hierarchy process (f-AHP) [8] embeds the fuzzy theory to basic Analytic Hierarchy Process (AHP), which was developed by Saaty [13].

Step 1: Decision maker compares the criteria or alternatives via linguistic terms shown in Table 1

Table 1: Linguistic terms and the corresponding triangular fuzzy numbers

Saaty Scale	Definition	Fuzzy Triangular Scale
1	Equally Important (Eq. Imp)	(1, 1, 1)
2	The intermittent values	(1, 2, 3)
3	Weakly Important (W. Imp)	(2, 3, 4)
4	The intermittent values	(3, 4, 5)
5	Fairly Important (F. Imp)	(4, 5, 6)
6	The intermittent values	(5, 6, 7)
7	Strongly Important (S. Imp)	(6, 7, 8)
8	The intermittent values	(7, 8, 9)
9	Absolutely Important (A. Imp)	(9, 9,9)

According to the corresponding triangular fuzzy numbers of these linguistic terms, for example if the decision maker state "Criterion 1 (C1) is weakly important than Criterion 2 (C2)", then it takes the fuzzy triangular scale as (2, 3, 4). On the contrary, in the pair wise contribution matrices of the criteria comparison of C2 to C1 will take the fuzzy triangular scale as (1/1, 1/3, 1/2). The pair wise contribution matrices is shown in Eq1. [12] Where d_{ij} indicates the k^{th} decision maker's preference of i^{th} criterion over j^{th} criterion, via fuzzy triangular numbers [11].

$$A^{-K} = \begin{bmatrix} d^{-k}_{11} & d^{-k}_{12} \dots & d^{-k}_{1n} \\ d^{-k}_{21} & d^{-k}_{2n} \dots & d^{-k}_{2n} \\ d^{-k}_{n1} & d^{-k}_{n2} \dots & d^{-k}_{nn} \end{bmatrix} \quad (1)$$

Step2: if there is more than one decision maker. Preferences of each decision maker ($\tilde{d}^{k}_{ij}$) are averaged and ($\tilde{d}_{ij}$) is calculate as in the Eq. 2.

$$\tilde{d}_{ij} = \frac{\sum_{k=1}^{k} \tilde{d}^{k}_{ij}}{K} \quad (2)$$

Step 3: according to averaged preferences, pair wise contribution matrice is updated as show in Eq. 3

$$\tilde{A} = \begin{bmatrix} \tilde{d}_{11} & \dots & \tilde{d}_{1n} \\ \vdots & \ddots & \vdots \\ \tilde{d}_{n1} & \dots & \tilde{d}_{nn} \end{bmatrix} \quad (3)$$

Step 4: the geometric mean of fuzzy comparison values f each criterion is calculated as show in Eq 4. Here, $\tilde{r}_i$ still represents triangular values.

$$\tilde{r}_i = \left(\prod_{j=1}^{n} \tilde{d}_{ij}\right)^{1/n}, \; i = 1,2,\dots\dots\dots,n \quad (4)$$

Step 5: The fuzzy weights of each criterion can be found with Eq 5.by incorporating next steps.

- Find the vector summation of each $\tilde{r}_i$. Find the (-1)' power of summation vector. Replace the fuzzy triangular number. To make it in an increasing order.
- To find the fuzzy weight of criterion i ($\tilde{w}_i$), multiply each $\tilde{r}_i$ with this reverse vector.

$$\tilde{w}_1 = \tilde{r}_1 \times (\tilde{r}_1 \times \tilde{r}_2 \times \dots\dots\dots \times \tilde{r}_n)^{-1} \quad (5)$$

$$= (lw_i, mw_i, uw_i)$$

Step 6: since $\tilde{w}_i$ are still fuzzy triangular numbers, they need to de-fuzzified by centre of area method proposed by chou and chang[17]. Via applying the Eq.6.

$$M_j = \frac{lw_i + mw_i + uw_i}{3} \quad (6)$$

VIKOR METHOD

The VIKOR method is a multi-criteria decision making (MCDM) or multi-criteria decision analysis method. It was originally developed by Serafim Opricovic to solve decision problems with conflicting and no commensurable (different units) criteria, assuming that compromise is acceptable for conflict resolution, the decision maker wants a solution that is the closest to the ideal, and the alternatives are evaluated according to all established criteria. VIKOR ranks alternatives and determines the solution named compromise that is the closest to the ideal.

The idea of compromise solution was introduced in MCDM by Po-Lung Yu in 1973[1] and by Milan Zeleny[2]. The VIKOR method was developed to solve multiple criteria decision making (MCDM) problems with conflicting and non-commensurable (different units) criteria, assuming that compromising is acceptable for conflict resolution, the decision maker wants a solution that is the closest to the ideal, and the alternatives are evaluated according to all established criteria.

The proposed methodology for reclaimer selection problem composed of VIKOR Method the MCDM method is very popular technique widely applied for determining the best solution among several alternatives having multiple attributes or alternatives. A MCDM problem can be presented by a decision matrix as follows:

Here, i A represents ith alternative, i =1, 2,....., m; j Cx represents the jth criterion, j =1, 2,.....,n; and xij is the individual performance of an alternative. The procedures for evaluating the best solution to an MADM problem include computing the utilities of alternatives and ranking these alternatives. The alternative solution with the highest utility is considered to be the optimal solution.

The following steps are involved in VIKOR method [6]

Step 1: Representation of normalized decision matrix

The normalized decision matrix can be expressed as follows:

$F = [f_{ij}]_{m \times n}$ (1)

$$\text{Here, } f_{ij} = \frac{x_{ij}}{\sqrt{\sum_{i=1}^{m} x_{ij}^2}}$$

$f_{ij} = xijx2ijmi$=1 , where I = 1, 2,…..and X_{ij} is the performance of alternative Ai with respect to the jth criterion.

Step 2: Determination of ideal and negative-ideal solutions

The ideal solution A^* and the negative ideal solution A^- is determined as follows:

Find **Best** i.e $(x_{ij})_{max}$ for beneficial, $(x_{ij})_{min}$ for non-beneficial criteria

And Worst $(x_{ij})_{min}$ for beneficial, e $(x_{ij})_{max}$ for non-beneficial criteria

$$x_i^+ = \{(\max x_{ij} \mid x \in X) or \min x_{ij} \mid x \in X'), i = 1,2,\dots\dots m\} = \{x_1^+, x_2^+ \dots\dots x_j^+ \dots . x_n^+\}$$

$$x_i^- = \{(\min x_{ij} \mid x \in X) or \max x_{ij} \mid x \in X'), i = 1,2,\dots\dots m\} = \{x_1^-, x_2^- \dots\dots x_j^- \dots . x_n^-\}$$

Where X = {x = 1, 2,……..n| X_{ij} , if desire response is maximum}

X' = {x = 1, 2,……..n| X_{ij} , if desire response is minimum}

Step 3: Calculation of utility measure and regret measure

The utility measure and the regret measure for each alternative are given as:

$$S_i = \sum_{j=1}^{m} \left(W_j * \frac{X_i^+ - X_{ij}}{X_i^+ - X_i^-} \right)$$

$$R_i = \max\left(W_j * \frac{X_i^+ - X_{ij}}{X_i^+ - X_i^-}\right)$$

Where, $S_i$and R_i, represent the utility measure and the regret measure, respectively, and w_j is the weight of the j_{th}criterion.

Step 4: Computation of VIKOR index

The VIKOR index can be expressed as follows:

$$Q_i = v * \frac{S_i - S^*}{S^- - S^*} + (1 - v) * \frac{R_i - R^*}{R^- - R^*}$$

Where, *Qi*, represents the i_{th}alternative VIKOR value, i =1, 2,..... , m;

$$S_i = \sum_{j=1}^{m}\left(W_j * \frac{X_i^+ - X_{ij}}{X_i^+ - X_i^-}\right)$$

$$R_i = \max\left(W_j * \frac{X_i^+ - X_{ij}}{X_i^+ - X_i^-}\right)$$

$S^* = \min S_i$, $S^- = \max S_i$;

$R^* = \min R_i R^- = \max R_i$

Where v is the weight of the maximum group utility (usually it is to be set to 0.5). The alternative have smallest VIKOR determined to be the best solution.

CASE STUDY

This study mainly focuses on the green Reclaimer selection problem of an oil company located in Amaravathi four possible Reclaimers have been determined by the expert. As a result of increasing consciousness of environmental issues and being under pressure from customers' demand, the company tends to incorporate environmental criteria into reclaimer selection process.

Table 2: Fuzzy weights of all the criteria

Attribute or Criteria	Price (Rs)	Quality	Environmental Competence	Technology Level Satisfaction
Price	(1,1,1)	(1,2,3)	(2,3,4)	(5,6,7)
Quality	(1/3,1/2,1)	(1,1,1)	(4, 5,6)	(2, 3,4)
Environmental Competence	(1/4,1/3,1/2)	(1/6,1/5,1/4)	(1,1,1)	(6,7,8)
Technology Level Satisfaction	(1/7,1/6,1/5)	(1/4,1/3,1/2)	(1/8,1/7,1/6)	(1,1,1)

$\tilde{r_i} = \left(\left[\prod_{j=1}^{n} \tilde{d_{ij}}\right]\right)^{1/n} = \left[(1*1*2*5)^{\frac{1}{4}}; (1*2*3*6)^{1/4}; (1*3*5*7)^{1/4}\right] = [1.778; 2.45; 3.03]$

Table3: Relative fuzzy values of quality weights

Price	1.778	2.45	3.03
Quality	1.278	1.65	2.21
Environmental Competence	0.707	0.83	1.00
Technology Level Satisfaction	0.258	0.30	0.36
Total	4.022	5.23	6.60
Inverse(1/Col Value)	0.249	0.19	0.15
Ascending Order	0.15	0.19	0.249

Hence the relative fuzzy weights of each criterion are given Table

Table: 4: fuzzy weights of all the criteria

Price	0.27	0.47	0.75
Quality	0.19	0.32	0.42
Environmental Competence	0.11	0.16	0.25
Technology Level Satisfaction	0.04	0.06	0.09

The relative non fuzzy weight of each criterion (M_i) is calculated by taking the average of fuzzy numbers for each criterion.

Ex: for price m1 = (0.29+0.47+0.75)/3 = 0.49

By using non fuzzy M_i 's, the normalize weights (N_i)of each criterion are calculated and tabulated in Table 5.

Table 5.Normalised values of criteria of reclaimer

Attribute	M_i	(N_i)
Price	0.49	0.49
Quality	0.29	0.29
Environmental Competence	0.15	0.15
Technology Level Satisfaction	0.07	0.07

Step 1: Representation of normalized decision matrix

Weightage →	0.49	0.29	0.15	0.07
Attribute or Criteria	Cost or Price	Quality	Environmental Competence	Technology Level Satisfaction
Reclamier -1	18000	95	5	95
Reclamier -2	12000	80	2	75
Reclamier -3	15000	90	4	80
Reclamier -4	10000	80	3	90

Step 2: Determination of ideal and negative-ideal solutions

Best i.e (x ij) max for beneficial, (x ij) min for non-beneficial and Worst (x ij) min for beneficial, e (x ij) max for non- beneficial

Weightage →	0.49	0.29	0.15	0.07
Attribute or Criteria	Cost or Price	Quality	Environmental Competence	Technology Level Satisfaction
Reclamier -1	18000	95	5	95
Reclamier -2	12000	80	2	75
Reclamier -3	15000	90	4	80
Reclamier -4	10000	80	3	90
Best (X_i^+)	10000	95	5	95
Worst(X_i^-)	18000	80	2	75

Step 3: Calculation of utility measure and regret measure

The utility measure and the regret measure for each alternative are given as:

Where, S_i and R_i, represent the utility measure and the regret measure, respectively, and w_j is the weight of the j_{th} criterion.

$$S_i = \sum_{j=1}^{m}\left(W_j * \frac{X_i^+ - X_{ij}}{X_i^+ - X_i^-}\right)$$

$$R_i = max\left(W_j * \frac{X_i^+ - X_{ij}}{X_i^+ - X_i^-}\right)$$

$$S^* = minS_i$$

Attribute or Criteria	Cost or Price	Quality	Environmental Competence	Technology Level Satisfaction	S_i	R_i
Reclamier -1	0.49	0	0	0	0.49	0.49
Reclamier -2	0.1225	0.29	0.15	0.07	0.6325	0.29
Reclamier -3	0.3063	0.0967	0.05	0.0525	0.505417	0.306
Reclamier -4	0	0.29	0.1	0.0175	0.4075	0.29
				S^*, S^-	0.4075	0.29
				R^*, R^-	0.6325	0.49

$$R^- = maxR_i$$

Step 4: Computation of VIKOR index

The VIKOR index can be expressed as follows:

$$Q_i = v * \frac{S_i - S^*}{S^- - S^*} + (1 - v) * \frac{R_i - R^*}{R^- - R^*}$$

Where, *Qi*, represents the i_{th}alternative VIKOR value, *i* =1, 2,..... , *m*;

Attribute or Criteria	S_i	R_i	Q_i	Rank based on Q_i
R-1	0.49	0.49	**0.683333**	**4**
R-2	0.6325	0.29	**0.5**	**3**
R-3	0.505417	0.306	**0.258218**	**2**
R-4	0.4075	0.29	**0**	**1**
S^*, S^-	0.4075	0.29		
R^*, R^-	0.6325	0.49		

R-Reclamier

Where v is the weight of the maximum group utility (usually it is to be set to 0.5). The alternative have smallest VIKOR determined to be the best solution.

Check the Conditions

C1-Acceptable advantage; C2- Acceptable stability in Decision making

Check first condition: C1-Acceptable advantage

$Q(A^2)-Q(A^1) \geq DQ$

Where DQ =1/(j-1)

j is number of alternative =4

$Q(A^2)-Q(A^1) \geq DQ$

0.258218 -0 = 0.258218

DQ= 1/(4-1) = 0.3

Check Second condition: C2- Acceptable stability in Decision making

If one of the conditions not satisfied, then a set of compromise solution is proposed, which consists of:

- alternative a^1 and a^2 if only condition C2 is not satisfied, or
- Alternative a1, a2, ... ,a(M) if condition c1 is not satisfied; and a(M) is determined by the relation $Q(a^{(M)}) - Q(a^1) < DQ$ for maximum M (the positions of these alternatives are " in closeness")

Condition 1 **X**	Condition 2 √

IV. CONCLUSION

Many researchers and scholars have mentioned the advantages of green supply chain management for environment sustainability. Creating a close and long term relation between the supplier and purchaser is one of the key elements of supply chain creation success to obtain competitive advantage. Therefore, the issue of supplier selection is the most important issue in effectively implementing supply chain. Reclamier selection is similar to supplier selection in reviser logistics in this study initial select the four Reclamiers by Delphi method later evaluated them by using Comprehensive AHP and VIKOR Method with four criteria such cost, quality, Technology level satisfaction and Environmental Competence. The Reclamier who receives the highest ranking (minimum loss score) will be selected to perform with the minimum VIKOR value as follows

Reclamier -1	**4**
Reclamier -2	**3**
Reclamier -3	**2**
Reclamier -4	**1**

REFERENCES

[8] Po Lung Yu (1973) "A Class of Solutions for Group Decision Problems", Management Science, 19(8), 936–946.

[9] Milan Zelrny (1973) "Compromise Programming", in Cochrane J.L. and M.Zeleny (Eds.), Multiple Criteria Decision Making, University of South Carolina Press, Columbia.

[10] Jiang, H. L., & Yao, H. X. (2013). Supplier Selection Based on FAHP-VIKOR-IVIFs. Applied Mechanics and Materials, 357-360, 2703–2707.

[11] Chatterjee, K., & Kar, S. (2017). Unified Granular-number-based AHP-VIKOR multi-criteria decision framework. Granular Computing, 2(3), 199–221. doi:10.1007/s41066-017-0039-4

[12] Fei, L., Deng, Y., & Hu, Y. (2018). DS-VIKOR: A New Multi-criteria Decision-Making Method for Supplier Selection. International Journal of Fuzzy Systems.

[13] Sonu Bansal, Madhukar Chhimwal and Arvind JayantA Comprehensive VIKOR and TOPSIS Method for Supplier Selection in Supply Chain Management: A Case Study Journal of Material Science and Mechanical Engineering (JMSME) Print ISSN: 2393-9095; Online ISSN: 2393-9109; Volume 2, Number 12; July-September, 2015 pp. 8-13

[14] Karuna Kumar G., M. Srinivasa Rao, Kesava Rao V.V.S., "Fuzzy multi objective technique for the quantity to be ordered on supplier" International Journal of Mechanical and Production Engineering Research and Development (IJMPERD) ISSN(P): 2249-6890; ISSN(E): 2249-8001 Vol. 9, Issue 1, Feb 2019, 509-522 © TJPRC Pvt. Ltd., SCOPUS Indexed Journal

[15] Karuna Kumar G., M. Srinivasa Rao, Kesava Rao V.V.S., "Fuzzy Optimization Technique in inventory cost minimization" International Journal of Mechanical Engineering and Technology (IJMET) Volume 9, Issue 13, December 2018, pp. 1527–1536, ISSN Print: 0976-6340 and ISSN Online: 0976-6359, Scopus Indexed

[16] Karuna Kumar G., M. Srinivasa Rao, Kesava Rao, V.V.S., "Supplier Selection and Order Allocation in Supply Chain" ScienceDirect ,Available online at www.sciencedirect.com, Published in Elsevier ,Materials Today: Proceedings 5 (2018) 12161–12173

[17] Karuna Kumar G., Kesava Rao V.V.S., "Supplier Selection and Evaluation in Supply Chain Management"International Journal of Science and Research (IJSR) ISSN: 2319-7064 Index Copernicus Value (2016): 79.57 | Impact Factor (2017): 7.296,Volume 7 Issue 12, December 2018,1042-1050

[18] Karuna Kumar G., B. Karuna Kumar, Kesava Rao V.V.S., "An Integrated Method for the Quantity to be ordered to Supplier" International Journal of Research in Advent Technology, Special Issue, March 2019,E-ISSN: 2321-9637:1-9

[19] T.L. SAATY, (1996) "Decision Making with Dependence and Feedback: The Analytic Network Process", *RWS*, Pittsburgh, PA.

[20] T.L. SAATY, (1980)*The Analytic Hierarchy Process*, McGraw-Hill, New York.

[21] K.G.Durga Prasad , M.V.Prasad 2, S.V.V.Bhaskara Rao3, C.S.PatroSupplier Selection through AHP-VIKORIntegrated MethodologySSRG International Journal of Industrial Engineering (SSRG – IJIE) – Volume 3 Issue 3 – Sep to Dec 2016

[22] Adhikary. P., Roy. P.K and Mazumdar.A (2015), "Selection of small hydro power project site: A multi criteria optimization technique approach", APRN Journal of Engineering and Applied Sciences, Vol.10, No.8, pp.3280- 3285.

[23] Rao.R.V (2007), "Decision making in the manufacturing environment: using graph theory and fuzzy multiple attribute decision making methods", Springer, London.

[24] Tzeng.G.H and Huang. J.J (2011), "Multi-attribute decision making: Methods and Applications, CRC Press, Boca Raton.

[25] Zavadskas, Edmundas Kazimieras; Govindan, Kannan; Antucheviciene, Jurgita; Turskis, Zenonas (2016). Hybrid multiple criteria decision-making methods: a review of applications for sustainability issues. Economic Research-Ekonomska Istraživanja, 29(1), 857–887. doi:10.1080/1331677x.2016.123730

 ISBN: 978-93-91420-02-4

Design of Eco-Friendly Road Cleaner

Siva Sankara Babu Chinka[1], M.ChetanSatya[2], Ch. Siva Srinivas Rao[3], D.Harish[4], K. Sai Babu[5], K.V.Viswanath[6]
Department of Mechanical Engineering, Lakireddy Bali Reddy College of Engineering, Mylavaram, Andhra Pradesh, India

***Abstract*—Cleaning has become a significant need in this advanced period for every one of the people and it is unavoidable in day-by-day schedule measure. It is important to keep streets, roads and floors of the multitude of public get-togethers are all around kept up because of the pattern and furthermore the pandemic across the globe. While cleaning and clearing the streets and roads the work was confronting extreme medical issues for all such issues this planning and created street cleaning machine would help a great deal for every one of the labourers and it is absolutely eco-accommodating. It includes roller brushes to the machine that is associated with cycle wheel where it cleans the streets or roads as the cycle pushes ahead. This machine is complete dependent on mechanical and its support is likewise simple. The brush in the machine is comprised of grating material where the movement of brush permits to drive the residue into capacity box. The principal objective of this is to spread this thought of Model Street cleaner to every single one who expects to diminish the work, time utilization. Henceforth, the current design is planned to foster a physically worked street cleaning machine which is eco-accommodating practical, convenient and less upkeep. The design expects to foster a cutting-edge street cleaning machine that would clean the waste particles lying in the streets successfully for different purposes in every one of the climate conditions.**

Keywords: Road cleaning, Eco-friendly, Roller Brushes and Storage Box.

I. INTRODUCTION

Successful cleaning helps to ensure the wellbeing of the people straightforwardly and in a roundabout way. Cleaning also develops the time span of usability of the floor, dividers and so forth because of customary cleaning and upkeep. As of late, the greater part of individuals like to use transport vehicles for driving and thus these spots are covered with bread rolls covers, cold drink bottles and so forth Thus, it is important to clean the transport stands and rail lines stations at ordinary stretch. .

Cleaning work can be physically demanding and a need has been identified and to develop methods for systematic efficiency evaluation of new products. The present work is aimed to design, development and evaluation of a pedal operated sweeping machine and this should reduce labour and time. An effort has been made to develop a mechanically operated sweeping machine so that it can be an alternative to decrease time consumption as well as labour cost for cleaning roads. On other hand in rural area the road cleaning is done by an manual operated which renders fatigue hazards like asthma, bronchitis etc. to the worker.

However, qualitatively India's roads are a mix of modern highways and narrow, unpaved roads are being improved. Our focus is to develop a machine which should be operated manually so that it can be alternative for conventional electric road cleaning machine. In this work we have done modelling and analysis of the road cleaning machine. The project introduces new technology of cleaning roads and making more comfortable to the people who involved in cleaning the roads. We used such type of materials for manufacturing of road cleaning machine finally. We have observed that all the components are with in safe limit in the manually operated road cleaning machine. Thus, Eco friendly environment can be obtained by the Modern cleaning vehicle because of the harmless energy sources.

While cleaning the roads with the machine, the roads and surfaces were differ from various seasons according to the change in weather conditions we were trying the equipment to be adjustable for multipurpose, where the height, contact of surface are taken into consideration for smooth function of machine and the large output that is to be connected to the cycle . The roller brushes place a crucial role in cleaning the roads in this machine, the brushes are made up of abrasive material which can resist high temperature and has high hardness and less wear and tear.

II. LITERATURE REVIEW

As the part of literature survey under the area of Static structural analysis on Body frame of Road Cleaner consisting of pedals for easy movement. Many research articles, conference papers, books and some research papers are referred, and the outcome of those research are discussed in detail as given below. In the recent years it is being observed that, Alloys materials structures are gaining good attention in the fields of automotive industry, aerospace and marine fields due to inherent properties like high stiffness to weight ratio, corrosion resistance, crash energy absorption, load bearing capacity etc.

Mohammad Kashif Shaikh Ghaffar (Et al) [01], [2018] clarified the plan and manufacture of cycle worked street cleaning machine with the connected hunt is thought of. They had announced that the task research works with an effective floor cleaning with clearing and wiping activities. They had presumed that there are sure restrictions in floor cleaning machines which can be worked upon. Cleaning machines are made with a mean to clean just dry surface of the floor and the machine can eliminate the residue in summer season and furthermore it can eliminate and clean the earth, water from floor in blustery season.In order to reduce the physical stress of workers the machine Is very usefull and covers more area in less time

Vivek Pal (Et al) [02]. – [2019] Planned and created that there is still a ton of endeavors are executed to clean the street for its upkeep. Additionally, a few group are flippant. They through coverings, plastic jugs, squander on streets. At the point when upkeep of street is to be done, a few laborers particularly ladies are designated to clear the street. They clean the street ordinarily like clearing. While clearing, there is more shot at spreading of air borne sicknesses and Present cleaning measure renders weariness to the hand and even it makes harm the shoulder. They reasoned that the plan of

machine would replaces and diminish the endeavours of individuals.

V.Kalaiselvan (Et al) [03] - [2018] Clarified the basic components utilized in the framework makes the vehicle simpler for activity. The machine will defeat the human exertion. They are worked through "Scotch burden instrument" with the assistance of the system, the rotational movement can be effortlessly changed over into responding movement. By utilizing this instrument, the waste particles present external the track path can likewise be adequately eliminated.

Dhananjay Kudche (Et al) [04]. – [2018] The creators has been planned the street cleaner foster a machine which will supportive for sweepers to gather waste and residue easily. They have seen that every one of the segments are with in safe breaking point in the physically worked street cleaning machine. They centred to foster a machine which ought to be worked physically that would clean the streets. At last, the creators reasoned those different applications are utilized with the plan of this machine.

Saravanan N (Et al) [05]. - [2020] They planned the floor cleaning machine is exceptionally minimal as contrast with other cleaning machine which are accessible on the lookout however has an alluring plan and high solidness. There are sure limits in floor cleaning machines which can be worked upon and furthermore while testing of machine, that the cleaning is less successful where the street is by all accounts exceptionally unpleasant and harmed.

S. Eswaran (Et al) [06]. – [2020] Their undertaking points guarantees a spotless climate by giving equally cleaned streets in towns and urban areas. This additionally implies less measure of residue in the encompassing, they likewise associated engine drives for cleaning roller and the going system to understand the programmed cleaning and reusing of trash. They presumed that the undertaking guarantees a perfect climate by giving uniformly cleaned streets in towns and urban communities are accomplished by this machine.

Praveen H (Et al) [07]. – [2018] Planned and fostered a double wheel street cleaning machine that would cleans the residue and soil by the roller brushes. They additionally expressed that the wheels are moved for an ideal situation with an assistance of manual power which can deal with is given to move. They further portrayed handle can be adapted to a necessary tallness and gave three changing openings to it. Subsequently the creators reasoned that with the assistance of manual power the machine would push ahead which upgrades the turn of roller brushes work that would gathers the residue and the exertion applied for the pushing is less when contrasted with the physically clearing.

M. Adil Arshad (Et al) [08]. – [2018]: Plan and creation of cycle worked street cleaning machine with the connected hunt is thought of. They had announced that the task research works with an effective floor cleaning with clearing and wiping activities. They had reasoned that there are sure impediments in floor cleaning machines which can be worked upon. Cleaning machines are made with a mean to clean just dry surface of the floor and the machine can eliminate the residue in summer season and furthermore it can eliminate and clean the earth, water from floor in blustery season.

N. Kapilan Kumar (et al)- [9] [2015] :"Plan and Investigation of Manually Operated Floor Cleaning Machine"- The creators has been planned and investigated physically worked floor cleaning machine. From his examination he finished up the anxiety in the physically worked machine is inside as far as possible.

Sandeep. J. Mesh ram (et al) [10] -. [2016] "Plan furthermore, Development of Tricycle Operated Street Cleaning Machine" – He has fostered the road cleaning machine by tricycle worked. In this examination article he outlined a model particularly for provincial region. He inferred that the cleaning is less powerful where the road is by all accounts very unpleasant and harmed.

Ali Kiapey (et al) [11] –[2014] : The author developed a farm truck of tractor automobile with using fossil fuels ,he plans for more development of the machine and made complete automation of machine and the machine he developed id about 45% efficiency and it is of high cost and maintenance .So he plans for further development of the machine in the manufacturing without high cost.

Abhishek Chakraborty, Ashutosh Bansal [12] –[2013] : Experimented work for cleaning with the disc arranged to the motor by the emerging technologies of the machine. He studies that the emerging technologies would cause reduce the dust in the roads and streets which would a present progressing Technology. He resulted that the machine is not produced sufficient results for cleaning by using disc using residue collector.

1. METHODOLOGY

In this design process the major methodology for working of this machine is briefly explained with the dramatic figure given below. While moving of the vehicle the brush follows the following method.

A. Methodology

In this project the different mechanism which are used are as follows

1. Roller mechanism
2.Belt and pulley mechanism
3.Conveyer belt mechanism

B. Roller mechanism

In our project a broomer is connected to a roller which is operated with the help of electric motor. The rolling force help the dust particles to move to the collector the lighter particles are directly connected to the secondary collector and the heaver particle are transfer to the conveyer belt and they are transfer to the primary collector.

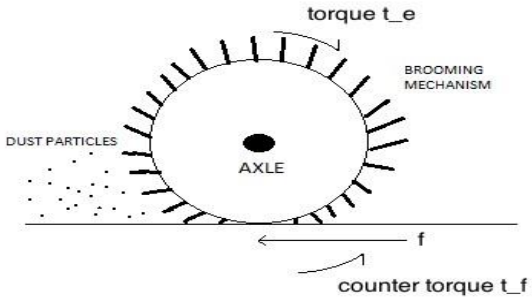

Fig 3.1 Roller mechanism

The broomer brushes are in directly contact with the dust particles when the roller rotates the force experienced by the roller is in forward direction hence it applies force on the dust particles in backward direction which is governed

 ISBN: 978-93-91420-02-4

by the newton third law. The brushes are also in compression while they are in contact with the ground so when they are released, they exert an upward thrust on the dust Particles which help them to be collected in the dust collector chamber.

C. Belt and pulley

Our project uses cross belt mechanism to drive broomer and conveyer belt. the power is directly transferred to the broomer via spur gear with the gear ratio. Then a belt and pulley arrangement transfer the power to the conveyor belt and conveyor pulley is connected to the secondary collecting chamber.

D. Conveyer Belt Drives

Conveyor belts are arranged to the angle of inclined so that dust easily collect in the collecting chamber. Conveyer belt are rotating with the help of cross belt drive which is operated by external force operated mechanism for transmission of power.

III. DESIGN AND MODELLING

Design and modelling of the vehicle that is Eco-Friendly Road cleaner is primarily designed and analyzed by the following necessary steps given below, where these steps make the complete outlet of vehicle with the necessary dimensions.

A. Procedure for Design of Road Cleaning Machine

(a). Open CATIA V5 Software
(b). Go to Mechanical design and part design.
(c). Draw the front part of cleaning machine frame by using line, circle ,arc ,polyline ,rectangle ,trim etc.. With the dimensions given in table.
(d). Repeat the same procedure for rear end i.e.. Cycle too as shown in figures below in the part design.
(e). Go assembly and import all drawings in one part design
f). Using different constraints like surface constraint, offset, Poly-array, mirror, Update commands etc. Make them a set.

B. Design Considerations

The design is performed using CATIA V5 software with required dimensions.

Main Dimensions of Design are:
Diameter of circle where load acting =25mm,
Length of load rod (Lr) = 253.854mm,
Distance between front wheels and rear wheel=415mm
Distance between two wheels in front end = 280mm
Diameter of Handle rib (rod) = 25mm
Diameter of Big Sprocket = 180mm,
Diameter of small sprocket = 60mm

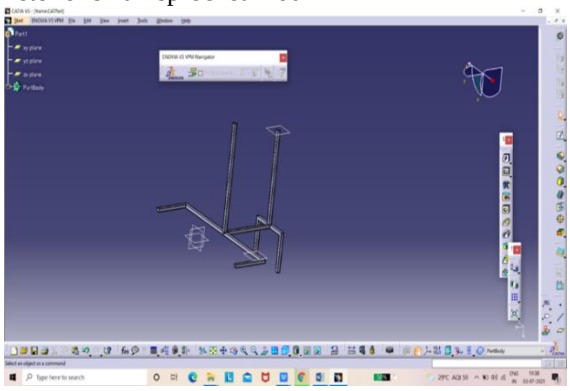

Fig.: 4.1 Model Frame of vehicle.

C. Design and Assembly of Individual parts

The Individual parts of Tires, rim and frame are imported from part design into assemble window. Using various tools and constraints the front part is assembled as follows.

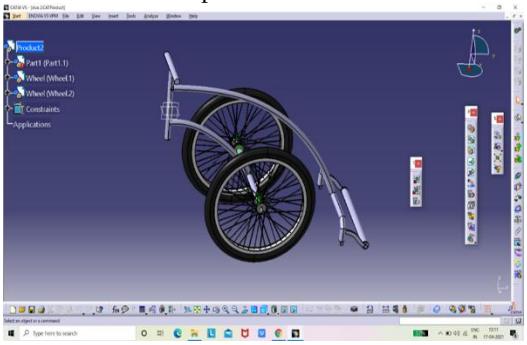

Fig.: 4.2 Assembly of individual parts

Fig.: 4.3 Overall Layout of vehicle

D. Design and Assembly of Sprockets and Chain

For the functionality purpose and the movement of vehicle the sprocket and chain are the main components. By using the various commands like pad, offset, fillet, polar array, pocket, rib etc.

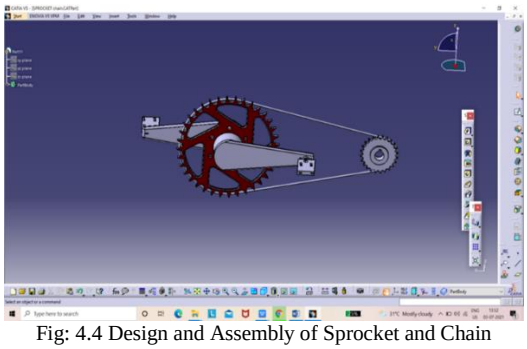

Fig: 4.4 Design and Assembly of Sprocket and Chain

E. Assembly of all Individual Parts to the Vehicle

Individual designs from the Part designs are imported to the assembly design for total outlet ofthe vehicle. The parts are assembled by using existing command in software and made the dimensions of the assembly drawing.

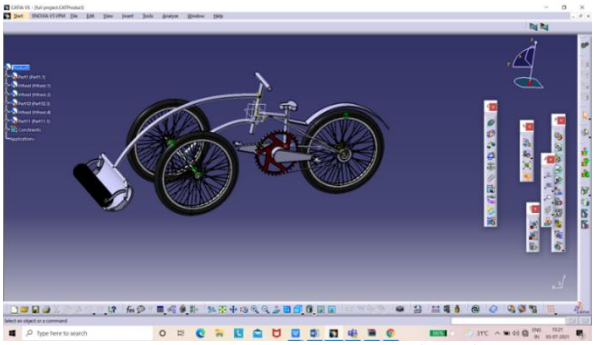

Fig.: 4.5 Complete Design and Assembly of Eco-friendly Vehicle.

CONCLUSION & FUTURE SCOPE

The physically worked eco-accommodating Street and floor cleaner is effectively planned, Designed and analyzed. This task works executes the physically worked eco amicable street cleaner for street cleaning that lessening the expense, human endeavors just as time. It is the best option for computerized street cleaning machine during power emergency. It is tracked down that the current street cleaning machines works with a human straightforward exertion. Manual cleaning may cause shoulder issue because of persistent clearing.

The physically worked street cleaning machine is elective idea for staying away from such issues. It works productively regarding covering region. It is exceptionally prudent to utilize. The physically worked eco-accommodating street and floor cleaner can work proficiently with deference to covering region, time and cost of street cleaning measure contrasted and the current hardware.

Utilizing this Simplified Road Cleaning Machine with Modified Technology, Suitable for Indian Conditions, in view of its unwavering quality and superfluity. Because of all out cost of the framework is extremely low and just one time speculation must be made for lessening work charges. It will lessen human endeavours definitely and exceptionally accommodating to clean streets even in rush hour gridlock.

As fuel is a non-renewable resource, we have to reserve fuels for future usage. We can reduce the fuel usage with this bicycle because of their light in weight and no need of any fossil fuels. Structural Steel using in the manufacturing of the automobile parts is a quite good replacement for conventional materials.

REFERENCES

[1]. Muhammad Kashif Shaikh Ghaffar, M. AadilArshad, Nandkishor S. Kale, Ansari M Bilal,Prof. D. M. Ugle - **"**Design and Development of floor cleaning Machine" ,International Journal of Advanced Engineering and Research Development(IJAERD) NSCOSET(2018),Volume 5, Issue 06,April 2018, India ISSN 2348-4470.

[2]. Vivek Pal, Vishal Ranjan Mall, Manish Prakash, Shubham Agrawal, Vivek Singh, Prof Dharmendra – "Design and Fabrication of Brooming Machine" , International Journal of Civil, Mechanical and Energy Science (IJCMES) [Vol-5, Issue-3, May-Jun, 2019] https://dx.doi.org/10.22161/ijcmes.5.3.2 ISSN: 2455-5304.

[3]. V.Kalaiselvan, P.Jagadeeswaran, M.Gopi and B.Rahulraj –"Design and Fabrication of modern cleaning Machine", First International conference NexGen Technologies, 05-06 Jan 2018, www.conferenceworld.in, ISBN: 978-9386171-90-0.

[4]. Dhananjay Kudche, Yadnyesh Kulkarni, Prof. Manoj Bauskar, "Design and Development of Eco-Friendly Road Cleaner", MAT Journals 2018, Journal of Advancement in Machines Volume 3 Issue 3.

[5]. Saravanan N, Sanjay S, Sreenithiyanandan R S – "Fabrication Of Floor Scrubber Machine", International Journal of Scientific & Technology Research Volume 9, Issue 02, February 2020, ISSN 2277-8616.

[6]. S.Eswaran, V.Logesh, U.Manojkumar, S.Mohanraj, R.Mowleeswaran – [2020] "Design and Fabrication of Pedal Operated Sweeper", Aegaeum Journal, Volume 8, Issue 4, 2020, http://aegaeum.com/, ISSN NO: 0776-3808.

[7]. Praveen H , Harish Gowda GR , Anil G Ramageri, Arunkumar Kallammanavar, Prasanna P Kulkarni, Girish B Kallihal – [2018] International Journal for Research in Applied Science & Engineering Technology (IJRASET) ISSN: 2321-9653; IC Value: 45.98; SJ Impact Factor: 6.887 Volume 6 Issue V, May 2018- Available at www.ijraset.com.

[8]. 01. Muhammad KashifShaikh Ghaffar, M. AadilArshad, Nandkishor S. Kale, Ansari M Bilal, Prof. D. M. Ugle - "Design and Development of floor cleaning Machine", International Journal of Advanced Engineering and Research Development (IJAERD) NSCOSET(2018),Volume 6, Issue 01,April 2018, Science journal for impact factor, India ISSN 2321-0613.

[9]. N. Kapilan-"Plan and Analysis of Manually Operated Floor Cleaning Machine" - Global Journal of Engineering Research and Innovation (IJERT) ISSN: 2278-0181 IJERT IS040912 [www.ijert.org] Vol. 4 Issue 04, April-2015.

[10]. Sandeep. J. Meshram, Dr. G.D. Mehta - "Plan and Improvement of Tricycle Operated Street Cleaning Machine" - Journal of Information, Knowledge And Examination In Mechanical Engineering ISSN 0975 – 668X| Nov 15 To Oct 16 | Volume–04, Issue-01.

[11]. Ali Kiapey, Ali Jafari-"Plan what's more, Fabrication of a farm truck controlled departs gatherer outfitted with attractions blower framework" - September, 2014 Agric Eng Int: CIGR Journal Open access at http://www.cigrjournal.org Vol. 16, No.3.

[12]. Abhishek Chakraborty, Ashutosh Bansal – "Plan of Residue Collector for Rear Wheel of Four-Wheeler" - Global Journal of Emerging Technology and Progressed Engineering, Volume 3, Issue 7, July 2013, 199- 216.

 ISBN: 978-93-91420-02-4

Mechanical and Microstructural Characterisation of Jute Hybrid Composite with Alkali Treatment

K. Venkatarao, Ch. Lakshmikanth, A. Bharathi Lakshmi and A. Venkata Jayasri
Department of Mechanical Engineering, Prasad V. Potluri Siddhartha Institute of Technology,Vijayawada, India

***Abstract*— This article presents the effects of alkali treatment (NaOH) on the mechanical properties of natural fiber reinforced polyester composites. In the current study, composite specimens are prepared using treated and untreated jute fiber and teak wood powder as reinforcement phase and polyester resin as a matrix through hand layup technique as per the ASTM D256M and ASTM D638M standards. The fabricated specimen was subjected to tensile and impact for both treated and untreated. The mechanical properties were analyzed through load-displacement curves. The mechanical properties increased with increasing fiber content. Further, the densities of composites were decreased with increasing fiber content. The fracture surface analysis on the failure region was studied through scanning electron microscopy (SEM) and the nature of the failure was reported.**

I. INTRODUCTION

In the present era, the natural fiber-reinforced composite is a key subject to many researchers, academicians, and scientists. Over the past, so many decades, different kinds of research were conducted to create novel natural fiber-reinforced polymer composites with superior mechanical characteristics [1]. This natural fiber-reinforced polymer composite material has huge potential to replaceable synthetic materials [2-4]. Now the major research has been focusing on those polymer matrices reinforced with various wood fillers.

The addition of wood particulate enhances the numerous features of polymer composites [5, 6]. The wood powder fillers are sufficiently available and it is cost-effective in the utilization of polymer composites as referred to as fillers like nano-clays, carbon nanotubes, and various inorganic fillers. The utilization of filler improves the mechanical properties of composites. The high-density polyethylene (HDPE) was loaded with Pinecone filler at various wt% like 5, 10, 15, and 20%. The experimental results exploit that the 10% addition of filler boosted the mechanical properties of composite as well its elastic and flexural modulus [7].

The sal and teak wood powders are used to fabricate hybrid epoxy composites with a distinct composition by keeping the composition of reinforcement within the matrix around 33%. This study reveals that the equal quantity powder reinforced composites have better tensile, flexural, and impact strength, and also it is also noticed that the inclusion of both powders reduces the water absorption [8]. The hardness was improved by reinforcing Fagus Orientalis wood flour in high-density polyethylene. The particle size of filler has a significant effect on the hardness of composites. The increase in the size of particulate reduces the hardness of the composite. On the other hand, 50% of retainment in mechanical properties was noticed and there is a slight decline in impact strength at an elevated proportion of reinforcement [9]. The jute fiber reinforced epoxies composite is fabricated by using Calotropis gigantean filler with various weight percentages and tested for mechanical characterizations. From the results, 10 wt% of filler composite laminates show excellent tensile, flexibility, and compression strength [10]. Chemically transformed powder fillers augment the thermal and mechanical qualities of polymer composites. The incorporation of alkali-treated Portunus sanguinolentus shell powder filler results in the enhancement of mechanical properties of composites [11]. The polyester -banana fiber laminates were loaded with nano green gram husk filler with various wt. % reinforcements. Among the all fabricated composites, the 5% nano green gram husk filler made known the addition of nanofiller improve the strength of laminate [12]. Spent Camellia sinensis kernel and Azadirachta indica kernel flours are utilized as a filler material for the fabrication of jute epoxy laminates. The test results of laminates testimony that morphological and physical characteristics of filler have a crucial part in the thermo-mechanical behavior of composites [13].

The banana fiber-based polyester hybrid composites were fabricated by using red mud filler to rise in vibration, chemical, and physical properties of the composite [14]. The results of clean and hybrid composites are fabricated from jute and coir fibers were tested for their mechanical and swelling characteristics. The results illustrated that coir-jute fibers utilization pick up size constancy and superior mechanical strength [15].

From the wide range of literature reviews, it was established that there are a few reports that were practically narrated to bio fillers and that too very little work related to teak wood powder as fillers in the polyester composites. In the present work, polystyrene was chosen as a matrix, jute fibers as reinforcements, and teak wood particulates as filler. The hand layup procedure is opted to make up the composites. The fabricated composite laminate was examined for mechanical characteristics. The fractography, destitute, teak powder disbursement qualities of the formed composites were researched by using SEM..

II. MATERIALS AND METHODS

The materials were used to prepare the specimens are teak wood powder, Jute fibre, and polyester resin. To improve the bonding strength between fiber and matrix heat treatment was conducted for jute fibre and teak wood powder.

The impact and tensile properties of the composite, the specimens are prepared according to ASTM D256, ASTM D638 standard by using hand lay-up technique with different weight ratios as shown in table 1.

 ISBN: 978-93-91420-02-4

Table.1 Composite specimen Preparation weight Percentages

Test specimen	Weight percentages of specimens
T1	1.5gm fiber (untreated)
T2	1.5gm fiber (treated)
T3	0.5gm Teakwood powder (untreated)
T4	0.5gm Teakwood powder(treated)
T5	0.3gm Teakwood powder +1.5g fiber (untreated)
T6	0.3gm Teakwood powder + 1.5g fiber (treated)
T7	0.5gm Teakwood powder +1.5g fiber (untreated)
T8	0.5gm Teakwood powder +1.5g fiber treated)

The tensile experiments are conducted on universal testing machine with transfer speed of 2 mm/min and the impact study was conducted izod impact testing machine.

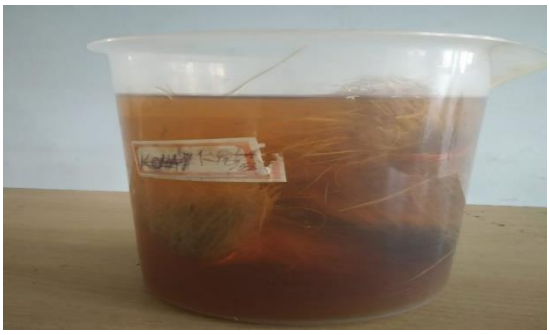

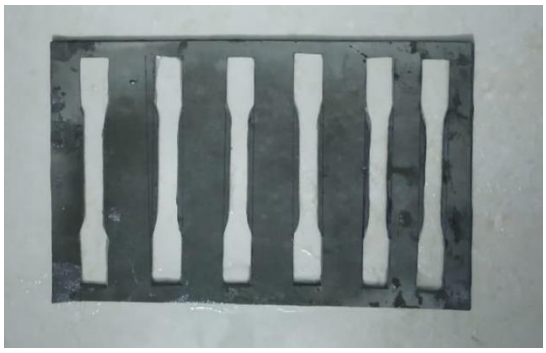

Fig.1 (a) Jute fiber, (b) Teak wood powder, (c) Chemical treatment, (d) Mould preparation, (e) Specimen for impact test (f) Specimen for tensile test

RESULTS AND DISCUSSIONS

The chemical treatment effect on composites specimens shows an important role in the tensile behavior of polyester composites and it was gradually increased with increase with reinforcement phase. The higher tensile load-bearing capacity was recorded for the T5 specimen because of its excellent bonding strength and combination of fiber and teak wood powder. In maximum cases the specimen shows high-level strength after chemical treatment because of surface roughness of fiber enhances the superior bonding strength, and it is observed from scanning electronic micrographs. The composite samples are exhibited lower level displacement with irrespective load and chemical treatment. The diminished tensile strength and bearing capacity are noted in the T3 sample. Figure 3 shows the load versus displacement curves for a better understanding of the mechanical behavior of polyester composites.

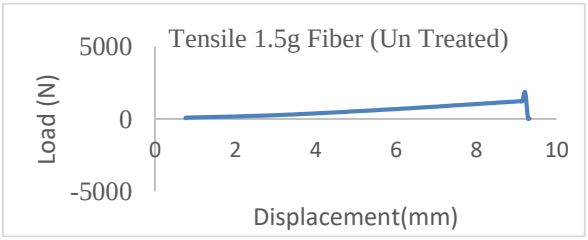

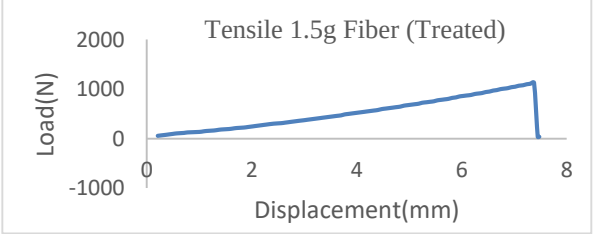

 ISBN: 978-93-91420-02-4

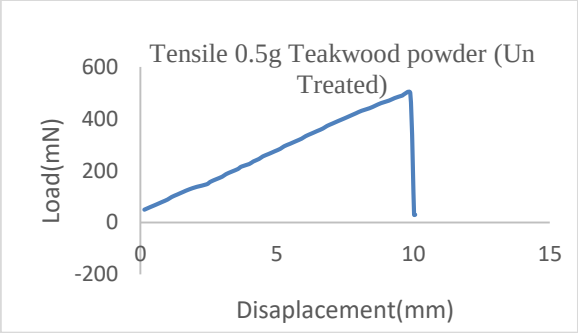

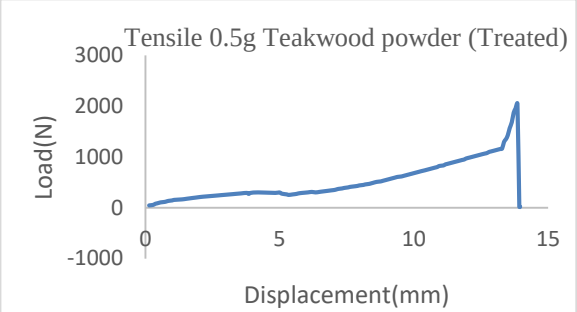

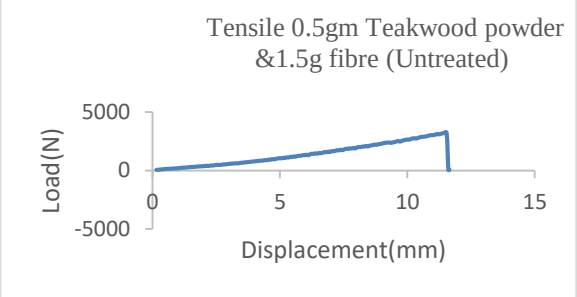

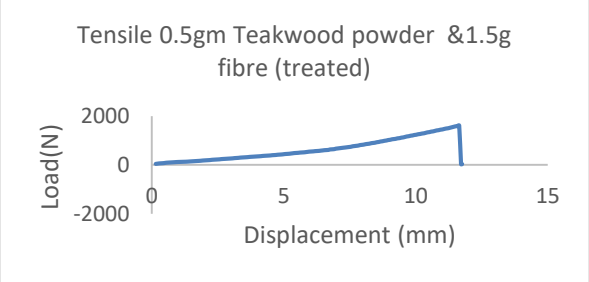

Fig.3 Tensile Behaviour of Composite Specimens

Figure 5 shows the impact strength of polyester composites. The impact strength was significantly enhanced through alkaline treatment of polyester composite. After chemical treatment, the impact strength of composite increased due to the roughness on the surface of fiber which affects the impact strength. The maximum impact strength is observed at the T6 specimen due to the presence of teak wood powder and bonding strength jute fiber insufficient level. The specimen T1 has low impact strength due to it contains untreated fiber which has lower bonding strength among the fiber and matrix phase. It is clearly noticed that the impact strength of composite was enhanced with treatment of fiber as well teak wood powder.

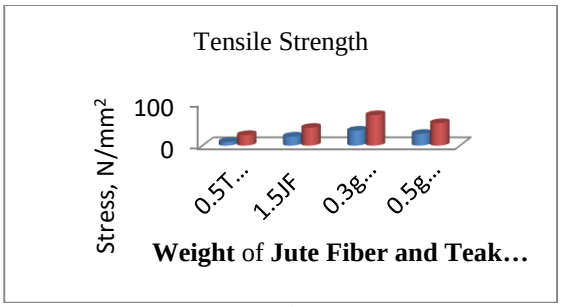

Fig.4 Tensile Behavior of Composite Specimens

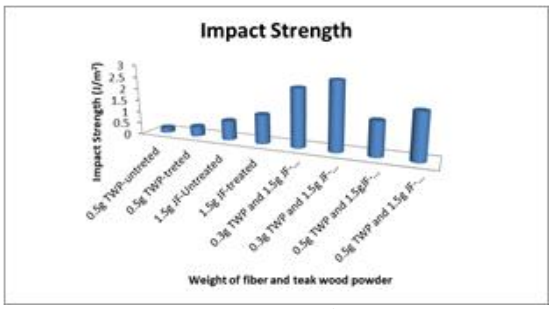

Fig.5. Impact strength of specimens

Fracture analysis of polyester jute fiber-reinforced composites The fracture surface was examined through the scanning electron microscope micrographs of T1, T6 under tensile loading condition, This micrographs discloses the nature of the failure of the composite specimen. Fig 5a discloses the uniform teak wood powder distribution in the polyester matrix. The internal cracks were noticed from figure 5b due to tensile load and exhibit the brittle failure of the specimen. The fiber pulls out and de-bonding is observed from the figure 5d for tensile specimen T6 under tensile load. The fiber distribution is captured in figure 5c.

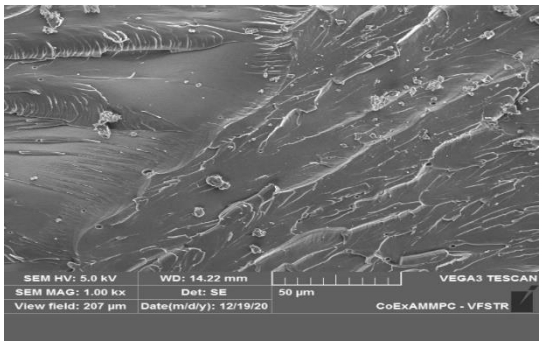

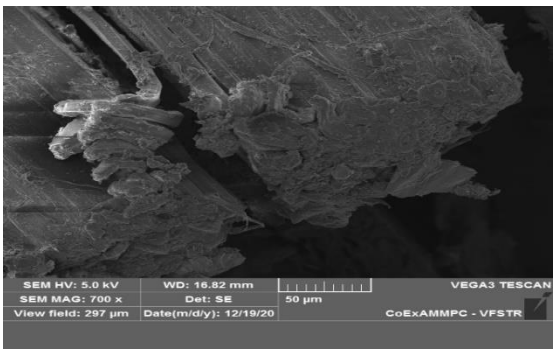

 ISBN: 978-93-91420-02-4

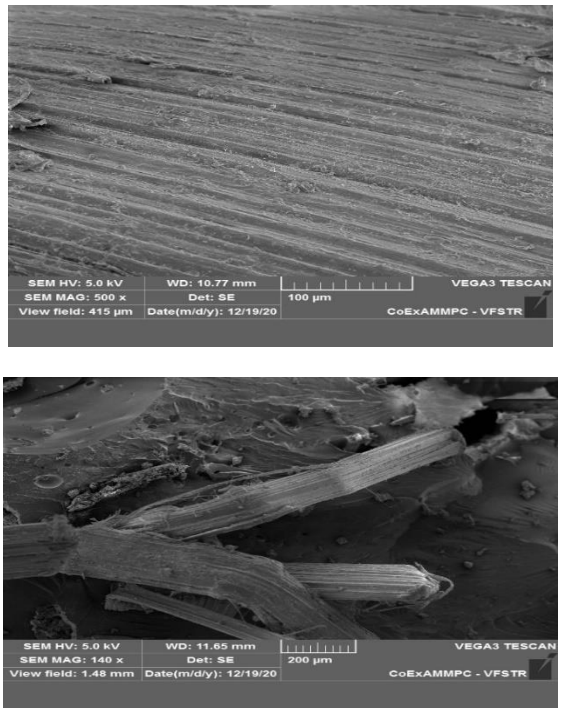

Fig 5. Sem Images of impact and Tensile samples

CONCLUSION

By the analysis, the following conclusions were stated

In this work, the fiber-reinforced polyester hybrid composites were prepared as per ASTM standards. The jute fiber and teak wood powder are available abundantly in nature and offer low material density. The impact strength and tensile strength of the investigated material composite with the fiber and teak wood powder were found to be comparatively higher than the novel composite material. The density of the composite decreased with increasing fiber content or increasing teak wood powder. Thus, the hybrid composites were found to be light in weight and proposed better mechanical properties and insulating properties. The fracture surface was studied through the SEM images.

REFERENCES

1. Thakur VK, Thakur MK, Gupta RK (2014) Review: raw natural Fiber-based polymer composites. Int J Polym Anal Charact 19: 256–271. https://doi.org/10.1080/1023666X.2014.880016.
2. Wang X, Wang L, Lian W, Zhou A, Cao X, Hu Q (2018) The influence of carbon spheres on thermal and mechanical properties of epoxy composites. J Polym Res 25:1–7. https://doi.org/10.1007/ s10965-018-1623-2.
3. Oladele IO, Akinwekomi AD, Agbabiaka OG, Oladejo MO (2019) Influence of biodegradation on the tensile and wear resistance properties of bio-derived CaCO 3 /epoxy composites. J Polym Res 26: 1–9. https://doi.org/10.1007/s10965-018-1676-2.
4. Tavassoli F, Razzaghi-Kashani M, Mohebby B (2018) Hydrothermally treated wood as reinforcing filler for natural rubber bio-composites. J Polym Res 25:1–11. https://doi.org/10.1007/ s10965-017-1394-1
5. Burzic I, Pretschuh C, Kaineder D et al (2019) Impact modification of PLA using biobased biodegradable PHA biopolymers. Eur Polym J 114:32–38. https://doi.org/10.1016/j.eurpolymj.2019.01. 060.
6. Ramesh P, Prasad BD, Narayana KL (2019) Morphological and mechanical properties of treated kenaf fiber/MMT clay reinforced PLA hybrid biocomposites. AIP Conf Proc. https://doi.org/10.1063/1.5085606.
7. Agayev S, Ozdemir O (2019) Fabrication of high density polyethylene composites reinforced with pine cone powder: mechanical and low velocity impact performances. Mater Res Express. https://doi.org/10.1088/2053-1591/aafc42.
8. Jain NK, Gupta MK (2018) Hybrid teak/Sal wood flour reinforced composites: mechanical, thermal and water absorption properties. Mater Res Express. https://doi.org/10.1088/2053-1591/aae24d.
9. Khonsari A, Taghiyari HR, Karimi A, Tajvidi M (2015) Study on the effects of wood flour geometry on physical and mechanical properties of wood-plastic composites. Maderas Cienc y Tecnol 17:545–558. https://doi.org/10.4067/S0718-221X2015005000049.
10. Vinod A, Vijay R, Singaravelu DL (2018) ThermoMechanical characterization of Calotropis gigantea stem powder-filled jute Fiberreinforced epoxy composites. J Nat Fibers 15:648–657. https://doi. org/10.1080/15440478.2017.1354740.
11. Kumaran P, Mohanamurugan S, Madhu S et al (2019) Investigation on thermo-mechanical characteristics of treated/untreated Portunus sanguinolentus shell powder-based jute fabrics reinforced epoxy composites. J Ind text:1–33. https://doi.org/10.1177/ 1528083719832851.
12. Movva M, Kommineni R (2019) Effect of green gram husk Nanocellulose on Banana Fiber composite. J Nat Fibers 16:287– 299. https://doi.org/10.1080/15440478.2017.1414658.
13. Vijay R, Vinod A, Kathiravan R et al (2018) Evaluation of Azadirachta indica seed/spent Camellia sinensis bio-filler based jute fabrics–epoxy composites: experimental and numerical studies. J Ind text:1–26. https://doi.org/10.1177/1528083718811086.
14. Arumuga prabu V, Uthayakumar M, Manikandan V, et al (2014) Influence of redmud on the mechanical, damping and chemical resistance properties of banana/polyester hybrid composites. Mater Des 64:270–279. doi: https://doi.org/10.1016/j.matdes. 2014.07.020.
15. Saw SK, Akhtar K, Yadav N, Singh AK (2014) Hybrid composites made from jute/coir fibers: water absorption, thickness swelling, density, morphology, and mechanical properties. J Nat Fibers 11: 39–53. https://doi.org/10.1080/15440478.2013.825067

 ISBN: 978-93-91420-02-4

Experimental Investigation and Optimization of Process Parameters in Wire Cut EDM of EN31 Steel

Kantheti Prasada Raju ,
Research Scholar, Department of Mechanical Engineering, Nirwan University, Rajasthan, India

Abstract **- Wire-cut electrical discharge machining (WEDM) is extensively used in machining of conductive materials producing intricate shapes with high accuracy. This study exhibits that WEDM process parameters can be altered to achieve betterment of surface roughness (SR). The objective of our project is to investigate and optimize the potential process parameters influencing the SR and Electrode Wear while machining of EN 31 STEEL using WEDM process. This work involves study of the relation between the various input process parameters like pulse-on time(Ton), pulse off time(Toff), pulse peak current(IP), Wire material and work piece material and process variables. Based on the chosen input parameters and performance measures L-9 orthogonal array is selected to optimize the best suited values for machining for steel alloys by WEDM.**

Keywords:Wire-cut EDM process, EN 31 steel, surface roughness, Taguchi approach.

I. INTRODUCTION

Wire electro discharge machining (WEDM) is the process of material removal of electrically conductive materials using the thermo-electric source of energy. It is one of the most extended non-conventional machining processes. Wire-cut EDM is typically used to cut plates as thick as 300mm and to make tools, punches, and dies from hard metals that are difficult to machine with other methods. Wire electric discharge machining is based on material removal through a series of repetitive sparks between electrodes i. e, work piece and tool. In WEDM, material is removed from the work piece by a series of discrete sparks that occurs between the work piece and the wire separated by a flow of dielectric fluid, which is continuously supplied to the machining zone. The process uses a thin wire of diameter about 0.1-0.3 mm as tool and the work piece is mounted on a computer numeric-controlled worktable. Complex two-dimensional shapes that can be cut on the work piece by controlled movement of the x-y worktable. Industry demands new materials showing high mechanical performance in terms of high strength-to-weight ratio, high toughness, and lower value of coefficient of thermal expansion.

1.1 Influence of Process Parameters on Wire Cut EDM Process

The main goal of WEDM manufacturers and users is to achieve a better stability of the process and higher productivity. As newer, more exotic materials are developed and more complex shapes are presented, conventional machining operations reach their limitations; hence the increased use of WEDM in manufacturing continues to grow at an accelerated rate. Wire electrical discharge machining manufacturers and user emphasize on achievement of higher machining productivity with a desired accuracy and surface finish. However, due to many variables even a highly skilled operator with a state-of the art WEDM is rarely able to achieve the optimal performance. The optimum utilization of the capacity of WEDM process requires proper selection of machining parameters. This part of literature review aims to investigate the effect of various process parameters on desirable output. WEDM is complex in nature and is controlled by large number of parameters.

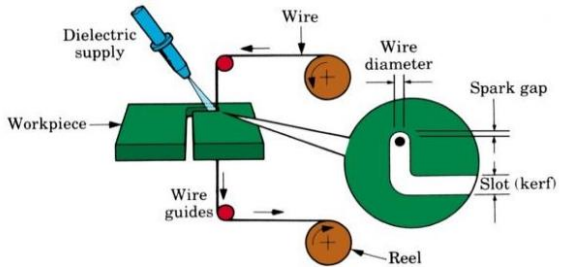

Fig :1 Working principle of WEDM

II. LITERATURE REVIEW

S. B. Prajapati, N. S. Patel [1] evaluates the effect of Ton, Toff, voltage, wire feed and wire tension on MRR, SR, kerf, and gap current in Wire EDM. A series of experiments have been performed on AISI A2 tool steel in form of a square bar. Analysis of data optimization and performance is done by Response Surface Methodology (RSM). Atul J. Patel, Prof. Satyam Patel [2] used Taguchi L9 orthogonal array to find out effects on AISI 304 Stainless Steel of thickness 10 mm in Wire EDM. Input parameters such as Ton,Toff, wire tension and input power have been used to evaluate their influence on Surface Roughness and Material Removal Rate. Mathematical relations between input parameters and performance characteristics were established by the linear regression analysis method by using MINITAB software. Rao and Sarcar [3] studied the influence of optimal parameters on cutting speed, surface roughness, spark gap, and material removal rate (MRR). He evaluated the optimal parameters such as discharge current, voltage at rated wire speed and tension for brass electrode of size 5-80 mm. Mathematical relation was developed for cutting speed, spark gap and MRR. Effect of wire material on cutting criteria was also evaluated for brass work piece with four wires of different copper percentages. This study is useful for evaluating cutting time for any size of job and to set parameters for required surface finish for high accuracy of cutting. Mathematical relations are helpful for estimating cutting time, cost of machining, process planning and accuracy of cutting for any size of job within machine range. Results obtained are helpful for quantification of parameters for quality cuts. Also, results are useful in manufacturing wire EDM system for die and tool steel electrodes. The effect and optimization of machining

parameters on kerf and material removal rate (MRR) in WEDM operations is addressed in [4]. Experimental studies were conducted using different pulse duration, open circuit voltage, wire speed, and dielectric flushing pressure. Importance levels of parameters were analyzed using analysis of variance (ANOVA). The optimum machining parameter combination was obtained by using the analysis of signal-to-noise (S/N) ratio. The variation of kerf and MRR with machining parameters is mathematically modelled by using regression analysis method. Objective of minimum kerf together with maximum MRR was performed. The experimental studies were performed on a Sodick A320D/EX21 WEDM machine tool. CuZn37 Master Brass wire with 0.25mm diameter was used in the experiments. As work piece material, AISI 4140 steel (DIN 42CrMo4) with 200mm × 40mm × 10mm size was used [5]. The effect of process parameter like Ton, Toff, voltage, wire feed and wire tension on MRR, SR, Kerf and Gap current. Output parameters of wire EDM of AISI A2 tool steel are predicted by using artificial neural network. Taguchi method is used for design of experiment. The control factors considered for the study are Ton, Toff, bed speed and current. Three levels for each control factor were used. In [6], authors investigated the effect of voltage, dielectric pressure, pulse on-time and pulse off-time on spark gap of Ti6AL4V alloy. It has been found that pulse on time and pulse off time have the more impact on the spark gap. The minimum spark gap was obtained as 0.040407mm. The WEDM experiments were conducted in electronic ultra-cut S1 machine using 0.25 mm brass wire as the tool electrode. 'Pulse on time', 'pulse off time', 'voltage' and 'dielectric pressure' are the four WEDM parameters that were selected for investigations. In this experimental study two level full factorial experiment is adopted because this gives all possible combinations of machine parameters. It can be noticed that corresponding to minimum value of pulse off time the spark gap decreases with increase in dielectric pressure, whereas the spark gap increases with increase in dielectric pressure corresponding to maximum value of pulse off time.

Authors in [7] aimed to investigate the influence of feed rate on the performance of WEDM on Titanium Ti-Al-4V. Brass wire was employed as the electrode for the investigation. The best combination of machining parameter viz. machine feed rate (4 mm/min), wire speed (8 m/min), wire tension (1.4kg) and voltage (60V) were identified. The selection of parameters depends on the requirements based on a better surface roughness or a maximum material removal rate. Hence an appropriate combination of variables can be selected accordingly. Furthermore, this combination can contribute to increase production rates perceptibly by reducing machining time. The outcome of this study will help in improving the quality of Titanium Ti-6Al-4V products as well as minimizing the machining cost to realize the economic potential to the fullest. Lodhi et al [8] investigated effect of parameter on machining of AISI D3 steel through wire cut EDM. The machining parameters selected are pulse-on-time, pulse-off-time, peak current, and wire feed. An orthogonal array, the signal-to-noise (S/N) ratio, and the analysis of variance (ANOVA) were employed to the study the surface roughness in the WEDM of AISI D3 Steel. It was observed that the discharge current was the most influential factors on the surface roughness. It was identified that the pulse on time and current have influenced more than the other parameters considered in this study. The conformation experiment has been conducted. Result shows that the error associated with SR is only 3.042 %. G. Selvakumar et al [9] investigated effect of parameter on machining of 5083 aluminum alloy through wire cut EDM. Based on the Taguchi experimental design (L9 orthogonal array) method, a series of experiments were performed by considering pulse-on time, pulse-off time, peak current and wire tension as input parameters. The surface roughness and cutting speed were considered responses. ANOVA test was performed to determine the level of significance of the parameters on the cutting speed and surface roughness. ANOVA revealed that the CS was independent on wire tension and Ra was independent on pulse-off time and wire tension. An optimum parameter combination for the minimum Ra and the maximum CS was obtained by the analysis of signal-to- noise (S/N) ratio. Pratik A. Patil et al [10] investigated effect of parameter on machining of AISI D2 cold work steel through wire cut EDM. This research deals with Response Surface Methodology approach for maximizing the material removal rate in wire electrical discharge machining. The investigated machining parameters were wire tension, pulse on time and peak current. After the experimentation, the effect of the parameters on MRR was determined by analysis of variance. From the investigation work MRR increases as the peak current increases. Also, the wire tension and pulse on time influences the MRR, but to a smaller extent.

III.ATERIALS AND METHODS

Due to the different melting point, evaporation and thermal conductivity, different materials show different surface quality and MRR at the same conditions of machining.EN 31 STEEL is the work piece material which is used in this experiment. TheEN 31 steel of 125mm x 100mm x 3mm size has been used as a work piece material and a profile of 5mm x 5mm x 2mm has been cut with the wire(Brass and Brass coated Nickel) traversing the through the kerf made and the performance analysis of output parameters with respect to input parameters is measured.

IV.EXPERIMENTAL SETUP

The experiments were carried out on a wire cut EDM machine (ELEKTRA SPRINTCUT 734).The WEDM machine tool has the following specifications.

- Experiments have been performed to investigate the effects of one or more factors of the process parameters on the surface finish of the wire cut machined surface.
- The main aim of the project is to determine the influence of time on, time off, wire feed and input power. The investigation is based on surface roughness during machining of EN 31 steel.

V.PROCESS PARAMETERS AND DESIGN

Input process parameters such as Pulse On time (TON), Pulse Off time (TOFF), Peak Current (IP), used in this thesis are shown in Table. Each factor is investigated at three levels to

 ISBN: 978-93-91420-02-4

determine the optimum settings for the WEDM process. Wire feed is 3m/min, Wire Tension is 7 Kgf and Servo Feed is kept constant at 2.1m/min.

The selection of parameters for experimentation is done as per taguchi design. An orthogonal array for three controllable parameters is used to construct the matrix of three levels of controllable factors. The L9 orthogonal array contains 9 experimental runs at various combinations of three input variables.

Table 1: Experimental parameters.

Experiments	Ton (µsec)	Toff (µsec)	IP (A)
1	116	52	210
2	116	54	220
3	116	56	230
4	123	52	210
5	123	54	220
6	123	56	230
7	128	52	210
8	128	54	220
9	128	56	230

Fig. 2: WEDM machine.

Fig. 3: Cutting process.

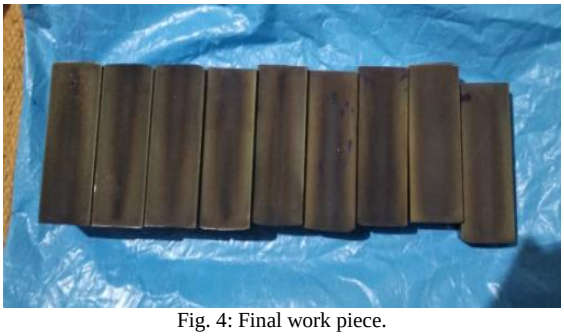

Fig. 4: Final work piece.

VII.SURFACE FINISH RESULTS

In this project most important output performances in WEDM such as Surface Roughness (Ra) is considered for optimizing machining parameters. The surface finish value (in µm) was obtained by measuring the mean absolute deviation, Ra (surface roughness) from the average surface level using a computer controlled surface roughness tester. Surface Finish Tester – Model Surtronic 3+, Rank Taylor Hobson Ltd., Made in England which is periodically calibrated using Reference Specimen Type 112/1534. Lab Temperature 20 $\pm 20^0$C.

Table 2: Surface finishing values for each piece.

Experiments	Ton (µsec)	Toff (µsec)	IP (A)	SR
1	116	52	210	4.12
2	116	54	220	3.85
3	116	56	230	3.80
4	123	52	220	4.00
5	123	54	230	4.82
6	123	56	210	4.10
7	128	52	230	4.90
8	128	54	210	4.60
9	128	56	220	4.26

VI.AGUCHI TECHNIQUE

Taguchi defines Quality Level of a product as the Total Loss incurred by society due to failure of a product to perform as desired when it deviates from the delivered target performance levels.

This includes costs associated with poor performance, operating costs (which changes as a product ages) and any added expenses due to harmful side effects of the product in use.

Taguchi Methods

- Help companies to perform the Quality Fix!
- Quality problems are due to Noises in the product or process system
- Noise is any undesirable effect that increases variability
- Conduct extensive Problem Analyses
- Employ Inter-disciplinary Teams
- Perform Designed Experimental Analyses
- Evaluate Experiments using ANOVA and Signal-to noise techniques

The Experimental results show the effect of three process parameters surface roughness.

Table 3: Response for S/N Ratios.

Level	Ton (µsec)	Toff (µsec)	IP (A)
1	-11.87	-12.71	-12.60
2	-12.65	-12.88	-12.11
3	-13.22	-12.15	-13.02
Delta	1.35	0.73	0.91
Rank	1	3	2

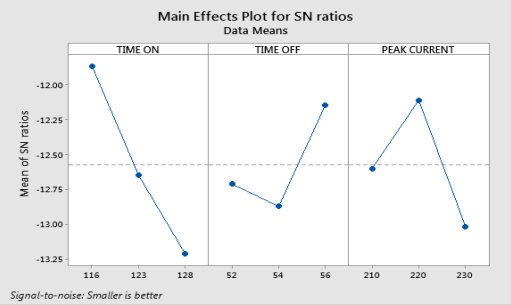

Fig. 5: Effect of parameters surface roughness for S/N ratio.

CONCLUSION

The objective of the present work is to investigate the effects of the various Wire cut EDM process parameters on the machining quality and obtain the optimal sets of process parameters so that the quality of machined parts can be optimized. Experiments are conducted on the pieces varying parameters. The materials used for machining are nickel alloy. The process parameters considered are Ton, Toff, and IP. The range of values varied are Time on – 116µsec, 123 µsec and 128 µsec, Time off – 52µsec, 54µsec, 56 µsec, Input current –210 amp, 220 amp, 230 amp. Wire feed, wire tension and servo voltage are kept constant. The optimization is done by using TAGUCHI technique by considering L9 orthogonal array. Finally, the optimal process parameter combination obtained at Ton-116µsec, Toff- 56 µsec, and IP-230amp for maximum surface finish values.

REFERENCES

[1] S. B. Prajapati, N. S. Patel, Effect of process parameters on performance measures of Wire EDM for AISI A2 Tool Steel. International Journal of Computational Engineering Research|, vol. 3, no. 4, 2013.

[2] Atul J. Patel, Prof. Satyam Patel, Parametric optimization of Wire cut EDM machine on hard steel alloy with multiple quality characteristics. Patel et al., International Journal of Advanced Engineering Technology.

[3] C V S Parameswara Rao and M MM Sarcar, Evaluation of optimal parameters for machining brass with Wire cut EDM. Journal of Scientific and Industrial Research, vol. 68, 2009, pp. 32-35.

[4] Nihat Tosun, Can Cogun and Gul Tosun, A study on kerf and material removal rate in wire electrical discharge machining based on Taguchi method. Journal of Materials Processing Technology, vol. 152, 2004, 316-322.

[5] S. B. Prajapati, N. S. Patel, V D Asal. Prediction of Process Parameters of Wire EDM for AISI A2 using ANN. vol. 3, no. 5, 2013.

[6] K. Basil, J. Paul, J. M. Issac. Spark Gap Optimization of WEDM Process on Ti6Al4V. International Journal of Engineering Science and Innovative Technology, vol. 2, no. 1, January 2013.

[7] A. Alias, B. Abdullah, N. M. Abbas. WEDM: Influence of machine feed rate in machining titanium Ti-6Al-4V using brass wire and constant current (4A). International Symposium on Robotics and Intelligent Sensors, 2012.

[8] B. K. Lodhi, S. Agarwal, "Optimization of machining parameters in WEDM of AISI D3 Steel using Taguchi Technique." Procedia CIRP, vol. 14, 2014, pp. 194-199.

[9] G. Selvakumar, G. Sornalatha, S. Sarkar, S. Mitra, "Experimental investigation and multi-objective optimization of wire electrical discharge machining (WEDM) of 5083 aluminum alloy." Trans. Nonferrous Met. Soc. China, vol. 24, 2014, pp. 373-379. |

[10] P. A. Patil, C.A. Waghmare, "Optimization of process parameters in wire-EDM using response surface methodology." Proceedings of 10th IRF International Conference, 01st June-2014, pp. 110-115.

 ISBN: 978-93-91420-02-4

Design and Analytics of Differential Gear Box

T.Ashok Kumar and P.Mokthar Bhasha
Department of Mechanical Engineering, Narasaraopeta Engineering College (A), Narasaraopet, India

***Abstract*- Gears are the most important component in a power transmission system. Advances in engineering technology in recent years have brought demands for gear teeth, which can operate at ever increasing load capacities and speeds. The gears generally fail when tooth stress exceeds the safe limit. Therefore it is essential to explore alternate gear material. The important considerations while selecting a gear material is the ability of the gear material to withstand high frictional temperature and less abrasive wear. Weight, manufacturability and cost are also important factors those are need to be considered during the design phase. Moreover, the gear must have enough thermal storage capacity to prevent distortion or cracking from thermal stress until the heat can be dissipated. It must have well anti-fade characteristics i.e. their effectiveness should not decrease with constant prolonged application and should have well anti-wear properties.**

The main objective of this project is to developed parametric model of differential Gearbox by using CATIA-V5 under various design stages. It is observed that composite material is best material for differential gearbox and is found to suitable for different revolutions (2500 rpm, 5000 rpm and 7500 rpm) under static loading conditions. Comparisons of various stress and strain results using ANSYS-19.2 with Glass filled polyamide composite and metallic materials (Aluminium alloy, Alloy Steel and Cast Iron) are also being performed and found to be lower for composite material.

I. INTRODUCTION

Gearboxes are used in almost every industry right from power to marine, and also include agriculture, textile, automobiles, aerospace, shipping etc. There are different types of gearboxes available for varying uses. These gearboxes are constructed from a variety of materials depending on their end use and the kind of industry they are being used in. The product has numerous industrial applications for providing high torque and smooth speed reductions. These gearboxes are also manufactured keeping certain specifications in mind, which will also vary depending on the application.

The upcoming requirement of power saving and efficiency of mechanical parts during the past few years increased the use of composite materials. Moreover the use of composite materials have also increased due to their properties such as weight reduction property with enough strength , high specific stiffness, corrosion free, ability to produce complex shapes, high specific strength, high impact energy absorption and many more. Product development has changed from the traditional serial process of design, followed by prototype testing and manufacturing but to more on computer aids. CAE (Computer Aided Engineering) has greatly influenced. The chain of processes between the initial design and the final realization of a product. CAE software helps in product designing, 3-D visualization, analysis, simulation and impacted a lot on time and cost saving to the industry. A Gear box is one of the important mechanical components of transmission system used in variety of machines. Differential Gear box increases effective weight of vehicle which in turn directly affects the performance and efficiency of the vehicle. So there is a requirement to make light and effective gears. Therefore, in the present work composite materials are used to make light weight gears in order to perform such duty efficiently.

A. Importance of differential gear box

A differential is a device, usually but not necessarily employing gears, capable of transmitting torque and rotation through three shafts, almost always used in one of two ways: in one way, it receives one input and provides two outputs this is found in most automobiles and in the other way, it combines two inputs to create an output that is the sum, difference, or average, of the inputs. In automobiles and other wheeled vehicles, the differential allows each of the driving road wheels to rotate at different speeds, while for most vehicles supplying equal torque to each of them. A vehicle's wheels rotate at different speeds, mainly when turning corners. The differential is designed to drive a pair of wheels with equal torque while allowing them to rotate at different speeds. In vehicles without a differential, such as karts, both driving wheels are forced to rotate at the same speed, usually on a common axle driven by a simple chain-drive mechanism. When cornering, the inner wheel needs to travel a shorter distance than the outer wheel, so with no differential, the result is the inner wheel spinning and/or the outer wheel dragging, and this results in difficult and unpredictable handling, damage to tires and roads, and strain on (or possible failure of) the entire drive train.

B. Definition

- A gearbox, also known as a gear case or gearhead, is a gear or a hydraulic system responsible for transmitting mechanical power from a prime mover (an engine or electric motor) into some form of useful output. It is referred to the metal casing in which a number of gears are sealed.
- A gearbox is also a set of gears for transmitting power from one rotating shaft to another. They are used in a wide range of industrial, automotive and home machinery application.
- Gearheads are available in different sizes, capacities and speed ratios. Their main function is to convert the input provided by an electric motor into an output of lower RPM and higher torque.

C. Functions of Gear box

- A gearbox is precisely bored to control gear and shaft alignment.
- It is used as a housing/container for gear oil.

 ISBN: 978-93-91420-02-4

- It is a metal casing for protecting gears and lubricant from water, dust and other

D. Transmission system

There are three types of transmission system**.**

- Manual Transmission System
- Automatic Transmission System
- Semi-automatic Transmission System

E. Manual Transmission

A manual transmission is often referred to as a stick shift or standard transmission, essentially used in the automobile industry. This type of transmission features gear ratios that are selected by engaging pairs of gears inside the transmission.

Figure 1: manual transmission

Types of Manual Transmission

Synchronized Systems**:** This type of transmission system or gearbox does not require synchronization with the driver while changing gears.

Unsynchronized Systems: This type of transmission system or gearbox allows free spinning of gears with their relative speeds synchronized by the driver for avoiding clashing and grinding of gears.

Types of Gearbox Available

There are different types of gearbox available and with different mountings. Some of them are:

- Floor Mounted Shifter
- Column Mounted Shifter
- Sequential Manual Shifter

Advantages of a Manual Transmission System

- Cheaper than the automatic transmission system.
- Better fuel economy than other transmission systems.
- Requires low maintenance.
- Does not require active cooling.

F. Automatic Transmission

- Automatic transmission is a type of gearbox, especially used in the automobile industry for changing gear ratios automatically. It does not require manual shifting of gears. The gearbox has a set of selected gear range.

- The system is hydraulically operated and makes use of a torque converter and a set of planetary gears.

Figure 2: Automatic transmission

Parts of an Automatic Transmission System

An automatic transmission consists of the following parts:

- *Torque Converte***r:** It is a device connecting engine and transmission. The instrument takes place of a mechanical clutch, allowing the engine to remain running. A torque converter that provides a variable amount of torque multiplication at low engine speeds.
- *Planetary Gearbox Set***:** The bands and clutches of this gear set are actuated with the help of hydraulic servos controlled by the valve body, thereby providing two or more gear ratios.
- *Valve Body***:** The system receives pressurized fluid from a main pump operated torque converter. The pressure coming from this pump is regulated and used to run a network of spring-loaded valves, check balls and servo pistons. The valves make use of pump pressure and the pressure from a centrifugal controller on the output side.

G. Semi-Automatic Transmission

- Semi-automatic transmission is a system that makes use of electronic sensors, processors and actuators for gear shifting. The system removes the need of a clutch pedal required for gear changing. This system is widely used in the automobile industry.

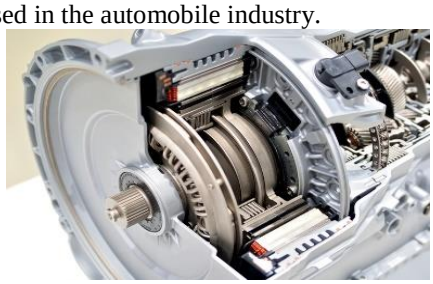

Figure 3: semi-automatic transmission

Types of Semi-Automatic Transmission

- Direct Shift Gearbox
- Dual Clutch Gearbox

The system allows for only forward and backward shift into higher and lower gears. It does not make use of the traditional H-pattern, normally used in automobiles. The system is also equipped with sensors that sense the direction of the shift. The input combines with the sensor placed in the gearbox and senses the current speed and selected gear. The unit also determines the torque required for smooth functioning. The system also reduces fuel consumption significantly.

Gearbox Specifications

 ISBN: 978-93-91420-02-4

II. GEARBOX SPECIFICATIONS

There are a number of performance specifications which must be considered while choosing a gearbox for different industrial application.

Some of the important specifications are:

- Gear ratio: The ratio may be specified as x: 1, where x is an integer.
- Output torque
- Maximum input power
- Maximum input speed
- Gearing arrangement
- Reducer output
- Shaft Alignment

A. About Gear Ratio

The gear ratios can be defined as the relationship between the number of teeth on two different gears meshed together or the circumference of two pulleys connected with a drive belt.

Generally the number of teeth on a gear is also proportional to the circumference of the gear wheel, so the bigger the wheel, the more teeth it has. Therefore the gear ratio can also be explained as the relationship between the circumferences of both wheels.

B. Explanation of the Term

The concept of gear ratio can be well explained with the help of an example as follows:

Suppose a smaller gear has 12 teeth, while the larger gear has 24 teeth. Therefore the gear ratios between the smaller and the larger teeth are 12/24 or 1:2

The first number in the ratio is generally the gear that power is applied to. The ratio also means that for one revolution of the smaller gear, the larger gear has made 1/2 or 0.50 revolutions. This further implies that the larger gear turns slowly as compared to the smaller one.

III. GEAR BOX

A. Gearbox Glossary

- ANSI**:** American National Standards Institute.
- Addendum**:** It can be defined as the radial or perpendicular distance between the pitch circle and the top of the teeth.
- Alignment**:** Accurate alignment of shafts on which gears are mounted is an important factor in gear life and performance. Shafts are set parallel in spur and helical gearboxes, and perpendicular in most bevel and worm gearboxes. Dis-alignment of shafts could lead to premature gear failure or other performance issues including noise.
- Brinell hardness number (BHN)**:** It is a measure of the hardness of a material such as steel.
- Backlash: It is the extent by which the width of a tooth space exceeds the thickness of the engaging tooth on the pitch circles.
- Backlash Variation**:** It can be defined as the difference between maximum and minimum backlash occurring in a complete revolution of the largest of a pair of mating gears.
- Bevel Gears**:** These are conical shaped gears designed to operate on intersecting axes. In most gearboxes the shafts will intersect at a 90o angle. Straight bevel gears and spiral bevel gears are the two common types.
- Bore**:** It is the diameter of the hole in a sprocket, gear, bushing, etc.
- Bottom Diameter: Also known as a root diameter, it is the diameter of a circle measured across the bottoms of opposite tooth spaces.
- Bull Gear: A bull gear is the larger gear in two or more gear set, the smaller one, known as a pinion.
- Burning**:** Cutting a steel plate with the help of a torch.
- Bushing**:** A mechanical device/tool used for mounting a sprocket or gear on a shaft.
- CD**:** Centre Distance.
- CP: Circular Pitch.
- Distance (CD): It is the shortest distance between non-intersecting axes of engaged gears.
- Circular Pitch (CP): It is the distance along the pitch line between corresponding profiles of adjacent teeth.
- Circular Thickness: It is the thickness of the tooth on the pitch circle.
- Coupling Sprockets, Chains, and Covers**:** A product line used for connecting two non- continuous shaft ends.
- DP: Diametral Pitch.
- Dedendum (DED): It is the radial or perpendicular distance between the pitch circle and the bottom of the gullet.
- Diametral Pitch (DP): It is the ratio of the number of teeth to the number of inches in the pitch diameter.

B. Gearbox Materials

A range of gearboxes are constructed from a variety of materials depending on the industry or the product in which they are being used for. Finest quality materials are used to manufacture gearboxes for ensuring reliability, ease of maintenance and long life. The specialty gearboxes materials undergo vibration and endurance test to ensure that the end product is of premium quality.

- Aluminum Gearbox
- Cast Iron Gearbox
- Bronze Iron Gearbox
- Stainless steel Gearbox

C. Types of Gearbox

A variety of gearboxes are manufactured from different superior quality materials and with different performance specifications depending on their industrial application. These gearboxes are available in a range of capacities, sizes and speed ratios, but the main function is to convert the input of a prime mover into an output with high torque and low RPM. A variety of gearbox find application in a large number of industries including agriculture, aerospace and mining, paper and pulp industry.

Some of the popular types of gear boxes in use are as follows:

- Bevel Gearbox
- Helical Gearbox
- Planetary Gearbox
- Sequential Gearbox
- Spiral Bevel Gearbox
- Worm Reduction Gearbox
- Cycloidal Gearbox

- Offset Gearbox
- Right Angle Bevel Gearbox
- Shaft Mounted Gearbox
- Worm Gearbox
- Crane duty gear box

Simple Differential Gearbox

D. Simple differential Gear box

Figure 4: simple differential gear box

IV. INTRODUCTION OF SIMPLE DIFFERENTIAL GEAR BOX

Bevel gearboxes are special speed reducers with their shafts lying perpendicular to each other and therefore used mainly in right-angle applications. The gearbox is a kind of right angle gear and is suitable for a right angle solution with a low ratio. These gearboxes save more energy as compared to worm gears and are available in varying gear ratios.

A. Materials Used:

These gearboxes are constructed from a variety of materials. Some of the popularly used materials are

- Cast Iron
- Aluminum Alloy
- Steel

The ratio of a bevel gearbox can be determined by dividing the number of teeth in the larger gear by the number of teeth in the smaller one. These gearboxes generate varying level of torque and can also be customized to suit individual requirements.

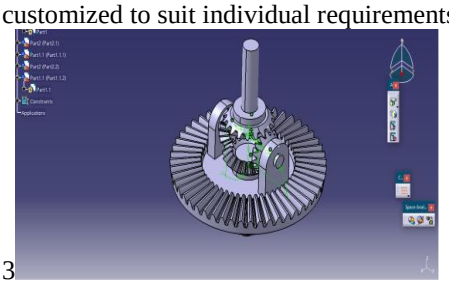

3

Figure 15: assembly of differential gearbox

The above picture shows the assembly of differential assembled in CATIA assembly design workbench. There is a constraints used to put gears on exact positions after the assembling gears, assembly was saved in IGS file format for analysis purpose.

V. ANSYS INTRODUCTION

The ANSYS program is a computer program for a finite element analysis and design. The operating conditions. The ANSYS program can also be used to calculate the optimal design for given operating conditions using the design optimization feature.

The ANSYS program is a multi-purpose program, meaning that you can use it for almost any type of finite element analysis in virtually any industry - automobiles, aerospace, railways, machinery, electronics, sporting goods, power generation, power transmission, and biomechanics, to mention just a few. “Multi- purpose” also refers to the fact that the program can be used in all disciplines of engineering – structural, mechanical, electrical, electromagnetic, electronic, thermal, fluid, and biomedical. The ANSYS program is also used as an educational tool in universities and other academic institutions.

ANSYS software is available on many types of computers – PCs (personal computers), workstations, minicomputers, super minis, mainframes, super mainframes, etc. Several operating systems are supported, as are multiple of graphic devices.

A total of six windows are opened when you start ANSYS.

- Utility Menu (top) – contains functions that are available for throughout the ANSYS session, such as file controls, selections, graphic controls and parameters. You also exit the ANSYS program from the file pull down menu.
- Main Menu (bottom left) – contains the primary ANSYS functions, organized by the pre-processor, solution, general, postprocessor, design optimizer.
- Toolbar (Middle Right) – contains push buttons that execute commonly used ANSYS commands. More push buttons can be added.
- Input window (middle left) – shows program prompt messages and allow you to type in commands directly.
- Graphic window (bottom right) – a window where graphics are shown and graphical picking are made.
- Output window (not shown here) – shows text output from the program, such as listing of data etc. It is usually positioned behind the other window and can be put to the front when necessary.

The steps in any finite element analysis can be divided in three phases:

- Pre-processing – define the model such as mesh, loads, and boundary conditions
- Solution – assembling and solving the system of equation.
- Post processing – extracting relevant result from the solution.

Ansys develops and markets engineering simulation software for use across the product life cycle. Ansys Mechanical finite element analysis software is used to simulate computer models of structures, electronics, or machine components for analysing strength, toughness, . Ansys is used to determine how a product will function with different specifications, without building test products or conducting crash tests. For example, Ansys software may simulate how a bridge will hold up after years of traffic, how to best process salmon in a cannery to reduce waste, or how to design a slide that uses less material without sacrificing safety.

Elasticity, temperature distribution, electromagnetism, fluid flow, and other attributes

Most Ansys simulations are performed using the Ansys Workbench system, which is one of the company's main products. Typically Ansys users break down larger

 ISBN: 978-93-91420-02-4

structures into small components that are each modelled and tested individually. A user may start by defining the

A. Geometry:

In this step import designed differential in to ansys design modular, this is ansys design work window where simple, moderate designs are can create. Differential is more complex design to do so we created in CATIA V5 application. The created design saved in IGS file format. The below picture shows the imported geometry of differential.

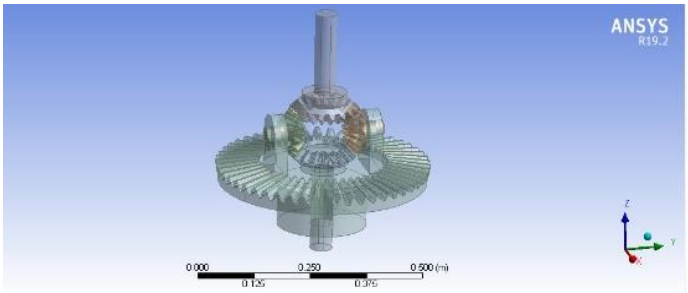

Figure 19: geometry

B. MESHING OF GEAR ASSEMLY

Meshing is the process which divides the whole assembly into small known parts. Those parts are called elements, those elements are connected to common points called nodes. Tetrahedrons element type is used for meshing and elements size is 40mm.

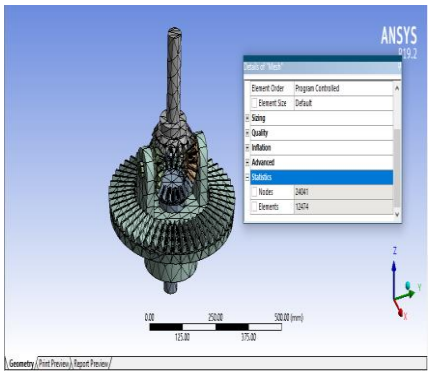

Figure 20: meshing

VI. RESULTS DISCUSSION

Analysis is the application of analytical techniques for checking the utility and feasibility of any design under workbench. Figure 19 shows Differential gearbox. Figure20 shows the meshed Differential gearbox. Figure 16 to Figure 18 shows properties of different materials used for Differential gear box. In the present work, Structural Analysis system is chosen in Ansys which is capable of providing solution for Equivalent (von-Misses) stress, Displacement (total Deformation) and Maximum Shear Elastic Strain for a different revolution i.e. 2500 rpm, 5000 rpm and 7500 rpm under static conditions for composite Material Differential Gear Box. Figure 22 to Figure 30 shows the Von-Misses stress, displacement and Maximum Shear Elastic Strain for tangential loading at 2500 rpm. Figure 31 to Figure 39 shows the Von-Misses stress, displacement and Maximum Shear Elastic Strain for tangential loading at 5000 rpm. Figure 40 to Figure 48 shows the Von-Misses stress, displacement and Maximum Shear Elastic Strain for tangential loading at 7500 rpmpredetermined specifications. The current work evaluates 3D modeled concepts for composite material Differential Gearbox using Finite Element Analysis (FEA). It is used to calculate deflection, stress, vibration, buckling behaviour and many other phenomena. In this work FEA is applied on solid CAD models developed on CATIA and deformation and stresses are evaluated on ANSYS.

A. Results for Aluminum alloy at 2500 rpm

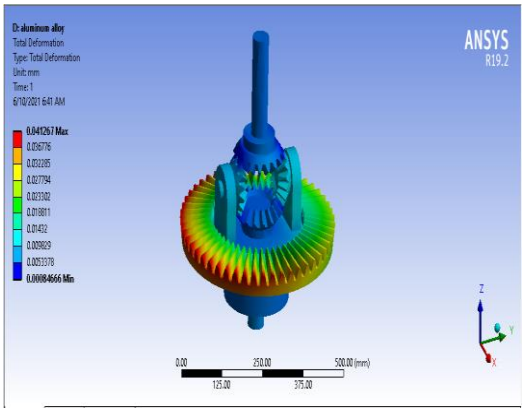

Figure 22: deformation of aluminium alloy

*Comparison tables***:**

2500 RPM:

	Cast Steel	Aluminium Alloy	Cast Iron
Tangential Load (N)	2093.8	2922.51	3243.08
Displacement(mm)	0.00615413	0.0241696	0.0100566
Stress (N/mm2)	2.29414	3.19018	3.57544
Strain	1.0400e-5	4.1593e-5	1.69558e-5
Static Load (N)	56141.9	18143.3	37933.7
Displacement (mm)	0.164988	0.150063	0.11763
Stress(N/mm^2)	63.5052	19.8068	41.8212
Strain	0.000280882	0.000258239	0.00019839
material	Total deformation	Equivalent stress	Shear strain
Aluminium alloy	0.041mm	17.75Mpa	0.00037

5000RPM:

TANGENTIAL	Cast Steel	Aluminum Alloy	Cast Iron
LOAD(N)	1818.54	1595.22	1770.24
DISPLACEMENT(mm)	0.0054118	0.0131944	0.00548866
STRESS (N/mm^2)	2.584	1.70369	2.01579
STRAIN	1.04958e^{-5}	2.2558e^{-5}	9.32532e^{-6}
STATIC			
LOAD(N)	56141.9	18143.3	37933.7
DISPLACEMENT(mm)	0.164853	0.150036	0.117614
STRESS (N/mm^2)	74.4963	22.6949	43.1949
STRAIN	0.000309415	0.000274774	0.000199826

 ISBN: 978-93-91420-02-4

CONCLUSION

In our project we have designed a differential for Ashok Leyland 2516M. Loads are calculated when the gears are transmitting different speeds 2400 rpm,5000 rpm. Structural analyses are done on the differential gearbox to verify the best material by taking in to account stresses, displacements, weight etc. By observing the structural analysis results using Aluminum alloy the stress values are within the permissible stress value. So using Aluminum Alloy is safe for differential gear. When comparing the stress values of the three materials for all speeds 2400rpm, 5000rpm the values are less for Aluminum alloy than Alloy Steel and Cast Iron. By observing analysis results, Aluminum Alloy is best material for Differential gearbox.

REFERENCES

1. J.O.Nordiana ,S.O.Ogbeide, N.N.Ehigiamusoe and F.I.Anyasi.,2007,"Computeraided design of a spur gear, "Journal of Engineering and Applied Sciences2(12);pp17431747.
2. ZepingWei., 2004" Stresses and Deformations in Involute spur gears by Finite Element method,"M.S,Thesis, College of Graduate Studies and research, University of Saskatchewan, Saskatchewan.
3. DarleW.Dudley, 1954, Hand book of practical geardesign
4. Alecstrokes,1970, High performance of gear design
5. Maitra,G.M,2004,HandBookofGearDesign,TataMcGrawHill, NewDelhi..
6. S.Md.Jalaluddin., 2006, "Machine Design,"Anuradha publications, Chennai.
7. ThirupathiChandrupatla,AshokD.Belegundu,"Introductionto finiteelementinEngineering",2003
8. PSG,2008."Designdata,"KalaikathirAchchagampublishers, Coimbatore, India.
9. S.Mahalingam,R.E.DBishop,1974,"Dynamicloading of Gear tooth", Journal of sound andvibration,36(2),pp179189